HOT ISOSTATIC PRESSING— THEORY AND APPLICATIONS

Conference Proceedings
Edited by M. Koizumi

CONFERENCE CHAIRMAN

M. Koizumi, Ryukoku University

PROGRAM COMMITTEE

M. Abouaf	CICESA, France
A. Asari	Kobe Steel Ltd, Japan
M. F. Ashby	University of Cambridge, UK
L. Delaey	Katholieke Universiteit Leuven, Belgium
T. Garvare	The Swedish Institute of Production Engineering Research, Sweden
R. Hayami	Ion Engineering Center Corporation, Japan
W. A. Kaysser	Max-Planck-Institut für Metallforschung, FRG
R. J. Schaefer	National Institute of Standard and Technology, USA
K. Watando	NKK Corporation, Japan
R. Widmer	Industrial Materials Technology, USA

ORGANIZING COMMITTEE

H. Udoguchi and M. Nishihara, *Advisors*

R. Hayami, *Chairman*	President of Japan Research Association of Isostatic Pressing and Processing
T. Doi	Nikkiso Co. Ltd
T. Fujikawa	Kobe Steel Ltd
T. Igarashi	Sumitomo Electric Industries Ltd
K. Ishizaki	Nagaoka University of Technology
Y. Kaieda	National Research Institute for Metals
M. Kinoshita	Government Industrial Research Institute, Osaka
S. Kubo	Government Industrial Research Institute, Nagoya
Y. Miyamoto	Osaka University
K. Okuda	Nippon Tungsten Co. Ltd
M. Shimada	Tohoku University
M. Takata	Sumitomo Special Metals Co. Ltd
I. Tanaka	Osaka University
K. Uematsu	Nagaoka University of Technology
R. Watanabe	Tohoku University
H. Nishio	NKK Corporation

HOT ISOSTATIC PRESSING—
THEORY AND APPLICATIONS

Proceedings of the
Third International Conference
Osaka, Japan
10–14 June 1991

Edited by

M. KOIZUMI

Sponsored by
The Japan Research Association of
Isostatic Pressing and Processing

ELSEVIER APPLIED SCIENCE
LONDON and NEW YORK

ELSEVIER SCIENCE PUBLISHERS LTD
Crown House, Linton Road, Barking, Essex IG11 8JU, England

Sole Distributor in the USA and Canada
ELSEVIER SCIENCE PUBLISHING CO., INC.
655 Avenue of the Americas, New York, NY 10010, USA

WITH 68 TABLES AND 447 ILLUSTRATIONS

British Library Cataloguing in Publication Data

Hot isostatic pressing: theory and applications.
I. Koizumi, M.
620.43

ISBN 1 85166 744 X

Library of Congress CIP data applied for

PREFACE

The HIP process was originally devised for diffusion bonding of nuclear fuel elements at Battelle Memorial Institute in the United States in the mid-1950s. This innovative technique has been a subject of global research and development, and was applied to the cemented carbide industry at the end of the 1960s by ASEA/ Sandvik. Since then this process has been applied to many kinds of industrial materials, including tool steel, superalloys and electronic and ceramic materials. In very recent years, HIPing technology has been applied even to R&D of high temperature superconducting materials and of a composite process with self-combustion reaction.

On this occasion we should recognize that the 3rd HIP Conference was held in the midst of such progress of HIP technology, and that it was the first international conference which was held in Asia in the field of HIP and CIP technologies.

The conference was very successful, with about 250 participants from 13 countries, including Japan. About 90 presentations, including nine invited lecturers, 44 oral and 35 poster presentations, were offered, and all contributions were at a high level and contained valuable results which had been attained in recent years.

It should be noted that the International HIP Committee (IHP) was established during this Osaka Meeting to unify the two series of international HIP conferences which were started independently in Sweden and in Belgium in 1987. The Committee successfully reached an agreement to unify the two conference series and decided to hold the next conference, the 4th HIP-HIP '93, at Antwerp in 1993.

Finally, I hope that the conference proceedings will be a valuable reference for scientists in the field of HIP technology. And I would like to express my hearty thanks to the Japan Research Association of Isostatic Pressing and Processing (JRAIPP) for their financial support, and to academic societies and associations, including The Japan Institute of Metals and The Ceramic Society of Japan, for their co-sponsorships.

MITSUE KOIZUMI
Conference Chairman

CONTENTS

4. METALS AND ALLOYS

5. BONDING

6. HIGH Tc SUPERCONDUCTORS

7. COMPOSITES

8. EQUIPMENT AND INSTRUMENTATION

9. NEW APPLICATION

1. PLENARY LECTURE

FUTURE PROSPECTS FOR HOT ISOSTATIC PRESSING

Robert Widmer
Industrial Materials Technology
Andover, MA, U.S.A.

ABSTRACT

The current status of HIP technology is briefly reviewed with the inclusion of some past success stories such as the densification of investment castings and the large tonnage production of powder billets.

In discussing future prospects for the method, the emphasis is primarily on projects which are expected to have an important commercial impact. Examples that are discussed are, among others, custom tailored materials and parts which are designed and manufactured by using HIP as a unique tool. Spray deposition combined with HIP densification is another area of obvious importance and good potential.

In considering expansion of HIP processing on a broad scale, the possibility of the use of dedicated equipment is being discussed. HIP of aluminum with all the equipment implications will be a prime target.

INTRODUCTION

Over the last 20 years hot isostatic pressing (HIP) has experienced a relatively rapid acceptance by several industries. This was accomplished, in part, due to innovative developments by materials R&D groups but equally as important was the availability of reliable equipment adapted to emerging needs. Once feasibility of a specific processing step was established, end users of the material or the part cooperated closely for the purpose of sensible specifications and subsequent integration of the HIP step into the manufacturing sequence. An outstanding example of this type has been the HIP application to casting densification where enlightened casting metallurgists quickly learned to combine casting technology with HIP densification and therefore often came up with an improved product at lower cost. The development of this win/win situation happened as soon as the goal was not just scrap recovery but rather total process improvement aimed at property amplification and extension of manufacturing capabilities.

On the other hand, these developments may have happened all too quickly since full understanding of the effects of the process step was often lacking and therefore conditions were not necessarily optimized. The material densified at the available pressure and the chosen temperature and

consequently the process conditions were frozen. In some instances of metallurgically complex alloys this turned out to be a premature action and HIP conditions had to be modified in order to get the maximum benefit.

HIP activities currently ongoing and as usually represented in technical meetings can be observed in four areas:

- -Commercial HIP processing of materials on a routine basis
- -Studies of new areas which may involve the development of new materials or new approaches to the processing of a conventional material
- -Modeling and mechanistic studies aimed at understanding the process and the ability to predict processing conditions and resulting structures and properties
- -Development of innovative features in equipment design and operations.

This paper will address the major current HIP applications of commercial importance and come to some conclusion with regard to future business developments in those areas. In addition, an attempt will be made to show the likely directions in which the HIP activities can move successfully and what development work should be done in order to accelerate the process. The latter may include both theoretical and applied materials investigations as well as equipment developments. Finally, it is necessary to look at consolidation methods that may compete with conventional HIP.

CASTING DENSIFICATION

Conventional HIP has been used on a high volume commercial basis for structural castings as well as rotating parts for a variety of industries but with aerospace applications in the forefront. By now the benefits of the treatment are well known: due to the elimination of shrinkage porosity one gets improved mean values and a significant decrease in scatter. This means that properties of a casting can resemble those of a forging, and a replacement of forged and fabricated parts has occurred in many instances with cost savings the obvious incentive. Furthermore and probably most important, with the marriage of modern casting technology and HIP, the capability for cast parts was significantly extended to larger dimensions and thinner sections. This example of concurrent engineering has worked perfectly for titanium and nickel base engine parts.

Looking into the future we can see a steady business for new aircraft engines for the next ten years. We will also see a marked increase in the build rate for industrial and marine gas turbines.

The same process is used for numerous other applications but mostly where high reliability is required or where a forging can be replaced by a less expensive casting with guaranteed properties. A few outstanding examples are surgical implants, parts for marine applications and automotive parts. The message is rather clear: the process application is a winner; it applies wherever the improved properties bring an advantage or wherever a casting can replace a more expensive part. There will certainly be many future success stories.

HIP OF ENCAPSULATED METAL POWDERS

The general advantage of direct HIP of loose powder is the resulting fine microstructure combined with theoretical density. The drawback is the need for encapsulation which is most often done with welded sheet metal

structures and sometimes with ceramic molds or glass (Ref. Table 3). Today metal containers are by far most frequently used. Since there is no final net shape capability with either of the methods, the removal of the metal capsule does not offer a particular problem. Ceramic molds allow for more accurate shape control whereas glass has the advantage of easy removal.

The biggest past and present commercial application is the conversion of high speed steel powder to mill products. Today almost the total production is done via powder metallurgy. The advantages are in scrap reduction and improved performance due to more uniform and fine microstructure.

Originally the economics of HIP near net shape jet engine parts made the process a success. In the meantime, one found that a material that was forged after initial consolidation was more forgiving with regard to foreign particles if properties such as fracture toughness are important. The isothermal forging process for near net shape structures was perfected and it is now the accepted method for jet engine discs.

Whereas HIP near net shape engine parts are in disrepute for aerospace there is no reason to disregard the method for other applications. In general the advantage with regard to properties is established and the choice of the method has to be based strictly on economics.

HIP OF PREVIOUSLY SINTERED OR SPRAY DEPOSITED MATERIALS

In using today's large HIP equipment it turns out that the HIP process step by itself is actually less expensive than the encapsulation. This is true even for relatively simple shapes like right cylinders and therefore there is a strong desire to avoid encapsulation if at all possible. Depending on the material there are a number of options available, usually with some limitations. Table 1 shows the most frequently used methods; it should also be pointed out that some methods are often used without HIP if

TABLE 1
Methods for Powder Consolidation and Shaping Prior to HIP

Method	Application (examples)	Approximate Density % of theoretical	Limitations
CIP + sinter	Ti alloy parts	95-98	Cold pressed density has to be quite high.
Metal injection molding (MIM) + sinter	Low alloy steel, others	96-97	Today small parts only
Spray deposition (Osprey and others)	Steels, Ni base, Al, other large parts such as plates, tubes, bars	98	Simple shapes only
Plasma sprayed coatings	Various	95-98	Shaping depends on substrate which has to be accessible

the somewhat inferior properties are acceptable. For all the approaches listed one can expect substantial growth over the next decade. HIP will undoubtedly play a vital role for the final densification of P/M titanium parts. The approach is particularly attractive from an economic viewpoint since it allows the use of a relatively inexpensive blend of titanium sponge and master alloy powder and yields properties comparable to those of wrought materials.

The use of injection molded metal powder parts is in its infancy and we can expect substantial growth. The shape capability as compared with conventional P/M technology is superior and full densification can be achieved via HIP.

Direct HIP of encapsulated powder has one advantage over sintering: the processing temperature is lower and therefore there is less grain growth.

PROCESSING OF CERAMICS

Although enormous efforts were spent in developing and applying high temperature ceramics such as silicon nitride and silicon carbide, large scale commercial developments have been lagging. Very good properties were achieved with HIP processed materials, either with glass encapsulation or densification after sintering, but the integration into high temperature machinery has been slow. On the other hand, HIP has found wide application in oxide ceramics as well as nitrides and carbides for tools, optical ceramics and others.

ENGINEERED OR TAILORED MATERIALS AND PARTS

HIP is playing an increasingly important role in the processing of some advanced materials tailored for specific applications. Some examples of this type are mechanically alloyed nickel and iron base alloys, ODS copper and rapidly solidified alloys. Since the major applications call for sheet and strip, the preferred method of powder consolidation is HIP at lowest possible temperature in order to maintain microstructural integrity.

Metal matrix composites (MMC) are excellent examples to illustrate the successful approach in combining a relatively soft matrix such as titanium with the properties of very strong silicon carbide fibers. The structures in the form of flat panels or profiles are built up by alternating fiber mats and metal foil or plasma sprayed powder. In order to maintain dimensional integrity, the assemblies are HIP consolidated with the aid of hard tooling. Although MMC and similarly ceramic matrix composites may have limited applications today, the concept will certainly be used on a much wider scale.

The approach of engineered microstructures can be applied equally as well on a macroscale. Subcomponents in the form of wrought, cast or powder parts can be advantageously consolidated and bonded into a composite part. Again HIP represents the ideal tool to achieve the desired goal. For example, it makes good sense to make a hot working roll by cladding a medium alloy steel with a better performing high temperature alloy. There are numerous applications where the working surface of a part should have rather stringent properties in terms of wear resistance, hardness or corrosion resistance, and the same requirement does not exist for the main body of the part.

HIP MAPS AND PROCESS SENSORS

Ashby and others have done pioneering work in HIP modeling and thus have given us a rather good understanding of the mechanisms involved in the HIP consolidation process. The HIP maps that were generated have been extremely helpful in the selection of suitable HIP conditions. At the same time, various researchers have developed sensors to be used in process in order to give us a good indication of the progress as well as the successful end of a HIP cycle.

In both instances the criterion for a successful cycle is full density which does not necessarily mean good metallurgical bonding. This is a shortcoming which may be overcome in the future.

COMPETING PROCESSES

There are several alternate routes for the consolidation of metal powders as well as for the densification of castings. It is appropriate to assess those methods vis-a-vis conventional HIP as to their specific applicability. Table 2 shows a comparison of the capabilities and limitations of the various approaches. They all seem to have two things in common: according to the proponents/inventors of the process, they are lower in cost than HIP but they lack extensive property data. It can be expected that some of those methods will find their niche within the range of manufacturing processes. Some of the processes such as spray deposition, CAP amd injection molding can be considered in combination with HIP in order to bring the material to full density.

TABLE 2
Comparison of Various Consolidation Methods

Process	Application	Advantages	Limitations	Need for More Information
Quick HIP	P/M parts and castings	Low cost	Small size parts only	Property comparison
ROC Process	P/M parts	Good shape control, low cost	Small size parts only	Property comparison
Ceracon Process	P/M parts and castings	Low cost	Small size parts	Property comparison
Spray deposition (e.g., Osprey)	Large bars, tubes, plates	No powder handling, good properties	No intricate shapes, some porosity	Further property comparison, combine with HIP
CAP	Preforms	Low cost	Needs further processing, some porosity	
Injection molding + sintering	Small intricate parts	Very good dimensional control	Very small parts only	Property comparison

EQUIPMENT IMPLICATIONS

It may be assumed that the growth in HIP related business has been growing at a steady although not dramatic rate (on the average in the U.S. and Europe probably about 20% or less/year). From this we must conclude that there is no increase in requirements for large HIP equipment for commercial processing. The business is flat at best and most likely erratic. However, the sale of small laboratory type units has increased from about 50 in 1970 to close to 500 in 1990 worldwide but this is not really an indication of a growing business but rather a growing interest on the part of researchers and strategic planners. If one can draw a parallel with other developments in industry, one might conclude that a more rapid growth, beneficial to the equipment industry, could come at some point. However, as the situation exists today there is overcapacity in large HIP equipment in the U.S. and in Europe.

In order to keep the momentum of the total scientific as well as the industrial effort going we need some commercial successes. This will support a HIP equipment industry which in turn is addressing the processing machinery to new challenges that come up with new applications.

We now ask ourselves the question: how can a more rapid growth be achieved with industrial HIP applications? One could broaden the field of applications and apply HIP to lower cost materials if the process can be accomplished at considerably lower cost. Up to a point the economy of size has been successfully used in reducing the unit cost for HIP processing but the improvement becomes at best marginal with furnace diameters much larger than 1000 mm. Also, the loads may become very heavy in the case of powder billets and parts which obviously has an impact on machine dwell time. For those reasons one can conclude that very large HIP units will be built only because one wants to process very large parts.

Since a further increase in size doesn't help, one has to change the mode of operation. Quick HIP represents one possibility. However, due to the high pressure requirements (400 MPa and more), the equipment would probably stay rather small. Although the throughput per time unit might be high the method is limited to relatively small parts.

Another possibility would be to set up equipment dedicated to one specific material and process. Densification of aluminum castings and/or powder billets might represent an outstanding example since considerable savings could be achieved in equipment as well as processing. The logistics and the cost of transportation might become a problem which would require for the HIP plant to be integrated into the aluminum plant.

There are some further features of equipment and process variations which can improve the economics, although not dramatically. Examples of this type are the combination of HIP and heat treatment, sinter and HIP, and others.

CONCLUSION

In identifying present and potential winners for the HIP process we are looking primarily for applications in which the method is unique and therefore cannot easily be replaced. Casting densification is certainly representative of this type, in particular as it applies to large pieces. In addition, the areas of major growth can be expected in combining current powder metallurgy techniques with HIP in order to produce engineered materials and multi component parts.

2. MODELING AND THEORY

CONSTITUTIVE EQUATION FOR COMPRESSIBLE MATERIALS AND ITS APPLICATION TO SIMULATION OF POWDER FORMING PROCESSES

SUSUMU SHIMA
Department of Mechanical Engineering, Kyoto University,
Sakyo-ku, Kyoto 606, Japan

ABSTRACT

Development of constitutive equations for compressible materials, such as powders and porous materials, is briefly described and the application of these equations to simulation of powder forming processes is presented. Some results of the analysis of CIP, HIP and closed-die compaction processes are given and discussed. Further, it is pointed out that anisotropy is evolved in the powder during compaction and an analysis is also carried out taking account of the anisotropy. The shape of the compact produced by isostatic compaction and density distribution seem to be quite dependent on the characteristics of the powder, and it is thus concluded that an intensive investigation into them must be undertaken for a more sophisticated simulation.

INTRODUCTION

Simulation of compacting processes with a view to predicting the shape of the compact in isostatic pressing and the density distribution is of great importance for near net-shape production and also for better qualities of the products. In order to simulate a powder compaction process, constitutive equations for the powder concerned should be properly given, however, there are not, at present, sufficient equations available. Recently, attempts have been made to simulate the behaviours of granular assemblies [1-3], however there is still a long way until we can make use of them for actual powder compaction processes. Therefore, approaches based on contiuum mechanics still play an important role in the simulation. We shall describe briefly the constitutive equations for compressible materials [4-7] and their application to simulation of some powder forming processes [6,8-11].

In our laboratory, we have been developing constitutive equations for metal powders [4] and ceramic powders [5,6]. To do this, it is necessary to examine relationship between stress and density ratio, which is called densification criterion, by pressing the powder with various stress ratios. Since the material is a granular medium, a particular testing apparatus should be utilized: a three-dimensional compaction apparatus [4,5] is very usuful for this purpose. An apparatus on which the stress ratio can be altered during a compacting process has also been developed [12].

CONSTITUTIVE EQUATION

Rate Independent Constitutive Equation

The constitutive equations developed by Shima et al. [4,5,7] are shown below.

Yield function: This may be called the "densification function".

$$F(\sigma_{ij}, \rho) = (3/2)\sigma'_{ij}\sigma'_{ij} + (\sigma_m / f)^2 - (\rho^n \bar{\sigma})^2 \tag{1}$$

where σ'_{ij} is deviatoric stress, ρ the density ratio and f is a function of ρ such as

$$f = 1/a(1-\rho)^n \tag{2}$$

σ, a, m and n are constants depending on the characteristics of the powder. The surface which is given by $F=0$ is an ellipsoid in the principal stress space. It is shown experimentally [4,5,7] that stress for a particular density ratio lies on a same elliptical curve, if these constants are determined properly.

Stress-strain rate relationship: This is obtained by partially differentiating F in Eq.(1) with respect to stress.

$$\dot{\varepsilon}_{ij} = \frac{3}{2} \frac{\dot{\bar{\varepsilon}}}{\rho^{2n-1}\bar{\sigma}} \left\{ \sigma_{ij} - \delta_{ij} \left(1 - \frac{2}{9f^2} \right) \sigma_m \right\} \tag{3}$$

where the elastic component is neglected and $\dot{\bar{\varepsilon}}$ is the equivalent strain rate, which is expressed by

$$\dot{\bar{\varepsilon}} = \rho^{n-1} \left\{ (2/3)\, \dot{\varepsilon}'_{ij}\dot{\varepsilon}'_{ij} + (f\dot{\varepsilon}_v)^2 \right\}^{1/2} \tag{4}$$

$\dot{\varepsilon}'_{ij}$ being the deviatoric strain rate and $\dot{\varepsilon}_v$ is the volumetric strain rate.

We have now fundamental constitutive equations, but these have been determined on a condition of a constant stress ratio throughout one compacting process. It is reported that anisotropy is induced during compaction depending on the stress condition [13]. If the anisotropy is significant, the preceding equations do not of course apply. It is also reported that the anisotropy induced during compaction also affects shrinkage during sintering [14]. Therefore, the anisotropy plays a very important role in the near net-shape production. To describe the anisotropic behaviour an evolution equation for the anisotropy has been developed based on the kinematic hardening [12,15]. This is described in a later section.

Rate Dependent Constitutive Equation

For simulation of HIP process, rate dependent constitutive equations should be developed; for this purpose, visco-plastic equations are proposed [10]. Total strain rate is given by

$$\dot{\varepsilon}_{ij} = \dot{\varepsilon}^{th}_{ij} + \dot{\varepsilon}^{p}_{ij} + \dot{\varepsilon}^{c}_{ij} \tag{5}$$

where $\dot{\varepsilon}^{th}_{ij}$ is thermo-elastic strain rate, $\dot{\varepsilon}^{p}_{ij}$ plastic strain rate and $\dot{\varepsilon}^{c}_{ij}$ is creep strain rate. Both $\dot{\varepsilon}^{p}_{ij}$ and $\dot{\varepsilon}^{c}_{ij}$ are derived by partially differentiating a potential similar to F in (1).

ANALYSIS

The finite element method (FEM) is one of the best tools for calculating distributions of stress and density or for predicting the shape of compact after isostatic pressing. In the following, FEM simulations, in particular, based on the rigid-plastic formulation are mainly dealt with.

The rigid-plastic finite element equations for analyzing the deformation of compressible materials [16] are obtained from a solution which minimizes the functional or potential

$$\Phi = \int_V \sigma_{ij}\, \dot{\varepsilon}_{ij} dV - \int_{S_\sigma} T_i u_i dS \tag{6}$$

Here, V is the volume of the body, u_i the velocity and T_i the prescribed traction on surface S_σ. The solution is obtained by an iterative technique. It should be noted that some feature arises depending on the boundary condition.

EXAMPLES OF ANALYSIS

Closed-die Compaction

There is not any particular difference between the ordinary analysis and the one for closed-die compaction, provided that friction is assumed at die-powder interfaces. If there is no friction, deformation is supposed to be uniform throughout, however, in the simulation it does not occur uniformly in an iterative step; it occurs layer by layer and it seems to propagate through the compact. This can be overcome by taking account of workhardening in one deformation step or by prescribing a threshold value for the equivalent strain increment.

Figure 1 shows density distributions for mean densisty ratios of (a) 0.333 and (b) 0.484 for a ceramic powder of an initial density ratio of 0.3, where the Coulomb friction is assumed with friction coefficient μ= 0.2 and the initial height to diameter ratio is 0.75. It is seen that there is a fairly large inhomogeneity in the compact.

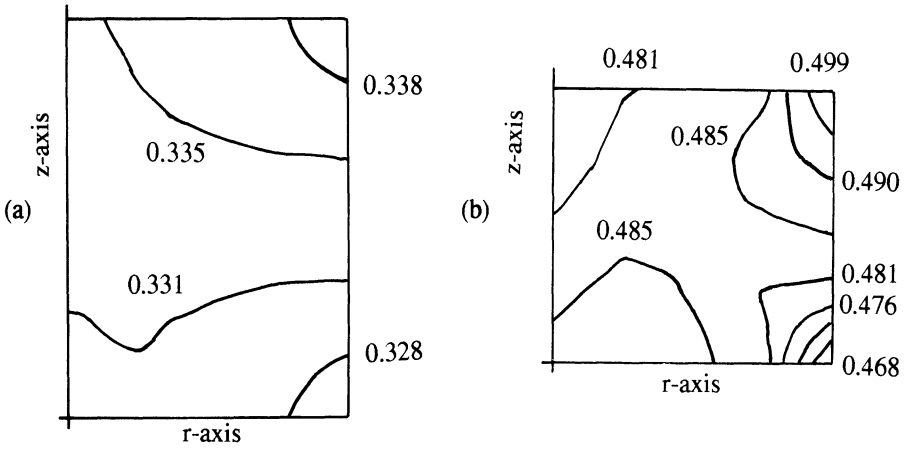

Figure 1. Density distributions after closed-die compaction at (a) p=0.26MPa, p=0.333 and (b) p=16.0MPa, p=0.484.

CIP

In case of isostatic pressing, whole boundary S is covered by S_σ (see Eq.(5)), and the traction T_i is expressed in terms of hydrostatic pressure p. The solution u_i, however, cannot be obtained because of the fact that there is no measure of the amount of deformation. To overcome this difficulty, a new scheme has been developed and it is thus shown that simulation is possible [8,9]. If the intial density is uniform and the strength of the capsule is neglected, the density and the stress are obviously uniform. In experiment, however, it is rigorously not homogeneous [17]; this may be due to the strength of the capsule and also the fact that the powder is not a continuum but a granular material may of course have some effect.

In the case of the elasto-plastic analysis, the difficulty described above does not arise, however elastic modulus, which is dependent on the density ratio, should be given. Matsumoto et al. [18] carried out elastici-plastic analysis with a constant Young's modulus. As seen in Figure 2, Young's modulus for an alumina powder changes significantly with density ratio. By taking account of the change in the modusus, elastic-plastic analysis was caried out.Figure 3 shows the shape of a compact and density distribution after CIP of the alumina powder with an intial density ratio of 0.246 in a cylindrical rubber capsule. It is obvously seen that the shape is distorted and the density becomes inhomogeneous. It seemed that the compaction behaviour is very much dependent on the values of the parameters in the constitutive equations

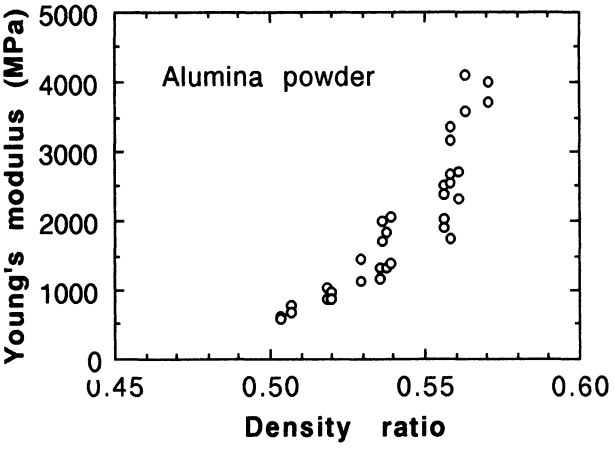

Figure 2. Variation of Young's modulus with density ratio for an alumina powder.

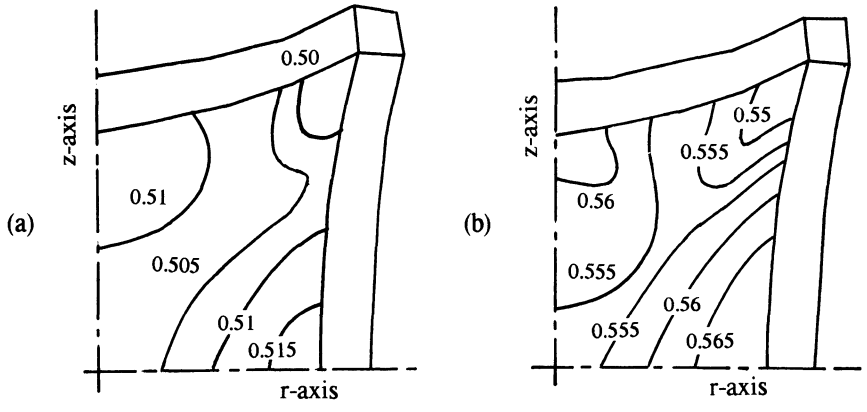

Figure 3. Density distribution of compacts after CIP (a) p=5MPa and (b) p=10MPa.

for the powder. It is, therefore, very important to investigate the properties of the powders concerned.

HIP

Since the material concerned is rate dependent, visco-elastic-plastic analysis [10] and visco-plastic analysis [11] are carried out. It was shown by the both analyses that there is fairly good agreement between the calculated and the experimentally obtained shape. To extend this simulation to different materials, it is necessary to prepare extensive materials data.

Psuedo-isostatic pressing is also simulated by the rigid-plastic formulation [19].

Analysis Taking Account of Anisotropy

Fig.4 shows the strain due to CIP after closed-die compaction; it is obviously seen that a remarkable anisotropy exists. In such a case, therefore, the constitutive equation as above is not applicable. A constitutive equation with kinematic hardening is proposed to describe the anisotropic behaviour of ceramic powders [15]. The densification function, F, is expressed by

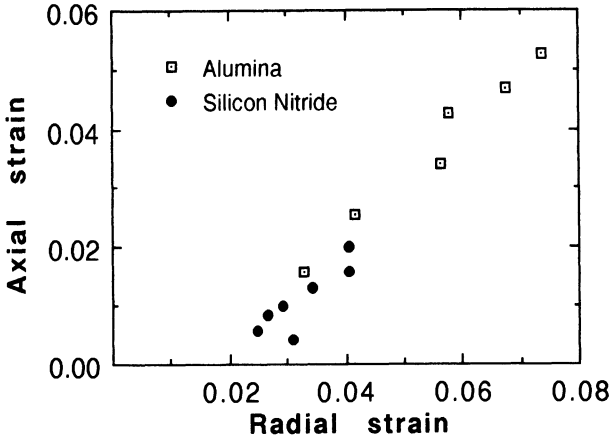

Figure 4. Relationship between axial and radial strains due to CIP after closed-die compaction of alumina and silicon nitride (Experiment)

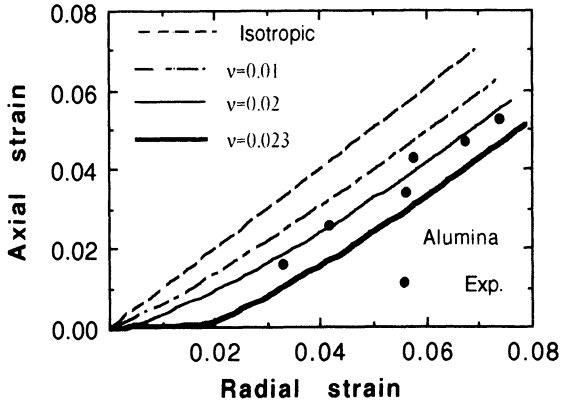

Figure 5. Calculated relationship between axial and radial strains due to CIP after closed-die compaction of alumina powder.

$$F = F(\sigma_{ij} - \alpha_{ij}, \rho) \tag{7}$$

where α_{ij} is back stress, which describes kinematic hardening. The evolution equation for α_{ij} is given either by

$$\dot{\alpha}_{ij} = \nu(\sigma_{ij} - \alpha_{ij}), \quad \nu = const. \tag{8}$$

or by

$$\dot{\alpha}_{ij} = C\rho^{N}\dot{\varepsilon}_{ij}, \quad C = const. \tag{9}$$

Figure 5 shows calculated results with Eq.(8). It is seen that the kinematic hardening is very useful to describe the anisotropic behaviour.

CONCLUDING REMARKS

Constitutive equations obtained by three-dimensional compaction were described and they were applied to the analysis by the FEM. Further, it was shown that anisotropy is induced

during the compaction process and therefore the conventional isotropic equations are not sufficient in some cases. Since the shape of the compact and density distribution seem to be quite dependent on the characteristics of the powder, such as particle size, its distribution, particle shape, surfaces characteristics of the particles, etc., an intensive investigation into them must be undertaken for a simulation with a better accuracy.

REFERENCES

1. Cundall, P. A. & Strack, O.D.L., A Discrete Numerical Model for Granular Assemblies, *Geotechnique*, 1979, 29, 47-65.
2. Aizawa, T. & Kihara, J. Direct Ball Element Method for Simulation of Mechanical Behaviours of the Ceramic and Metal Powders, *Advances in Plasticity, Proc. Plasticity '89*, 1989, 7-10.
3. Shima, S., Ohta, T. & Kada, O., *Proc. 1991 Japanese Spring Conf. Tech. Plasticity*, 1991, 653-656.
4. Shima, S., Inoue, T., Oyane, M. and Okimoto, K., Study on Compaction of Metal Powders (2nd Report): Investigation of Compaction Criterion by Three-dimensional Compaction, *J. Japan Soc. Powder and Powder Metall.*, 1976, 22, 257-263.
5. Shima, S. and Mimura, K., Densification Behaviour of Ceramic Powder, *Int. J. Mech. Sci.*, 1986, 28, 53-59.
6. Shima, S. and Nakanishi, T., Compaction Characteristics of Si_3N_4 Powder and its Application to Analysis of Isostatic Compaction, *J. Japan Soc. Mat. Sci.*, 1988, 37, 70-76.
7. Shima, S. and Oyane, M., Plasticity Theory for Porous Materials, *Int. J. Mech. Sci.*, 1976, 18, 285-291.
8. Shima, S. and Nakanishi, T., Analysis of Isostatic Compaction of Powder by Rigid-Plastic Finite Element Method, *J. Japan Soc. Tech. Plasticity*, 1988, 29, 139-144.
9. Shima, S. and Nakanishi, T., Rigid-Plastic Finite Element Analysis of the Isostatic Compaction of Ceramic Powder, *Current Japanese Mater. Res., Vol. 7, Computational Plasticity*, 1990, 117-133.
10. Abouaf, M., Chenot, J. L., Raisson, G. and Baudin, P., Finite Element Simulation of Hot Isostatic Pressing of Metal Powders, *Int. J. Num. Meth. Eng.*, 1988, 25, 191-212.
11. Nohara, A., Nakagawa, T., Soh, T. and Shinke, T., Numerical Simulation of the Densification Behaviour of Metal Powder during Hot Isostatic Pressing , *ibid.*, 1988, 25, 213-225.
12. Shima, S., Hirata, N. & Saleh, M. A., Effect of Loading Path on Compaction Behaviour of Ceramic Powders, *Proc. 1991 Japanese Spring Conf. Tech. Plasticity*, 1991, 341-344.
13. Shima, S., Saleh, M. A. & Hirata, N., Evolution of Structura l Anisotropy in Powders during Compaction, *Adv. Tech. Plasticity, Proc. 3rd ICTP*, 1990, 883-888.
14. Shima, S., Saleh, M. A. & Hirata, N., A Study of Internal Structures in Ceramic Powders during Compaction, *Pre-print 1990 Spring Conf. Powder & Powder Metall.*, 1990, 30-31.
15. Shima, S. & Hirata, N., A Study of Shape of Compacts Produced in Closed-die Compaction Followed by Isostatic Pressing, *Proc. Japanese Joint Conf. Tech. Plasticity*, 1990, 471-473.
16. Mori, K., Shima, S. & Osakada, K., Finite Element Method for Analysis of Plastic Deformation of Porous Metals, *Bull. JSME*, 23, 1980, 516-522.
17. Abe, O., Kanzaki, S. Tabata, H., Structural Homogeneity of CIP Formed Green Compacts (Part2): Influence of Applying Pressure, *J. Japan Ceramic Soc.*, 1989, 97, 32-37.
18. Matsumoto, H. & Kikuma, T., Elastic-Plastic FEM for Compressible Materials Allowing Large Incremental Deformation, *Adv. Tech. Plasticity, Proc. 3rd ICTP*, 1990, 933- 938.
19. Shima, S. and Inaya, A., Simulation of Psuedo-isostatic Pressing of Powder Compact, *Proc. 3rd HIP*, 1991.

HIP OF BI-MODAL POWDER MIXTURES: MODELING AND EXPERIMENT

P.D. Funkenbusch and E.K.H. Li
Materials Science Program
Dept. of Mechanical Engineering
Univ. of Rochester, Rochester, NY 14627-0133, USA

ABSTRACT

Models of the HIPing process have often assumed a uniform, spherical powder. However it is known that "inhomogeneities", in the form of particles of differing composition and/or size, will alter both initial powder packing and subsequent HIPing behavior. We have investigated these effects using the simplest form of mixture; a bi-modal powder with various size ratios and particle fractions. Modeling is based on the Arzt/Ashby et al. HIP map concept, with appropriate modification to produce a determinate and self-consistent model for this more complex case. Experiments have been performed with a 316L stainless steel powder, with particle size ratios varying from 1:1 to 6:1 and fractions from 0 to 100% small particles. Packing experiments confirm the existence of "optimum" packing fractions for which the density is maximized over both monosized and the as-received (continuously distributed) powders. During HIPing these powder mixes remain relatively more dense, but densify more slowly than monosize packings. The implication of these results with respect to problems such as differential densification/distortion and the modeling of composite powder mixes is discussed.

INTRODUCTION

Particle packing has been a subject of both theoretical and practical interest for many years [1,2]. In powder materials control of initial packing is of interest because of its influence on subsequent consolidation. For example, changing from dry-pressing to slip casting of a composite ceramic powder improves packing and sintering behavior [3]. Alternatively, packing can be directly altered by adjusting the size and volume fractions of the components in a powder mixture.

Tri-modal or higher order packings of spheres can be used to obtain very high initial packing densities. However, in order to produce such packings the size ratio between the largest and smallest particles must be very large, presenting problems with mixing and segregation. For maximum size ratios of less than about 10:1, bi-modal mixtures turn out to be a more effective means of increasing packing [1]. Further, although the packing density increases with the size ratio, significant improvements can be

obtained even for comparatively small ratios.

Several advantages of an increased packing density are apparent. Higher initial density will mean less total shrinkage and potential distortion. The thermal conductivity and initial mechanical "integrity" may also be improved, further reducing the effects of thermal-stresses and differential-densification. Finally, if the interstices between coarse particles in a packing can be filled with a smaller component, the final stage pore size will be reduced, decreasing the overall densification time.

In this communication we report on the densification behavior of bi-modal powder mixes in the first stage (i.e. less than 90% dense) of HIPing. Both the consolidation mechanism (particle re-arrangement, yielding, power-law creep) and the consolidation rate are of interest. Since most of the time required for consolidation is concentrated in the final stages of HIPing, this behavior has only a secondary influence on the total consolidation time. However, it is in the first stage that the compact is most vulnerable to the effects of differential heating and densification and it is in this stage that the subsequent morphology (e.g. pore size/distribution, defects/voids, recrystallization, distortion) is chiefly determined. For example, geometrical considerations may force smaller particles in a mix to undergo more extensive deformation [4], controlling subsequent re-crystallization behavior (e.g. in Ni_3Al [5]).

EXPERIMENTS

A commercially available 316L stainless steel powder with a continuous size distribution and a nearly spherical shape (Hoeganaes) was used for our experiments. This powder was sieved to produce powder fractions for subsequent mixing. Particle sizes used for subsequent experimentation ranged from 37-44 μm to 212-250 μm. Packing experiments were performed in a copper tube of 1.46 cm diameter. 35 grams of powder with the desired size ratio and volume fraction of small particles were poured into the tube and then "agitated" by repeatedly tapping them from the top with a small weight. (Details may be found in [6,7]). Density was measured by determining the final height of the powder in the tube. Repeated tapping increased the packing density appreciably but 500 taps were found sufficient to approach the maximum packing density [6,7]. Results of 500 tap experiments are shown in figure 1. As anticipated [1], a large peak in the packing density occurs for a certain "optimal" fraction of the small powder. This fraction is a function of the particle size ratio, and the maximum peak height is also increased by increasing the size ratio. For HIP experimentation we chose to work with bi-modal mixtures of size ratios 2:1 and 4:1. (The maximum ratio being limited by the small quantities of powder available at the extremes of the size distribution.) Mixtures near the optimum (i.e. at 40 volume % small particles) were chosen in both cases. We have also HIPed "mono-sized" (i.e. as sieved) powders and an as-received mix for comparison.

An as-poured ("0-tap") density for these powders was also measured. Poured/500-tap packing densities were 62/64, 63/68, and 70/73 for the mono-sized, 2:1 bi-modal, and 4:1 bi-modal powders, respectively. It is thus seen that the bi-modal powders pack to significantly higher densities in either condition.

Powders for HIPing were poured into 0.64 cm diameter copper tubes, evacuated and sealed. These were subsequently HIPed at 840°C, 44.3 MPa. At various intermediate times during the at-temperature "hold", the HIP cycle was interrupted, the chamber ramped-down to ambient conditions, and the sample density measured (using a modified Archimedes technique), before reloading, and continuing the HIPing. A heating rate of 20°C/minute was used

during the ramp-up/ramp-down of the HIP. Preliminary experiments were performed to test the effects of the tube size and of multiple rampings on the density, and the differences were found to be minor [6]. We were thus able to examine the density of a large number of samples at various times during the temperature/pressure plateau. Each of the data points we will show represents between five and ten separate samples. (This type of "interrupted" HIP technique [8] is more cumbersome than direct monitoring of sample density, but does not require a special internal sensor, and the results are less subject to interpretation of the sensor output.)

HIPing results are shown in figures 3 and 4. The first (t = 0) data point is the density measured after ramping to the HIPing temperature and pressure and then immediately ramping back down (i.e. zero-hold time). While time-dependent processes during the ramping may play some role in producing the densification observed (and the yielding process itself is strictly speaking not rate independent [9]), the increase in density observed at t = 0 is an indication of the role of yielding (as well as particle rearrangement) on densification. Subsequent densification represents the contribution of time-dependent mechanisms. Several monosize powders, with as much as a factor of three difference in their sizes, exhibited essentially identical behavior in these experiments, supporting an assumption that power-law creep is the dominant mechanism. This is also consistent with the relatively high pressure and temperature and the low sample density chosen for these experiments.

MODELING

At least two models exist for predicting the behavior of bi-modal particle systems. Nair and Tien's modeling [10] was based on assumption of equal interparticle forces. Large differences between the densification mechanism maps of mono-sized and bi-modal sized powder were predicted. In contrast, our modeling has been based on an assumption of uniform contraction, requiring a varying contact force, but producing a more internally self-consistent result [4]. Differences in the densification maps were again predicted. However, by comparing mono-sized and bi-modal mixtures with similar initial densities the differences were substantially reduced. A full description of this model may be found in [4].

As an input to the HIP model, radial distributions functions (RDFs) are necessary. For each bi-modal mix we need four separate RDFs. To estimate these values the following model was adopted. Initial contact numbers were found from the model of Suzuki and Oshima [11]. This model requires as input the size ratio and volume fraction of the two particle types, as well as the contact number expected in a monosized bed ("N_c", set equal to 6 in [11]). Although there is no explicit dependence on packing density in this model, we incorporated this effect by making the value of N_c a function of the initial packing density. Since Suzuki and Oshima's original model is based on the area fraction of particles in a mixture, it seems most consistent to adjust N_c based on the total particle surface area expected as density is increased. This of course is just proportional to the density, D_o (i.e. proportional to the number of particles per unit volume), giving $N_c = 6 * (D_o/0.636)$.

At large distances from the particle center in question, the increase in the RDF (dN_{ij}/dr, for type j particles around a type i particle) with distance (r) is dictated by the necessity that the total volume fraction of each type of particle enclosed within r, must be consistent with the fraction of such particles in the mixture. Although this relationship will generally not be true for smaller r (the presence of the reference particle

at r = 0 biases the result) we assume that it is still approximately true. We thus use:

$$dN_{ij}/dr = (3 \times D_o \times f_j \times r^2) / R_j^3$$

where D_o is the total initial packing density, f_j the volume fraction of j particles in the mixture, and R_j the radius of a type j particle. RDFs calculated by this technique (absent the density adjustment in N_c) have been shown to approximate a variety of measured bi-modal packings [6]. Use of the density adjustment in N_c further improves the fit.

Material parameters for the 316L stainless steel were estimated using a combination of literature data for 316 stainless [9,12] and comparison with the experimental results. A yield stress of 180 MPa gave a good match between the first (time = 0) point on the monosize densification curve and the HIP data and is also within the range of values found experimentally for 316 at 840°C [12]. There are two power law creep parameters (n and A, see ref. 4 for definitions)."n" = 7.9 was taken from Frost and Ashby's compilations for 316 stainless steel [9]. We estimated "A" = 3.5×10^{-72}/(sec x $Pa^{7.9}$) at 840 C by fitting the model curve to the experimental data for monosized powders. This value is within a factor of two of the value obtained using Frost and Ashby's constitutive laws for 316 [9], a reasonable agreement given that "A" is dependent on the diffusivity and other parameters which are known only to an order of magnitude approximation. Notice that we have, in effect, used the monosized data to estimate the material parameters for subsequent comparison with bi-modal results.

DISCUSSION

In our HIPing experiments powder was poured loose into the copper containers (not agitated). During the initial compaction of the can, therefore, there is a potential for densification to occur by particle rearrangement. One might expect increased re-arrangement in a bi-modal mix and, given the large difference between the poured and well-packed densities, such rearrangement would significantly increase the initial densification. Figure 2 shows the relevant data for the 1:1, 2:1, and 4:1 mixtures. The left hand bar in each case represents the "as-poured" (0-tap) data for the specimens as well as the density predicted from yielding under the pressure/temperature conditions used here. The right hand bars represent similar predictions for a "well-packed" (500-tap) mixture. The center bar gives the experimental results. Although some density increase by re-arrangement may be occurring in the bi-modal mixtures, their behavior is similar to that seen in the monosize mix (recall that we have normallized against the monosized data). Hence the role of particle re-arrangement in densification does not appear to be greatly increased in the bi-modal mixtures.

The increased density observed for bi-modal mixes during packing and initial yielding is also maintained during subsequent creep (fig. 3). Modeling does a good job of predicting the 4:1 data and, while it underestimates the data in the 2:1 case, the qualitative trend is correct. The as-received powder, with a continuous size distribution, initially packs to a density similar to that of the monosize. During HIPing it exhibits an intermediate behavior, densifying somewhat more rapidly than the monosize but remaining significantly below the 4:1 curve (figure 4).

Separating out the direct effects of increased packing density from those inherent in having a bimodal mixture is difficult. One cannot simply use a monosize model with an increased initial density to predict bimodal

behavior. Random monosized packings with the high initial packing densities obtainable from bi-modal mixes do not exist. The RDF for such a packing may be "created" using the simple packing model presented above and used for HIP modeling, but the results do not match those obtained for the actual bi-modal packing. Moreover such an approach is unable to predict more subtle effects (such as differences in the deformation of different particles in the mix) which can profoundly influence the final microstructure.

Beyond interest in powder packing to alter HIP behavior, use of modeling techniques similar to those illustrated here is, of course, also of interest for composite applications. To account for contacts between particles of the same composition within a composite mix, there is no need to alter the current approach, provided particle rearrangement is not greatly increased in the composite (an assumption consistent with the bi-modal results presented above). Therefore properly accounting for the behavior of contacts between dissimilar particles is the critical step in developing such models. The bi-modal case represents one extreme (particles with identical properties in which we have assumed that the deformation is equally "split" between the particles [4]). At the opposite extreme, for composites with one component with much more resistance to flow than the other one can easily envision allowing the softer material to undergo nearly all of the deformation within the shared particle contacts. Development of such a model is currently under way.

ACKNOWLEDGEMENTS

This work is supported under National Science Foundation grant MSM-8657038. We would also like to thank Wenjea Tseng and Chun-Wei Shih for useful discussions and the Hoeganaes Company (Mr. Walter Blovis) for supplying the 316L powders used in this study.

REFERENCES

1. R.M. German, Particle Packing Characteristics, Metal Powder Industries Federation, Princeton, 1989
2. D.J. Cumberland and R.J. Crawford, The Packing of Particles, Elsevier, Amsterdam, 1987
3. W.J. Tseng and P.D. Funkenbusch, manuscript in preparation
4. E.K.H. Li and P.D. Funkenbusch, Acta Metall., 1989, 37, 1645-1655
5. R.N. Wright, R.L. Williamson, and J.R. Knibloe, Powder Metall., in press
6. E.K.H. Li, Ph.D. thesis, University of Rochester, Rochester, NY, USA, (1991)
7. E.K.H. Li and P.D. Funkenbusch, manuscript in preparation
8. D. Bouvard and M. Lafer, Powder Metal. Int., 1989, 21, 11-15
9. Harold J. Frost and Michael F. Ashby, Deformation Mechanism Maps, Pergamon Press, Oxford, 1982
10. S.V. Nair and J.K. Tien, Metall. Trans. A, 1987, 18a, 97-107
11. Michitaka Suzuki and Toshio Oshima, Powder Technol., 1983, 35, 159-166
12. Metals Handbook, ASM, 8th edition, 1961, page 504

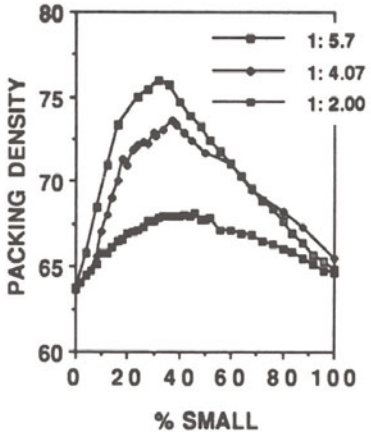

Figure 1. Packing density of various bi-modal powder mixes after 500 "taps" as a function of the volume fraction of small particles and the size ratio between the particles.

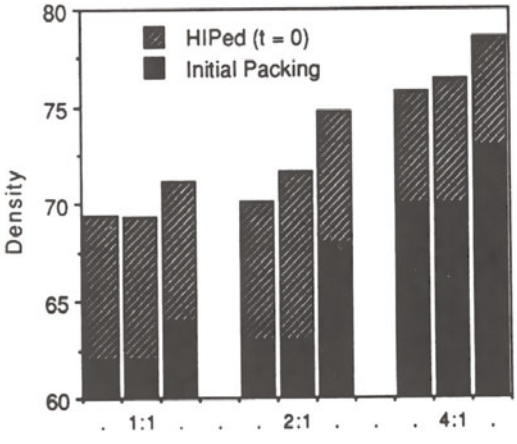

Figure 2. Initial (time = 0) HIPing behavior for 1:1, 2:1, and 4:1 mixes. Left and right bars are model predictions for "as-poured" and "well-packed" mixes respectively. Center bars are experimental results.

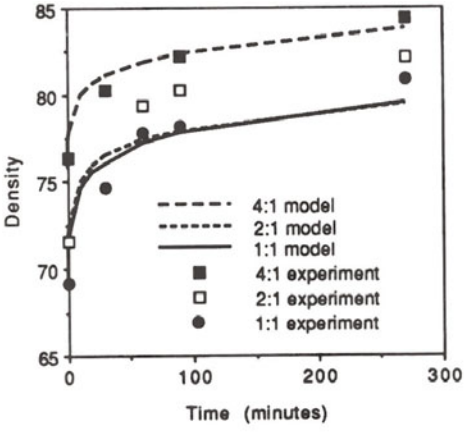

Figure 3. Density as a function of HIPing time for various particle size ratios. Model predictions are also shown.

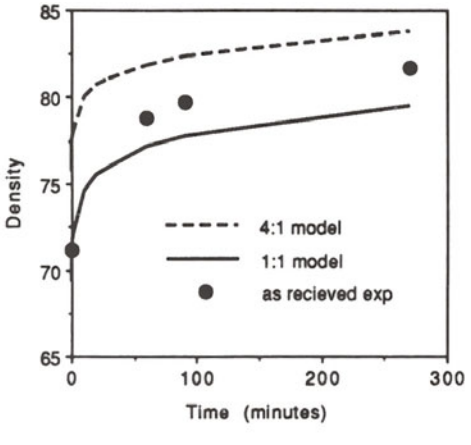

Figure 4. Density as a function of HIPing time for the as-received powder. Model predictions for various size ratio mixes are also shown.

THE EFFECT OF NON-UNIFORM DENSIFICATION DURING HOT ISOSTATIC PRESSING

W.B. Li and K.E. Easterling
Department of Engineering Materials
University of Luleå
S-951 87 Luleå, SWEDEN

ABSTRACT

Hot isostatic pressing (HIPing) is an extremely efficient way of densifying ceramic and metallic powders, or for healing porosity in castings. However, depending on the parameters of pressure, temperature, heating rate and sample size, can result in a non-uniform mode of densification. This mainly occurs when a rapidly heated sample, or a sample of large size, densifies quickly at the surface to produce in effect a fully dense, hard shell. It is shown in this paper that there can be a number of negative factors resulting from this, including reduced rates of densification, decrease of effective pressure, sample shape change, non-uniform shrinkage and the development of residual stresses in the sample etc.

INTRODUCTION

It has previously been established [1, 2] that a dense thick skin can form at the surface of a powder compact during HIPing. This occurs as follows. When the temperature of a powder compact is raised, heat diffuses inwards from the surface. As heat diffuses into the powder, the hotter surface layers sinter faster than the porous interior, producing in effect a dense shell around a porous core. Heat is then conducted through the denser skin faster than through the less-dense interior, further adding to the temperature differences between the dense region and the interior. As the HIP process continues, the interface between the dense skin and the porous core, termed "the densification front", propagates inwards at a certain rate until the entire compact becomes fully dense.

It has been pointed out [2] that a dimensionless parameter $C = KRo/a_S$ gives the criterion as to whether a dense shell forms (K is a kinetic constant of densification, Ro the initial radius of a cylindrical compact and a_S the thermal diffusivity of the material). Physically, the parameter C is simply the ratio of the time required for heat to diffuse through the compact to the time required for full densification [2]. It was shown when $C > 1$, there is a tendency for a densification front to form. When $C < 1$,

a densification front is unlikely to occur.

Once non-uniform densification or a dense shell forms, it will be shown in this paper that there are a number of important consequences.

SHELL EFFECT DUE TO NON-UNIFORM DENSIFICATION

Effective pressure

At any given time during HIPing, it is assumed that the sample being HIPed is made up of a solid shell with an enclosed porous core. The solid shell creeps under pressure, while the porous core densifies by the various mechanisms of densification. It is evident that, if the pressure were uniform throughout the sample, the creep rate of the solid shell would not match the densification rate of the porous core; the difference in contraction results in the development of stresses. These stresses act such as to make the contraction rates equal, so that the overall deformation remains compatible. In order to maintain compatibility, therefore, the internal pressure acting at the solid/porous interface termed "effective pressure", Pi, should be different from the applied pressure P. It is Pi not P that brings about densification of the remaining porous part of the sample. This feature of HIPing can be brought out more clearly by the following (over-idealised) example.

Consider a spherical compact of radius Ro. The surface is heated and almost immediately, a pressure is applied. The hot surface has a lower yield strength than the cold core. The hot surface layer densifies to give a dense skin of thickness ΔR (= Ro-Ri), completely enclosing the colder, not-yet-densified core. A stress Pi acts radially between the skin and the core. For simplicity consider the case when $\Delta R \leq Ro$. The skin now acts like a thick, strong can containing the remaining powder. Any further densification requires a compressive yielding of the can wall, compatible with a volume shrinkage (i.e. densification) of the core. The circumferential stress in the skin, σ, is given by $\sigma = (P - Pi)Ri/2\Delta R$. The skin will yield if σ exceeds σ_S, the yield strength of the skin. For Von Mises yield criterion, yield requires that $P - Pi = 2\Delta R\sigma_S/Ri$. The pressure on the powder in the core, Pi, is thus less than the applied pressure P by the amount $2\Delta R\sigma_S/Ri$. As the densification front of thickness ΔR sweeps inwards, the difference between P and Pi increases, and the remaining powder densifies more and more slowly.

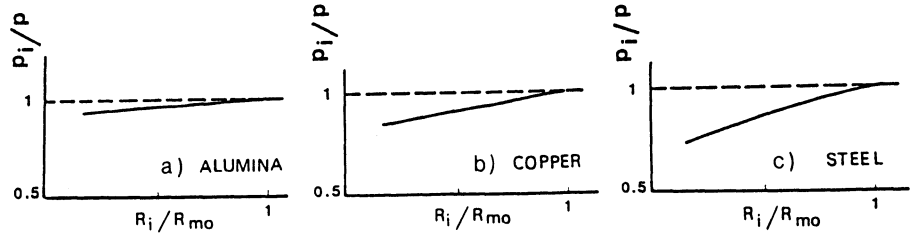

Fig. 1. Change in internal pressure, Pi/P at the inside of a dense skin interface, as a function of the skin thickness: a) alumina (HIPed at 150 MPa amd 1623K); b) copper (150MPa and 823K); c) steel (150MPa and 1423 K).

This approach is oversimplified, of course. The effective pressure,

Pi, is in fact related to the creep rate of the outer shell and the densification rate of inner core. Both the creep and densification rates depend on the temperature distribution. Therefore Pi is a complex function of the parameters of creep, densification, heat conductivity and sample size etc. Indeed, the calculation of Pi requires extensive numerical analysis [3]. Examples of how Pi varies as a function of degree of densification in 3 materials are shown in Fig 1. As the shell thickens the effective pressure, Pi, continuously drops, and it can be shown that this drop in pressure can be significant.

Densification rate
It should be emphasized that in the case of non-uniform densification, i.e. when the shell-effect occurs, the effective pressure Pi acts as the actual HIPing pressure. The drop in Pi retards densification, prolongs the time to full density and specially makes densification of the last part of the sample very difficult. Our results show that a sharp increase in HIPing (furnace) temperature is likely to have a negative effect on the total HIPing time, due to the onset of the shell-effect and continuous reduction of P to Pi.

Shape change
When a powder compact is consolidated by HIP-ing, the final shape of HIPed parts is almost always different from that of the starting preform. There are a number of reasons for possible change of sample shape [4]. The origin of the shape change by shell formation is illustrated in Fig 2. This shows that when densification is uniform, the cylinder shrinks uniformly. However, when non-uniform densification takes place and a dense shell forms, its shape transforms to that of a dog-bone as shown.

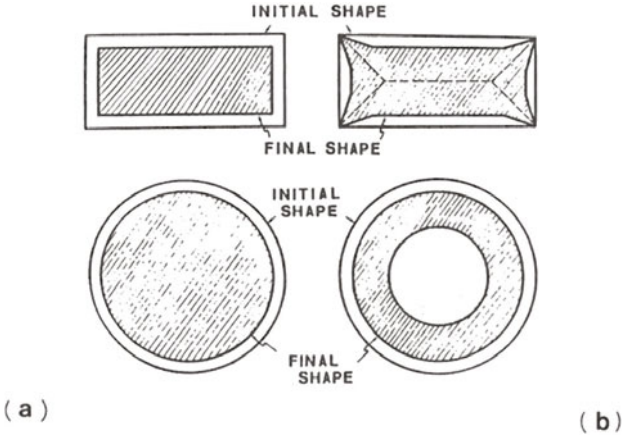

Fig.2. a) When densification is uniform,the final shape is the same of that of the preform. b) when a densification front forms, shape changes.

Transient shell stresses
The creep of a dense shell is governed by the stress distribution in the shell during HIPing. As mentioned above, there is a pressure difference across the solid shell during HIPing. This difference in pressure results in an unequal stress distribution and this can be formulated by the equations given in our earlier paper [1].

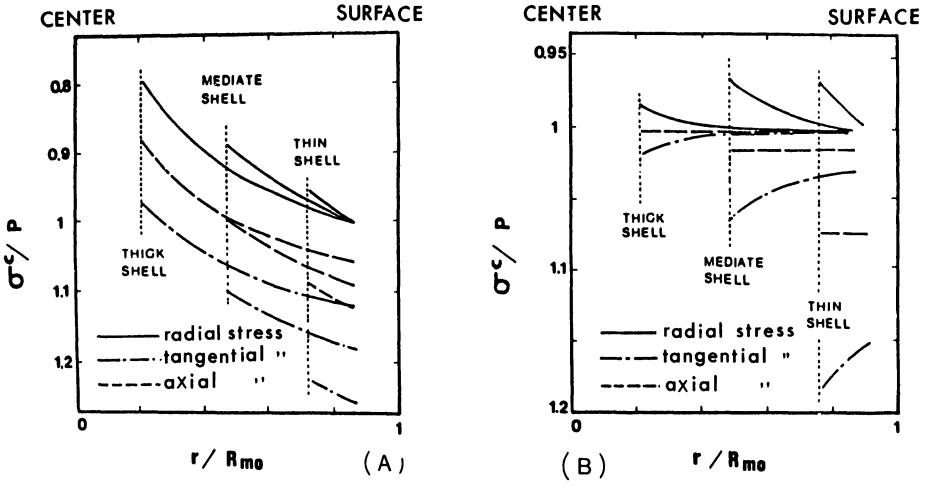

Fig. 3. Distribution of instantaneous stress at different stages of the HIPing process within the dense shells of a) steel (HIPed at 150 MPa and 1323 K) and b) alumina (150 MPa and 1623 K).

The distributions of the various stresses within the dense parts of cylindrical steel and alumina samples have been evaluated and are shown in Fig 3 [3]. The stress state is far from isotropic, in spite of the fact that the external pressure remains isostatic. This anisotropic stress distribution during HIPing must result in anisotropic creep of the dense shell, and may partly be responsible for the shape changes.

Sample shrinkage

The shrinkage encountered in different directions in a sample during HIPing is typically unequal, and may even vary from one product geometry to another. Some empirical values of shrinkage for HIPed cylinders are illustrated in Fig 4 [5]. In this figure, the filling density ($D_o = \varrho_o/\varrho$) is the free parameter and the lines correnspondingto different values of D_o indicate theoretically the relationship between axial and radial shrinkage (S_L and Sr) based on the formula: $D_o = (1-Sr)^2(1-S_L)$. The 45^0-line in Fig 4 corresponds to equal shrinkage in both directions. The experimental data (shaded area in Fig 4) show that $Sr > S_L$. The deviation from isotropic shrinkage makes accurate shape prediction and the attainment of near net shape, more difficult. There are many factors, such as non-uniform filling density, relative container wall thickness etc, which are often advocated in the literature to account for anisotropic shrinkage of HIPed samples [4, 5, 6]. However, non-uniform densification is also an important cause of unequal shrinkage. This can be understood through the following simple argument. Let us consider two preforms being HIPed: a) a long cylinder ($L \gg R$); b) a flat disk ($L \ll R$). For the long cylinder, heat diffuses mainly along a radial direction during HIPing and a temperature gradient thus occurs over the sample's radius. The densification front, in this case, is therefore parallel to the cylindrical surface, resulting in $Sr > S_L$. If, on the other hand, a disk (short cylinder) is HIPed, the densification front lies parallel to the plane surface of the disk. Obviously, this leads to $Sr < S_L$. To prove this point, a short cylindric compact of steel powders (R/L = 3) is HIPed at

150 MPa and 1423 K with the heating rate of 50 K/min. The experimental result represented by a solid circle in Fig 4, supports the argument presented above.

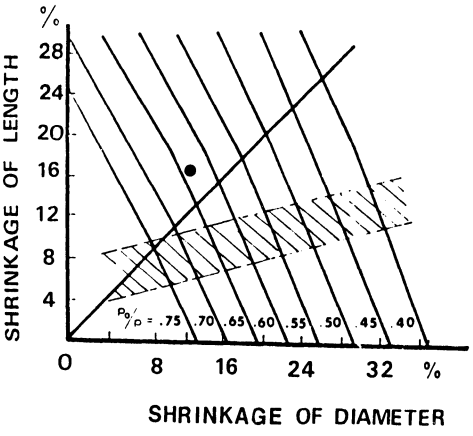

Fig 4. Shrinkage relationship of solid cylinders [5].

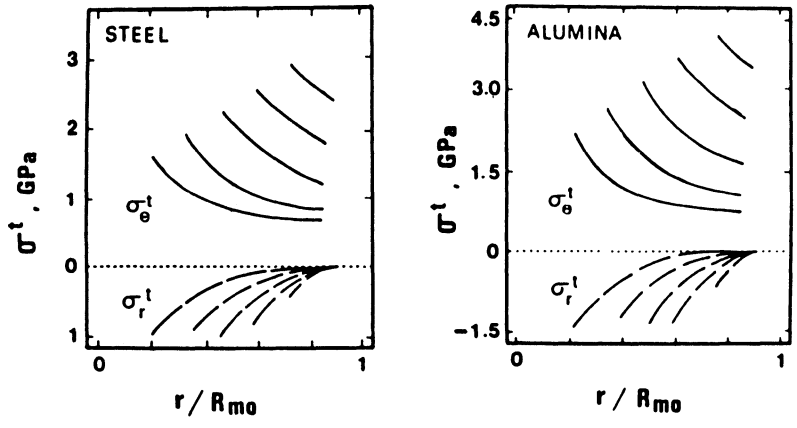

Fig 5. Variation in radial and tangential residual stress, as a function of thickness attained by the densified skin of the sample: (a) steel (b) Alumina [3]. Note different scales.

Residual stresses and surface cracking

Another consequence of non-uniform densification is that after cooling the preform to ambient temperature, residual stresses may occur in the sample [1, 3]. If the HIP treatment is interrupted before the sample is completely densified, the displacement of the inner face of the solid shell has to be compatible with the displacement of the outer face of the

porous core. The shell is in effect acted on by an internal stress exerted by the core and thermal stress. In this case, the residual stresses may be significant, and can be calculated by the equation given in ref. [3]. Fig. 5 shows plots of residual stress against distance from the centre of a solid shell for 2 materials. The different curves show the residual stresses at different thickness of the shell forming at different instants after the HIP treatment is interrupted. As expected, alumina gives larger residual stresses than the metal because its thermal conductivity is lower (note the different scales used). Obviously, the magnitude of the residual stresses is dependent on the presence of residual porosity.

SUMMARY AND CONCLUSIONS

Depending critically on the processing cycle, densification during HIPing can be non-uniform across the sample. A parameter C which measures the ratio of the densification rate to the rate of heat flow can be used to approximately indicate whether or not non-uniform densification may occur. For non-uniform densification several undesirable effects may occur:

1) a reduction of the effective pressure Pi;
2) a prolonging of the HIP-ing time to reach full density;
3) a shape change in the sample being HIPed;
4) anisotropic shrinkage of the sample;
5) residual stresses and surface cracking due to thermal stresses acting on the unevenly densified sample.

The ways of avoiding these problems can be evaluated using software developed for use on a micro-computer.

REFERENCES

1. Li, W-B and Easterling, K.E., Stresses developed in the hot isostatic pressing of metals and ceramics, Proceedings of 1st Int HIP Conf., ed. Garvare T., Centek Publishers, Luleå, SWEDEN, 1987, pp 97-105.

2. Li, W-B., Ashby, M.F. and Easterling, K.E., On Densification and Shape Change during Hot Isostatic Pressing, Acta Met., 1987, Vol 35, No 12, pp 2831-2842.

3. Li, W-B., Easterling, K.E. and Ashby, M.F., Instantaneous and residual stresses developed in hot isostatic pressing of metals and ceramics, Met. Trans., 1991, Vol 22A, May, pp 1071-1078.

4. Aren, B.and Li, W-B., The approach of near net shape by direct hot isostatic pressing of powders, Technical Report of Luleå University, SWEDEN, 1985:053T.

5. Fällman S., Jaktlund L-L., Tegman R. and Garvare T., Numerical modelling of shrinkage during HIP, Proceedings of 1st Int HIP Conf., ed. Garvare T., Centek Publishers, Luleå, SWEDEN, 1987, pp 89-96.

6. Aren B. and Li W-B., Investigation of Hot Isostatic Pressing of Metal Powder to Near Net shape, Proceedings of 1st Int HIP Conf., ed. Garvare T., Centek Publishers, Luleå, SWEDEN, 1987. pp 117-124.

FINITE ELEMENT SIMULATION OF NONUNIFORM SHRINKAGE DURING SINTERING OF CERAMIC PRODUCTS

Ken-ichiro MORI, Kozo OSAKADA and Toshiaki HIRANO
Department of Mechanical Engineering, Faculty of Engineering Science,
Osaka University, Machikaneyama, Toyonaka, Osaka 560, Japan.

ABSTRACT

A method for simulating nonuniform shrinkage in sintering of ceramic compacts is proposed on the basis of the rigid-plastic finite element method. The effects of the density distribution, the dead weight and the pressure on the nonuniform shrinkage are taken into consideration. The method makes it possible to predict the shape of a ceramic product after sintering. Sintering of pipes with a flange is chosen as an example of the simulation. The deforming shape and the distribution of density during sintering are computed. The wall thickness near the bottom of the sintered pipe becomes large because of nonuniform shrinkage due to the dead weight. The curvature of the flange increases as the length of the flange increases.

INTRODUCTION

Ceramic products are manufactured by compacting ceramic powders and subsequently sintering the compacts at elevated temperatures. Ceramic products are fully densified by sintering. Shrinkage of a ceramic compact during sintering is fairly large, i.e. 20%–50% of the volume. Since the compact has a distribution of density depending on the geometry and the friction of the die, the compact shrinks nonuniformly during sintering due to the density distribution. Also, a large compact is nonuniformly shrunk during sintering by the dead weight. The nonuniform shrinkage makes it difficult to predict the shape of the product after sintering. It is desirable in the ceramic industry to develop a method for predicting the shape change in the sintered product. Such a method would play a significant role in net shape manufacturing of ceramic products, because the trial and error procedure for minimizing the finishing operation by grinding is then quickly carried out. It is not easy to modify the shape of the ceramic products after sintering, because they are extremely hard.

The finite element method has been applied to powder forming processes[1–4]. The authors [5] have proposed a method for simulating plastic deformation in compaction and

sintering of ceramic powder on the basis of the rigid-plastic finite element method. In this method, the effect of the density distribution of the compact on nonuniform shrinkage during sintering has been taken into consideration.

In the present paper, a method for simulating the deformation behaviour in sintering of ceramic compacts is proposed on the rigid-plastic finite element method. In this method, nonuniform shrinkage of compacts during sintering due to the density distribution, the dead weight and the pressure is dealt with.

METHOD OF SIMULATION

A compact of powder undergoes a change in apparent density during sintering. To treat the density change, the following densification criterion for powders proposed by Shima et al. [6,7] is used;

$$(\sigma_x-\sigma_y)^2+(\sigma_y-\sigma_z)^2+(\sigma_z-\sigma_x)^2+6(\tau_{xy}^2+\tau_{yz}^2+\tau_{zx}^2) + 2(\frac{\sigma_m}{f})^2 - 2(\rho^n\bar{\sigma})^2 = 0, \quad (1)$$

$$f = 1/a(1-\rho)^m, \quad \bar{\sigma} = F\dot{\bar{\varepsilon}}^b$$

where σ_m is the hydrostatic stress, ρ is the relative density and a, m, n, F and b are the material constants. By assuming the left-hand side of equation (1) to be a plastic potential, the stress-strain-rate relations for the porous rigid-plastic material are expressed by,

$$\{\sigma\} = [D]\{\dot{\varepsilon}^p\}, \quad (2)$$

where [D] is the matrix correlating the stress with the strain-rate and $\{\dot{\varepsilon}^p\}$ is the plastic strain-rate.

The amount of shrinkage in sintering varies with the density of the compact; the shrinkage is small when the density is high and is large when it is low. The strain in sintering obtained for a compact with a uniform density distribution is called the shrinkage strain. The normal shrinkage strain in sintering is a function of the relative density of the compact, ρ_c;

$$\varepsilon_{ii}^s = \varepsilon_{ii}^s(\rho_c). \quad (3)$$

The relationship between the shrinkage strain and the relative density is measured from sintering experiment of compacts with a uniform density distribution. The average shrinkage strain-rate is expressed by

$$\dot{\varepsilon}_{ii}^s = \varepsilon_{ii}^s/t, \quad (4)$$

where t is the time of the shrinkage in sintering. The shrinkage strain-rate during sintering is approximated to be the average strain-rate, because it is not easy to measure the change in the shrinkage strain-rate.

Consider that a compact having a density distribution caused in compaction shrinks nonuniformly during sintering. In the compact with a density distribution, the shrinkage strain in sintering is not uniform in the material according to equation (3). It is considered that plastic deformation is induced by the difference of the shrinkage strain. Since a change in

volume is caused also by the plastic deformation, the shrinkage in sintering is not uniform. The plastic deformation during sintering is simulated by a rigid-plastic finite element method.

The total strain-rate in sintering is assumed to be composed of two parts;

$$\dot{\varepsilon}_{ij} = \dot{\varepsilon}_{ij}^{s} + \dot{\varepsilon}_{ij}^{p}. \tag{5}$$

The strain-rate components within the element in the finite element analysis are expressed by

$$\{\dot{\varepsilon}\} = [B]\{v_e\}, \tag{6}$$

where [B] is the matrix correlating the strain-rate with the nodal velocity $\{v_e\}$. By substituting equations (5) and (6) into equation (2), the stress components in sintering are given by

$$\{\sigma\} = [D][B]\{v_e\} - [D]\{\dot{\varepsilon}^s\}. \tag{7}$$

From the principle of virtual work, the nodal forces for each element are obtained;

$$\{P\} = \int_{V_e} [B]^T\{\sigma\}dV + \int_{V_e} g\rho\gamma\{N\}dV, \tag{8}$$

where g is the gravity, γ is the density and $\{N\}$ is the shape function of the element. From equations (7) and (8), the nodal forces are expressed by

$$\{P\} = \left[\int_{V_e} [B]^T[D][B]dV\right]\{v_e\} - \int_{V_e} [B]^T[D]\{\dot{\varepsilon}^s\}dV + \int_{V_e} g\rho\gamma\{N\}dV. \tag{9}$$

The nodal forces of the surrounding elements at each nodal point are equilibrated;

$$\sum^{\text{element}} P_i = \begin{cases} 0 \ \text{(in material)} \\ F_i \ \text{(on surface).} \end{cases} \tag{10}$$

where F_i is the external force obtained from the pressure applied in the sintering or from the friction between the tool and the workpiece. The equilibrium simultaneous equations (10) are solved by the direct iteration without partial differentiation. In the equilibrium equations (10), the effects of the density distribution, the dead weight and the pressure on the nonuniform shrinkage of compacts during sintering are taken into consideration.

RESULTS

Nonuniform shrinkage in sintering of cylindrical pipes having a flange without pressure is simulated by the present rigid-plastic finite element method. To examine only the effect of the dead weight in sintering, the density of the compact before sintering is set to be uniform. Thus, the compaction process has not been computed. The working conditions used in

simulation of sintering are given in Table 1. The material constants F, b, n, a and m in equation (1) were measured for alumina compacts.

The element meshes of the pipes after sintering for the flange length l_f=60mm and 100mm are shown in Fig. 1. Deformation is axi-symmetrical. The number of the deformation steps in simulation of sintering is 50. The flange is bent by the dead weight after sintering.

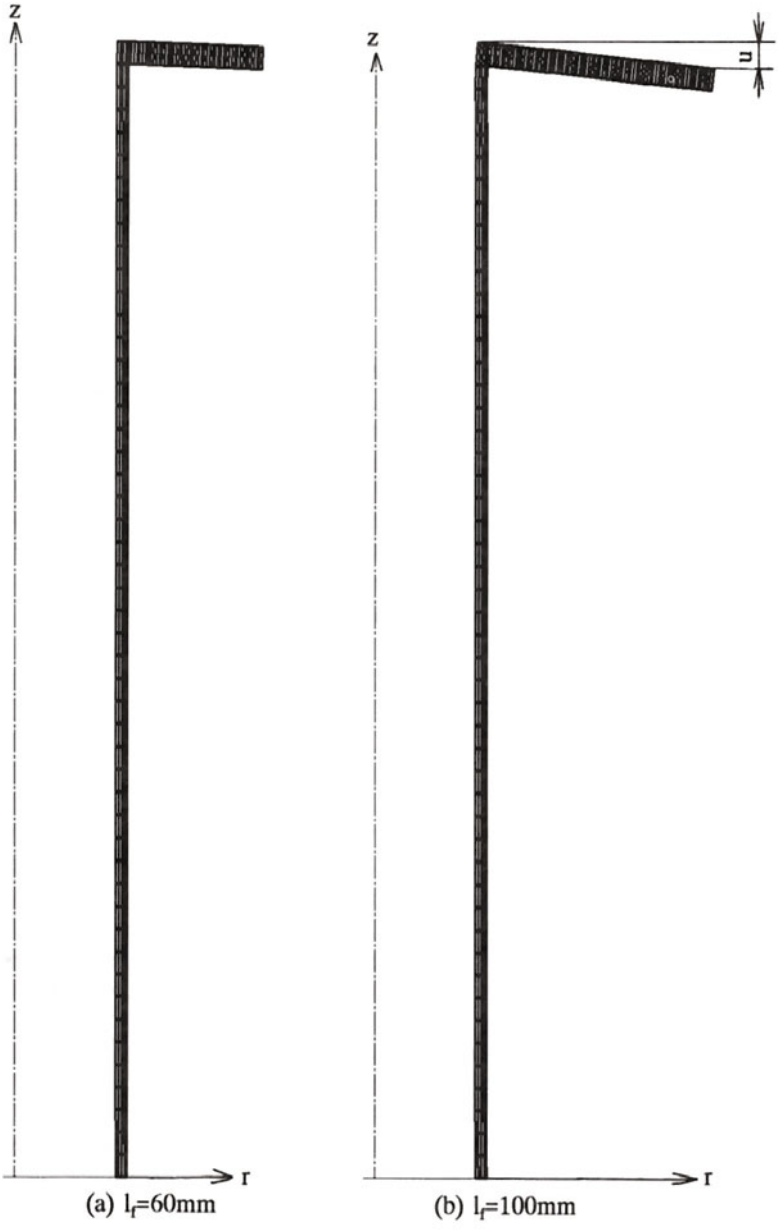

Fig. 1 Element meshes of pipes with flange after sintering.

The relationship between the flange displacement u after sintering and the flange length is given in Fig. 2. The curvature of the flange increases as the flange length increases.

Fig. 3 shows the distribution of the calculated relative density after sintering for l_f=100mm. The relative density has a minimum value around the outer corner of the flange.

The wall thickness distribution of the pipe without a flange (l_f=0mm) after sintering is illustrated in Fig. 4, where h is the height of the pipe after sintering. The thickness of the pipe is the largest around the bottom due to the dead weight. The inhomogeneity of the thickness distribution increases as the flow stress decreases.

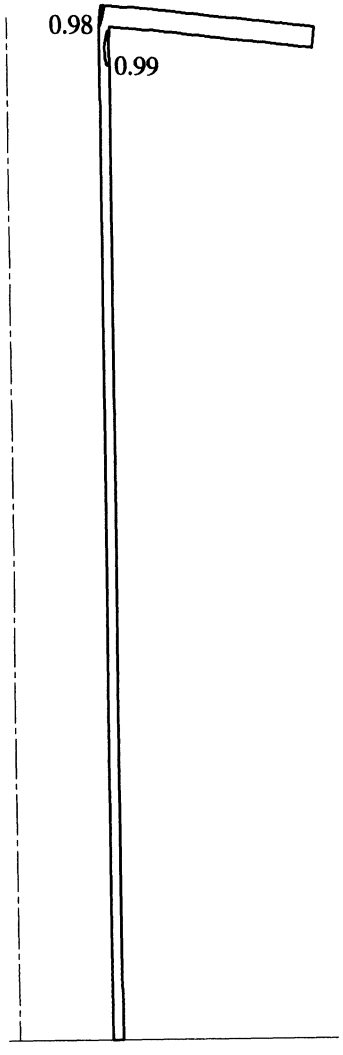

Fig. 3 Distribution of calculated relative density after sintering for l_f=100mm.

Table 1 Working conditions used in simulation of sintering.

Height	500mm
Wall thickness	t_0 = 5mm
Outer diameter	100mm
Flange length	l_f = 0,20,40,60,80,100mm
Relative density	0.4
Density of alumina	3990kg/m^3
Material constants in equation (1)	F=3100GPa, b=1, n=3.4, a=2.61, m=0.799
Coefficient of friction	0.3

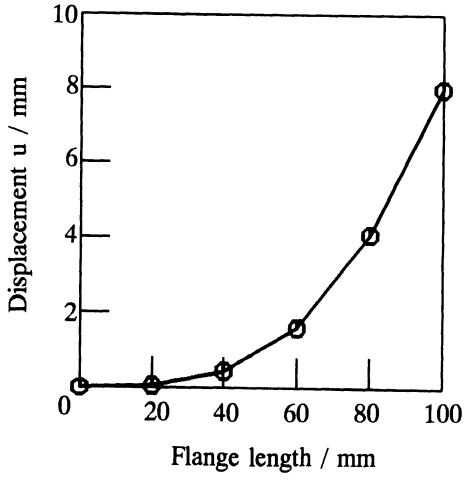

Fig. 2 Relationship between flange displacement after sintering and flange length.

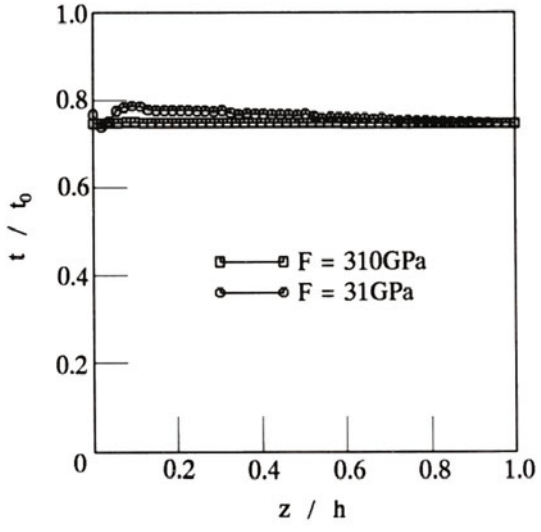

Fig. 4 Thickness distribution of pipe without flange after sintering.

CONCLUSIONS

To predict the shape of the ceramic product after sintering, a finite element method for simulating the sintering process was developed. The method is based on the plasticity theory of porous materials to deal with the density change during sintering. In the method for sintering, plastic deformation induced by the difference of the shrinkage strains, the dead weight and the pressure is simulated. The method is useful for net shape manufacturing of ceramic products.

REFERENCES

1. Mori, K., Shima, S. and Osakada, K., Finite element method for the analysis of plastic deformation of porous metals. Bull. JSME, 1980, 23, 516–522.

2. Mori, K. and Osakada, K., Analysis of the forming process of sintered powder metals by a rigid–plastic finite–element method. Int. J. Mech. Sci., 1987, 29, 229–238.

3. Abouaf, M., Chenot, J.L., Raisson, G. and Bauduin, P., Finite element simulation of hot isostatic pressing of metal powders. NUMIFORM 86, ed. K. Mattiasson et al., Balkema, Rotterdam, 1986, pp.79–83.

4. Nohara, A., Nakagawa, T., Soh, T. and Shinke, T., Numerical simulation of the densification behaviour of metal powder during hot isostatic pressing. Int. J. Numer. Methods Eng., 1988, 25, 213–225.

5. Mori, K. and Osakada, K., Prediction of shape of ceramic product after sintering by a rigid–plastic finite–element method. Int. J. Mech. Sci., submitted for publication.

6. Shima, S. and Oyane, M., Plasticity theory for porous metals. Int. J. Mech. Sci., 1976, 18, 285–291.

7. Shima, S. and Mimura, K., Densification behaviour of ceramic powder. Int. J. Mech. Sci., 1986, 28, 53–59.

FURTHER EVIDENCE FOR PROPER FUNCTION OF HIP PHASE DIAGRAM

Kozo Ishizaki
Dept. of Materials Science and Engineering
School of Mechanical Engineering
Nagaoka University of Technology
Nagaoka 940-21, Japan

ABSTRACT

The author describes a fundamental method to promote new applications of HIP technology. Just like all other materials engineering, there are two fundamental aspects; how fast materials can be produced, i.e. kinetics, and what can be obtained, i.e. thermodynamics.

In HIPping technology the former is rather well established by "a HIP map" proposed by Ashby and others, but no special methods have been established to obtain thermodynamical information for HIPping technology. A phase diagram, or "a HIP phase diagram" to apply in HIP process was proposed by the group of the author. In the diagram, stable phases can be determined under varying temperature, total pressure and partial pressure of related chemical reactions. In the present work, first of all, the method to obtain the diagrams is briefly explained. To provide a further evidence to evaluate HIP Phase Diagrams, capsule free HIP case for aluminum nitride is discussed. Aluminum nitride ceramics of large grain size with clean grain boundary phases without loosing impurity oxygen solute atoms ($\sim$2wt%) were obtained. On the other hand, oxygen contents of normal sintered AlN decreased from 2.8 to 0.9 wt% by increasing sintering temperatures from 1773 to 2173K. This phenomenon was only possible to explain by using HIP phase diagram.

INTRODUCTION

Since the invention of sinter HIP process by Romp in 1941[1], there have been many applications of HIP processes. The advantage of HIP densification is an established fact. What is needed now are:

1. New applications, such as to produce porous materials by HIP process [2-4], or
2. To use advantage of high pressure to obtain new Phases.

In this paper, a HIP Phase diagram is discussed to examine the second point.

An Ellingham (ΔG^0-T) diagram is used to examine which is the most stable material at a given temperature and oxygen partial pressure. A total pressure axis must be added to the diagram to obtain a chemical stability (i.e. Phase) diagram as a function of temperature, total pressure and partial oxygen pressure. Some aspects of the method to obtain this diagram were discussed by the first time by the group of the author [5-10].

The pressure effects, say 200MPa, have rather secondary effects for normal solids compared to gases. At a given temperature the value of standard free energy difference ΔG^0 with pressure is,

$$\left(\frac{\partial \Delta G^0}{\partial P} \right)_T = \Delta V. \qquad (1)$$

Using this relation, we obtain a HIP Phase Diagram. The diagram is used to sinter AlN with good grain boundary properties without loosing oxygen contents.

ALUMINUM NITRIDE

Aluminium nitride ceramics have excellent thermal and mechanical properties. In the case of normal-sintering, extremely high sintering temperatures and long periods are usually required to obtain a fully compacted and high thermal conductive AlN. A HIP method densifies AlN thoroughly with less defects and better mechanical properties by an additional driving force provided by the applied gas pressure at even lower sintering temperatures than a normal-sintering process, and is expected to be a better method for obtaining a higher thermal conductivity material.

The thermal conductivity of capsule-free-HIP, capsule-HIP and normal-sintered AlN was compared. Despite expectations, the thermal conductivity of HIPped AlN was lower than that of the normal-sintered one. The cause of this phenomenon is explained by using the HIP Phase Diagram.

A commercial AlN powder (Tokuyama Soda) with the average partial size (0.6 μm) and the specific surface area (3.2 m^2/g) was used. An Y_2O_3 powder (average particle size: 1.6 μm, specific surface area: 8.4 m^2/g, supplied by Shin-Etsu Chemical) as a sintering aid was added to 1 mol% in the raw AlN power. The mixed powder was pressed into cylinders (14 mm diameter and 10 mm height), CIPped under 400 MPa for 60 s, and sintered by the following two different procedures.

(1) Capsule-HIP sintering: The CIPped samples were coated by boron nitride powder and placed in Vycor glass capsules. After being degassed for 1 h under vacuum (1 Pa or lower pressure) at 1000 K, they were sealed and HIP sintered at temperatures between 1773 and 2073 K under an argon gas pressure of 60 MPa for 1 h.

(2) Normal-sintering: The CIPped samples were normal-sintered in a graphite-resistance furnace at temperatures between 1773 and 2173 K under nitrogen gas atmosphere of 1 MPa for 1 h.

(3) Capsule-free-HIP: After removing the capsule, the AlN specimens obtained by capsule-HIP sintering were wrapped in graphite foils and then HIPped at a temperature of 2773K with a graphite heater for 1h under a nitrogen gas pressure of 100MPa. The equipment and detailed procedures for the ultra-high temperature HIP sintering have been described elsewhere [11,12]. The bulk density was measured by a displacement method in toluene. Its thermal conductivity, specific heat and thermal diffusivity were measured by a laser flash technique. The detailed procedures have been reported elsewhere [13]. Impurity oxygen contents were measured by a radioactive analysis method.

The thermal conductivity is shown in Fig.1. The values were calibrated by the total porosity of the sintered AlN. The mean thermal conductivity of the HIP sintered AlN was about 100 W/(m.K). The values were independent of the sintering temperatures. On the contrary, the thermal conductivity of the normal-sintered AlN increased linearly as the sintering temperature augmented.

The oxygen content remained almost constant (～2 wt%) with the increasing HIPping temperature, as seen in Fig.2. During capsule-free-HIP, samples were wrapped in graphite foil, but oxygen content was also 1.9 wt%. The grain size was 40μm (about 1μm for capsule-HIP) but the thermal conductivity did not improve. However, the oxygen content of the normal-sintered AlN linearly decreased from 2.8 to 0.6 wt% as the sintering temperature increased from 1773 to 2073 K. The oxygen content, which influences thermal conductivity of AlN, is evaluated by using the HIP Phase Diagram for the oxidation reactions of carbon, the related metals and AlN in the previous work [2-11]. In the previous work HIP sintering was performed at 2073K. It is proven also by capsule-free-HIP at 2773K that the HIP Phase Diagram function properly.

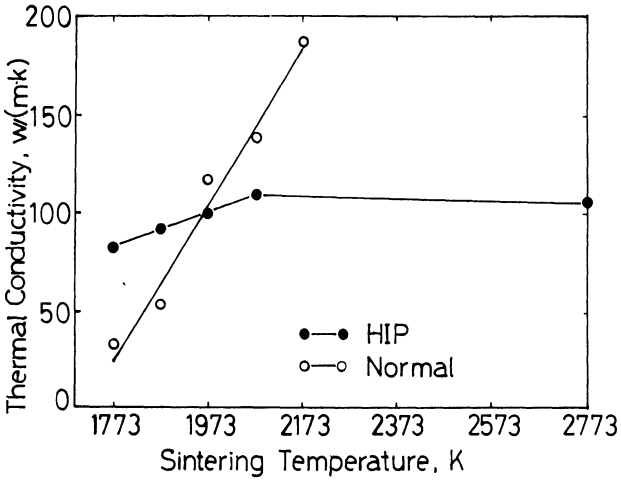

Figure 1. Thermal conductivity depending upon sintering temperature for the cases of HIP and normal sintering. The sample at 2773K is obtained by capsule-free-HIPing.

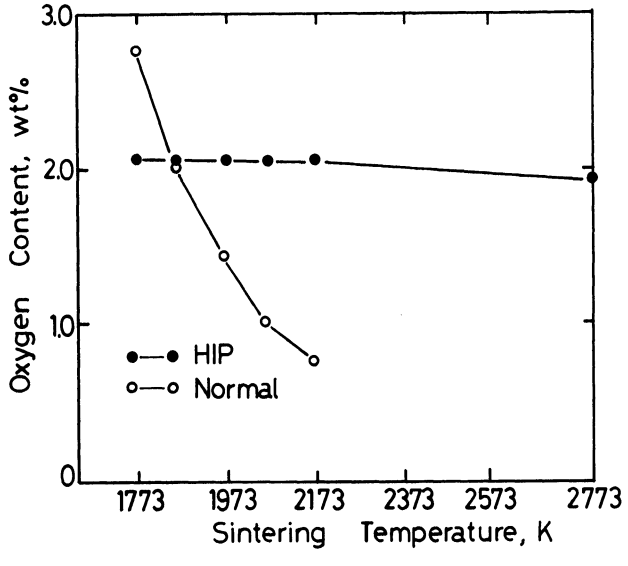

Figure 2. The influence of oxygen contents of the sintered AlN on sintering temperature for the cases of HIP and normal-sintering. The sample at 2772K is obtained by capsule-free-HIPing.

SUMMARY

The HIP Phase Diagrams proposed in the previous works clarifies many HIP sintering problems which could not be solved previously. The HIP Phase Diagram was constructed to add the total pressure axis in a ΔG^0 (i.e., the partial pressure of oxygen) - T space. Exactly the same argument may be applied for nitriding reactions in a N_2 atmosphere. In this case, the HIP Phase Diagram has the ΔG^0 (i.e., P_{N2}), P_{total} and T axes. The main difference between the normal Ellingham diagram and the HIP Phase Diagram is that the former considers $P_{total} = P_{O2}$ (or P_{N2}, etc.), but the latter has P_{total} as an independent variable.

The oxygen content of capsule-HIPped AlN was almost equal to that of the capsule-free-HIPped one. The grain size of AlN specimens obtained by capsule-HIP sintering increased from 1 to 40μm by ultra-high temperature HIPping at 2773K for 1h under a nitrogen gas pressure of 100MPa. However the room temperature thermal conductivity of both specimens were almost the same. The explanation of this phenomena was easily done by HIP Phase diagram. This was true even at the extreme HIPping condition at 2773K. The oxygen contents do not decreased as the HIP Phase diagram predicted.

This is just a example that shows how new applications are easily visualized and programmed by using HIP Phase diagrams, and a further evidence of proper function of HIP Phase diagrams.

ACKNOWLEDGEMENTS

This work was partially supported by Mon-busho (Ministry of Education and Culture) under a cooperative program (Kyo-do Kenkyu) with Kobe Steel, Ltd.(KOBELCO).

REFERENCES

1. J. Romp, U.S. pat. 2,263,520 (Nov. 18, 1941).
2. K. Ishizaki, A. Tanaka and S. Okada, "Mechanically Enhanced Open Porous Materials by a HIP Process", J. Ceram. Soc. Jpn. International Ed., 98, 545- 551 (1990)
3. A. Takata, K. Ishizaki and S. Okada, "Inprovement of a Porous Meterial Mechanical Property", in "Mechanical Properties of Porous and Cellular Materials", Ed. by Z. J. Gibson, D. Green and K. Sieradzki, MRS (1991).

4. K. Ishizaki, "Stronger Open Porous Ceramics and Metals Produced by HIP", Materials and Processing Report, 5, 4-5 (January 1991).
5. K. Watari, K. Ishizaki and M. Kawamoto, J. Ceram. Soc. Jpn. Internatle. Ed. 96, 128-134 (1988).
6. K. Watari and K. Ishizaki, J. Ceram. Soc. Jpn. Internatle. Ed. 96, 535-540 (1988).
7. K. Watari, K. Ishizaki and M. Kawamoto, J. Ceram. Soc. Jpn. Internatle. Ed. 96, 741-748 (1988).
8. K. Ishizaki, "Phase Diagrams under High Gas Pressure-Ellingham Diagrams for Hot Isostatic Press Process", Acta. Met. et Mat., 38, 2059-2066 (1990).
9. K. Ishizaki, "Thermodynamics for HIP Sintering of Ceramics- Proposed HIP Phase Diagrams", (invited) pp.129-138, in "Hot Isostatic Pressing: Theory and Applications", the 2nd International HIP Conference, NIST, Washington D.C. (1989) Ed. by R. J. Schaefer, and M. Linzer, ASM Internatinal, Metals Park, Ohaio (1991).
10. K.Ishizaki, "Oxygen Partial Pressure and HIPping of Ceramics-Proposed HIP Phase Diagrams", in "Euro-Cermics, Processing of Ceramics", Eds. G. de With, R. A. Terpstra and R. Metselaar, Elsevier Appl. Sci., London and New york, Vol.1, pp.314-318 (1989).
11. K. Uehara and Y. Sakashita, "Recent Trends in HIP Equipment", pp.31-35 in Proc. of the 9th HIP seminar, Edited by Kobe Steel Ltd., Kobe Japan, 1989.
12. Y.Sakashita, C.Manabe, K. Muramatsu, S. Kofune, T. Fujikawa and T. Kanda, "Development and Application of Ultra-High-Temperature HIP by Means of an Optical Tempareture Measurement System," pp.355-359, loc. cit. ref. 9.
13. K. Watari, Y. Seki and K. Ishizaki, J. Ceram. Soc. Jpn. Internatle. Ed., 97, 53-59 (1989).

SIMULATION OF PSEUDO-ISOSTATIC PRESSING OF POWDER COMPACT

SUSUMU SHIMA and AKIO INAYA
Department of Mechanical Engineering, Kyoto University,
Sakyo-ku, Kyoto 606, Japan

ABSTRACT

To investigate the deformation behaviour of the workpiece, pressure characteristics, etc. in pseudo-isostatic pressing, a rigid-plastic finite element simulation in an axi-symmetric case and, for simplicity, at room temperature is carried out. The formulation is based on the plasticity theory for compressible materials. Further, an experimental method of estimating the pressure exerted on the workpiece is developed and carried out. As a model material for the workpiece, sintered copper and sintered aluminium are utilized; an alumina powder with or without graphite powder admixed is used for a pressure medium. Deformation and stress state in the workpiece, which have not been well-understood so far, are thus investigated. It is also confirmed that the density increase and deformation of the workpiece are well simulated.

INTRODUCTION

Cold isostatic pressing (CIP) and hot isostatic pressing (HIP) of powder or powder compacts have been successful in obtaining the products of more or less homogeneous density distribution throughout. These processes require a proper design of the capsule for material saving or near net-shape production, but since they possess various advantages, they will be utilized more and more in future.

HIP, which is done at elevated temperatures, possesses some difficulties in handling, since gas is used as a pressurizing medium. To overcome the difficulties, pseudo-HIP process was developed [1]. Since a powder is used in this process as a pressurizing medium, the apparatus is simpler and handling is much easier. It has, therefore, its potential to be employed in various fields. However, the feature of the process is not known except that the stress state in the workpiece is not isostatic. For near net-shape production, the shape of the products should be predicted and this, in tern, requires the fundamental characteristics to be investigated.

Motomura et al. carried out experiments with workpieces of various shapes and derived some empirical formula for predicting the shape of the product [2]. Mizunuma et al. studied experimentally the deformation characteristics of preforms [3]. However, there has been little work done in the past on a theoretical basis.

In this study, simulation is carried out, based on the plasticity theory for compressible materials [4,5], to investigate the stress state in the workpiece, the increase in density ratio and thus the shape of the product in pseudo-isostatic pressing; also a particular experimental procedure is developed to evaluate the stress state experimentally. For convenience, the experiment is first described and followed by simulation. Let compression be positive.

EXPERIMENTAL EVALUATION OF STRESS STATE

Furguson et al. [1] measured pressure distribution at the inner surface of the container in pseudo-isostatic pressing by amounting pressure pins, but the pressure actually exerted on the workpiece surface may not be the same. Since it is difficult to measure the pressure directly, an indirect method was developed as follows:

1) A porous material whose mechanical behaviour is known is used as the workpiece; sintered copper and sintered aluminium were used in the present study.

2) Pseudo-isostatic pressing is carried out in a stepwise manner and the density ratio and strains are measured.

3) The plasticity theory for compressible materials is used to calculate stress state. Stress is expressed in terms of strain increments as [4,5]

$$\sigma_{ij} = \frac{\rho^{2n-1}\bar{\sigma}}{\dot{\bar{\varepsilon}}} \left\{ \frac{2}{3}\dot{\varepsilon}_{ij} + \delta_{ij}\left(1 - \frac{2}{9f^2}\right) f^2 \dot{\varepsilon}_v \right\} \tag{1}$$

Substituting the strain increments measured in 2), one can calculate the stress during the process. In the stress calculation, the flow stress-strain curve of the pore-free matrix (copper and aluminium) is necessary; the curves for both of these materials were obtained by the method described in [4]. Note that in this experiment and calculation it was assumed that the workpieces deform uniformly throughout the process.

EXPERIMENT

Cylindrical workpieces of sintered copper and aluminium were used for the workpieces. An alumina powder was used for the pressure medium; the same powder mixed with graphite powder was also used to examine the effect of the properties of the pressurizing medium on the deformation characteristics of the workpiece. The inner surface of the container was lubricated with stearic acid to reduce the friction at the powder-container interfaces.

The cylindrical workpieces remained almost cylindrical, but a little distorted after pseudo-isostatic pressing; the diameter at the bottom was 1 to 3% larger than that at the top after about 30% reduction in height. The assumption of uniform deformation would have been reasonable. The increase in the density ratio in the workpieces was plotted against axial strain. Based on this curve, the stress was calculated.

To carry out the simulation, on the other hand, the characteristics of the powder, or the pressure medium, are necessary and therefore compaction tests of the powders were carried out in plane-strain [6] and also in a closed-die.

Experimental Results

Relationship between density ratio and compacting pressure for the alumina powder and for the graphite-mixed alumina powders in simple closed-die compression was obtained; it was observed that the higher the graphite content, the higher is the density ratio reached for a constant pressure. This means that the graphite has reduced the internal friction in the powder. On the other hand, the ratio of the lateral pressure to the compacting pressure was increased only to a small extent by adding the graphite powder and was more or less of a constant value of about 0.5.

Since the effect of graphite content was not so significant, we shall be concerned with powder A, which is alumina powder with 0% graphite, and powder B, which is the same alumina powder but mixed with graphite of 15% in volume.

Figure 1 shows the relationship between the density ratio and the axial strain for both copper and aluminium, where A refers to powder A and B to powder B. It is clearly seen that the density increase in aluminium is greater than that in copper; it is also obvious that adding the graphite increases the density increase in aluminium whereas in copper there is no apparent difference. This is due to the fact that the latter material is higher in strength than the former and therefore this material is insensitive to the characteristics of the pressure medium. Since the density increase in the workpieces of copper were more or less constant regardless of the graphite content, we shall focus mainly on the results for the workpieces of aluminium.

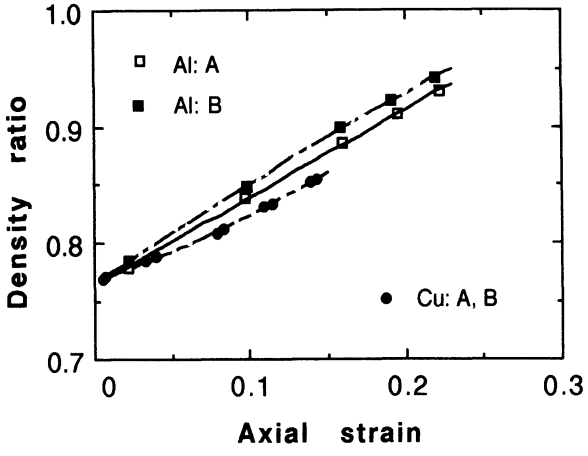

Figure 1. Relationship between density ratio and axial strain.

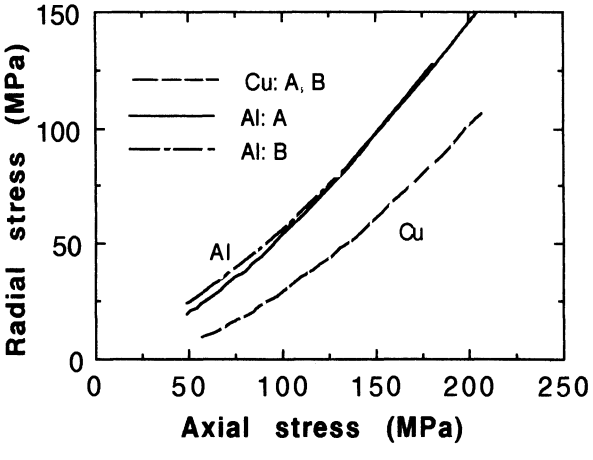

Figure 2. Relationship between radial stress and axial stress in pseudo-isostatic pressing.

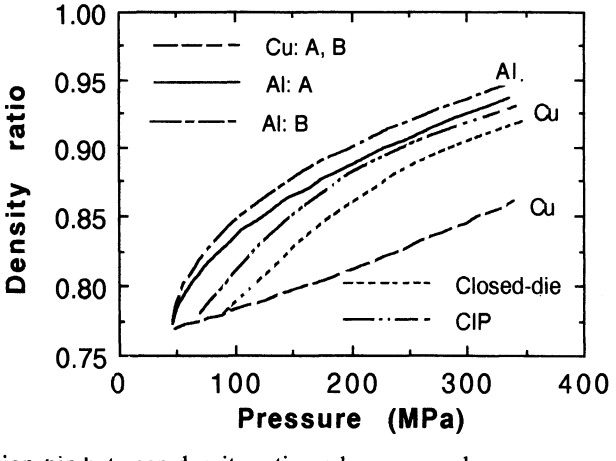

Figure 3 . Relationship between density ratio and mean punch pressure.

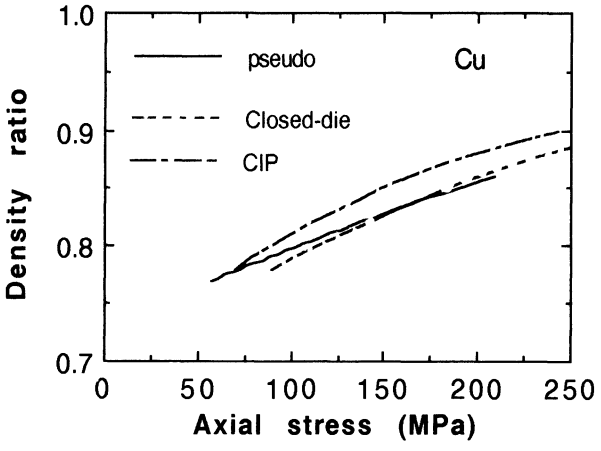

Figure 4. Relationship between density ratio and axial stress.

Figure 2 shows the radial stress vs. axial stress in aluminium and copper with an initial density ratio of 0.77. Considering the fact that the ratio of radial pressure to axial pressure in simple closed-die compression of the pressure medium was about 0.5, one sees that the ratio in the aluminium in pseudo-isostatic pressing is greater than that in the pressure medium itself. There is no significant effect of graphite observed on stress state.

In Fig.3 the density is plotted against mean punch pressure. The calculated relationship between density ratio and pressure in isostatic and closed-die compression for copper are also shown for comparison. It is clearly seen that the density increase is far below in pseudo-isostatic compaction. However, if the density ratio is plotted against axial pressure exerted on the workpiece, the increase is more or less the same in pseudo-isostatic and closed-die compression and is a little less than in isostatic case (Fig.4). This can be explained by considering the yield surface of the compressible material [4,5]; the pressure required to achieve a certain density ratio by closed-die compression is higher than by isostatic pressing and also the maximum pressure such as in pseudo-isostatic pressing lies in between.

SIMULATION

To carry out a simulation of pseudo-isostatic pressing process by the FEM, the constitutive equations for compressible materials [4,5] are used to describe the behaviour of the pressurizing media; the parameters which appear in the equations for the powders were determined from the results of plane-strain and closed-die compression. The values of the parameters are listed in Table 1.

TABLE 1
Material parameters for pressure medium

Powder	$\bar{\sigma}$ (MPa)	n	a	m
Alumina (powder A)	14500	9.00	1.75	0.8
Alumina (5% Gr.)	9500	8.25	1.70	0.8
Alumina (10% Gr.)	7200	7.85	1.65	0.8
Alumina (powder B) (15% Gr.)	5800	7.60	1.60	0.8

The rigid-plastic formulation for FEM was carried out based on the variational principle [7]; its details have been given elsewhere [8,9]. The simulation can similarly be done to the case of closed-die compaction process, but care must be taken that the material properties of the pressure medium are quite different from those of the workpiece and therefore, difficulties are sometimes encountered in convergence.

The Coulomb friction was assumed at the powder-container interfaces. Simulated results showed that the higher the friction coefficient the lower the increase in density ratio of the workpieces. This is of course due to the loss in pressure transmission from the top tothebottom of the container. Comparing the result and the experimental one, we assumed that the friction coefficeint was 0.3.

COMPARISON BETWEEN SIMULATED AND EXPERIMENTAL RESULTS

Both experimental and calculated results will be shown. Figure 5 shows the relationship between the density ratio and the mean punch pressure. It is seen that for aluminium the density increases more significantly for the larger graphite content and there is fairly good agreement between the calculated and experimental results, whereas for copper, agreement between the results is not satisfactory. This may be due to the fact that although the flow stress of copper is much higher compared with that of the pressure medium in the beginning of the process, we have not still considered any sliding between the workpiece and the powder. In Fig.6 the increase in density ratio is plotted against axial strain for aluminium. There is good

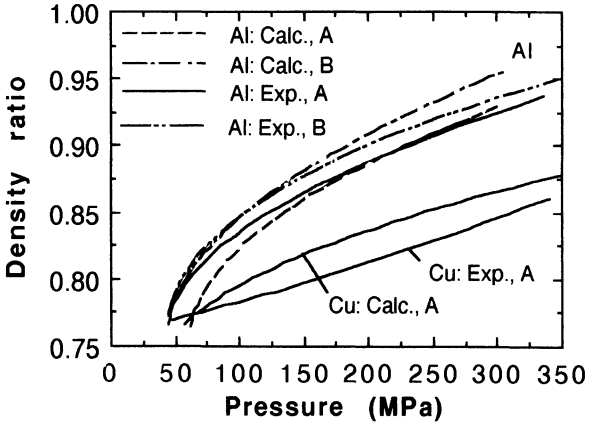

Figure 5. Relationship between density ratio and mean punch pressure.

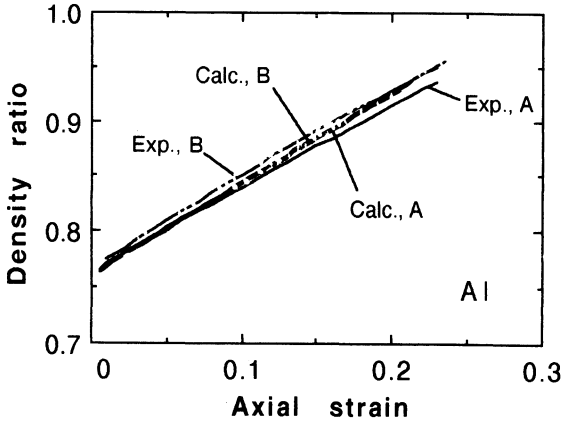

Figure 6. Relationship between density ratio and axial strain.

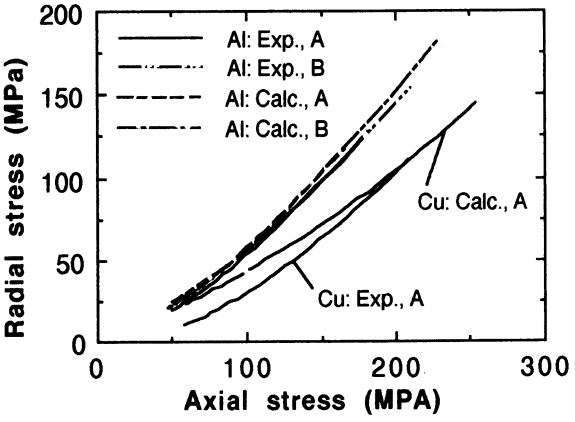

Figure 7. Relationship between radial stress and axial stress.

agreement between experiment and simulation. Figure 7 shows the relationship between the axial stress and radial stress for aluminium and for copper; it is seen that the calculated radial stress is a little larger than the experimentally derived one for a smaller axial stress for copper, but on the whole there is very good agreement between the calculated and experimental results.

CONCLUSIONS

An indirect method of estimating the pressure characteristics in pseudoisostatic pressing was developed. Sintered aluminium and copper were used for workpiece material and it was observed that the deformation of aluminium, the flow stress of which is lower than that of copper, was influenced more significantly by the property of the pressure medium. Simulation was also carried out by FEM. comparing the experimental and simulated results, it can be said that they agreed fairly well. In the present study, the experiments and simulation were both for room temperature, but since it was shown that we can rely on the simulation it can be extended for pseudo-HIP provided that the material properties for both pressure medium and the workpiece. This should be undertaken for future work.

REFERENCES

1. Ferguson, B. L. & Smith, O. D., Ceracon Process, *Metals Handbook, 7, Powder Met, ASM*, 1984, 537-541.
2. Motomura, M. & Uehara, M., Forming of SiC by Pseudo-hot Isostatic Pressing, *Proc. 1990 Japanese Spring Conf. for Tech. Plasticity*, 1990, 209-212.
3. Mizunuma, S., Yamazaki, T. & Kikuma, T., *ibid.*, 133-136.
4. Shima, S. and Oyane, M., Plasticity Theory for Porous Materials, *Int. J. Mech. Sci.*, 1976, 18, 285-291.
5. Shima, S. and Mimura, K., Densification Behaviour of Ceramic Powder, *Int. J. Mech. Sci.*, 1986, 28, 53-59.
6. Shima, S., Saleh, M. A. & Hirata, N., Evolution of Structural Anisotropy in Powders during Compaction, *Adv. Tech. Plasticity, Proc. 3rd ICTP*, 1990, 883-888.
7. Hill, R., *The Mathematical Theory of Plasticity,* Oxford University Press, London, 1950, pp. 60-69.
8. Mori, K., Shima, S. & Osakada, K., Finite Element Method for Analysis of Plastic Defor mation of Porous Metals, *Bull. JSME*, 23, 1980, 516-522.
9. Shima, S. and Nakanishi, T., Rigid-Plastic Finite Element Analysis of the Isostatic Com paction of Ceramic Powder, *Current Japanese Mater. Res., Vol. 7, Computational Plasticity*, 1990, 117-133.

3. ADVANCED CERAMICS

DEVELOPMENT OF GAS PRESSURE SINTERED SILICON NITRIDE CERAMICS

YASUSHI MATSUO
Research & Development Center
NTK Technical Ceramics, NGK Spark Plug Co., Ltd.
2808 Iwasaki,Komaki,Aichi,485 Japan

ABSTRACT

Gas pressure sintering (GPS) process is one of the most promising sintering techniques for the fabrication of high performance silicon nitride ceramics. Almost pore-free densified compacts with low amounts of sintering additives can be obtained by this process. They present high strength with high reliability and good heat resistance. These properties make them one of the best candidate materials for heat engine component as well as other industrial fields application. The gas pressure sintered silicon nitride (GPSSN) ceramics densified to high density have already been applied in turbocharger rotors for automotive application, cutting tools and bearing balls for industrial applications, etc., and have been highly evaluated for high strength and reliability.

INTRODUCTION

As the self-diffusion in silicon nitride is extremely slow,it is necessary to use sintering additives, and at the same time,it is desirable to raise the sintering temperature in order to minimize the amounts of additives.

However,as the sintering temperature is raised, silicon nitride starts to decompose into silicon and nitrogen. Possible solution for this problem without lowering the sintering temperature is the atmosphere control. Figure 1 shows the maximum sintering temperature as a function of nitrogen pressure. Gas pressure sintering (GPS) is the sintering under overpressure of nitrogen gas which suppresses the decomposition of silicon

nitride at higher sintering temperatures. Effectiveness of GPS has been reported by several investigators.[1),2),3),4)]

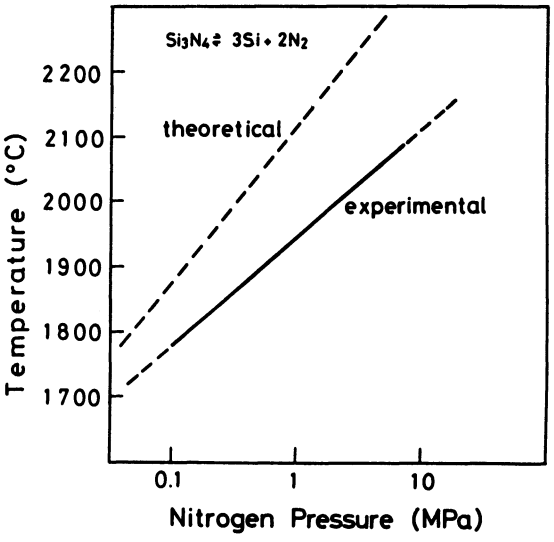

Figure 1. Decomposition map

THE CONCEPT OF GPS

Figure 2 shows the summary of the concept of GPS. GPS is carried out under overpressure of nitrogen gas and consequently higher sintering temperature is possible without significant decomposition. Advantageous effects of higher nitrogen pressure and temperature during sintering process are prevention of pore formation and promoted densification behavior. Therefore, it is possible to minimize amounts of additives, and the selection of additives can be widened.

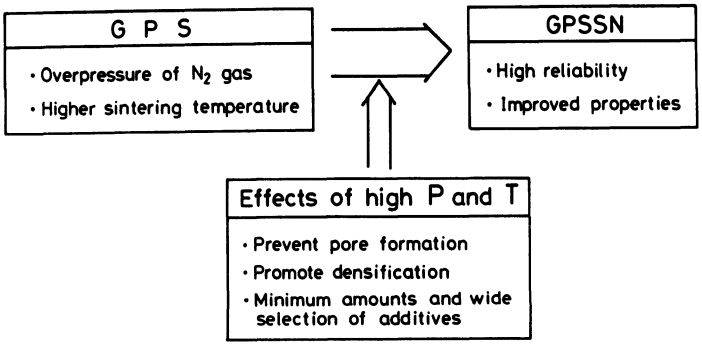

Figure 2. Concept of GPS

As a result, GPSSN can exhibit high reliability and improved properties.

At this point, it would be appropriate to compare GPS and HIP, which are somewhat similar but two different processes. Working gas has to be nitrogen for GPS, whereas it could be other gasses for HIP. GPS employs lower pressure and usually higher temperature than HIP. One of the advantages of GPS is that any pre-treatment is unnecessary.

In GPS, major contribution for densification is due to high temperature, and a role of overpressure is to suppress the decomposition of silicon nitride. On the other hand, major contribution for the densification is a high pressure in HIP. Because of these differences, characteristics of the resultant densified materials are also different. Due to the high sintering temperature, amounts of sintering aids can be reduced and grain growth is promoted by the GPS. Grain growth is effective in achieving high fracture toughness in silicon nitride.

In the HIP, it has been shown that the full densification is possible without adding sintering aids. Also, as the densification at low temperature is possible by the HIP, very fine microstructure can be produced by HIP, which could result in high strength of the materials.

These two densification processes have their own advantages and disadvantages. Therefore, I would suggest that we should choose either process depending on what we want. For instance, if we want high toughness material with coarse microstructure, GPS would be a choice. If we want high density, high strength material with fine microstructure, then HIP would be a choice.

PROPERTIES OF GPS SILICON NITRIDE (GPSSN)

In the following, properties of GPSSN are described. Emphasis is placed on reliability, durability and other properties pertinent to the piston engine application in which maximum temperature is 1000°C.

One of the advantages of GPSSN is the high reliability. Three point flexural strength was measured according to the Japanese standard (4 X 3 X span 30mm) for specimens of 240 each produced by GPS and NS. It is seen that the strength distribution is narrower and the minimum strength level is much higher for GPSSN. Residual pore distribution are dramatically different between the two materials (i.e., almost no pores vs. many pores), and this would in part account for the difference in the strength distribution.

Other distinctive features of GPSSN, compared with normal sintered silicon nitride (SSN), include better oxidation resistance, higher thermal conductivity and higher thermal shock resistance. The first two features presumably result from the lower content of additives used for GPSSN.

APPLICATIONS OF GPS SILICON NITRIDE

Due to the excellent properties and high reliability of GPSSN, many applications to the automotive and industrial field have been intensively pursued.

AUTOMOTIVE APPLICATIONS

Figure 3 shows a ceramic turbocharger rotor. The ceramic turbocharger rotor made of GPSSN was first introduced in 1985, and since then production volume has dramatically increased. There are several key technologies in the production process of the ceramic rotor, that include shaping, sintering, joining and reliability assurance.

For the shaping, we have developed a new shaping method, in which the blade is formed by injection molding and the core region is formed by cold isostatic pressing. The two preforms are then joined by the cold isostatic pressing into one unit and gas pressure sintered.

One of the advantages of this shaping method is that dewaxing process becomes much easier and faster than the single injection molding method. Therefore, this method is particularly effective for larger rotors, for example, gas turbine rotors.

Joining was another important technology for the development of the rotor. Ceramic wheel is joined with the metal shaft by the active brazing method. And multi-buffer layer was developed to reduce the residual stress due to the difference in thermal expansion coefficients between the ceramic and metal.

The major advantage of the ceramic rotor is the improvement in acceleration response due to the reduction of moment of inertia. This was confirmed by applying stepped input torque and measuring the charge in rotational speed for ceramic and metal rotors. Comparison of the time required to reach one hundred thouand rpm shows that the improvement in acceleration response, which is about 36%, corresponds closely to the amount of reduction in the moment of inertia.

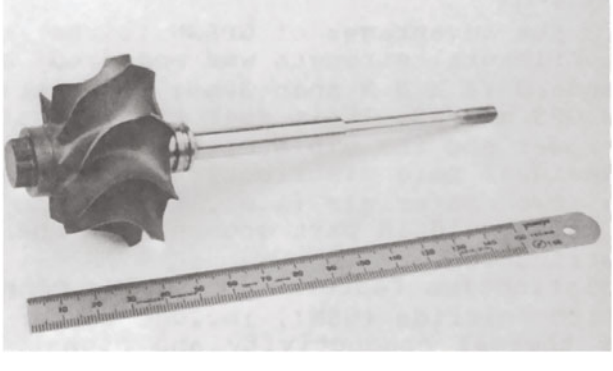

Figure 3. Ceramic turbocharger rotor

Due to the excellent mechanical properties and high reliability of the GPS material, application to other heat engine components have been attempted. Valves, piston pins and tappets have been tested successfully.

INDUSTRIAL APPLICATIONS

Silicon nitride ceramics are applied to bearings used under high temperature or corrosive atmosphere where metal bearings cannot be used and for ultra-high speed bearings where performance is greatly affected by the inertia of the rolling elements. Generally, all-ceramic bearings are used for the former application, and the hybrid bearing consisting of metal races and ceramic rolling elements are used for the latter applications.

Materials for the bearings need to have very high reliability. Defects such as pores, inclusion, and other inhomogeneities could become sources of failures due to the rolling contact fatigue. Therefore, starting powders, powder processing conditions and densification conditions have to be carefully optimized to eliminate these defects. Commercially available materials for the bearings are densified by either hot-pressing, HIP or gas pressure sintering.

Silicon nitride is more heat resistant than tool-steel and tungsten carbide, and shows superior toughness and thermal shock resistance to alumina. These features made silicon nitride ceramics be widely applied as cutting tool materials. They have become popular because they allow vastly higher metal removal rates and subsequent productivity increase. The gas pressure sintered material has high fracture toughness due to the presence of elongated silicon nitride grains, and because of this high toughness, it has a higher resistance to breakage compared with conventional hot-pressed silicon nitride and alumina-TiC materials.

CONCLUSIONS

In summary, the gas pressure sintering has been proven to be an effective sintering method for the production of high performance silicon nitride materials. Because of the improved properties, the gas pressure sintered materials has been used for automotive and industrial applications.

REFERENCES

1. Hattori,Y., Tajima,Y., Yabuta,K., Matsuo,Y., Kawamura,M. and Watanabe,T., Gas Pressure Sintered Silicon Nitride Ceramics for Turbocharger Application. In Ceramics Materials and Components for Engines. ed. W. Bunk and H. Hausner, Deutche Keramiche Gesellshaft, 1986, pp. 165-72.
2. Mitomo. M., Pressure Sintering of Si_3N_4, J. Mater. Sci.,1976, 11, pp.1103

3. Greskovich, C. D., Preparation of High-Density Si_3N_4 by a Gas-Pressure Sintering Process, J. Am.Ceram.Soc.,1981,64,pp.725
4. Yabuta,K., Kito, T., Hattori, Y., Kato,N., Development of Gas Pressure Sintered Silicon Nitride and Its Automotive and Industrial Application. SAE Technical Paper Series, 1989, 890423.

MECHANICAL PROPERTIES OF POST-SINTERED SILICON NITRIDE FABRICATED BY HIPING

YOSHIRO NODA, TORU SHIMAMORI AND MASAKAZU WATANABE
Materials Research Department, Research & Development Center,
NTK Technical Ceramics, NGK Spark Plug Co.,Ltd.
2808 Iwasaki, Komaki, Aichi 485, Japan

ABSTRACT

Mechanical properties of post-sintered Si_3N_4 doped with Sc_2O_3 and Sc_2O_3+Y_2O_3 as sintering additives were investigated. Post-sintering was carried out by sinter-hiping with the hiping condition being at 1800°C for 2 hours under nitrogen pressure of 200MPa. For the post-sintered Si_3N_4 doped with Sc_2O_3, flexural strength at room temperature and 1400°C was nearly constant when presintering temperature was from 1770°C to 1830°C. On the other hand, for the post-sintered Si_3N_4 doped with (Sc_2O_3 + Y_2O_3), flexural strength had a tendency to decrease as presintering temperature was higher. When presintering temperature was 1700°C, flexural strength at room temperature and 1400°C was 800 MPa and 615 MPa, respectively. From the quantitative microstructure analysis, it is considered that flexural strength and microstructure for the post-sintered Si_3N_4 doped with (Sc_2O_3 + Y_2O_3) was closely related.

INTRODUCTION

Si_3N_4 ceramics have been developed in recent years for structural applications at high temperatures.[1] These materials show good high temperature strength, good oxidation resistance, creep behavior compared with those of metals, and good thermal shock resistance compared with other ceramic materials.

Si_3N_4 ceramics can be fabricated by sintering, hot-pressing and hot isostatic pressing. Those fabrication methods are mainly carried out for Si_3N_4 powder compacts with sintering additives. On the other hand, post sintering(PS), which starts with silicon powder, has been developed as one of the advanced sintering tech-

niques for fabrication of Si_3N_4 ceramics.[2] PS has several advantages over the conventional sintering techniques, among which near net shape capability due to low shrinkage is most well-known. Post-sintering methods which densify reaction-bonded Si_3N_4 (RBSN) are in present carried out by means of hot pressing, hot isostatic pressing and so on.[3),4)]

Generally,microstructure of dense-Si_3N_4 is known to influence mechanical properties, and thus analyses of microstructures of dense-Si_3N_4 are performed to understand densification behavior and mechanical properties.[5)-7)]

In this paper, mechanical properties and microstructure of post-sintered Si_3N_4 fabricated by means of sinter-hiping was evaluated and the influence of microstructure on mechanical properties is discussed.

Experimental procedure

Si powder and additives were milled in acetone for 40 hours by using Si_3N_4 balls and pots. The compacts formed from these mixtures were nitrided at temperature below 1450°C in mixture of nitrogen and hydrogen. The compositions of post-sintered Si_3N_4 used in this investigation were 2.4wt%Sc_2O_3 and 4.8wt%Sc_2O_3 + 2.4wt%Y_2O_3 for 100wt%Si_3N_4. Post sintering was carried out by sinter-hiping. Sintering before hiping (i.e. presintering) was at 1700°C - 1830°C for 4 hours, and hiping was at 1800°C for 4hours under the nitrogen pressure of 200MPa.

Density of the samples was determined according to the Archimedean principle at room temperature in water. The strength of the diamond wheel-ground samples after hipping was measured by four-point bending tests at room temperature and 1400°C according to JIS-R1601 and JIS-R1604. Phases of hipped samples were determined by a X-ray diffraction method and quantitative microstructural analyses were performed on etched samples after hiping to determine the diameter(d), length(L) and aspect ratio(L/d) of grains by an image analyzer.

RESULTS AND DISCUSSION

DENSITY AND FLEXURAL STRENGTH OF POST-SINTERED Si_3N_4

Density of the post-sintered Si_3N_4 doped with Sc_2O_3 and (Sc_2O_3+Y_2O_3) before hiping increased with increasing sintering temperature and the density of them after hiping reached full density. The relation between flexural strength and presintering temperature is shown in Fig.1 and Fig.2. The flexural strength of post-sintered Si_3N_4 doped with Sc_2O_3 was nearly constant at presintering temperature between 1770°C and 1830°C and showed 680 - 700 MPa at room temperature and 440 - 450 MPa at 1400°C. On the other hand, the flexural strength at room temperature and 1400°C of the material doped with (Sc_2O_3 + Y_2O_3) decreased with increas-

ing presintering temperature. When presintering temperature was 1700°C, the strength was 800 MPa at room temperature and 615 MPa at 1400°C.

Microstructure of post-sintered Si_3N_4 was observed by scanning electron microscope. For the post-sintered Si_3N_4 doped with Sc_2O_3, no clear correlation between microstructure and presinterintg temperature was observed. On the other hand, microstructure of the post-sintered Si_3N_4 doped with (Sc_2O_3 + Y_2O_3) showed a tendency of grain growth with increasing presintering temperature.

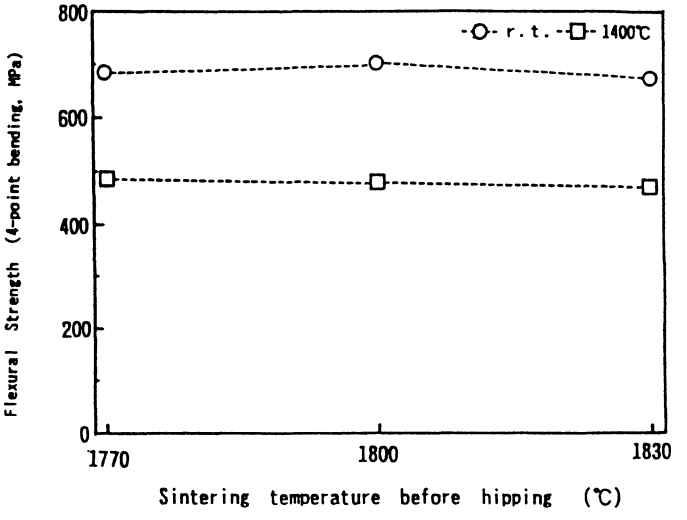

Fig.1 Relation between density and sintering temperature before hiping of post-sintered Si_3N_4 doped with Sc_2O_3.

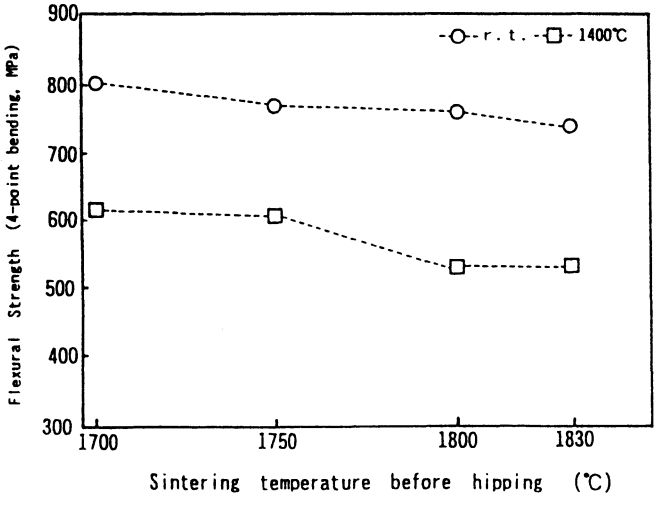

Fig.2 Relation between density and sintering temperature before hiping of post-sintered Si_3N_4 doped with (Sc_2O_3 + Y_2O_3).

Phases of the Sc_2O_3 doped Si_3N_4 presintered at 1770°C - 1830°C were nearly the same. Also, phases of the (Sc_2O + Y_2O_3) doped Si_3N_4 presintered at 1700°C - 1830°C were nearly equal. Accordingly, influence of microstructure on flexural strength was considered. Next, microstructure analysis of post-sintered Si_3N_4 was performed.

Microstructure analysis of post-sintered Si_3N_4

Microstructures of the post-sintered Si_3N_4 were analyzed by using the image analyzer. Presintering temperature of the samles analyzed was 1770°C and 1830°C for the post-sintered Si_3N_4 doped with Sc_2O_3, and 1700°C and 1830°C for the Si_3N_4 doped with (Sc_2O_3 + Y_2O_3). For the Sc_2O_3 doped Si_3N_4, the difference of grain size was not clear. The results of microstructure analysis on length of grains for the post-sintered Si_3N_4 doped with (Sc_2O_3 + Y_2O_3) are shown in Fig. 3. The length of grains became longer as presintering temperature was higher. Also, the distribution became broader for the sample with higher presintering temperature, and a proportion of length longer than 2 μm increased as the presintering temperature was higher. As mentioned before, almost no difference in phases was observed for these samples. Therefore, it was considered that the microstructure has a considerable influence on the flexural strength at room temperature and 1400°C for the material with (Sc_2O_3 + Y_2O_3). The diameter of grains was also observed to grow as the presintering temperature was higher.

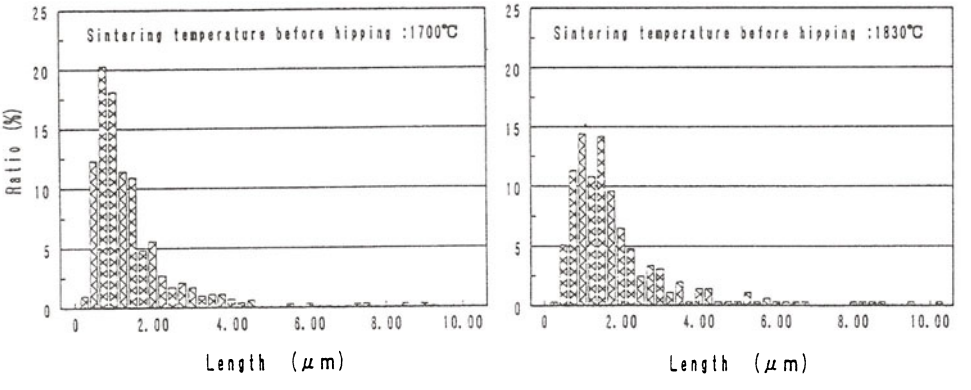

Fig.3 Grain size distribution of post-sintered Si_3N_4 doped with (Sc_2O_3 + Y_2O_3). (Length of grain)

Next, the relation between flexural strength and average length of grains is shown in Fig.4. The data of the length for

the post-sintered Si_3N_4 doped with (Sc_2O_3 + Y_2O_3) at presintering temperature of 1750°C and 1800°C were added in this figure.

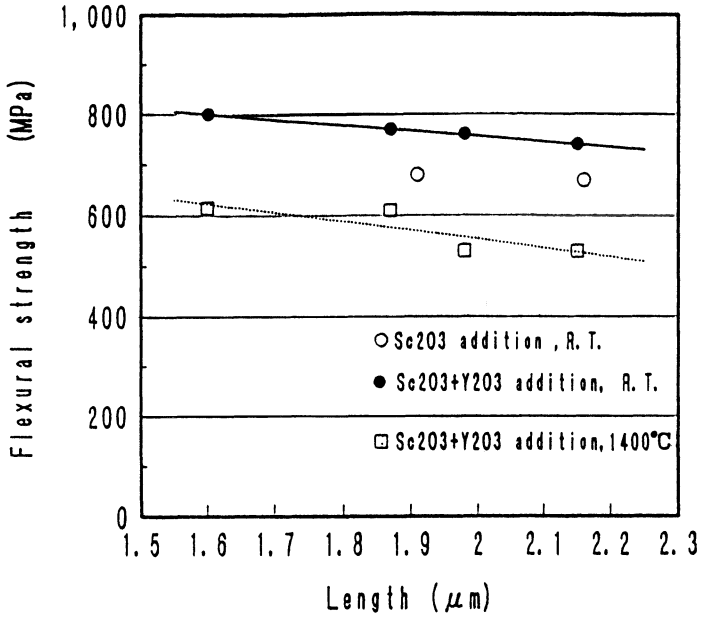

Fig.4 Relation between flexural strength and the diameter of grain for post-sintered Si_3N_4

For the post-sintered Si_3N_4 doped with (Sc_2O_3 + Y_2O_3), flexural strength had a tendency to increase with decreasing length of grain. On the other hand, for the post-sintered Si_3N_4 doped with Sc_2O_3, the relation between flexural strength at room temperature and microstructure was not clear.

It was considered that intrinsic flaw size was smaller as grain size decreased, and therefore flexural strength at room temperature and 1400°C increased if heat resistance of grain boundary was high enough. Microstructure of Si_3N_4 ceramics is well-known to influence mechanical properties, especially strength at room temperature and fracture toughness. In this investigation, microstructure seemed to influence not only strength at room temperature but also strength at high temperature of 1400°C. From the analyses using the image analyzer, strength of both room temperature and 1400°C was considered to be influenced by grain size of post-sintered Si_3N_4 fabricated by the sinter-hipping and had a tendency to increase with decreasing grain size.

SUMMARY

Mechanical properties and microstructure of post-sintered Si_3N_4

doped with Sc_2O_3 and (Sc_2O_3 + Y_2O_3) as sintering additives were investigated. Post-sintering was carried out by sinter-hiping.

Experimental results are summarized as follows.

1. Flexural strength at room temperature and 1400°C had a tendency to increase with decreasing grain size for the post-sintered Si_3N_4 doped with (Sc_2O_3 + Y_2O_3).
2. Flexural strength of post-sintered Si_3N_4 doped with (Sc_2O_3 + Y_2O_3) was higher than post-sintered Si_3N_4 doped with Sc_2O_3.

ACKNOWLEDGEMENT

This work was performed under the management of Engineering Research Association for High Performance Ceramics as a part of the national R&D project " Research and Development of Basic Technology for Future Industries " supported by NEDO (New Energy and Industrial Technology Development Organization).

REFERENCES

1. Hattori,Y., Tajima,Y., Yabuta,K., Mastuo,Y., Kawamura,M. and Watanabe,T., Gas Pressure Sintered Silicon Nitride Ceramics for Turbocharger Application.In Ceramics Materials and Components for Engines. ed. W.Bunk and H.Hausner, Deutshe Keramische Gesellschaft,1986,pp.165-72.
2. Shimamori T.,Kato T. and Mastuo Y., Development of oxidation resistant Si_3N_4 material. In Proceedings of the 1st symposium of the national R&D project,1983,pp.47-65.
3. Heinrich, J.,Backer E. and Bohmer M., Hot Isostatic Pressing of Si_3N_4 powder Compacts and Reaction-Bonded Si_3N_4.J.Am.Ceram. Soc., 1988, C-28 - C-31.
4. Ziegler, G. and Wotting, G., Post-treatment of Pre-sintered Silicon Nitride by Hot Isostatic Pressing. Int. J. High Technology Ceramics, 1985, 1, 31-58.
5. Mitomo, M. Tsutsumi, M.,Tanaka, H.,Uenosono,S. and Saito, F., Grain Growth During Gas-Pressure Sintering of B-Silicon Nitride. J. Am. Ceram. Soc., 1990, 73, [8], pp.2441-45.
6. Selkregg K. R., Microstructural Characterization of Silicon Nitride Ceramics Processed by Pressureless Sintering, Overpressure Sintering, and Sinter HIP. Ceram. Eng. Sci. Proc. 1990,11,[7-8] pp.603-615.
7. Mastuhiro, K. and Takahashi, T., The Effect of Grain Size on the Toughness of Sintered Si_3N_4. Ceram. Eng. Sci. Pro. 1989,10,[7-8],pp.807-816.

EFFECTS OF HIP CONDITIONS UPON THE CHANGES OF MECHANICAL PROPERTIES WITH SINTERED SILICON NITRIDE

Yushi Horiuchi, Kyoichi Ichinoseki, Yoshio Nakamura

R & D Center, Toshiba Ceramics Co.,LTD,
Soya 30, Hadano, Kanagawa 257,Japan

ABSTRACT

Three types of pre-densified silicon nitride were HIPed in various conditions. HIP effects upon bulk density and flexural strength were different between these materials. SEM observation suggested this is due to the difference of morphology. HIPing temperature was one of the most critical factors for mechanical properties. By HIPing at 1700℃ (in 98MPa N_2, for 2hours), flexural strength was improved from 840MPa to 1100MPa. With optimum temperatures, only moderate nitrogen gas pressure was needed to improve mechanical properties. Also the nitrogen gas pressure did not influence high temperature strength or microstructures.

INTRODUCTION

Post-HIP is thought to be an effective method to improve mechanical properties of pre-densified materials. Many experimental results on fabrication of silicon nitride have been reported [1)2)3)4)5)]. Whether post-HIP is effective or not depends upon the HIP conditions and characteristics of the pre-densified materials.
In this study, three types of silicon nitride pre-sintered with Y_2O_3-Al_2O_3 additives (different starting powder or sintering method) were HIPed without canning in various conditions. And the changes of mechanical properties and microstructures were investigated in detail. Finally the mechanism of the changes of mechanical properties by post-HIPing was estimated.

EXPERIMENTAL

Characteristics of pre-sintered Si_3N_4 are shown in table 1.
Post-HIP conditions investigated are as followings;

- ·Pressurizing gas : N_2 and Ar
- ·HIPing temperatures : 1400～2000℃
- ·HIPing gas pressures : 15～196MPa(153～2000kgf/cm^2)
- ·Keeping times : 1～6h

The characteristics of pre-densified and post-HIPed materials were obtained by the following methods.

- ·Bulk density measured by Archimedes method
- ·3-point flexural strength at room temperature and high temperatures (1000℃;1200℃),[sample size=3mm×4mm×40mm,span=30mm]
- ·Fracture toughness measured by IF method
- ·SEM observation of fracture surface or polished and etched sections

Table 1 Characteristics of pre-densified Si_3N_4

No.	Starting Powder[1)]	Sintering Method	Sintering Temperature	Bulk Density (g/cm^3)	Flexural Strength (MPa)	Fracture Toughness (MPa$\sqrt{m}$)
A	R	PLS	1750℃	3.203	840	6.5
B	D	PLS	1770℃	3.190	580	6.0
C	R	HP(49MPa)	1750℃	3.211	900	7.0

[1)] R:Produced by Reduction of SiO_2
D:Produced by Direct Nitridation of Si

RESULTS and DISCUSSION

Types of pre-densified materials

Each pre-densified material (A, B, C) was HIPed at 1700℃ in 98MPa gas pressure for 2 hours. Introduced gas species were Nitrogen or Argon. The changes of bulk density and flexural strength of each sample are shown in Figure 1.

As for A and B, bulk density was improved by HIPing both in N_2 and Ar atmosphere. However, that of sample C, which was hot-pressed, remains almost at the same level as pre-densified.

Improvement of flexural strength was found in each atmosphere. The value was higher in N_2 than in Ar. The maximum value was about 1100MPa (which is about 30% increase of that of pre-densified). On the other hand, flexural strength of B was not improved either in N_2 or in Ar. That of sample C was slightly improved only in N_2 atmosphere.

Generally, these experimental results indicate that nitrogen is more effective than argon and the effects of HIPing are strongly influenced by the types of pre-densified materials. The reason will be discussed later.

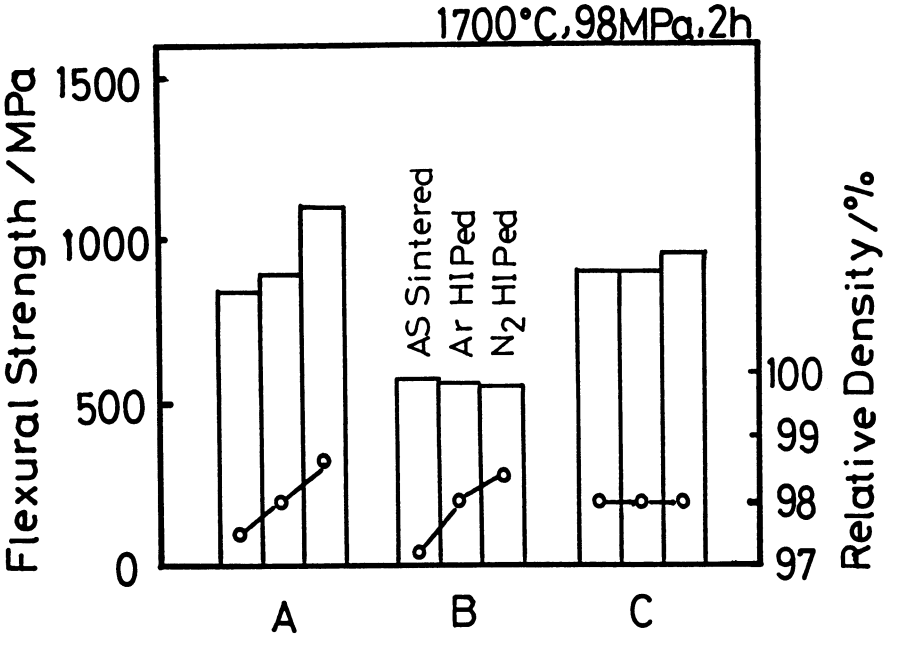

Figure 1. Effects of gas species on bulk density and flexural strength with three types of pre-sintered Si_3N_4

HIPing Conditions

For sample A, the effects of HIPing conditions (keeping time, temperatures and gas pressures) on densification and flexural strength were investigated in detail.

Keeping time: The other conditions were fixed to 1700℃, 98MPa N_2 gas pressure. Bulk density reaches to 3.235 g/cm^3 (98.4% of T.D.) after 1 hour, and this value remains almost at the same level even after 6 hours. However, it takes at least 2 hours to get an optimal value of flexural strength (1100MPa).

Temperature: The effects of HIPing temperatures (in 98MPa N_2 for 2 hours) on bulk density and flexural strength are shown in Figure 2. At 1500℃, bulk density reaches a maximum value of 3.239 g/cm^3 (98.6% of T.D.), which is not changed with increasing temperature. On the other hand, flexural strength is improved with increasing temperature and shows a maximum value of 1100MPa at 1700℃. At higher temperatures it decreases to almost the same value (850MPa) of the pre-sintered. Fracture toughness was not improved by HIPing at each HIPing temperature.

Gas pressure: With nitrogen as pressure medium when HIPing Si_3N_4, it is possible for the nitrogen gas to dissolve into the materials and change the characteristics of secondary phase[2]. Therefore the gas pressure may be a controlling factor for the high temperature strength of HIPed Si_3N_4. The effects of gas pressure upon the flexural strength at room temperature and high temperatures are shown in Figure 3. Optimal

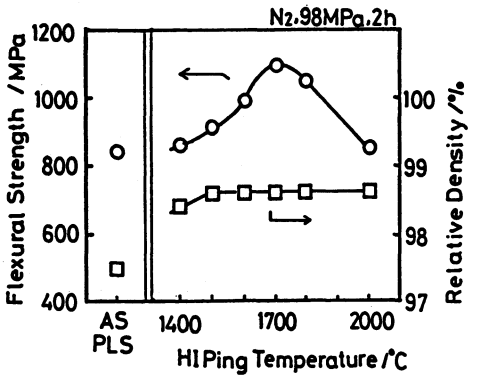

Figure 2. Effects of HIPing Temperature on Bulk Density and Flexural Strength of material A

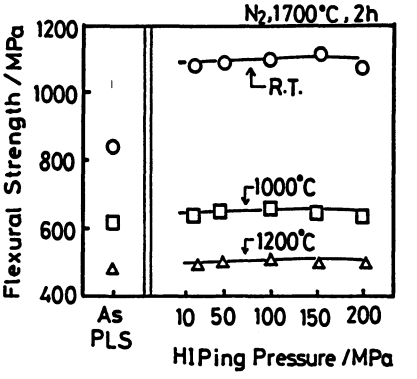

Figure 3. Effects of HIPing Pressure on flexural strength at room temperature and high temperatures of material A

strength at room temperature is achieved, 1100MPa, even at the lowest pressure of 15MPa (the minimum limit at this temperature). Only small deviations are observed at all tested pressures up to 196MPa (the maximum limit of this HIP instrument). The high temperature strength was also independent on gas pressures as shown in Figure 3.

Microstructures

At HIPing condition of Figure 1, any significant changes of particle size and shape of Si_3N_4 particles were not observed after HIPing in all tested materials. An example of material A is shown in Figure 4. However, SEM observation of fracture origin of material B reveals that, even in HIPed materials, there still remain macropores (about $\phi 20\mu m$, Figure 5-a), inside which elongated large grains were observed (Figure 5-b). These residual macropores seemed to inhibit the increase of strength, although bulk density was improved. For HIPed materials of A and C, fracture origin was not clearly identified.

Figure 6-a and 6-b show the fracture surface of material A HIPed at 1700℃ and 2000℃, respectively. Exagerated grain growth was observed when HIPed at 2000℃. This grain growth seems to cause an extreme reduction of flexural strength. On the other hand, any remarkable differences in microstructure were not observed in the materials HIPed at different gas pressures. The gas pressure does not seem to have an influence either on the Si_3N_4 matrix or on secondary phase. However, certain materials in this study changed color (from grey to black) by HIPing. At some HIPing condition, also color distribution was observed in HIPed body (inside:green, outside:black). Some chemical reaction between nitrogen and material must occur, as some authors reported before[2)6)7)].

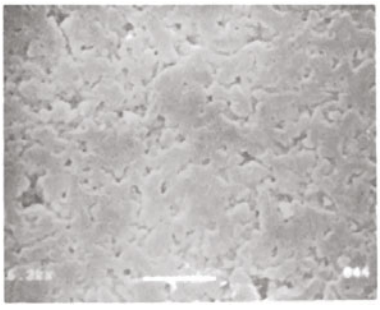

a) before HIPing $\overline{2\mu m}$

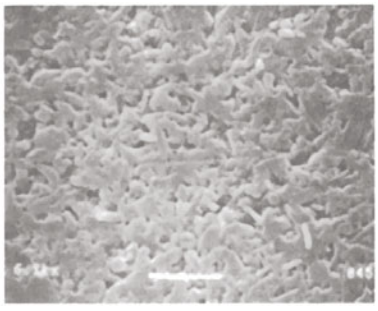

b) after HIPing $\overline{2\mu m}$

Figure 4. SEM of Polished and etched sections of material A (HIPing condition:1700℃,in 98MPa N_2, for 2h)

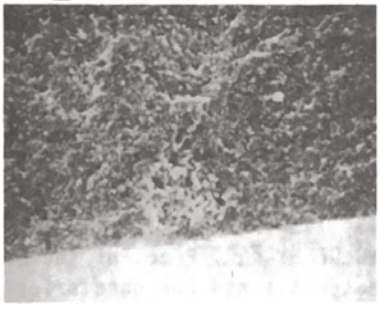

a) fracture origin $\overline{20\mu m}$

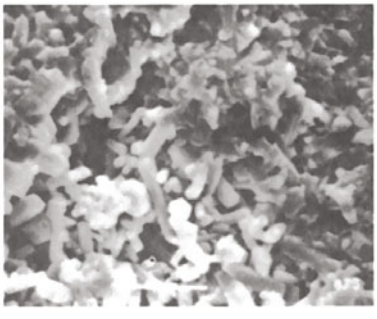

b) inside the origin $\overline{5\mu m}$

Figure 5. SEM of fracture origin observed in material B after HIPing, a) fracture origin b) inside the origin (HIPing condition:1700℃,in 98MPa N_2, for 2h)

a)1700℃HIP $\overline{2\mu m}$

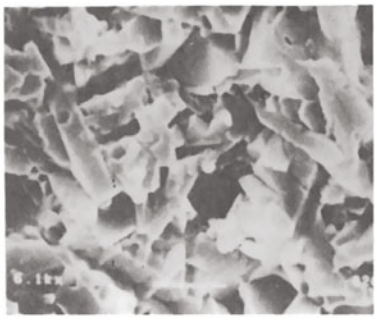

b)2000℃HIP $\overline{2\mu m}$

Figure 6. SEM of fracture surface of material A after HIPing (HIPing condition:1700℃ and 2000℃, in 98MPa N_2, for 2h)

CONCLUSION

From the experimental results, the mechanism of improvement (or degradation) of flexural strength was estimated as follows,

1. The elimination or reduction of macropores by the high pressure used increases both bulk density and flexural strength.
2. Softening and sliding of grain boundary leads to the rearrangement of particles or the healing of residual minute cracks, causing improved flexural strength, although bulk density is almost unchanged.
3. Coalescence and Coarsening of Si_3N_4 particles results in remarkable reduction of flexural strength at high HIPing temperatures.

REFFERENCES

1. Katuhiko Honma, Tuneo Tatuno, Hiroshi Okada, Nobuyasu Kawai and Masao Nishihara, "HIP treatment of Sintered Silicon Nitride" (in Japanese with English summary), Zairyo - Journal of the Society of Materials Sciense Japan, 30, 1005-1011 (1981)
2. Kazushi Hirota, Tetsuo Ichikizaki, Yasutoshi T. Hasegawa and Hiroshige Suzuki, "DENSIFICATION OF Si_3N_4 BY HOT ISOSTATIC PRESS IN N2 ATMOSPHERE", Proc. of International Symposium on Ceramic Components for Engine, 1983 Japan, 434-441
3. G.Wotting and G.Ziegler, "POST-HIPING OF Si_3N_4", Proc. of the Second International Symposium on Ceramic Materials and Components for Engine, 1986 FRG, 235-242
4. G.Ziegler and G.Wotting, "Post-treatment of Pre-sintered Silicon Nitride by Hot Isostatic Pressing", Int.J.High Technology Ceramics 1, 31-58 (1985)
5. Takao Fujikawa, Yasuhiko Inoue, Tsuneo Tatsuo and Hiroshi Okada, "Hot Isostatic Pressing of Ceramics", (in Japanese with English Summary), KOBE STEEL ENGINEERING REPORTS, 37, 65-68 (1987)
6. Yasuhiro Goto, Hiroyasu Ohta, Katsutoshi Komeya and Takao Fujikawa, "Silicon Nitride Grain-Boundary Alteration by Capsule-Free Hot Isostatic Pressing(HIP)", J.Electron Microsc., 35, 365-370 (1986)
7. Yasuhiro Goto, Katsutoshi Komeya and Takao Fujikawa, Sintering of Advanced Materials - Applications of Hot Isostatic Pressing - (in Japanese), UCHIDA ROKAKUHO PUBLISHING CO.,LTD., Tokyo, 1987, 89-108

HOT ISOSTATIC PRESSING OF SINTERED SILICON NITRIDE

SANG S. KIM and SUNGGI BAIK*
Pohang Institute of Science and Technology
Department of Materials Science and Engineering
Pohang, 790-600 Korea

ABSTRACT

Silicon nitride ceramics were fabricated by pressureless sintering and then hot isostatic pressed under 150 MPa of nitrogen at 1800°C. Density changes by hot isostatic pressing (HIPing) varied significantly depending on sintered densities before HIPing and on the compositions of sintering additives and their amounts. Moderate increases in densities were observed when sintered densities exceeded 90% of the theoretical. However, fully dense components could not be obtained; even occasional density reduction was observed when the amount of additives exceeded 12 wt %. Further reduction in the final density were observed as HIPed silicon nitride was reannealed at 1650°C under 0.1 MPa of nitrogen. It is thus concluded that sinter-HIPing of silicon nitride is severely limited by the increase in solubility of nitrogen in glassy phases under high pressure. HIPing under similar conditions using mixed gas of nitrogen and argon produced fully dense components.

INTRODUCTION

Sinter-HIPing has been applied to the production of silicon nitride components frequently[1-5]. In theory, sinter-HIPing should be able to remove all the isolated pores except those located very close to the surface of the components and open to ambient pressure. In practice, however, the application to silicon nitride to obtain fully dense components is not straight forward.

Homma et al.[1] and Hirota et al.[3] achieved near theoretical densities by applying HIPing to sintered silicon nitride. On the other hand, Fujikawa et al. [2] and Ziegler et al. [4] found that the increase in final densities was only marginal and failed to obtain full densities under similar experimental conditions. Such inconsistency was also observed in the results on mechanical properties such as fracture toughness and flexural strength after HIPing treatment. Only exception was the significant improvement of Weibull modulus after HIPing regardless of post-HIPing densities or microstructural characteristics. Ziegler and Wotting [4] suggested

that a "bridging effect" originated from the interlocking network formation of large β-grains during pre-HIP sintering was responsible for the failure in complete removal of residual pores by subsequent HIPing.

Recently, we found that the "bloating" of intergranular glass phase saturated with nitrogen during HIPing was real and severe under certain experimental conditions[6]. The success of sinter-HIPing of silicon nitride critically depends on the control of the bloating effect. In this paper, we summarize various factors influencing the bloating of glass phases during HIPing, and several methods to overcome it.

EXPERIMENTAL PROCEDURE

The silicon nitride powder (LC12, H.C. Starck, Inc.) used in the experiment consists of 97% of α phase with an average particle size of 0.7 μm. Amounts of the additives were 1.5 - 9.0 wt% of MgO or 1.5 - 18.0 wt% of Al_2O_3-Y_2O_3(1:2 wt ratio). Mixed slurry was prepared with ethyl alcohol doped with additives in the form of nitrate solutions. Details of the procedure of specimen preparation and sintering prior to HIPing were described elsewhere [6]. The sintered specimens were placed in a BN-coated graphite crucible, and isostatically pressed in a HIPing unit (Kobelco, Inc.) at 1800°C for 1h under 150 MPa of pure nitrogen or of argon with 7 v/o of nitrogen. The heating and cooling rates were 10°C/min and 50°C/min, respectively. Densities, weight fractions of β phase, and cross-sectional microstructures were analyzed before and after HIPing. A few HIPed samples were selected randomly and reannealed at 1650°C for 3h in 1atm of nitrogen in order to investigate if any density change occurred. Theoretical density (TD) was computed by a rule of mixture from the starting composition.

RESULTS AND DISCUSSION

Fig. 1 shows the variation in relative densities after sintering at 1700°C for 1h and thier changes after HIPing with pure nitrogen as a fuction of wt % of Al_2O_3-Y_2O_3. The minimum 9

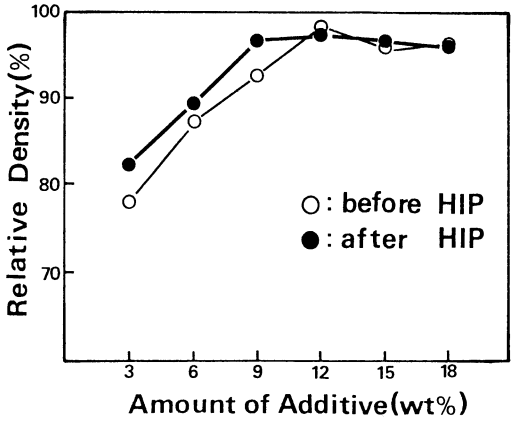

Fig. 1. Relative densities of Si_3N_4 before and after HIPing at 1800℃ for 1h under 150MPa of pure N_2 gas as a function of wt % of Al_2O_3-Y_2O_3.

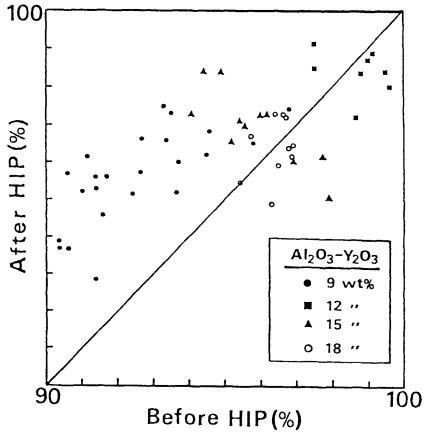

Fig. 2. Relative densities after HIPing as a function of those before HIPing in Si_3N_4 containing various amounts of Al_2O_3-Y_2O_3.

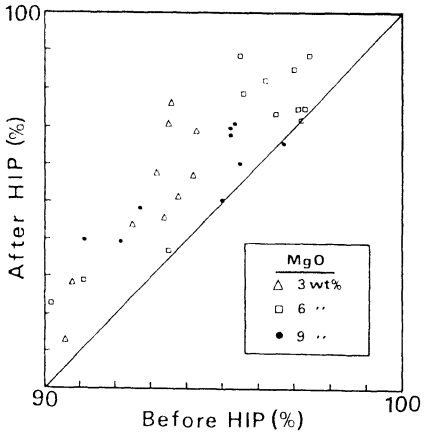

Fig. 3. Relative densities after HIPing as a function of those before HIPing in Si_3N_4 containing various amounts of MgO.

wt % of Al_2O_3-Y_2O_3 or 3 wt % of MgO was required in order to achieve > 90% of TD after sintering as long as the sintering temperature and time exceeded 1600°C and 10 min, respectively. However, full density could not be achieved after HIPing in any cases; even slight reduction in the final densities was observed occasionally. Fig. 2 shows the densities after HIPing as a function of the densities before HIPing for the samples containing Al_2O_3-Y_2O_3. Regardless of wide variations in additive contents and pre-HIPing sintering conditions, final densities fell within the range of 95-98% of TD. Weight changes after HIPing were always less than 1 % of the total weight of pre-HIPed samples, which suggested that it was not the cause of the density reduction. In the case of Si_3N_4 containing 3 - 9 wt % of MgO, as shown in Fig. 3, such density reduction was not observed. Although, increase in relative densities was only slight with no evidence of reaching TD.

An extensive formation of tightly interlocked network of β grains could be observed in

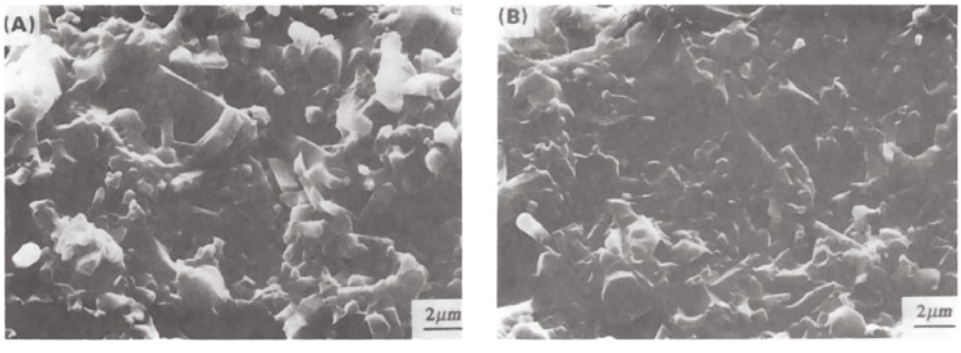

Fig. 4. Extensive formation of interlocking network of β-grains is evident in Si_3N_4 - 3wt% MgO (A) before, and (B) after HIPing.

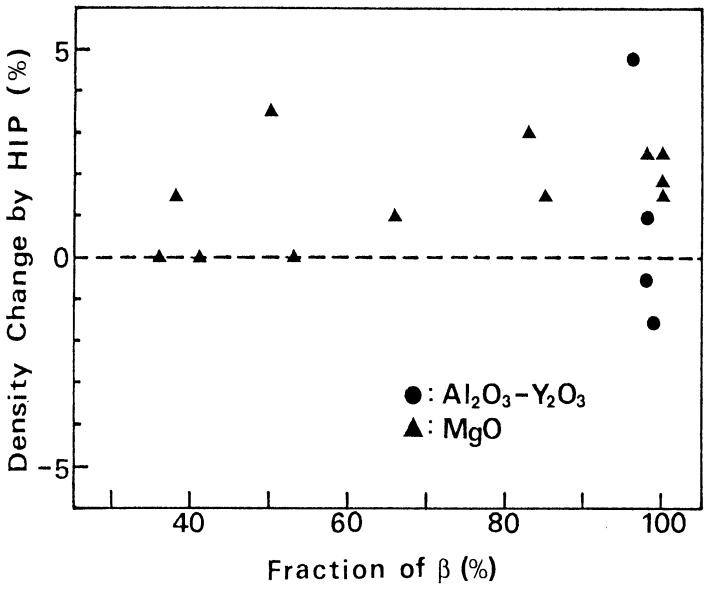

Fig. 5. Density change by HIPing as a function of the fraction of β phase in sintered Si_3N_4 prior to HIPing.

the sintered Si_3N_4 as shown in Fig. 4, which compares the microstructures before and after HIPing for the system containing 3 wt% of MgO. It suggested that the "bridging effect" might indeed prohibit elimination of pores trapped within the tight network unless they could be deformed under high external pressure. However, when plotting the density change as a fuction of the fraction of β phase in sintered samples, no significant correlation could be established, as shown in Fig. 5. It was also demonstrated recently that large residual pores could be removed by glass infiltration under external pressure of less than 0.5 MPa as long as intergranular glass formed continous channels [7]. In this situation, larger amount of glass-forming additives is beneficial for achieving fully dense components. Nevertheless, as the density changes by HIPing were plotted against the amounts of oxides added (Fig. 6), the occasional reduction in densities was observed in the systems containing above 12 wt% of additives. It was thus concluded that the bridging effect was not primarily responsible for the failure in achieving full densities by HIPing with pure nitrogen gas.

We found that spontaneous bloating of intergranular glass during a de-pressurizing cycle of HIPing operation was more likely responsible for the density reduction and severely limiting the complete removal of residual porosities. The results in Fig. 7 were obtained as a few samples were randomly selected and annealed again at 1650°C for 3h in an atmospheric pressure of pure N_2. Significant reduction in densities were observed for the HIPed samples; some were even ruptured. Whereas, the sintered samples remained unchanged or showed a slight increase in the final density. Internal porosity after the annealing was found indeed increased in the cross-sectional micrographs. This clearly demonstrates that the HIPed samples still were supersaturated with nitrogen, and density reduction occurs as the supersaturated nitrogen precipitates in the residual pores during annealing. It is thus highly possible that full density has been achieved during the pressurizing stage in HIPing operations. However,

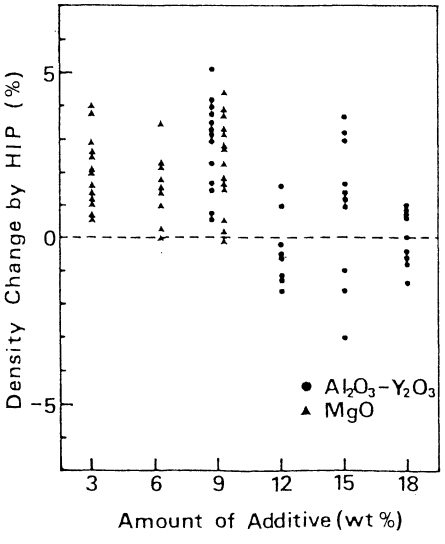

Fig. 6. Density change by HIPing sintered Si_3N_4 as a function of the amount of glass-forming oxide additives, MgO and Al_2O_3-Y_2O_3.

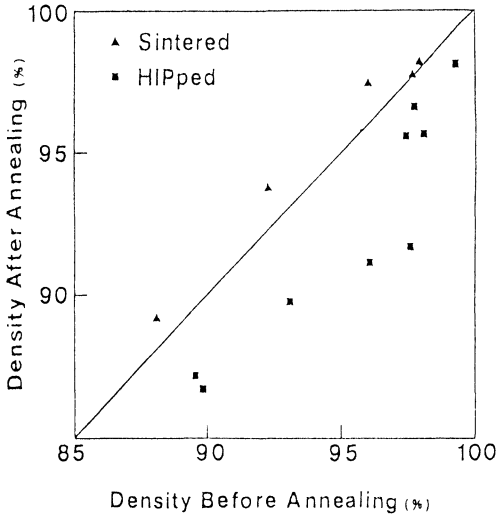

Fig. 7. Relative densities after annealing as a function of those before annealing

excessive nitrogen is dissolved in the glassy phase at the same time. If the cooling and de-pressurizing is faster than the rate of diffusion of nitrogen out of the specimen through glass channels, it precipitates internally resulting in the density reduction. In this situation, desintering is more likely with larger amounts of glassy phase, which is consistent with our experimental observation.

One may take several approaches to circumvent the adverse effect due to spontaneous bloating of glass by dissolved gas. The cooling an de-pressurizing schedule can be designed, for instance, by introducing an intermittent

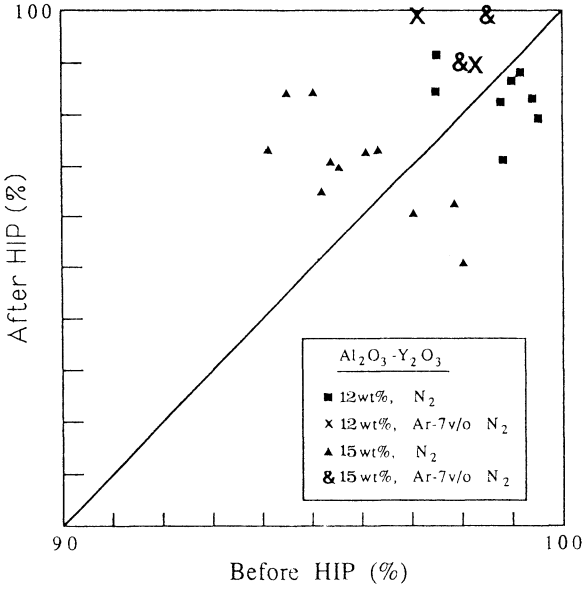

Fig. 8. Relative densities after HIPing with a mixed gas of Ar and N_2 as a function of those before HIPing.

internal gas pressure through diffusion. However, a simpler but more efficient way is to use argon gas. HIPing using pure Ar would induce weight losses[1]. It is desirable to add a small amount of N_2 just enough to avoid the weight losses. We selected the compositions and sintering conditions which had been particularly prone to the bloating effect, and sinter-HIPed using a mixed gas in order to test our hypothesis. Fig. 8 compares final densities after HIPing with pure nitrogen and those with Ar -7 v/o N_2. Pore-free components were obtained using the mixed gas during HIPing.

CONCLUSIONS

Hot isostatic pressing of sintered Si_3N_4 using pure nitrogen failed to produce fully dense components. It was discovered that the failure was most likely due to "bloating" of intergranular glass. It occurs when excessive nitrogen dissolved during pressurizing period precipitates out internally during cooling and depressurizing period of a HIPing process. The bloating effects could be circumvented by using a mixed gas of Ar and N_2.

ACKNOWLEDGMENT

The authors thank to POSCO for financial assistance through Research Institute of Industrial Science and Technology (RIST).

REFERENCES

1. Homma, K., Tatuno, T., Okada, H. and Fujikawa, T., HIP Treatment on Non-oxide Ceramics. Proceedings of 25th Japan Congress on Materials Research. Society of Materials Science, Kyoto, Japan, 1982, pp. 213-17.

2. Fujikawa, T., Moritoki, M., Kanda, T., Homma, K. and Okata, H., Hot Isostatic Pressing: Its Application in High-Performance Ceramics. Proceedings of International Sym. on Ceramic Components for Engines. Edited by Somiya, S., Kanai, E. and Ando, K., KTK Scientific, Tokyo, Japan, 1983, pp. 425-33.

3. Hirota, K., Ichikizaki, T., Hasegawa, Y.T. and Suzuki, H., Densification of Si_3N_4 by Hot Isostatic Press in N_2 Atmosphere. *ibid.*, pp. 434-41.

4. Ziegler, G. and Wotting, G., Post-treatment of Pre-sintered Silicon Nitride by Hot Isostatic Pressing. Int. J. High Technol. Ceramics. 1985, 1[1], 31-58.

5. Goto, Y., Ohta, M., Komeya, K. and Fujikawa, T., Silicon Nitride Grain Boundary Alteration by Capsule-Free Hot Isostatic Pressing. J. Electron Microsc., 1986, 35[4], 365-70.

6. Kim, S.S. and Baik, S., Hot Isostatic Pressing of Sintered Silicon Nitride. to appear in J. Am. Ceram. Soc., 1991, 74[7].

7. Kang, S.L., Greil, P., Mitomo, M. and Moon, J.H., Elimination of Large Pores During Gas-Pressure Sintering of β'-Sialon. J. Am. Ceram. Soc., 1989, 72[7], 1166-69.

HIPed Si_3N_4 FOR HIGH TEMPERATURE STRUCTURAL APPLICATIONS AT 1400°C

Isao TANAKA, Giuseppe PEZZOTTI,
Taira OKAMOTO, Yoshinari MIYAMOTO and Koichi NIIHARA
The Institute of Scientific and Industrial Research (ISIR),
Osaka University, Ibaraki, Osaka 567, JAPAN

ABSTRACT

Excellent time-dependent strength up to 1400°C has been demonstrated in HIPed high-purity Si_3N_4 without additives. Lifetime at 1400°C under static loading of 300 MPa was found to be >240 h with very small creep deformation rate of about 1×10^{-5} h^{-1}, which were far better than presently available non-HIPed Si_3N_4s appeared in literatures. Selected additives have been systematically doped onto this pure system and their effects on the time dependent mechanical properties at around 1400°C were analyzed by a new convenient method proposed by the authors.

INTRODUCTION

The technology for fabricating high-strength and tough silicon nitride ceramics for structural applications at below 1000°C such as wear resistant tools and some automobile-engine components has been considerably improved in the last decade. These materials are usually sintered under < 3 MPa of nitrogen gas pressure or by uniaxial hot-pressing, and contain oxide additives for 5 to 20 vol% as sintering aids. The addition often gives rise to the degradation of delayed failure resistance at high temperatures during operative cycles because common mechanisms operate in opposite stress directions for sintering and delayed fracture processes. At temperatures >1200°C most of these "conventional" silicon nitrides suffer considerable time-dependent strength degradation phenomena and therefore they become practically useless for such structural applications in which long-term strength is required at these temperatures for example in gas-turbine engines.

HIP encapsulation technique enables the full densification of silicon nitride powders without or with small amount of optimum additives, which was already clearly shown in 1977 by Larker et al[1]. Despite their intuitive advantage, however, lack of clear experimental evidences for the real advantages of HIPed materials as well as their high production cost impeded the research and development. In 1987, Adlerborn et al[2] and Homma et al[3] reported the success in densifying high-purity silicon nitride

powder with metallic impurity content of < 100 ppm. The present authors have examined systematically the role of impurities in starting powders and found that delayed failure resistance can be significantly improved in additive-free silicon nitrides only when such high-purity powders are carefully sintered[4-7].
The excellent high temperature properties of HIPed silicon nitrides can be demonstrated most clearly by means of appropriate testing methods. In the present paper, factors determining the high-temperature time-dependent strength are described based on data obtained by newly developed testing procedures.

WHY HIPed Si_3N_4 FOR HIGH TEMPERATURE APPLICATIONS ?

The major advantages for HIPed Si_3N_4 can be summarized as follows:
1) Superior high temperature time-dependent strength can be expected.
2) High-purity and dense Si_3N_4 only with high-purity glassy silica as intergranular phase can be obtained, which is useful as a reference system for basic investigation of the effects of specific impurities, solute atoms and reinforcements.
3) Near-net shaping of complicated parts without need of finish machining is possible. Compared with CVD process, it is easier to manufacture high-purity and large/complex components.

Highest service temperature and stress of the present turbo-charger rotor is about 900°C and 170 MPa[8]. On the other hand, for gas turbine engine material, the inlet gas temperature is expected to be about 1370°C [9] which is about 500°C higher than the former. Figure 1 summarizes the temperature at which lifetime under static loading becomes 100 h and creep rate becomes 1×10^{-5} h^{-1} under bending load of 300 MPa for some typical Si_3N_4 materials based on recent reports appeared in scientific papers[6,7,10-16]. Because of the absence of a standard evaluation method for such time-dependent phenomena at high temperatures, some data are extrapolated by assuming that the activation energy for creep and slow crack growth is 600 kJ/mol and the creep exponent is 1.4.
It is important that the above two conditions are satisfied at around 1400°C only in HIPed Si_3N_4 sintered without additives or small amount of Y_2O_3 at least within this figure, showing that HIPed materials may be exclusively useful for long-term structural applications at around 1400°C. Of course improvement of non-HIPed materials are in active progress: Some of pressureless-sintered Si_3N_4 already showed lifetime of >100 h under 300 MPa at 1371°C [17]. But such materials seem to exhibit low creep deformation resistance[18], which gives rise to the blunting of pre-existing flaw and elongation of apparent lifetime in compensation for large plastic deformation.

HOW TO EVALUATE THE HIGH TEMPERATURE TIME-DEPENDENT STRENGTH ?

Two delayed failure modes appear at stress levels lower than the fast-fracture strength, depending both on loading rate and testing temperature. They are slow crack growth (SCG) failure originating from pre-existing flaws, and damage accumulation appearing mostly at grain boundaries. For structural application in which requirement for dimension-tolerance is strict, creep deformation rate of the specimen at the service temperature

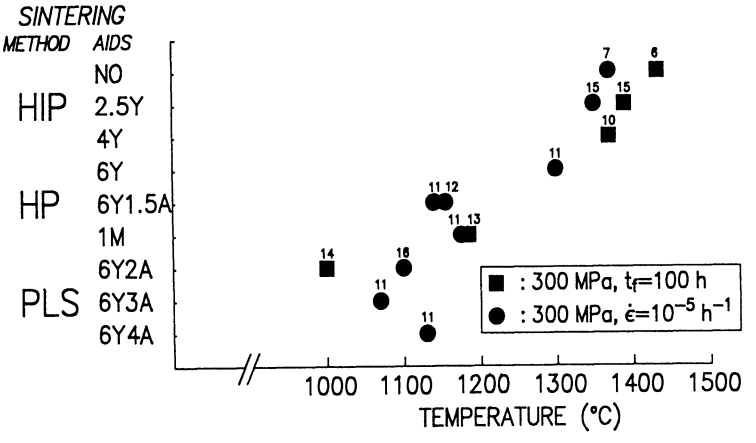

Figure 1. Temperatures at which lifetime under static loading of 300 MPa and bending steady state creep strain rate under 300 MPa become a fixed value. As sintering aids, A, Y and M denote Al_2O_3, Y_2O_3 and MgO, respectively. Small numbers indicate the reference numbers. HP and PLS denote hot-pressing and pressureless sintering.

and stress should be very small: No crack blunting can be virtually expected under such a condition. Consequently, the flaw severity for SCG of the material determine its lifetime.

Regardless of testing procedures, lifetime of a specimen under pure SCG condition is determined simply by the initial flaw geometry and the applied stress as a function of time. We have proposed[6] the use of the stress intensity given by

$$K_I^* = Y \; a_0^{1/2} \quad \sigma_f \tag{1}$$

as the measure of the SCG resistance where a_0 and σ_f are the initial flaw size and fracture stress, respectively. This value gives the initial stress intensity corresponding to the equivalent static-load lifetime that can be calculated analytically when applied stress is given as a function of time. Figure 2(a) shows the SCG resistance, K_I^*, for three HIPed Si_3N_4 materials and two pressureless sintered SiCs only with B and C addition as a function of temperature. The values of K_I^* were determined by stepwise loading of 10 MPa/10 min started from 140 MPa for precracked specimens (Vickers Indentation by 49 N). For this loading condition, the equivalent static load lifetime can be calculated as about 1000 s[6]. It means that a specimen with initial flaw size of a_0 is expected to show SCG failure after 1000 s when static load of σ_f is applied. Based on these data, lifetime by SCG can be estimated as shown in Fig. 2(b). Calculations were made by assuming that initial flaw size is 20 or 40 μm and the SCG exponent is 20. The calculated values show fairly good agreement with lifetime measured by real-time experiments indicated by open circles in the figure. Time-deflection data were recorded during the experiments of unindented specimens and used as four-point bending creep data. The creep rate of high-purity material at 1400° C was found 1 to 3 x 10^{-5} h^{-1} between 200 and 360 MPa. The very low creep rate well support the assumption that the delayed failure mechanism under these static load is predominantly SCG.

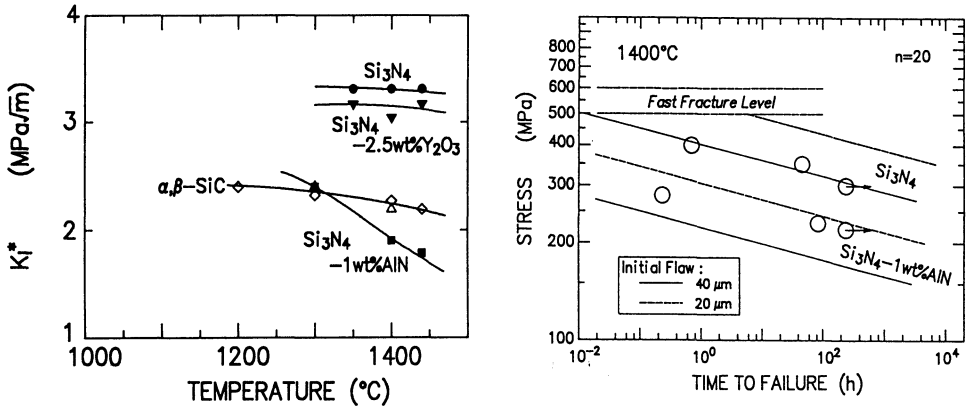

Figure 2. (a) Slow crack growth resistance for lifetime of 10^3 s as a function of temperature. (b) Estimated lifetime by assuming that initial flaw size of 20 and 40 μm and SCG exponent is 20. Open circles are obtained lifetime by real-time experiments.

HOW MATERIAL PARAMETERS AFFECT HIGH TEMPERATURE PROPERTIES ?

Impurity Contents in Starting Powders

High temperature time dependent strength was found significantly affected by the impurity levels of a few hundred ppm[5]. Figure 3 shows the 4-point bending strength measured according to Japan Industrial Standard (JIS) as a function of temperature. Both materials were sintered without additives. Material A contained < 100 wtppm of total cation impurities; and that of material B was about 500 wtppm. Considerable strength degradation was only found in low-purity material, B. Detailed investigation revealed that the impurities localized at the intergranular glassy phase enhance the cavity nucleation rate significantly when external tensile load is applied at elevated temperatures: It gives rise to the enhancement of macroscopic

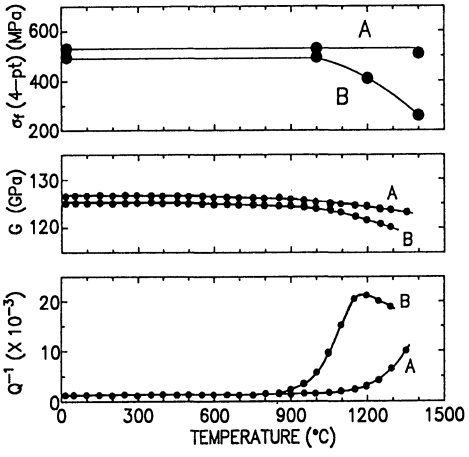

Figure 3. (Top) Bending strength as a function of temperature for two Si_3N_4 materials sintered without additives. (Middle) Shear modulus and (Bottom) internal friction measured by torsion pendulum method as a function of temperature.

SCG rate and consequently the strength degradation. A clear relaxation peak of internal friction located at around 1100°C, which is close to the onset temperature of strength degradation, was found only in material B as shown in Fig. 3. The presence of the impurity enhanced cavity formation mechanism may be effectively detected by the internal friction measurement up to high temperatures.

Solution Effects

Some elements, such as Al, Be and Li, were found to make solid solution with β-Si_3N_4 with concurrent substitution of N by O[19]. Solution effects of such elements have not been examined in details partly because of the lack of high-purity system which can be used as a reference system of such effects. The present authors succeeded to obtain high-purity and dense β-sialon solid solutions as well as β-Si_3N_4 and compared their high temperature properties[20,21]. Contrary to the generally accepted view that such solute atoms do not affect so much the high temperature properties, even 0.3-0.6 wt% of Al (corresponding to 0.5-1.0 wt% AlN or 0.6-1.2 wt% Al_2O_3) considerably degraded the delayed failure resistance, as already shown in Fig. 2. The Al atoms are found almost dissolved into Si_3N_4 matrix and no segregation of impurities was detected even by EDX analyzer equipped with high spatial-resolution (field emission gun) transmission electron microscope. Moreover, internal friction measurements found practically no difference between undoped Si_3N_4 and 1wt%AlN-added materials. Such an effect by solute atoms has been called "solution effect"[21] and its atomistic origin can be explained by the formation of virtual defect of covalent bonding based on electronic structure calculations by the present authors[22].

The Amount of Intergranular Glassy Phase

Higher content of intergranular glassy phase has been believed to provide worse effect for the high temperature strength of Si_3N_4, and many investigators have tried to decrease the glass content by decreasing the amount of sintering aids or by changing their composition feasible to intergranular crystallization. Recently, Zeng et al. have found that increase of high-purity silica glass content up to 10 wt% does not degrade the high temperature strength of high-purity Si_3N_4[23,24], contrary to the above ideas. In the region in which cavity formation rate limits the high temperature strength of the material, the cavitation rate may be strongly affected by the presence of impurities as mentioned above, but not so much by the amount of high-purity silica glass.

Secondary Phase as Reinforcements

Addition of reinforcing phase, such as SiC particles, platelets, and whiskers, has been thought to have positive contribution on both toughening at room temperature and increase in delayed failure resistance at elevated temperatures. Pezzotti et al have studied such effects systematically in high-purity Si_3N_4 based composites without sintering aids[25], and found that some thick SiC whiskers bridged the subcritically propagating cracks. But, the macroscopic SCG resistance of such composites was found strongly affected by impurities introduced from the reinforcements.

REFERENCES

1. Larker, H., Adlerborn, J., and Bohman, H., Fabrication of dense silicon nitride parts by hot isostatic pressing, Society of Automotive Engineers, Technical paper No.770335, 1977.
2. Adlerborn, J., Burstroem, M., Hermansson, L., and Larker, H., Development of high temperature high strength silicon nitride by glass encapsulated hot isostatic pressing, Mater & Design, 1987, **8** 229-32.
3. Homma, K., Okada, H., Fujikawa, T., and Tatuno, T., HIP sintering of silicon nitride without additives, Yogyo-Kyokai-Shi, 1987, **95**, 229-34.
4. Tanaka, I., Pezzotti, G., Okamoto, T., Miyamoto, Y., and Koizumi, M., Hot isostatic press sintering and properties of silicon nitride without additives, J. Am. Ceram. Soc., 1989, **72**,1656-60.
5. Tanaka, I., Pezzotti, G., Matsushita, K., Miyamoto, Y., and Okamoto, T., Impurity enhanced cavity formation in Si3N4 at elevated temperatures, J. Am. Ceram. Soc. 1991, **74** 752-59.
6. Tanaka, I., and Pezzotti,G., Slow crack growth resistance in ceramics for high temperature applications, J. Am. Ceram. Soc. submitted.
7. Tanaka, I., and Pezzotti,G., Delayed-failure resistance of high-purity Si3N4 without additives at 1400°C, J. Am. Ceram. Soc., submitted.
8. Soma, T., Ishida, Y., Matsui, M., Oda, I., Ceramic component design for assuring long term durability, Adv. Ceram., Mater., 1987, **2**, 809-12.
9. Helms, H.E., Haley, P.J., Emerging ceramic components for automotive gas turbines, Ceramic Materials and Components for Engines, The Am. Ceram. Soc., Ohio, 1988, pp. 1347-64.
10. Yeckley, R.L. and Siebein, K.N., High temperature cavitation of HIP silicon nitride, ibid, pp.751-65.
11. Pasto, A.E., Van Schalkwyk, W.C., and Mahoney,F.M., Creep behavior of yttria and alumina-doped silicon nitride, ibid, pp.776-85.
12. Baldoni, J.G. and Buljan, S-.T., ibid, pp.786-95.
13. Quinn, G.D., Static fatigue resistance of hot pressed silicon nitride, Fracture Mechanics of Ceramics **8**, Plenum, New York, 1986, pp.319-32.
14. Khandelwal, P.K., Chang, J. and Heitman, P.W., Slow crack growth in sintered silicon nitride, ibid, 351-62.
15. Tanaka, I., unpublished data.
16. Todd, J.A. and Xu, Z.Y., The high temperature creep deformation of Si3N4-6Y2O3-2Al2O3, J. Mater. Sci., 1989, **24**, 4443-52.
17. Hamano, Y., Development of ceramic engine components in Kyocera, (in Japanese) Application of Ceramic Components to Engine, Uchida-Roukakuho, Tokyo, 1990, pp.367-93.
18. Hecht, N.L., McCullum, D.E., Graves,G.A., Investigation of selected Si3N4 and SiC ceramics, Ceramic Materials and Components for Engines, The Am. Ceram. Soc., Ohio, 1988, pp.806-17.
19. Gauckler, L.J., Lukas, H.L., Tien, T.Y., Crystal chemistry of beta-Si3N4 solid solutions containing metal oxides, Mat. Res. Bull., 1976, **11**, 503-12.
20. Fujiwara, Y., Tanaka, I., Okamoto, T., Kume, S., and Miyamoto, Y., Hot isostatic pressing of synthesized beta-sialon powders, J. Ceram. Soc. Japan., 1990, **98**, 360-64.
21. Tanaka, I., Pezzotti, G., Okamoto, T., Niihara, K., Solution effects on the slow crack growth resistance of dilute sialons at high temperatures, J. Mater. Sci., submitted.
22. Tanaka, I., Nasu, S., Adachi, H., Niihara, K., Electronic mechanisms behind the mechanical properties of beta-sialons, Acta Met. Mater., submitted.
23. Zeng, J., Yamada, O., Tanaka, I., and Miyamoto, Y., Hot isostatic pressing and high-temperature strength of silicon nitride-silica ceramics, J. Am. Ceram. Soc., 1990, **73** 1095-97.
24. Zeng, J., Tanaka, I., Yamada, O.,Miyamoto, Y., and Niihara, K., High temperature strength and cavitation threshold of silicon nitride-silica ceramics, J. Am Ceram. Soc., submitted.
25. Pezzotti, G., Tanaka, I., and Okamoto, T., Si3N4/SiC whisker composites without additives-III High temperature behavior, J. Am. Ceram. Soc., 1991, **74** 326-32.

PROPERTIES OF SILICON NITRIDE-SILICA CERAMICS SINTERED BY HIP

Jianren Zeng, Isao Tanaka, Yoshinari Miyamoto,
Osamu Yamada* and Koichi Niihara
The Institute of Scientific and Industrial Research,
Osaka University, Ibaraki, Osaka 567, Japan;
*College of General Education,
Osaka Industrial University, Daito, Osaka 574, Japan

ABSTRACT

High-purity Si_3N_4 containing 2.5 to 20 wt% SiO_2 additions were fabricated by hot isostatic pressing. Addition of SiO_2 promoted densification and delayed the α-β transformation rate. The fracture toughness was insensitive to the microstructure and glass content, but the Vickers hardness depended strongly on both. The room temperature strength decreased with SiO_2, probably due to increase in the initial flaw size. Vickers hardness showed no drastic degradation up to 1200°C regardless of SiO_2 content and sintering temperature.

INTRODUCTION

Si_3N_4 is one of the most important high-temperature materials. It has been successfully used as turbo-charger rotor for temperatures up to ~1000°C, but applications at higher temperatures are still limited due to strength degradation caused by the intergranular glassy phase. Therefore, great effort is being paid to improve the refractoriness of the intergranular glassy phase by, for example, the use of high-purity Si_3N_4 powders and suitable sintering aids.

Recently we succeeded in fabricating a series of high-purity Si_3N_4-SiO_2 ceramics [1,2,3], by hot isostatic pressing (HIP) of Si_3N_4 and SiO_2 powders using a glass encapsulation technique [4]. In these ceramics, the added SiO_2 remained as glassy phase at the grain boundaries, but fracture strengths of these ceramics were not degraded at 1400°C when the SiO_2 addition was $\leqq$10 wt%.

As a part of the study towards better understanding of the basic properties of Si_3N_4 ceramics, this paper reports on the mechanical properties of Si_3N_4-SiO_2 ceramics from room temperature to high temperatures.

MATERIALS AND METHODS

The starting Si_3N_4 powder and SiO_2 powder both contained < 0.01% of cation impurities. The Si_3N_4 powder had an oxygen impurity content of 1.3 wt%, and a specific surface area of 10 m^2/g. This powder was composed of 97% α-Si_3N_4 and 3% β-Si_3N_4. The SiO_2 powder had a specific area of 170 m^2/g. These two powders were mixed by ball-milling for 12 h in ethanol using Si_3N_4 balls and polyethylene container. The Si_3N_4-SiO_2 ceramics were prepared by HIPing of these mixtures at 1900~2000°C in argon gas of 170 MPa for 1 h using the glass encapsulation method.

Density, phases of the sintered bodies were characterized by Archimedes method and X-ray diffraction [5], respectively. Fracture toughness and hardness were measured by Vickers indentation method with a 49 N load and 15 s loading time [6].

RESULTS AND DISCUSSION

Sintering behaviors

The densification and phase transformation behaviors of Si_3N_4 were found to depend strongly on SiO_2 content. Figure 1 shows the results at 1900, 1950 and 2000°C. Addition of 10 wt% SiO_2 led to complete densification at a sintering temperature 100°C lower than that required for full densification of additive-free Si_3N_4, and resulted in a retention of > 60% α-Si_3N_4: It

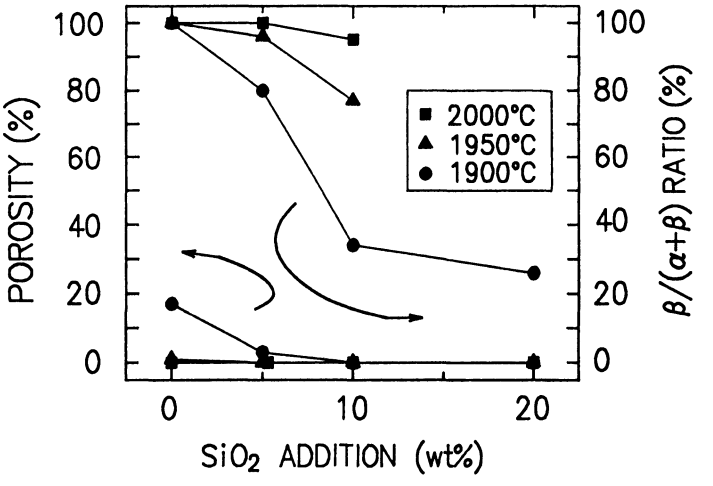

Figure 1 Dependence of porosity and $\beta/(\alpha+\beta)$ ratio on SiO_2 content at different sintering temperatures.

transformed into β-Si_3N_4 at 1800°C in the additive-free Si_3N_4. The addition of SiO_2 is thus considered to play dual roles in the HIP sintering of Si_3N_4: Promotion of densification and retardation of phase transformation. Consequently, the microstructure and phase compositions of densified Si_3N_4 ceramics can be controlled by proper addition of SiO_2.

Si_2N_2O phase was formed only in Si_3N_4 with 20wt% SiO_2 at temperatures higher than 1900°C, showing that the formation of Si_2N_2O depends on both composition and temperature. Sintering behaviors of the Si_3N_4-SiO_2 are discussed in detail elsewhere [3].

Fracture toughness, strength and hardness

Figure 2 summarizes the results of fracture toughness and fracture strength at room temperature as a function of SiO_2 addition at different sintering temperatures. Despite the different SiO_2 content and sintering temperature, the fracture toughness remained constant at ~ 3 MPa$\cdot m^{1/2}$. It was also found that all these materials exhibited transgranular fracture behavior independently of SiO_2 addition and temperature. When the transgranular fracture is dominant, the effect of some important toughening mechanisms, such as crack deflection, crack bridging or grain pull-out may not operate so much. This may be the reason why the fracture toughness is low.

The fracture strength at room temperature decreased with the increase of SiO_2 addition. The fracture-origin size is thus considered to increase with SiO_2 content, because the fracture toughness was almost independent of SiO_2 addition. Observations of fracture surfaces showed that the fracture

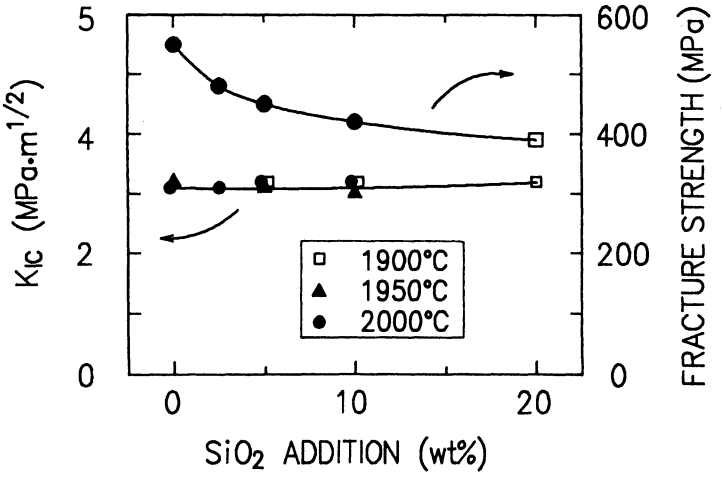

Figure 2 Fracture toughness and strength at room temperature as a function of SiO_2 content and sintering temperature.

origins were mainly surface flaws introduced during machining. Materials with higher glassy content are suggested to suffer such damage more severely. Crack healing treatments such as annealing may be useful to improve the fracture strength of these materials.

Figure 3 shows the dependence of Vickers hardness on SiO_2 content and sintering temperature. The Vickers hardness was, contrary to fracture toughness, strongly dependent on SiO_2 content and sintering temperature. The hardness decreased reasonably with SiO_2 content for the materials sintered at 2000°C, but was almost independent of SiO_2 content for those

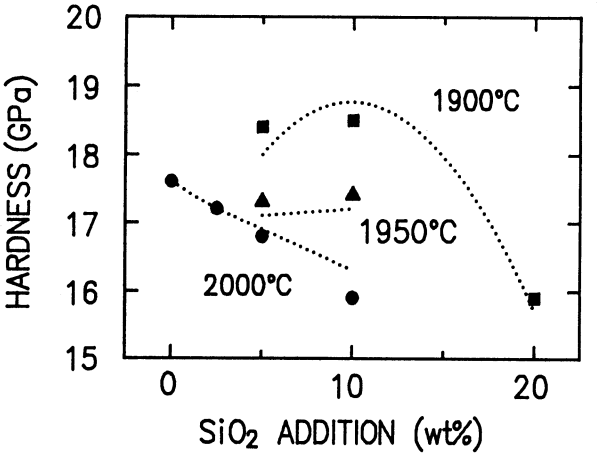

Figure 3 Dependence of Vickers hardness on SiO_2 content and sintering temperature.

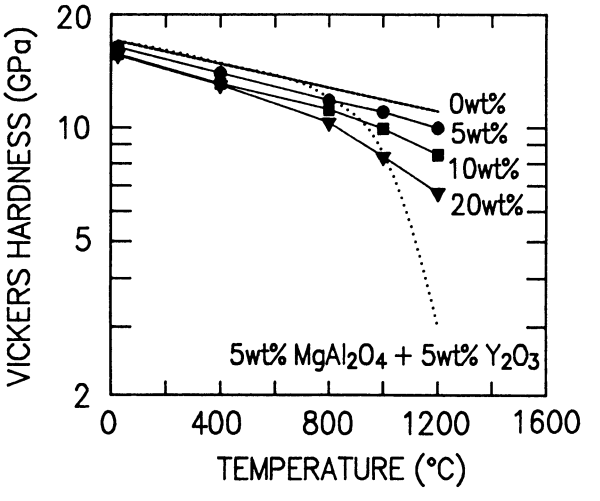

Figure 4 Temperature dependence of Vickers hardness for Si_3N_4 with different SiO_2 additions.

sintered at 1950°C or 1900°C. For the Si_3N_4 with 10 wt% SiO_2 addition, the hardness decreased with increasing sintering temperature. The only difference between these materials are mean grain size [3] and $\beta/(\alpha+\beta)$ ratio (see Figure 1) of the matrix Si_3N_4. Because α-grain size was smaller than that of β-grains, contributions by grain size and phase composition were superposed in the present experiments. Assuming that the latter contribution is larger than the former, the apparent hardness of α-grains can be estimated and the hardness values can be simulated. The calculated results with 23 GPa for the apparent hardness of α-phase are shown by broken curves in Figure 3: They roughly show agreement with the experimental data.

Figure 4 shows the temperature dependence of Vickers hardness for Si_3N_4 with different SiO_2 additions, together with that for Si_3N_4 without additives [7] and for Si_3N_4 sintered with 5wt% $MgAl_2O_4$+5wt% Al_2O_3 by hot-pressing [8]. At room temperature, the difference in hardness was relatively small. But it expanded with the increase of temperature: Materials with more SiO_2 lost more hardness: This is simply due to the softening of the pure glassy phase. But it is noticed that, unlike the Si_3N_4 with 5wt% $MgAl_2O_4$+5wt% Al_2O_3 that suffered a drastic loss in hardness at above 1000°C, the Si_3N_4-SiO_2 ceramics did not show abrupt decrease up to 1200°C. This is consistent with the result that addition of up to 10 wt% did not cause strength degradation even at 1400°C [2].

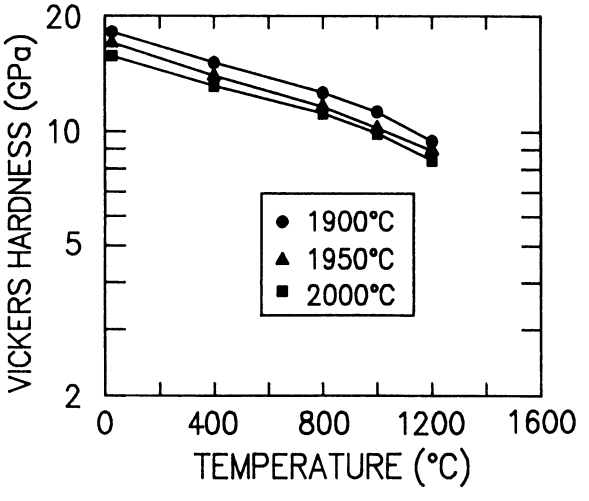

Figure 5 Temperature dependence of Vickers hardness for Si_3N_4-5wt% SiO_2 material sintered at different temperatures.

Figure 5 shows the temperature dependence of Vickers hardness for Si_3N_4-10 wt% SiO_2 sintered at different temperatures. As mentioned above, drastic decrease in hardness was not found regardless of sintering temperature.

CONCLUSIONS

Dense Si_3N_4-SiO_2 ceramics with various SiO_2 contents were successfully prepared by HIP sintering using the glass encapsulation technique. The effects of SiO_2 addition on the sintering behavior and mechanical properties of Si_3N_4 were studied, and summarized as follows:

(1) Densification was promoted, but α-β transformation was delayed by SiO_2 addition.

(2) The fracture toughness was independent of SiO_2 content and sintering temperature.

(3) Vickers hardness depended on both sintering temperature and SiO_2 content.

(4) Vickers hardness exhibited no drastic decrease up to 1200°C despite up to 10 wt% SiO_2 addition.

REFERENCES

1. Zeng, J., Yamada, O., Tanaka, I., and Miyamoto, Y., Hot iso-static pressing and high temperature strength of silicon nitride-silica ceramics. J. Am. Ceram. Soc., 1990 73 1095-97.

2. Zeng, J., Tanaka, I., Miyamoto, Y., Yamada, O., and Niihara, K., High temperature strength and cavitation threshold of silicon nitride-silica ceramics. J. Am. Ceram. Soc., in press.

3. Zeng, J., Tanaka, I., Miyamoto, Y., Yamada, O., and Niihara, K., Sintering behaviors of silicon nitride-silica ceramics during hot isostatic pressing. Submitted to J. Am. Ceram. Soc..

4. Larker, H., Adlerborn, J., and Bohman, J., Fabricating of dense silicon nitride parts by hot isostatic pressing. SAE Technical Paper, 1977, No 770335.

5. Gazzara, G.P., and Messier, D.P., Determination of phase content of Si_3N_4 by X-ray diffraction analysis. Am. Ceram. Soc. Bull., 1977, 56 777-80.

6. Niihara, K., Morena, R., and Hasselman, D.P., Further reply to "comment on "elastic /plastic indentation damage in ceramics the median/radial crack systems"". J. Am. Ceram. Soc., 1982 65 C116-17.

7. Tanaka, I., Pezzotti, G., Okamoto, T., Miyamoto, Y., and Koizumi, M., Hot isostatic pressing and properties of Si_3N_4 without additives. J. Am. Ceram. Soc., 1989, 72 1656-60.

8. Tsukuma, K., Shimada, M., and Koizumi, M., Thermal conductivity and microhardness of Si_3N_4 with and without additives. Am. Ceram. Soc. Bull., 1981, 60 1281-88.

MECHANICAL PROPERTIES OF SIALON SINTERED AT DIFFERENT PRESSURES

ANDRÁS KELE, PÉTER ARATÓ, ELIZABETH BESENYEI,
JÁNOS LÁBÁR, FERENC WÉBER
Research Institute for Technical Physics
of the Hungarian Academy of Sciences
POB 76, H-1325, Budapest, Hungary

ABSTRACT

We studied the effect of sintering techniques on the mechanical properties of sialon probes. Samples were densified applying high pressure processes without encapsulation. In some cases the sintering process was interrupted at different temperatures to study the pore closure. The flexural strength, the modulus of elasticity, the hardness and the indentation toughness were used to characterize the samples. The microstructure and the local composition were studied by SEM and EDAX. Although high density was attained for most of the samples, the mechanical properties considerably depended on the details of the HIP process. The results can be explained by the mechanical effect of the applied pressure.

INTRODUCTION

Silicon nitride based ceramics are among the most promising materials for high temperature structural applications. These materials can be densified in the presence of additives which provide liquid phase during sintering. The liquid formed allows an easy rearrangement of particles and a subsequent solution of α Si_3N_4 and reprecipitation of α' and β' sialons. High pressure can be applied not only to promote sintering but to hinder the decomposition of silicon nitride [1]. With the development of new sintering techniques such as sinter HIP methods at different pressures where no encapsulation of the green body is used [2,3], it becomes of crucial importance to investigate the processes during densification. When high pressure is applied a better understanding of the initial stage is inevitable.

In this paper it is shown on silicon nitride based ceramics sintered by sinter HIP techniques at different pressures, how some details of the sintering process can affect

the microstructure and the mechanical properties. This may help in revealing the relationship of processing parameters, microstructure and mechanical properties.

EXPERIMENTAL PROCEDURE

The compositions of the materials are given in Figure 1. Mixtures of Si_3N_4, AlN, Al_2O_3 an Y_2O_3 powders were milled in ethanol in a planetary type alumina ball mill. Samples were compacted by dry pressing.

All sintering experiments were carried out in an ABRA SHIRP 8/16-200-2000 apparatus. The heating rate was 25 ^oC/min. The sintering temperature was 1640-1800 ^oC. The atmosphere was high purity nitrogen of 1-2 MPa during heating and in the first period of holding. Then the pressure was increased to 10 MPa, or 20 MPa within a few minutes. In other experiments argon was pumped into the furnace. It took about 30-60 minutes to reach 200 MPa. Post HIP treatments at 20 or 200 MPa were also performed on samples sintered previously at different pressures (0.1-200 MPa). In some cases the sinter HIP process was interrupted during heating or in the first period of holding, and the furnace was cooled down quickly.

We measured the density by the Archimedes method. The modulus of elasticity and the 4 point flexural strength were measured at room temperature with a span of 40 by 20 mm. Hardness and indentation fracture toughness were determined using a Vickers diamond indenter on a polished surface. X-ray diffraction phase analysis was carried out on the same samples. Microstructure of the fractured surface was investigated by scanning electron microscopy. The distribution of silicon, aluminium and yttrium was measured by EDAX on polished surfaces.

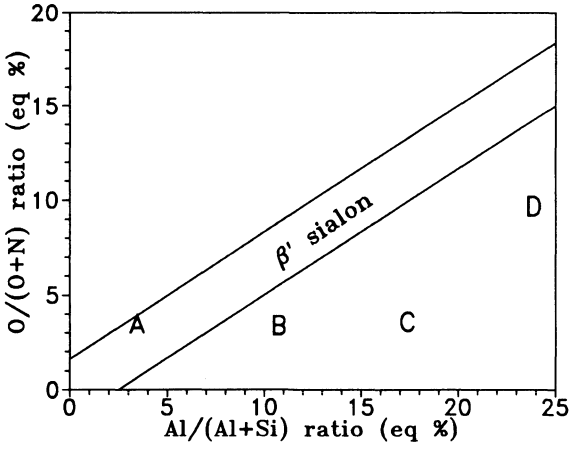

Figure 1. Composition of materials.

TABLE 1
Properties after sinter HIP treatment

Sample No.	Composition	Pressure (MPa)	Density (g/cm^3)	Strength (MPa)	Mod. elast. (GPa)	Hardness (GPa)	K_{IC} ($MPa*m^{1/2}$)	$\frac{\alpha'}{\alpha'+\beta'}$ (%)
1	C	20	2.9	211		14.6	7.3	82
2	C	20	3.02	302	266			71
3	C	20	2.98	278	241	19.1	4.7	74
4	A	200	3.13	391	272	19.1	5.7	47
5	A	20	3.13	364	250	15.5	4.2	20
6	A	20	3.17	401	263	15.5	4.4	26
7	A	20	3.24	553	279	17.8	5.1	22
8	A	200	3.24	602	310	16.9	5.3	8

RESULTS AND DISCUSSION

The HIP treatments on sialon samples resulted in a wide variety of properties and microstructures depending on composition, pressure and some other processing parameters. Some examples are shown in Table 1.

Sample 7,8 are the reference ones showing the properties that could be obtained in an appropriate treatment.

The sintering of the first three samples was started at high pressure. The densities are rather low, closed porosity was not reached (Figure 2a), the development of a connected solid structure can not be expected. It explains the low mechanical strength of these samples.

Sample 4,5,6 were densified in sinter HIP processes. The pressure was applied before the completely closed porosity developed. The density of these samples is increased, but it is much lower than that of the reference samples. The pores became closed, but the materials did not densify properly (Figure 2b) which explains the low value of strength. The high pressure gas remaining inside the pores may hinder the densification in this case.

The first essential condition of obtaining good properties for almost all compositions is that no open porosity can remain in the structure when high pressure is applied. The density belonging to the pore closure can be determined by measuring the apparent and bulk densities of the samples obtained from the sintering processes which were interrupted at different temperatures. The two kinds of density approach a common value corresponding to the density of the material with closed porosity (Figure 3).

The closed porosity before applying pressure is a necessary but not sufficient condition of obtaining high strength. The properties of some sialon samples subjected to post HIP treatments are shown in Table 2. In all cases the density achieved in the first step of sintering exceeded the value belonging to the closed porosity state. The application of high pressure in the second sintering step resulted in high density, the flexural strength increased for some samples while for others it decreased.

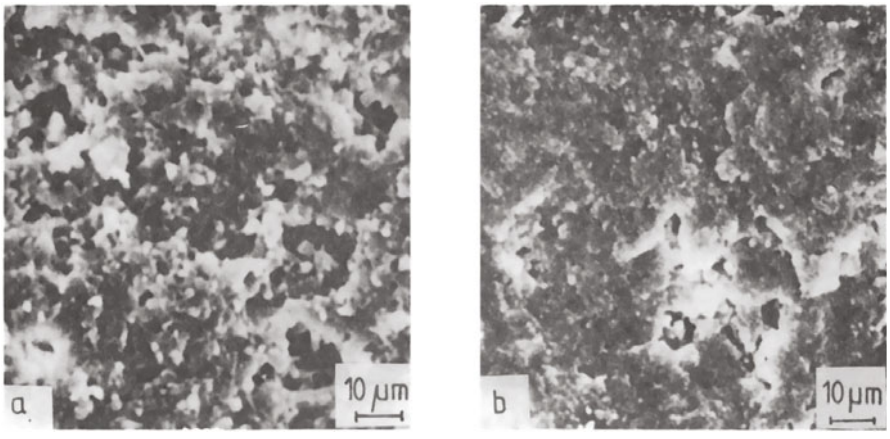

Figure 2. Microstructure of partially densified samples (a/Sample 1 ; b/Sample 4)

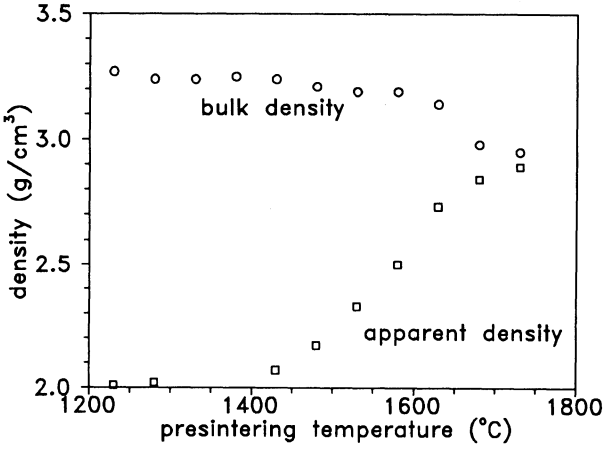

Figure 3. The apparent and bulk densities as a function of presintering temperature for material A.

These observations can be attributed to the effect of different processes. In high pressure liquid phase sintering the residual macropores are eliminated either by a mixed flow of both the liquid phase and the grains, or by the flow of the liquid phase alone. The latter case may result in soft spots and inhomogenous microstructure [4].

If the solid structure developed during sintering is strong and connected enough, the liquid phase will be pushed into the pores without moving the solid phase. If a solid structure has been developed but it is not strong enough the liquid of high viscosity can deteriorate it. When the pore healing occurs by the movement of the liquid phase alone the

TABLE 2
Properties before (b) and after (a) post HIP treatment

Sample No.		Composition	Pressure (MPa)	Density (g/cm^3)	Strength (MPa)	Mod. elast. (GPa)	Hardness (GPa)	K_{IC} ($MPa*m^{1/2}$)	$\frac{\alpha'}{\alpha'+\beta'}$ (%)
9	b	D	20	3.09	238	270	17.6	5.3	4
	a		200	3.25	352	303	18.2	5	23
10	b	D	20	3.09	284	271			5
	a		200	3.24	298	292			
11	b	A	20	3.22	521	307	16.1	5.3	2
	a		200	3.25	594	304	16.1	4.9	3
12	b	A	1	3.07	415	266			
	a		20	3.25	370	305	16.8	5	
13	b	A	200	3.25	607	310			
	a		200	3.25	523	287			

density of the sample is increased without improving the strength (see Sample 10 and 12), as the strength is mainly determined by the solid structure. However the modulus of elasticity increases when this process takes place.

Pores filled by the glassy phase can be seen on a polished sample if the glassy phase is removed by etching (Figure 4). The results of the EDAX analysis also point to the presence of pores filled by a material of different composition from that of the matrix.

The strength can be improved if the high pressure is applied on a structure with a few small pores (Sample 11).

If the structure has already developed the high pressure may damage it, decreasing the strength of the sample (Sample 13). On the damaged parts the intergranular phase is loaded instead of the structure. The modulus of elasticity is expected to decrease because the intergranular phase is believed to be more flexible. The damage caused by the high pressure may not be healed in the further course of sintering. The heat treatment decreasing the strength of the sample above gave high strength when there was no pretreatment (Sample 8).

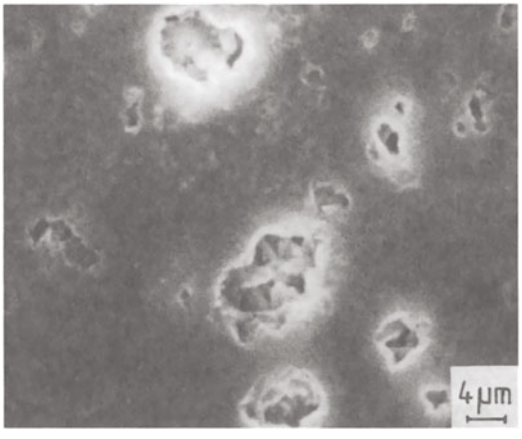

Figure 4. Healed pores on polished surfaces after etching.

When the pressure is increased in sinter HIP treatments the flow of the liquid phase may occur, too. The results obtained at 20 MPa and 200 MPa are shown on Figure 5. The higher pressure resulted in higher hardness and higher modulus of elasticity while the strength values were similar.

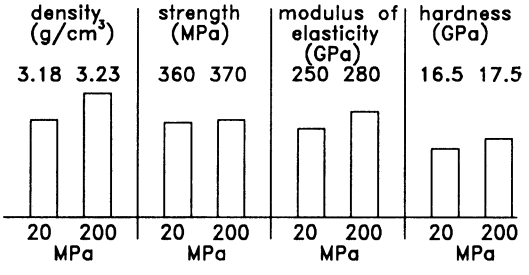

Figure 5. Dependence of the mechanical properties of material D on the sintering pressure.

CONCLUSION

We have shown that the initial stage of the sintering significantly affects the final mechanical properties. The density belonging to the closed porosity can be determined by measuring bulk and apparent densities simultaneously. The faults developed in the initial stage can hardly be corrected by high pressure. Even a good material can be deteriorated if the conditions of the high pressure process are not properly chosen. The results can be explained by the mechanical effect of the applied pressure.

We are grateful to Mrs É. Hajdu, Mrs M. Mészáros and Mrs. J. Zsoldos for technical assistance. This work was supported by the government Committee of Research and Development.

REFERENCES

1. Ziegler, G., Heinrich, J., Wötting, G., Relationships between processing, microstructure and properties of dense and reaction-bonded silicon nitride, J. Mat. Sci. 1987, **22**, 3041-86.

2. Tanaka, I., Pezzotti, G., Okamoto, T., Miyamoto, Y., Hot isostatic press sintering and properties of silicon nitride without additives, J.Am.Ceram.Soc. 1989, **72** [9], 1656-60.

3. Iturriza, I., Echeberria, J., Castro, F., Sinter-HIP of silicon nitride ceramics with oxide additions, in Proc. Int. Conf. Hot Isostatic Pressing, (Antwerpen, 1988), 5.27-5.33.

4. Frisch, A., Kaysser, W. A., Petzow, G., Defect healing during sinter/HIP, in Proc. PM '90, The Institute of Metals, London, 1990, 237-50.

PREPARATION OF HIGH-DENSITY AND HIGH-STRENGTH ALUMINA BY HIP

KIICHI ODA, HIROYUKI MIZUTA, YASUO SHIBASAKI, MASAKI MAEDA
and MICHIHIDE MACHIDA
Government Industrial Research Institute, Nagoya
1-1 Hirate-cho, Kita-ku, Nagoya 462, Japan
KAZUYUKI OHSHIMA
Toshiba Ceramics Co. Ltd., 1 Kogakie-cho Minamifuji, Kariya 448, Japan

Abstract

Well-dispersed slurry was prepared for high-purity and submicron alumina powder, and dense green compact was formed by the slip casting system assisted with vacuum-pressure. The sample, sintered at 1240^{o}C for 2 h in air, was subjected to the HIP treatment without capsule at 1050^{o}-1400^{o}C for 1 h in argon atmosphere. Extremely high-density (99.9%) and fine-grain (0.7-15 um in diam.) alumina ceramics were obtained. The HIP'ed sample showed high bend strength (~780 MPa).

Introduction

It is important to fabricate high-strength alumina ceramics for the practical application. CIP(cold isostatic pressing) can provide easily dense green compact, but machining must be necessary to form complicated object. In general, slip casting can provide complicated green compact and has the advantage of low cost. We have been studying the application of slip casting to the forming of structural ceramics. The preparation conditions and the characteristics of the slurry for the submicron alumina were investigated and also the slip casting system has been developed. As the results, high-density alumina could be prepared by the sintering at lower temperature(at 1250^{o}C for 3 h in air) via slip casting[1,2,3]. In the present work, the effect of the HIP(hot isostatic pressing) temperature on the density, the grain size and the bend strength of alumina was examined, and the relationship between grain size and bend strength were studied.

Experimental

A commercially available alumina (Taimicron TM-DAR;Taimei Chemicals) was used in this work. The optimum batch composition of the slurry is shown in Table 1. After the slurry batch was mixed in a ball-mill for 16 h, the slurry was supplied into the slip casting system and the green compact(about 11 cm in diam. x 2 cm in thickness) was formed by using polymer resin porous mold. The green compact was dried adequately and then sintered at 1240^{o}C for 2 h in air before HIP treatment.

TABLE 1
The composition of the slurry

Alumina	Taimicron TM-DAR	77 wt%
Water		23
Deflocculant	$NH4^{+}$ salt of polymethacrylic acid	0.5 wt%
Binder	D-Sorbitol	0.3
Defoamer	Polyethylenegrycol	0.1

The sintered sample was isostatically pressed at various temperatures of 1050^{o}-1400^{o}C without capsule at 150 MPa for 1 h in argon atmosphere. The bend strength of the sample(3 x 4 x 40 ^{L} mm) was measured by a 3-point bend testing machine under the cross-head speed of 0.5 mm/min. Each datum point was obtained from the measurement of twenty test pieces.

Results and Discussion

The slip casting can provide the high-density green compact (relative density=62%), that value was considerably high in comparison with that formed by other methods. The green compact was sintered at 1240^{o}C for 2 h in air. The sintered sample(relative density >98%) was subjected to the HIP treatment without capsule. The disk (8 cm in diam. x 1.5 cm in thickness) has been prepared as shown in Fig.1.

The microstructures of the samples HIP'ed at various temperatures of 1200^{o}-1400^{o}C were investigated. It was found that all samples consisted of fairly uniform grain and extremely pore-free microstructure. The density increased from 98.2 to 99.9% with raising HIP temperature from 1050^{o} to 1200^{o}C. The ultimately densified alumina(relative density=99.9%) was obtained at lower temperatures of 1200^{o}-1400^{o}C by HIP without capsule.

The grain size increased rapidly from 0.7 to 15 um with raising HIP temperature. Both the extremely high-density and the fine-grained microstructure were attained by the HIP treatment at lower temperatures. It can

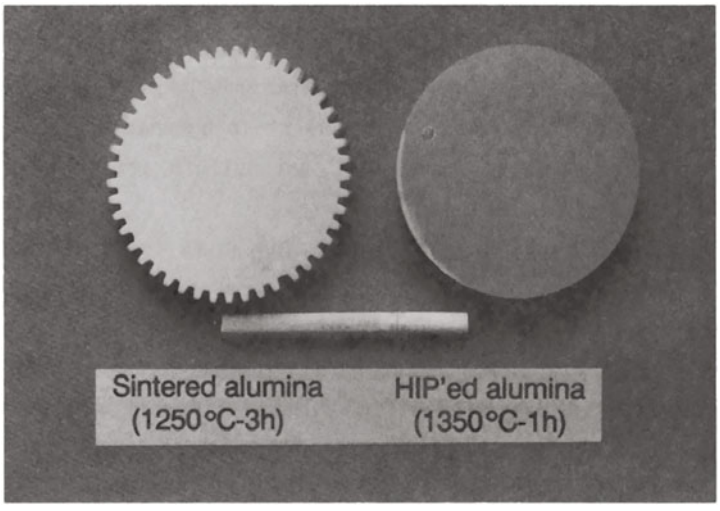

Figure 1. Sample appearance(left;sintered, right;HIP'ed).

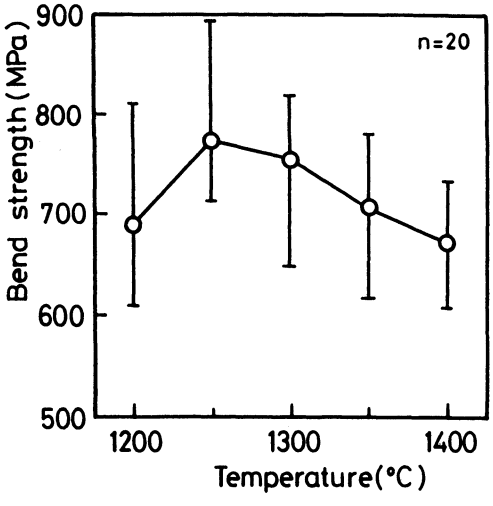

Figure 2. Plot of the bend strength of the alumina vs HIP temperature.

be considered that the high-density of the HIP'ed sample is attributed to the sample prepared from the high-purity and submicron alumina powder by the slip casting assisted with vacuum-pressure.

The plot of the average bend strength of the sample vs HIP temperature is shown in Fig.2. Bar means the maximum and minimum values of bend strength. The bend strength increases from 690 to 780 MPa with raising HIP temperature from 1200^{0} to 1250^{0}C, however, decreases slightly from 780 to 680 MPa with raising HIP temperature from 1200^{0} to 1400^{0}C. The slight reduction in strength seems to be due to the growth of the fracture origins such as pore and impurity precipitated at grain-boundary. It is noted that the high-density alumina with the fine and uniform grain shows extremely high bend strength.

The plots of the bend strength of the alumina vs the grain size and the porosity is shown in Fig.3. The HIP'ed sample shows high values of 680-780 MPa. The relation between bend strength and grain size of alumina has been studied by Passmore et al.[4]. Referring to their experimental equation, the bend strength of fully densified alumina increases with decreasing grain size. This tendency is recognized as follows: defect, origin of fracture, becomes smaller when the grain of alumina becomes smaller. But, it is actually difficult to prepare fully densified alumina with submicron grain. Therefore, the density decreases below a certain grain size. Based

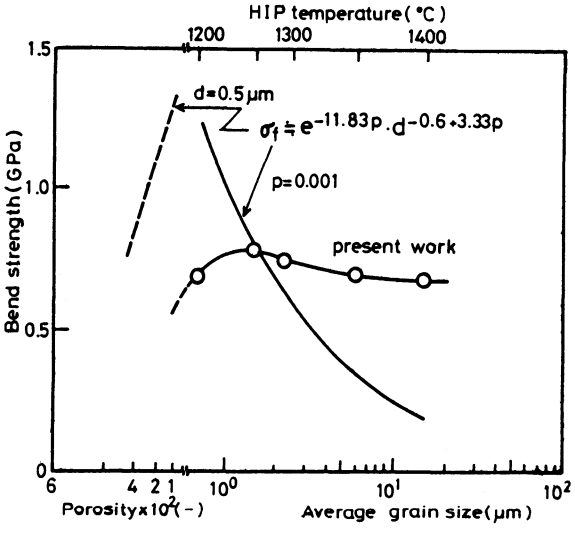

Figure 3. Plots of the bend strength of the alumina vs the grain size and the porosity.

on their equation, the grain size dependence of the bend strength of alumina can be expressed by the two equations. One is the bend strength depending upon mainly porosity, where the grain size is constant (0.5um in diam.). The other is the bend strength depending upon mainly grain size, where the ultimate densification (relative density=99.9%) is attained. As seen in Fig.3, the bend strength decreases below 0.5 um, on the other hand, the bend strength increases with decreasing grain size above 0.5 um. The relation between bend strength and grain size is qualitatively explained as mentioned above. However, the grain size dependence of the bend strength of the HIP'ed alumina is far small than that expected from their equation. It is found that the alumina with less fracture origins such as pore, impurity and etc. does not show the strong grain size dependence of the bend strength.

Conclusion

In order to prepare high-density and high-strength alumina ceramics the slip casting and HIP were employed. The slurry was prepared carefully by considering both lowering viscosity and higher content of solid. The dense green compact has been formed by using the slip casting system assisted with vacuum-pressure. The alumina ceramics were prepared by normal sintering at 1240^{o}C for 2 h in air and subjected to the capsule free HIP.

1)Extremely fully densified alumina ceramics can be obtained by HIP at the temperature range of 1200^{o}-1400^{o}C for 1 h (argon gas ; 150MPa).

2)The sample HIP'ed at 1250^{o}C showed high-strength of 780 MPa at R.T.

The high-strength is attributed to the high-density and the fairly uniform microstructure of HIP'ed sample prepared from the high-purity and submicron starting powder.

References

1. H.Mizuta, Y.Shibasaki, S.Sakai, M.Katagiri and H.Fujimoto, Funtai Oyobi Funmatsuyakin, **35**[7]619-624(1988)(in Japanese)

2. H.Mizuta, Y.Shibasaki, M.Maeda, S.Sakai, M.Itoh and K.Ohshima, Reports of the Government Industrial Research Institute, Nagoya, **39**[1]25-32(1990)(in Japanese)

3. H.Mizuta, K.Oda, M.Maeda, Y.Shibasaki, M.Machida and K.Ohshima, ibid, **39**[6]284-291(1990)(in Japanese)

4. E.M.Passmore, R.M.Spriggs and T.Vasilos, J.Am.Ceram.Soc., **48**[1]1-7(1965)

MECHANICAL PROPERTIES AND MICROSTRUCTURES OF TiB_2-ZrO_2-SiC FABRICATED BY HIP

SHIRO TORIZUKA, HIROAKI NISHIO, ATSUSHI CHINO AND YOUICHI ISHIBASHI
Advanced Technology Research Center,
NKK Corporation
1-1 Minamiwatarida-cho, kawasaki-ku, kawasaki, 210, Japan

ABSTRACT

Ceramic TiB_2 composites with up to 40wt% of ZrO_2, 2mol%Y_2O_3-ZrO_2 or 2.5wt%SiC were fabricated by hot isostatic pressing (HIP) both with and without glass encapsulation. The effects of these additions on the mechanical properties and microstructure of TiB_2 were investigated. The addition of ZrO_2 or 2mol%Y_2O_3-ZrO_2 was very effective in improving the 3-point bend strength of TiB_2. The 3-point bend strengths of TiB_2 with 10wt% ZrO_2 and TiB_2 with 10-20wt% (2mol%Y_2O_3-ZrO_2) were 1160-1200MPa, which is three times higher than that of monolithic TiB_2 (450MPa). The 3-point bend strength was dependent on the monoclinic ZrO_2 content in the HIP'ed composite. To obtain high strength HIP'ed materials with strengths greater than 1000MPa, the content of monoclinic ZrO_2 must be less than 10wt%. The fracture toughness was also affected by the addition of ZrO_2 or 2mol%Y_2O_3-ZrO_2. The fracture toughness of TiB_2 with 30wt% ZrO_2 was 8.2MPam$^{1/2}$. TiB_2 with ZrO_2 and TiB_2 with (2mol%Y_2O_3-ZrO_2) lacked sinterability. The addition of 2.5wt%SiC was very effective in improving the sinterability of TiB_2 with (2mol%Y_2O_3-ZrO_2). The mechanism of sinterability improvement was thought to be liquid phase sintering.

INTRODUCTION

TiB_2 should be an excellent wear and erosion resistant material because of its high hardness and high melting point. However, fully dense, high strength monolithic TiB_2 products are difficult to fabricate because grain growth occurs easily at the sintering temperature[1-3]. Thus, sintering additives or second phases are required. In this work the authors used ZrO_2, 2mol%Y_2O_3-ZrO_2 (tetragonal stabilized ZrO_2) and SiC as second and third phase additions to TiB_2 to improve mechanical properties [4-10]. The effect of these additions on the mechanical properties of TiB_2 was studied. 2mol%Y_2O_3-ZrO_2 is abbreviated as 2Y-ZrO_2 in following text.

EXPERIMENTAL WORK

The chemical compositions of TiB_2, ZrO_2, 2mol%Y_2O_3-ZrO_2 and SiC are shown in Table 1. These components were mixed in ethanol using a ball mill and then dried and sieved through 300μm mesh. The dried powder was compressed at 9.8MPa and cold isostatically pressed (CIP) at 300MPa. The resulting green compacts had a theoretical density of 59%. These were sintered at 1700°C for 14.4ks under a 0.013MPa vacuum and then HIP'ed with or without glass encapsulation. The HIP'ing conditions were 1600°C for 7.2ks under 200MPa of Ar. The HIP'ed specimens were evaluated for bulk density, three point bend strength and fracture toughness. The bars for three point bend strength tests were 3x4x36mm and the crosshead speed was 0.5mm/min. Fracture toughness was measured by the IM method. Microstructures were analyzed using SEM and TEM, and phases were identified by X-ray diffraction. Quantitative analysis was performed on ZrO_2 to determine the amount of monoclinic and tetragonal phases.

Table 1 Specific surface area and chemical composition of TiB_2, SiC, 2mol%Y_2O_3-ZrO_2 and ZrO_2 powder.

Powder	Specific surface area (m^2/g)	Chemical composition (wt%)				
		B	O	C	N	Fe
TiB_2	5.20	29.7	1.57	0.18	0.11	<0.15
		Al	SiO_2	C	Fe	-
SiC	17.5	0.03	0.3	0.4	0.04	-

Powder	Specific surface area (m^2/g)	Chemical composition (wt%)				
		Y_2O_3	Al_2O_3	SiO_2	Fe_2O_3	Na_2O
2%Y_2O_3-ZrO_2	14.2	3.74	0.066	0.091	0.029	0.004
ZrO_2	14.6	-	0.005	0.002	0.003	0.007

RESULTS AND DISCUSSION

Density

As shown in Figure 1., the TiB_2 - ZrO_2 and TiB_2 - (2Y-ZrO_2) composites attained up to 63% of their theoretical density, as calculated by the complex rule. The glass encapsulation HIP technique [11] was required to achieve nearly full density. On the other hand, TiB_2 - 20wt%(2Y-ZrO_2) - 2.5wt%SiC densified up to 98% by vacuum sintering alone. This density (98%) was high enough for HIP without glass encapsulation. The addition of 2.5wt%SiC was found to be very effective in improving the sinterability of TiB_2 - 20wt%(2Y-ZrO_2).

Microstructure

Figure 2. shows microstructures of TiB_2 - 20wt%(2Y-ZrO_2) and TiB_2 - 20wt%(2Y-ZrO_2) - 2.5wt%SiC as observed with SEM. The black grains are TiB_2 and white ones are ZrO_2. The grain size of TiB_2 in TiB_2 - 20wt%(2Y-ZrO_2) was 2-5μm, as shown in Figure 2(a). On the other hand, the grain size of TiB_2 - 20wt%(2Y-ZrO_2) - 2.5wt%SiC was 1-3μm, as shown in Figure 2(b). The addition of SiC was also effective in retarding grain growth.

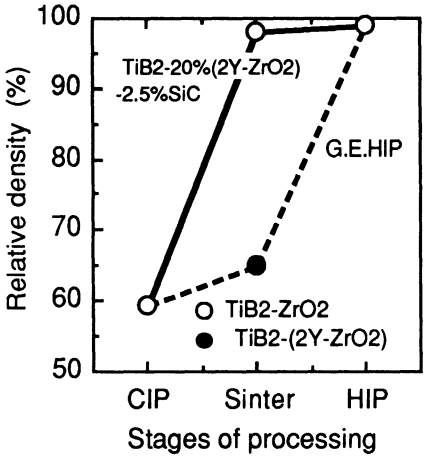

Figure 1. Relationship between stages of processing and relative density.
CIP; 300MPa,
Sinter; 1700°C, 0.013MPa vac., 14.4ks,
HIP; 1600°C, 200MPa of Ar, 7.2ks.

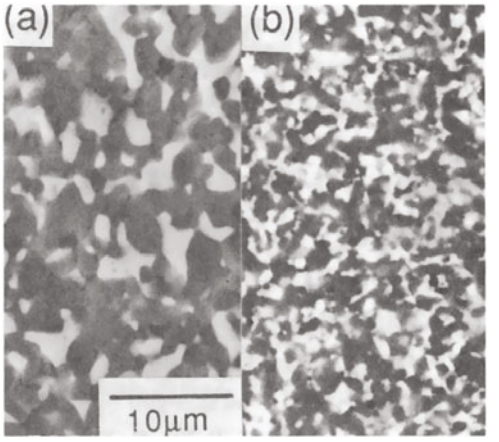

Figure 2. Microstructures of (a)TiB_2 - 20wt% (2mol% Y_2O_3-ZrO_2) and (b)TiB_2 - 20wt% (2mol%Y_2O_3-ZrO_2) - 2.5wt%SiC observed with SEM.

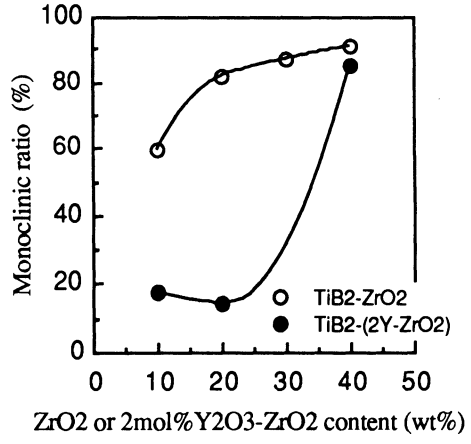

Figure 3. Monoclinic ZrO_2 ratio of ZrO_2 in TiB_2 - ZrO_2 and TiB_2 - (2mol%Y_2O_3-ZrO_2).

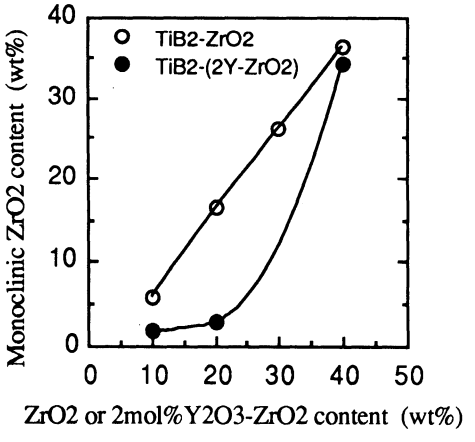

Figure 4. Monoclinic ZrO_2 content in TiB_2 - ZrO_2 and TiB_2 - (2mol%Y_2O_3-ZrO_2).

Phase identification

Monoclinic and tetragonal phases of ZrO_2 were found by X-ray diffraction in both TiB_2 - ZrO_2 and TiB_2 - (2Y-ZrO_2) HIP'ed specimens. As shown in Figure 3., the monoclinic to (monoclinic + tetragonal) phase ratio increased with increasing ZrO_2 content. The tetragonal phase is stable at sintering and HIP'ing temperatures, but transforms to monoclinic during cooling. The greater the ZrO_2 content, the more this transformation occurs. The monoclinic phase ratio of TiB_2 - 20wt%(2Y-ZrO_2) was less than that of TiB_2 - 20wt%ZrO_2, because Y_2O_3 stabilizes the tetragonal phase. Figure 4. shows the monoclinic phase content in both HIP'ed specimens, calculated by multiplying the monoclinic ratio by the ZrO_2 content. The monoclinic content increases linearly with increasing ZrO_2 in TiB_2 - ZrO_2. On the other hand, the monoclinic content was less than 5% in TiB_2 - 10-20wt%(2Y-ZrO_2) and was greater for the 40wt%(2Y-ZrO_2) specimen, but was slightly less than that of TiB_2 - 40wt%ZrO_2.

Mechanical properties

3-point bend strength: Figure 5. shows the 3-point bend strength of TiB_2 - ZrO_2 and TiB_2 - (2Y-ZrO_2) HIP'ed specimens. The 3-point bend strengths of TiB_2 was 450MPa. However, the addition of ZrO_2 or 2Y-ZrO_2 was very effective in improving the 3-point bend strength of TiB_2. High 3-point bend strengths of 1160-1200MPa were obtained with the TiB_2 - 10wt%ZrO_2 and TiB_2 - 10-20wt%(2Y-ZrO_2) HIP'ed specimens. The addition of 10wt%ZrO_2 or 10-20wt%(2Y-ZrO_2) made TiB_2 three times stronger. The maximum strength of TiB_2 - ZrO_2 was obtained at a ZrO_2 content of 10wt%; however, the strength decreased with increasing ZrO_2 content above 10wt%. On the other hand, the maximum strength of TiB_2 -

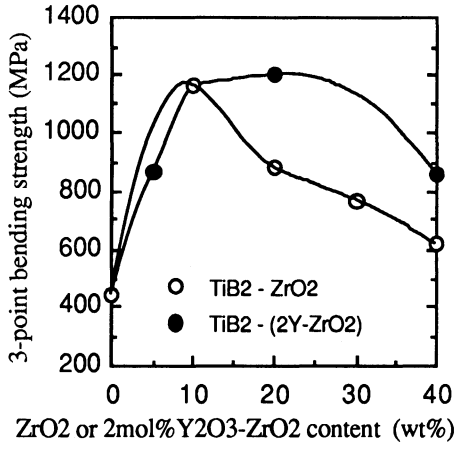

Figure 5. 3-point bending strength of TiB2 - ZrO_2 and TiB_2 - (2mol%Y_2O_3-ZrO_2).

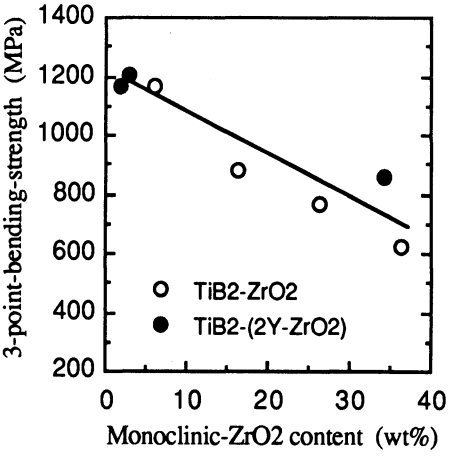

Figure 6. Effect of monoclinic ZrO_2 content on 3-point bending strength.

(2Y-ZrO_2) was obtained with a content of 10-20wt%(2Y-ZrO_2), above which the strength also decreased. The strength of TiB_2 - (2Y-ZrO_2) was greater than TiB_2 - ZrO_2, regardless of ZrO_2 content. The relationship between the 3-point bend strength and monoclinic ZrO_2 content is shown in Figure 6. The open marks represent TiB_2 - ZrO_2 and the closed marks TiB_2 - (2Y-ZrO_2). The 3-point bend strength decreased linearly with increasing monoclinic ZrO_2 content, suggesting that the monoclinic phase was the cause for the decrease in strength. Tetragonal ZrO_2 expands 4% when it transforms into the monoclinic phase, which causes microcracks [12]. Monoclinic ZrO_2 has almost no strength due to these microcracks. Therefore, the decrease in the strength of TiB_2 - ZrO_2 and TiB_2 - (2Y-ZrO_2) was caused by microcracks in the ZrO_2. To obtain high strength HIP'ed parts with strengths greater than 1000MPa, the monoclinic content must be less than 10wt%.

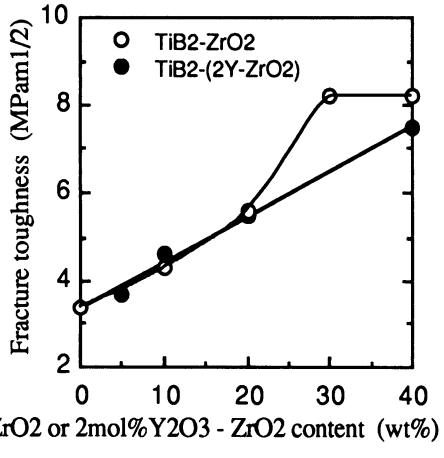

Figure 7. Effect of ZrO_2 or 2mol%Y_2O_3-ZrO_2 content on fracture toughness of TiB_2.

Table 2 The difference of monoclinic-ZrO_2 ratio between the original surface and the fracture surface.

Sample	The ratio of monoclinic-ZrO_2	
	Original surface	Fracture surface
TiB_2 - 10wt%ZrO_2	0.46	0.33
TiB_2 - 20wt%ZrO_2	0.85	0.82
TiB_2 - 30wt%ZrO_2	0.89	0.89
TiB_2 - 40wt%ZrO_2	0.93	0.93
TiB_2 - 10wt%(2Y-ZrO_2)	0.20	0.12
TiB_2 - 20wt%(2Y-ZrO_2)	0.14	0.13
TiB_2 - 40wt%(2Y-ZrO_2)	0.87	0.88

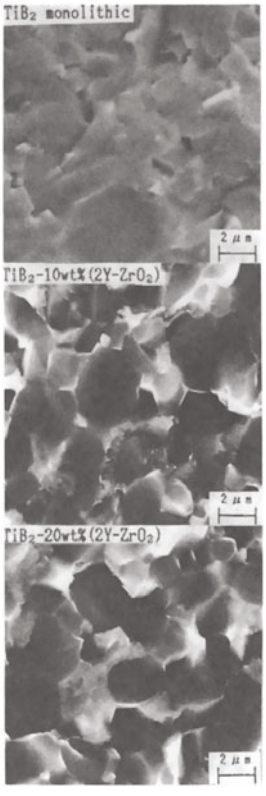

Figure 8. Fracture surfaces of TiB_2 and TiB_2 - (2mol% Y_2O_3-ZrO_2) observed with SEM.

Fracture toughness: The results of fracture toughness tests are shown in Figure 8. Fracture toughness increased with increasing ZrO_2 content. TiB_2 - ZrO_2 was tougher than TiB_2 - (2Y-ZrO_2). The addition of ZrO_2 or 2Y-ZrO_2 was very effective in improving fracture toughness. The 3.5MPam$^{1/2}$ toughness of monolithic TiB_2 increased to 5.5MPam$^{1/2}$ for TiB_2 - 20wt%ZrO_2 and TiB_2 - 20wt%(2Y-ZrO_2), to 8.2MPam$^{1/2}$ for TiB_2 - 30wt%ZrO_2 and to 8.2MPam$^{1/2}$ for TiB_2 - 40wt%(2Y-ZrO_2). Generally, fracture toughness is improved by crack deflection, microcrack and transformation toughening. Figure 9. shows fracture surfaces observed with SEM. The fracture surface of monolithic TiB_2 is flat. However, the TiB_2 - 10-20wt% (2Y-ZrO_2) fracture surfaces were very complex. This suggests crack deflection, which is one method of fracture toughness improvement. Microcrack toughening also contributed to the improvement in fracture toughness, judging from the fact that the fracture toughness of TiB_2 - 40wt%ZrO_2 is higher than that of TiB_2 - 40wt%(2Y-ZrO_2). Contributions to fracture toughness improvement from transformation toughening were not observed. Table 2 shows the difference in the monoclinic ZrO_2 phase ratio between the original surface and the fracture surface. The monoclinic phase ratio should be higher on the fracture surfaces if transformation occurs, although no increase is apparent in Table 2.

Sinterability: As mentioned in the paragraph on density, the addition of 2.5wt%SiC was found to be very effective in improving the sinterability of TiB_2 - 20wt%(2Y-ZrO_2). This phenomenon was strange because the amount of SiC was as low as 2.5wt% and SiC is difficult to sinter by itself. The addition of 2.5wt% SiC is not sufficient to retard the grain growth of TiB_2, but grain growth was well retarded as shown in Figure 2.(b). Figure 10 shows grain boundaries of TiB_2 - 20wt%(2Y-ZrO_2) - 2.5wt%SiC as observed with TEM. A grain boundary phase was observed between the TiB_2 grains. EDAX analysis showedthat this phase consist of Ti and Si. Therefore SiC reacted with TiB_2. A model of this reaction is as follows: SiC reacts with TiO_2 that exists on the surface of TiB_2, creating titanium silicide.

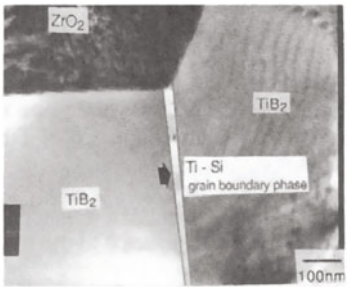

Figure 9. Grain boundary of TiB_2 - 20wt%(2mol%Y_2O_3-ZrO_2) -2.5wt% SiC observed with TEM.

$$TiO_2 + 2SiC \text{ ----- } TiSi_2 + 2CO$$

$TiSi_2$ has a relatively low melting point, at 1526°C and melts at the sintering temperature. TiB_2 and 2Y-ZrO_2 was densified by this liquid phase.

CONCLUSIONS

(1) The addition of ZrO_2 or 2Y-ZrO_2 was very effective in improving the 3-point bend strength of TiB_2. The strength of TiB_2 - 10wt%ZrO_2 and TiB_2 - 10-20wt%(2Y-ZrO_2) HIP'ed specimens were as high as 1160-1200MPa. The 3-point bend strength was dependent on the monoclinic ZrO_2 content in the HIP'ed composite. To obtain high strength HIP'ed materials with strengths greater than 1000MPa, the content of monoclinic ZrO_2 must be less than 10wt%.

(2) The addition of ZrO_2 or 2Y-ZrO_2 was also effective in improving the fracture toughness of TiB_2. The fracture toughness of TiB_2 - 30wt%ZrO_2 was 8.2MPam$^{1/2}$. Crack deflection contributed to the fracture toughness improvement.

(3) The addition of 2.5wt%SiC was very effective in improving the sinterability of TiB_2 - 20wt%(2Y-ZrO_2). TiB_2 - 20wt%(2Y-ZrO_2) - 2.5wt%SiC densified up to 98% of its theoretical density by vacuum sintering at 1700°C. The mechanism of sinterability improvement was thought to be liquid phase sintering.

REFERENCES

1. Finch, C.B., Becher, P.F., Angelini, P., Baik, S., Bamberger, E.and Brynestad, Effect of impurities on densification of submicrometer TiB_2 powders. J., Advanced Ceramics Materials, 1986, **1**, 50-54.
2. Baik, S.and Becher, P.F., Effect of oxgen contamination on densification of TiB_2. J. Am. Ceram. Soc., 1987, **70**, 572-530.
3. Watababe, T. and Tokunaga, Y. Bull. Jpn. Inst. Met., 1986, **25**, 1018-1025.
4. Torizuka, S. and Nishio, H., Fabrication and mechanical properties of TiB_2 - ZrO_2 sintered material. J. Jpn. Soc. Powder and Powder Metallurgy, 1989, **36**, 100-104.
5. Torizuka, S. and Nishio, H., High strength TiB_2. Ceramic Engineering and Science Proc., 1990, **11**, 1454-1460.
6. Torizuka, S. and Nishio, H., Mechanical properties of Titanium Diboride fabricated by HIP. Proc. Fall Meeting Ceram. Soc. Jpn., 1988, 297-298.
7. Torizuka, S. and Nishio, H., Fabrication and mechanical properties of TiB_2 - ($2Y_2O_3$-ZrO_2) sintered material. Proc. Ann. Meeting Ceram. Soc. Jpn., 1989, 408.
8. Torizuka, S. and Nishio, H., Fabrication and mechanical properties of TiB_2 - ($2Y_2O_3$-ZrO_2) - SiC sintered material. Proc. Fall Meeting Ceram. Soc. Jpn., 1989, 530-531.
9. Torizuka, S. and Nishio, H., Effect of SiC on the sinterability and microstructure of TiB_2. Proc. Ann. Meeting Ceram. Soc. Jpn., 1991, 338.
10. Watanabe, T. and Shobu, K., Watanabe, T., J. Am. Ceram. Soc., 1985, **62**, C34-35.
11. Larker, H., Industrial Heating, 1984, Jan., 39-42.
12. Claussen, N., J. Am. Ceram. Soc., 1976, **59**, 49-51.

HIP OF ZnO

Akio Watanabe, Hajime Haneda, Takayasu Ikegami,
Junzou Tanaka, Yusuke Moriyoshi, and Shin-ichi Shirasaki
National Institute for Research in Inorganic Materials
Namiki, Tsukuba-shi, Ibaraki 305
JAPAN

and

Taisei Yamamoto

Hakusui Chemical Industries Ltd., Central Laboratory
KRP Annex, 17-Chudojiminamimachi, Shimogyo-ku, Kyoto 600
JAPAN

ABSTRACT

ZnO was HIPed at 1250^{o}C in Ar for 2h under various pressures from 50MPa to 200MPa. Almost all the pores were eliminated at a pressure higher than 130MPa. The HIPed sample was transparent. The maximum transmittance was 47% at 800nm (0.8mm thick). The grain size increased during HIP. This grain growth may be caused by elimination of pores. The changes of the transmittance and electrical resistance of the samples before and after annealing showed that the effect of reduction during HIP was not so significant.

INTRODUCTION

Zinc oxide is a typical n-type semiconductor[1] and is used for electric devices such as varistors[2] and gas sensors[3]. It is also known that ZnO does not sinter to high density because of its high

volatility[4]. Dense ceramics of ZnO has been requested for electric measurements and for some analyses such as SIMS, STEM etc. We have already reported that HIP is effective to densify Zn-containing compounds[5]. HIP may be also effective to densify ZnO. This study describes HIP of ZnO.

EXPERIMENTAL PROCEDURE

As a starting material, reagent grade zinc oxalate was chosen. It was decomposed at 500°C in O_2 for 2h. In this paper, this zinc oxide is written ZnO-1. For comparison, commercial zinc oxide powder(Hakusui Chemical) which was made by oxidation of metal zinc powder was also HIPed. This zinc oxide is written ZnO-2. The powder characteristics of these materials are shown in Table 1.

For sintering, they were pressed at 30MPa into discs 12mm in diameter and 6mm in length, and then CIPed at 160MPa. Thereafter they were sintered in O_2 for 5h at various temperatures ranging from 1000°C to 1300°C. The highest sintered density obtained was about 94% of theoretical at between 1150° and 1250°C.

The samples pre-sintered at 1250°C were HIPed at 1250°C under various pressure from 50MPa to 200MPa in Ar without any capsul. They were annealed in O_2 at 1000°C for 5h.

For characterization of HIPed samples, microstructure was observed by using a optical micrograph. Light transmittance was determined by a double beam spectrometer (Model 228, Hitachi Ltd.) Electric measurement was done by the DC, 2-terminal method at room temperature using In-Ga electrode.

TABLE 1
Powder characteristicsof ZnO

	ZnO-1	ZnO-2
surface area(m^2/g)	9.7	3.2
average particle size(um)	0.70	0.47
impurities	Si - 20ppm Mg - 10ppm Al - 5ppm Cu - 5ppm	Na - 40ppm Mg - 10ppm Pb - 4ppm

RESULTS AND DISCUSSION

1. Microstructure of HIPed ZnO

Figure 1 shows photomicrographs of ZnO-1 before and after HIP. Table 2 shows their porosity and grain size. Before HIP, there were two kinds of pores. One was a small pore which occupied grain boundary. The other was a large pore which located at grain corner[Figure 1a]. At 50MPa, only the pores occupying grain boundaries were eliminated[Figure 1b]. When the pressure became higher, the porosity became smaller. Almost all the pores were eliminated at a pressure higher than 130MPa[Figure 1d].

The grain size increased during HIP. However, its change does not seem to be affected by pressure. In contrast to this result, the change of grain size of ZnO-2 was very large. Figure 2 shows photomicrographs of ZnO-2 before and after HIP. The average grain size before HIP was about 14μm, and that after HIP (130MPa) was about 150μm. As alkali metals enhance grain growth rate of ZnO[6], such a change of grain size may be caused by sodium which was included in ZnO-2 as a impurity.

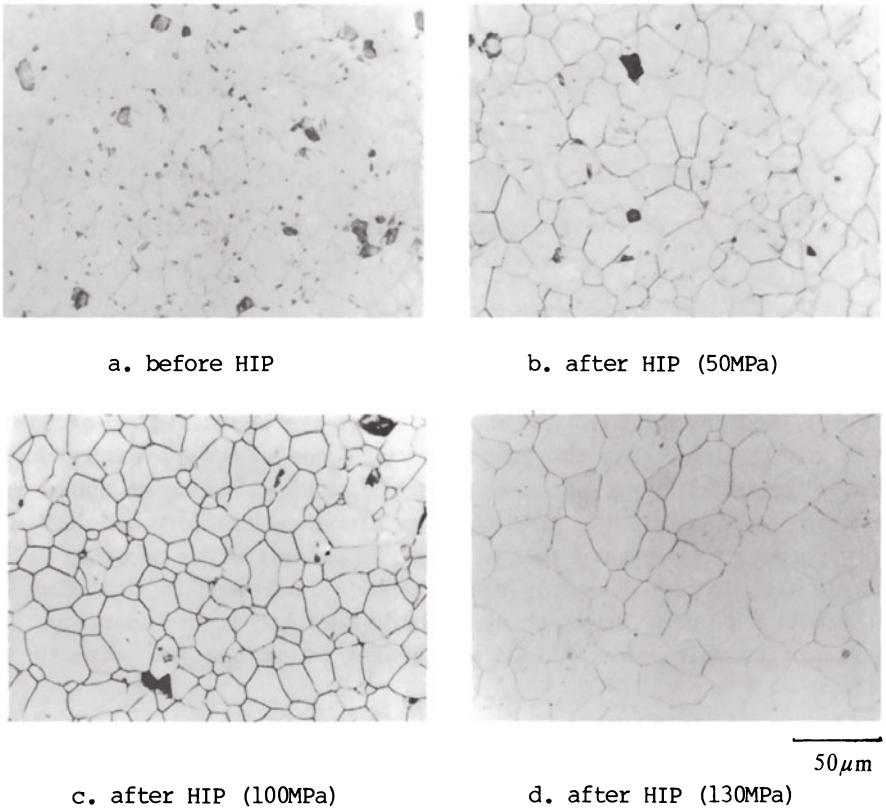

a. before HIP

b. after HIP (50MPa)

c. after HIP (100MPa)

d. after HIP (130MPa)

Figure 1. Photomicrographs of ZnO-1 before and after HIP

TABLE 2
Porosity and grain size of HIPed ZnO-1

Pressure(MPa)	Porosity(%)	Grain size(μm)
before HIP	5.6	19
50	1.5	26
100	0.2	30
130	0.1	36
200	0.1	30

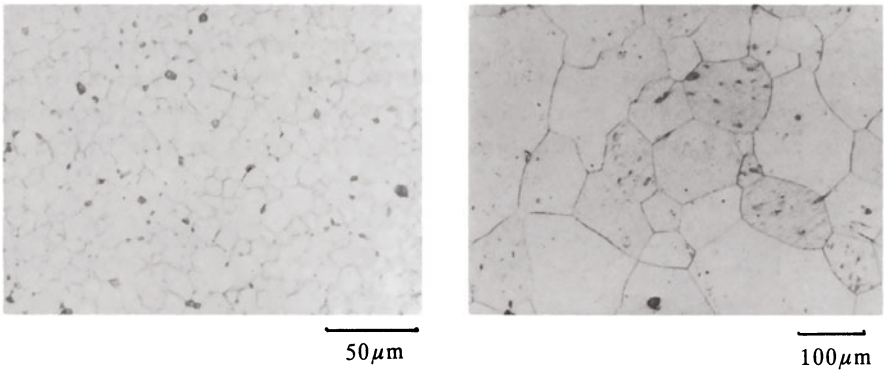

a. before HIP b. after HIP (130MPa)

Figure 2. Photomicrographs of ZnO-2 before and after HIP

2. Transmittance

Figure 3 shows the typical transmittance as a function of wave length (0.8mm thick). The solid line shows the result of the sample HIPed at 130MPa, and the dotted line shows that of the sample HIPed at 50MPa. This result shows that the transparency depended upon pressure during HIP. Figure 4 shows the change of the transmittance at 800mn as a function of pressure. The transmittance increased rapidly near 100 MPa. This change corresponded to the change of porosity. The porosity of the sample also decreased rapidly near 100MPa. These results show that the elimination of pore led to an appreciable increase in transparency. The maximum transmittance obtained was 47% at 800nm and its porosity was 0.1%.

3. Reduction during HIP

To investigate the effect of reduction during HIP, the transmittance of the sample HIPed at 130MPa was measured before and after annealing. Figure 5 shows the transmittance of the sample before and after

annealing. The dotted line shows the result before annealing. The transmittance slightly decreased around 400nm. This result was different from the result of $SrTiO_3$ ceramics[7]. In case of $SrTiO_3$, the transmittance decreased at all wavelength. This differece may be caused by the difference of the formation of defects.

The electrical resistance was also measured before and after annealing. The electrical resistance was about 0.77ohm before annealing and about 2.27ohm after annealing.

The changes of the transmittance and electrical resistance showed that the effect of reduction during HIP was not significant. In this study, the heater unit was made of Pt-Rh wire heating element and alumina-based refractory; No reduction is caused by the unit. The only source which causes reduction during HIP was decrease of oxygen partial pressure in Ar[7].

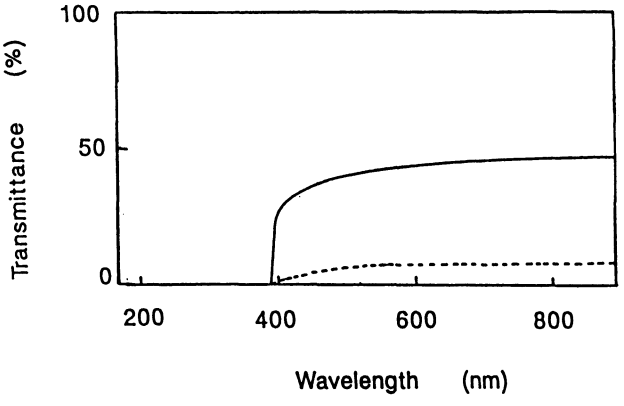

Figure 3. Typical transmittance of HIPed ZnO-1

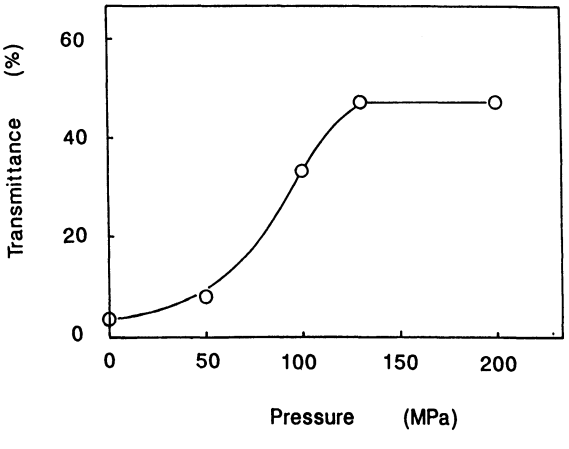

Figure 4. Change of transmittancs at 800nm as a function of pressure

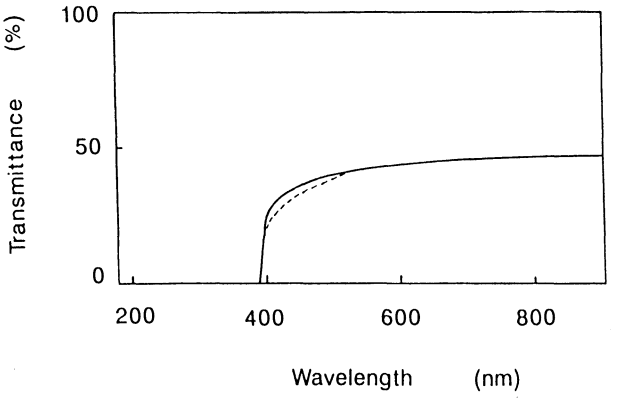

Figure 5. Change of transmittance before and after annealing

REFERENCES

1. W.D.Kingery, H.B.Bowen and D.R.Uhlman, Introduction to ceramics (second edition), John Wiley & Sons, 1976, pp.891-895
2. M.Matsuoka, Nonohmic properties of zinc oxide ceramics, Jap.J.Appl.Phys., 1971, 10, 736-746
3. T.Seiyama, A.Kato, K.Fujiishi and M.Nagatani, A nem detector for gaseous components using semiconductive thin films, Anal.Chem., 1962, 34, 1502-3
4. H.Schaffer and H.Maywald, Untersuchungen uber die Verdampfung von ZnO mit einem hohen Fehlordnungsgrad, Z.Phy.Chem. 1970, B244 289-304
5. A.Watanabe, H.Haneda, Y.Moriyoshi, S.Shirasaki and H.Yamamura, Preparation of Zn_2TiO_4 by co-precipitaion method and hot-isostatic press, J.Mat.Sci., 1989, 24, 2281-2284
6. Y.Moriyoshi, O.Maruyama, T.Ikegami, H.Yamamura, A.Watanabe and S.Shirasaki, Structural defects in hot-pressed zinc oxide, Z.Phy.Chem.Neue Folge, 1980, Bd. 122, 225-235
7. A.Watanabe, H.Haneda, S.Hishita, Y.Moriyoshi, S.Shirasaki and H.Yamamura, Effective oxygen partial pressure during HIP, J.Ceram.Soc.Jap.Int.Edition, 1990, 98, 541-4

CHARACTERISTICS OF HIGH DENSITY NON-MAGNETIC CERAMICS BY HIP

HEIKI HOSHI, SACHIO NAGAYAMA
TOKIN Corp. , Sendai. Miyagi 982. JAPAN

ABSTRACT

High density non-magnetic ceramics have been produced. They have thermal expansion coefficient suitable for ferrites, alloy thin films and amorphous thin films for digital recording heads. The relation between the thermal expansion coefficient and main composition, some additives were investigated. Grain structure, sintering and HIP condition were also investigated. Zn ferrites with the thermal expansion coefficient of 87×10^{-7}/℃, the average grain size of 10μm, and the porosity of 0.02% was obtained at HIP condition of 1150-1170℃ under the pressure of 100MPa. αFe_2O_3 ceramics with the thermal expansion coefficient of 115×10^{-7}/℃, the average grain size of 6μm, the porosity of 0.02% was obtained at HIP condition of 1060- 1080℃ the pressure of 100MPa. MgO-NiO ceramics with the thermal expansion coefficient of 130×10^{-7}/℃, the averge grain size of 4μm, the porosity of 0.05% was obtained at HIP condition of 1320-1340℃ under the pressure of 100MPa.

INTRODUCTION

Magnetic recording heads are used for recording all kinds of informations, such as voice, image, document, etc. Recent developments of magnetic recording techniques have been remarkable, and research is proceeding to obtain a high performance device, a small device, a light weight device with a high memory capacity. For these reasons, the design improve function, to make a device small, and to satisfy to high-reliability is made in order to correspond to the performance of magnetic recording media in the field of the magnetic recording heads.[1,2] For example, the following developments are proceeded steadily. The one is the MIG (Metal in Gap) head, which have both excellent characteristics of high wear resistance of ferrites and metal magnetic materials with high saturation magnetic flux density. The another is the thin film magnetic head, which makes a truck narrow by putting metal magnetic film on a substrate of ceramics. The another is the multilayer head where metal magnetic film is put by means of non-magnetic ceramics. In this way, with high performance magnetic recording heads, not only ferrites but also metal thin film and amorphous are used as magnetic materials for the magnetic recording heads. The materials having the thermal expansion

coefficient corresponding to the magnetic materials are required in the non-magnetic materials consisting of part of a head because of distortion generation and other defects in making conjunction. We have developed the high density non-magnetic materials corresponding to these various magnetic materials by using HIP method, and then discuss about the several characteristics.

EXPERIMENTAL PROCEDURE

Zn ferrites
Raw materials of Fe_2O_3 and ZnO were mixed in a ball mill with distilled water, dried, calcined at 900℃, and then milled. The mixture was granulated by spray dryer, and pressed at 200MPa. The samples were sintered at 1200℃ for 3 hours in air. The presintered samples were HIP' ed at 1130-1190℃ for 2 hours under the pressure of 100MPa.

αFe_2O_3
Three different raw materials of Fe_2O_3 and additives of CeO_2, MgO, ZnO were mixed in a ball mill with distilled water, dried, granulated by spray dryer. The powder was pressed at 200MPa. The samples were sintered at 1100℃ for 3 hours in air. The presintered samples were HIP' ed at 1040-1100℃ for 2 hours under the pressure of 100MPa.

MgO-NiO ceramics
Raw materials of MgO and NiO as the main element, TiO_2 and MnO_2 as the sub-element, and the additives of $CaCO_3$ and Y_2O_3, were mixed in a ball mill, calcined, at 1200℃ and then milled. The mixture was granulated by spray dryer, and pressed at 200MPa. The samples were sintered at 1400℃ for 3 hours in air. The presintered samples were HIP' ed at 1300-1380℃ for 2 hours under the pressure of 20-150MPa.

RESULTS AND DISCUSSION

Zn ferrites
TABLE 1 shows the relation between the composition of Zn ferrites and the secondary phase precipitation. The secondary phase begins to precipitate, if ZnO exceeds 50mol%. If the ZnO amount increases furthermore, the amount of the secondary phase precipitation increases. The ZnO precipitation was confirmed by analyzing result of the secondary phase. It is possible to prepare for the single phase of $ZnFe_2O_4$ by reducing the ZnO amount less than 50mol%. Figure 1 shows the relation between HIP temperature and the relative density, the average grain size of Zn ferrites. Densified Zn ferrites are obtained above 1150℃. On the other hand, average grain size increases largely, as the HIP temperature is close to the sintering temperature. Zn ferrites having the thermal expansion coefficient of 87×10^{-7}℃, the average grain size of 10μm and the porosity of 0.02% was obtained under the HIP temperature of 1150-1170℃ and the pressure of 100MPa.

TABLE 1
Conposition and secondary phase precipitation of Zn ferrites

Fe_2O_3(mol%)	49.0	49.5	50.0	50.5	51.0
ZnO (mol%)	50.0	50.5	50.0	49.5	49.0
Secondary phase precipitation	+++	++	+	-	-

- non-observed
\+ observed in small numbers
\+ + observed
\+++ ovserved in large numbers

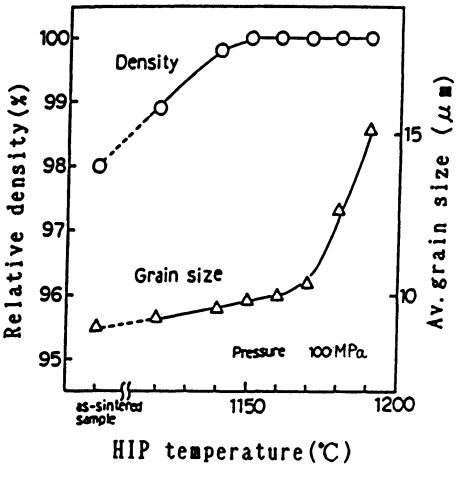

Figure 1. Relation between HIP temperature and relative density, av. grain size of Zn-ferrites.

αFe_2O_3

TABLE 2 shows the purity, impurities and particle size of the used three raw materials. In case of raw materials containing a large amount of impureties, grain growth is easy. Uniformed αFe_2O_3 with a small grain are obtained by using raw material having a low impurity. The average grain size and the relative density become low, by adding additives. CeO_2, MgO and ZnO have grain growth depression effect. Especially, the relative density goes down by adding ZnO. Figure 2 shows the relation between amount of additives (CeO_2, MgO, ZnO)and initial permeability of sintered αFe_2O_3. When using the MgO as an additives, the initial permeability increases as its amount increases. Its reason can be thought in this way that spinel phase of $MgFe_2O_4$ generates because of MgO addition. The most suitable additive and its amount is 0.2-0.5wt% CeO_2.

Figure 3 shows the relation between the HIP temperature and the relative density, the average grain size. αFe_2O_3 having the thermal expansion coefficient of $115\times10^{-7}/℃$, the average grain size of 6μm and the porosity of 0.02% was obtained under the HIP temperature of 1050-1070℃ and the pressure of 100MPa.

TABLE 2
Analysis of raw material of Fe_2O_3

Raw material	Fe_2O_3(%)	SiO_2(%)	CaO(%)	MnO(%)	B.E.T(μm)
A	99.2	0.003	0.003	0.006	0.15
B	99.3	0.005	0.006	0.16	0.3
C	99.3	0.004	0.001	0.03	0.15

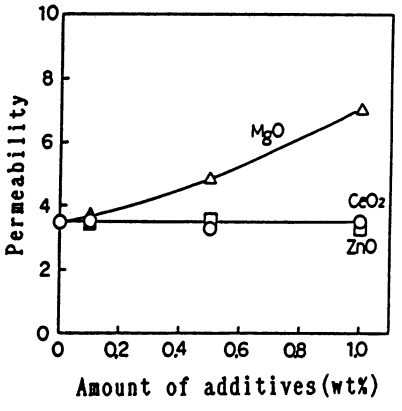

Figure 2. Relation between amount of additives and permeability of αFe_2O_3.

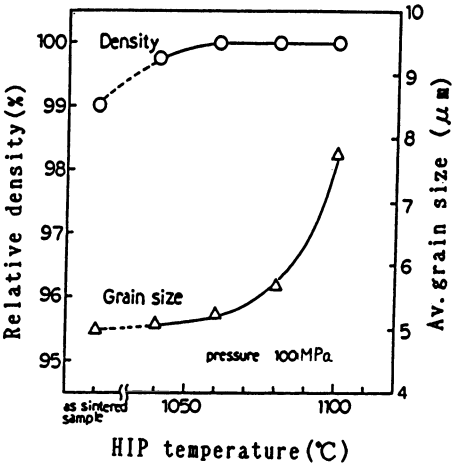

Figure 3. Relation between HIP temperture and relative density, av. grain size of αFe_2O_3.

MgO-NiO ceramics

Figure 4 shows the relation between MgO-NiO composition and the thermal expansion coefficient. The thermal expansion coefficient increases as NiO composition increases. Figure 5 shows the relation between the HIP temperature and the relative density, the average grain size. Figure 6 shows the relation between the HIP pressure and relative density, average grain size. MgO-NiO ceramics having the thermal expansion coefficient of $130\times10^{-7}/℃$, the average grain size of 4μm and the porosity of 0.05% was obtained at HIP condition of 1320-1340℃ and the pressure of 100MPa.

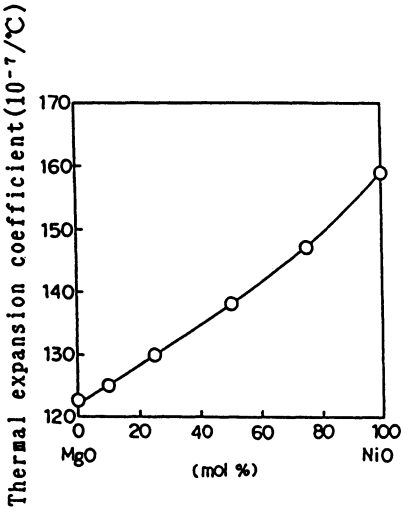

Figure 4. Relation between MgO-NiO composition and thermal expansion coefficient of MgO-NiO ceramics.

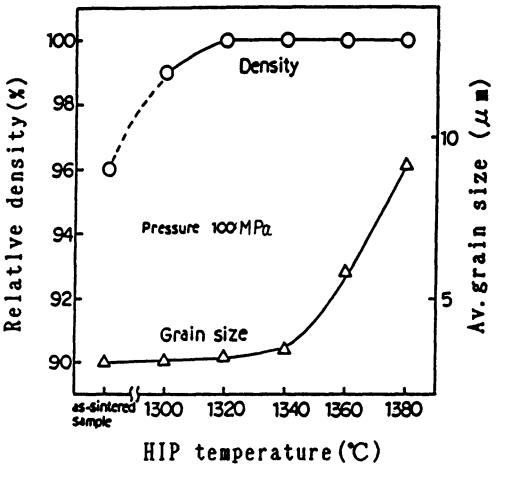

Figure 5. Relation between HIP temperature and relative density, av. grain size of MgO-NiO ceramics.

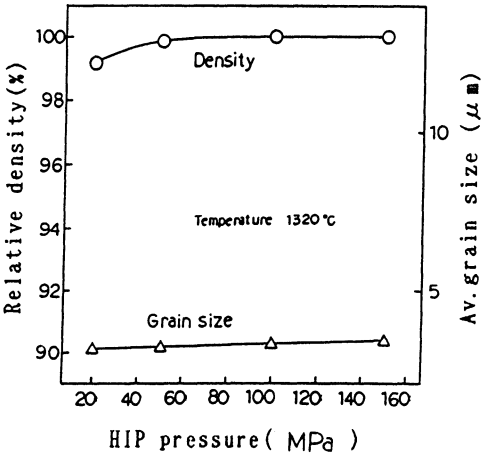

Figure 6. Relation between HIP pressure and relative density, av. grain size of MgO-NiO ceramics.

CONCLUSION

We have developed the high density non-magnetic ceramics having the thermal expansion coefficient corresponding to the magnetic materials for the magnetic recording heads by means of HIP method.

TABLE 3 shows the various properties of high density non-magnetic ceramics.

TABLE 3
Various properties of high density non-magnetic ceramics

Item	Zn ferrites	αFe_2O_3	MgO-NiO ceramics
Vickers hardness	650	900	800
Bending strength(kg/mm^2)	14	30	22
Average Grain size(μm)	10	6	4
Density(g/cc)	5.3	5.2	4.5
Thermal expansion coefficient($\times 10^{-7}$/℃)	87	115	130
Resistivity(Ωcm)	10^2	10^{10}	10^8
Porosity(%)	0.02	0.02	0.05

Zn ferrites
The single phase of $ZnFe_2O_4$ was obtained under the condition of less than 50mol%ZnO. The high density Zn ferrites having the thermal expansion coefficient of 87×10^{-7}/℃, the average grain size of 10μm and the porosity of 0.02% was obtained under the HIP temperature of 1150-1170℃ and the pressure of 100MPa.

αFe_2O_3
The uniformed αFe_2O_3 having small grain was obtained by using law material containing a small amount of impurities by adding 0.5wt%CeO_2. The high density αFe_2O_3 having the thermal expansion coefficient of 115×10^{-7}/℃, the average grain size of 6μm and the porosity of 0.02% was obtained under the HIP temperature of 1050-1070℃ and the pressure and the pressure of 100MPa.

MgO-NiO ceramics
It was found that the thermal expansion coefficient increased as NiO composition increased. TiO_2, MnO_2, CaO and Y_2O_3 are effective for making 75MgO-25NiO ceramics densified and for controlling the grain growth.
The high density MgO-NiO ceramics having the thermal expansion coefficient of 130×10^{-7}/℃, the average grain size of 4μm and the porosity of 0.05% was obtained under the HIP temperature of 1320-1340℃ and the pressure of 100MPa.

ACKNOWLEDGMENTS

We are grateful to Mr. M. Takeuchi, Mr. M. Okabe for helpful and useful discussions in this work.

REFERENCES

1) S. Ohara, Y. Koshimoto, and T. Kita, Ferrites(1980)690.
2) H. Shibaya, H. Kitayama, H. Abe, and A. Nagura, Ferrites (1980)685.

DENSITY AND REFRACTIVE INDEX OF DENSIFIED SILICA GLASS

Naoyuki Kitamura, Yutaka Toguchi*, Shigeki Funo*, Isao Kondoh, and Hiroshi Yamashita
Government Industrial Research Institute Osaka
1-8-31, Midorigaoka, Ikeda, Osaka 563, JAPAN
*Osaka Electro-Communication University
1-18, Hatsumachi, Neyagawa, Osaka 572, JAPAN

ABSTRACT

Silica glasses with the OH content about 1200ppm and 100ppm have been densified with a HIP apparatus at temperatures of 1000-1300^{o}C under pressures of 100-200MPa for 2 hours. The density of both glasses increases in proportion to the pressure at a fixed temperature. Under a fixed pressure, the density increases with the increase of temperature up to about 1100^{o}C and reaches at constant values. The temperature to attain the constant density is slightly lower in the high-OH glass than in the low-OH glass, because the OH species decrease the viscosity of glass. Refractive index increases almost linearly with the increase in density with the same slope for both glasses. The relationship is explained well by the extended point dipole theory.

INTRODUCTION

When crystals are submitted to high pressures, they show continuous and reversible increases in density but phase transitions may occur. Contrary to this behaviour, glasses show gradual structural reconstructions resulting in increased density even after the release of pressure. Optical properties of densified glass have been studied by many authors[1-3]. Specifically the refractive index increases with the increase in density. This would give us a method to control the refractive index other than the traditional annealing method using thermal processes. This new method is superior to the traditional method due to the wide range of the refractive

index values attainable and the shorter time to reach a target value.

Silica glass is the simplest glass in the silicate glasses and is most suitable for studying the process of densification under the high pressure. The glass is used widely as a UV-transmitting glass for its excellent durability against the UV light[4]. A UV-transmitting glass, which has a different refractive index than silica glass, is needed on a compensation of the aberration in a UV lens system. However, there are no glasses which have good transparency and durability like a silica glass. Therefore, silica glass has been densified by hot isostatic pressing for the purpose of improvement of refractive index. Moreover, the relationship between density and refractive index has been investigated with the view of controlling the refractive index by density.

MATERIALS AND PROCEDURES

Silica glasses synthesized by the direct(CVD) and soot(VAD) method were used. The OH content in the CVD and VAD glasses was ∿1200ppm and ∿100ppm, respectively. Cubic glass blocks of 40mm edge length were densified with a hot isostatic pressing apparatus (Autoclave Engineers, IsoHIPPER) in argon gas at temperatures of 1000-1300^{o}C under pressures of 100-200MPa for 2 hours. The operating conditions for each glass sample are listed in the left column of table 1.

TABLE 1
Operating conditions of HIP for each sample. The density and refractive index are measured at 25.0^{o}C.

Condition			Sample			
Press. (MPa)	Temp. (^{o}C)	Time (hrs.)	direct(CVD)		soot(VAD)	
			ρ(g/cm^3)	n(248nm)	ρ(g/cm^3)	n(248nm)
0.1	1200	2	2.2001	1.508921	2.2019	1.509067
100	1200	2	2.2091	———	2.2109	———
150	1200	2	2.2134	1.511778	2.2149	1.512014
200	1200	2	2.2170	1.512783	2.2192	1.512873
150	1000	2	2.2047	———	2.2103	———
150	1100	2	2.2135	1.511831	2.2137	1.511834
150	1300	2	2.2126	———	2.2148	———

The densified blocks were cut and ground into 60^{o} prisms with the faces of 30mm square. The faces were polished to flat within $\lambda/4$. Although the argon gas diffuses into silica glass under the high pressure and temperature[5], the Ar content inside the prism cut from the block is negligibly small, because the profile of the Ar content was observed to decrease in a way of exp(-t/100) against the removed thickness t(μm) from the surface by using a fluorescence X-ray spectrometer (Rigaku, 3370). Optical homogeneity of the prism was proved to be better than $\Delta n=\pm 1\times 10^{-6}$ cm^{-1} from the observation with an interferometer.

Density of the prisms was measured by the Archimedes method within an error of $\pm 3\times 10^{-4} g/cm^{3}$. Refractive index was measured by the minimum-deviation method with a precision spectrometer (Gaertner, L-124) equipped with a mercury lamp as a light source and with a photomultiplier as a light detector[6,7]. Refractive index was determined in the Visible and UV regions, and also at 248nm. Temperature of the prism was controlled at $25.0\pm 0.3^{o}C$, because silica glass shows a temperature dependence of refractive index as large as 1.5×10^{-5} $^{o}C^{-1}$ in the UV region[8]. Total errors arising from these experimental conditions did not exceed $\pm 1\times 10^{-5}$.

RESULTS

Density and refractive index are listed in the right column of table 1. Figure 1 shows the density of the glasses densified

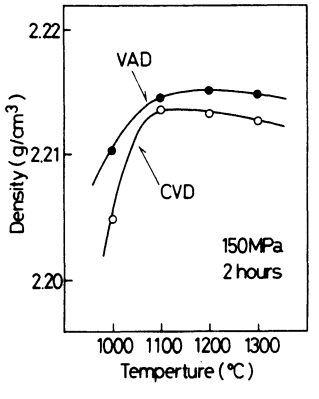

Figure 1. Density of silica glasses under the pressure of 150MPa versus the operating temperature.

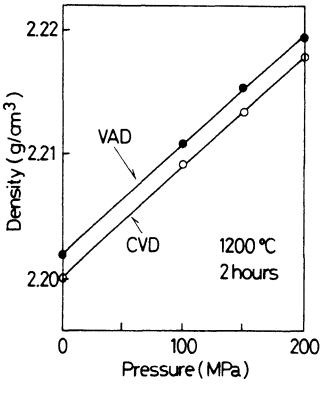

Figure 2. Density of silica glasses under the temperature of $1200^{o}C$ versus the operating pressure.

under 150MPa versus the operating temperature. The density increases with the increase of the pressing temperature up to about 1100°C and reaches at a constant value above the temperature for both(CVD and VAD) glasses. When the temperature is kept at 1200°C, the density increases with the increase of the applied pressure for both glasses as shown in figure 2. The density of the CVD glass is slightly lower than that of the VAD glass at each operation as shown in figures 1 and 2.

Refractive index increases almost linearly with the increase in density for both glasses as shown in figure 3. The refractive index and density of the CVD glass were slightly smaller than those of the VAD glass on each HIP operation.

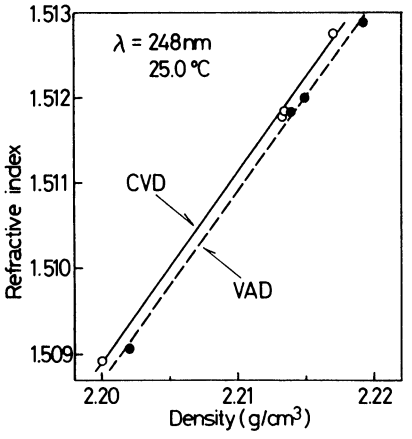

Figure 3. Refractive index and density for the CVD glass(o) and the VAD glass(●). The solid(CVD) and dashed(VAD) lines are the fitting results by using the extended point dipole theory.

DISCUSSIONS

The density of both silica glasses saturates above 1100°C as shown in figure 1. This saturation will be due to the decrease of viscosity, because the saturation temperature agrees well with the annealing point of silica glass around 1100°C[9]. Above the annealing point, the reconstruction of glass structure would bring the glass to a stable state of high density, whereas below the annealing point, the relaxation to the original density would take place due to the elastic property of the glasses. This is the reason why the density saturates above the temperature of 1100°C. On the other hand,

a slight difference of saturation points between the CVD and VAD glasses can be due to the difference of the OH content, because the OH species are believed to decrease the viscosity.

Above the annealing point, the density increases with the operating pressure in a linear relation as shown in figure 2. This behaviour is quite similar to the compression of a liquid or a gas and can be explained by the packing of molecules into a unit volume. There is no catastrophic break down of glass network up to this pressure.

Refractive index increased almost linearly with the increase of density as shown in figure 3. The relationship between density and refractive index was explained well by Arndt and Hummel[10] by following formula:

$$\frac{n^2-1}{4\pi+b(n^2-1)} = \frac{\alpha}{M}\rho \ , \qquad (1)$$

where α, b and M are molar polarizability, overlap parameter and molar weight of SiO_2, respectively. Molar polarizability α and overlap parameter b are adjustable parameters. This formula becomes equivalent to the Lorentz-Lorenz(ideal point dipole model) or the Newton-Drude(continuum model) formula when the parameter $b=4\pi/3$ or $b=0$, respectively. This formula was fitted to experimental data by a least square method. The results are shown in figure 3 by a solid(CVD) and a dashed(VAD) lines. The overlap parameter b values of 1.60 and 1.56 can explain the data well for the CVD and VAD glasses, respectively. Therefore, the refractive index is determined uniquely by the number of molecules in a unit volume. This behaviour is consistent with the relation between the density and the operating pressure. On the other hand, the b value of 1.60 or 1.56 is obviously different from that of 1.3 obtained by Arndt and Hummel from the measurement of refractive index at 589nm(Na-D line). This difference cannot be due to the difference of the wavelength in the measurement of refractive index, because the overlapping of the electron distribution is independent of the wavelength of light. The possible reason would arise from the difference in the operating temperature. In their experiment, glass was densified at the temperature up to 800^{o}C, while in ours it was done above 1100^{o}C. Several kinds of defects can be induced during the densification process. However, the defects will vanish by the reconstruction of glass structure above the annealing point. On the other hand, the defects will remain in the glass if it

is operated below the annealing point and may affect the electronic states through which refractive index can vary. Therefore, the difference is probably due to the defects in the glass.

CONCLUSION

The refractive index increases with the increase in density. The relationship between refractive index and density can be explained well by the extended point dipole theory as described by formula (1). Therefore, refractive index of silica glass can be controlled by densifying it without adding any other materials. Moreover, this method can be applied to gradient refractive index materials, for example, rod lenses, optical fibers and so on.

REFERENCES

1. Cohen, H.M. and Roy, R., Densification of glass at very high pressure.
   Phys. Chem. Glasses, 1965, **6**, 149-161.
2. Arndt, J. and Stoffler, D., Anomalous changes in some properties of silica glass densified at very high pressures
   Phys. Chem. Glasses, 1969, **10**, 117-124.
3. Williams, Q. and Jeanloz, R., Spectroscopic evidence for pressure-induced coordination changes in silicate glasses and melts.
   Science, 1988, **239**, 902-05.
4. Bruckner, R., Properties and structure of vitreous silica.
   J. Non-Cryst. Solids, 1970, **5**, 123-175.
5. Faile, S.P. and Roy, R., Strengthening of glass by high-pressure Ar impregnation.
   J. Am. Ceram. Soc., 1971, **54**, 532.
6. Hayakawa, J., Kitaoka, T., Yamashita, H. and Iwasa, M., Bulletin of the Government Industrial Research Institute Osaka, 1975, **26**, 266.
7. Kitamura, N., Hayakawa, J. and Yamashita, H., Optical properties of fluoroaluminate glasses in the UV region.
   J. Non-Cryst. Solids, 1991, **126**, 155-160.
8. Malitson, I.H., Interspecimen comparison of the refractive index of fused silica.
   J. Opt. Soc. Am., 1965, **53**, 1205-09.
9. Elmer, T.H. and Nordberg, M.E., Corning Research, 1961,225.
10. Arndt, J. and Hummel, W., The general refractivity formula applied to densified silicate glasses.
    Phys. Chem. Minerals, 1988, **15**, 363-69.

MICROSTRUCTURE DESIGNING OF HYDROXYAPATITE CERAMICS BY HIP POST-SINTERING

KOJI IOKU* and MASAHIRO YOSHIMURA
Res. Lab. Engineering Materials, Tokyo Institute of Technology
4259, Nagatsuta, Midori, Yokohama 227, Japan
*Now with Res. Lab. Hydrothermal Chemistry, Faculty of Science
Kochi University, 2-5-1, Akebono, Kochi 780, Japan

ABSTRACT

Microstructure-designed hydroxyapatite ceramics were prepared by HIP post-sintering. Hydroxyapatite single crystals of about 25 nm × 90 nm in size synthesized hydrothermally at 200 °C under 2 MPa for 10 h were sintered normally in air for 3 h. The obtained ceramics were HIP'ed at the temperatire from 900° to 1100 °C under 200 MPa of Ar for 1 h without any capsules. This post-sintering brought about densification up to nearly 100% for the samples more than 90% dense having closed pores. The fully dense ceramics with a grain size of about 0.54 μm showed transparency. Furthermore, dense/porous layered hydroxyapatite ceramics could be prepared by the same technique from the fine crystals and coarse powders with relatively low sinterability.

INTRODUCTION

Hydroxyapatite ($Ca_{10}(PO_4)_6(OH)_2$; HAp) ceramics have long been investigated and used as tooth roots and bone implant materials because of HAp's bio-compatibility due to similarity to natural tooth and bone mineral. Implant materials require not only bio-compatibility but mechanical strength and porosity to promote the connection with tissues [1, 2] . Therefore micro-structure designing, i.e., grain size, pore size and porosity et al. is necessary to be tailored in the application as bioceramics. The present work deals with the preparation of transparent HAp ceramics and dense HAp ceramics on porous layer (dense/porous HAp) by HIP post-sintering.

MATERIALS AND METHODS

Fine single crystals of HAp were prepared by hydrothermal treatment of a precipitate from solutions of $Ca(NO_3)_2$ and $(NH_4)_2HPO_4$ at 200 °C under 2 MPa for 10 h [3, 4] . The crystals were pressed isostatically (CIP) under 200 MPa for 5 min into disks. When dense/porous layered ceramics were prepared, the HAp single crystals and commercial HAp coarse powders with relatively low sinterability (BN grade, Central Glass Co., Ltd., Tokyo) were molded in layers without any operation such as mixing, then CIP'ed into disks. These disks were sintered normally in air for 3 h, then the disks were post-sintered by a hot isostatic pressing (HIP; Model Dr. HIP, Kobe Steel, Tokyo) at the temperature from 900° to 1100 °C under 200 MPa of Ar for 1 h without any capsules.

The produced phases were identified by powder X-ray diffractometry (XRD). Lattice parameters were determined by the precise angle-measurements corrected by the lattice parameter of standard Si with a least-square method. Crystallite sizes were calculated by the Sherrer's formula. The morphology of HAp particles was observed with a transmission electron microscope (TEM). Infrared (IR) spectra were measured by KBr method. The Ca/P ratio of HAp was analyzed by a standard EDTA titration for Ca^{2+} and the phosphorus-molybdate method for PO_4^{3-} . Sinterability of HAp powders was evaluated by dilatometry during sintering. The relative density of disks was calculated against the theoretical density (3.16 g/cm^3). The grain shape of the HAp ceramics were observed by a scanning electron microscope (SEM). Vickers hardness and fracture toughness were estimated by the indentation microfracture method [5] .

RESULTS AND DISCUSSION

Properties of Starting Powders

TEM observation of the HAp synthesized hydrothermally indicated uniform and nonaggregated particles [3, 4] . The particles had hexagonal prismatic shape of about 90 nm in length with a median aspect ratio of 3.8. The sizes of the particles agreed completely with crystallite sizes measured by XRD, therefore the particles can be

regarded as well-crystallized single crystals. Lattice parameters of the HAp (a = 0.9420 nm, c = 0.6880 nm) were in good agreement with the values of previous investigations [6] . The chemical analysis gave a Ca/P ratio of 1.67 being identical with the correct HAp stoichiometry (Ca/P = 1.67). The HAp single crystals had a high sinterability. According to dilatometry, densification started at about 800 °C to result in linear shrinkage of about 16% at 1100 °C. TEM observation of commercial HAp coarse powders indicated aggregated grains consisted of needle-like shaped particles of about 1 to 5 μm in length. No phases other than HAp were revealed by XRD. The Ca/P ratio was 1.67 by the chemical analysis. The commercial HAp powders had a lower sinterability than the HAp crystals. Densification started at about 1000 °C to result in linear shrinkage of about 2 % at 1100 °C.

Transparent HAp Ceramics

The HAp ceramics normally sintered at 900 °C for 3 h had a relative density of 60% with homogeneous pore distribution. The grain size was about 0.5 μm, which was almost same as that of pores. The HAp ceramics sintered at 1050 °C for 3 h in air had more than 90% density with few pores and the median grain size of 0.52 μm. The post-sintering at 1000 °C for the ceramics more than 90% dense having closed pores brought about further densification up to nearly 100% density to yield transparent ceramics (Fig.1), but barely increased the density of samples with lower density (Table 1).

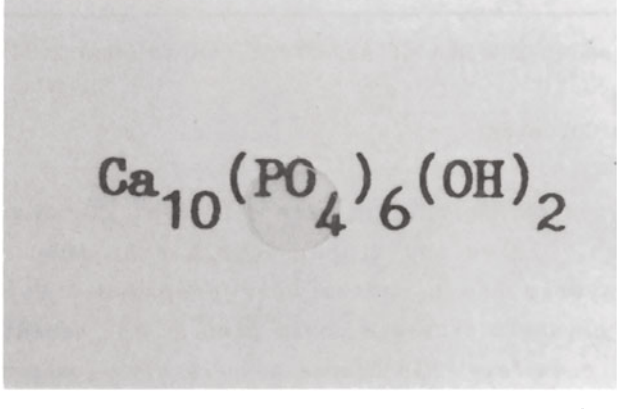

Figure 1. Post-sintered HAp ceramics by HIP at 1000 °C under 200 MPa of Ar for 1 h, after normal sintering in air at 1050 °C for 3 h.

Vickers hardness of the HAp ceramics was increased by post-sintering due to significant densification to result in 6.3 GPa, which is a highest value for pure HAp ceramics reported previously [7] . The grain size of the HIP'ed ceramics was almost same as that of the ceramics before HIP'ing. The grain growth was gradual until 1100 °C, but become rapid above that temperature. IR spectra showed very sharp adsorption band at 3570 cm^{-1} of OH^- for the sample post-sintered at 1000 °C, whereas those for the sample post-sintered at the temperature above 1100 °C are reduced in intensity. These dehydrated samples can be regarded as oxyhydroxyapatite with vacancies located on OH^- sites [8] . Thus the post-sintering of HAp must be carried out at the lower temperature than 1100 °C. Transparent HAp ceramics can be applied to a percutaneous device [9] .

Table 1

Properties of post-sintered hydroxyapatite.

Normal sintering	Post-sintering*	Relative Density/%	Hv** GPa	K_{Ic}** $MPam^{1/2}$	Remarks
900 °C, 3h	----------	60.0	2.7	---	
1050 °C, 3h	----------	90.0	4.1	1.2	
1050 °C, 3h	900 °C, 1h	99.3	6.0	1.1	
1050 °C, 3h	1000 °C, 1h	>99.9	6.3	1.1	Transparent
1050 °C, 3h	1100 °C, 1h	>99.9	6.1	1.1	Transparent
1100 °C, 3h	----------	97.2	5.4	1.2	
1100 °C, 3h	1000 °C, 1h	>99.9	6.0	1.1	Transparent

*post-sintered under 200 MPa of Ar, ** Vickers: Load 2.94 N

Dense/Porous HAp Ceramics

When two types of HAp powders with different sinterabilities were molded in layers, CIP'ed and sintered in air at 1050 °C for 3 h, dense/porous layered HAp ceramics were prepared. Hydrothermally synthesized HAp crystals provided dense part of the ceramics with >90% density, and the commercial HAp coarse powders with lower sinterability provided porous part of the ceramics with 56% density. The post-

sintering at 1000 °C brought about further densification for the ceramics of more than 90% dense having closed pores up to nearly 100% density. The dense part of the ceramics showed transparency with the median grain size of 0.54 μm, while the porous part of the ceramics remained unchanged with about 43% porosity and the pore size of about 1 $\sim$10 μm (Fig.2). That is, only the dense layer of the ceramics became denser by the post-sintering. Microstructure-designed ceramics on the porous part with controlled pore shape, size and porosity can be prepared by using other HAp powders with appropriate particle shape, size and sinterability. Vickers hardness of the interface between the dense part and the porous part of the dense/porous layered HAp ceramics was about 3.3 GPa. The hardness on the porous part of the ceramics was unchanged after post-sintering. The hardness on the dense part of this ceramics was increased by the post-sintering, but fracture toughness was unchanged after the post-sintering (Table 1). Unfortunately, mechanical properties of pure HAp ceramics, especially their low toughness preclude their use for many hard-tissue prosthetic applications. The authors have reported that HAp ceramics could be toughened by zirconia dispersion [10, 11] and/or whiskers dispersion [12]. Therefore tougher HAp ceramics can be prepared by ZrO_2 particles and/or Si_3N_4 whiskers dispersion into the dense part. The dense/porous layered HAp ceramics can be expected to have good bonding-osteogenesis with adequate mechanical properties.

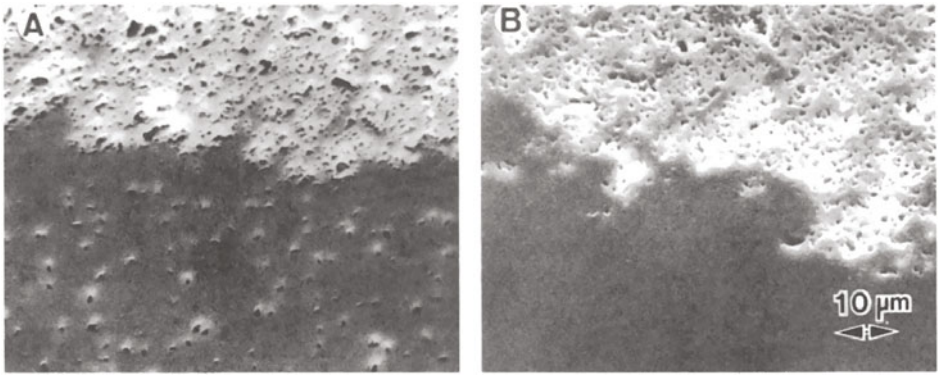

Figure 2. SEM photographs of the polished and thermally-etched cross section of dense/porous HAp ceramics. (a) before HIP'ing (normal sintering at 1050 °C for 3 h) and (b) after HIP'ing at 1000 °C under 200 MPa of Ar for 1 h.

CONCLUSIONS

The results described in this paper allow to draw the following conclusions. (1) Post-sintering by HIP without any capsuls produce a good effect on densification of HAp ceramics with over 90% density. (2) Transparent HAp ceramics were prepared by post-sintering at 1000 °C under 200 MPa of Ar for 1 h. (3) Dense/Porous layered HAp ceramics were also prepared by the post-sintering.

REFERENCES

1. Kurosawa, H., Shibuya, K., Murase, K., Sato, S., Masujima, A., Bessatsu Seikei Geka (Orthopedic Surgery) No.8, ed. Masumi, S., Nankodo, Tokyo, 1985, pp.58-63.
2. Hori, M., J. Jpn. Soc. Biomaterials, 1990, 8, 11-22.
3. Ioku, K., Yoshimura, M. and Sōmiya, S., Nippon Kagaku Kaishi (J. Chem. Soc. Japan), 1988, 1565-70.
4. Sōmiya, S., Ioku, K. and Yoshimura, M., Mater. Sci. Forum, Vol. 34-36, ed. Sorrell, C.C. and Ben-Nissan, B., Trans Tech Publications Ltd., Switzerland, 1988, pp. 371-8.
5. Niihara, K., Ceramics Japan, 1985,20, 12-18.
6. Eysel, W. and Roy, D.M., J. Crystal Growth, 1973, 20, 245-50.
7. Hirayama, Y., Ikata, H., Akiyama, H., Naganuma, K., Ojima, S. and Kawakami, M., Sintering '87, Vol.2, ed. Sōmiya, S., Shimada, M., Yoshimura, M. and Watanabe, R., Elsevier Applied Science, Tokyo, 1988, pp. 1332-7.
8. Kijima, T. and Tsutsumi, M., J. Am. Ceram. Soc., 1979,62, 455-60.
9. Shin, Y. and Aoki, H., Bioceramics; Development and Clinical Applications, ed. Aoki, H. and Niwa, S., Quintessence, Tokyo, Berlin, Chicago, London, Sao Paulo, Hong Kong, 1987, pp. 175-9.
10. Ioku, K., Yoshimura, M. and Sōmiya, S., Biomaterials, 1990, 11, 57-61.
11. Ioku, K., Sōmiya, S. and Yoshimura, M., Seramikkusu Ronbunshi (J. Ceram. Soc. Jpn.) 1991, 99, 196-203.
12. Ioku, K., Noma, T., Ishizawa, N. and Yoshimura, M., ibid., 1990, 98, 1337-42.

DIRECT OBSERVATION ON THE PORE ELIMINATION DURING HIP

JIN-YOUNG KIM, NOZOMU UCHIDA, ZENJI KATO, AKIRA MIYAMOTO* and
KEIZO UEMATSU
Department of Chemistry
Nagaoka University of Technology
Kamitomioka, Nagaoka, Niigata, Japan 940-21
*Advanced Technology Research Center, Nippon Kokan Steel
Minamiwatarida-cho, Kawasaki, Kawasaki, Kanagawa, Japan 210

ABSTRACT

Changes of pore size and shape during encapsulation HIP was examined directly with the novel liquid immersion technique, which can reveal great details of micro-structure and characterize flaw-forming defects of micron-size in undensified specimens. The results were supplemented by the pore size measurement with the mercury porosimetry, and compared to the corresponding results for normal sintering. The behavior in the change of pore size and shape was different in HIP and normal sintering. Elimination of large pores of micron-size starts from the beginning of densification in HIP, whereas it does not start in initial stage of densification in normal sintering. The shape of large pores changes drastically in HIP, but hardly changes in normal sintering. These observations were discussed in terms of current sintering theory.

INTRODUCTION

Elimination of processing defects is one of the most important objectives in hot isostatic pressing technique. Drastic improvement of properties is reported in many materials[1]. Apart from the practical success, we have limited and indirect understanding on the behavior of processing defect during hot isostatic pressing; On the pore shrinkage, the effectiveness of hot isostatic pressing is evaluated mostly through the density achieved. This parameter represents the average property, and provides no information on the characteristics of individual pores. Direct studies have been reported only for the removal of large artificial pores in the final stage of densification[2]. No direct study is reported on the pore

shrinkage during the initial stage of densification nor the behavior of natural pore in capsule hot isostatic pressing. A strong obstacle against the attempt of direct study has been the difficulty involved in the characterization of pores. Recently, we removed this difficulty by developing a unique method to be used for characterizing pores in green/low- density bodies[3]. The method was successfully applied to show the direct relationship between forming pressure and structure of the green body. The objective of the present study is to understand the behavior of large processing pores during the initial densification of capsule hot isostatic pressing. The present paper will be followed by another investigation which directly examines the removal of pores in the final stage of densification during capsule hot isostatic pressing.

EXPERIMENT

Active alumina powder granules* were used as starting material. The granules were molded into bars (15mm x 15mm x 80mm) at 10 MPa and isostatically pressed at 300MPa. After heating at 600^{o}C for 1 h in air for binder removal, the specimen was coated with BN powder and placed in a glass capsule. The capsule was evacuated for 1 h at 600^{o}C and sealed. The encapsulated specimen was hot isostatically pressed in a commercial equipment at 800^{o}C for 1h at 80MPa. Another specimen compact was normally sintered at 1150^{o}C for 1h. The internal structures of green, normally sintered and hot isostatically pressed bodies were characterized with the same immersion liquid technique[3] with bromonaphthalene as an immersion liquid. The specimen was thinned to 0.3 mm on sand paper and made transparent by the immersion liquid. An optical microscope in transmission mode was used for characterizing defects. The microstructure of the specimen was also examined with SEM on fractured surface. Density of specimen was measured with Archimedes method. Mercury porosimetry was used to characterize pore size distributions.

RESULTS

The densities of green, normally sintered and hot isostatically pressed bodies were 59.4, 75.3 and 75.5% of theoretical, respectively. The approximately equal densities for the latter two specimens simplify the

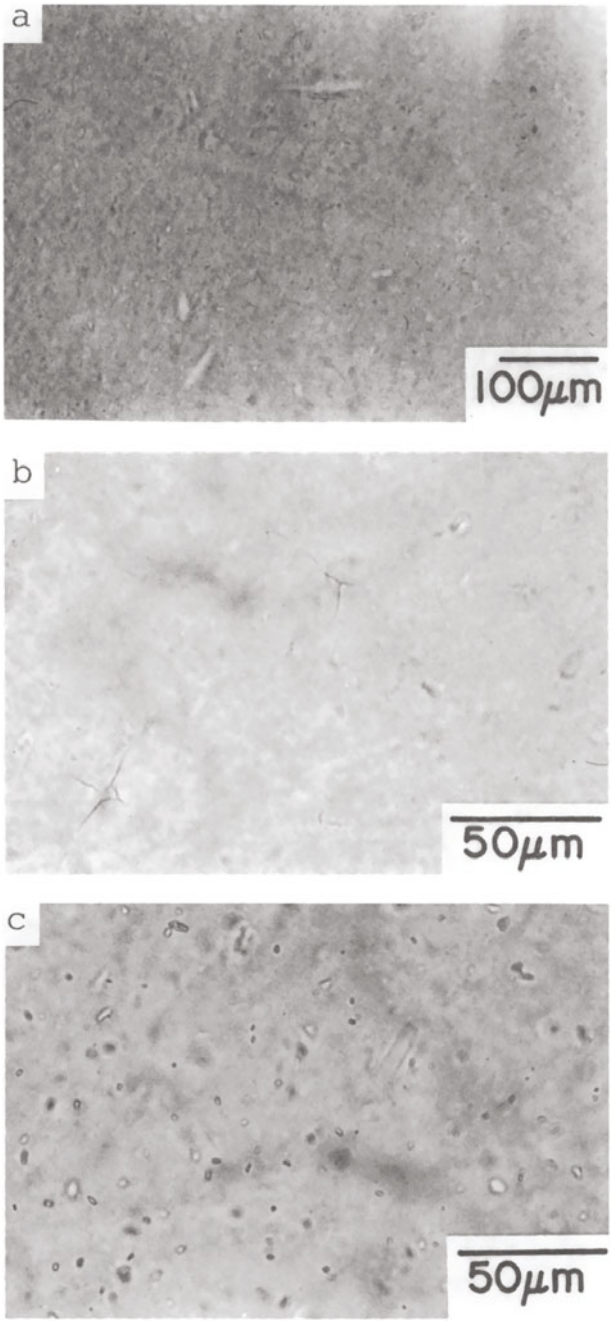

Figure 1. Internal structures of specimens examined with the liquid immersion technique
(a) Green body, (b) Sintered body, (c) Hot isostatically pressed body

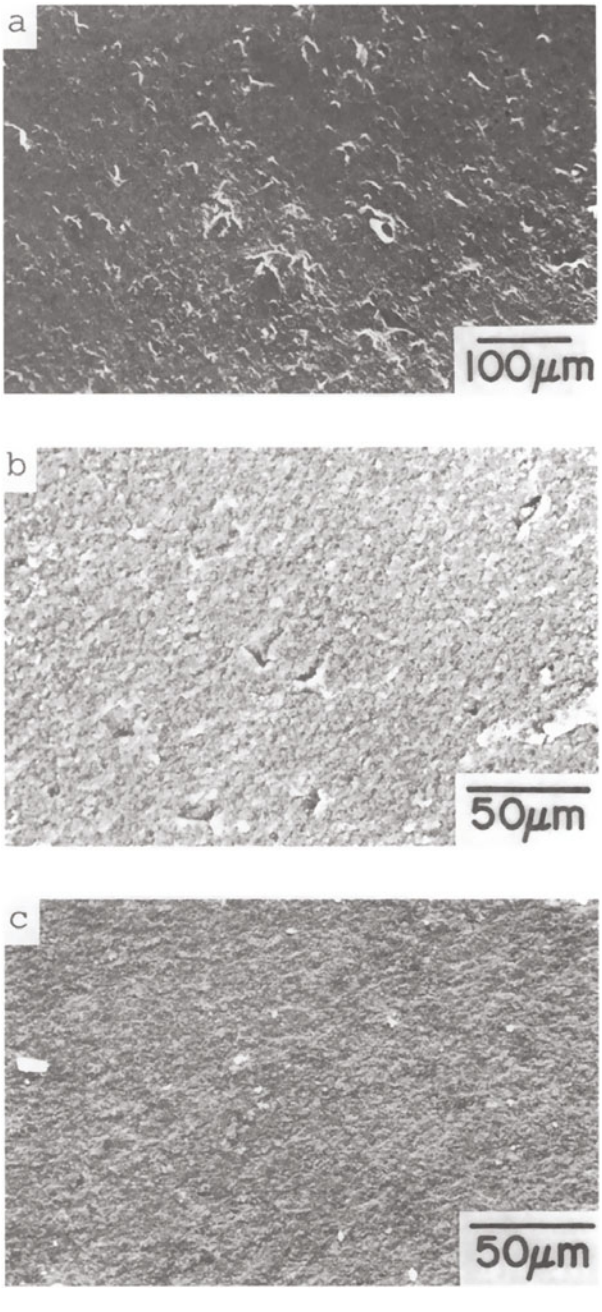

Figure 2. Fractured surfaces of specimens examined with SEM
(a) Green body, (b) Sintered body, (c) Hot isostatically pressed body

comparison of their microstructural characteristics.

Fig. 1 shows the structure of green, normally sintered and hot isostatically pressed bodies examined with the liquid immersion method. Crack-like features of approximately the same size and concentration are present in the green and normally sintered bodies. These crack-like features correspond to the processing pores formed at the junctions of three granule boundaries. Examination at higher forming pressure showed that the crack-like features were also present in the green and normally sintered bodies formed at 600 MPa. In the hot isostatically pressed body, only small isolated pores and platelets were found. These platelets correspond to aggregated particles in the starting material.

Fig. 2 shows the SEM micrographs of green, normally sintered and hot isostatically pressed bodies. The green and normally sintered bodies contain many crack-like pores. The fractured surface is much smoother and the concentration of pores is much lower in hot isostatically pressed specimen than in the normally sintered specimen.

Fig. 3 compares the micro-pore size distribution for various specimens. The pore size distribution was narrow in all specimens. These pores correspond to the matrix pores located between primary particles. Processing pores can not be evaluated by mercury porosimetry. Applying

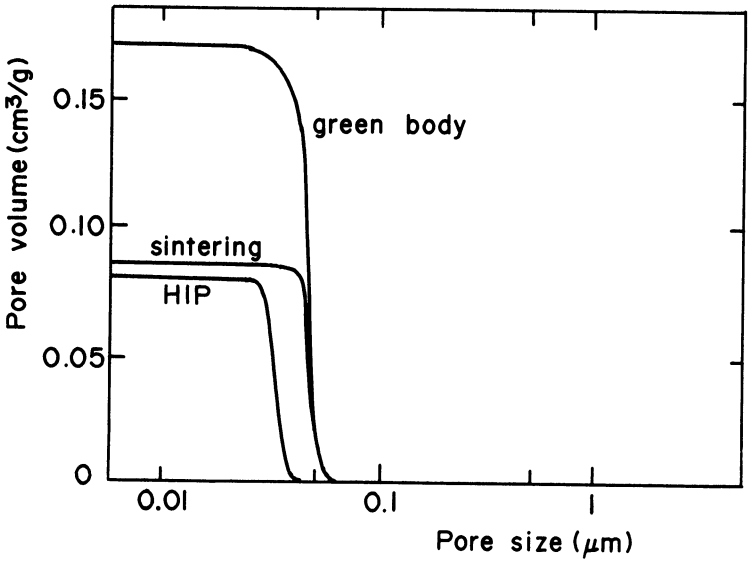

Figure 3. Pore size distributions of various specimens

normal sintering, the most frequent pore size was approximately the same in green and sintered bodies; the pore size does not change appreciably with densification. Whereas, the pore size decreased significantly with hot isostatic pressing.

DISCUSSION

The behavior of natural pores during initial-stage densification is very different for normal sintering when compared to hot isostatic pressing. Large processing pores located at three granule junctions do not shrink in normal sintering. Whereas they shrink and disappear in the early stage of densification in hot isostatic pressing.

Reduction of pore size was found to start in the early stage of densification in hot isostatic pressing. This is the first direct observation reported in this research field. With normal sintering, no significant change was found in pore size. This result is consistent with past observation; the pores can even grow in the initial stage of densification[4].

The difficulty of removing large processing pores by normal sintering is explained by their thermodynamic stability[5]. The driving force for pore removal is the surface curvature of pore in normal sintering. The curvature is mainly governed by the relative size between pore and grain. For pores with sizes much larger than the grain size, the curvature makes the pore grow.

With hot isostatic pressing, the driving force for pore removal is the high externally applied pressure. This driving force is much higher than that created by surface curvature for pore growth. The net effect is the reduction of pore size in the initial stage of densification.

REFERENCE

1. F. F. Lange, J. Am. Ceram. Soc., 1983, **66**, 396-98
2. A. G. Evans and C. H. Hsueh, J. Am. Ceram. Soc., 1986, **69**, 444-48
3. K. Uematsu, J.-Y. Kim, M. Miyashita, N. Uchida and K. Saito, J. Am. Ceram, Soc., 1990, **73**, 2555-57.
4. J. Zheng and J. S. Reed, J. Am. Ceram. Soc., 1989, **72**, 810-17
5. B. J. Kellett and F. F. Lange, J. Am. Ceram. Soc., 1989, **72**, 725-34

ATMOSPHERE CONTROL IN THE HIP TREATMENT OF CERAMICS

TAKAO FUJIKAWA, YASUO MANABE
Technology Development Center, Engineering & Machinery Division,
Kobe Steel, Ltd., Kobe, Hyogo 651, JAPAN

TSUNEO TATSUNO
Materials Research Laboratory, Kobe Steel, Ltd.,
Kobe, Hyogo 651, JAPAN

AND TAKAYUKI MIYATAKE
International Superconductivity Technology Center
Tokyo 135, JAPAN

ABSTRACT

Hot Isostatic Pressing (HIP) of ceramics has been recognized as an ideal process to produce fully dense and highly reliable parts in the course of application to ferrite magnetic recording heads, alumina cutting tool inserts, and automobile engine parts made of silicon nitride. Usually these parts are processed by the so-called capsule-free method in which the processed parts are exposed directly to the pressure medium gas. In this case, some interactions between the processed parts and the gas may occur and this phenomenon has to be carefully considered for some nitrides and oxides. Here, the influence of the surrounding gas is termed as an atmosphere and discussed from the viewpoint of thermo-dynamics. Three practical methods to create the desired atmospheres are explained and some examples in the application are given for silicon nitride, superconductive ceramics, and calcium carbonate.

INTRODUCTION

HIP has been used for a long time as a pressing technique to achieve full densification of sintered parts and castings, diffusion bonding, pressure impregnation, and so on. Here, high pressure gas is merely utilized as a pressing force and for this reason completely inert argon has been used as the pressing medium to avoid redundant chemical reactions. However, several recent studies on HIPing of ceramics have suggested that complete inertness often degrades nitride and oxide ceramics when they are processed by capsule-free HIPing. These degradations have been proven to be due to the decomposition of the constituent materials. To suppress

this decomposition, atmosphere control in the HIP treatment has been attracting attention. This paper discusses the thermo-dynamic aspects of the stability of some ceramics under high partial pressure of a specific constituent and practical techniques to control the atmosphere in HIPing of specific ceramics.

BASIC CONCEPT

In the HIP treatment of metallic materials, any sort of chemical reactions are not expected to occur and the densification, or deformation phenomenon is mainly dominated by plastic deformation rather than diffusional creep, except the final stage of densification. Furthermore the diffusion of some constituent elements are not necessarily important except for the solid phase diffusion bonding. Thus, the HIP treatment of metals is a very simple operation like other usual heat treatments widely used in industries.

On the other hand, in the case of ceramics, there are some important points that have to be taken into consideration. First, ceramics are basically compounds of a metallic element and a non-metallic element such as oxygen, nitrogen, and so on, so there are always some possibilities of decomposing reaction to occur. Second, in many cases ceramics have a composite microstructure consisting of crystal grains and secondary grain boundary phases and these grain boundary phases are quite sensitive to the surrounding gas atmosphere. Here, the influence of high pressure gas atmosphere is briefly reviewed in terms of chemical stability and reaction rate.

Chemical Stability

When a ceramic is subjected to high temperatures, it may decompose to a metal and a gaseous material depending on the surrounding atmosphere. Generally this decomposition can be expressed by the following equation:

$$AmBn \longrightarrow mA + oBp(gas) \qquad (1)$$

where A and B represent a metallic element and non-metallic element respectively, and between the coefficients n, o, and p there is a relation of $n = o \times p$. In many cases this reaction is reversible. As can be seen from the equation (1), the higher the pressure of Bp, the more effectively this decomposition is suppressed.

In order to discuss the stability of AmBn at a specific temperature and pressure condition, the most common approach is to evaluate the Gibb's free energy change for the reaction. There are some papers which discuss the stability of nitride ceramics from this point of view using the so-called Ellingham diagrams [1]. One problem with this approach for reactions under high pressures is that we have to treat the gaseous component as an ideal gas and this makes it difficult to evaluate the Gibb's free energy change precisely. This approach is, however, very useful and sometimes necessary to make qualitative evaluation, when new materials are targeted for HIP treatment.

Reaction And Diffusion Rate

Another important factor in the consideration of reaction is its rate. In the HIP treatment, time is a very important factor as well as temperature and pressure and it governs heat and mass transfer which are closely

connected with the reaction between the processed material and surrounding gas. This reaction occurs from the surface of the material and its front plane proceeds into the interior of the material with time. This propagation rate, namely the practical reaction rate, is dominated by diffusion. When diffusion becomes imperative, the microstructural nature of ceramics stated earlier affects the homogeneity of the ceramics itself because of the migration of a certain constituent element, impurity in the pressure medium gas, or pressure medium gas itself. Here, three types of diffusion may be assumed, that is, surface diffusion, grain boundary diffusion, and volume diffusion. The surface diffusion plays a role more or less in the mass transfer and densification as far as pores exist. The grain boundary diffusion in ceramics with composite structure may be divided into two types. One is the usual grain boundary diffusion which can be seen in metals and the other may be technically deemed as a kind of volume diffusion because the grain boundary phases in this type of ceramic consist of secondary phase in the form of migration paths with considerable thickness. Some components of concern may diffuse through these paths. When these phases are glassy and easily soften at high temperatures, a gaseous component dissolves into this softened glassy phase and diffuses at a considerably high rate. In this case, pressure, especially the partial pressure of the gaseous components, promotes their dissolution into these grain boundary phases. The volume diffusion is usually defined for within a crystal grain and its rate is considered to depend on the vacancy concentration in the grain. Thus, volume diffusion may be promoted by pressure when crystal grains include lattice defects.

PRACTICAL METHODS TO CREATE A TARGETED ATMOSPHERE

Three typical methods have been proposed and some of them are already applied industrially in the production of electronic ceramics. The conceptions of these three methods are summarized below.

Full Gas Pressure Method

In this method almost pure gas of Bp in the equation (1) is used as the pressure transmitting medium. The most popular application of this method is the nitrogen HIPing of Si_3N_4 based ceramics. The decomposition of Si_3N_4 at temperatures above 1700°C can be effectively prevented by using high pressure nitrogen. The "Gas Pressure Sintering Method" may be considered in the same category, although the pressure is not as high as in the ordinary HIP treatment.

Gas Mixture Method

Usually the pressure needed to densify the presintered ceramics and to suppress their decomposition are not identical. In such a case, the Bp in the equation (1) may be diluted with an inert gas such as argon in order to obtain total pressure for densification and an appropriate partial pressure of Bp for the prevention of the decomposition. A good example of this will be cited in the next section. This method is also advantageous when oxygen or a flamable gas, such as hydrogen, is preferred, because diluting these gases by inert gas enables safer operation of a HIP unit. Oxydizing atmosphere HIPing of superconductive ceramics are carried out by this method with the consideration of safety.

Powder Embedding Method

This method has been used for the production of soft ferrites, such as Mn-Zn-ferrite and Ni-Zn-ferrite and lead titanate ceramics. Presintered blocks are packed with powders of the same composition or other chemically stable materials in a container made of chemically stable material with a lid. This container is charged into an ordinary HIP unit and processed. During heating some oxygen will be emitted from the packing powders to form a equilibrium partial pressure of oxygen at the corresponding temperature. To avoid the reduction of the processed blocks, the space inside the container has to be densely packed with powder or the processed material itself and at the same time, the convection of high pressure gas near the product must be prevented [2]. The greatest advantages of this method are that: 1) this method utilizes a natural phenomenon and an appropriate atmosphere can be spontaneously created, and 2) under high pressures, the partial pressure of the desired constituent can be higher than 1 atom which is the absolute limit at ambient pressure.

EXPERIMENTAL

Three methods outlined in the previous section will be explained here by citing some actual examples.

Full Gas Pressure Method

Nowadays the HIP densification of Si_3N_4 ceramics on a commercial scale are carried out by this method using nitrogen as a pressurizing gas. There are several papers [3,4] which demonstrate the advantages over the conventional argon gas HIPing. However, the most effective utilization of this method seems to be the nitridation of metals or the reaction sintering of nitride ceramics [4]. The nitridation of molybdenum is another interesting topic in this field.

It is general knowledge that molybdenum cannot be nitrided by nitrogen at ambient pressure. However, H. Jehn and P. Ettmayer made an investigation on the preparation of Mo - N system phase diagram under high pressures [5] and postulated that dissociation pressure of Mo_2N could be represented by the equation:

$$\log(^{P}N_2) = 5.63 - 5990/T \qquad (2)$$

for $^{P}N_2$ in atm and T in K.

The authors have attempted the formation of molybdenum nitride under pressures up to 180 MPa. Some of the results are shown in Fig. 1(a) [6]. In this experiment, molybdenum powder with the particle size of - 44 um was used. The retention time at the maximum temperature was kept at 1 hour based on a preliminary experiment for 0.5 mm thickness wires to evaluate the nitrogen diffusion rate in molybdenum. The crystalline structure identified by X-ray diffractometory was $MO_{16}N_7$ according to the ASTM data. It is very interesting to note that the amount of nitride varied with pressure at a fixed temperature, because for other materials it was not greatly affected by pressure as shown in Fig. 1(b) for NbN. At higher temperatures, MoN which has been drawing attention as a high Tc B1 type superconductor may be synthesized.

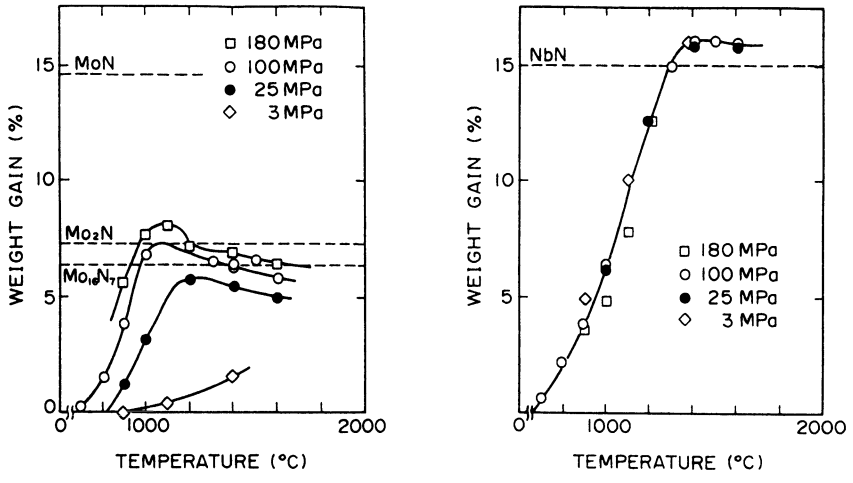

Figure 1. Weight gain observed in the nitridation of Mo (a) and Nb (b).

Gas Mixture Method

A good example of this method may be the oxydizing atmosphere HIPing of oxide ceramics. Several reports on the partially stabilized zirconia [7,8] and on alumina [8] have been published. In these studies pressurizing gas used was prepared by mixing oxygen with argon in the range of $O_2 \leq 20$ vol% from the viewpoint of safety. Another interesting application of this oxydizing atmosphere HIPing may be the synthesis of high temperature superconductive ceramics. In addition to the advantage in the shortening of the processing time due to the acceleration of volume diffusion rate, it was found recently that high pressure is effective to shape a neat lattice structure as shown in Fig. 2. This seems to contribute to the enhancement of Tc of the oxide superconductor family [10].

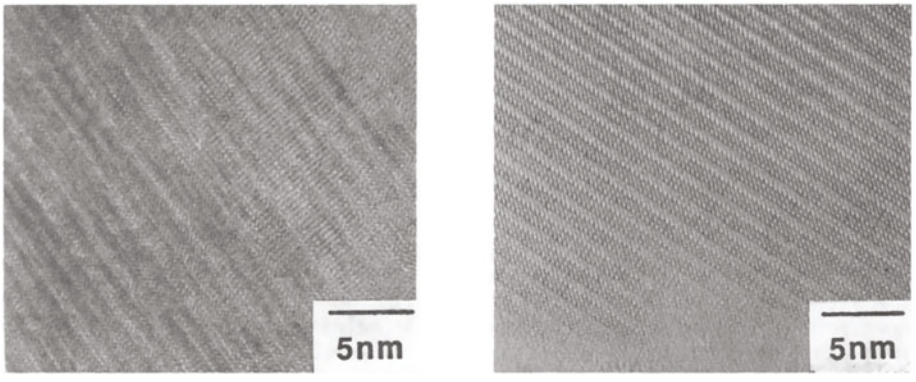

Figure 2. Lattice images of $YBa_2Cu_4O_8$ processed at pO_2=3atm, 850°C, 160hrs (a) and at pO_2=200atm (total p=1000atm), 1000°C, 5hrs.

In the HIP treatment of Si_3N_4 ceramics, nitrogen HIPing is popular as stated above, though some problems with their high temperature bending strength was recognized for a Si_3N_4 -Y_2O_3 -Al_2O_3 system. As illustrated in Fig. 3, an increase in weight during nitrogen HIPing was observed and this was considered to be one of the causes of the degradation of the high temperature strength for this material. A closer examination on the microstructure revealed that the crystalized grain boundary phase (mellilite) changed to glassy phases or other crystalline phases. This phenomenon was considered to be due to the desolution of nitrogen into the grain boundary phase which can be conjectured from the above mentioned weight gain, since the weight gain was prominent for the materials with more grain boundary phases, namely, normally sintered Si_3N_4 (SSN). In order to solve this problem, HIPing using a gas mixture of argon and nitrogen has been carried out for this material and improvement in high temperature strength at temperatures of about 1400°C was achieved. The details will be reported in the near future.

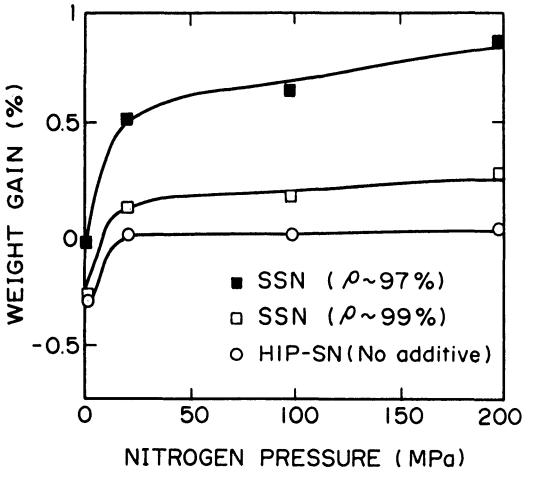

Figure 3. Weight gain observed in Si_3N_4-Y_2O_3-Al_2O_3 sample after nitrogen gas HIPing at 1700°C, 1hr.

Powder Embedding Method

As stated earlier, this method is widely used in the HIPing of oxide electronic ceramics and similar methods have been used in the normal sintering for a long time. The greatest advantage is that it can form a partial pressure of the desired constituent higher than 1 atm. Calcium carbonate has been successfully sintered by this method. At ambient pressure calcium carbonate decomposes to calcium oxide when heated above 600°C and cannot be sintered.

Calcium carbonate powder with about 6 wt% magnesium carbonate was pressed in a metal mold to form green bodies with dimensions of 10 x 30 x 5 mm and then sintered in a HIP unit under high pressures using argon gas. These samples were placed in an alumina crucible with a lid and then this crucible was packed with calcium carbonate and alumina powder. The

TABLE 1
Sintering conditions and densities after sintering

No.	Temperature (°C)	Pressure (atm)	Retention time (hr)	Density (g/cm^3)	Remarks
1	1000	1000	1	2.362	
2	1000	2000	1	2.392	
3	1100	20	1	2.142	
4	1100	100	1	2.348	
5	1100	100	1	2.601	Sinter/HIP
	+ 1000	1000	1		

sintering conditions and the densities after this sintering are given in TABLE 1 and the SEM micrographs are in Fig. 4. The sample with the highest density was processed by the so-called sinter/HIP pattern operation. This was the first successful experiment in which dense calcium carbonate was artificially obtained.

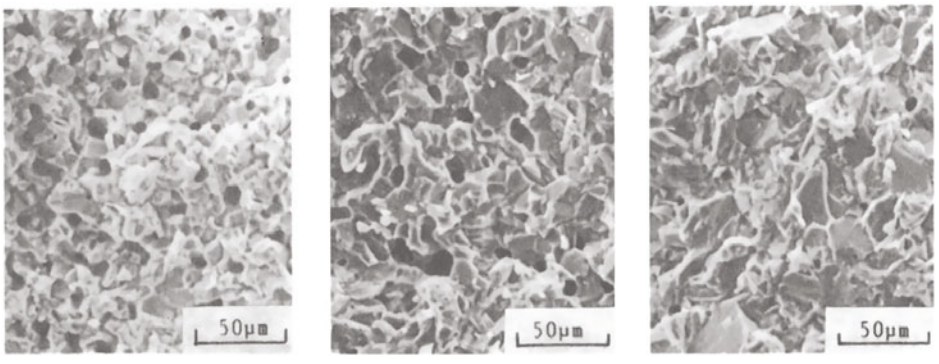

(a) No. 1 (b) No. 4 (c) No. 5

Figure 4. Microstructure of $CaCO_3$ based ceramics sintered by powder embedding method under high pressure.

FUTURE PROSPECT

In the '90s the HIP treatment of ceramics will become more important than ever especially in the area of functional ceramics, such as electronic ceramics. The requirement for these materials seems to be getting more severe year by year. The need for microscopically homogeneous and pore-free structure will become mandatory. In order to achieve the homogeneity in microstructure the atmosphere control is believed to be inevitable. The methods explained above or integrated methods will play an important role here. As for HIP equipment for this purpose, recently some improvement has been achieved for the HIP impregnation and carbonization of tar/pitch or some sort of resins to fabricate dense C/C composites. The concept of this HIP equipment is illustrated in Fig. 5. This type of HIP unit has a special casing to the inside the heaters to form a desired atmosphere within this casing without causing any influence on the heaters or other furnace parts and may be the ideal equipment to materialize the atmosphere control discussed above.

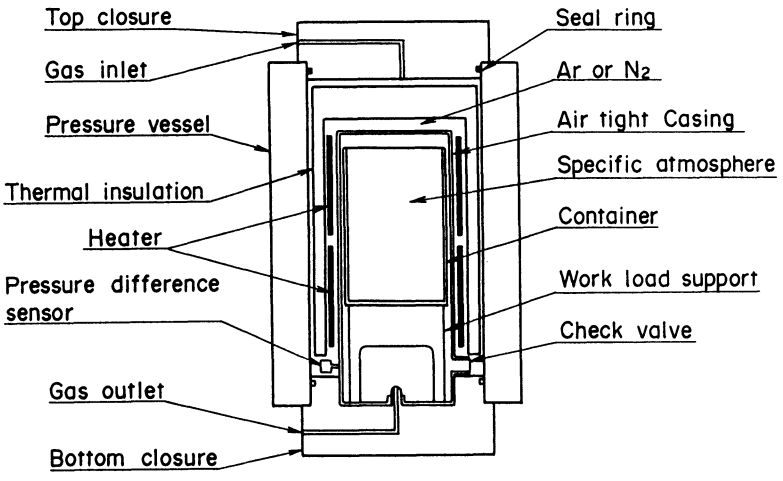

Figure 5. Schematic view of the Insulation Chamber HIP equipment for atmosphere control HIP treatment.

ACKNOWLEDGEMENT

The authors wish to express their gratitude to Mr. K. Yamaguchi for his support in the preparation of TEM micrographs of superconductive ceramics.

REFERENCES

1. Ishizaki, K., Phase diagrams under high total pressure - Ellingham diagrams for Hot Isostatic Pressing. Acta. Metal. Mater., 1990, 38, 2059-66.
2. Takata, M., Isostatic Pressing - Technology And Applications, ed. M. Koizumi and M. Nishihara, Elsevier Applied Science, London and New York, 1991, pp239-54.
3. Homma, K., Tatsuno, T., Okada, H. and Fujikawa, T., HIP treatment of non-oxide ceramics. Proc. 25th Japan Congress on Material Research, Kyoto, Japan, 1982.
4. Fujikawa, T., Moritoki, M., Kanda, T., Homma, K. and Okada, H., Hot Isostatic Pressing: its application in high performance ceramics. Proc. Int. Symp. Ceram. Comp. for Engine, Hakone, September 1983.
5. Jehn, H. and Ettmayer, P., The molybdenum - nitrogen phase diagram. J. Less-Common Met., 1978, 58, 85-98.
6. Takagi, I. and Fujikawa, T., unpublished data.
7. Masaki, T., Nakajima, N. and Shindo, J., J. Mat. Sci. Letters, 1988, 5, 1115-1118.
8. Manabe, Y., Fujikawa, T., and Narukawa, Y., Effect of O_2 HIP for oxide ceramics. Proc. Second. Int. Conf. HIP, Gaithersburg, MD, USA, June 1989.
9. Miyatake, T., Synthesis and superconducting properties of $YBa_2Cu_4O_8$. Text of KOBELCO 10th HIP Seminar, Kobe, Japan, December 1990.
10. Fujikawa, T., Manabe, Y., Narukawa, Y. and Inoue, Y., Influence of Pressure transmitting gas in HIPing of ceramics. Proc. Fall Meeting, The Ceramic Society of Japan, Nagaoka, Japan, September 1988.

GAS-PRESSURE SINTERING MAP FOR SILICON NITRIDE-BASED MATERIALS

Naoto Hirosaki and Akira Okada
YM0, Central Engineering Laboratories, Nissan Motor Co., Ltd.,
1, Natsushima-cho, Yokosuka 237, Japan

ABSTRACT

The effect of N_2 gas pressure on the sintering of silicon nitride-based ceramics (α and β sialon) is examined. When gas pressure is low, reactions occur between Si_3N_4 and oxides and dense compacts are not obtained. Using the gas-pressure sintering method, dense compacts are produced at an elevated N_2 gas pressure. However, N_2 gas pressures higher than 10 MPa result in lower density because high pressure gas inside the closed pores inhibits densification in the final stage of sintering. These results suggest that silicon nitride-based materials should be sintered at an appropriate gas pressure to minimize thermal decomposition and to promote shrinking after pore closure. A gas-pressure sintering map is proposed for sintering silicon nitride-based ceramics under suitable gas pressure and temperature conditions.

INTRODUCTION

The gas-pressure sintering method (GPS) [1] has been applied for sintering silicon nitride-based materials. Thermal decomposition of silicon nitride limits the firing temperature to $< 1800°C$ under a condition of the pressureless sintering. The GPS method permits firing at higher temperatures because high-pressure nitrogen gas suppresses the thermal decomposition of silicon nitride, thus promoting better sintering. High-pressure nitrogen gas, however, inhibits densification of silicon nitride in the final stage of sintering[2].

In this paper, the effect of N_2 gas pressure on the sintering of silicon nitride-based ceramics is examined and a gas-pressure sintering map is proposed for sintering silicon nitride-based ceramics under suitable gas pressure and temperature conditions.

EXPERIMENTAL PROCEDURE

The raw materials were Si_3N_4 powder [Grade H1, H. C. Starck], Y_2O_3 [Shinetsu Chemical, 99.9% pure], AlN [Japan Metals and Chemicals], and Al_2O_3 [Alcoa, A16SG grade]. The Y_2O_3-AlN and Al_2O_3-AlN systems were used for sintering additives. In the Y_2O_3-AlN system, Y_2O_3 and AlN were added to a composition of x=0.2 (A02) and 0.4 (A04) in the general expression for Y-containing α-sialon:

$$Y_x(Si, Al)_{12}(O, N)_{16}. \quad (1)$$

In the Al_2O_3-AlN system, Al_2O_3 and AlN were added to a composition of z=2 (B2) in the general expression for β-sialon:

$$Si_{6-z}Al_zO_zN_{8-z}. \quad (2)$$

These powders were ball-milled in ethanol for 94 h, dried, die-pressed, and then isostatically pressed under 200 MPa; the resultant pressed specimens were about 6 by 12 by 50 mm. The specimens were fired at 1700°C to 1900 °C for 1 h in 0.1 to 100 MPa N_2 gas using a graphite resistance furnace. The density of the sintered specimens was measured by the Archimedes method.

RESULTS

Figures 1 (a)–(c) show the effect of N_2 gas pressure on the density and weight loss of silicon nitride fired at 1700°C to 1900°C for 1 h. Weight loss increased with rising temperature but decreased with increasing N_2 gas pressure. This weight loss occurred because of thermal decomposition during firing. Specimens experiencing a large weight loss did not show sufficient densification. Density increased with higher gas pressure up to 10 MPa because of reduced thermal decomposition. However, specimens fired in 100 MPa N_2 gas tended to have lower density than those fired at 10 MPa. This tendency was most pronounced for the Al_2O_3-AlN system (B2). When B2 was fired at 0.1 MPa, the weight loss was extremely high and shrinkage was not achieved. Using the GPS method, weight loss decreased and density increased. The density, however, peaked at 10 MPa and decreased at 100 MPa.

DISCUSSION

Thermal Decomposition

Weight loss occurred during firing because of thermal decomposition. Thermal decomposition is discussed here in terms of two stages, before and after formation of sialons, because the material in this study formed α- or β-sialon during firing.

First, thermal decomposition before sialon formation is discussed. The powder mixtures for the Y_2O_3-AlN system contained Si_3N_4, Y_2O_3, SiO_2, AlN, and Al_2O_3, where SiO_2 and Al_2O_3 were impurities present in the silicon nitride and aluminum nitride raw powder, respectively. The powder mixtures for the Al_2O_3-AlN system contained Si_3N_4, SiO_2, AlN, and Al_2O_3, where SiO_2 was an impurity present in the silicon nitride raw powder. In these systems, the following thermal decomposition reactions can occur:

$$Si_3N_4 \rightarrow 3Si + N_2 \quad (3)$$

$$Si_3N_4 + 3SiO_2 \rightarrow 6SiO + 2N_2 \quad (4)$$

$$Si_3N_4 + Al_2O_3 \rightarrow 3SiO + 2AlN + N_2 \quad (5)$$

$$2AlN + SiO_2 \rightarrow SiO + Al_2O + N_2 \quad (6)$$

$$4AlN + Al_2O_3 \rightarrow 3Al_2O + 2N_2 \quad (7)$$

Figure 2 shows the decomposition partial pressure of Si, SiO, and Al_2O as a function of N_2 gas pressure at 2000K. These results were calculated using thermodynamic data [3]. Thermodynamic calculations indicated that reactions (4) and (5) contributed more to weight loss than reactions (3), (6), and (7).

After sialons are formed, α-sialon is reported to decompose by the reaction [4]:

$$Y_{0.6}(Si_{9.3}, Al_{2.7})(O_{0.9}, N_{15.1}) = 7.2Si + 0.6YSi_2 + 2.7AlN + 0.9SiO + 6.2N_2 \quad (8)$$

and β-sialon is reported to decompose by the reaction [5]:

$$\beta_1\text{-sialon} + \text{X-sialon} = \beta_2\text{-sialon} + 6\text{SiO} + 2\text{N}_2 \quad (9)$$

$$\beta\text{-sialon} = 15\text{R-sialon} + 4\text{SiO} + 2\text{N}_2 + \text{Si} \quad (10)$$

Equations (9) and (10) are for the reactions of two-phase sialon and single-phase sialon. β_2 had a larger z value than β_1 in reaction (9). In this study, Si, YSi_2, and AlN were not detected for the Y_2O_3-AlN system and 15R-sialon and Si were not detected for the Al_2O_3-AlN system by X-ray diffraction. Moreover, the Al_2O_3-AlN system had the same lattice constant under all firing conditions. Therefore, reactions (8) – (10) contributed little to the weight loss whereas reactions (4) and (5) contributed greatly.

Densification

When reaction (4) and/or (5) occurred, the oxygen content in the composition of sialon was reduced. For β-sialon, reduced oxygen content caused a decline in siterability because the amount of low melting temperature liquid decreased [5]. For α-sialon, where a glassy phase existed [6], reduced oxygen content was also presumed to degrade sinterability, because of the decrease in the liquid phase or the increase in viscosity during sintering. These decomposition reactions were the reason for insufficient densification of A04 when it was fired in 0.1 MPa N_2 at 1700°C and for the attainment of high density when the gas pressure was increased.

Thermal decomposition reactions (3) to (10) were accelerated with increasing temperature because of the result in increase in the equilibrium partial pressure of the volatile gas. On the other hand, the densification rate increased as the temperature rose because of the acceleration of diffusion and/or the decrease in liquid phase viscosity. In actual firing, thermal decomposition was suppressed as sintering progressed because of the reduction in specific surface area. This is thought to be the reason why A04 fired at 1800°C in normal N_2 gas pressure, where decomposition was suppressed by this effect, densified to 3.28 g/cm^3.

Obstruction of Final-Stage Sintering by High-Pressure Gas

Greskovich [2] has reported that densification of Si_3N_4 containing $BeSiN_2$ and SiO_2 was obstructed when N_2 gas pressure was too high because of the presence of high pressure gas in the closed pores. In this study, excessively high N_2 gas pressure was also observed to obstruct densification in the final stage of sintering, which resulted in insufficiently dense compacts.

The effect of gas pressure on the density was small for A02 fired at 1700°C and 1800°C. With this material, the open pores permitted free movement of gas to the outside. In contrast, all materials which were affected by gas pressure were very dense and had more closed than open pores. Gas pressure did not affect densification at the early or middle stage of sintering but only during the final stage after the pores had closed. This result is consistent with Greskovich's observation.

Gas-Pressure Sintering Map

Figure 3 shows the temperature and gas pressure region where high density was achieved. Although the conditions where dense compacts were obtained differed according to the additive compositions, a region of suitable temperature and pressure conditions is evident. Based on these results, a sintering map is proposed, where a good sintering region is determined as a function of temperature and pressure (Figure 4). Using this sintering map, the region where good sintering is obtained can be explained by the four following conditions.

1. Minimum temperature-I (line 1):
   This is the temperature at which the liquid phase for promoting sintering appears, or the minimum temperature at which sintering occurs in the form of liquid phase sintering. Thus, little densification takes place at temperatures below this level (region A).

2. Maximum pressure (line 2):
   This is the pressure at which high pressure gas sealed in closed pores obstructs densification in the final stage of sintering. Sufficient densification is impossible to obtain anywhere beyond this level (region B).

3. Maximum temperature (line 3):
   This is the temperature at which Si_3N_4 and the product (sialon) decompose. The maximum temperature increases with N_2 gas pressure. Dense compacts can not be obtained at temperatures beyond this level (region A) because the raw materials or products undergo thermal decomposition.

4. Minimum temperature II (line 4):
   The temperature at which SiO gas is actively generated by the reaction between Si_3N_4 and oxides (SiO_2 or Al_2O_3) is shown as line 5 in Fig. 4. This temperature increases with rising N_2 gas pressure and beyond this temperature, decomposition increases. When a decomposition reaction occurs, the liquid formation temperature (line 1) increases. Because thermal decomposition is accelerated with decreasing N_2 gas pressure, the liquid formation temperature also increases. As a result, densification is inhibited in region D.

It is concluded that dense materials can be obtained in region E, which satisfies all four conditions.

CONCLUSIONS

A gas-pressure sintering map was proposed to explain suitable sintering conditions (gas pressure and temperature) for silicon nitride-based ceramics. When silicon nitride was sintered at low N_2 gas pressure, reactions occurred between Si_3N_4 and oxides (SiO_2 or Al_2O_3) and dense compacts were not obtained. Using the gas-pressure sintering method, dense compacts were produced at an elevated N_2 gas pressure. However, N_2 gas pressures higher than 10 MPa resulted in lower density because high pressure gas inside the closed pores inhibited densification in the final stage of sintering. These results suggested that silicon nitride-based materials should be sintered at an appropriate gas pressure to minimize decomposition and to promote shrinking after pore closure.

REFERENCES

1. M. Mitomo, M. Tsutsumi, E. Bannai and T. Tanaka, "Sintering of Si_3N_4", *Am. Ceram. Soc. Bull.*, 1976, **55** [3] 313.

2. C. Greskovich, *J. Am. Ceram. Soc.* 1981, **64**, 725-30.

3. D. R. Stull and H. Prephet, *JANAF Thermochemical Tables, 2nd Ed.*, National Bureau of Standards, 1971.

4. M. Mitomo and O. Fukunaga, "The stability of α-sialon at high temperatures", *Yogyo-Kyokai-Shi*, 1981, **89** 631-33.

5. M. Mitomo, N. Kuramoto, and Y. Inomata, "Fabrication of high strength β-sialon by reaction sintering", *J. Mater. Sci.*, 1979, **14** [10] 2309-16.

6. M. Mitomo, F. Izumi, Y. Bando and Y. Sekikawa, in *Proceedings of the First International Symposium on Ceramic Components for Engine*, ed. S. Somiya, "Characterization of α-Sialon Ceramics", KTK Scientific Publishers, Tokyo, 1983, pp. 377-86.

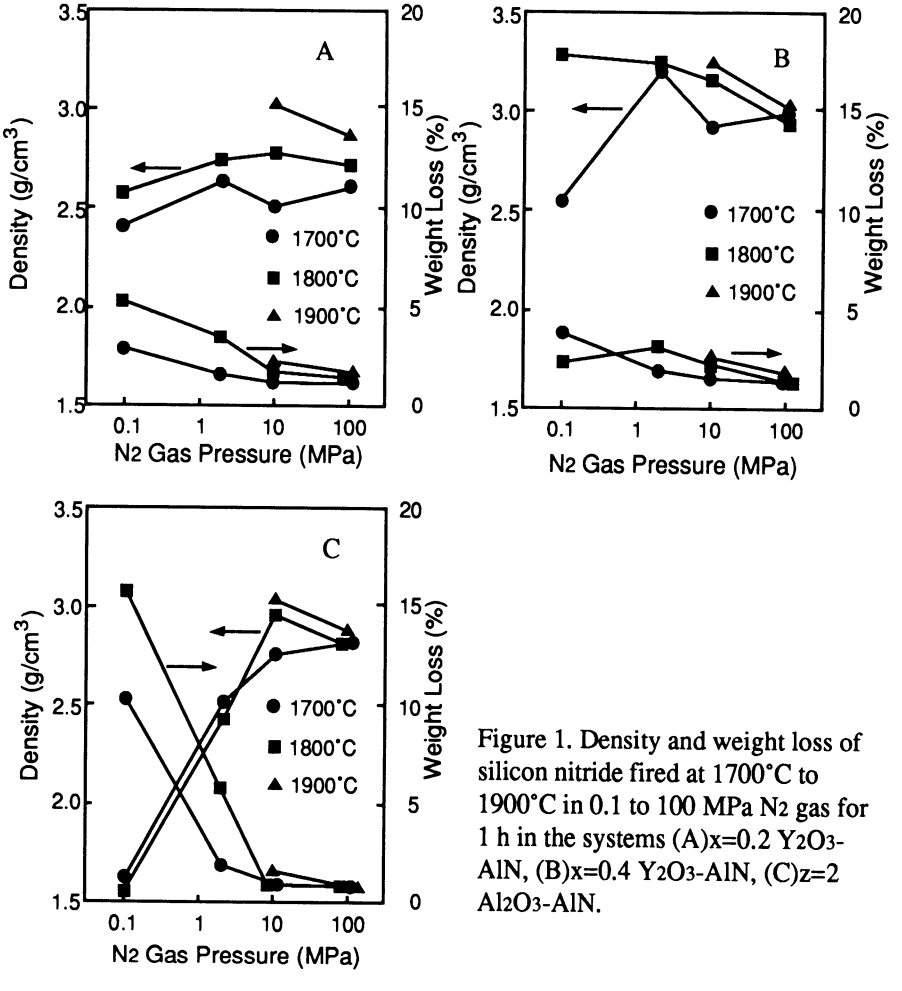

Figure 1. Density and weight loss of silicon nitride fired at 1700°C to 1900°C in 0.1 to 100 MPa N_2 gas for 1 h in the systems (A)x=0.2 Y_2O_3-AlN, (B)x=0.4 Y_2O_3-AlN, (C)z=2 Al_2O_3-AlN.

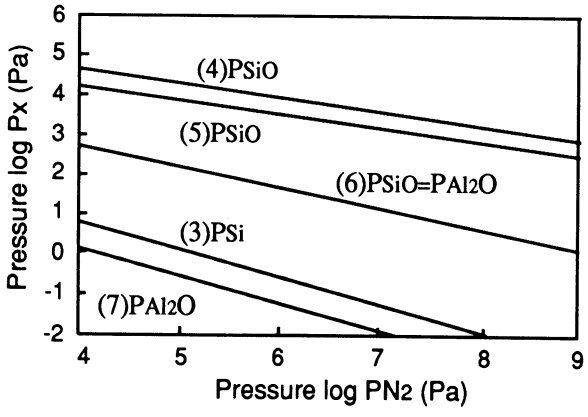

Figure 2. Equilibrium partial pressure vs. N_2 pressure at 2000K.

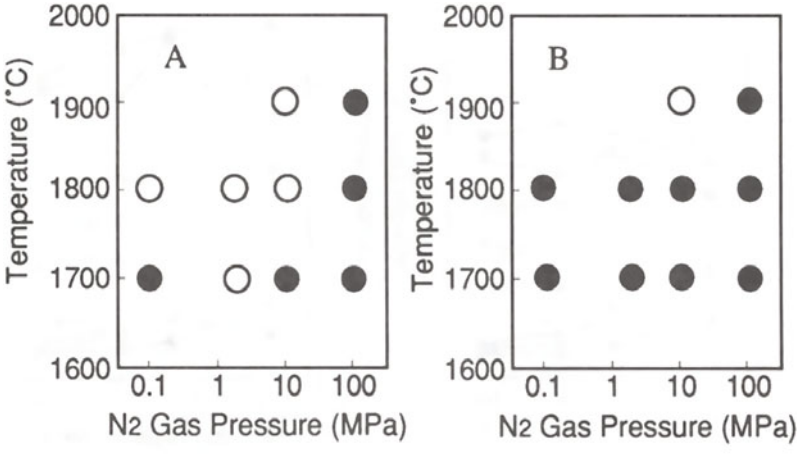

Figure 3. High density region of (A) x=0.4 and (B) x=0.2 Y_2O_3-AlN.
(●<3.0g/cm^3, ○≥3.0g/cm^3)

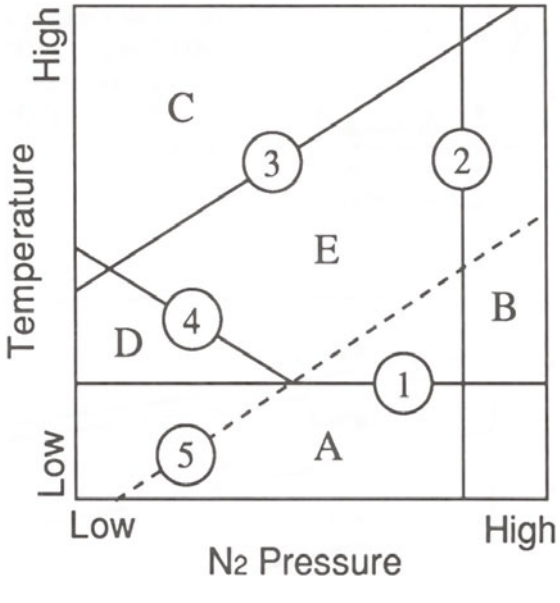

Figure 4. Gas-pressure sintering map for silicon nitride.

POST-SINTERING HOT ISOSTATIC PRESSING OF SILICON NITRIDE BASED CERAMICS

Tanguy ROUXEL, Jean-Francois ANGER, Jean-Louis BESSON and Paul GOURSAT,

Laboratoire "Ceramiques nouvelles", U.A. 320, Universite de Limoges, France.

ABSTRACT

It is well known that the degradation of the high temperature properties of silicon nitride ceramics is due to the presence of intergranular glassy phases which result from oxide additives necessary to promote densification.

One way to improve their high temperature behaviour is to recrystallize these phases. Another way is to reduce the glass content by exuding it on the surface. In order to reach the latter goal, samples are introduced in a borosilicate capsule where they are embedded in SiC powder. The capsule is then outgassed and sealed. Finally, the H.I.P. treatment is performed. Above the softening temperature of the capsule, the pressure is transmitted to the nitride grains by the SiC particles. The temperatures of the heat-treatment were carefully selected to insure that, during the rearrangement of the silicon nitride grains in an improved grain packing, the intergranular glassy phases were fluid enough to be squeezed out toward the SiC powder, through the porosity existing between the SiC particles.

After such a treatment, the creep deformation in 3-point bending (1200°C, 240 MPa) was divided by 3. A crystallization treatment of the glassy pockets remaining at triple junctions may be added, which results in a further improvement of the creep resistance.

INTRODUCTION

Hot Isostatic Pressing is suitable for the preparation of dense materials with an homogeneous microstructure. Thus, this technique has been extensively used to produce high performance ceramics[1,...,4]. SiAlON(s) are silicon nitride based ceramics exhibiting excellent properties for high temperature structural applications. When sintered within 1700-1800°C they are constituted of elongated grains separated by a mainly glassy interphase which contains the major impurities and sintering additives. Since the glass viscosity decreases dramatically above the transition temperature, this latter phase controls the high temperature properties. Performed on SiAlON(s), H.I.P. treatments were

found to improve their density as well as their mechanical properties at room temperature. Drawbacks are grain coarsening and globularization, accompanied by the appearance of micro-cracks and brittle secondary crystalline phases (Y.A.G.). Furthermore, most of the treatments involve temperatures close to that of sintering and high pressure (200-300 MPa). This tends, on one hand, to enlarge the glassy phase content and, on the other hand, to develop micro-cracks due to the cooling under pressure of secondary crystalline phases (also appeared during cooling)[5,6]. Therefore, no improvement of the high temperature properties, but a degradation of the creep strength is generally reported[7,8]. In this paper we present a new route for decreasing the glassy phase content of presureless sintered silicon nitrides (SSN), by means of a "low temperature" H.I.P. treatment. The principle of the technique is first detailed, together with the characteristics of the required encapsulation. Based on microstructural observations and chemical analysis, the feasibility is then demonstrated. Creep behaviour is significantly improved by the treatment. This strengthening is related to an improve grain packing and an important reduction of the glassy phase amount. The residual intergranular phase was recrystallized to further ameliorate the mechanical properties. The total creep deformation could be reduced by a factor six with respect to the as-sintered (untreated) ceramic.

MATERIALS AND METHODS

SiAlON(s) materials were prepared from mixed powders of silica, aluminium and yttrium oxide dispersed in alcohol. After drying, the mixture was nitrided at 1400°C and then, after shaping, sintered (SSN) at 1700°C under nitrogen atmosphere for an hour. Sintered materials are composed of β' $Si_{6-z}Al_zO_zN_{8-z}$ grains with a substitution coefficient z=0.8, and a glassy YSiAlON intergranular phase. The major impurities are iron and calcium. The nominal composition is given in table 1 together with some room temperature properties.

TABLE 1

Weight %			ppm		HV (30kg)	σ_r (3pts)	K_{1c} (SEPB)
Si	Al	Y	Fe	Ca	GPa	MPa	$MPa.m^{0.5}$
86.0	5.4	8.6	525	65	14.0	533	4.2

The used H.I.P. equipment allows to perform treatments up to a 200 MPa argon pressure and 2000°C. The sample holder is in graphite. Creep tests were carried out in air on specimen 3(large)x4(height)x25 mm^3 with a 3 point bending device (span=21 mm) under constant load.

Principle of the technique

Specimens (4x3x25 mm^3) are introduced in a cylindrical capsule (10-12 mm internal and external diameters) and embedded in a refractory powder. Capsules are then sealed under vacuum and set in the H.I.P. furnace. Above the softening temperature of the encapsulating material, the pressure is transmitted to the inside powder and further to the specimen. The latter is stressed in a discontinuous manner through the

numerous contacts with the particles. Since presureless areas remain on the surface of the specimen and between the powder grains, the glassy phase is exuded through the porosity toward the capsule. A schematic drawing of the principle is given in figure 1.

- Figure 1 -

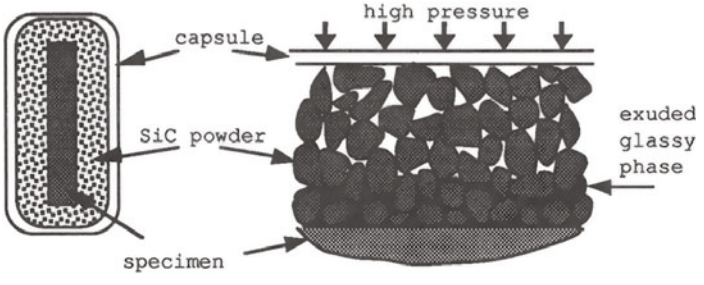

The powder does not act as a diffusion barrier only, but also as a pressure transmitting medium. Requirements for the capsule are : thermal stability, good refractoriness, chemical neutrality with the powder, convenience for disencapsulation and a softening temperature below the glass transition temperature of the SiAlON glassy phase. The powder must be highly refractory, so that the particles remain still very hard during the treatment. With regards to these conditions, a borosilicate glass and silicon carbide have been selected as suitable materials for encapsulation and powder respectively. From dilatometric experiment, the softening temperature of the glass is close to 610 °C. The SiC powder has an average grain size of 20 microns. Temperature during the heat treatment must be high enough to allow the flowing of the intergranular glassy phase but moderate to prevent against the formation of additional glassy phases that would balance the positive effect. Viscosities of oxynitride glasses have already been reported[9,10] and Tg for YSiAlON glasses ranges within 850-1000°C, depending on their nitrogen contents.

RESULTS AND DISCUSSION

The sample holder being in graphite, capsules are black after the H.I.P. treatment (figure 2).

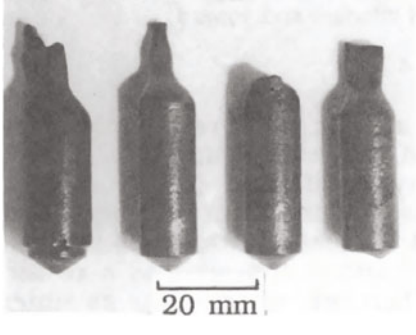

- Figure 2 -

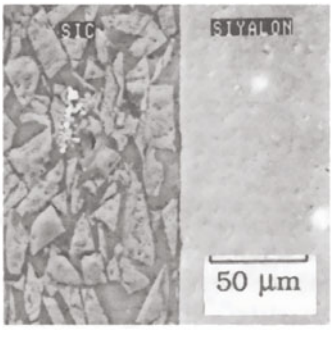

- Figure 3 -

An observation of a section reveals that the specimen is surrounded by a conglomerate composed of SiC particles embedded in an extraneous glassy phase, forming a few micron thickness film at the boundary with the SiAlON/SiC interface (figure 3). The recuperation of the specimen can be achieved by etching the capsule (easily etched by hydrochloric acid without any alteration of the specimen surface). After the experiment, powder is constituted of fractured SiC grains with many debris, demonstrating that particles transmitted the pressure applied to the envelope. The composition of the glassy phase surrounding the SiC grains has been analyzed by an E.D.S. micro-probe along a transverse axis (xx'), going through the center of the specimen at various distances from the SiAlON/SiC interface. The weight fractions of the metallic cations were measured with an accuracy better than 10 % for each spectrum. Results are plotted together in figure 4. According to the diffusion profiles, it appears that some yttrium atoms spread out of the specimen, through the SiC powder. Whereas yttrium was exclusively present in the intergranular phase of the SiAlON previous to the experiment, a centrifugal mechanism has induced a composition gradient from the specimen and up to more than 2 mm away. However, since potassium and sodium were also detected between the SiC particles, a concurrent centripetal diffusion from the borosilicate glass has occurred.

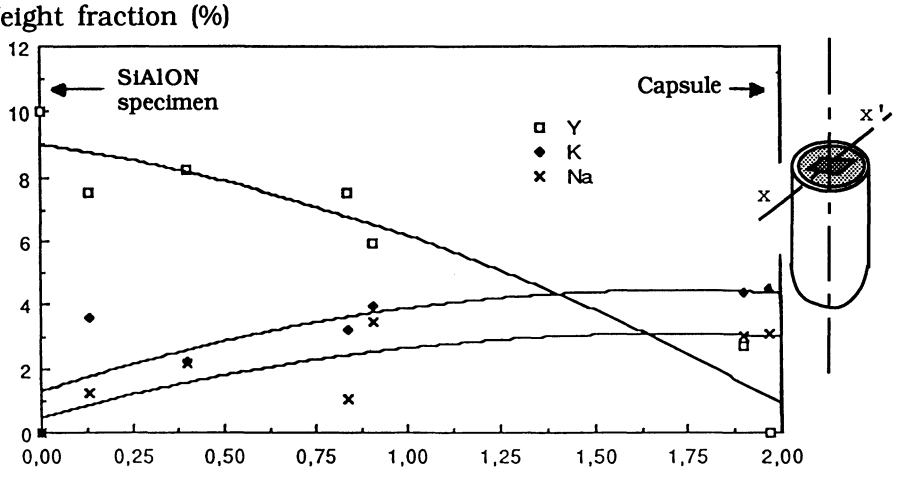

- Figure 4 -

Microstructure of samples before and after testing are roughly similar. The average grain size is identical and the grain shape didn't change. From X.R.D. analysis, no secondary crystalline phase appeared. Nevertheless, with regard to T.E.M. observations (figure 5), heat-treated samples seem to have a more compact microstructure, exhibiting many grain/grain contact areas, where dislocations appeared as a result of high pressure and high temperature. Therefore, whereas the as sintered SiAlON contains a lot of glassy phase pockets, the H.I.P. treated specimen is expected to be less dependent on its intergranular phase.

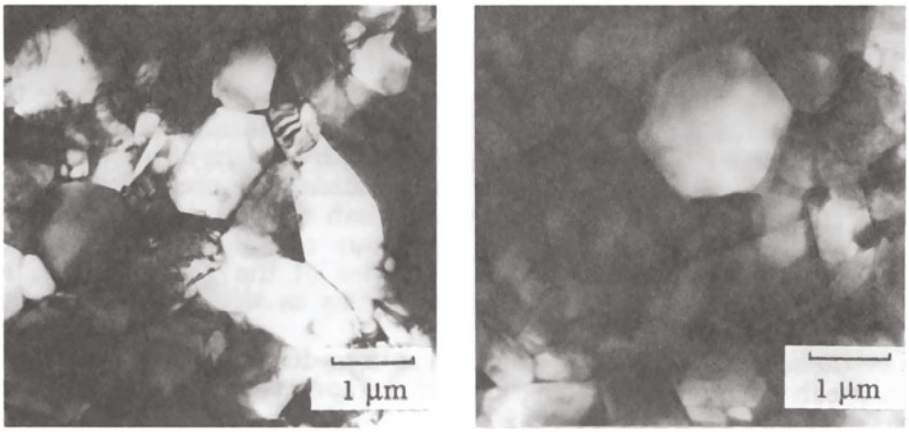

As-sintered After HIP treatment

- Figure 5 -

Creep curves obtained at 1200°C under 240 MPa are plotted together in figure 6 for samples as-sintered, after H.I.P. treatment and after an additional recrystallization heat-treatment at 1250°C under nitrogen for 48 hours.

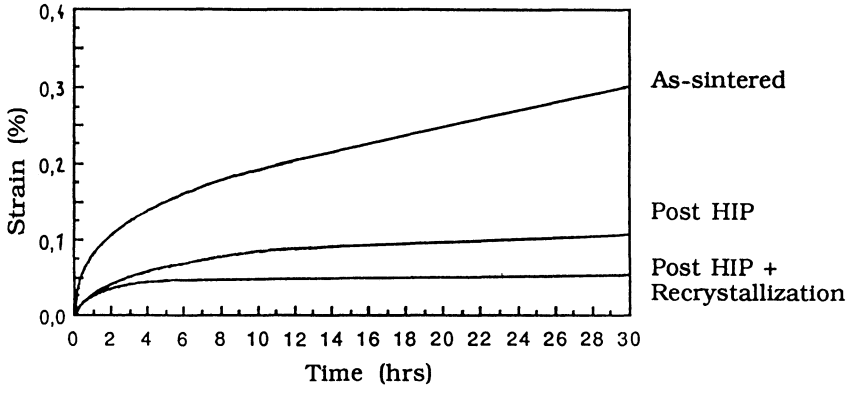

- Figure 6 -

The total strain of the specimen after H.I.P. treatment is about one third of that for the as-sintered body. SiAlON(s) having elongated grains, it is impossible to remove all the glassy intergranular phase. Whatever the pressure is during the treatment, a residual fraction of the vitreous phase is trapped in close domains as the grains rotate and slide each with regard to the other. A further improvement of the creep resistance can be achieved by recrystallization of the residual glassy phase. In such case, the total strain is further reduced by a factor 2. It means that for SiAlON(s) ceramics containing some glassy phase, the creep deformation is divided by a factor 6 after H.I.P. and recrystalliszation treatments. It is noticeable that the recrystallization step may be easily include in the H.I.P. cycle for convenience.

CONCLUSION

We have presented a post sintering H.I.P. treatment that is able to greatly improve the creep resistance of SSN β' SiAlON(s) ceramics. The improvement derives from the exudation of a significant fraction of the intergranular glassy phase. A recrystallization treatment of the remaining glassy pockets results in a further amelioration. The creep deformation of the treated sample is six times lower than the one of the untreated material. The high temperature behaviour of silicon nitride based ceramics being governed by the properties of the glassy phase, an improvement of all the mechanical properties as well as the oxidation resistance can be expected.
Since the feasibility of the technique has been demonstrated, we suggest that it can be applied to strengthen any ceramic containing some glassy phase.

Acknowledgement:
We are grateful to MM. W. Mustel and L. Minjolle, from 'Ceramiques et Composites' (Bazet, France), for providing the silicon nitride materials and for fruitful discussions.

REFERENCES

[1] A. Miyamoto, 'Hot isostatic pressing and application for high performance ceramics', Taikabutsu Overseas 1 [6] (1983).
[2] J.C. UY and E.R. Herman, 'Isostatic densification and strengthening of reaction sintered Si_3N_4', Proc. Fifth Army Mater. Tech. Conf. Cer. High. Perform. Appl. 2 1011-21 (1977).
[3] H. Okada, K. Homma, T. Fujikawa and T. Kanda, 'Fabrication of dense Si_3N_4 by hot isostatic pressing', High Tech. Cer. 38A 1023-32 (1987).
[4] R.L. Tsai and R. Raj, 'The role of grain boundary sliding in fracture of hot pressed Si_3N_4 at high temperatures', J. Am. Ceram. Soc. 63 9-10 (1980).
[5] C.C. Ahn and G. Thomas, 'Microstructure and grain-boundary composition of hot pressed silicon nitride with yttria and alumina', J. Am. Ceram. Soc. 1 66 (1983).
[6] G. Ziegler and G. Wotting, 'Post-treatment of pre-sintered silicon nitride by hot isostatic pressing', High Tech. Cer. 1 31-58 (1985).
[7] D. Bethge, 'High temperature creep and slow crack growth properties of HPSN as an example of ceramics containing a glassy phase', J. High Tech. Cer. 3 199-230 (1987).
[8] J.L Besson and P. Goursat, 'Post-sintering Hot Isostatic pressing of SiYAlON(s) materials', Ecole Nationale Superieure de Ceramique Industrielle (Limoges, France), internal report (1985).
[9] T. Rouxel, J. L. Besson, C. Gault, P. Goursat, M. Leigh and S. Hampshire, 'Viscosity and Young's modulus of an oxynitride glass', J. Mat. Sci. Lett. 8 1158-60 (1989).
[10] S.Hampshire, R.A.L. Drew and K.H. Jack, 'Viscosities, glass transition temperatures, and microhardness of YSiAlON glasses', Com. Am. Cer. Soc. [3] C.46-47 (1984).

HIGH STRENGTH HIPRBSN - AN OPTIMIZATION BY STATISTICAL METHODS

PETRA DÖTSCH, MATTHIAS STEINER, JÜRGEN HEINRICH
Hoechst CeramTec AG, Wilhelmstrasse 14, 8672 Selb, Germany

ABSTRACT

Because of the high content of the beta modification in sintering additive containing RBSN it was assumed that this typ of Si_3N_4 cannot be densified by sintering or HIP to a high strength material. By using statistical methods it could be shown however that the homogeneity of the microstructure - regardless of the beta content - is the most important strength controlling factor. By carrying out 32 Taguchi tests, 2048 experiments have been simulated concerning the influence of the starting silicon powder, the typ and concentration of additives and the prepararion parameters on the microstructure and the resulting mechanical strength. By combining the optimum processing parameters Weibull moduli $sigma_0$ of about 1000 MPa and m of about 30 could be achieved in 4-point bend testing in HIPRBSN with beta contents of about 50 percent in the starting RBSN material.

INTRODUCTION

Application of dense silicon nitride is nowadays particularly discussed in the field of engine construction with regard to valves, valve guides, valve seat rings, diesel pre-combustion chambers, turbocharger rotors or wearing parts. Due to its good mechanical characteristics HIPRBSN is in particular reputed to be a promising material for such applications. The mechanical characteristics of this material are first of all dependent on the structural parameters varying according to the production process involved |1|. Similar as for the densification of pressed parts made from silicon nitride powder it is presumed that the starting material (in this case RBSN) should have a highest possible alpha content. If sintering additives are con tained liquid phases will develop on the particle surfaces during the sintering process together with SiO_2 which is always available for thermodynamic reasons. In liquid phase sintering the alpha crystallites will dissolve in the liquid phase and precipitate as beta crystallites in case of supersaturation |2|. The hexagonal beta crystallites show a higher growth rate towards the crystallographic c-axis than towards the a-axis which results in a rod-like grain morphology and in an interlocked high strength microstructure.

To produce high strength components, however, it is also necessary to distribute the sintering additives which use to reappear as amorphous

grain boundary phase after sintering in a homogenous way and to avoid moulding faults which may result in even worse microstructural faults. That is why it is required to optimize the milling and mixing procedures and especially the moulding process. As even the temperature/time programs and the gas composition during the sintering process will affect the homogenity of the component there are numerous factors to be considered that may be studied only with enormous difficulties in a serial production with full factorial test plans.

For this reason the statistical test planning according to Taguchi has been used to optimize the strength of HIPRBSN, by studying such factors affecting its use like silicon powder, type of additives, concentration of additives, pretreatment of additives and preparation. By full factorial test planning this would have required 2048 experiments while by means of the statistical test planning by Taguchi these experiments could be reduced to 32 studies.

DESIGN OF EXPERIMENT BY TAGUCHI

The design of experiment by G. Taguchi's method is an effective means to explore the influence both of individual parameters and of their interaction on the characteristics of test samples. Using highly condensed fractional factorial plans the test efforts are reduced to a fraction of full factorial plans. The so-called orthogonal array will simultaneously reduce the misinterpretation of results that might occur due to disturbing (noise) factors respectively unknown interactions.

A precondition for the use of design of experiment is the exact knowledge of all details of the production process and of their effects as well as the determination of reference values and tolerances which allow the part to be passed over from one production step to another. The novelty of G. Taguchi's method is on the one hand the extreme reduction of the test effort and on the other a target concentrated quality definition as well as the introduction of the signal/noise concept.

The basis of Taguchi's testing are orthogonal arrays. Such arrays are available for double-, three-, four- and five-stage parameters and specify which parameters will have to be set for the respective tests. Orthogonal means here that the stages of one parameter are equally often available in the test.

While two- and multi-parameter interactions had been strictly ignored in the beginning, these special test plans allow now to verify the theoretically possible maximum number of parameters (resulting from the mathematical statistics as per the degrees of freedom of the parameters to be tested), based on the number of tests specified. As an example Plan L 16 is to be indicated here where 5 four-stage parameters can be treated by 16 tests only. In a full factorial plan 1024 test would be required. If required parameter interactions can of course at any time be verified explicitely, thus reducing the number of parameters to be tested accordingly.

The second part of the Taguchi method is the strict application of the signal/noise analysis. This analysis refers to the deviation of the measured values from the average value, weighted as per the root mean

square, the value thus received being rescaled in Dezibel, so that a high S/N value (signal to noise ratio) corresponds to a minimum dispersion. In case a measurable variable is to be minimized, maximized or set to a specified reference value there are similar S/N value calculation methods available to weight simultaneously minimum dispersion and distance from a reference value. The variance analysis and the application of the f-value statistics indicate the percentage of effectiveness of the tested parameters.

A detailed explanation of the proceedings is to be seen from |3|.

EXPERIMENTAL DETAILS

Hot-isostatically post densified reaction-bonded silicon nitride is produced by nitriding silicon powder mouldings that contain sintering additives and by subsequent post densification (HIP) of those RBSN parts. The production process starts by a milling run to disperse the sintering additives homogeneously in the powder mix, shatter agglomerates, reduce the initial grain size and increase the specific surface area of the powder mix. The powder mix obtained is then cold-isostatically pressed at 200 MPa or organic plastifying constituents are added and then it is injection moulded or further processed to samples by slip casting. In the subsequent nitriding process the mouldings from silicon powder are transformed into silicon nitride at 1100°C to 1450°C in nitrogen atmosphere under atmospheric pressure. The temperature-time program of this exothermal reaction depends on the geometry of the components and the particle size of the silicon powder. Thereafter the RBSN specimens are hot-isostatically post-densified using nitrogen-argon mixes as pressure transmitting medium. Under gas pressures of up to 200 MPa and densifying temperatures of up to 1900°C as well as in variable temperature-time programs and by means of the sinter canning technique |4| the mouldings achieve almost a theoretical density. Due to the multiple factors affecting the strength very high efforts are required to verify all parameters in a factorial testing. The design of experiment by Taguchi provides for a method to minimize the test numbers required.

All tests have been run according to Taguchi's method by elaborating two successive test plans of an L16-design, each, i.e. 16 tests of 5 respectively 6 influencing factors (parameters) being varied in 4 respectively 2 stages. In a full factorial test plan 2048 experiments would have been required instead of such 32.

In the first Taguchi test plan 4 different silicon starting powders have been tested, varying in their grain morphologies, grain size distributions, specific surface areas and chemical impurities (Table 1).

TABLE 1
Specification of the silicon starting powders

Si Starting Powder	d_{90}	d_{50}	d_5	spec. surface area	chemical impurity content
1	29,0 µm	10,0 µm	0,7 µm	2,8 m²/g	Fe: 0,58 % Al: 0,26 % Ca: 0,13 % Ti: 0,05 %

2	4,4 µm	2,3 µm	0,6 µm	6,3 m²/g	Fe: 0,42 % Al: 0,36 % Ca: 0,07 %
3	8,0 µm	4,5 µm	1,0 µm	2,6 m²/g	Fe: 0,08 % Al: 0,10 % Ca: 0,01 %
4	25,0 µm	9,0 µm	1,3 µm	2,0 m²/g	Fe: 0,07 % Al: 0,13 % Ca: 0,01 %

These starting powders have been doped by 4 different combinations of sintering additives (Y_2O_3, Nd_2O_3, CeO_2, MgO always in combination with Al_2O_3), varying the content of sintering additives as well by 4 stages (2,5%, 5%, 7,5%, 10%). The sintering auxiliaries have been added either directly to the silicon powder or premilled in wet condition in a laboratory ball mill respectively attritor mill and then mixed with the silicon powder. As a forth variation the sintering additives have been melted to a pre-homogenized glas phase, then powdered and added to the silicon powder. These starting powders are prepared in four different ways, either by dry milling respectively wet milling in a laboratory ball mill or as further alternative by means of a kneading process. This results in 16 tests with 5 four-stage parameters. Full factorial testing would require 1024 experiments (Table 2).

TABLE 2
Comparison of a full factorial test plan with the Taguchi test plan I

Factor	Level	Number of Experiments Taguchi	Full Factorial
Silicon Powder	4		
Additive Types	4		4^5
Additive Contents	4	16	=
Additive Treatment	4		1024
Refining	4		

Based on the results of this first test plan another program has been elaborated. Again 4 different silicon powders to which the best additive combination of the first plan had been added (Y_2O_3/Al_2O_3) have been tested. The additive content has again been varied in 4 stages (5%, 10%, 12,5%, 15%). The only way of refining was the wet milling as it had in the first test plan brought the best results with regard to strength and should therefore be further studied in the second plan. Milling media used have been Isopropanol and Ethanol and the milling time has been varied in 4 stages (12h, 24h, 36h, 48h). The solids content of the milling slip has been set so that every slip showed the same viscosity. The powder mixes obtained have been further processed both by slip casting and by cold-isostatic pressing. Before the hot-isostatic post-densifying the test specimens are encapsulated in 4 different ways. Thus, the elaborated test plan consists of 4 four-stage parameters and 2 two-stage parameters, resulting in 16 Taguchi experiments. Full factorial testing would again require 1024 tests (Table 3).

TABLE 3
Comparison of a full factorial test plan with the Taguchi test plan II

Factor	Level	Number of Experiments Taguchi	Full Factorial
Silicon Powders	4		
Additive Contents	4		$4^4 \times 2^2$
Milling Time	4	16	=
Milling Medium	2		1024
Shaping	2		
Encapsulation	4		

As to the starting powders and the prepared powder mixes the specific surface area of the powders has been determined according to BET method and the grain size distribution by means of a sedigraph. Measurement of RBSN- and HIPRBSN density has been done according to Archimed's principle at room temperature in mercury respectively in water. The share of alpha respectively beta Si_3N_4 phases has been determined by quantitative x-ray diffraction analysis. Structure analysis by scanning electron microscope has been done in HIPRBSN condition. Strength in HIPRBSN condition has been determined by test bars of the dimensions 3 mm x 4 mm x 45 mm, three sides being ground and one side polished. The method applied was the four-point bending test with an outer span of 40 mm and an inner span of 20 mm. Evaluation is based on the Weibull statistics.

RESULTS AND DISCUSSION

The mechanical strength of HIPRBSN at room temperature is influenced by a lot of productions parameters (see above). By means of design of experiment and evaluation it is possible to find out the effects of the individual control variables on a certain target characteristic, here the strength at room temperature. To determine the effect of the control variables Taguchi refers to the variance analysis.

By such variance analysis the contribution of a single variance of each tested parameter towards the overall variance can be determined. The evaluation of table 1 refers to Taguchi's first test plan.

TABLE 4
Variance analysis according to Taguchi for strength

Control Variable	Effect %
Type of Si Powder	23,31
Type of Additive	15,42
Additive Content	13,65
Pretreatment of Additive	8,70
Refining of powder	36,74
Error (fault due to Disturbing Effects)	2,18
Total	100,00

From the calculation it can be seen that for an increase of the room temperature strength first of all the type of powder preparation and the starting silicon powder are decisive as they show the highest effect on strength. Of less importance as to an increase of the strength are type and content of sintering additives while a pretreatment of the additives

has hardly any influence as to the strength due to the low percentile. These "variables" will no longer be taken into account for the following considerations.

The variance analysis has been made out in both of the test plans for all measurable variables (specific surface area, grain size distribution (d_{50}), green density, alpha-Si_3N_4 share and density in RBSN condition, strength and density in HIPRBSN condition).

Moreover, the effect of each variable on the scattering behaviour of the measured values can be looked upon separately by means of the signal/noise (S/N) ratio. In its most simple form the S/N ratio represents the standard deviation of the series of measurements. For the strength variable a S/N ratio has been calculated for 20 specimens in each case. The higher the S/N value calculated the better the result with regard to strength and dispersion behaviour. Halfing the dispersion will result in an approximate increase of the S/N value by 10, doubling the strength level in an increase by 6. Evaluation of the signal/noise analysis is done by means of the Taguchi graphs. The way of powder preparation is shown as an example as it shows the highest effect on strength according to the results of the variance analysis (Fig. 1). The highest signal/noise ratios have been obtained by wet prepared powder mixes. This means that wet preparation, apart from highest strength values, will also lead to the lowest dispersion of the individual values. Low dispersion, again, is connected with high values for the Weibull modulus. The high strength values are based on the very good mixing efficiency of this type of preparation. The signal/noise ratio has also been determined in both of the test plans for every influencing variable with regard to all measured values.

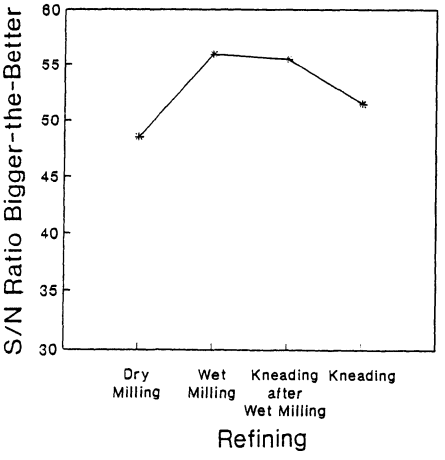

Figure 1: Signal/Noise analysis of the type of refining with regard to strength

Due to this evaluation especially the wet milling has been further studied in the second Taguchi plan. By wet milling and increasing the milling time as well as by using pure fine grain silicon starting powder a further increase in strength could be achieved (Fig. 2).

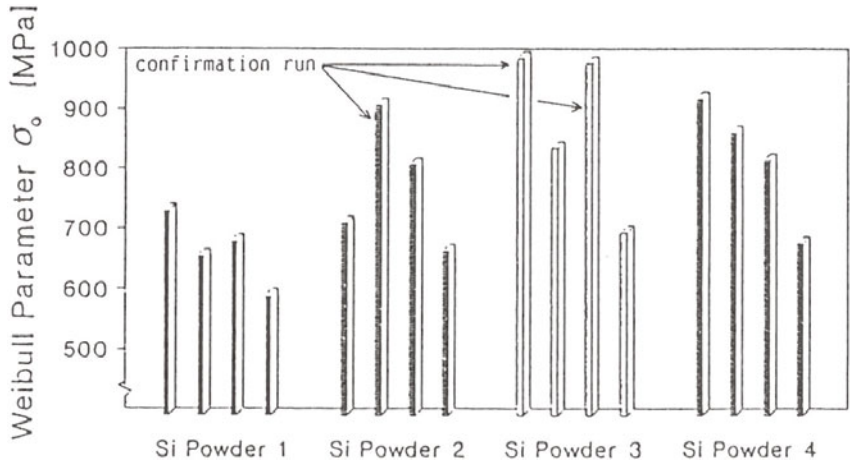

Figure 2: 4-point-bending-strength of HIPRBSN using different starting silicon powders, additive contents, milling time and medium, type of moulding and of encapsulation according to Taguchi-plan II (table 3) including the confirmation runs (table 5).

Guided by these results another important step can be taken, i.e. the proof of analysis. The confirmation run includes one or even several tests combined of the respective optimum parameters of the test plan. The measurable values to be obtained are precalculated and the demonstration experiment must correspond to these predictions. When combining the optimum parameters such variables have been selected that had achieved high strength values before, all other points have been disregarded.

By the tests of the confirmation run average room temperature strength values between 900 and 1000 MPa have been obtained with Weibull modules up to 30. All material modifications that had been realized achieved almost theoretical density in HIPRBSN condition, independent of their alpha-Si_3N_4 share and their density in RBSN condition. At starting RBSN condition densities ranged from 2,07 g/cm³ to 2,26 g/cm³ and the share in alpha-Si_3N_4 phase between 24% and 93% (Tab. 5).

TABLE 5
Material characteristics of RBSN and HIPRBSN produced in the confirmation run

Confirmation run	Density RBSN	Alpha-Share RBSN	Density HIPRBSN	σ_0 HIPRBSN	m HIPRBSN
1	2,11 g/cm³	24 %	3,16 g/cm³	894 MPa	13
2	2,07 g/cm³	93 %	3,26 g/cm³	953 MPa	15
3	2,26 g/cm³	54 %	3,25 g/cm³	978 MPa	30

Before this test program had been run the room temperature strength of HIPRBSN was approx. σ_o = 686 MPa with a Weibull modulus of 10. The main reason for this enormous increase in strength is the very good mixing efficiency by wet preparation of the starting powder mixes. Wet milling results in very fine powder mixes with high specific surfaces and homogeneously distributed sintering additives. The RBSN microstructures involved are very uniform and fine porous of relatively low density and also homogene distribution of the sintering additives. A very fine grain

structure is produced from these RBSN structures by hot isostatic post densification where the individual silicon nitride grains have a good interlocking and a rather high aspect ratio of 6-7, independent of the starting alpha-Si_3N_4 share (Fig. 3).

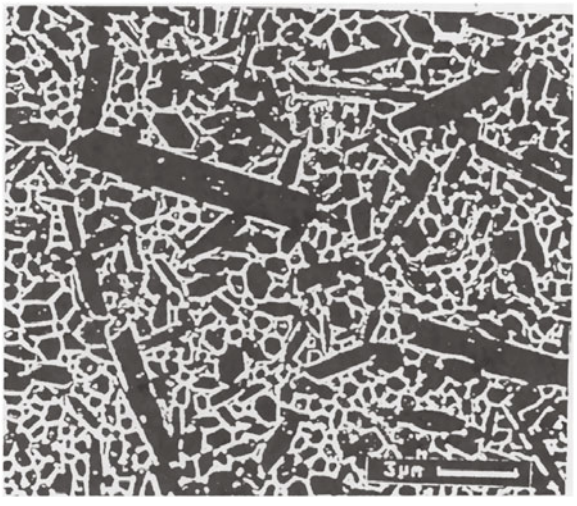

Figure 3: HIPRBSN microstructure, SEM, polished and etched microsection

According to these experiments strength in HIPRBSN condition is no function of the alpha share in RBSN condition as both with low and with very high alpha-Si_3N_4 contents good strength values are obtained (Table 5). Meanwhile, the results have been translated to components (valves). The room temperature strength values measured on specimens worked out of such components are σ_o = 870 MPa at a Weibull modulus of m = 14 (Fig. 4).

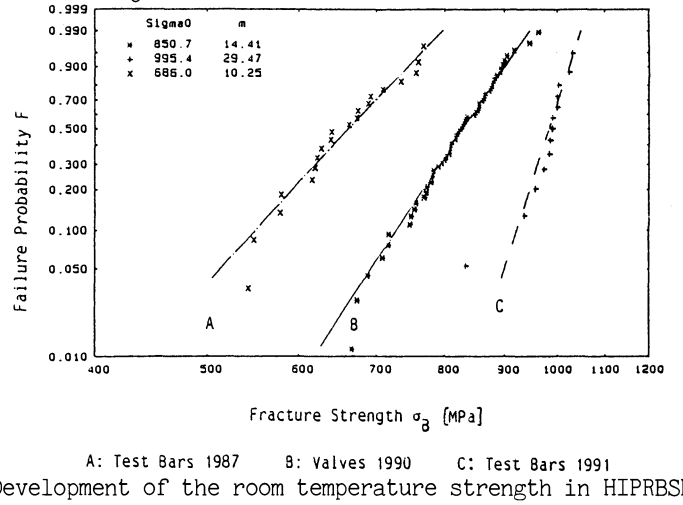

A: Test Bars 1987 B: Valves 1990 C: Test Bars 1991

Figure 4: Development of the room temperature strength in HIPRBSN by using design of experiment by Taguchi

OUTLOOK

By means of design of experiment by Taguchi characteristics like the strength of HIPRBSN can be optimized with a minimum of testing. The scientific interrelationship between production parameters, structure and strength, however, cannot be definitely clarified this way. To obtain positive results it is a prerequisite to have a certain knowledge of fundamental relations between production parameters, structural parameters arising and the characteristics to be optimized.

This procedure is certainly suited to optimize a ceramics production process as to a special characteristic. For the fundamental research of relations in natural science now as before the full factorial test plan will be required.

REFERENCES

1. Ziegler, G., Heinrich, J., Wötting, G.: Review; Relationship between Processing, Microstructure and Properties of Dense and Reaction-bonded Silicon Nitride, J. Mat. Sci. 22 (1987) 3041-3086

2. Lange, F.F.: Silicon Nitride Polyphase Systems: Fabrication, Microstructure and Properties, International Metals Reviews 1 (1980) 1-20

3. Taguchi, G.: System of Experimental Design. American Supplier Inst., Dearborn, Mich., (1987)

4. Heinrich, J., Böhmer, M.: Process by compacting a porous structural member for hot isostatic pressing, US Patent 4,812,272

OPTIMIZED FABRICATION OF SILICON NITRIDE BALL BEARING PARTS

H.-J. RITZHAUPT-KLEISSL, A. KÜHNE,* R. OBERACKER*

Institut für Materialforschung, Kernforschungszentrum Karlsruhe GmbH, Postfach 3640, D-7500 Karlsruhe, Federal Republic of Germany

* Institut für Keramik im Maschinenbau (IKM), Universität Karlsruhe, Postfach 6980, D-7500 Karlsruhe, Federal Republic of Germany

ABSTRACT

An optimized fabrication route for silicon nitride (Si_3N_4) with low amounts of sintering additives was established. By careful powder preparation, near net cold forming and by a well controlled Sinter/HIP process ball bearing parts with full density, good mechanical properties and a fine-grained microstructure of high aspect ratio were achieved. As a main advantage of this process, no encapsulation is required to obtain fully dense material.

INTRODUCTION

Silicon nitride (Si_3N_4) is one of the most promising materials with respect to ceramic ball bearing applications. Low specific weight, high strength combined with rather high toughness, good abrasion behaviour and corrosion resistance as well as the suitability for high temperature application are favouring this material. Possible fields of application for those ball bearings are e.g. high-precision tool-machines due to the material's high stiffness. The low specific weight of silicon nitride reduces the centrifugal forces of high-speed bearings and favours aerospace application. Low abrasion, even with poor or no lubrication, high temperature strength and good corrosion resistance allows operation in special environments. Furthermore Si_3N_4 is non magnetic and is a good thermal as well as an electrical insulator.

Nevertheless, all these positive properties have to be seen together with the problems arising from the fabrication of such high performance ceramics. A general review on production routes and properties of Si_3N_4-ceramics is given e.g. by Ziegler et al. [1]. To overcome these problems a fabrication route with a consequent optimization of each processing step must be realized.

OBJECTIVES

Considering the application as high performance ball bearings and in order to meet the requirements for these it is necessary to establish a fabrication route finally resulting in a product which can meet the specifications and demands. To reach this, all the fabrication steps must be optimized.

First there must be an optimized powder composition with the amount of sintering additives kept as low as possible. This will avoid the formation of amorphous grain boundary phases which deteriorate the mechanical properties.

Another step, which must be optimized is the procedure of powder preparation, which consists of mixing/milling, drying and granulation of the powder. Here, the objective is a homogeneous mixture consisting of granulates which give a high tap density but can easily be destroyed and compacted by low pressures during the cold forming process.

Cold forming is another important step in the fabrication route. A high green density is favourable for several reasons: with respect to near net shape forming, a large - not well controllable - shrinkage shall be avoided and an already high density before the heat treatment can perhaps allow lower processing temperatures and shorter times. With respect to minimize expensive grinding of the sintered bodies a preshaping or calibration should be performed on the cold-pressed parts, taking into account the shrinkage during the final densification step.

As the last step, a capsule free Sinter/HIP process with optimum process parameters must be applied to obtain dense material with a fine grain size and best mechanical properties. Furthermore economical aspects like wear of the HIP and spent of gas as well as time must be taken into account.

EXPERIMENTAL PROCEDURE

Starting materials and powder preparation

The starting materials were as follows:

- Silicon nitride, type UBE-SN E10. This powder has a specific surface area of about 12 m^2/g, a particle size of about 0.2 μm and an alpha-phase content of ~95%.
- Yttrium oxide and aluminium oxide from Ventron were used as sintering additives.

The standard mixture of Si_3N_4 + 5 w% Y_2O_3 + 1.5w% Al_2O_3 gave satisfactory results.

The preparation of a homogeneous mixture was done by intimate wet milling and mixing the starting powders under ethanol. This was carried out in a ball mill with the lining and the balls made from Si_3N_4. Using this equipment contamination of the powder with undesirable elements could be avoided.

One of the most important needs in ceramics development is the avoidance of the formation of inner flaws in the sintered material. To maintain this, a granulate must be fabricated, consisting of granules which are stable enough to give a good flowing behaviour and tap density, but which, on the other hand are soft enough to be easily destroyed and compacted by dry pressing. Therefore various parameters for drying the powder slurry in a rotation evaporator were tested. A fast and easy quantitative classification of the granules resulting from these experiments was performed using a special granules tester developed at the IKM [2]. Measurements on different granules showed that the drying temperature has a major influence. Powders

from the same milling process could be dried to granules with a difference in fracture strength of one order of magnitude. This reduction of the fracture strength was reached just by reducing the drying temperature from 80 to 30 °C at constant boiling temperature. Taking into account all the aforementioned facts and experimental experience, a homogeneous granulate consisting of submicron size primary powder particles could be reached.

Cold forming/ Cold isostatic pressing (CIP)

The precompaction steps were chosen differently for the balls and for the rings. Precompaction of the balls was done in a dry-bag CIP with special ball moulds followed by a subsequent pre-shaping and calibration step. The rings at first were prepressed in an axial press with special tools, then they were CIP'ed in a wet-bag CIP and also pre-shaped.

Final densification by Sinter/HIP

The determination of optimum process parameters for a capsule free Sinter/HIP process requires knowledge of the materials densification behaviour during all stages of the thermal treatment. For continuous monitoring of the material's shrinkage during heat treatments even at highest pressures a special HIP-dilatometer for use in a Sinter/HIP equipment had been developed [3].

In former experiments a maximum temperature of 2000 °C with a pressurization to 200 MPa and a holding time of 2h was used. With help of HIP-dilatometer measurements the process parameters could be optimized within only a few Sinter/HIP cycles. As shown in fig.1 a maximum temperature of 1950 °C and a maximum pressure of 50 MPa is sufficient, if the pressurization is started just after the stage of pore-closure

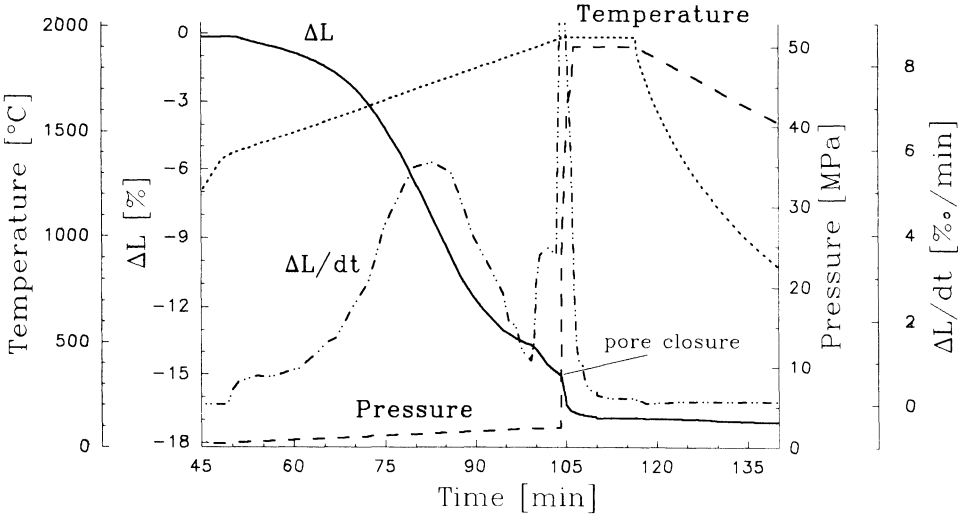

Fig. 1: Part of the optimized Sinter/HIP-cycle as monitored by the HIP-dilatometer

(at about 92 %TD) has been reached. Furthermore, due to the exact process supervision and control the holding time at maximum temperature and maximum pressure could be reduced to about 15 minutes, as no

further increase in densification occured. With these process improvements not only better material properties, but also a significant reduction of the process costs could be achieved.

RESULTS

When following the fabrication route as described above, ceramic ball bearing parts could be obtained which show good values with respect to density, microstructure, surface and mechanical properties. An overview of the data is given in table 1.

TABLE 1

Mechanical properties of the Si_3N_4 ball bearing ceramics

Max. bending strength	[N/mm^2]	930 - 1300
Vickers hardness HV10	[-]	~1600
Fracture toughness K_{Ic} (Indentation method)	[Mpa$\sqrt{m}$]	~8

The open porosity was measured by mercury intrusion porosimetry. As shown in fig. 2, the values lie well below 0.5%, giving a density of more than 99.9%TD.

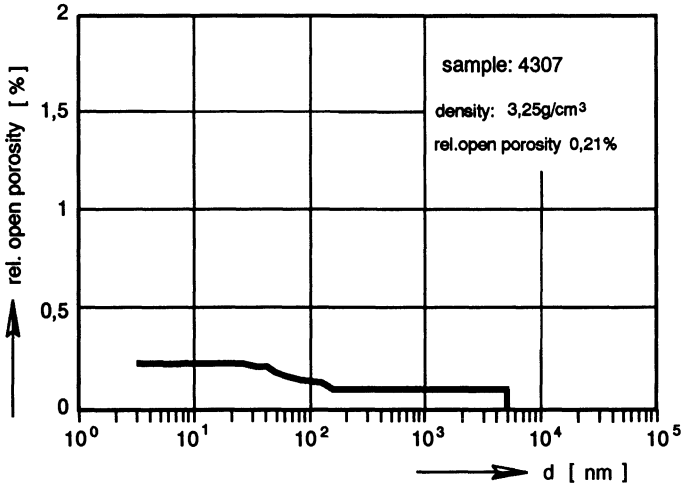

Fig. 2: Cumulative open porosity versus intrusion channel diameter

Characterization of the material was done by X-ray diffractometry, ceramography and by SEM- and EDX-analysis. Fig. 3 shows fracture surface SEM pictures of non optimizd (left) and optimized material. As can be seen, an undesirable grain coarsening occured during the former processing. After process optimization a very fine, homogenious microstructure of high aspect ration with a grain size of about 1μm could be achieved. No glass phases were detected by X-ray diffractometry.

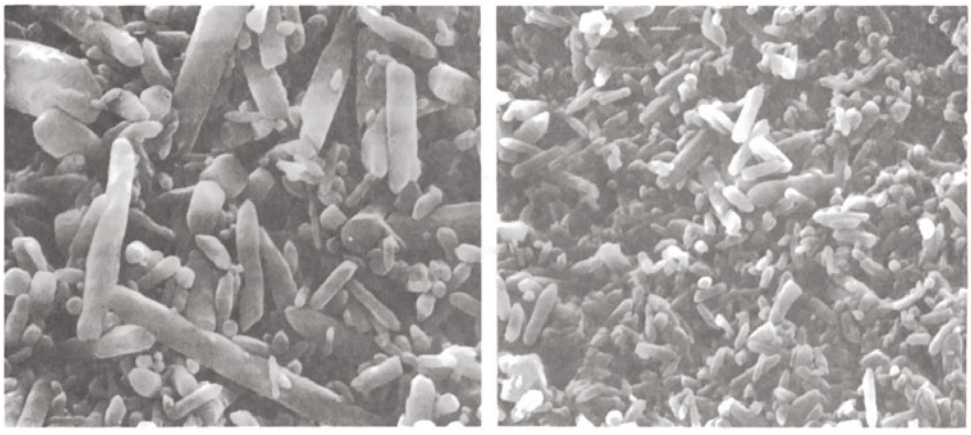

Fig. 3: SEM pictures of etched fracture surfaces: a) former fabrication b) optimized fabrication

A final surface finishing by grinding was done for a set of balls as shown in fig 4. A very smooth surface could be reached.

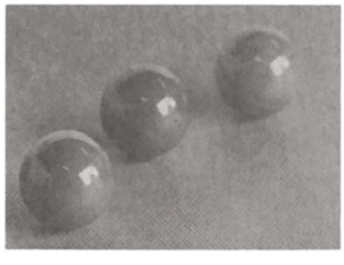

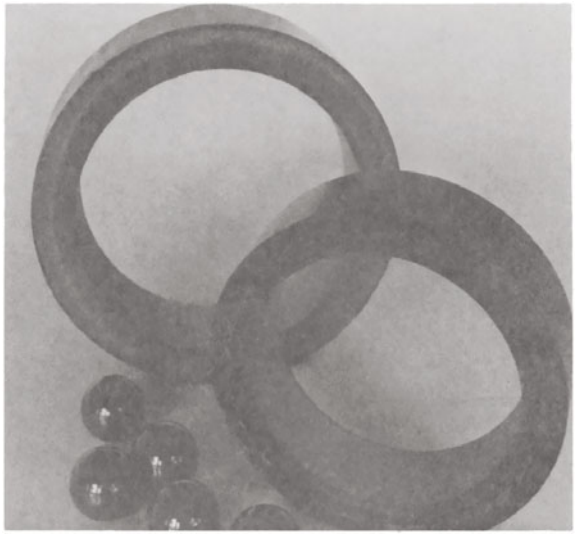

Fig. 4: Si_3N_4 ball bearing parts

CONCLUSIONS

As could be shown, it is possible to obtain fully dense Si_3N_4-ceramic parts for high performance application such as for ball bearings by use of a combined Sinter/HIP process without any expensive encapsulation prior to final densification. Neither glass nor metal canning is needed. However, to meet the requirements it is necessary to develop a well defined production route with detailed process supervision and control.
As an outlook it should be mentioned that there is still a great potential for further improvement of Si_3N_4-ceramics with respect to properties as well as with respect to processing, especially in the field of powder treatment, such as mixing, drying, preparation of an optimized granulate and cold forming of the green bodies.

REFERENCES

[1] Ziegler, G., Heinrich, J. and Wötting, G., Realtionships between Processing, Microstructure and Properties of Dense and Reaction-bonded Silicon Nitride. J. Mater. Sci., 1987, **22**, 3041 - 3086.

[2] Oberacker, R., Ottenstein, A. and Thümmler, F., Characterization of granules by measurement of load-deformation curves with newly developed strength tester. In Proc. 2nd Int. Conf. on Ceramic Powder Processing Science, ed. H. Hausner, G.L. Messing, S. Hirano, DKG, Köln 1989, pp. 415-24

[3] Kühne, A., Oberacker, R. and Thümmler, F., HIP-Dilatometer for Process Development in Powder Materials. Powder Met. Int., 1991, **23**, 113 - 119.

PREVENTION OF THE COLOR CHANGE IN HIP'ING OF ZIRCONIA CERAMICS

AKIRA KITAMURA, SHOJI KUBODERA, HIDEHARU YAMAMOTO, AKIRA MIYAMOTO, and TAKASHI TSUKUI*
Advanced Technology Research Center, NKK Corporation
Kawasaki-ku, Kawasaki 210, Japan
*Helios Inc., Chiyoda-ku, Tokyo 101, Japan

ABSTRACT

The color of ZrO_2 ceramics (PSZ) changes from white to black by HIP'ing under reducing conditions, though mechanical properties of the material such as strength and toughness are much improved. The white color can readily be recovered by an appropriate heat treatment in an oxidizing atmosphere, whereas the strength markedly decreases by this heat treatment. A plain answer to this problem is the introduction of HIP equipment mounted with oxygen furnaces. The authors, however, have found an alternative solution from the viewpoint of utilizing conventional HIP facilities, HIP units that are equipped with graphite or molybdenum furnaces. The use of oxide crucibles and/or oxide powder bedding, as convection-preventive measures and also oxygen potential buffers, eliminated the problem caused by the extremely low partial pressures of oxygen in these furnaces.

INTRODUCTION

Some research results have already been reported on the color change of ZrO_2 in HIP treatment under reducing conditions. Masaki et al. and also Fujikawa et al. noted that carbon was detected in HIP'ed black ZrO_2 when they used graphite furnaces [1, 2]. Fujikawa et al. further mentioned that the color change was unavoidable even though molybdenum furnaces were used instead. On the other hand, Sasaki et al. reported that impurities in ZrO_2 such as Fe, Ti and C gave blackish colors to the material [3]. These results suggest that the color change of ZrO_2 during HIP'ing be caused by

(1) deoxidation and/or (2) carbon contamination of ZrO_2. The authors, therefore, propose the use of oxide crucibles and oxide powder bedding to avoid both deoxidation and carbon contamination. These oxide materials are expected to play an important part in HIP'ing as barriers against impurities and also create a local oxidizing atmosphere. Zirconia ceramics used in this study were 3mol%Y_2O_3-stabilized PSZ (partially stabilized zirconia).

EFFECT OF OXIDE CRUCIBLE AND OXIDE POWDER BEDDING

A preliminary test was conducted to find optimum setting configurations of ZrO_2 materials in HIP furnaces. Test pieces of round bars were set [I] in double crucibles of $A\ell_2O_3$, [II] in double crucibles of alumina together with $A\ell_2O_3$ powder, and [III] on an $A\ell_2O_3$ plate, as shown in Fig. 1. The bars had the dimensions of 3.2 mm in diameter and 10 mm in length. The $A\ell_2O_3$ materials were of 99.9% purity and the average size of the powder was 100 μm in diameter. The results, or the appearance of specimens after HIP'ing, are given in Table 1, along with the HIP'ing conditions. They ensured the effectiveness of the use of oxide crucibles and oxide powder bedding for the prevention of the color change of ZrO_2. In spite of carbon-free atmosphere the bars set on an $A\ell_2O_3$ plate in a molybdenum furnace showed the same results as those HIP'ed in graphite furnaces. It was concluded that the color change of ZrO_2 in HIP'ing was caused by de-oxidation of ZrO_2 rather than carbon contamination, or the diffusion of carbon into ZrO_2.

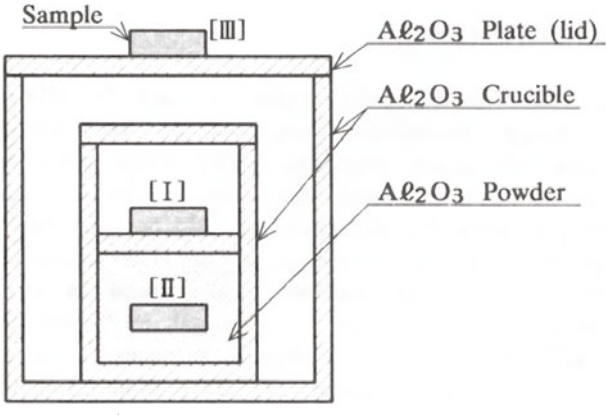

Figure 1 Setting of PSZ Samples in HIP'ing

TABLE 1 Preliminary-Test Results

Temperature (°C)	1400			
Pressure (MPa)	200			
Holding Time (hr)	2.0			
Pressure Medium	Ar Gas			
Furnace	Graphite			Molybdenum
Setting	[I]	[II]	[III]	[III]
Appearance after HIP'ing				

MECHANICAL PROPERTIES OF MODIFIED-HIP'ED ZrO_2

To evaluate the proposed, modified-HIP technique, the strength and toughness were measured of as-HIP'ed and post-HIP, heat-treated materials. HIP parameters in the test were the same as in Case [I] presented in Table 1, except temperatures, which ranged from 1300 to 1500 ℃. Post-HIP heat treatment (hereafter referred to as 'ageing') was conducted in an oxidizing atmosphere at 1000 ℃ for 1000 hrs. Four-point bending test and fracture toughness (K_{Ic}) measurement were carried out in accordance with JIS/R1601 and JIS/R1607 (SEPB method), respectively. The specimen size was 3x3x4 mm in both cases.

The change in flexural strength by ageing for modified-HIP'ing are illustrated in Fig. 2, together with the results for a conventional technique (Case [Ⅲ] with a graphite furnace). A maximum strength of 1715 MPa was achieved by modified-HIP'ing at 1500 ℃. No significant change in strength was recognized after ageing with the modified-HIP'ed zirconia, while the strength of conventional-HIP'ed PSZ markedly decreased by ageing. The K_{Ic} value, 4.5 $MPa\sqrt{m}$, of PSZ before HIP'ing was almost constant in all cases of HIP'ing.

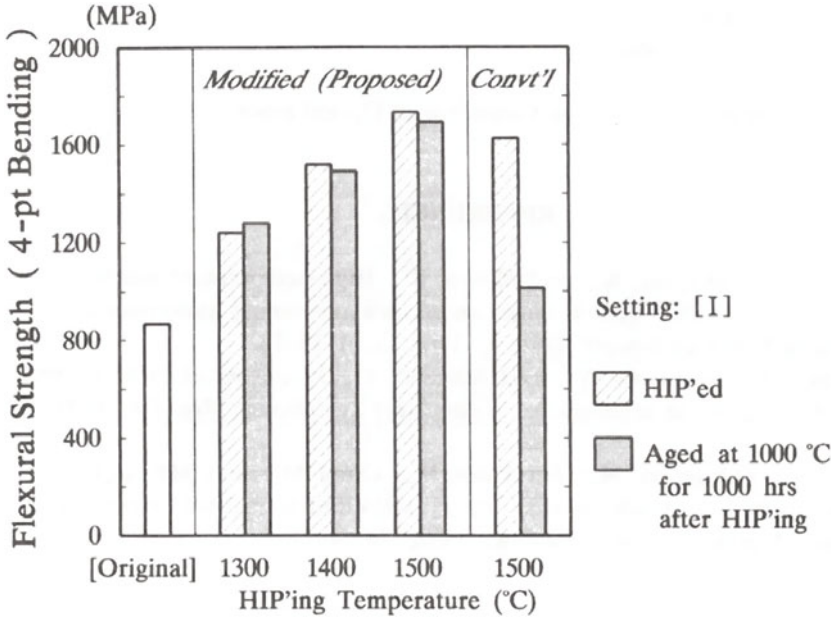

Figure 2 Change in Flexural Strength by Ageing for Modified- and Conventional-HIP'ed ZrO_2

From the above results, the modified HIP'ing, which employs oxide crucibles and oxide powder bedding, significantly improve the strength of ZrO_2 materials without the necessity of ageing procedure.

APPLICATION FOR OPTICAL COMMUNICATION USE

An application of this modified HIP is ZrO_2 sleeves used for optical communication, small sleeves that are connected with ferrules as illustrated in Fig. 3. The sleeves made of 3mol%Y_2O_3-PSZ had the dimensions of 3.2 mm in outer diameter, 2.5 mm in inner diameter, and 9.4 mm in length. HIP'ing temperature was 1500 °C and other HIP'ing conditions were the same as in the successful case previously mentioned. The modified-HIP'ed sleeves, with no change in their colors, demonstrated satisfactory clamping forces in the test of JIS/C5961. Fatigue tests are yet to be done.

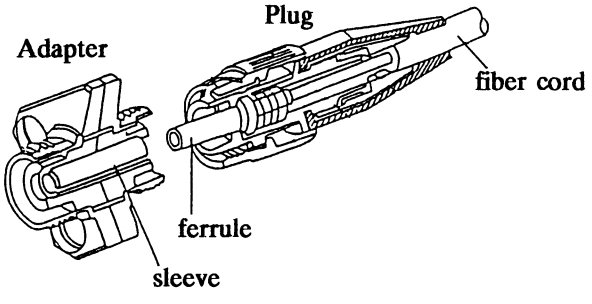

Figure 3 FC-type Connector of Optical Fiber

REFERENCES

[1] Masaki, T., Nakajima, K., and Shinjo, K., High-temperature mechanical properties of Y-PSZ HIPed under an oxygen-containing atmosphere. Journal of Materials Science Letters, 1986, 5, 1115-18.

[2] Fujikawa, T., Narukawa, Y., and Manabe, Y., Properties of oxide ceramics HIP'ed in oxidizing atmosphere. Kobe Steel Engineering Reports, 1990, 40, 73-6.

[3] Sasaki, T., Shiroyama, M., Furukawa, M., Ohno M., and Masaki,T., Analytical study of black-colored Y_2O_3-stabilized tetragonal zirconia polycrystals. Nippon Tungsten Review, 1987, 20, 4-11.

OPTICAL CHARACTERISTICS OF PLZT SINTERED BY O_2- AND Ar-HIP

SACHIO TOYOTA AND MITSUHIRO TAKATA
Sumitomo Special Metals Co., Ltd.
2-15-17 Egawa, Shimamoto-cho, Mishima-gun, Osaka, 618, Japan

ABSTRACT

Grain sizes and optical characteristics of PLZT(9/65/35) sintered by various methods, that is, O_2-HIP, Ar-HIP, vacuum sintering and atmospheric pressure sintering in air or oxygen, were compared. A transmittance increased with the loss of Pb (PbO) in firing process. Maximum transmittance at 400 nm wavelength was found in vacuum sintered samples, in which the amount of Pb was 7 at% short. Sintering by O_2-HIP or Ar-HIP improves the transmittance at wavelength above 500 nm without serious increase of the grain size.

Optical shutters of an electrophotographic page printer were made of these PLZT ceramics with fine grain size and high optical transmittance, and worked well as high speed printer.

INTRODUCTION

Lead lanthanum zirconate titanate ceramics (PLZT) have been used as switching devices of an electrophotographic printer [1] and as optical modulators for displays [2] because PLZT have large electrooptic coefficients and fast electrooptic responses. For the application of PLZT to microdevices such as printing machines, it is important to obtain defect-free and homogeneous polycrystalline state. In the case of optical shutters for an electrophotographic printer, a diameter of the individual shatter is 85 μm (300 dots per inch), therefore inhomogeneities in ceramics will cause the printed pictures improper shades. To obtain optical uniformity, usually it is desirable to suppress grain growth. We reported in a previous paper that PLZT ceramics with small grain size and high optical transmittance were manufactured by a combination of vacuum sintering and HIP.[3] Improvement of transmittance at long wavelength region was due to

the annihilation of pores.

In the present study, the influence of sintering atmosphere on grain sizes and optical characteristics of PLZT(9/65/35) was investigated. Sintering methods were as follows, O_2-HIP, Ar-HIP, vacuum and atmospheric pressure in air or oxygen. The HIP'ed PLZT ceramics are most suitable for optical shutters of an electrophotographic page printer with high printing speed and dot density.

MATERIALS AND METHODS

PLZT powder was prepared from chemical co-precipitation process and mixed oxide process according to the formula $Pb_{0.91}La_{0.09}(Zr_{0.65},Ti_{0.35})_{0.9775}O_3$. In the chemical co-precipitation process, $Pb(NO_3)_2$, $La(NO_3)_3$, $ZrO(NO_3)_2$ and $TiO(NO_3)_2$ were used as starting materials. They were dissolved in water and then PLZT compound was precipitated by adding ammonium hydroxide. The resulting slurry was filtered, calcined and milled. Specific Surface area of this powder was 1×10^4 m^2/kg by BET method. In the mixed oxide process oxide powders of 99.9 % or better purity were used as starting materials. They were blended, calcined and milled. Powder of 9×10^3 m^2/kg specific surface area was obtained by partially stabilized zirconia milling balls. Ceramics manufactured by the above two methods showed no difference in optical characteristics.

The powder was isostatically pressed at 500 MPa by CIP. The green density was 5 to 6 Mg/m^3. A firing process consisted of two stages. In the first stage, the green body was sintered at 1200 ℃ for 2 hours in vacuum. The grain diameter and density was 1.67 μm and 7.76 Mg/m^3 respectively. In the second stage, it was fired at 1100 to 1250 ℃ for 2 h by the following various methods, O_2-HIP, Ar-HIP, firing in vacuum and firing in air or oxygen at atmospheric pressure. Working gas used in HIP was 100 % argon or mixed gas of 90 % argon and 10 % oxygen and final pressure was 60 MPa.

Compositional ratios of Pb, La, Zr and Ti were determined by ICP-AES (Inductively Coupled Plasma-Atomic Emission Spectroscopy) and the change of Pb amount after firing was estimated from the formula, $Pb_{0.91}La_{0.09}(Zr_{0.65}, Ti_{0.35})_{0.9775}O_3$. ICP method is suitable for quantitative analysis of the amount of Pb and La in PLZT, but inadequate to determine whether the lost component is Pb or PbO.

An optical shutter array shown in Figure 1 was formed by grooving the ceramic thin plate with diamond blades. These shutter arrays were assembled into an electrophotographic copier.

RESULTS AND DISCUSSION

Optical properties of PLZT ceramics

Grain sizes for various second stage firing conditions are shown in Table 1.

Grain growth depends on sintering temperature. The rate of grain growth is lower in the case of HIP. As for firing time, the grain size reached about 10 μm after 100 h (1200℃, O_2, 100 kPa).

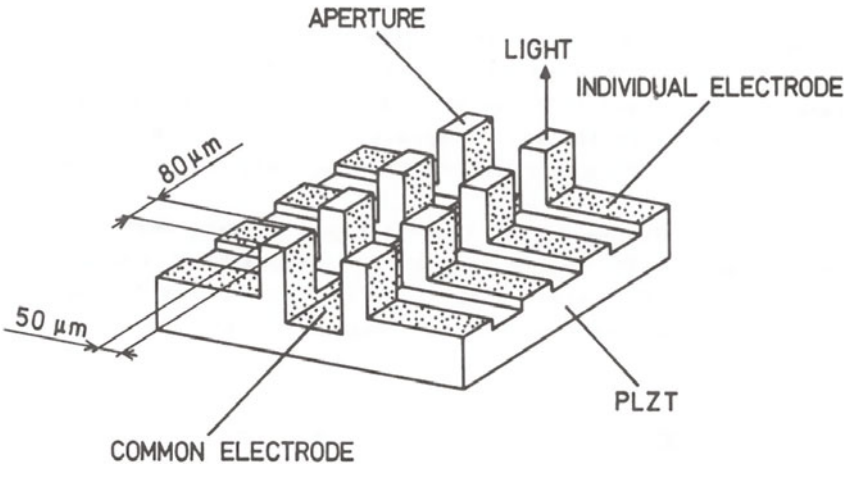

FIGURE 1. PLZT optical shutter array configuration.

TABLE 1
Average grain sizes by intercept method for various second stage firing conditions.

temp.＼method	O_2-HIP	Ar-HIP	VACUUM	AIR	O_2
1100℃	1.72	1.75	2.00	2.00	1.92
1150℃	2.04	1.92	2.50	2.56	2.38
1200℃	2.38	2.33	2.70	2.70	2.56
1250℃	2.78	2.63	3.33	3.13	3.23

(μm)

TABLE 2
Differences of Pb amount from stoichiometric compositional ratio after the second firing processes.

temp.＼method	O_2-HIP	Ar-HIP	VACUUM	AIR	O_2
1100℃	-5.65	-5.78	-6.74	-6.51	-6.23
1150℃	-6.13	-6.38	-7.02	-6.83	-6.57
1200℃	-6.77	-7.06	-7.27	-7.18	-6.84
1250℃	-7.68	-7.62	-7.95	-7.84	-7.81

(at%)

As an airtight container was not used in the second stage firing processes, Pb content in the ceramics decreased. Differences of Pb amount from stoichiometric compositional ratio after the second firing processes are shown in Table 2. According to the work of G. Wolfram, optically homogeneous hot-pressed PLZT can be obtained by evaporating some excess of lead oxide over stoichiometric composition.[4] In this study, ceramics with insufficient Pb under stoichiometric composition showed higher transmittance.

As shown in Figure 2, the transmittance at wavelength of 750 nm is almost constant for Pb content, but the transmittance at 400 nm depends on the deficiency of Pb content significantly. As for the firing in vacuum and air, the transmittance at 400 nm increases with the loss of Pb content

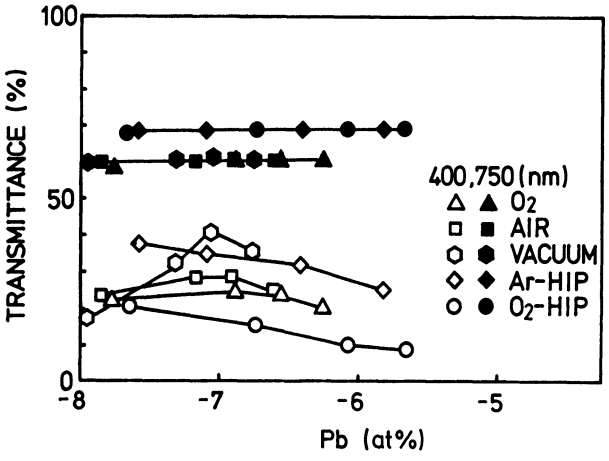

FIGURE 2. Transmittance for the deficiency of lead content.

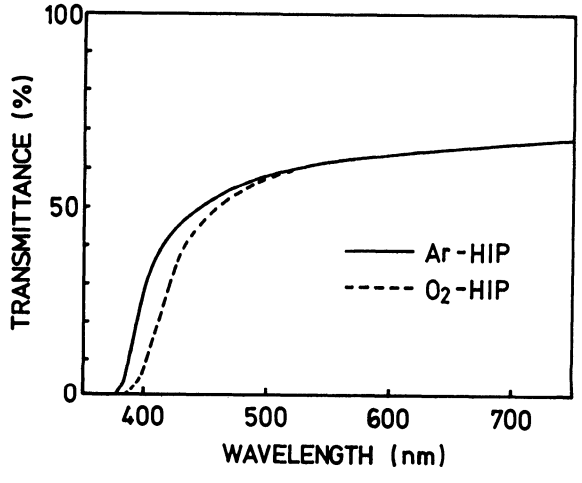

FIGURE 3. Transmittance as a function of wavelength for O_2-HIP and Ar-HIP.

and has a maximum value at about -7 at% of Pb. The transmittance at 750 nm is higher for HIP'ed specimens, which is due to the annihilation of pores. But at 400 nm, the transmittance of specimens fired in vacuum and Ar-HIP is higher than that of specimens fired in oxygen. Figure 3 shows transmittance as a function of wavelength for O_2-HIP and Ar-HIP. At the wavelength above 500 nm, the transmittance of HIP'ed specimens was higher than that of the

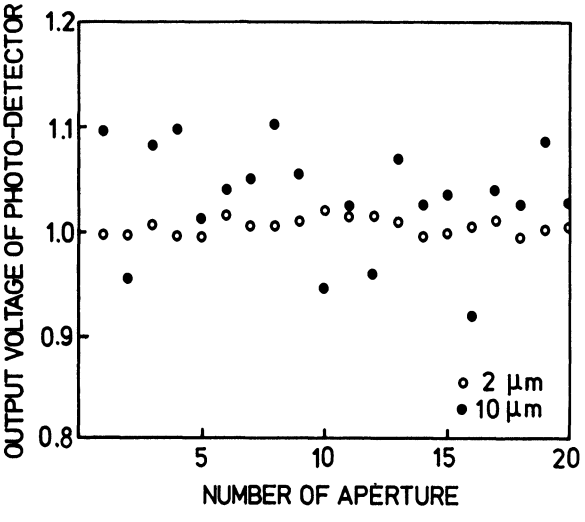

FIGURE 4. Variations of the light intensity among individual apertures.

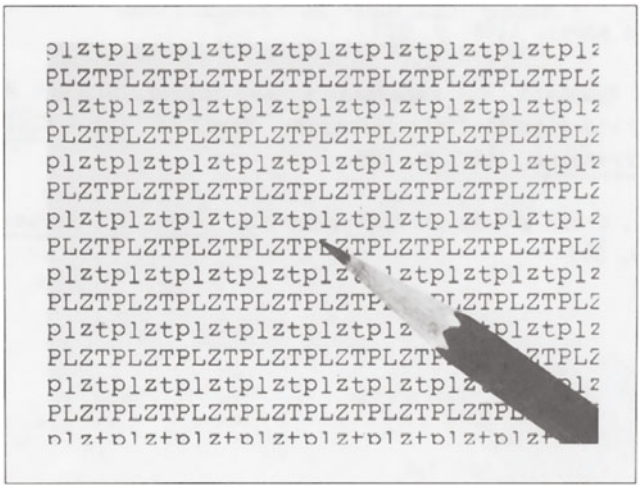

FIGURE 5. A printout of the electrophotographic printer with the PLZT shutter array. (Courtesy of Minolta Camera Co., Ltd.)

specimens fired by other processes. The reason of the above phenomenon is not yet clear.

Application to optical shutters of an electrophotographic printer

Figure 4 shows variations of the light intensity among individual apertures (Figure 1) made from PLZT ceramics with 2 and 10 μm grain size. It is obvious that the grain size should be small for this application. Figure 5 shows a printout of the electrophotographic printer with the PLZT shutter array.

CONCLUSIONS

The transmittance of PLZT ceramics at shorter wavelength increases with the loss of Pb in firing process. The treatment with O_2-HIP or Ar-HIP improves the transmittance at wavelength longer than 500 nm. The rate of grain growth in HIP is low in comparison with vacuum and atmospheric pressure sintering. The optical shutter array made from HIP'ed PLZT satisfied the required performances of an electrophotographic printer.

ACKNOWLEDGEMENT

The authors would like to thank K. Ohta, I. Saito and H. Kitano of Minolta Camera Co., Ltd. for providing the test results of printing.

REFERENCES

1. Wessel, G., Electro-optical ceramic (PLZT) as light-gate array for non-impact printer. Proc. SPIE, 1983, 396 , p. 53.

2. Buchanan, R. C., Ceramic Materials for Electronics, Marcel Dekker, Inc., New York and Basel, 1986, p. 221.

3. Takata, M., Kawahara, S., Kageyama, K. and Toyota, S., The HIP treatment of magnetic and piezoelectric ceramics. Proc. of Int. Conf. on Hot Isostatic Pressing, 1987, p. 399.

4. Wolfram, G., Grain growth in PLZT ceramics. Ber. Dt. Keram. Ges. 1978, 55, Nr. 7, p. 365.

Effect of Processing on the Micro-Structure and Properties of Hot Isostatically Pressed Alumina Added with Rare-Earth Elements

MASAYASU KOMURO, NOZOMU UCHIDA, ZENJI KATO, JUN HARADA* and KEIZO UEMATSU
Department of Chemistry
Nagaoka University of Technology
Kamitomioka, Nagaoka, Niigata, Japan 940-21
*Advanced Technology Research Center, Nippon Kokan Steel
Minamitoda-cho, Kawasaki, Kawasaki, Kanagawa, Japan 210

ABSTRACT

To control the formation of defects and development of uniform microstructure in powder compact during hot isostatic pressing, the effects of solvent and drying method were examined. Freeze dried powder mixture was found to have better characteristic than thermally dried samples. Homogeneously distributed rare-earth elements develop excellent microstructure and improve properties.

INTRODUCTION

Defects in powder compacts are preserved in ceramics even after hot isostatic pressing and affect their properties. In the production of high quality ceramics, it is essential to control defects in powder compact [1]. In a typical production process of ceramics, a slurry of powder and additive is often involved and thermal evaporation is used to remove solvent in the slurry. The dried powder contains hard agglomerates that are formed by capillary force and surface

tension[2]. It also contains a segregated layer of additives formed by the migration of solvent to the surface region. Powder compact formed with this powder contains many defects. In freeze drying[3], solvent is removed from frozen slurry by sublimation. Agglomerates produced are soft and can be easily broken during pressing. Additives are expected to be homogeneously distributed without segregation. Thus freeze drying is expected to produce superior powder compact and better ceramics than thermal evaporation process. Homogeneous distribution of additive is expected to give uniform grain growth. Improved properties will be achieved though secondary phase precipitated at grain boundary[4].

EXPERIMENT

Raw material used were fine alumina powder (TM-D:TAIMEI CHEMICALS CO., LTD.) and $PrCl_3$, $NdCl_3$, and $ErCl_3$ as additives. Alumina and a additive were weighed (1wt% oxide) and ball milled for 16h with a small amount of distilled water or alcohol added. The slurry was dried by thermal evaporation or by freeze drying. The dried mixture was uniaxially pressed at 30MPa and cold isostatically pressed at 300MPa to form powder compact(15mm x 15mm x 80mm). These were then sintered at 1300-1500°C for 2h. The sintered bodies were hot isostatically pressed at 1400°C, 100MPa for 2h. Densities were measured by the Archimedes method. The microstructure of specimens were examined by SEM. The grain size distribution was examined with the Spector method. The fracture strength was measured by 3-point bending(3mm x 4mm x 40mm), and the fracture toughness by IM method. Phases present were examined by the powder X-ray diffraction analysis.

RESULTS

Relative densities of samples with various additives reached over 99% of theoretical above 1400°C. Results reported hereafter are for samples sintered at 1400°C.

Figure 1 shows the effect of drying method and solvent on the microstructures of specimens without additive. Freeze dried samples have the most homogeneous grain distribution among these samples and slightly larger grain size than others.

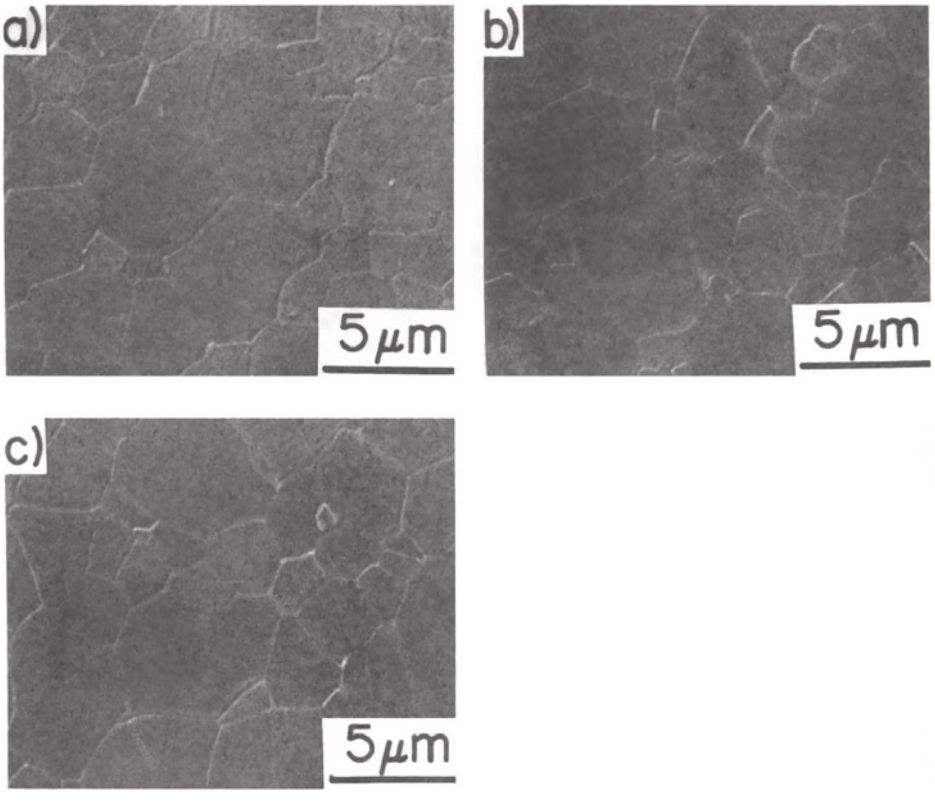

Figure 1 The effect of drying method and solvent on microstructures of specimens without additive : a) thermal evaporation by alcohol, b) thermal evaporation by distilled water, c) freeze drying by distilled water.

Figure 2 shows the effect of drying method and solvent on microstructures of specimens added with $PrCl_3$. Powder X-ray diffraction and EPMA microanalysis showed that light points in the micrographs represent secondary phase of praseodymium aluminate. Freeze dried sample had more uniformly dispersed secondary phases and more homogeneous grain size than other samples. Clearly, grain size of sample having additive is smaller than that of sample without additive. Similar results were found with other additives.

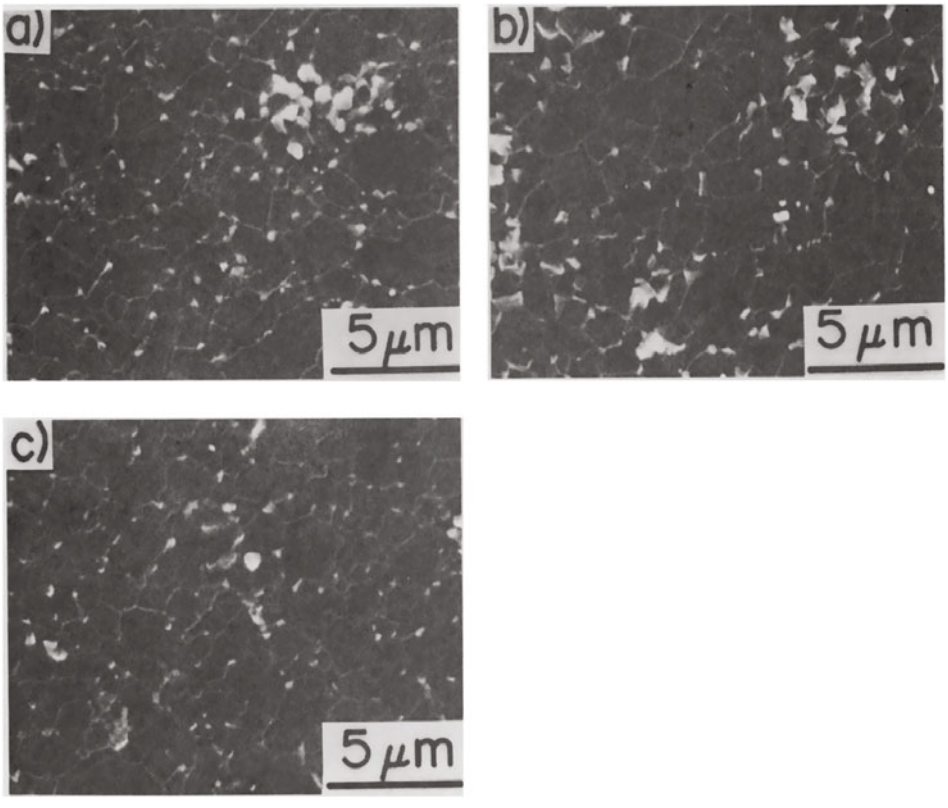

Figure 2 The effect of drying method and solvent on microstructures of specimens added with $PrCl_3$: a) thermal evaporation by alcohol, b) thermal evaporation by distilled water, c) freeze drying by distilled water.

Table 1 summarizes the characteristics of specimens. Average grain size was reduced by the addition of rare-earth elements. The grain size distribution was narrowed by freeze drying. The lattice constant of sample with additive is sightly larger than that without additive; only small amount of rare-earth element is dissolved into the alumina matrix. Fracture strength and fracture toughness are increased by the addition of rare-earth elements. Secondary phase precipitated in grain boundaries is responsible for these results. Among specimens having additives, the freeze dried specimen has the highest strength and toughness.

Table 1
The characteristics of specimens.

		GS(μm)	σ	d(A)	MOR(MPa)	K_{1C}(MPa•$m^{1/2}$)
no-	TE(A)	3.19	1.52	1.0424	538	3.17
additive	TE(W)	3.10	1.61		589	2.93
	FD(W)	3.81	1.46		551	2.90
	TE(A)	1.67	1.45	1.0430	601	3.64
$PrCl_3$	TE(W)	1.79	1.45		598	3.47
	FD(W)	1.84	1.35		690	3.69
	TE(A)	1.76	1.40	1.0429	648	3.94
$NdCl_3$	TE(W)	1.75	1.40		647	3.76
	FD(W)	1.95	1.34		783	3.97
	TE(A)	1.35	1.52	1.0428	616	3.89
$ErCl_3$	TE(W)	1.35	1.52		611	3.69
	FD(W)	1.38	1.43		652	3.95

Figure 3 shows a typical fracture origin in a low strength sample. This is a large pore surrounded by large grains produced by abnormal grain growth. Fracture origins in low-strength sample added with rare-earth elements and dried by thermal evaporation was mostly pore near surface. Fracture origin of high-strength specimens could not be identified

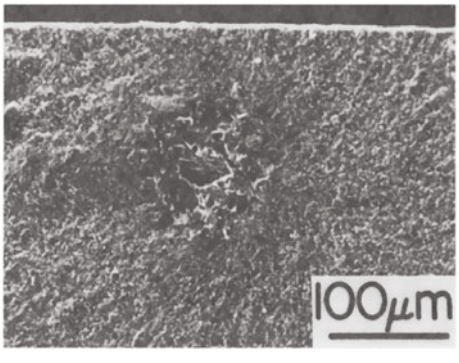

Figure 3 Fracture origin of low-strength sample.

DISCUSSION

Drying method affects the microstructure of hot isostatically pressed bodies and segregation of additive. The formation of hard agglomerate is responsible for more non-uniform microstructure in the thermally dried powder. Sublimation of solvent without solute migration clearly helps uniform distribution of additive. Uniformly distribution additive inhibits abnormal grain growth, and improved properties are obtained after hot isostatically pressing. The pinning effect of secondary phase at grain boundaries clearly reduces the grain growth.

The freeze drying method can clearly produce powder mixture with better characteristic than thermal evaporation process. Homogeneously distributed rare-earth elements develop excellent microstructure and improve properties.

REFERENCE

1. Evans, A.G., Consideration of Inhomogenety Effects in Sintering., J. Am. Ceram. Sci., 1982, 65, 497-501.

2. Horn, R.G., Surface Forces and Their Action in Ceramic Materials., J. Am. Ceram. Sci., 1990, 73, 1117-1135.

3. Dogan, F. and Hausner, H., THE ROLE OF FREEZE-DRYIHG IN CERAMIC POWDER PROCESSING., Ceram. Trans., 1988, 127-134.

4. Taylor, R.I., Coad, J.P., and Hughes, A.E., Grain-Boundary Segregation in MgO-Doped Al_2O_3., J. Am. Ceram. Sci., 1976, 59, 374-375.

APPLICATION OF HIPING TO SINTERING CHROMIUM CARBIDE

OSAMU NAKANO and MITSUHIKO FURUKAWA
First R&D Department, Nippon Tungsten Co., Ltd.
20-31, Shimizu 2-Chome, Minamiku, Fukuoka , Japan

INTRODUCTION

Cr_3C_2 ceramics are expected to be applied to auxilially equipment for in the steel-making industry because of their good chemical properties, that is, high temperature stability oxidation and scale-reaction resistance [1)2)]. We have reported some properties of HIP-mamufactur Cr_3C_2 ceramics [3)4)]. However the effects of HIP conditions on the properties of Cr_3C_2 ceramics have not been ascertained. In present paper, We report the effects of HIP conditions on the mechanical properties of chromium carbide (Cr_3C_2+Cr_7C_3phase) having lower carbon content than theoretical carbon content of Cr_3C_2.

MATERIALS AND METHODS

Chromium carbide sintered compact was fabricated from commercially available high purity Cr_3C_2 powder, with particle size was below 1μm. The powder contaned 13.1wt% carbon. This value was lower than theoretical combined carbon content of Cr_3C_2(13.3wt%). Cr_3C_2 and sintering agent powder were wet-mixed in a ball mill. After wax-addition, the powder was uniaxially prsssed at 70MPa to form plates, 30×10×7mm, before cold isostatic pressing 100MPa. After de-waxing, the green compacts were presintered at 1723K to 1773K for 3600s under a vacuum of 0.13Pa. After presintering, the surface of some specimens was planned off by gliding. Hot isostatic pressing was performed at three different pressures, 50MPa, 100MPa and 150MPa at 1603K for 3600s. The bulk density of presintered and HIPed bodis was determined by Archimedes' technique. The bodies were cut into 20 ×7×4mm specimens by diamond wheel and the edge were beveled with 600grit diamond paper. Specimens were subjected to three

point bending test using a crosshead speed 1×10^{-5}m/s and span length 20mm.Five specimens were fractured.After polishing, specimen microstructure was observed under optical microscope. The surface and internal phase of sintered compacts was identified by X-ray diffraction.

RESULTS AND DISSCUSSION

The microstructure near the surface consists of surface layer

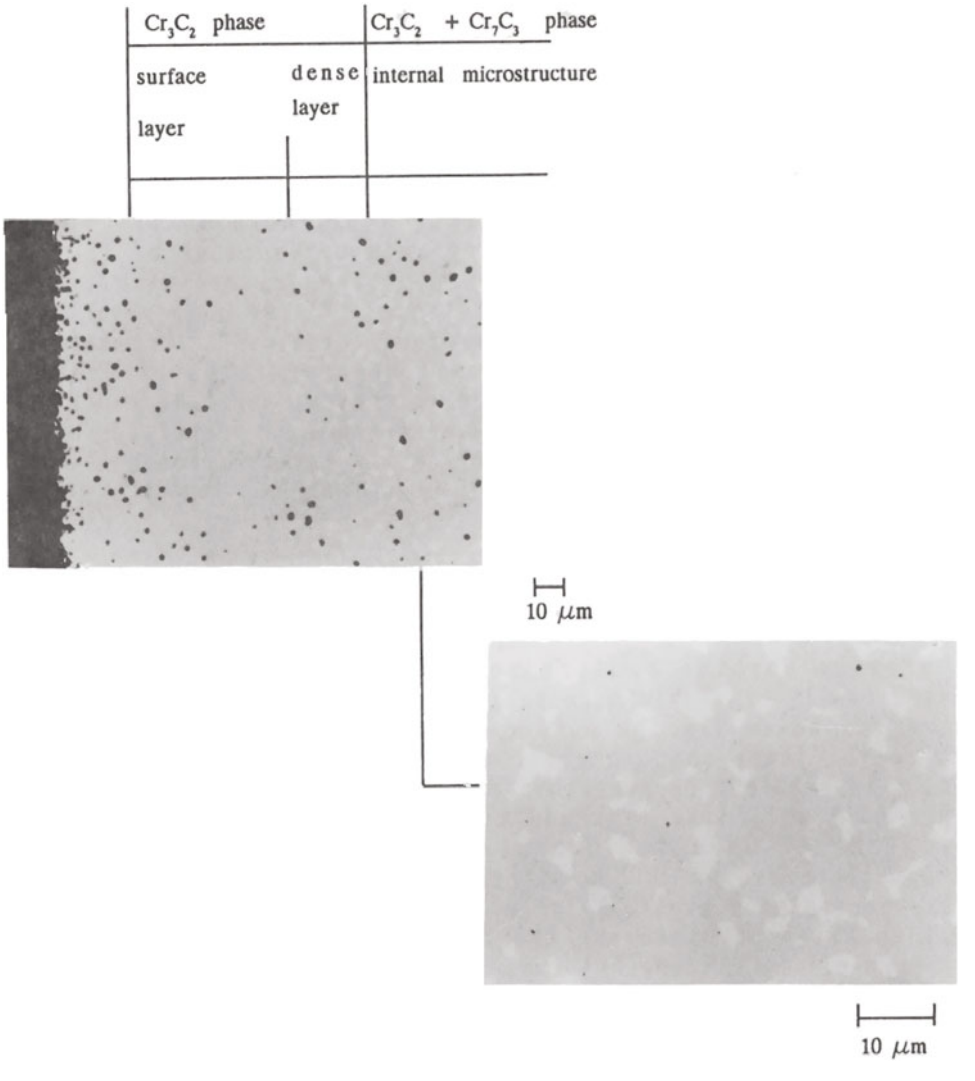

Fig.1 Surface microstructure of presintered chromium carbide

with many pores and a dense internal layer.This surface layers identified as Cr_3C_2 phase,with a thickness of about 100μm.The internal microstructure consists of Cr_3C_2 phase and Cr_7C_3 phase,see Fig.1.The results of density measurement in HIPed specimens are shown below.The relationship between relative density of the presintered compact before HIP(D_b) and relative density after HIP(D_a) is summarized in Fig.2.In the sintered compacts with a dense layer,the density steeply increases the relative density of 89%,in spite of the HIP pressure.In a pressure of 50MPa,after a steep increase,the relative density is constant in spite of increasing D_b.In 100MPa,the relative density slightly increases with increasing D_b and above D_b of 98%,D_a reaches theoretical density.However,in the spcimens with the dense surface layer planed off,D_a reaches theoretical density above D_b of 94%.The relationship between bending stress in HIP and non-HIP treated specimens and D_b are summarized in Fig.3.When D_b is below 95%,the effect of HIP showed an extreme increase in bending stress.In lower D_b of 93%,the bending stress of HIPed specimens is higher than that

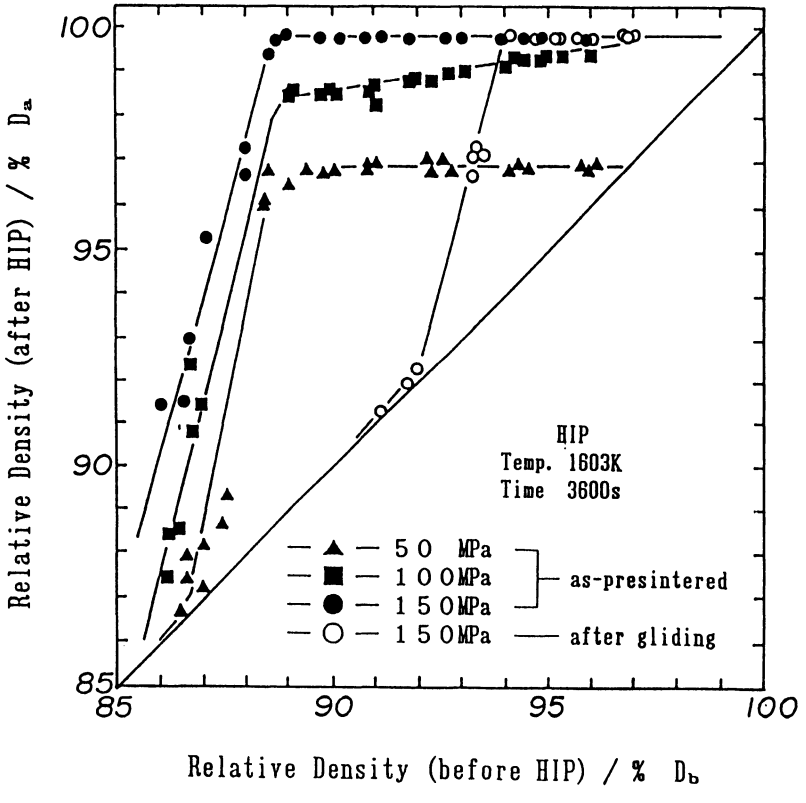

Fig.2 Relative density before and after HIP of chromium carbide

of hot-pressed specimen. Futhermore, fracture toughness hardly changed with an increase in D_b. The differances in microstructures for various D_b HIP were observed. In result, with a low D_b, fine grains equiaxed in shape are observed, and as D_b increases the grain size and shape is larger and irregular. This results indicate that bending stress depends on the defect size accompanied by change in grain size. The surface layer which consists of Cr_3C_2 phase can be utilized as a capsule and the effect of HIP on strngth was confirmed.

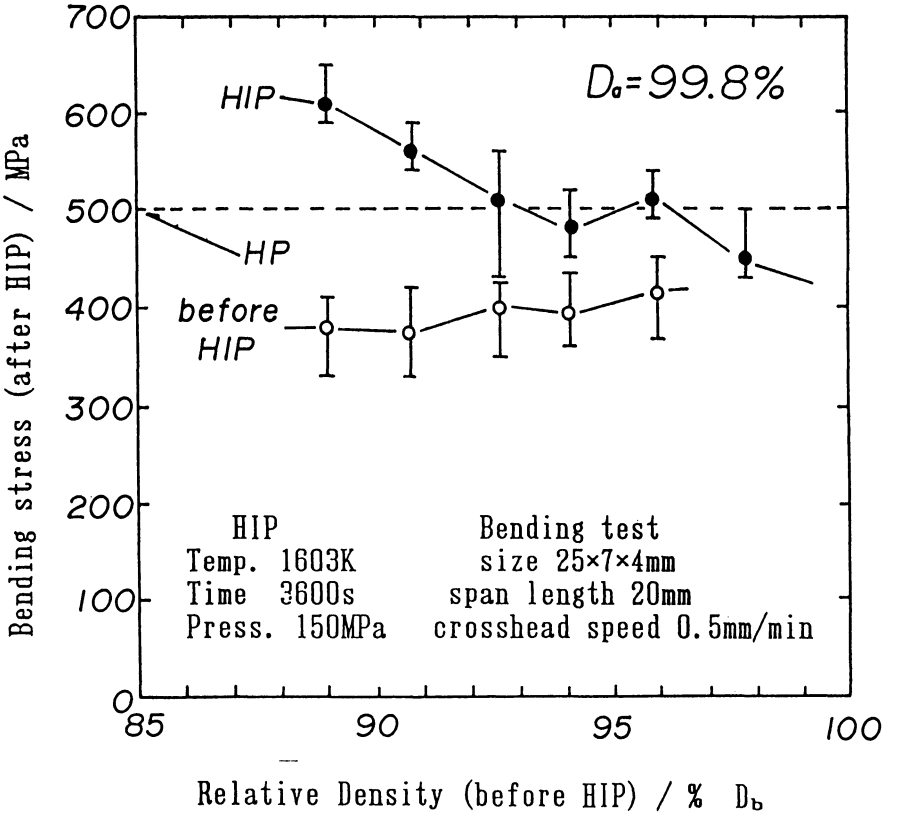

Fig. 3 Bending stress versus relative density after HIP in chromium carbide (150MPa in Ar)

Fig. 4 shows the effect of the carbon content on consolidation in chromium carbide green compact. The green compact with theoretical carbon content of Cr_3C_2 readily consolidated in comparison with other carbon content. However, for the mechanism of the formation of Cr_3C_2 phase at the surface it is presumed that there is a difference between the carbon content at the surface and that of the interior in sintering, and this difference influences consolidation.

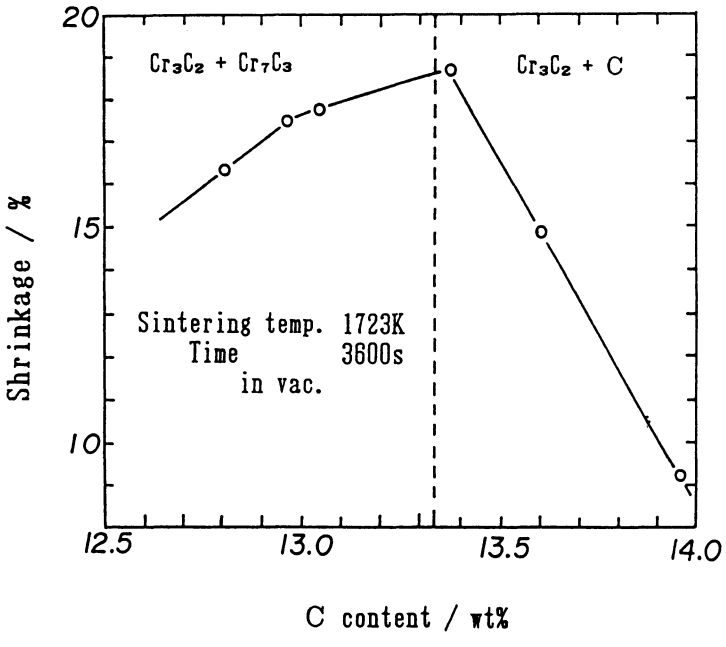

Fig.4 Sinterbility of chromium carbide as a function of carbon content

CONCLUSIONS

Chromium carbide readily consolidated but as consolidation proceeds there is a decrease on bending stress due to abnormal grain growth. Above relative density of 95%, the effect of HIP on bending stress was comfirmed in comparison with no HIP. Furthermore, chromium carbide green compact forms the dense layer by presintering. This presintered compact can be consolid ated by HIP above a relative density of 89%. This HIPed compact has a high bending strength.

REFERENCES

1. M. Tanaka, T. Maeda, E. Kuboyama, H. Hiraishi and M. Furukawa, J. Iron and Steel Inst. Japan, 71, S835(1985)
2. M. Tanaka, T. Maeda, H. Hiraishi, Y. Yamagami, M. Furukawa and O. Nakano, J. Iron and Steel Inst. Japan, 71, S836(1985)
3. M. Furukawa, M. Saito, O. Nakano, T. Kitada, H. Hiraishi and Y. Yamagami, Nippon Tungsten Review, 19, 6-10(1986)
4. M. Furukawa, M. Saito, O. Nakano, T. Kitada, H. Hiraishi and Y. Yamagami, Nippon Tungsten Review, 20, 18-25(1986)

4. METALS AND ALLOYS

HIP STEEL COMPONENTS FOR THE MANUFACTURING INDUSTRY

KRISTER TORSSELL
ABB Powdermet AB
Box 209
S-735 23 Surahammar, Sweden

ABSTRACT

The hot isostatic pressing of gas atomized powders is today a fabrication method for steel components of simple and complex shapes. Applications are found in areas such as steam turbines, boilers, centrifugal separators, off-shore piping, tool manufacture etc. The advantages of this manufacturing method relative to conventional techniques are among others:
- homogeneous material leading to isotropic properties
- near net or net shape design
- low tooling costs and short series economy
- short delivery times
- compound products with optimized material properties

INTRODUCTION

Why Powder Metallurgy (PM) and Hot Isostatic Pressing (HIP) for the manufacture of components to the manufacturing industry? Powder metallurgy in this case means gas atomized powders and thereby rapid solidification and as a consequence "no" segregation. Hot Isostatic Pressing gives uniform pressure compaction and therefore a homogeneous and isotropic material. This technology also adds new degrees of freedom in shaping the products. The advantages of PM/HIP steels relative to other conventional manufacturing methods are among others:
- homogeneous material
- isotropic properties
- often improved material properties
- new alloys
- new freedoms in shape and integrated design (NNS or NS)
- components in two or more materials, compound solutions
- short series economy
- short delivery times

The intention of this paper is to illustrate these points and to show the technical and economical feasibility of this technology as a supplier of components to the manufacturing industry.

PROCESS

The manufacturing process for a typical machine component such as a hollow cylinder comprises the following steps, as shown in Figure 1.

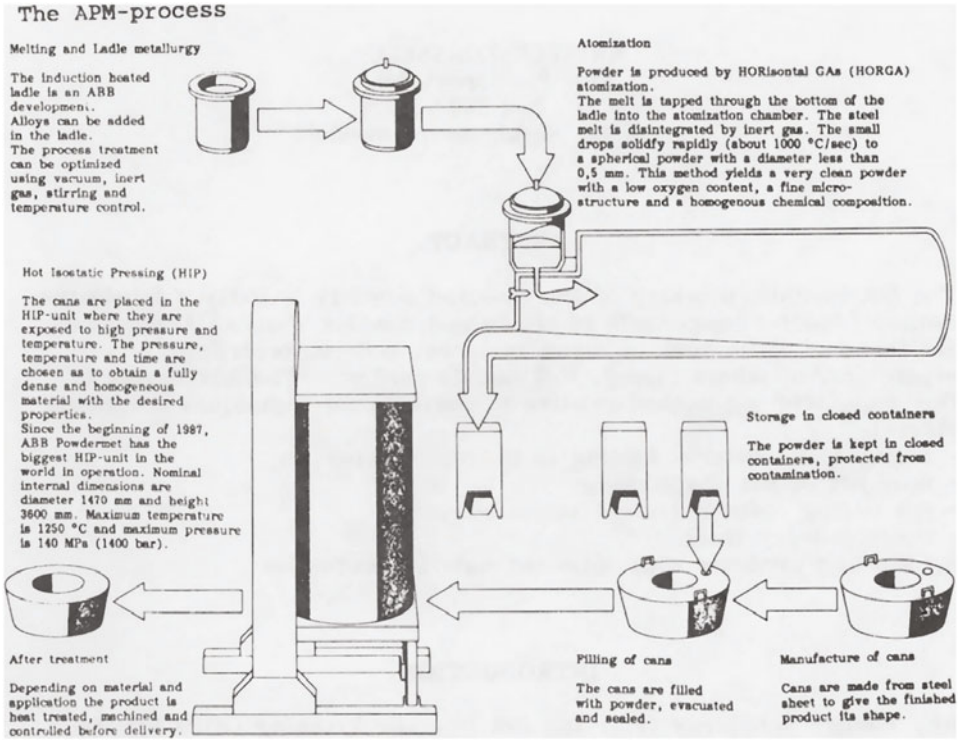

Figure 1. Schematic view of process and equipment at ABB Powdermet

1. Powder manufacture including melting of the alloy, control of composition and atomization of the melt by inert gas at high pressure. In this way a clean and rapidly solidified powder is obtained.

2. Powder filling into a steel sheet capsule giving the shape to the product. The filling density is about 70 % of the fully dense product so a corresponding shrinkage will take place but the shape of the capsule will be maintained.

3. Hot isostatic pressing is typically performed at a temperature above 1100 °C at a pressure above 100 MPa during 3 hours at full temperature and pressure. The total cycle time lasts approximately 12 hours. Main features of HIP-equipment are:

Max temperature	1250 °C
Max pressure	140 MPa
Inner diameter	1,47 m
Inner height	3,6 m

4. Heat treatment is made in the conventional way although the parameters may vary somewhat to obtain the best material properties. It is also possible to include heat treatment in the HIP-cycle.

5. Machining which often includes removal of the sheet of the capsule.

6. Quality control before delivery including non destructive examination and mechanical testing.

In order to meet the high demands on functional reliability a comprehensive Quality Assurance System covers all parts of the manufacturing procedure.

APPLICATIONS IN THE POWER GENERATING INDUSTRY

In the gas and steam turbine industry strong efforts are being made to increase the output and efficiency of the turbines and to lower the production costs. New materials with better properties and more effective ways of manufacturing are means to meet these demands. [1-3].

The properties of greatest interest for turbine parts are toughness, fatigue strength, good yield strength at elevated temperatures, good creep and creep rupture strengths, low thermal expansion, high thermal conductivity and resistance to stress corrosion cracking.
The task of the designer when designing a new turbine is not only to consider the function of the turbine but also the availability of the components and how to assemble it. Everyone knows more or less the possibilities of such techniques as casting, forging, welding, machining etc. to manufacture parts for a turbine. A new technology such as HIP-steels adds new possibilities, which if they are known to the designer gives him more possible solutions.

Blading rings for radial counter rotating steam turbine
In a radial steam turbine rings are used to carry the blades as is shown in Figure 2.

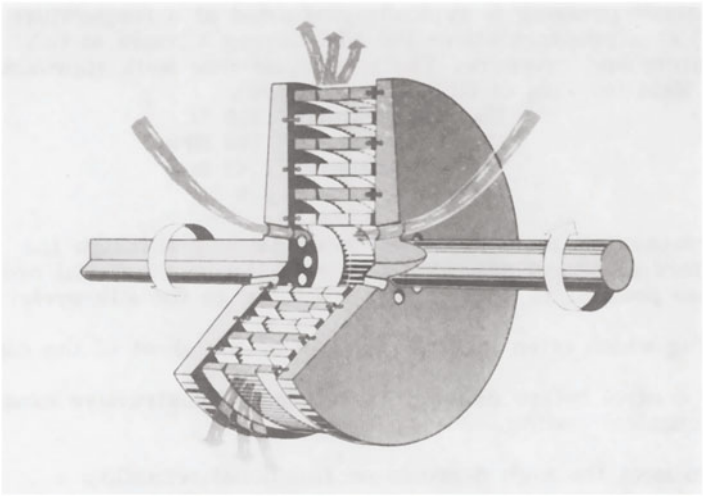

Figure 2. Principle of a radial flow steam turbine.

These rings are counter rotating driving two generators, one on each side of the turbine itself. The temperature of the steam which flows from the center to the periphery can be 540 °C in the center and perhaps 70 °C at the outer part of the turbine. The same material APM 2390 (a 12 % Cr-steel) is used in all rings in order to have the same coefficient of thermal expansion.
In the central rings high creep strength at elevated temperature is neccessary while the outer rings demand high yield strength at lower temperature and good toughness.
The change to PM/HIP-steel has given a material with improved toughness and maintained good strength at ambient and elevated temperature.
When these improved properties are utilized it will be possible to increase the performance of the turbine. About one thousand such rings have been produced during the last 6 years and put into operation.

Turbine disks
The disks for radial flow turbines are also made from the same 12 % Cr-steel, APM 2390. An example is shown in Figure 3.

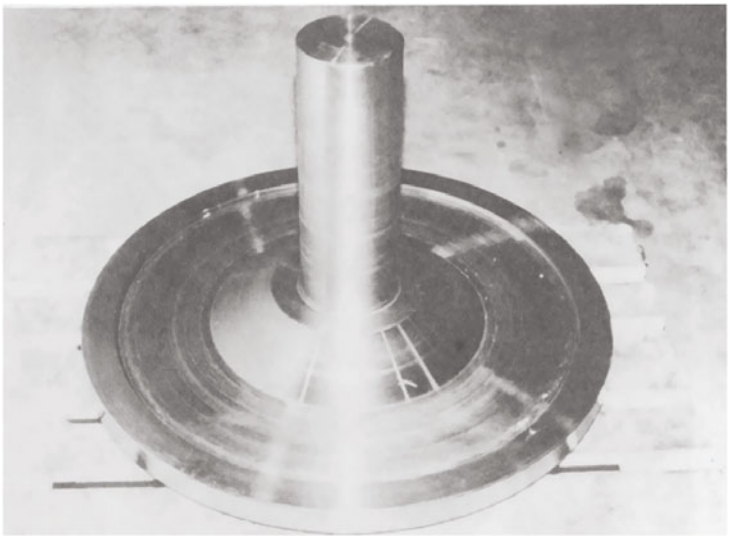

Figure 3. Turbine disk from PM/HIP steel in APM 2390 for a radial turbine.

Steam chests

Steam chests for radial steam turbines are used for the distribution of steam. Figure 4 shows the intricate shape of the interior of the capsule before powder filling and Figure 5 the capsule after HIP'ing and partial machining.

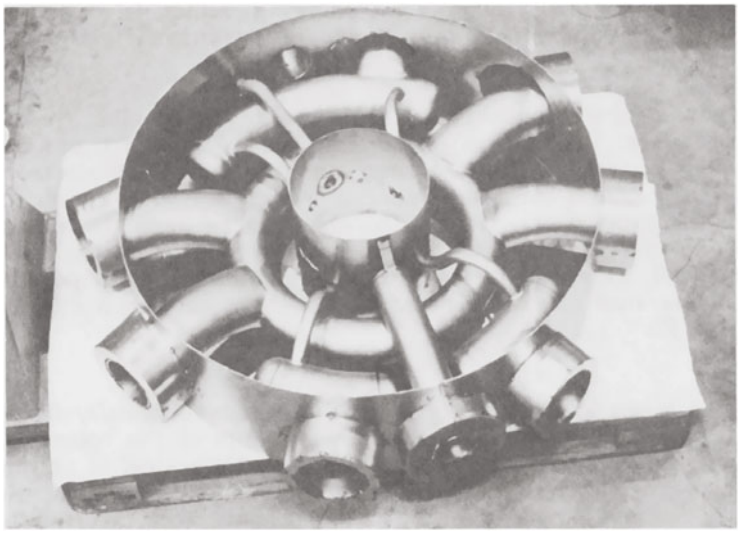

Figure 4. Can for steam chest for radial turbine in APM 2218 before powder filling.

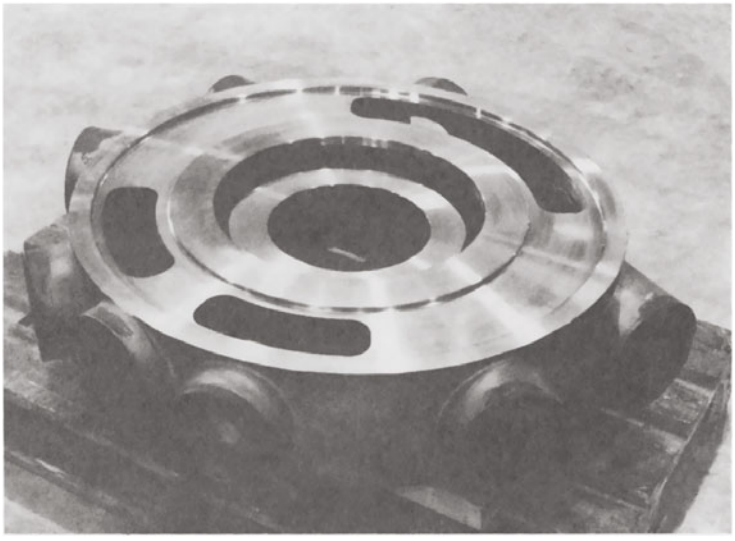

Figure 5. Steam chest for radial turbine after HIP'ing, APM 2218.

The material that is used is APM 2218, corresponding to T22. The HIP'ed component will then be heat treated to obtain the mechanical properties and machined on the outer surfaces.
The advantages of this solution is that the steam channels can be introduced by welding them into the capsule as tubes. As these tubes are open and therefore filled by argon at high pressure during the hot isostatic pressing they will remain open.
Conventional manufacturing means forging a solid piece and then machining the channels followed by plugging, which is a costly process and does not give channels as suitable for the steam flow.

Diaphragms
The use of ceramic cores inside the can makes it possible to form net shape products. Diaphragms for axial steam turbines are manufactured conventionally from two forged rings and the vanes are electron beam welded into position by a very special technique. With the aid of a core, which is removed after HIP'ing, the channels between the vanes can be formed and allowing the integregation of the vanes into the vane-carrying wall, (Figure 6). By this technique it has been possible to obtain a tolerance of the diameter of 350 $\pm$ 0,2 mm and a surface roughness Ra $\leq$ 1,3 µm.

Rotors
Rotors for steam and gas turbines are made conventionally by forging an ingot to shape or by welding together segments of the rotor. If the rotor is to operate at high temperature a 12 % Cr-steel is chosen to give it the necessary creep strength and other properties needed. Such a rotor has to have a weld overlay in the bearing area in order to avoid the wooling effect associated with 12 % Cr-steels. The total delivery time for such a rotor is in the range of 6 to 12 months.

By using the HIP-route it is possible to avoid both forging and the overlay welding and to reduce the delivery time to 2-3 months. The short delivery time is especially valuable for service and retrofits. Rotors weighing up to 10 tonnes have been produced so far.
For the bearing area APM 2218 (T22) has been used and a very good metallurgical bound is obtained. Figure 7 shows a steam turbine rotor ready for delivery.

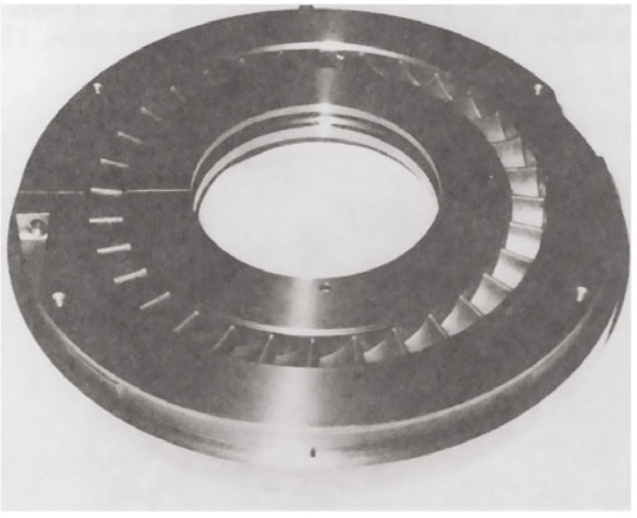

Figure 6. Diaphragm wall for axial steam turbine.

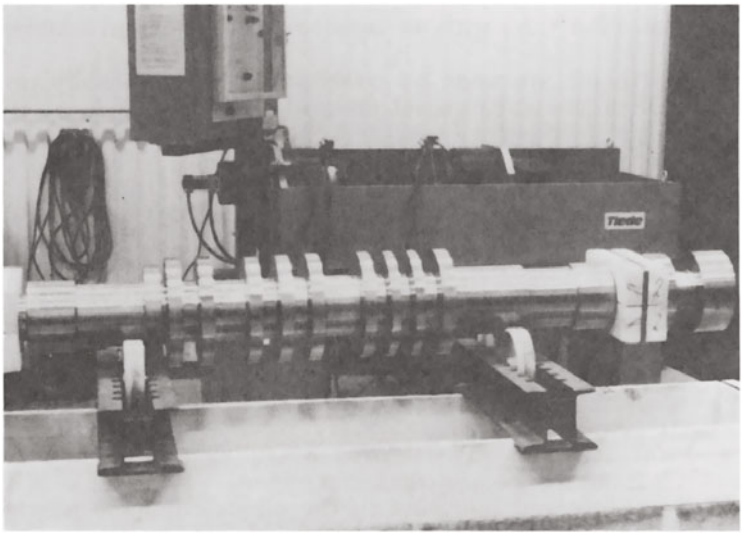

Figure 7. Steam turbine rotor made in APM 2390 with APM 2218 in the bearing area.

BOILER APPLICATIONS

Several applications have also been found in the boiler area of power generation. Two examples are presented.

Compound tubes
In coal fired fluidized beds erosion resistant tubing at high temperature is needed. Such compound tubes can be manufactured with an erosion resistant material on the inside or on the outside. The use of such tubes in boilers is of great interest using a pressure vessel material on one side and an erosion resistant material on the other side, (Figure 8).

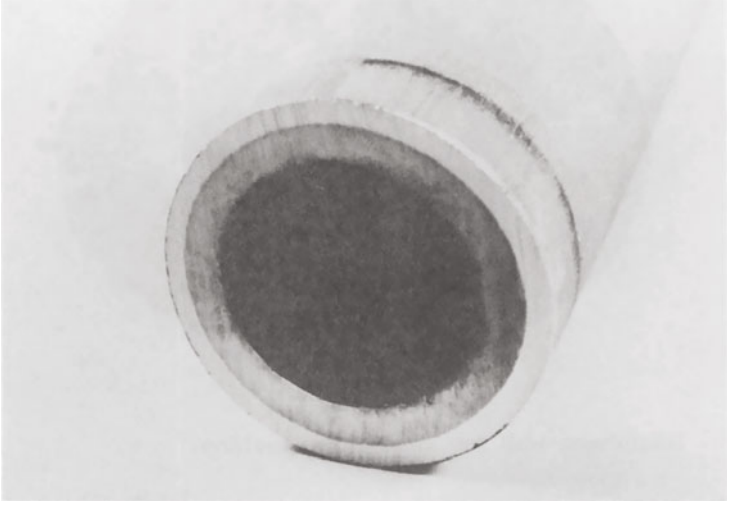

Figure 8. Compound tube with an inner erosion resistant material.

Blanks for extrusion are made by combining a conventionally produced hollow cylinder of pressure vessel steel with an erosion or corrosion resistant material in powder form. It is possible to make different combinations of materials to optimize properties and to obtain fully dense layers with a complete diffusion bonding.
A very erosion resistant material has been used for this application is APM 2311, (26Cr2C-alloy). This alloy, produced by gas atomization, lends itself very well to HIP and extrusion. Depending on heat treatment a hardness of 400-680 HV is feasible. Several thousand meters of such tubes have been supplied for ash transport and fluidised bed tubes.

Header for Steam Boiler
In a COST-project a part of a real size header for a steam boiler has being tested, (Figure 9). [4].
This component has been manufactured by filling powder into a welded capsule of the same shape and then compacted. The capsule is then removed by pickling and the holes in the nipples and the nozzles are machined afterwards.

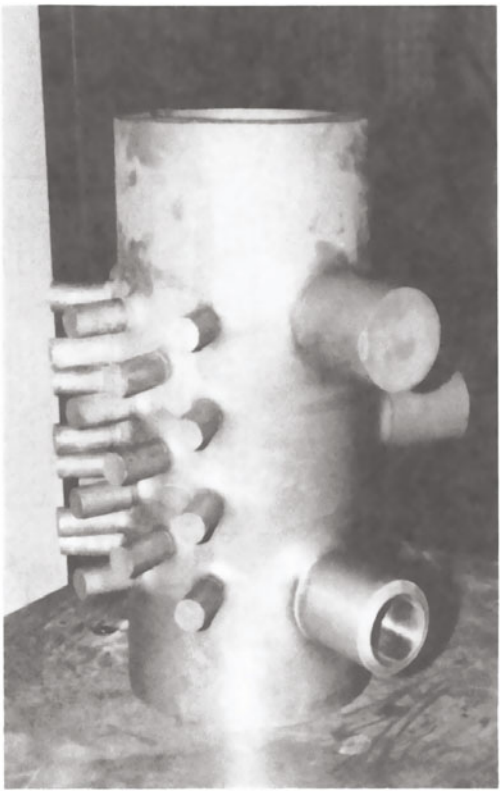

Figure 9. Header specimen for a steam boiler.

Conventional manufacture consists of drilling holes in the main pipe, welding the nipples and the nozzles at elevated temperature followed by a stress relieving treatment and X-ray control of all the welds. This is a very expensive manufacturing process when the number of welds is large.
The homogeneity and isotropy of a header made from HIP-steel are illustrated by the mechanical properties in different directions as shown in Figure 10 and by the creep data given in Figure 11.

The aim of this COST project is two fold: To manufacture a thick wall steam header by PM/HIP steel and to show its technical viability and to use an improved material which allows increased pressure and temperature. The first part was demonstrated using 12 % Cr-steel (APM 2390), and for the second part the steel T91 was chosen. A T91 header has been manufactured and is at present under testing.

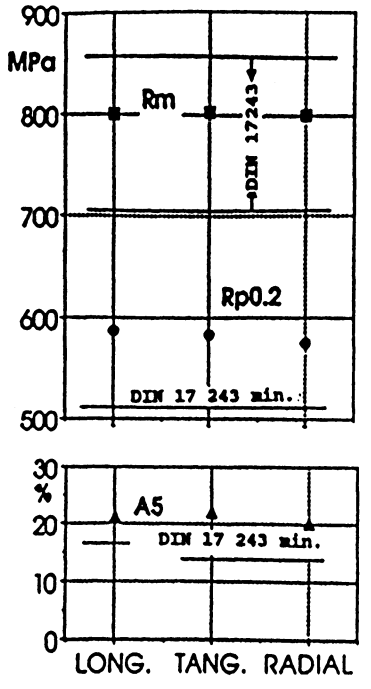

Figure 10. Results of tensile tests at room temperature for APM 2390 taken from a header.

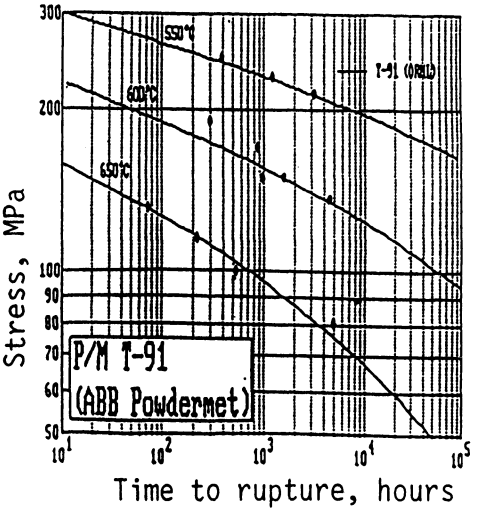

Figure 11. Creep rupture tests for APM 2390.

OFF SHORE

Off shore applications for the production of oil and gas are increasing all the time. There are a number of reasons for chosing HIP-technology to manufacture certain parts. The materials which are needed are duplex stainless steel with good corrosion resistance and relatively high mechanical properties. These steels are highly alloyed and prone to segregation during solidification which make them difficult to hot work without cracking. Especially flanges, fittings, tees, valve bodies, manifolds, piping and pump components are suitable to be manufactured from gas atomized powders and hot isostatic pressing. They are often components with irregular shape and small series of each type and size.

Depending on series length and shape of the components differents ways of manufacturing the can are used. Flanges as in Figure 12 are manufactured from sheet material formed by spin forming and then welding of the elements to produce the can.

A further example of can making is illustrated in Figure 13 where the sheet elements have been formed by pressing them in a fluid cell press. Such a press works with a membrane that forms the sheet against a tool. These tools are relatively simple and can be made from wood, plastic or metal whatever is the most convenient.

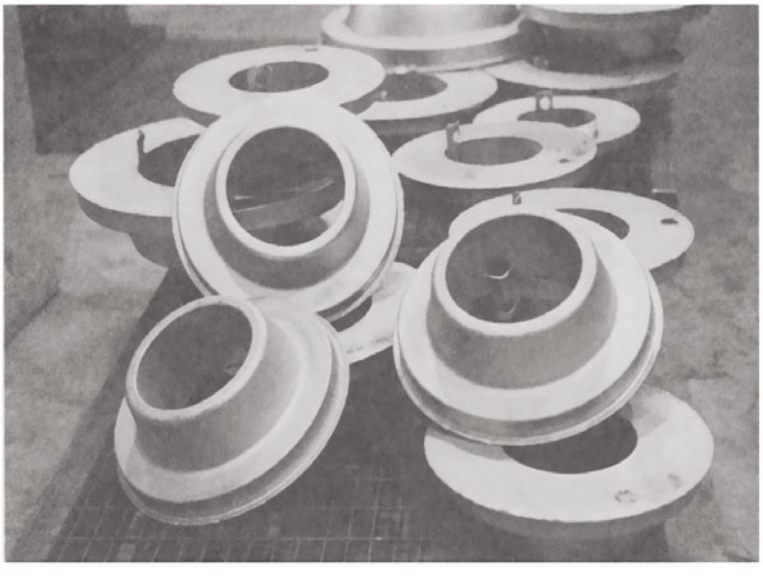

Figure 12. Flanges for tube welding used in off shore.

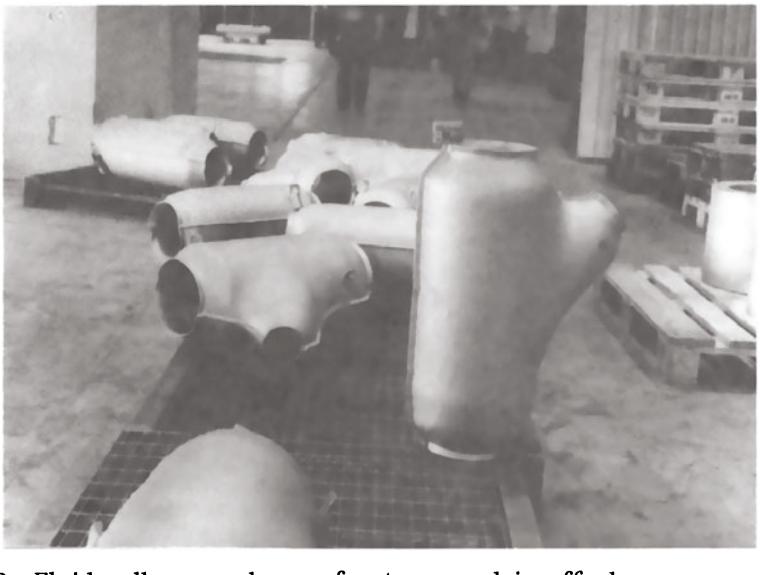

Figure 13. Fluid cell pressed cans for tees used in off shore.

A third alternative is to form sheet elements in the workshop by bending and then welding them together. Figure 14 shows a valve component manufactured to shape. Proper allowance has to be made for the shrinkage of course.

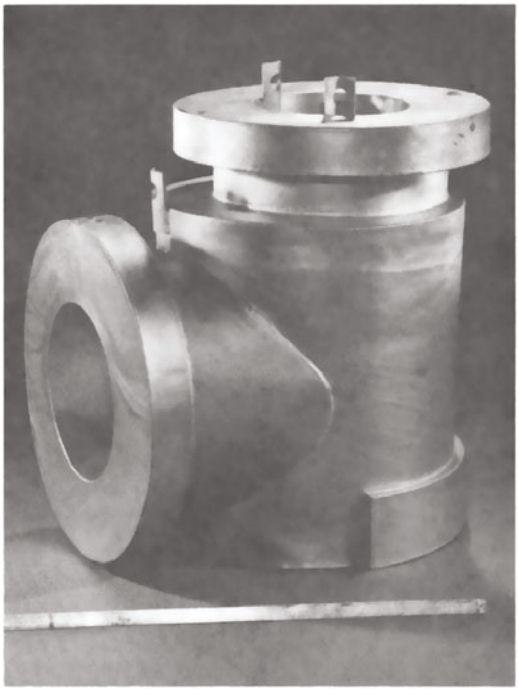

Figure 14. Valve component used in off shore.

After HIP'ing and heat treatment the encapsulation is removed by pickling and the relevant surfaces are machined.

When the powder is available from stock the delivery times for most components is quite short. The material properties are excellent and equal or better than a corresponding forged product thanks to the homogenity of the material and its isotropy. An added advantage is also that these alloys can be ultrasonically tested when produced from powder and HIP, while conventionally solidified material has a too coarse microstructure.

AS-HIP'ED PM HIGH SPEED STEEL

Until recently the ASEA-Stora process [5] and the Crucible process have dominated the production of high performance PM high speed steels. Both processes comprise gas atomization of a powder which is then encapsulated. The capsule is preheated and hot loaded into a HIP unit where it is densified to a standardized billet which is then hot worked to required sizes.

The APM process also comprises gas atomization, encapsulation and HIP'ing but there are two major differences as compared to the previous processes:

* The capsule is cold loaded into the HIP and temperature and pressure are applied simultaneously.

* HIP'ing is done directly to required size and shape i.e. the steel is not hot worked.

The APM process offers the following characteristics:

When heating at ambient pressure the low heat conductivity of the powder mass produces a steep temperature gradient that drives a segregation of sulphur and oxygen towards the centre of the capsule. Considerable hot working is then necessary to avoid reduction in strength. This segregation is prevented when temperature and pressure are applied simultaneously.

Distorsion in heat treatment is expensive when producing hobs and other big complex shaped tools. The shape changes are smaller and more predictable with as-HIP'ed high speed steels than with hot worked PM high speed steels.

Other important properties such as machinability, hardenability, strength, grindability and coatability are at least as good as for PM high speed steels produced by the previous processes.

Shorter lead time and smaller minimum quantities per size give a flexibility that allows a new market strategy where availability can be guaranteed with less stockholding.

For the production of small bar sizes direct HIP'ing is more expensive than HIP'ing and rolling. The boarder line seems to be approximately 60 mm diameter.

It is possible to produce directly hollow bars, compound materials and near net shapes as shown in Figure 15.

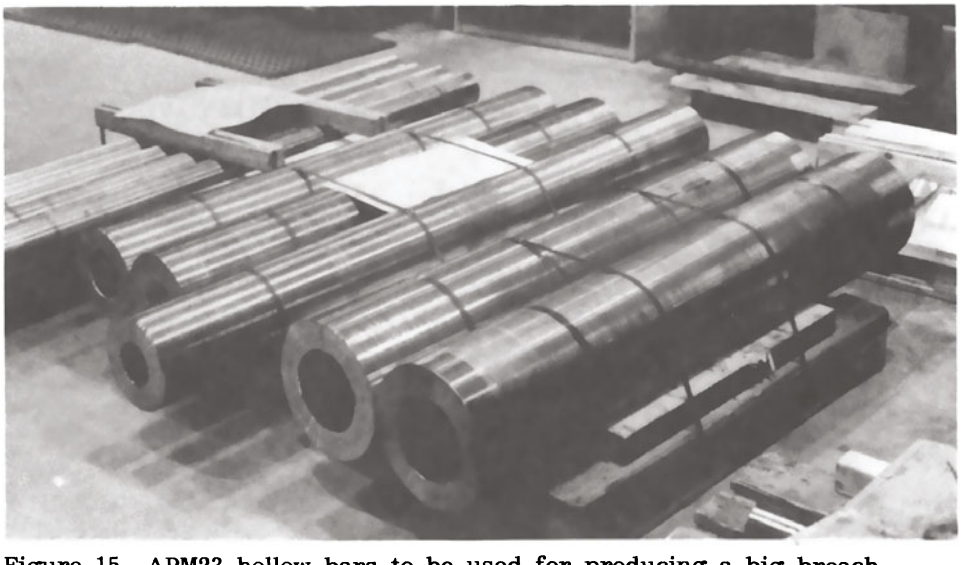

Figure 15. APM23 hollow bars to be used for producing a big broach.

CONCLUSIONS

The future of HIP-steels looks very promising in many areas of engineering and construction materials such as new PM based alloys, high alloy steels prone to segregation, corrosion resistant off shore applications, high temperature applications, steels difficult to hot work etc.

The examples given above illustrated clearly some applications in the manufacturing industry.

The economy of this method of manufacturing is of course essential to the user. The scale of application has a very large influence on the cost. The scaling up of powder production and the compaction equipment has lowered the price per kg considerably. The short delivery times and the great flexibility of the process are other important cost factors.

Finally it is not the purchase price but the value of the function in the machine that should be considered. With improved properties and an integrated design leading to NNS or NS this technology is very competitive for many applications. The ultimate proof of this technology's commercial viability is of course the fact that these products have been manufactured, sold on the market and put into use regularly for the last 6 years and that new applications are found all the time.

REFERENCES

1. Ekbom, R. (1988), The application of PM/HIP Technique For Gas and Steam Turbines. Modern Developments in Powder Metallurgy. Volumes 18-21, 1988, MPIF, Princeton N.J.

2. Torssell, K. High Performance Steel by Hot Isostatic Pressing - Processing, Applications and Perspectives. Liége. High Temperature Materials for Power Engineering 1990. Kluwer Academic Publishers Dordrecht p. 1513-1532.

3. Torssell, K. Eigenschaften Pulvermetallurgisch Hergestellter Teile für Hochtemperatureinsatz. VDI Werkstofftag 1991 München. VDI Berichte Vol 852, p. 353-367.

4. Heisel, U., Hollstein, T., Schepp, P., Torssell, K., Schumacher, G., Pulvermetallurgische Herstellung von Dampfleitungs-Komponenten mit komplizerter Geometri. VDI-Werkstofftag 1990, München. VDI Berichte Vol. 797. p. 447-458.

5. Hellman, P. The ASEA-Stora Process, Modern Developments in Powder Metallurgy, 4, (1970), p. 578-582.

6. Dulis. E.J., Neumeyer. T.A. Particle-Metallurgy High-Speed Tool Steel, Materials for Metal Cutting, BISTRA-ISI, 1970, London.

DENSIFICATION BEHAVIOUR OF PARTICLE-REINFORCED SUPERALLOY POWDER DURING HOT ISOSTATIC PRESSING

M. LAFER*, D.BOUVARD*, P. STUTZ*, M. PIERRONNET** and G. RAISSON**
* Institut de Mécanique de Grenoble, 38041 Grenoble, France
** Tecphy S.A., 58160 Imphy, France

ABSTRACT

In this paper understanding of the role of inclusions in the consolidation process of powder composite is attempted. A nickel base superalloy powder was mixed with alumina particles and consolidated by hot isostatic pressing. Densification kinetics were estimated from interrupted HIP tests, and compacted specimens were observed by microscopy. Simple compression tests were also performed at high temperature on dense samples. From these results explanations for the retardation in densification due to the inclusions are suggested.

INTRODUCTION

Mechanical properties of a metal alloy can be improved by introducing hard inclusions. It has been shown that fiber reinforcements usually increase the bulk strength, whereas particulate inclusions improve particularly the wear resistance. Powder metallurgy is a major way of processing this type of composites, requiring novel investigation on the role of inclusions during consolidation , since processing capability, as much as final-property requirement, controls the choice of reinforcement characteristics (morphology, volume fraction, disposition).

In this paper the consolidation of particle-reinforced metal powder is adressed by reporting the densification by hot isostatic pressing (HIP) of a superalloy powder mixed with alumina particles. From densification kinetics and microscopic observations the effect of the inclusions on the densification is displayed and its possible causes are discussed.

MATERIAL AND EXPERIMENTS

The matrix powder is nickel-base superalloy Astroloy powder obtained by argon atomization with a diameter lower than 150 μm. The inclusions are alumina particles obtained by grinding of melt alumina. As seen in Figure 1 their shape is angular and irregular, whereas the superalloy powder is mostly spherical, with many satellites particles. Although it is difficult to estimate a particle size distribution, alumina inclusions appear to be roughly of the same size as superalloy particles.

Two compositions with respectively 18 and 35 % volume fraction of inclusions were prepared by mixing. Their tapped density is 3.86 and 4.39 g/cm^3 respectively (about 60 and 59 % of the full density of each material), whereas the tapped density of pure Astroloy powder is 5.02 g/cm^3 (63 %).

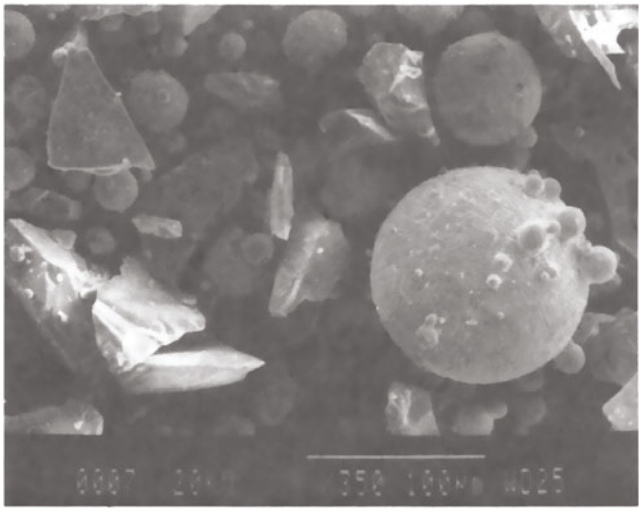

Figure 1: Micrograph of loose powder composite

To estimate the densification kinetics of each material HIP tests interrupted after different holding times were performed. A complete presentation of this method and of previous applications can be found in Reference 1. The powder was filled and tamped into stainless steel cans (internal diameter 15 mm, internal height 45 mm, thickness 2 mm) and next outgassed at 400°C under vacuum during 4 hours. The cans were next sealed by electron bean welding. After a rapid rise in pressure and temperature the holding values, 1000°C and 50 MPa, were maintained during a certain time between 5 and 180 minutes. A sudden depressurization and natural cooling ended the tests. The compacted samples were extracted by machining and their density measured by impregnation and immersion, with a precision of about 0.3 %. Polished surfaces of porous and dense specimens were also observed by electron and optical microscopy.

The materials were also hipped at 1000°C under 200 MPa during 3 hours to get dense specimens. For the most reinforced powder only 96 % of the theoretical density has been obtained, while the other mixture was found fully dense. Simple compression tests were performed on these specimens at the same temperature, 1000°C. Various strain rates, between $1.4\ 10^{-5}$ and $5\ 10^{-4}\ s^{-1}$, were successively applied.

To characterize the densification and creep behaviour of the matrix powder, results obtained in the same experimental conditions with a 0-80 μm particle-size distribution of the same Astroloy powder have been used, because results on the 0-150 μm distribution were not available yet. A previous study [2] on argon-atomized superalloy powder showed a slight effect of the particle-size distribution on the densification kinetics, but this effect is not of the same order as the differences due to the presence of hard inclusions, that will be displayed next.

RESULTS

The relative density ρ of the compacted samples is presented in Figure 2 as function of the holding time. It appears that, as expected, the densification is hindered by the inclusions. For 35 % volume fraction of inclusions the relative density obtained after 3 hours is only 86 % compared to 95% obtained with the 18 % alumina mixture and 99.5 % obtained with Astroloy powder.

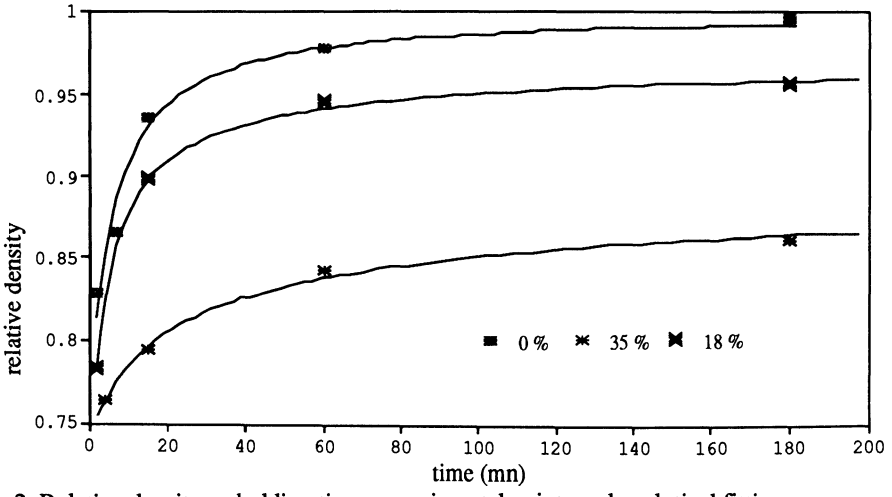

Figure 2: Relative density vs holding time: experimental points and analytical fitting

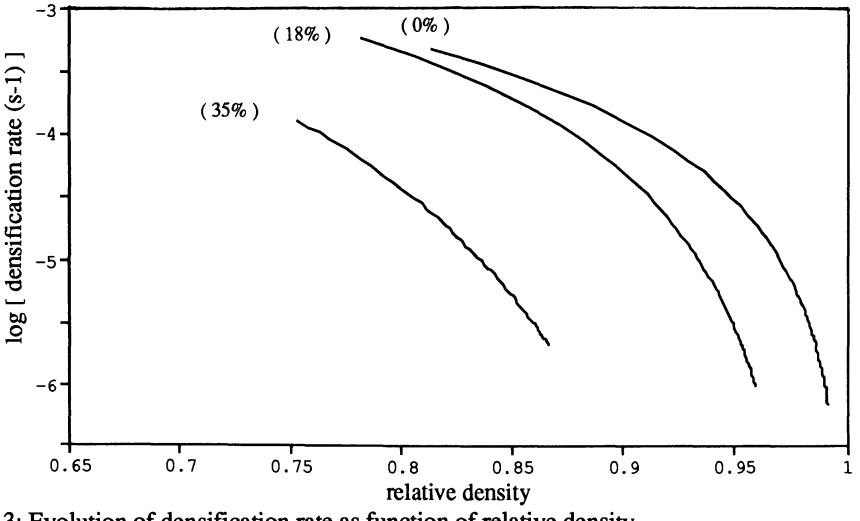

Figure 3: Evolution of densification rate as function of relative density

The densification rate $\dot{\rho}/\rho$ was estimated by derivating the analytical functions fitted to density vs time points (Figure 3). The 18 % alumina mixture has about the same densification rate as the matrix powder up to about 85 % of relative density, and next its densification rate gets progressively lower, to be about 10 times smaller than the densification rate of the matrix powder at 95 % of relative density. On the other hand the densification of the 35 % alumina composite is much slower from the lowest density. At 85 % of density the densification rate is about 100 times smaller than the densification rate of the matrix powder.

Simple compression tests on dense - or close-to-dense - specimens permitted assessement of the effect of reinforcements on the creep behaviour. The inclusions significantly increase the strength of the material (Figure 4). Although it was not fully dense, the 35 % alumina specimen had a resistance between 3 - at high strain rate - and 10 - at low strain rate - times higher than the resistance of the dense superalloy specimen. Power functions $\dot{\varepsilon} = A\ \sigma^n$

have been fitted using the stabilized stress values. It was obtained $A = 4\ 10^{-7}$ and $n = 1.84$ for Astrolloy, $A = 1.2\ 10^{-8}$ and $n = 2.58$ for the 18% alumina mixture, and $A = 2.1\ 10^{-12}$ and $n = 4.03$ for the 35% alumina mixture, the strain rate $\dot{\varepsilon}$ being expressed in s^{-1} and the stress σ in MPa. The stress exponent n rises from about 2 to 4 with increasing fraction of inclusions.

To correlate the effect of the inclusions on the densification rate and on the creep resistance, the densification rate divided by $A.P^n$ has been plotted in Figure 5 as function of relative density (P is the HIP pressure, and A and n the creep coefficients of each material). As the curves corresponding to each powder get very close around 0.8 of relative density, this representation suggests that the inclusions affect in about the same way the initial stage of the densification process and the creep behaviour

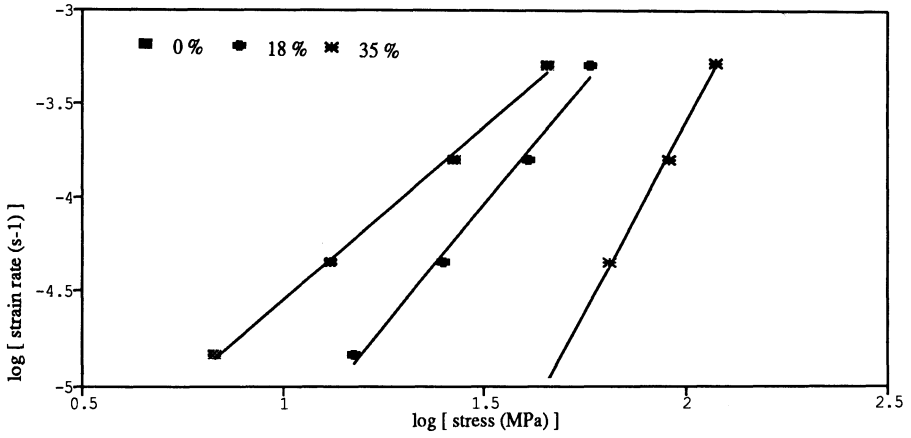

Figure 4: Results of creep tests

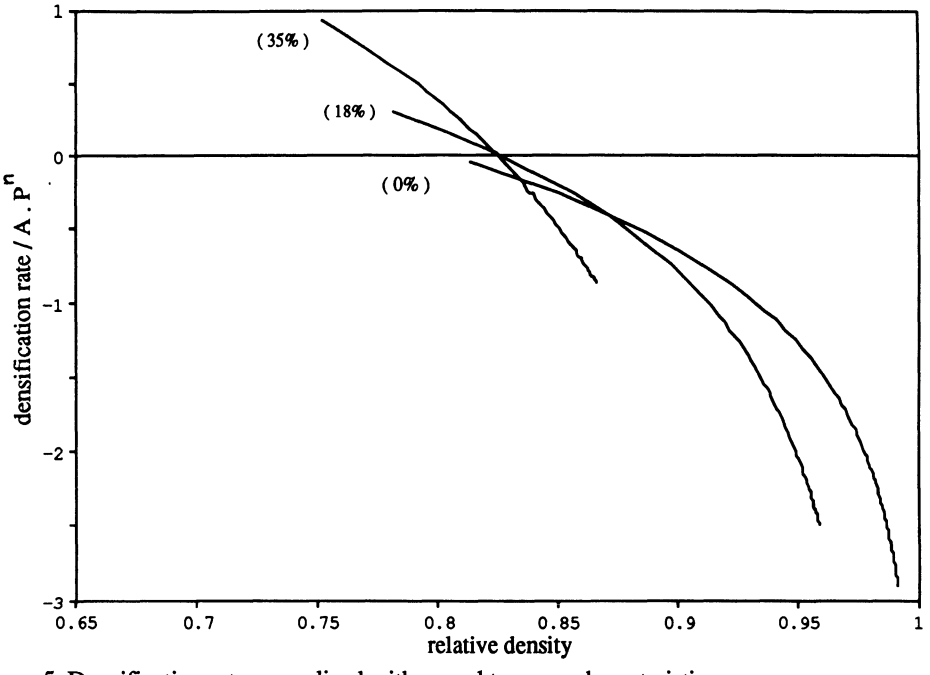

Figure 5: Densification rate normalized with regard to creep characteristics

DISCUSSION

After studying the compaction of mixtures of hard and soft spherical metal spheres, Lange et al [3] proposed two explanations for the retardation in densification due to the presence of hard inclusions in a matrix powder. The first one concerns the large deformation required for the matrix particles to fill the so-called "excluded volume", which is the volume located around the contacts of inclusions between eachother and inaccessible to matrix particles during the initial packing. The second explanation is related to the formation of a continous inclusion network capable of supporting a significant part of the applied pressure, which is therefore no longer available for the densification of matrix particles.

The macroscopic and microscopic results presented above suggest that both mechanisms occur during the consolidation of the alumina-reinforced superalloy powder. Because of the excluded volume at contacts of inclusions between each other, but also because of the irregular shape of alumina particles, superalloy particles must be largely deformed in order to reach a high density (Figure 6), what of course requires longer HIP times. This phenomenon likely caused the slowing down of the 18 % alumina mixture from a relative density of 85 % .

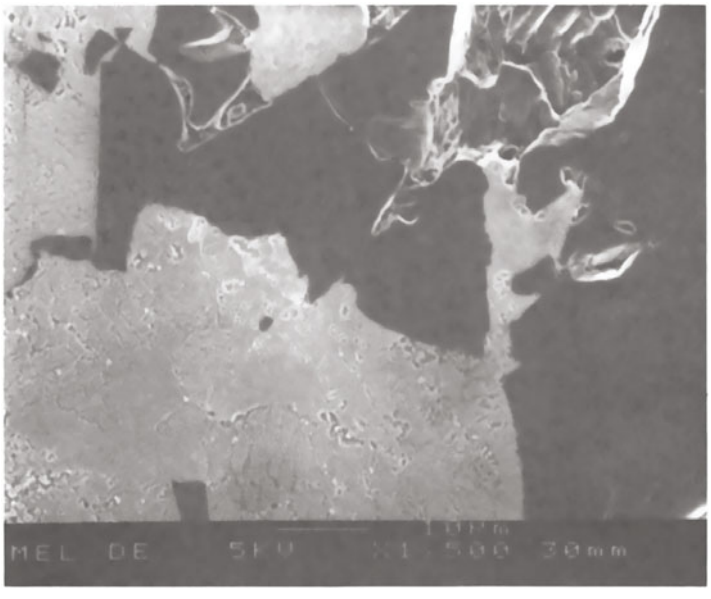

Figure 6: Large deformation of superalloy particles around alumina inclusions

However this first mechanism cannot explain the very low densification rate measured for the 35 % alumina mixture at low density, when matrix particles are still slightly deformed. This low densification rate may be due to the second mechanism, i.e. the formation of a continuous network of inclusions transmitting a portion of the applied pressure. Breaking of alumina particles observed in most specimens (Figure 7) supports this hypothesis. Furthermore superalloy-filled cracks prove that this breaking did not happen during the cooling, but during the early stage of the consolidation. The supportive inclusion network is also likely responsible with the very high resistance of the 35 % alumina specimen during creep tests - quantitatively consistent with densification measurements, as shown in Figure 6.

The developement of long range connectivity - or percolation - in a bimodal powder mixture with increasing volume fraction of inclusions has been studied through numerical

simulations [4]. This study suggested that for spherical matrix particles and inclusions of the same size a supportive inclusion network forms when the volume fraction of inclusions relative to all space is about 0.27, what corresponds for a solid volume fraction of 35 % to a relative density of 0.77. Although the morphology and the size distribution of the present material are quite different, this value is roughly consistent with the densification results displayed above.

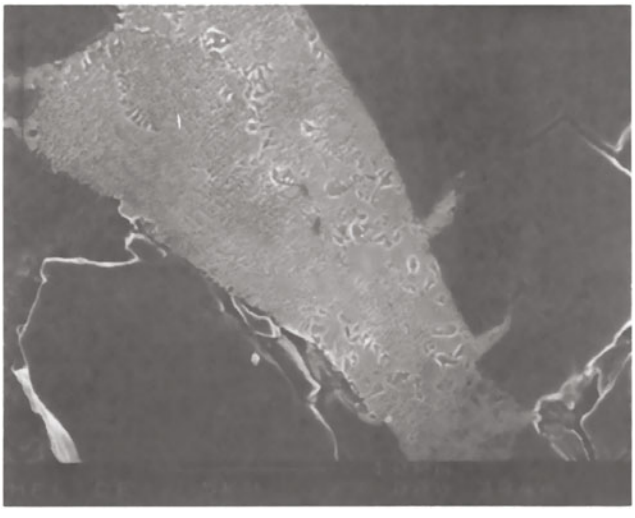

Figure 7: Broken alumina inclusion

CONCLUSION

For "low" fraction of inclusions (18 %) the densification is likely hindered because of the large deformation required to fill the volume around inclusion-inclusion contacts and to surround the irregularly-shaped inclusions. For "high" fraction of inclusions (35 %) the retardation in densification is much more important and may be due to the formation of a continuous inclusion network, supporting part of the applied pressure.

REFERENCES

1. Bouvard D. and Lafer M., Determination of the densification kinetics of metal powders by interrupted hot isostatic pressing tests. Powder Metal. Int., 1989, **21**, pp. 11-15.

2. Bouvard D., Cheynet M.C. and Saint-Antonin F., Densification behaviour of argon atomized powders during hot isostatic pressing. In Proceedings of the 3rd Int. Conf. on Isostatic Pressing, MPR Publishing Services, Stratford/Avon, 1986.

3. Lange F.F., Atteraas L., Zok F., and Porter J.R., Deformation consolidation of metal powders containing steel inclusions. Acta Metall. Mater., 1991, **39**, pp. 209-219.

4. Bouvard D. and Lange F.F., Correlation between percolation and particle coordination in binary powder mixtures. Submitted to Acta Metall. Mater., 1991.

ACKNOWLEDGEMENTS

The authors acknowledge the support grant from Ministère de la Recherche et de la Technologie under contract n° 90.A.0570.

HIP AND SINTER-HIP OF TERNARY NiAl-X ALLOYS

W.A. Kaysser[+], R. Laag[+], J.C. Murray[+*] and G Petzow[+]

[+] Max-Planck-Institut für Metallforschung, Pulvermetallurgisches Laboratorium, Heisenbergstraße 5, D-7000 Stuttgart 80, Germany.

[*] General Electric Aircraft Engines, 1 Neuman Way, Evendale, OH 45215 USA.

ABSTRACT

Prealloyed powders of NiAl, NiAl-5Ti and NiAl-5Nb (at.-%) were gas atomized with an average particle size of 90 μm and attritor milled under Ar atmosphere reducing the average particle size to 1.5 μm. Sintering CIP compacts developed microstructure and density disributions, which allowed subsequent containerless HIPing to near full density (>98.5%) and a final grain size < 8 μm. Alloying of NiAl with 5at% Nb or Ti increased its hardness, Young's modulus, toughness and creep resistance. The room temperature fracture path changed from primarily intergranular (NiAl) to primarily transgranular (Nb, Ti alloyed), increasing the K_{Ic} values from 3.8 to 14.4 and 15.3 $MPa\sqrt{m}$, respectively. For comparison, HIPed materials from the as-atomized powders were also tested.

INTRODUCTION

In the development of new high temperature structural materials the P/M processing route for the compounds of NiAl-X type is competitive to the Ti--Aluminides because the higher melting point enables higher service temperatures in comparison to TiAl. Due to the formation of a stable Al_2O_3 surface layer, stoichiometric NiAl exhibits an excellent oxidation resistance together with a density advantage of about 30% compared to Ni-based superalloys. Currently, the use of NiAl is limited by its creep resistance and its low room temperature toughness and room temperature brittleness.

It has been proposed that alloying or dispersion hardening may improve the mechanical properties of NiAl [1],[2]. Vedula et al. [1] have studied the effects of a variety ternary alloying additions on the creep resistance of NiAl. The materials for these experiments were prepared by HIPing or hot extruding mixtures of - 80 mesh

nonstoichiometric prealloyed Ni-44.6at% Al powder and -325 mesh elemental Ti and Nb powders respectively, followed by homogenization heat treatment. This processing method yielded a final grain size in the order of 100 μm with precipitates that formed were mainly isolated to the grain boundaries although the ternary additions were inside the solubility limits of the β-phase [3]. These materials gave some insights to the high temperature behavior of alloyed NiAl, nevertheless it is expected that they would have shown poor ductility at room temperature. Schulson and Barker [4] have observed a maximum grain size much below 20 μm to extend the ductility of the NiAl phase at 400 °C.

The present study examines the effect of ternary alloying with Nb and Ti on the consolidation behavior and mechanical properties of stoichiometric NiAl-X at room temperature and on the creep properties in the high temperature regime. In order to avoid uncontrolled embrittlement of the NiAl alloys by coarse grains [5], an alternate processing route was used to make ternary alloys with small grains and more uniform distribution of alloying elements. The minor alloying elements were selected based on phase diagram considerations. Titanium has 10% solubility in stoichiometric NiAl at room temperature [6], thus 5 at.% Ti may act as a solid solution strengthener. Niobium has 1% solubility in stoichiometric NiAl [7], thus 5 at.% Nb may act as a precipitation strengthener. Prealloyed powders were gas atomized so that rapid solidification of the particles would prevent gross segregation of the elements. Using prealloyed material removes the need for a homogenization heat treatment which causes grain growth.

POWDER PROCESSING

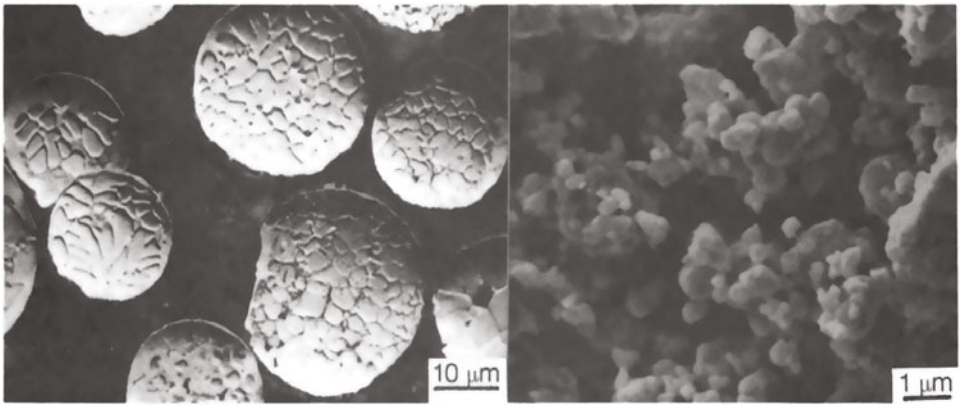

(a) (b)

Fig. 1: As atomized powders of single phase NiAl (a) and the same powder after attritor milling (b).

Powders with nominal compositions of Ni-50at%Al (NiAl), (Ni-50at%Al)-5at%Ti (NiAl-5Ti), and (Ni-50at%Al)-5at%Nb (NiAl-5Nb) were gas atomized with Argon (99,995) yielded cooling of the droplets and particles between 32 and 90 μm at rates of $4 \cdot 10^4$ and $8 \cdot 10^4$ K/s [8]. The powders were protected from air using glove box facilities for further processing.

For all alloys the spherical powders had an average diameter of 90 μm and internal equiaxed grains averaging 8 μm diameter (fig. 1a). Optical metallography

and x-ray diffraction revealed all powders to be single phase and of B2 type [9]. The microhardness of the as atomized powders was highly different for the different compositions, with 369 ± 16 $HV_{0.1}$, NiAl, 433 ± 8 $HV_{0.1}$, NiAl-5Nb and 567 ± 23 $HV_{0.1}$, NiAl-5Ti. That means a 53% increase in hardness with 5 at.% Ti and a 17% increase with 5 at.% Nb compared to binary NiAl.

Attritor milling of batches from the atomized alloyed powders was performed under flowing Argon without fluid milling agents. Milling caused brittle fracture of the atomized powders to form small angular particles (fig. 1b). The average particle size was reduced from 90 μm to 1.5 μm. The oxygen impurity content was 377.9, 390.5 and 314.6 ppm for NiAl-5Nb, NiAl-5Ti and NiAl respectively. Comparative milling of NiAl in isopropanol increased the oxygen content to 2.1wt%.

POWDER CONSOLIDATION

The parameters for HIP consolidation of the as-atomized powders were calculated with a modified version of the HIP-487 program [10]. The material parameters required for the HIP-diagram calculations were partly obtained using the single particle dilatometer (SPD) [11]. Figure 2 shows the relative creep resistance at test temperature T_V = 1200 °C, 1/E, in units of 1/MPa, obtained from the SPD experiments, whereby 1/E is given as the deformation normalized to the initial

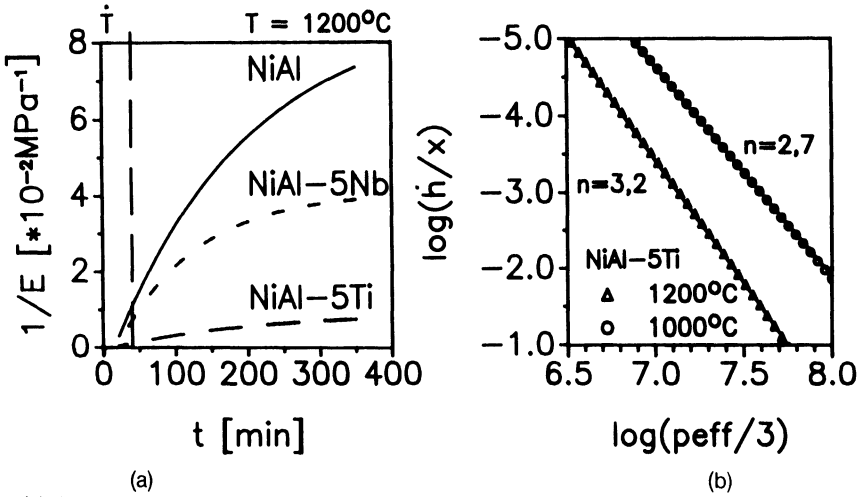

(a) (b)

Fig. 2: (a) Deformation curves for NiAl, NiAl-5Nb and NiAl-5Ti under a constant load of 0.4N. (b) Creep of NiAl-5Ti at different temperatures calculated from (a).

particle radius and the applied pressure on the particle contact. Special attention was given to the determination of the reference stress for P-L-Creep, which was found to be one of the important parameters in the HIP diagram calculation (Tab. I). Using SPD, the reference stress for P-L-Creep can be taken directly from the actual material.

In HIP diagram calculation, power law creep is described by

$$\frac{\dot{h}}{x} = \left[\frac{9\pi}{16}\,\dot{\epsilon}_0\,\sigma_0^{-n}\right]\cdot\left[\frac{p_{eff}}{3}\right]^n \qquad <1>$$

and the creep exponent,n, can be taken from the Arrhenius plot

$$\log\left[\frac{\dot{h}}{x}\right] = B + n \cdot \log\left[\frac{p_{eff}}{3}\right] \qquad <2>$$

The activation energy for P-L-Creep can be determined from the slope of an Arrhenius plot $\ln(p_{eff})$ vs. $1/T$, where the slope is $m = -Q_c/R$ using the results from the SPD. Using the equation

$$\frac{\dot{h}}{x} = A \cdot \sigma^n \cdot \exp\left[\frac{-Q_c}{R\,T_V}\right] \qquad <3>$$

and after transformation of eq.<2> and dividing eq. <2> / eq. <3> this results in

$$\sigma_{Ref} = \left[\frac{10^{-6}}{10^B} \cdot \exp\left[\frac{Q_c}{R} \cdot \left[\frac{2}{T_m} - \frac{1}{T_V}\right]\right]\right]^{1/n} \qquad <4>$$

using eq. <1>, with Q_c = Activation Energy for P-L-Creep, $\dot{\epsilon}_0$, σ_0 = Material Constants, R = Universal Gas Constant, p_{eff} = Applied pressure on particle contact, T_m = Melting Temperature. The calculated parameters are collected in Table II.

Property	Unit	NiAl	NiAl-5Ti
Melting Point	K	1911.2	1863.2
Surface Energy	J/m²	2.2	1.9
Youngs Modulus	GPa	200.0	201.0
T-dependence of Modulus		*	*
Yield Stress at RT	**MPa**	**736.1**	**1000.0**
T-dependence of yield		*	*
Atomic Volume	m³	$1.0 \cdot 10^{-29}$	$1.3 \cdot 10^{-29}$
Pre-exp. Volume Diff.	m²/s	$4.8 \cdot 10^{-5}$	$4.5 \cdot 10^{-4}$
Activ.Energy, Vol.Diff.	kJ/mol	335.0	307.3
Pre-exp. Boundary Diff.	m³/s	$1.6 \cdot 10^{-15}$	$1.4 \cdot 10^{-15}$
Activ.Energy, Bound. Diff.	kJ/mol	289.8	184.4
Pre-exp. Surf. Diff.	m³/s	$6.3 \cdot 10^{-10}$	$6.3 \cdot 10^{-10}$
Activ.Energy, Surf. Diff.	kJ/mol	325.0	307.3
Power Law Creep Exponent		**4.2**	**2.7**
Ref. Stress, P-L creep	**MPa**	**368.1**	**176.0**
Activ.Energy for P-L creep	**kJ/mol**	**257.2**	**304.3**
Solid Density	g/cm³	5.9	5.8
Particle Diameter	**µm**	**100.0**	**100.0**
Grain Diameter in Particle	µm	8.0	8.0

Tab. I: Material property table for HIP diagrams calculated for T = 1200 °C. **Highlighted** values from SPD. Diffusion data are partially taken from literature, or calculated using scaling relations [10]. (*) indicates values which are approximated by a function.

Hot isostatic pressing of as-atomized powder compacts was carried out with each Ni aluminide. According to the calculated HIP diagram the specimen prepared for mechanical property measurements were heated at 30 K/min up to 1000 °C (NiAl, NiAl-5Nb) and 1200 °C (NiAl-5Ti) respectively. They were pressed with 100 MPa for 120 min in an ASEA HIP (QHI-9) to full dense material.

Cold isostatic compaction of as-atomized powders at pressures between 150 and 350 MPa was unsuccessful. The green compacts crumbled during die ejection. Cold isostatic pressing of the attrited fine powders provided a reasonable green strength and relative green densities between 0.55 and 0.62. For sinter experiments the green compacts were prepared by tapping 25 to 30 g of attrited powder into a bar shaped rubber die and CIPing at 350 MPa. Density measurement was performed using Archimedes' method based on theoretical densities for NiAl of 5.9 g/cm³, NiAl-5Ti of 5.8 g/cm³, and NiAl-5Nb of 6.0 g/cm³.

T_V [K]	1273	1473
B	-23.9	-26.1
n	2.7	3.2
Q [kJ/mol]	304.3	304.3
T_m [K]	1863	1863
σ_{Ref} [MPa]	176	141

Tab. II: Parameters for the calculation of reference stress for P-L-Creep.

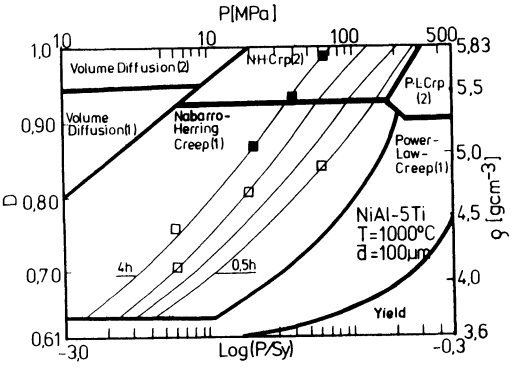

Fig. 3: HIP diagram for as atomized NiAl-5Ti powder with an average particle size of 100 um.

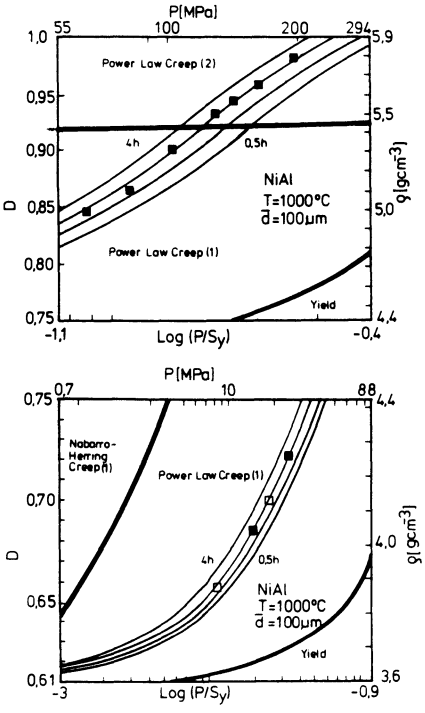

Fig. 4: HIP diagram for as atomized NiAl powder with an average particle size of 100 um.

As atomized loose powder, tapped into an alumina crucible and heated to temperatures as high as 1500° C for 2 h, showed minimal evidence of sintering. The CIPed NiAl compacts from the attrited powders were sintered 2 h at 1400° C with heating rates of 10 K/min to 500° C and 20 K/min to the sintering temperature. After sintering densities of 95±2% of theoretical were obtained in the surface regions of the specimens and are almost independent of the alloy composition, which indicates closed porosity and the possibility of containerless subsequent HIPing. The specimens were consolidated according to the Sinter-HIP diagram at 1250° C with 150 MPa for 2 h (fig. 5). The final density of the HIP specimens is listed in table III. Samples, indicated by an asterisk, were mechanically tested.

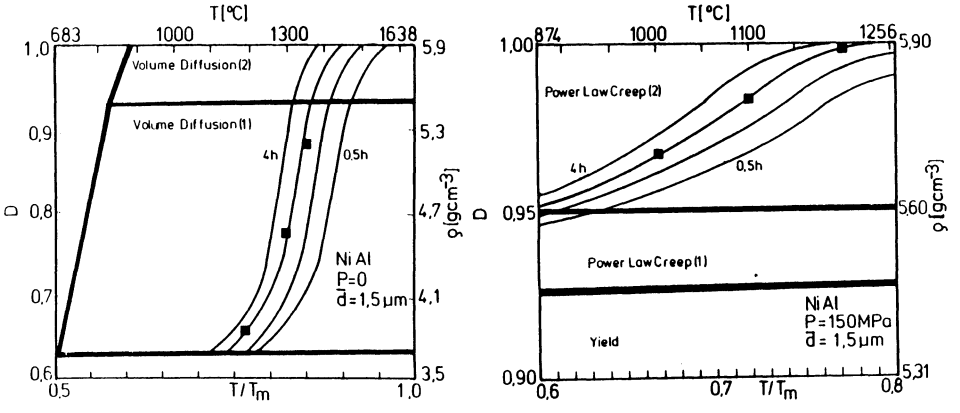

Fig. 5: Sinter-HIP diagram for NiAl: Sintering 2 h in vacuum at 1400 °C to closed surface porosity; HIP with 150 MPa Argon gas pressure for 2 h at 1200 °C to full density.

MECHANICAL PROPERTIES

Young's modulus, Poisson's ratio, and fracture toughness at room temperature were tested. These data are summarized in table II. Dynamic elastic modulus and Poisson's ratio were measured on polished parallel-surface specimens by the impulse-echo method. The small increase in the measured elastic modulus of the ternary alloys relative to binary NiAl is statistically not significant.

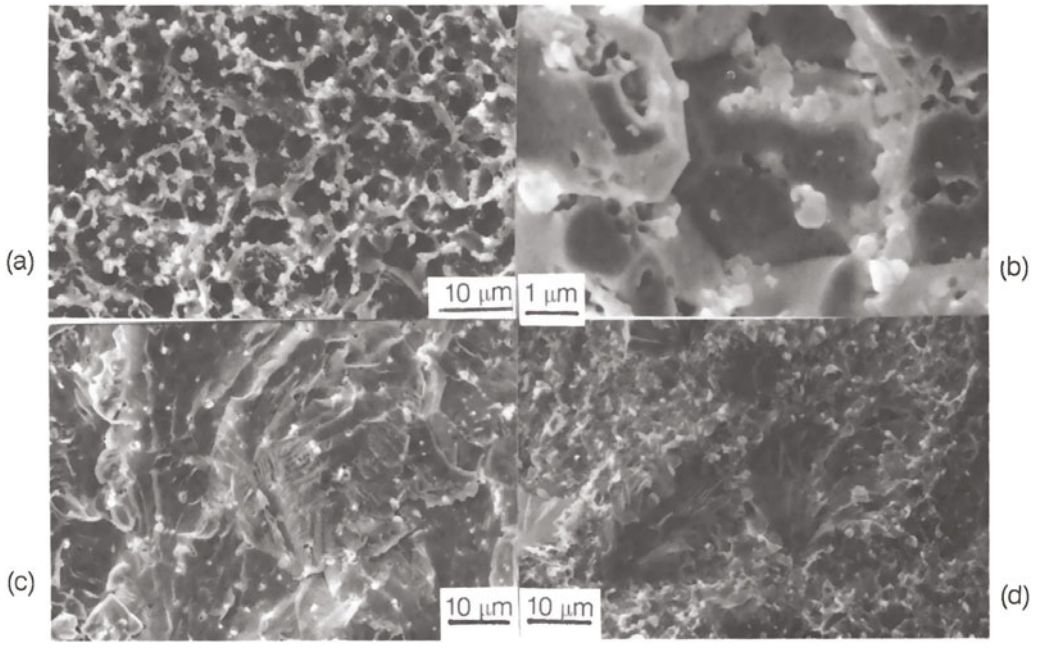

Fig. 6: Fracture surfaces of the binary and ternary specimen made from atomized and attrited powders. (a,b) NiAl, (c) NiAl-5Ti and (d) NiAl-5Nb.

Fracture thoughness of the alloys was measured by the single edge notch beam method with 40/20 or 30/20 mm (upper/lower distance of the support) four-point bend specimens. The impact velocity for all measurements was 0.1 mm/min. The cross-section of the specimen was 4 x 5 mm with a length of 50 or 40 mm, respectively. The data are given in table III. There was an approx. 4-fold increase in fracture toughness of the ternary alloys over binary NiAl. The 12% increase in the measured fracture toughness of NiAl-5Nb over NiAl-5Ti is not significant because it falls within the experimental error.

There was a significant difference in the fracture surface of the binary and ternary alloys. Binary NiAl fractured along the grain boundaries (fig. 6a,b). This reflects that the toughness represents grain boundary cohesion, crack deflection and crack branching, rather than the crack propagation resistance in the grains. The ternary alloy NiAl-5Ti and NiAl-5Nb, fractured through the grains (fig. 6c,d), so the measurements were representative of the ternary alloy toughness.

Alloy	Cons.	ρ_{rel} [%]	E [GPa]	ν	K_{Ic}[MPa$\sqrt{m}$]
NiAl-5Nb	C,S	86.3	180.51	0.29	12.2±3.2
NiAl-5Nb	C,S,H	98.6	200.32	0.29	15.4±3.2
NiAl-5Nb	H (*)	100.0	131.15	0.28	13.1±1.4
NiAl-5Ti	C,S	84.9	121.73	0.28	4.7±0.4
NiAl-5Ti	C,S,H	99.1	206.32	0.33	14.5±3.0
NiAl-5Ti	H (*)	100.0	149.10	0.27	11.2±2.6
NiAl	C,S	86.8	168.32	0.28	2.7±1.0
NiAl	C,S,H	100.0	199.56	0.34	3.8±0.4
NiAl	H (*)	100.0	199.10	0.34	3.4±1.3

Tab. III: The density depending on consolidation after CIP (C), sintering (S), final stage consolidation by containerless HIP (H) and encapsulated HIP of as atomized powders (H(*)). Abbreviations for relative density (ρ_{rel}), Young's modulus (E), Poisson number (ν) and fracture toughness (K_{Ic}).

DISCUSSION

Relative deformation of NiAl, NiAl-5Ti and NiAl-5Nb alloys was measured by single powder particle dilatometry using as-atomized powders. The data clearly indicate that both Nb and Ti increase the creep resistance of NiAl at 1200 °C and Ti is a more effective strengthener than Nb. The reported solubilities of Ti in NiAl (B2-phase) indicate that the presence of Ti leads to solid solution strengthening (deformation experiments), whereas for Nb the presence of a second phase was identified. The presence of Ti as an alloying element is very likely to improve the interface cohesion between the NiAl matrix and coherent precipitation hardeners.

Sintering prealloyed NiAl powders to high density was driven by the high surface energy of the small attrited particles. The formation of layers of high density at the surface of sintering compacts allowed containerless HIPing as a final densification method even for sintered samples with overall densities as low as 84.9%.

During consolidation, the ternary alloys behaved similarly to the binary NiAl, yet the mechanical behavior of the alloys differed considerably. There was only a discernible difference in the Young's modulus and Poisson's ratio between the binary and ternary alloyed specimens made from as atomized powders. In the fine

grained material this difference is negliable. A large effect was not expected because these properties are dependent on atomic interactions which are still dominated by the high Ni and Al contents of the alloys.

ACKNOWLEDGEMENT
This work was supported by the Deutsche Forschungsgemeinschaft under contract Ka 664/1-5 and partially by the Bundesministerium für Forschung und Technologie under contract 03M0032C.

LITERATURE CITED

[1] K. Vedula, V. Pathare, I. Aslandis, R.H. Titran, "Alloys Based on NiAl for High Temperature Applications", Materials Research Symposium Proceedings, vol. 39, 1985, pp. 411-421.

[2] M. Sherman, K. Vedula, "High Temperature Dispersion Strengthening of NiAl," Journal of Materials Science, Vol. 21, 1986, pp. 1974-1980.

[3] V. Pathare, K. Vedula, "Structure-High Temperature Property Relationships for Powder Processed Ternary NiAl Alloys", Modern Developments in Powder Metallurgy, vol. 16, 1984, pp. 695-704.

[4] E.M. Schulson, D.R. Barker, "A Brittle to Ductile Transition in NiAl of a Critical Grain Size", Scripta Metallurgica, vol. 17, 1983, pp. 519-522.

[5] J.D. Rigney, P.S. Khadkikar, J.J. Lewandowski, K. Vedula; "Strength and Toughness of Composite Meterials based on Nickel Aluminide Martrices", Materials Research Symposium Proceedings, vol. 133, 1989, pp. 603-608.

[6] A. Raman, K. Schubert, "Über den Aufbau einiger zu $TiAl_3$ verwandten Legierungsreihen III", Zeitschrift f. Metallkde., vol. 56, 1965, pp.99-105.

[7] B.B. Argent, "Phase Diagrams of Alloys Based on Niobium", Niobium Conference Proceedings, TMS/AIME, San Francisco, California, Nov. 1981, pp. 325-415.

[8] R. Laag, W.A. Kaysser, G.Galinski, R. Maurer, "The Prediction of HIP Parameters of Ar-Atomized NiAl Powders with Soichiometric Variations", in: PM into the 1990's - International Conference on Powder Metallurgy London 1990; The Institute of Metals, London; 2 (1990) pp. 278-288.

[9] R. Maurer, G. Galinski, R. Laag, W.A. Kaysser; "Structural and Chemical Composition of Ni-Al Powders", Materials Research Symposium Proceedings, vol. 133, 1989 pp 421-426.

[10] M.F. Ashby; HIP-487: A Program for Constructing Hot Isostatic Pressing Diagrams, University of Cambridge, UK (1987).

[11] R. Laag, W.A. Kaysser, R. Maurer, G. Petzow; "The Influence of Stoichiometry on the Prediction of HIP Parameters for Intermetallic Prealloyed Ni-Al Powder", Proceedings of the 2nd International Conference on Hot Isostatic Pressing. ASM International 1991, pp 101-113.

FULLY DENSE HIP COMPACTION OF MECHANICALLY ALLOYED AMORPHOUS POWDERS

Hiroshi Kimura, Kazutoshi Toda* and Tutomu Yuine**
Department of Mechanical Engineering,
National Defense Academy, Yokosuka 239, Japan
* On leave from Koyo Seiko Co., Ltd., Kashiwara Osaka 582, Japan
** Koyo Seiko Co., Ltd., Tokyo 104, Japan

ABSTRACT

We develop novel HIP processing of mechanically alloyed amorphous powders with an insufficient time and/or temperature range between crystallization and glass transition, with which it is possible to obtain a fully dense amorphous compact. Our HIP processing mainly consists of short-time powder consolidation via viscous flow in an amorphous alloy and the pore shrinkage by compressive deformation of metal-sealed amorphous HIP compact. At 853 K near a temperature at the onset of crystallization, HIP compaction of amorphous $Co_{79.5}Nb_{15}Zr_{5.5}$ powders, encapsulated in vacuumed copper can, shows an amorphous product with a relative density of 98 % for a holding time of 5 min and an almost fully dense, but partially crystallized bulk for 30 min. The compressive deformation of the short-time HIP'ed amorphous compact leads to an increase in density, approaching to a theoretical one, when average stress of axial component exceeds 196 MPa which is the level of HIP pressure. The fracture stress(σ_F) in compression for amorphous HIP compact shows a great increase with a decrease in porosity(P) by compressive forming, this increase is expressed by a power law of $\sigma_F = BP^{-0.5}$.

INTRODUCTION

Mechanical alloying(MA) is becoming one of the most promising solid state powder processing by which to prepare non-equilibrium phase materials such as amorphous alloys and nanometer sized crystals[1]. These non-equilibrium phases could transform into a more stable phase at a higher consolidating temperature which is necessary for the production of a high density powder compact by a conventional P/M technique. Recently, we have succeeded in obtaining relatively high dense compaction of large scale and a near-net shape forming, via viscous flow above a glass temperature, of amorphous CoNbZr powders by hot isostatic pressing(HIP)[2], using high quality MA amorphous powder with an active and clean surface[3], prepared by a rotating-arm reaction ball mill[4]. Then, we found constitutive equations of viscous flow with which to optimize HIP variables of temperature, time and heating rate for a full densification of amorphous compacts of Co-rich CoNbZr[5], TiAl[6]. While, amorphous powders prepared by rapid solidification such as gas atomization and melt spinning could not be consolidated to a high density amorphous compact by HIP that do not provide macroscopically shearing, due to the oxide surface layer.

In order to realize the development of high performance bulk materials using a variety of MA amorphous powders, we here are going to develop a HIP processing for a fully dense compact of amorphous alloy having a narrow temperature range between glass transition and crystallization.

EXPERIMENTAL PROCEDURES

Rotating-arm reaction ball milling(Mitui Miike attritor, model MA1D-X) was used to prepare high quality mechanically alloyed powders of amorphous $Co_{79.5}Nb_5Zr_{5.5}$. The temperatures(T_x, T_p) at the onset and peak of crystallization for as attritted amorphous $Co_{79.5}Nb_{15}Zr_{5.5}$ were measured from a constant heating rate experiment at various rates in a differential scanning calorimeter(DSC). The pre-compacted sample, obtained by HIP of a cold isostatic pressed bulk for 20 min at 813 K was tested under an applied compressive stress(σ) using a heating rate of 0.22 K s^{-1} in a thermal mechanical analyzer to measure viscous flow above glass transition. MA amorphous $Co_{79.5}Nb_{15}Zr_{5.5}$ powders were encapsulated in vacuumed copper can with an outer diameter of 10 mm, and then HIP'ed under Ar gas pressure of 196 MPa for 5 and 30 min at 853 K using a heating rate of 0.22 K sec^{-1}. X-ray diffraction with radiation of CrKα was used to characterize a structure of HIP compact. The compressive deformation of metal-sealed HIP compact specimen were carried out using an Instron testing machine. For HIP compacts, the surface was observed by scanning electron microscopy(SEM), and then the porosity is obtained by lineal analysis. The density was measured by an Archimedean method.

RESULTS AND DISCUSSION

HIP Compaction of MA Amorphous Powders

Figure 1 shows compressive displacement versus temperature for the pre-compact of MA amorphous $Co_{79.5}Nb_{15}Zr_{5.5}$, HIP'ed for 20 min at 813 K under an applied stress of $7x10^{-3}$ MPa, together with a DSC trace. It can be seen that a drastic displacement via viscous flow in amorphous $Co_{79.5}Nb_{15}Zr_{5.5}$, following a contraction, appears above approximately 800 K;this temperature corresponds to the onset of an endothermic DSC peak due to glass transition. We obtain strain rate($\dot{\varepsilon}$) from the slope(dl/dT) of displacement(l)-temperature(T) curve and then deduce the viscosity(η) of the pre-compact using a equation of Newtonian flow, $\eta = \sigma_{eff}\mu/3\dot{\varepsilon}$ where σ_{eff} is effective stress and μ is internal friction coefficient{;see ref.(5) for a detail derivation}. The apparent viscosity for the pre-compact of amorphous

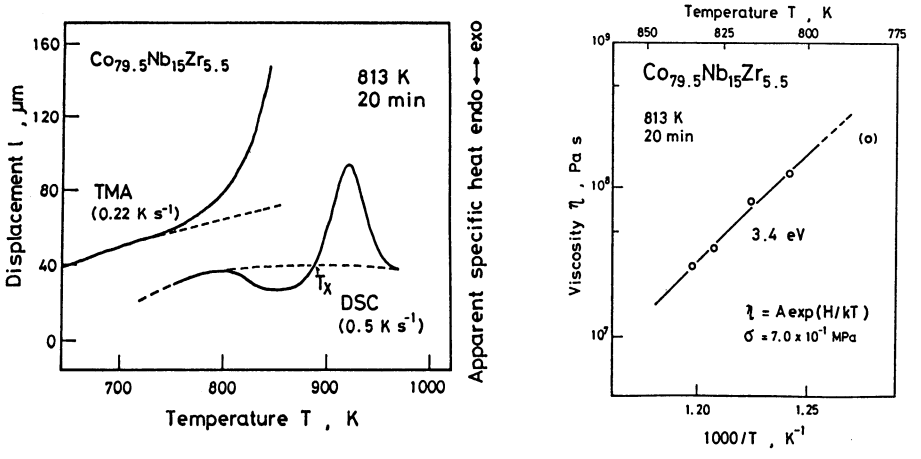

Figure 1. Compressive displacement versus temperature for pre-compact of mechanically alloyed amorphous $Co_{79.5}Nb_{15}Zr_{5.5}$, HIP'ed for 20 min at 813 K following cold isostatic pressing under an applied compressive stress of $7x10^{-3}$ MPa, using a heating rate of 0.22 K sec^{-1}. This figure also includes an apparent specific heat vs. temperature.

Figure 2 Apparent viscosity of pre-compact of MA amorphous $Co_{79.5}Nb_{15}Zr_{5.5}$, HIP'ed for 20 min at 813 K as a function of reciprocal temperature.

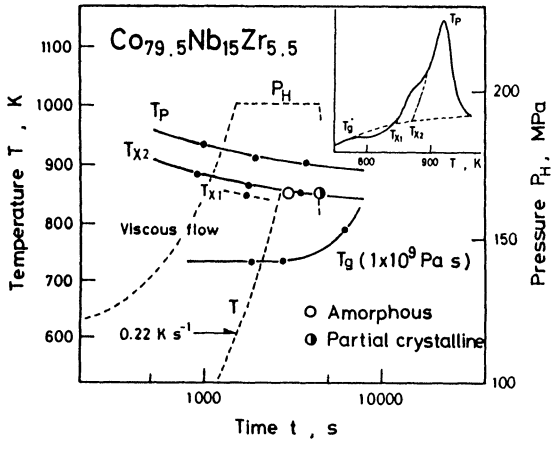

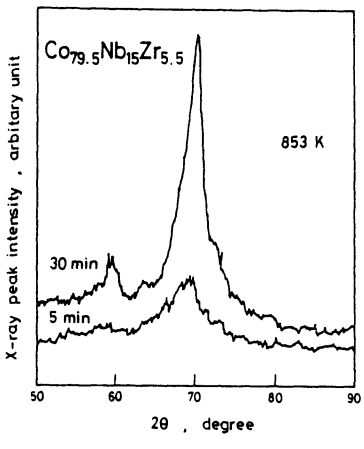

Figure 3. HIP temperature and pressure used in this study for consolidating high quality amorphous $Co_{79.5}Nb_{15}Zr_{5.5}$ powder as a function of time. This figure also describes T_{X1}, T_{X2} and T_g at various heating rates, showing a range of the occurrence of viscous flow.

Figure 4. X-ray diffraction patterns for MA amorphous $Co_{79.5}Nb_{15}Zr_{5.5}$ compacts, HIP'ed for 5 and 30 min at 853 K.

$Co_{79.5}Nb_{15}Zr_{5.5}$ shows the level of a undercooled liquid below glass transition temperature(T_g) and decreases with increasing temperature. This decrease is fairly well expressed by an Arrhenius relation, $\eta = A\exp(H/kT)$ with the activation energy(H) for viscous flow of 3.4 eV as shown in Fig.2.

The temperature range for the occurrence of viscous flow in amorphous $Co_{79.5}Nb_{15}Zr_{5.5}$ is T_g(at 10^9 Pa s)$<T<T_p$ above a heating rate of 0.8 K s^{-1}[5] as shown in Figure 3. We conducted HIP compaction of as attritted amorphous $Co_{79.5}Nb_{15}Zr_{5.5}$ powder for 5 and 30 min at 853 K under a pressure 196 MPa as depicted in Fig.3. The compacts, HIP'ed for 5 and 30 min were confirmed to be amorphous and partially crystallized by X-ray diffraction respectively, as predicted by a time-temperature curve of crystallization without pressure, as shown in Figure 4. The short-time consolidated sample shows a distribution of submicron sized pores mainly at the triple point of particles with a porosity(P) of 2 %, while partially crystallized bulk is almost fully dense(P = 0.4 %) as shown in Fig.5.

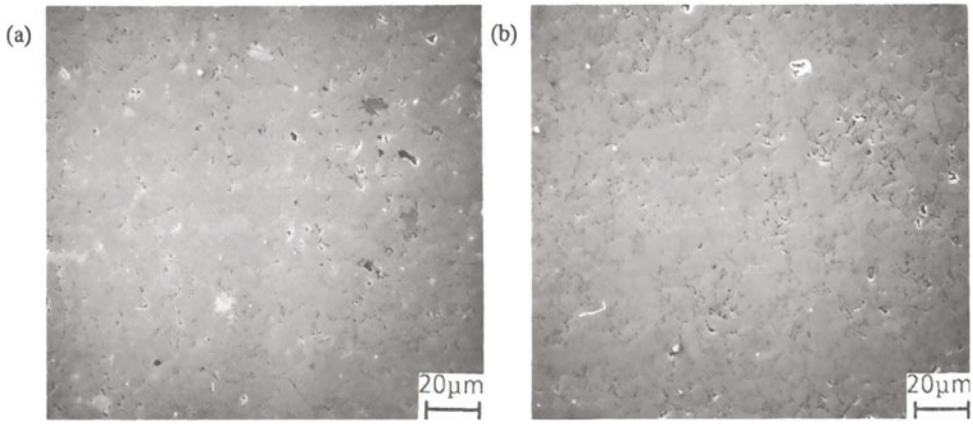

Figure 5. SEM image of surface of MA $Co_{79.5}Nb_{15}Zr_{5.5}$ HIP compact at 853 K, (a) 5 min, (b) 30 min.

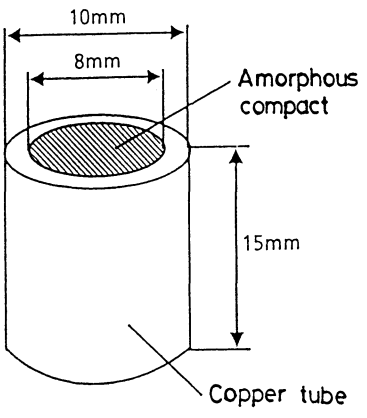

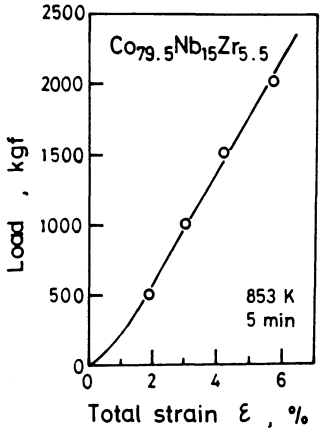

Figure 6. A schematic of metal-sealed HIP compact used in this study as a model experiment of secondary compressive forming.

Figure 7. Applied load versus total strain for compressive deformation of copper-sealed amorphous $Co_{79.5}Nb_{15}Zr_{5.5}$ HIP compacts, subjected to short-time consolidation of 5 min at 853 K.

Compressive Forming of Metal-Sealed HIP Compact

Figure 6 illustrates a schematic of metal-sealed HIP compact used in this study as a model experiment of secondary compressive forming for a full densification. Figure 7 shows the total strain under various compressive loads of 500, 1000, 1500 and 2000 kgf for different copper-sealed HIP compacts of amorphous $Co_{79.5}Nb_{15}Zr_{5.5}$ with the porosity of 2 %, subjected to short-time consolidation of 5 min at 853 K as shown in Fig.5(a). We see the linearity in the plotting of load vs. total strain, this indicating that the compressive forming of the copper-sealed amorphous HIP compact macroscopically proceeds in an elastic way up to an applied load of 2000 kgf. In other words, elastic stresses resulted from constant constrained(forced) elastic displacement apply to the metal-sealed HIP powder compact.

Figure 8 shows SEM image of the cross-section of copper-sealed amorphous $Co_{79.5}Nb_{15}Zr_{5.5}$ HIP

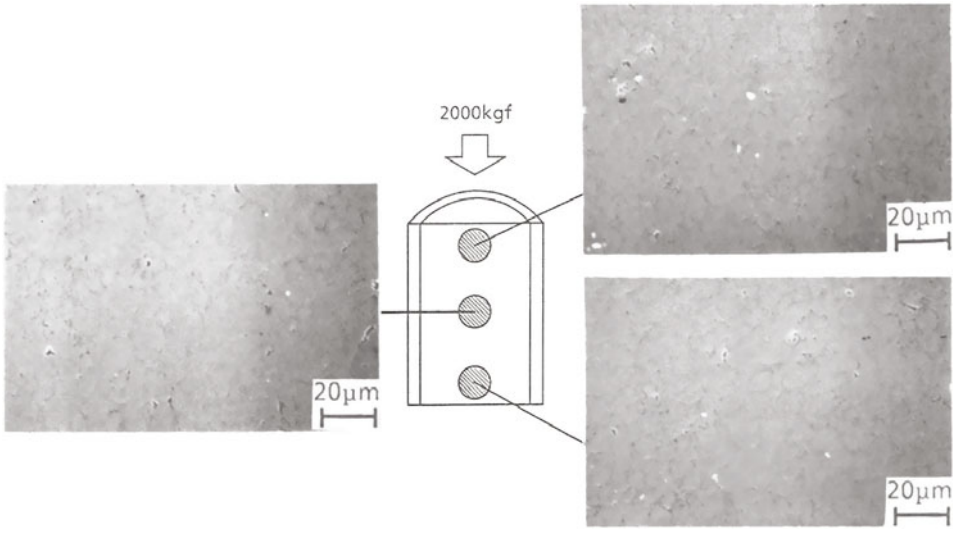

Figure 8. SEM image of a cross-section of metal-sealed HIP amorphous $Co_{79.5}Nb_{15}Zr_{5.5}$ compact, subjected to compressive forming under a load of 2000 kgf.

compact after compressive deformation under the load of 2000 kgf. A distributed pore shows a contradiction by compressive forming, comparing with as HIP'ed sample as shown in Fig.5(a). Furthermore, note that this pore contradiction has the almost same degree everywhere in the cross section of the amorphous HIP compact as shown in Fig.8. An elastic analysis of finite element method for three dimensional solid of copper-sealed amorphous Co-rich CoNbZr do not show any distribution of the axial stress in the direction of compressive axis, while other principle stress present a significant stress distribution. So, the compressive axial stress plays a dominant role in the contradiction of submicron sized pores at the triple points, uniformly distributed throughout the amorphous $Co_{79.5}Nb_{15}Zr_{5.5}$ HIP compact. On the other hand, the compressive axial stress presents a distribution(:i.e. a decrease) in a transverse direction in amorphous $Co_{79.5}Nb_{15}Zr_{5.5}$ HIP powder compact close to sealed copper and the outer copper tube(;a detail result of FEM analysis will be reviewed).

We here deduce an average stress (σ_a) of axial component as the net stress applied to the amorphous HIP compact. Figure 9 shows the density and the relative density, obtained from the porosity as a function of thus-defined axial stress for copper-sealed amorphous $Co_{79.5}Nb_{15}Zr_{5.5}$ after compressive forming under loads of 500, 1000, 1500, 2000 and 2400 kgf. We find that the relative density drastically raises from the level of as HIP'ed compact when compressive axial stress exceeds approximately 200 MPa, which is nearly equal to HIP pressure. Further increase in axial stress leads to an almost fully dense amorphous $Co_{79.5}Nb_{15}Zr_{5.5}$ HIP compact (P = 0.4 %) at 365 MPa. This finding further supports the idea that submicron sized pores can be easily diminished by compressive axial stress, not by shear stress as stated above.

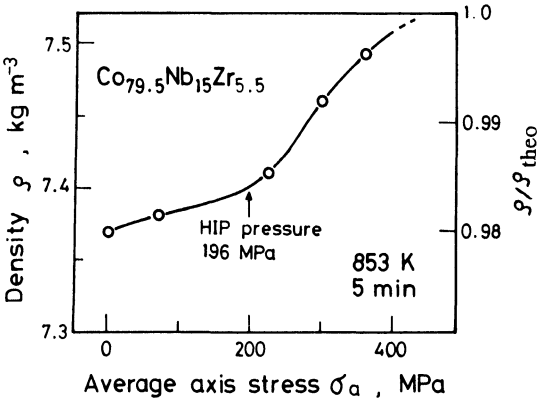

Figure 9. Density and relative density versus average stress of compressive axial component, deduced from FEM analysis for amorphous $Co_{79.5}Nb_{15}Zr_{5.5}$ compact after forming.

Strength of Amorphous HIP Compact

Figure 10 shows the fracture strength in compression for as HIP'ed amorphous $Co_{79.5}Nb_{5.5}Zr_{5.5}$ for 5 min at 853 K, amorphous HIP compact subjected to compressive forming under 2000 kgf, copper-sealed HIP compact under 2400 kgf, and partially crystallized HIP compact(30 min). This figure also describes the compressive fracture strength for amorphous $Co_{79.5}Nb_{15}Zr_{5.5}$ with a different porosity, HIP'ed at various consolidating temperature and time[5]. For short-time consolidated amorphous compact, the compressive strength drastically increases with decreasing porosity. This increase in compressive strength for the amorphous $Co_{79.5}Nb_{15}Zr_{5.5}$ compacts subjected to compressive forming accords to a power law[5] of $\sigma_F = BP^{-0.5}$ where B is constant. Note that the pore contradiction by compressive forming even at ambient temperature leads to a significant improvement of fracture strength for an amorphous HIP compact. Besides, the fracture strength for the almost fully dense, but partially crystallized compact is higher than that of the short-time HIP'ed amorphous compact(P = 2 %). The pore size could be a dominant parameter to discuss a fracture of amorphous HIP compact.

Figure 11 shows the mid-section at fracture for a compressive specimen of the amorphous $Co_{79.5}Nb_{15}Zr_{5.5}$ HIP compact after compressive forming under 2000 kgf and the copper-sealed HIP compact at the compressive load of 2400 kgf. For two almost fully dense amorphous compacts subjected to compressive forming, cracks propagates in axial direction, similar to a fracture path of ductile fracture in compression for crystalline alloys. This fracture occurs in a process of the coalescence of pores with the aid of hydrostatic tension due to local plastic constraint in ductile amorphous alloy.

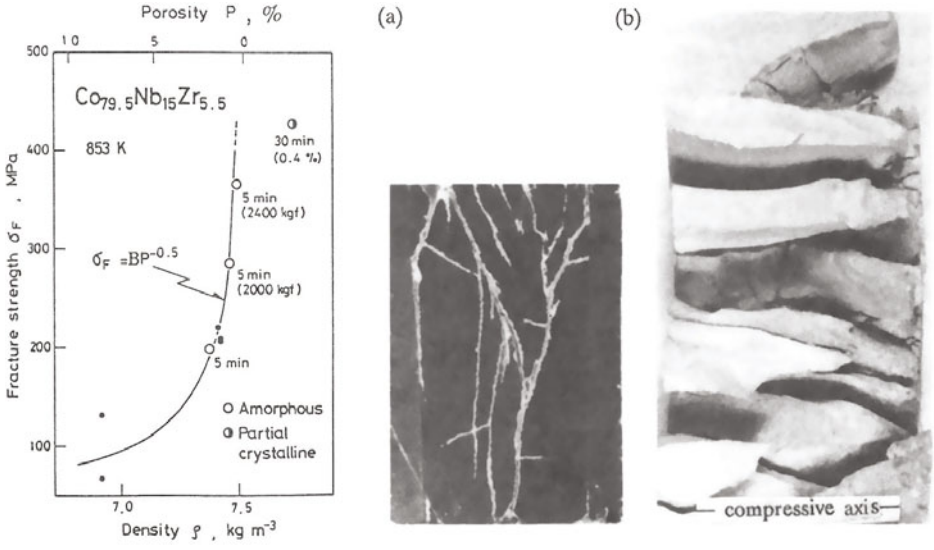

Figure 10. Compressive fracture stress as a function of density and porosity for various HIP compacts of MA amorphous $Co_{79.5}Nb_{15}Zr_{5.5}$.

Figure 11. Mid-section at fracture in compression for amorphous $Co_{79.5}Nb_{15}Zr_{5.5}$ HIP compacts with 8 mmΦ, subjected to compressive forming under applied loads, (a) 2000 kgf, (b) 2400 kgf.

CONCLUSIONS

This article described the novel HIP processing by which it is possible to obtain a full densification of mechanically alloyed amorphous powder having an insufficient time and/or temperature range between glass transition and crystallization. This processing consists of short-time HIP consolidation via viscous flow and successive compressive forming of metal-sealed HIP compact. Even for 5 min at 853 K, HIP compaction makes it possible to consolidate mechanically alloyed amorphous $Co_{79.5}Nb_{15}Zr_{5.5}$ powders to a relatively high density amorphous product with a distribution of submicron sized pores at triple points of particles without a crack. We found that the compressive deformation of short-time HIP'ed amorphous compact shows an increase in density, approaching to theoretical one, when average stress of axial component, deduced from FEM analysis, exceeds the level of HIP pressure(196 MPa). The fracture strength for amorphous $Co_{79.5}Nb_{15}Zr_{5.5}$ HIP compact increases by a decease in porosity by compressive forming, this increase obeys the power law of $\sigma_F = BP^{-0.5}$.

REFERENCES

1. For instance, Solid State Amorphizing Transformations, eds. by R.B.Schwarz and W.L.Johnson (Los Alamos USA, 1987 Aug.), Elsevier Sequoia S.A., J. Less-Common Metals, 140(1988).
2. H. Kimura, Bull. Japan Electronic Materials Society, 22,2(1990).
3. H. Kimura, M. Kimura and F. Takada, J. Less-Common Metals, 140,113(1988).
4. M. Kimura, H. Kimura and T. Ban, Trans. Japan Institute of Metals, 29,65(1988).
5. H. Kimura, W.-N. Myung, M. Kimura, S. Kobayashi and K. Toda, to be published in J. Japan Institute of Metals.
6. H. Kimura and S. Kobayashi, Sixth JIM Int. Sympo. on Intermetallic Compounds,(Sendai Japan, 1991 June), Trans. Japan Inst. Metals in the press.

DESIGN AND MANUFACTURE OF ENGINEERED COMPONENTS CLAD BY HIP

Jean-Pierre AUGER, Gérard RAISSON, Michel PIERRONNET
TECPHY, Powder Metallurgy Division, 58160 IMPHY, FRANCE

INTRODUCTION

The use of coatings is a widely accepted technique for improving the surface properties (as corrosion and wear resistance) of components produced from relatively low-cost materials. Numerous processes can be used, such as plasma or flame spraying, weld overlay coating, etc. Hot isostatic pressing is also used industrially for the production of clad or multi-material components, based on the densification and/or diffusion bonding of powdered or solid materials [1,3]. The advantages of the HIP-cladding technique have already been exploited for the manufacture of components combining nickel, cobalt or titanium alloys with structural or stainless steels, particularly for corrosion or wear resistant applications :

- valve bodies, wellheads and various oil and gas drilling rig components,
- components for marine engineering and transport of corrosive fluids,
- extrusion dies,
- twin-screw extruder bodies and screws, etc.

In order to determine the most suitable process for manufacturing a part, the functions to be performed must first of all be clearly identified, enabling comparison of different materials and property combinations, geometrical requirements, etc. The choice of the HIP-cladding process involves both technical and economic considerations, and must incorporate three indissociable elements :

- a partnership-like dialog with the user at the conception and design stage,
- an economic analysis, compared to alternative techniques,
- overall control of the complete industrial process.

1 - PARTNERSHIP WITH THE USER

Detailed discussions between the designers and technical engineers from both the user and producer companies are essential from the outset, in order to :

- ensure that the application and its associated property requirements are fully understood,
- integrate the HIP-cladding solution at the design stage,
- optimise the metallurgical and mechanical characteristics by overall control of the complete industrial process.

In this way, it is possible to optimise the geometry of the clad components and of the container (in the case of powder coating), together with the nature and form (powder or solid) of the materials to be used.

1.1 Design

The geometrical design of the blank is an extremely important stage in the HIP-cladding process. Certain allowances or simplifications can be made on the pre-machined blank, calculated where necessary by modelling the deformation during the HIP process. Moreover, the geometry of the container, in the case of a powder coating, can also be optimised as a function of the cladding profile and its thickness (uniform or variable), taking into account forming and assembling constraints, and the associated manufacturing costs. At this stage, a powder/solid route can often reveal to be advantageous, on both technical and economic grounds.

Two parameters which it is important to consider in the design of the premachined blank are the post-HIP heat treatment, which is often necessary to restore the mechanical properties of the substrate, and possible deformations during the HIP process. Conditioning operations should also be taken into account (mechanical or chemical elimination of the container, final machining), bearing in mind that the functional dimensions can often be obtained with acceptable tolerances in the as-HIPed component.

1.2 Metallurgical and mechanical aspects

Control over the complete industrial process (powder manufacture, encapsulation, HIP, post-HIP heat treatment) facilitates product design, giving maximum flexibility as regards :

- the choice of cladding material to suit the intended application,
- the compatibility of materials (possibility of an intermediate metallic layer),
- the structure and properties of the cladding,
- the influence of the HIP cycle on the substrate properties,
- residual stresses after heat treatment (due to differences in expansion coefficients and phase transformations),
- the introduction of compressive stresses in the clad surfaces, etc.

2 - ECONOMIC ANALYSIS COMPARED TO ALTERNATIVE PROCESSES

The economic analysis must incorporate two essential aspects :

- the relationship between the coating technology employed and the resulting properties, for a given combination of materials,
- the specific costs for each technique considered.

Some of the functional property criteria for which the HIP-cladding process is particularly advantageous, and which have a first-order influence on the overall component cost (including manufacturing, maintenance and repair costs) are :

- cladding geometry (variable thickness and profile),
- cladding density (100 % density via HIP),
- machinability and grindability improved by the homogeneous microstructure.

In certain cases, and for certain material combinations, the HIP-cladding process is the only technique possible and enables the final dimensions to be obtained without subsequent machining (e.g. coating with a Stellite 1 type alloy) :

- hardness,
- mechanical and tribological properties of the cladding. For example, figure 1 reveals the differences in microstructure and mechanical properties between a cast cobalt base alloy and the same grade obtained by powder metallurgy,
- corrosion behaviour.

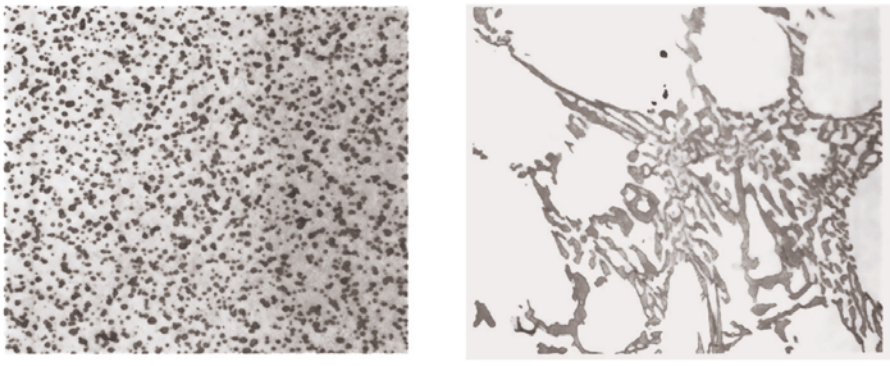

Figure 1. Microstructure and properties of Stellite 6 type alloy.

The specific production costs can vary greatly from one coating process to another, particularly when taking into account :

- the thickness of the coating to be guaranteed (no limit for HIP),
- the accessibility of the component to be coated (fewer constraints for HIP),
- series or batch production.

3 - CONTROL OF THE OVERALL INDUSTRIAL PROCESS

The various stages of the HIP-cladding process, which must be controlled by the producer, can be perfectly integrated in a quality assurance system, which for the customer represents an additional guarantee of product reliability.

3.1 Choice of materials and cladding technique

Two techniques can be used, depending on the nature of the noble material (powder or solid). In the case of a powder cladding, the premachined and cleaned substrate blank constitutes part of the container. A shaped container is then welded to the blank, and after filling with powder is evacuated and sealed, to make it gas-tight, enabling the powder to be fully densified and diffusion bonded to the substrate during the HIP cycle. When the clad layer is produced from solid material, the elements to be joined are previously machined. After appropriate surface preparation and assembly, the elements are welded round the edges of the joints, to ensure that the latter remain perfectly gas-tight during the HIP-bonding operation (figure 2).

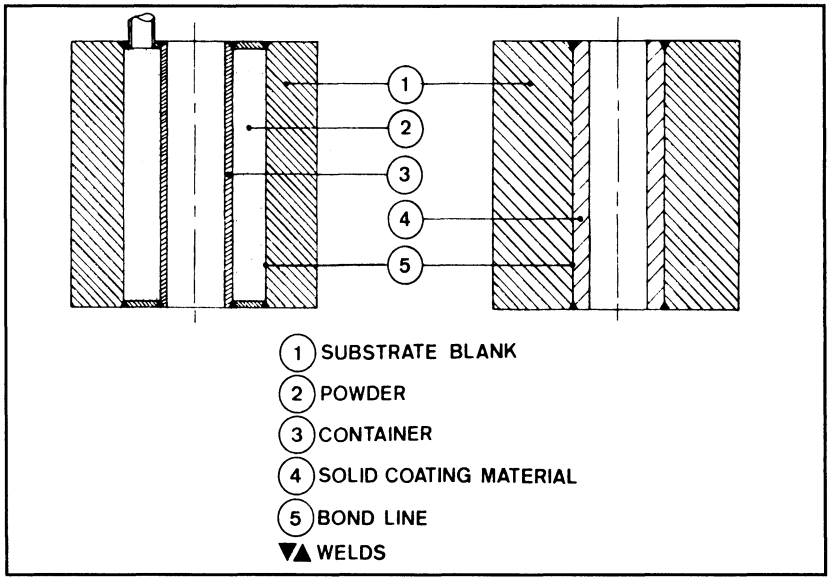

Figure 2. Assembly of sub-components for HIP cladding.

It is important to emphasize that the properties of the coating (corrosion and spalling resistance, mechanical strength) can be significantly affected by the quality of the powder used. Particular care must therefore be taken in the choice of particle size range, in the intrinsic cleanness of the powder, and in the avoidance of cross-pollution by other powder grades, during all handling and de-gassing operations carried out before densification. Figure 3 clearly illustrates the effect which an extraneous particle can have on the corrosion resistance of the nickel base alloy SY 625 in the standard ASTM G28 test, preferential attack having taken place at this point.

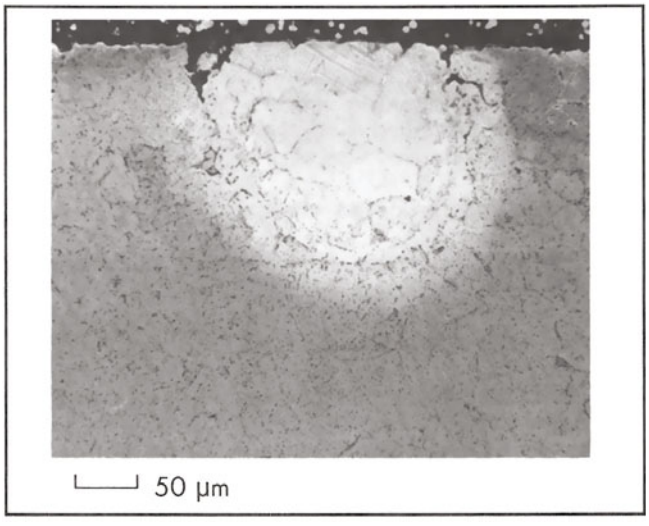

Figure 3. Preferential attack on extraneous particle in SY 625 alloy.

3.2 Physical-chemical preparation of surfaces

This parameter is particularly important in the case of solid/solid cladding configurations [3]. In effect, the mechanical strength of the bond, which can be arbitrarily characterized by the ratio 100.Rb/Rw, where Rb and Rw are respectively the ultimate tensile strengths of the bond zone and the weakest of the two constituent materials, is essentially conditioned by the physical-chemical preparation of the surfaces. Depending on the materials, certain operating parameters must be optimized, such as the roughness and adjustment of the surfaces, special machining of certain surfaces in order to increase the specific bond area, chemical treatments such as pickling.

TABLE 1

Effect of surface preparation on the efficiency of the HIP bond
Alloy 718/316 stainless steel assembly.

Roughness (Ra)	1.6 µm	3.2 µm	1.6 µm
Acid Pickling	YES	YES	NO
Bond Efficiency	88 %	75 %	35 %

In certain difficult cases [4] (e.g. structural or stainless steel/TA6V), it is possible to insert an intermediate metallic layer (foil or electrochemical deposit), to act as a diffusion barrier, in order to prevent the formation of intermetallic phases which could embrittle the bond.

3.3 Encapsulation and HIP cycle

This stage of the process is especially important, since it comprises a series of critical operations which determine the conformity of the product to customer requirements :

- design of the container (for powder coatings), possibly optimised by one or more iterative model-based finite element calculations, in order to predict the deformation during the HIP process [5],
- manufacture of the container with well-defined type and quality materials, together with stringent welding procedures (qualified welders, certified processes),
- verification that the containers are leakproof before filling,
- filling of the containers, bearing in mind that insufficient filling (possible gradients) can have deleterious consequences on the geometry of the cladding,
- optimisation of the HIP cycle parameters depending on the type of materials and the geometry of the component.

3.4 Post-HIP heat treatment

It is recalled that this operation must be integrated in the process from the design stage, in order to ensure the ultimate geometry of the clad component after final machining, and to take into account differences in physical properties (differences in the expansion coefficients between the two constituents, or volume changes associated with phase transformations, can lead to disbonding at the interface). The heat treatment necessary to obtain the required mechanical properties in the substrate must not have a deletereous effect on the characteristics of the cladding, such as its corrosion resistance.

3.5 Non-destructive testing

The HIP-cladding process is perfectly compatible with conventional non-destructive testing techniques. An ultrasonic examination methodology has been developed [3,6] enabling inspection of :

- the density and soundness of the cladding,
- the adherence between the coating and the substrate, and the presence of defects at the interface. The method has been tested with real defects simulated by alumina grains embedded along the interface of an alloy 718/316 stainless steel assembly, as shown in figure 7. The technique enables the detection of bonding defects 400 microns or more in size,
- the coating thickness, with an accuracy of ± 0.4 mm.

The ultrasonic inspection can be supplemented by dye penetrant examination in acoustically dead zones, such as at the ends of a component.

CONCLUSIONS

The design of a given component must be integrated within an overall analysis, based primarily on the functions to be fulfilled. However, the optimisation of the properties and cost of a HIP-clad component requires close collaboration between the user and producer, starting at the design stage. With this essential proviso, it is then the required functional properties which will guide the definition of an optimum manufacturing procedure, integrating both a design compatible with the HIP-cladding technique and metallurgical considerations related to the choice of material combinations and the specific characteristics of the HIP process.

REFERENCES

[1] G.Raisson, L.Buekenhout, "The manufacture of wear-resistant parts by hot isostatic pressing", 28th Special Steel Days, Liège, May 24-25, 1989.

[2] G.Raisson, M.Rouby, L.Buekenhout, "Diffusion bonding of low alloy steel and nickel base superalloy (SY 625) - metallurgical aspects", Proceedings of the International Conference on Hot Isostatic Pressing of Materials - Applications and Developments, Antwerp, April 25-27, 1989.

[3] M.Pierronnet, G.Raisson, "Production of clad and bimetal components by HIP-asisted diffusion bonding of steels and superalloys", Proceedings of the 4th International Conference on Isostatic Pressing, Stratford-upon-Avon, November 5-7, 1990.

[4] Z.Nizenholz, J.Mironi, N.Nir, "Diffusion bonding of 304 L stainless steel to TA6V alloy", Proceedings of the 3rd International Conference on Isostatic Pressing, vol. 1, pp. 33-1 to 33-10.

[5] M.Abouaf, JL.Chenot, P.Bauduin, G.Raisson, Mém. Sci. Rev. Mét., June, 1986 pp. 325-334.

[6] G.Raisson, P.Clément, M. Costedat, M. Meurtin, M. Brun, "Quantitative evaluation of the cleanness of HIP + forge Astroloy disks produced from AA powders of controlled inclusion contents", Metal Powder Report, vol. 43, N° 10, October, 1988.

APPLICATION OF P/M HSS COMPOUND PARTS TO STEELWORKS

Hoshiaki Terao, Teruhisa Ohki*, Jun Oota*,Masato Togawa*and Hideyuki Tokuda*
Niigata Works, Advanced Materials Division, NKK Corporation,
Niigata 950, Japan
*Ceramics Development, Advanced Materials Division, NKK Corporation,
Tokyo 100, Japan

ABSTRACT

The pursuit of high productivity, cost reduction and high-quality products at steel mill works requires high performance materials for wear parts such as rolls and guides. P/M HSS (high speed steel) is one of the promising candidates that surpass the conventional cast, sprayed or welded materials. NKK introduced P/M HSS compounds -compounds with carbon steel- to give a higher ductility to the material. NNS (near net shape) technique was employed to manufacture cost competitive parts. This report describes various examples of applications for the compound wear parts successfully used at NKK steelworks.

INTRODUCTION

Japanese steel makers are struggling to maintain strong competitiveness in the world market, where political and economical circumstances are intensively changing. They are making efforts for rationalization and for the commercialization of high quality products that the Japanese market requires. In order to manufacture products with high productivity and to manufacture high quality products (e.g. high precise shape products, high surface quality strip), rolls and guides are used under severe conditions and higher performance is required.

Conventional rolls [1.2] and guides, such as an Adamite cast iron

roll and a Stellite sprayed guide roller, do not necessarily satisfy the requirement. P/M HSS is one of the promising hard materials. A combination of the P/M HSS as an outer layer and carbon steel as a core should satisfy the requirement.

We have studied the applicability of P/M HSS compound parts through experimental use of various kinds of rolls and guide rollers at the steelworks of NKK and its subsidiary. The compound parts were produced at Niigata Works, where a large HIP unit is installed.[3] This report introduces some successful applications.

FEATURES OF P/M HSS COMPOUND

P/M HSS that is consolidated by HIP from gas atomized powder to full density has fine-grained and no-segregation structure, showing high mechanical properties with a narrow scatter. The P/M-HIP process is the only one that can produce highly alloyed HSS such as ASP60 (4Cr-6W-7Mo-7V-10Co).

Table 1 shows comparison of the mechanical properties of P/M HSS and of the conventional materials for hot-rolling rolls. Two highly alloyed NKK's products, NKP50 and NKP100, were used in this study.

Table 1
Mechanical properties of P/M HSS and the conventional cast materials for hot-rolling rolls

Material	Hardness (H_{RC})	Tensile strength (MPa)	Charpy impact value (J/mm²)
NKP50(Modified AISI M3/2)	64-68	1600-1800	880-1180
NKP100(Modified AISI T15)	67-70	1100-1400	590- 880
Adamite cast iron(Ni-Cr-Mo)	37-41	390- 690	150- 200
Indefinite chilled(Ni-Cr-Mo)	55-60	340- 490	245- 295
Hi-Chromium cast iron(14-18Cr)	50-60	640- 840	120- 150

Temperature dependence of the hardness of P/M HSS and conventional materials is given in Figure 1. These data show the excellence of P/M HSS, which have high strength with high toughness and high hardness up to elevated temperatures.

P/M HSS compounds that should demonstrate higher ductility lead to

cost reduction. Further reduction can be expected, if produced through the following NNS process: the highly alloyed HSS powder is first packed around a carbon steel core with minimized thickness and then is consolidated and diffusion bonded by HIP. The HIP conditions are determined by the perfect bonding between HSS powder and carbon steel core. The perfect bonding can be easily checked by a tensile test. The specimen has a diffusion-bonded interface in the middle. The tensile strength of the perfect bonding should be equal to that of the carbon steel, since the fracture occurs in the carbon steel. An example of tensile strength is 1070 MPa for perfect bonding of the NKP50/0.5% carbon steel compound.

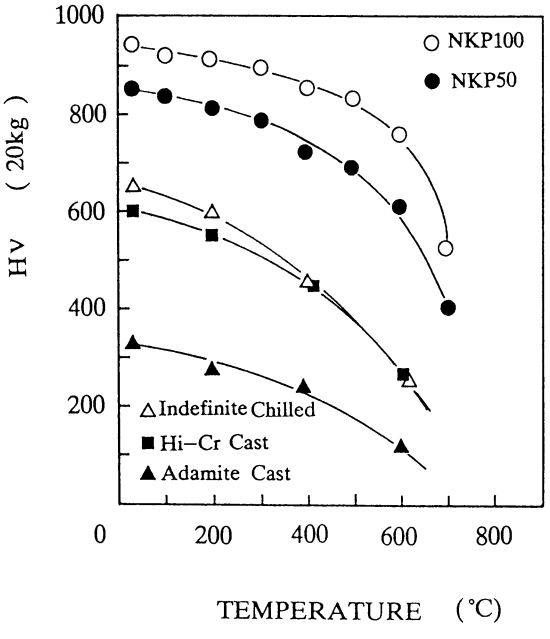

Figure 1. Temperature dependence of Vickers microhardness.

APPLICATION [1]: ROLLS FOR HOT ROLLING

Wear resistance of rolls for hot rolling is largely dependent on rolling conditions such as applied load, rolling temperature, rolled material and a roll cooling system.[4] In some cases the wear rate is attributed to thermal fatigue cracking and is not correlated with the hardness of the roll. In others the roll life depends on the resistance of adhesion to the rolled material.

For the evaluation of the wear resistance of the rolls, NKK uses the following roll-wear simulator. The tested rolls of 72 mm in diameter and 40 mm in length are placed as working rolls in a four-high and one-stand rolling mill. The rolls were passed through by a 20 mm wide hoop heated

about 1000℃ with a 2-tons load and water cooling. Figures 2 and 3 show the test results of P/M HSS and Adamite cast iron. The P/M HSS rolls proved to be superior to the Adamite ones, especially in rutting wear resistance.

Figure 4, an example of actual test results, shows the comparison of the wear rate of the P/M HSS compounds and chilled cast iron on the hot forming-mill rolls of the small-seamless pipe-mill works. The wear rate of the P/M HSS was 1/9 that of the chilled cast iron. The application of NKP50 compound rolls, shown in Figure 5, to the hot forming-mill led to much higher productivity of pipes due to the decrease of the roll changing frequency and to cost reduction.

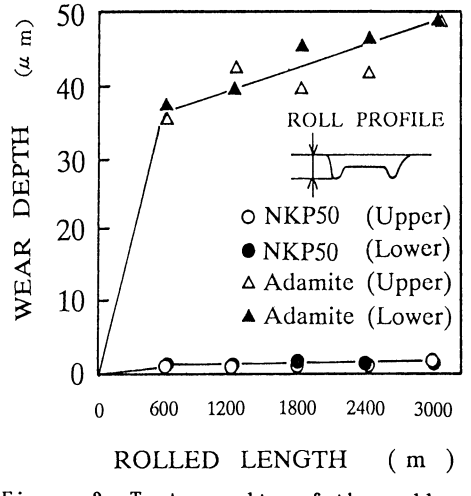

Figure 2. Test results of the roll-wear simulator.
(Rutting wear)

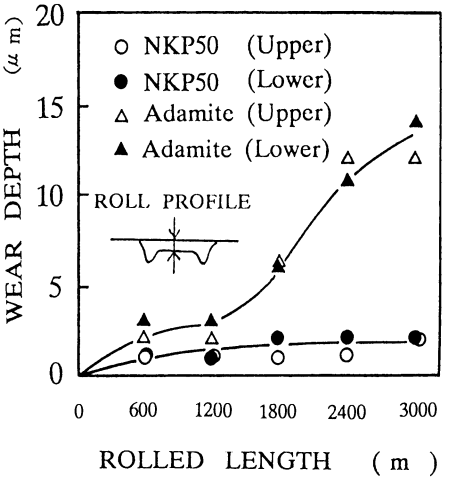

Figure 3. Test results of the roll-wear simulator.
(Wear in the middle of roll)

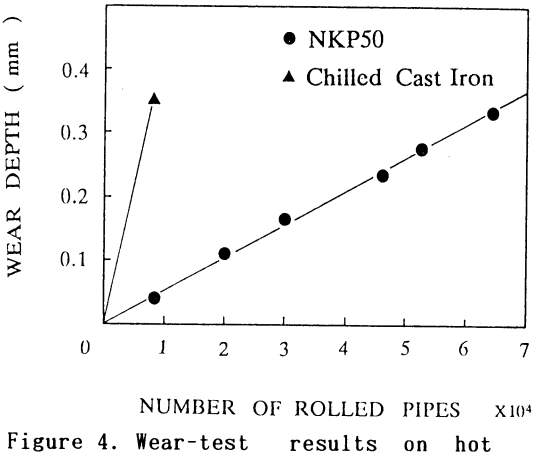

Figure 4. Wear-test results on hot forming-mill rolls

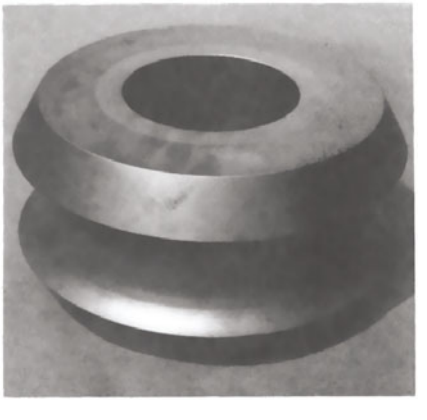

Figure 5. Appearance of hot forming-mill roll

APLLICATION [2]: GUIDE ROLLERS

Wear resistance of guide rollers has become decisive problems in steel works. For example, a worn-out guide roller causes run-down of the production line. In order to prolong the life of rollers, the following three properties are required:

1. High hardness up to high temperature
2. High resistance to wear and adhesion under high applied-load
3. Resistance to collision with the tips of the rolled steel

Figure 6 shows the results of the Amsler wear test for evaluation of guide rollers. The P/M HSS proved to be highly resistant to wear under high applied-load. A good example to figure out how the P/M HSS compounds meet the requirement is the support roller of the finishing mill for high-precise shape steel in the shape-mill works. The conventional Hi-Chromium welded roller was worn 1.5 mm in depth and had to be replaced when 500tons of the rolled steel had been passed. In the case of the Hi-Chromium cast roller, breakage of the rollers often occured due to the collisions with the rolled steel. The NKP100 compound roller was worn only 0.03 mm in depth after 5500 tons of steel had been rolled. The application of the NKP100 compound roller benefited the roller cost, the productivity and the surface quality of the products.

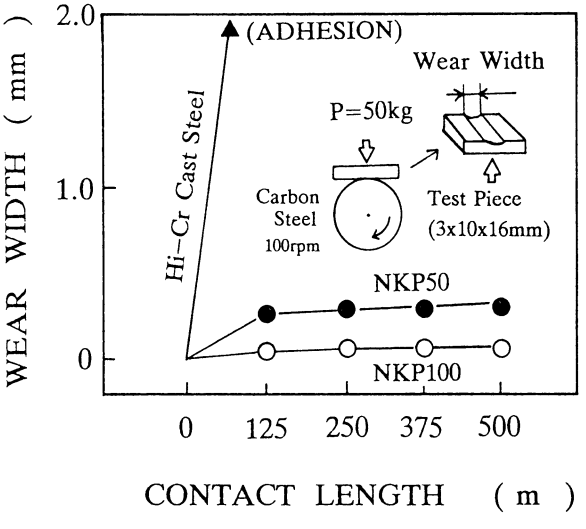

Figure 6. Test results of the Amsler wear test

LIST OF THE APPLICATION OF THE COMPOUND PARTS AT NKK

The list of the P/M HSS compound parts successfully applied at NKK steelworks is given in table 2.

Table 2
List of the application of P/M HSS compound parts at NKK steelworks

Works	Parts
Hot strip mill works	Side guide roller
Cold strip mill works	Side guide roller
Shape mill works	Roll of finishing mill
	Support roller
	Side guide roller
Pipe mill works	Roll of hot forming mill
	Pinch roll
	Support roller
Bar mill works	Pinch roll
	Support roller
	Guide roller

CONCLUSIONS

Various kinds of P/M HSS compound parts were applied successfully at NKK steelworks. The excellence of the P/M HSS compound parts in wear resistance has led not only to cost reduction of the parts but also to improvements of the productivity and the quality of the products.

REFERENCES

1. Muller, H.E., High-Chrome work rolls in a modern hot strip mill, Iron and Steel Engineer, October 1975, pp. 63-70.
2. McManus, G.J., Iron Age, October 6, 1980, pp.7-13.
3. Terao, H, HIP operation techniques in NKK, Proceedings of the 23rd meeting of Japan Research Association of Isostatic Pressing and Processing, 1990.
4. Sekimoto,Y, Wear mechanism of rolls, The 67-68th Nishiyama memorial seminar, ISIJ, Tokyo, 1980, pp.137-165.

EXPERIMENTAL STUDIES OF THE EQUILIBRIUM BETWEEN ZIRCALOY AND TRITIUM DURING HOT ISOSTSATIC PRESSING OF SPENT FUEL HULLS

Y,FUKUZAWA* , R.TEGMAN** AND T.WALTERSTEN***
* Taisei Corporation, Energy Engineering Dept., Shinjuku Center Building, 1-25-1, Nishi-Shinjuku, Shinjuku-ku, Tokyo, 163 Japan
** The Swedish Institute of Production Engineering Research, Laboratoriegränd 8, S-951 87 Luleå, Sweden
*** ABB Atom AB, Dept. SF, S-721 63 Västerås, Sweden

ABSTRACT

The purpose of the study is to establish the HIP conditions, that results in a complete densification of Zircaloy-2 hulls and also gives a minimum of tritium (T) contamination of the HIP gas.

At HIPing only 20-40 ppm of the added T was released to the HIP gas, which corresponds to specific tritium activity of 5-10Bq/L gas at 20℃, 1 atm. To gain a better understanding of the system Zr-H-T-experimental result have been compared with equilibrium calculations. Tritium containing Zircaloy hull and probably also reactor hulls can be HIP-ed at a temperature of 1000-1050 ℃ for a time of 2 hours at a pressure of 100 MPa without much tritium contamination of the HIP gas and result in a fully dense Zircaloy block suitable for an efficient self containment of rad waste.

INTRODUCTION

All the activity in zircaloy hulls can quantitatively be confined in a HIPed capsule with one exception, tritium, which can diffuse from the hulls through the HIP capsule wall and contaminate the HIP gas to some small extent.

The release of tritium from hulls to the HIP gas is very complex process and is determined by both equilibrium and kinetic factors in the system consisting of HIP furnace with argon gas, HIP capsule of steel and zircaloy waste.

By assuming that the equilibrium conditions prevail at HIP, the amount of tritium in the HIP gas can be calculated at all given conditions. An equilibrium calculation at a temperature of 700℃ gives that only about 20×10^{-6} parts of all the tritium in the system is present in the HIP gas, and the rest of the tritium is present as a solid solution of tritium in solid zirconium.

EXPERIMENT

HIP-Equipment
The test has been accomplished in a HIP-unit of ASEA-Quintus design with the designation QIH9. The hot zone for this unit; diam 150 mm, height 310 mm. The total volume of cold and hot zone in the pressure vessel is 20.7 dm^3.

The standard gas system of the HIP equipment was modified for HIP of tritium doped zircaloy and collection and dumping of tritium containing gases. A special gas sampling and purging device was made.

HIP capsules and HIP samples
The HIP capsules were all made of stainless steel tubes with a wall thickness of 2 mm. The shape of the capsules were cylindrical with an outer diameter of 60 mm, a length of 100 mm and with a lid TIG-welded gastight to the cylinder. For closing and evacuation of the HIP capsule after filling with hulls a top lid with evacuation pipe was used.

Each HIP capsule was filled with the chopped in 25 mm long and flattened Zircaloy-2 hulls and was added with about 170 mg $TiT_{0.5}$ foil with about 0.8 GBq tritium for tritium source. And then they were doped with hydrogen at a temperature of 750 ℃ in about 24 hours.

HIP and Gas Sampling
Preliminary HIP experiments were performed using tritium free Zircaloy-2 hulls as case Ⅰ, Ⅱ and Ⅵ and HIP using tritium doped hulls were performed as case Ⅲ, Ⅳ and Ⅴ.

The summary of performed HIP-experiments (caseⅢ, Ⅳ and Ⅴ), heating and cooling rates as well as HIP-parameters and gas sampling points are given in Fig. 1. The capsules prepared for HIP are given in Table 1.

The Results of Gas Sampling (caseⅢ, Ⅳ and Ⅴ)
The results of gas sampling analysis are summarized in Table 2. In Table 3 an evaluation of tritium release from the Zircaloy-2 hulls are made and compared with the calculated values assuming equilibrium.

DISCUSSIONS

Evaluation of the Tritium and Hydrogen Doping of Zircaloy-2
Three HIPed samples have been analysed for the tritium content. There was a considerable difference between the weighted values in tritium amount, which was considered to give the most reliable values and the analysed values. The doping level was between 1.5-4.7 times lower than expected. There is no straight forward explanation to the differences but the result could be explained by an unproper analysis of the tritium content, an extremely sluggish movement of tritium in the hulls, a nonuniform tritium content of the used titanium foil or a nonuniform tritium content in small $< 1g$ sized zircaloy samples used for analysis.

Behaviour of Hydrogen and Tritium During HIP of Zircaloy-2
The movement of tritium and hydrogen from the hulls to the HIP gas

is impaired by thin oxide layers on the hulls and on the capsule walls. During the beginning of the sustain time at full HIP parameters, the hull will densify fast and completely, and the oxide layer on the hulls starts to dissolve in the hull but that will take some time. Some oxidation of the stainless steel capsule will take place by reaction with $H_2O(g)$,CO and CO_2 in the gas forming $Cr_2O_3(s)$ but no FeO(s) due to the reducing condition in the system.

The increase of tritium in the HIP gas at cooling down, see Table 2 and 3, can be explained by the shift in HT/HTO ratio at lower temperature. This tendency can be even more strengthened by adsorption of H_2O and HTO at the cool bottom of the HIP. At the gas sampling to the gas bottles some of the adsorbed HTO at the bottom of the HIP will be washed away by the hot argon gas and give a higher tritium content of the gas samples than in the HIP gas in general.

CONCLUSION

It was found that HIP of Zircaloy-2 hulls can be performed at a temperature of 1000-1050°C, a pressure of 100 MPa for a time of 2 hours and result in fully dense block of zircaloy. The HIP process gives a volume reduction factor of 7. The reaction between the capsule and the hulls is very limited at temperatures below 1050°C.

Equilibrium calculations as well as experimental studies have shown that the tritium present in zircaloy hull can quantitatively be confined in the zircaloy phase at HIPing.

Very small amount of the tritium in the hulls diffuse through the HIP capsule at heating and contaminate the HIP gas. Typically 20-40 ppm of the added tritium was lost to the HIP gas at HIP.

At HIP of tritium doped Zircaloy-2 hulls a latent time of about 4 hours was observed before the tritium concentration of the HIP gas reached the expected calculated level.

At cooling down from the HIP temperature there was no decrease of the tritium content of the HIP gas which indicates that the back diffusion of tritium to the zircaloy is very limited after the densification of the hulls have been completed.

The behaviour of tritium in the Zircaloy-2 hulls at HIP seems to be very much dependent on kinetic factors. Further experiments will be necessary to investigate the characteristics of kinetic factors.

ACKNOWLEDGEMNETS

This project has been financed by TAISEI CORPORATION. The work has been performed under a contract between TAISEI CORPORATION and ABB-Atom and with IVF as a subsupplier to ABB-Atom.

REFERENCES

1. Ausing, J. H., Elleman, T. S. and Verghese, K. "Tritium Diffusion

in Zircaloy-2 in the Temperature Range -78 to 204℃". J. Nucl. Master. 51, (1974), 321-329

2. Smith, T. "Kinetics and Mechanisum of Hydrogen Permeation of Oxide Film on Zirconium". J. Nucl. Master. 18, (1966), 323-336

3. Gulbransen, E. A. and Andrew, K. F. "Mechanism of the Reaction of Hydrogen with Zirconium. I. Role of Oxide Films, Pretreatments, and Occluded Gases. J. Elecrochem Soc. 101, 7, (1954), 348-353.

4. Mallett, M.W. and Albrecht, W. M. "Low-Pressure Solubility and Diffusion of Hydrogen in Zirconium". J. Electrochem. Soc. 104, 3 (1957), 142-146

5. Tegman, R. "Evaluation of Confinement of Tritium in Zircaloy Fuel Hulls at Hot Isostatic Pressing". Technical report: ABB Atom AB and Swedish Institute of Production Engineering Research, Dec. 1988. IVF, Laboratoriegränd 8, S-951 87 Luleå, Sweden.

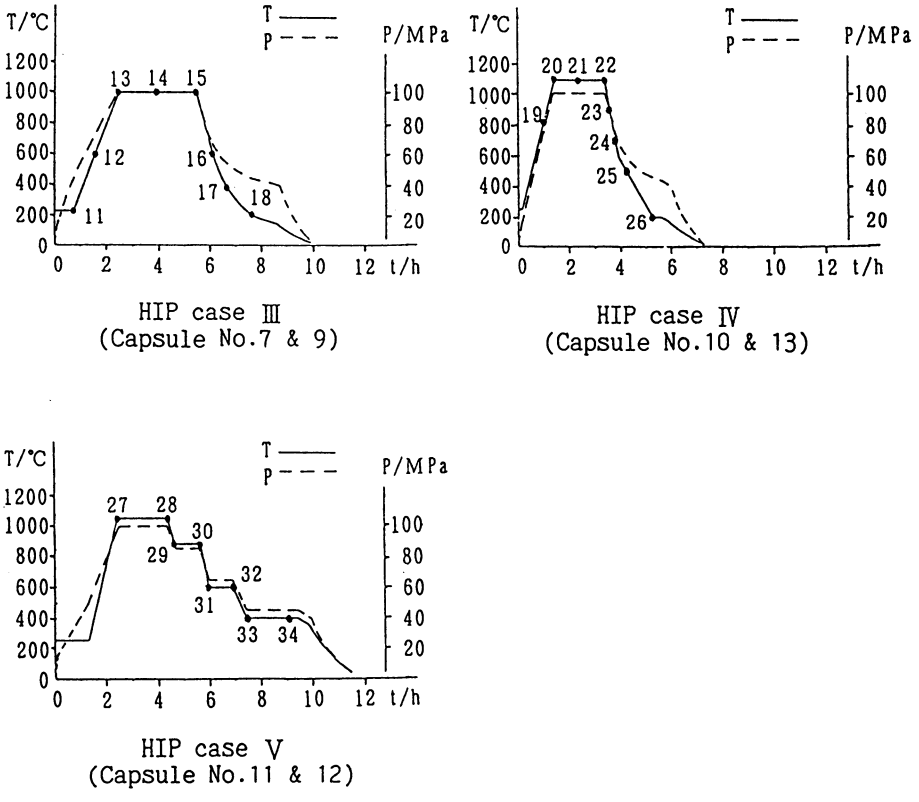

HIP case Ⅲ
(Capsule No.7 & 9)

HIP case Ⅳ
(Capsule No.10 & 13)

HIP case Ⅴ
(Capsule No.11 & 12)

Fig.1 The summary of performed HIP-experiments
The signs [· and No] indicate gas-sampling point and gas analysis number.

Table 1. Capsule sample number, total weight of sample, weight of stailess steel capsule and Zircaloy-2, weight of zirconium, hydrogen and added tritium and tritium activity of hulls prepared for HIP.

Capsule No	Total [g]	Steel Capsule [g]	Zircaloy 2 [g]	Zirconium [g]	Hydrogen [mg]	Tritium [μg]	Tritium activity [MBq]
7	1313.52	459.23	854.16	837	122	1.98	707
8	1354.42	466.68	887.62	870	120	2.64	943
9	1377.64	472.94	904.58	886	118	1.96	699
10	1390.47	468.43	921.92	903	118	2.19	780
11	1379.86	472.66	907.07	889	128	1.97	703
12	1361.78	465.92	895.76	878	103	1.71	609
13	1400.47	473.86	926.50	908	112	2.26	806
14	1379.21	465.90	913.18	895	131	1.89	673

Table 2. Tritium analysis data with gas sampling number, HIP parameters, amount and volume of argon gas in HIP vessel given at 1 bar pressure and 23 ℃ temperature, tritium amount, measured tritium activity per liter of HIP gas at normal temperature and pressure and total tritium gas activity in the HIP vessel

Gas samples No	HIP Temp [℃]	Argon gas pressure [MPa]	Argon amount [mole]	Tritium amount [p mole]	Argon gas vol [m^3]	Specific activity [Bq/l(NTP)]	Tritium activity [kBq]
11	255	46	260	< 0.6	6.38	< 0.1	< 1
12	600	73	280	3	6.87	0.4	3
13	1000	99	281	7	6.89	1.1	8
14	1000	100	280	24	6.87	3.7	26
15	1000	100	280	21	6.87	3.2	22
16	600	70	275	82	6.74	13.0	88
17	400	58	270	209	6.62	34.0	225
18	205	44	263	61	6.50	10.0	66
19	810	80	274	3	6.72	0.4	3
20	1100	100	268	2	6.57	0.3	2
21	1100	100	268	6	6.57	0.9	6
22	1100	100	268	12	6.57	2.0	13
23	900	89	266	17	6.52	2.7	18
24	700	70	262	31	6.42	5.2	33
25	500	57	254	41	6.23	7.1	44
26	200	40	246	61	6.01	11.0	66
27	1050	101	280	1	6.87	0.9	1
28	1050	100	277	6	6.79	0.9	6
29	880	86	277	5	6.79	0.7	5
30	880	82	269	2	6.60	0.4	2
31	600	65	264	3	6.48	0.4	3
32	600	61	250	32	6.13	5.5	34
33	400	49	242	25	5.93	4.5	27
34	400	46	230	30	5.64	5.7	32

Table 3. Evaluation of the tritium release from Zircaloy-2 hulls at HIP with gas sample number, HIP temperature, zirconium and hydrogen content and tritium activity in solid Zircaloy-2, total tritium activity in HIP-gas, ideal system vol., experimental and calculated ratio of tritium in the HIP-gas/total tritium content

Gas samples No	HIP Temp [°K]	Zr(s) [mole]	H(ss) in Zr [m mole]	T(ss) in Zr [GBq]	T-tot (g) [kBq]	system vol [dm³]	$\frac{n(T(g))}{n(T(ss))}$ [$\times 10^{-6}$]	$\frac{n(TH(g))}{n(T(ss))}$* [$\times 10^{-6}$]
11	528	18.89	237	1.41	< 1	24.8	< 0.5	— **
12	873	18.89	237	1.41	3	27.8	2.1	17.6
13	1273	18.89	237	1.41	8	30.0	7.1	432
14	1273	18.89	237	1.41	26	29.6	18	426
15	1273	18.89	237	1.41	22	29.6	16	426
16	873	18.89	237	1.41	88	28.5	62	17.6
17	673	18.89	237	1.41	225	26.8	160	0.167
18	478	18.89	237	1.41	66	23.9	47	—
19	1083	19.85	228	1.59	3	24.4	2	257
20	1373	19.85	228	1.59	2	30.6	1	861
21	1373	19.85	228	1.59	6	30.6	4	861
22	1373	19.85	228	1.59	13	30.6	8	861
23	1173	19.85	228	1.59	18	31.6	11	153
24	973	19.85	228	1.59	33	30.3	21	81.0
25	773	19.85	228	1.59	44	28.6	28	2.13
26	473	19.85	228	1.59	66	24.2	42	—
27	1323	19.37	229	1.31	1	24.2	1	614
28	1323	19.37	229	1.31	6	30.5	5	614
29	1153	19.37	229	1.31	5	30.9	4	128
30	1153	19.37	229	1.31	2	31.4	2	131
31	873	19.37	229	1.31	3	29.5	2	17.2
32	873	19.37	229	1.31	34	29.7	26	17.3
33	673	19.37	229	1.31	27	—	21	0.159
34	673	19.37	229	1.31	32	—	24	0.169

* Calculated values.

** The sign - indicates that equilibrium calculations have no significance due to the low temperature and lack of relevant thermodynamic data.

PROPERTIES OF HOT ISOSTATICALLY PRESSED TANTALUM

MARCEL BONCOEUR, FREDERIC VALIN, GERARD RAISSON *, HERVE MICHAUD *
Commissariat à l'Energie Atomique, Centre de Saclay
DTA/CEREM/DTM/SERC
91191, Gif/sur/Yvette Cedex, France
* Tecphy, Powder Metallurgy Division
58160, Imphy, France

ABSTRACT

Rough parts and near net shape pieces were prepared by hipping a tantalum powder. The products were characterized : density, microstructure, chemical analysis, mechanical properties. The characteristics of hipped tantalum compared with those of electron-beam melted tantalum can be very attractive for certain applications.

INTRODUCTION

Owing to its properties, tantalum is a very attractive candidate for high temperature systems. In addition, chemical inertness towards various compounds allows its use in a wide range of applications. A drawback of this metal is its relatively high cost. HIP proves to be a very competitive shaping technique for this material, allowing direct production by powder technology of near net shape parts, thereby reducing the amount of raw materials and the machining costs.

We have studied a commercial powder densification and characterized the densified material : density, microstructure and mechanical properties. The HIP tantalum characteristics are compared to those of the electron beam melted tantalum (EBM-Ta).

EXPERIMENTAL PROCEDURE

Powder characteristics

Its main characteristics are as follows :

Chemical analysis (provided by manufacturer see Table 1).

The main impurities are the following interstitial elements : oxygen, carbon, nitrogen, hydrogen. Except for iron which is present at 10 ppm, other elements are present at less than 3 ppm. Tungsten at 250 ppm is not an impurity, since it is added on purpose to limit grain growth at high temperature.

TABLE 1
Elements (ppm)

H	N	O	C	Fe	Ni	Cr	Na	K	Ca	Mg	Si	W
< 10	< 20	500	15	10	< 3	< 3	< 3	< 3	< 3	< 3	< 3	250

Particle size analysis
The Fisher diameter (FSSS) is larger than 25 µm. The particle size analysis obtained by sieving is given in Table 2.

TABLE 2
Powder screen analysis

Size (microns)	< 25	25-32	32-40	40-50	50-63	63-80	80-100	100-125
Weight %	9.8	7.7	10.7	10.3	5.9	12.6	18.7	24.3

The grains have an angular shape. It is supposed that they are made up of several crystal pieces from the original rod.

Density
Bulk density (Scott density)is 6.40 g/cm^3; tap density is 8.52 g/cm^3.

HIP densification
Tantalum powder is first dry-heated at 100°C, then introduced in a container made of titanium or steel. The powder is introduced in the container equipped with a tube allowing the degassing at 300°C for 12 hours under a vacuum of approximately 10^{-2} Torr. The tube is then pinched and welding performed to ensure leaktightness. The container thus prepared is introduced in the press where it is treated four hours under an argon atmosphere at 150 MPa. The temperature increase and decrease rate is 300°C/hour.

RESULTS

Manufactured parts
Figures 1 and 2 show different parts fabricated by the HIP method. They are rough or near net shape parts for final machining. It is noted in particular that it is possible to make parts including cylindrical or parallelepipedic cavities, and complex and accurate shape pieces. Visual examinations does not reveal macroscopic defects; no cracks are found, the material seems to be homogeneous.

All the following characteristics of HIP Ta concern the as fabricated product without any thermal treatment.

Density and Microstructure
The products density determined by water displacement is equal to 99.5% of theoretical density (d_{th} = 16.65 g/cm^3). The 0.5% difference is partially explained by the presence of a few isolated pores, and probably also by an increase of the lattice parameter due to the presence of oxygen.

Figure 1. Rough parts

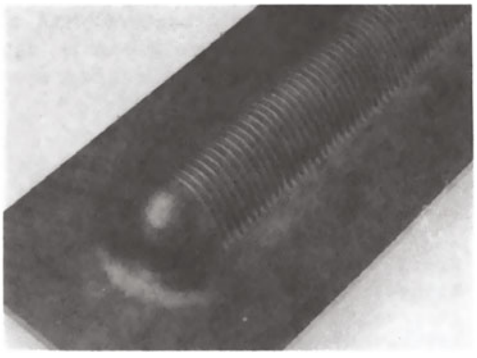

Figure 2. Near net shape parts

The product microstructure is shown in Figure 3. A good material homogeneity is noted and the grain size, which is regular, can be estimated to be 60 µm (interception method). Let us also report that this microstructure is very stable; indeed, a 300 hours thermal treatment at 900°C under 10^{-5} Torr vacuum does almost not affect the grain size which is then determined to be 65 µm. This thermal treatment causes an important grain growth namely 22 - 45 µm to 65 - 130 µm on an EBM Ta partially recrystallized. One can already note that the 250 ppm of tungsten added to slow down grain growth explains at least in part the above observation.

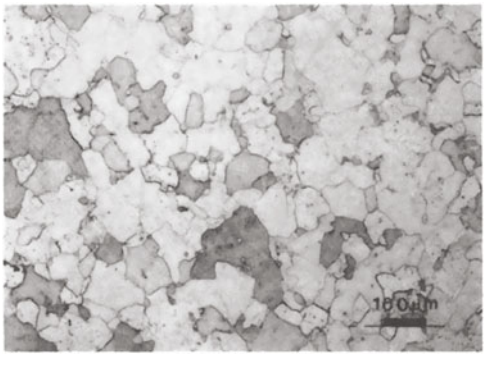

Figure 3. HIP Ta microstructure

Analysis

The average interstitial and tungsten amounts obtained by mass spectrometry are reported in Table 3.

TABLE 3
Chemical analysis

Element	O	N	H	C	W
ppm	230-370	40	# 5	10-50	250

The SIMS analysis shows the simultaneous presence of O, C, N in areas of a few square micrometers with a random distribution in the grains. No trace of these elements can be detected at grain boundaries even with a high resolution analysis. Hydrogen is homogeneously distributed in the sample.

Mechanical properties

The microhardness of this product, measured at room temperature under 1 N is comprised between 160 and 185 HV.

In Figure 4, we show as a function of temperature the variations of yield stress at 0.2% (YS), of ultimate tensile strength (UTS), and of elongation. It can be noted that the ultimate tensile strength starts to increase, reaches its maximum around 300°C (which cannot be accurately determined due to lack of measurements), then decreases in a very classical manner as the temperature increases further. Yield strengths decrease very slightly in the 20 - 300°C range, then more quickly above the latter temperature. As for elongations, one can note a continuous decrease in the 200 - 600°C range, then a strong increase beyond 600°C.

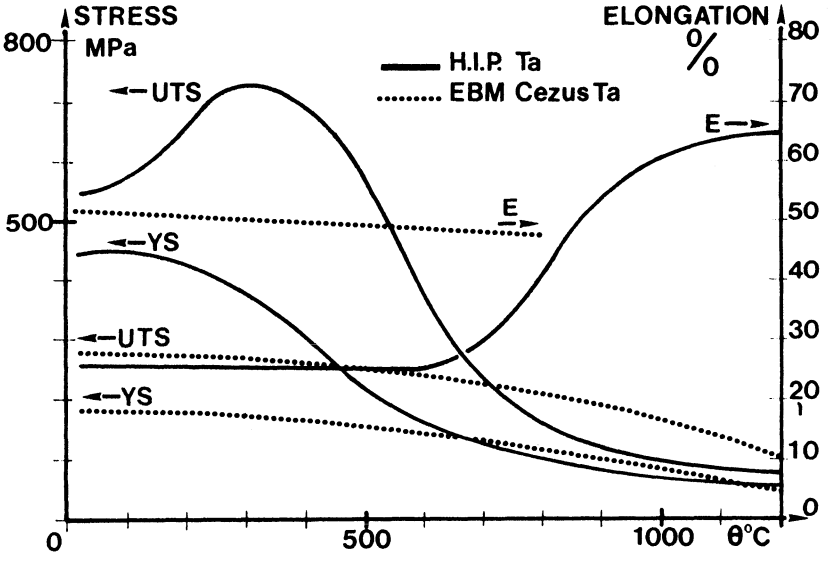

Figure 4. Comparison of UTS, YS, E% versus temperature for HIP Ta and EBM CEZUS Ta.

DISCUSSION

Comparison of EBM Ta and HIP Ta characteristics

In Table 4, are listed the main characteristics at room temperature of these two tantalum types. The EBM CEZUS tantalum is a laminated and annealed sheet of 3 mm thickness with partially recrystallized structure.

TABLE 4
Characteristics of HIP and EBM Ta

		HIP Ta	EBM Ta (CEZUS)
Microstructure		Homogeneous	Rolling texture
Grain size µm		60	22 - 40
Analysis of inter-stitials im ppm	O	232 - 370	50
	N	40	20
	H	# 5	5
	C	10 - 50	20
Microhardness HV 1N		165 - 185	110
Mechanical properties RT			
0,2% YS (MPa)		438	262
UTS (MPa)		552	334
Elongation %		27	52

Compared to the EBM Ta, the HIP tantalum is featured by its high oxygen content. Oxygen together with nitrogen and carbon is concentrated in precipitates homogeneously distributed in the grains. However it is clear that part of these elements is in solid solution form in HIP tantalum. At room temperature, its hardness, yield strength and ultimate tensile strength are larger whereas its elongation is smaller by about 50%. It exhibits a more homogeneous microstructure with a grain size around 60 µm; under the effect of a thermal treatment grain growth is smaller for the hipped tantalum.

In Figure 4 the dotted curve shows the average variations for UTS and 0.2% YS for the CEZUS EBM Ta. Regarding total elongation only a trend can be estimated because of the scarceness of experimental data and of the scattering of the results. One can note that these curves are significantly different from those of HIP Ta. The presence of oxygen can explain the difference in behaviour.

Oxygen effect on the characteristics of tantalum

F.F. SCHMIDT [1] has studied the variation of the mechanical characteristics of very pure EBM Ta, without and with 560 ppm oxygen, between 20°C and 500°C. Results obtained for yield strength, ultimate tensile strength are plotted in Figure 5. HIP tantalum results are also displayed in this figure. One can note that our results and SCHMIDT'S ones are very similar. It can be thought that the presence of 232 to 370 ppm of oxygen in HIP tantalum explains the difference in mechanical characteristics with those of the CEZUS EBM Ta with low O, N content. HIP tantalum is harder though its oxygen content is less than 560 ppm. This can be explained either by the presence of nitrogen and carbon (hardening elements though to a minor extent than (oxygen) or by the uncertainty

on the chemical analysis of the interstitials elements in Ta.

DRENNEN [2] showed that less than 0.1% tungsten in tantalum does not significantly affect mechanical characteristics.

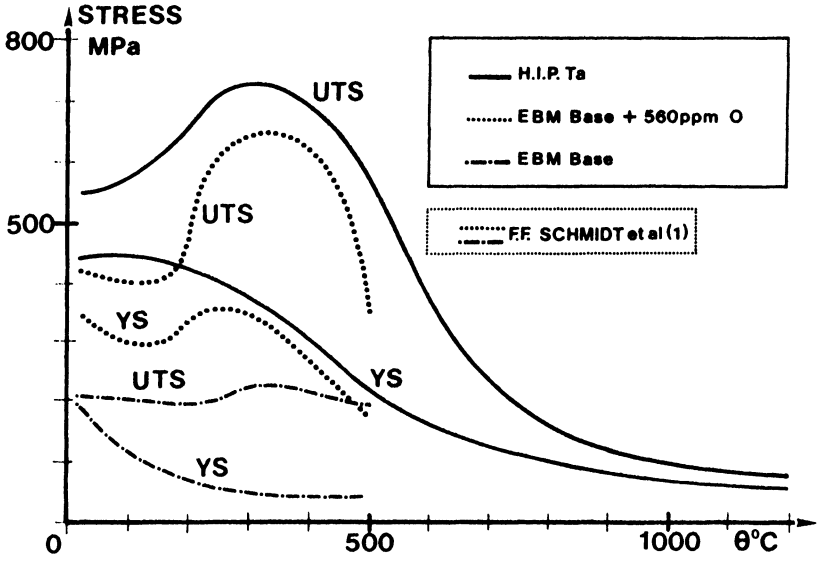

Figure 5. Comparison of UTS and YS versus temperature for HIP Ta, EBM base Ta and EBM base Ta + 560 ppm O [1].

Advantages of HIP for fabrication of large tantalum

The advantages of the HIP technique for the manufacture of tantalum parts are, in uses where the mechanical strength requirements are high, the superior mechanical strength of this materials which still provides fully acceptable elongation. Two other advantages of this method are the saving in raw materials and the reduction in manufacturing costs. On the near net shape part shown in Figure 2, the material saving is superior to 80%.

CONCLUSION

This study has shown that tantalum powder can very well be densified by HIP, and that the densification obtained is entirely adequate.

The saving in raw materials and machining costs can be quite high in the manufacture of certain parts.

The obtained products offer microstructural characteristics and mechanical properties which can be attractive in certain uses since they are superior to those of the rolled EBM tantalum. These advantages are mainly attributed to the effect of oxygen.

REFERENCES

1. F.F. Schmidt, W.D. Klopp et al., Investigation of the properties of Tantalum and its Alloys. Battelle Mem.Inst.Summary Rept WADD TR-59-13, AD236957, AF 33 (616) 5688, May 1958 - Dec 1959 (March 1960)

2. D.C Drennen et al. Development of Container Materials for LAMPRE Applications, BMI 1500, Feb 15, 1961.

THE DEVELOPMENT OF THE COMPOSITE ROLLS FOR HOT ROLLING MILLS BY HIPING

Hideo FUJITA, Jun FUNAKOSHI, Suejiro YOSINO, Yutaka NAKAI,*Takao MIHARA
Materials Consolidated Div., KUBOTA Corporation
64 Nishimukojima-cho,Amagasaki,Hyogo 660,JPN
*1-1-1 Ohike,Nakamiya,Hirakata,Osaka 573,JPN

ABSTRACT

The composite rolls by Hot Isostatic Pressing (HIP) which could attain high toughness and hardness due to minute structure and simultaneously diffusion bonding with other tougher materials were developed.
HIPing (temperatures between 1073 and 1473K, pressure 120 MPa, pressing times between 0.5 and 4 hours) was applied for the consolidation of high speed steel (HSS) powder bearing high carbon and the diffusion bonding to alloy steel. The influence of HIPing conditions on density, microstructure and bonding strength was studied.
Under the most suitable condition, cylindrical composite roll sleeve could be produced, which had homogeneous microstructure dispersed fine carbides, uniform hardness distribution in the whole HSS layer and defect-free bonding zone. The composite rolls were applied to actual hot rolling.

INTRODUCTION

To cope with the recent demand for the most advanced rolled products, high quality roll materials which can be used under the severer condition have been needed. The conventinal cast iron rolls sometimes could not meet this demand, because the ingot metallurgy method has limit to control the carbide distribution and to refine carbides. Therefore, the roll surface detriorates in rolling operation as coarse carbides distribute inhomogeneously. On the other hand, the powder metallurgy method can offer advantages of the homogeneous and fine microstructures[1][2]. Furthermore, full dense sintered body and diffusion bonding to other solid material can be achieved by HIPing. From above reason, the composite rolls have been developed by HIPing.

Based on thorough consideration of rolling conditions and material properties of conventional cast iron rolls, the first goals of material properties have been set. These are hardness Hs 90 ~ 95, bonding strength above 600 MPa, tensile strength above 1000 MPa, bending strength above 2000

MPa and carbide size under 10 μm.

This paper presents some results of an investigation about the influence of HIPing conditions on material properties, trial manufacture under more suitable condition and application of composite rolls for hot rolling.

MATERIALS AND METHODS

Experimental Procedure :

The powder selected in this study was HSS powder bearing high carbon. This powder was encapsulated in AISI 4140 steel container which was inner-layer material of composite roll (Fig.1). Chemical composition of HSS powder and AISI 4140 is shown in Table 1. The container was degassed under pressure $3X10^{-2}$ Pa and sealed by electron beam welding. The consolidation of these materials was carried out at temperatures between 1073 and 1473K, pressing times between 0.5 and 4 hours and pressure of 120 MPa. After HIPing, these materials were annealed and then machined as the tensile test and bending test specimens with the dimensions ϕ 6X30 and 3X4X50 respectively. In order to harden, all the specimens were austenitized in controlled atmosphere at 1453K for 1 hour and followed by high nitrogen gas pressure 0.6 MPa quenching. Specimens were triple tempered at 833K.

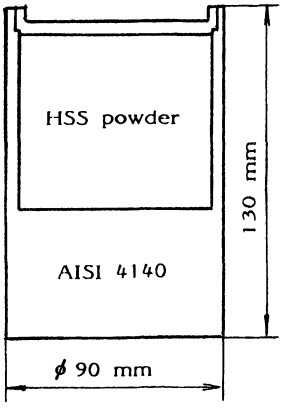

Figure 1. Configuration of container for consolidation and diffusion bonding experiment.

TABLE 1
Chemical composition of high speed steel powder and AISI 4140

Material	C	Si	Mn	Cr	Mo	W	V	Co
High speed steel powder	2.35	0.40	0.15	4.35	7.05	5.78	5.95	10.30
AISI 4140	0.38	0.30	0.73	1.02	0.16	-	-	-

Tensile tests and bending tests were carried out at room temperature. Density was determined by the Archimedes method. Microstructures of specimens were observed by scanning electron microscope. In order to compare conventional cast irons with HIP'ed HSS, same tests were carried out.

In order to design materials respectively to apply rolling conditions, the relationship between C content and mechanical properties on HSS consolidated powders bearing 1.7 ~ 2.6 wt.%C, 4.0 ~ 6.0 wt.%Cr, 4.1 ~ 8.9 wt.%W, 2.1 ~ 5.1 wt.%Mo, 5.0 ~ 7.3 wt.%V was investigated. And bending tests and Ogoshi type wear tests were carried out.

Application :

In order to manufacture composite roll by HIPing, HSS powder for outer layer and AISI 4140 for inner layer of the same kinds shown in Table 1 were used. The processing flow diagram is shown in Fig.2. Computer simulation was applied to control final shape of container and to decide most suitable HIPing condition on which real density would be obtained.

After manufacturing, quality of composite roll was confirmed. Composite rolls for hot rolling by HIPing were evaluated as the finishing roll for flat bar, finishing roll for angle bar and pre-finishing roll for plain bar.

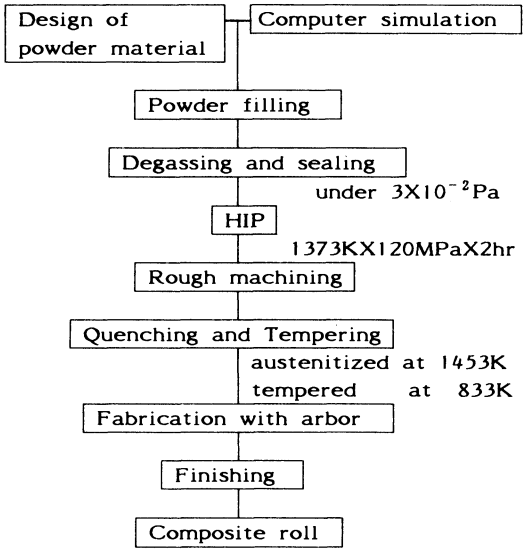

Figure 2. Processing flow diagram.

RESULTS AND DISCUSSION

Density and microstructure :
The dependence of relative density on HIPing temperature is shown in Fig.3. In the case of pressing time 0.5 hr, relative density is 93% at the temperature 1073K and increases with rising temperature and then reaches to theoretical density at the temperature 1373K. In the case of pressing time 4hr, relative density is nearly 99% even at the temperature 1073K. The microstructure at temperature 1073K and pressing time 0.5hr shows early stage of densification and the triangular pore is observed. At the pressing time 4hr, the pore becomes spherical and smaller but still exists. At the temperature 1273K and pressing time 0.5hr, the pore is almost eliminated (Fig.4).

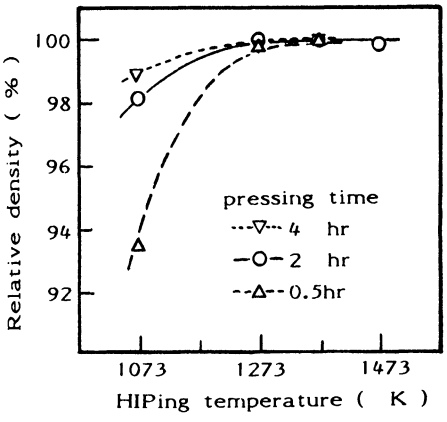

Figure 3. Relationship between relative density and HIPing temperature.

Tensile strength σ_T of HSS layer :
The relationship between σ_T of HSS layer and HIP temperature is shown in Fig.5. σ_T of test specimens fabricated at temperature 1073K and pressing time 0.5hr and 2hr, which are not theoretical densities, is low and varied widely. The tendency of σ_T to temperature is the same as density.

Tensile strength σ_T of bonding zone :
The relationship between σ_T of bonding zone and HIPing temperature is shown in Fig.6. Test specimens fracture in AISI 4140 except the case of HIPing at the temperature 1073K and pressing time 0.5hr. Therefore, σ_T of bonding zone is above AISI 4140. Test specimen fabricated at the temperature 1073K and pressing time 0.5hr fractures in HSS.

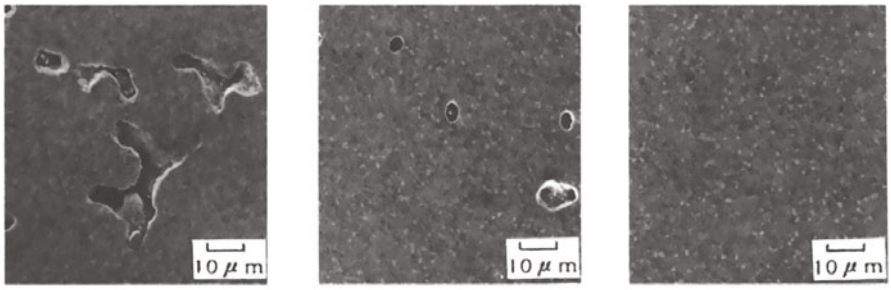

Figure 4. Microstructures produced under different HIPing conditions.

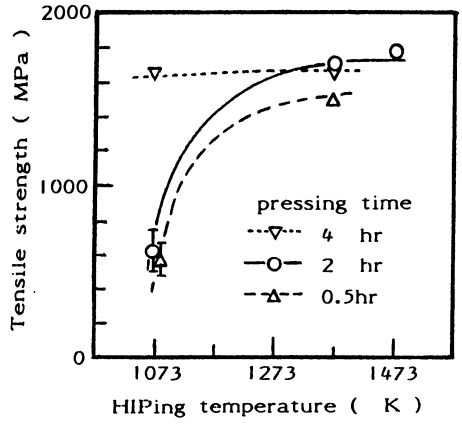

Figure 5. Relationship between tensile strength of HSS layer and HIPing temperature.

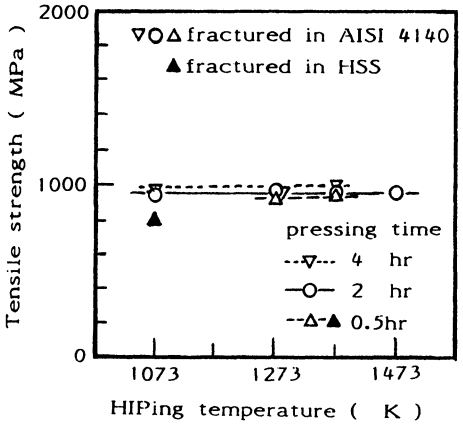

Figure 6. Relationship between tensile strength of bonding zone and HIPing temperature.

Relationship between C content and mechanical properties :
Mechanical properties of HIP'ed HSS powders bearing various C content are shown in Fig.7. C content is in stoichiometric balance with Cr, W, Mo and V in this experiment. Consequently, C content is given as stoichiometry (C_{stoich}%) which is described following in general[3].

$$C_{stoich}\%=0.06Cr\%+0.033W\%+0.063Mo\%+0.2V\%$$

Relationship between carbide volume fraction and C_{stoich}% is linear and carbide volume fraction increases with increase of C_{stoich}%. Wear rate decreases (wear resistance increases) with increse of C_{stoich}%; however bending strength σ_B decreases. According to these results, wear rate and σ_B are correlative with carbide volume fraction in HIP'ed HSS powder.

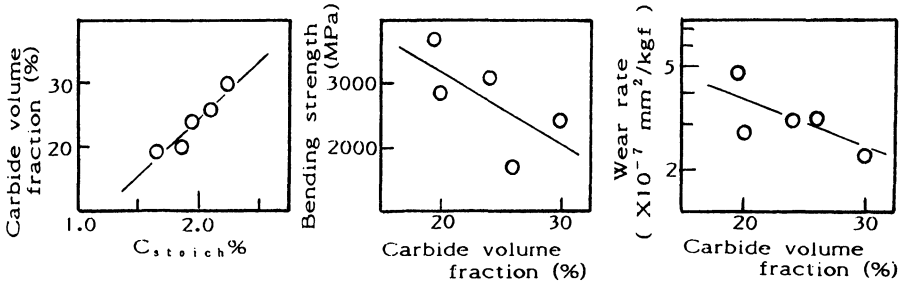

Figure 7. Relationship between C content and mechanical properties.

Material properties of manufactured composite roll by HIPing :
By penetration test and ultra-sonic test, defect-free whole HSS layer and bonding zone are confirmed. Hardness distribution of HSS layer measured in axial direction on the roll surface is uniform (Fig.8). Tensile strength of HSS layer and bonding zone is shown in Table 2. Homogenious micro-structure dispersed fine carbides is observed (Fig.9).

TABLE 2
Mechanical properties of HIP'ed HSS powder and conventional cast irons

Material	σ_T (MPa)	σ_T(bonding) (MPa)	σ_B (MPa)	Hs
HIP'ed HSS powder	1280	>890(fracture in AISI 4140)	2350	93
Chilled cast iron	280	-	540	78
Spheroidal graphite(S.G.) cast iron	420	-	800	66

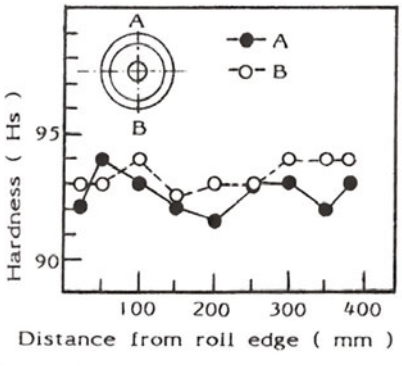

Figure 8. Hardness distribution of roll surface.

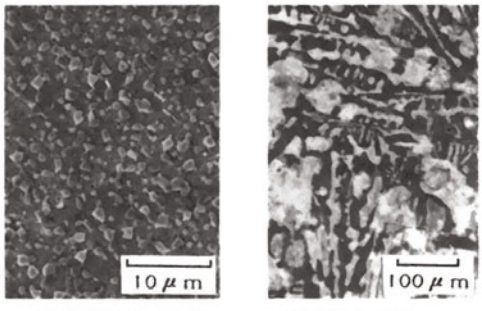

Figure 9. Microstructure of composite roll by HIPing and chilled cast iron.

Results of application :
The applied results of composite rolls as the finishing roll for flat bar, finishing roll for angle bar and pre-finishing roll for plain bar are shown in Table 3. Fig.10 shows one of the composite rolls by HIPing. As an example of composite roll superiority, the relationship between surface roughness and amount of rolled products is shown in Fig.11. Roughness of rolled products by composite roll is very smooth even in the case of large amount of rolling. On the other hand, roughness of rolled products by conventional

cast iron roll becomes rough in the early stage of rolling. The difference of these capability is considered as the diferrence of microstructure (Fig.9), morphology of carbides (MC, M_6C for HSS (M=Fe,W,Mo,V,Cr); $(Fe,Cr)_3C$ for conventional cast iron) and mechanical properties (Table 2).

TABLE 3
The applied results of composite rolls for hot rolling

Rolling	Roll	Amount of rolled products (ton)	Wear loss of roll (mm dia.)	Multiple
Finishing for flat bar	Composite	252	0.12	X 5.1
	Chilled	58	0.14	
Finishing for angle bar	Composite	140	0.6	X11.7
	S.G.I.	20	1.0	
Pre-finishing for plain bar	Composite	1355	1.5	X 5.4
	S.G.I.	500	3.0	

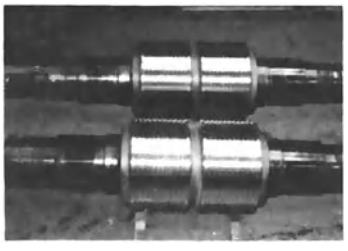

Figure 10. Composite roll by HIPing.

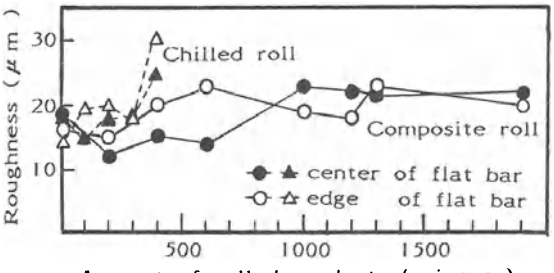

Figure 11. Relationship between roughness and amount of rolled products.

CONCLUSIONS

1. The consolidation of HSS powder bearing high carbon and simultaneous diffusion bonding to AISI 4140 can satisfactorily be carried out on condition of temperature in range of 1273 ~ 1473K, pressing time 2 ~ 4hr and pressure 120MPa.
2. Under the condition of temperature 1373K, a pressure 120MPa and pressing time 2hr, cylindrical composite roll sleeve which has homogeneous microstructure dispersing fine carbides, uniform hardness distribution in the whole HSS layer and defect-free bonding zone can be produced.
3. This composite roll has five to ten times resistance against wear and deterioration than conventional cast iron roll in the case of applying as hot rolling mill roll.

REFERENCES

[1] Y.Arata, A.Omori, H.Nishihara, T.Mihara, J.Funakoshi and Y.Nakagawa, Preprints of the National Meeting of Japan Welding Society, 1986, 38,102
[2] H.Nishihara, T.Mihara, J.Funakoshi, Y.Nakagawa, H.Fujita and J.Honda, J. The Iron and Steel Institute of Japan, 1987, 73, No.5, S669
[3] G.Steven, A.E.Nehrenberg and T.V.Philip, Trans. ASM, 1964, 57, pp.925-948

TECHNOLOGY OF HIPing COMPLEX SHAPE PARTS WITH DUAL CHEMICAL COMPOSITION AND PROPERTIES FROM METAL POWDERS: TRENDS OF ITS DEVELOPMENT IN THE USSR

Kratt E.P., Samarov V.N., Haykin R.A.*
All-Union Institute of Light Alloys (NPO VILS)
20 Gorbunov st. 121596 Moscow USSR
"ISOSTATICA"
*16 Vyborgskaya st. 125212 Moscow USSR

ABSTRACT

Recently the need for powder parts operating at high temperatures, stresses and in agressive media has grown greately. Complex shape parts with dual chemical composition and properties made with the help of HIP method can fully meet the operation requirements. The main trends of developing such technology in the USSR are:
-production of high strength powder parts by HIP method without consequent plastic deformation;
-using high quality powders;
-production of parts with variable cross-sectional properties meeting the operational requirements;
-introduction of aerospace technologies into national economy.

INTRODUCTION

Some 15 years ago HIP began to develope in the USSR on an industrial scale due to Academician A.F.Belov's innitiative. It was aimed at solving the problem of production of disks and other rotating parts of aerospace engines and of highly loaded power machines.

At present time there are about 50 industrial HIP units in our country and many pilot units as well.

HIP was introduced into industry as a process, providing 100% density of material and by now it has formed an area of its most efficient application. It includes production of quality parts made of powder of special composition, complex "near-net" and "net-shape" parts made of expensive and hardly-machined materials and parts of various composition and rationally distributed properties.

If one analyzes the tendencies of HIP development in

the USSR, he can observe the combination of world trends and some national peculiarities. The latter exist, on the one hand, due to the long-term isolation of soviet specialists because of certain export restrictions in Western countries (COCOM), and on the other hand, due to the prevailing aerospace orientation of the research in the field of HIP.

Furthermore, the complex shape parts production approach was greately influenced by the economical peculiarities of industrial development in the USSR. Unlike the West with its accurate and diverse division of labour, most of the soviet industrial facilities were developing with the tendency to a closed technological cycle with minimum of cooperation, trying to implement all the operations at one plant. In the case of HIP it means the complete technological chain beginning with the cast and its atomizing ending with the final shape part. This has the following important consequences:

1. Lack of powerful presses for vacuum isothermal forging and advanced machining equipment led to the acceptamce of "as-HIP" method for the production of large-size parts. This method soon showed its unique advantages in extra-complex shape parts production.

2. Strict requirements for powder purity from non-metallic particles, oxygen, carbon etc. were stated and kept in serial production.

3. Industrial use of this profitable and technologically promising method required a thorough mathematical and physical modelling of all major steps of the technological cycle, such as:

-atomization of powder and structurizing of particles;
-evacuation and encapsulation of powder;
-vacuum heating of loose powder;
-shrinkage under HIP conditions of the capsule filled with powder ;
-formation of materials structure and properties during densification. All this brought about the problem of optimization of the HIP cycle as a whole and development on its basis a HIP cycle control system.

4. As a result a team of skilled and broad-minded researchers has been formed.

HIP of complex shape parts with variable chemical composition - a concept approach

Two major technological processes of producing semiproducts for machine-building - precision casting and forging - have intensively developed during the recent decades and achieved outstanding results in shape precision and perfomance characteristics. However, the majority of semiproducts and parts posess either high precision and complexity, or high strength properties with poor shape and dimensional correspondence between the workpiece and final part. Illdeveloped vacuum-isothermal forging complexes, which can successfully combine these characteristics, are very few in number and can't be seriously relied upon.

HIP is the method which makes it possible to combine

both precision and high strength for a variety of parts and materials in one technological process, so we have the following motto enscribed on our banner: "Combination of the dimensional accuracy of precision casting with perfomance characteristics of forged material".

Up-to-date machine-building units and parts usually work under high temperature and stress gradients and in agressive media. Furthermore they need to combine high perfomance characteristics with special technological or physical properties, e.g. good welding, magnetic or tribological characteristics, machinability etc.

HIP process enables to bond different materials in a solid state (i.e. without loss of properties) with high strength of the border which is not less than the strength of bonded materials. Sometimes we can obtain boundary zone with smooth transfer from the material with one chemical composition to another. So NPO VILS can produce dual and multy property parts with the optimized combination of characteristics, meeting the operational conditions. The possibilities of providing high precision, complexity, geometrical reproducibility, the optimized combination and high level of properties are only the potentials of HIP, but their practical realization can be carried out only through number of iteration steps of experiment made while developing the particular technology. This requires a lot of time and expense.

As we are short of time and money, we have chosen another way - the way of physical and mathematical modelling of all steps of HIP. The main of them are: densification and shrinkage simulation.

During HIP the capsule acts as a plastically deformed shape-forming tool. That leads to the non-uniform stresse-state of the powder bulk and its complex shrinkage. The latter is greately influenced by the temperature and pressure as functions of time. The same capsules HIP-treated with "hot-hot" and "cold-cold" cycles, have different ways of shrinkage. It happens because the strength, plasticity, viscosity and thermophysical characteristics of capsule and powder are complex functions of temperature and density. Therefore, the HIP process trajectory should be taken into account when making complex shape parts.

While producing dual and multy property parts, optimal HIP regimes may occupy a very wide range of parameters. Therefore the adequate simulation of the process is necessary to define those of the parameters, which provide, for example, full densification of superalloy powder with negligible deformation of ceramic insert while producing a bladed wheel.

So only the complex simulation is able to provide a profitable production of complex shape parts. The corresponding software is developed at our institute on the FEM basis and is supported on PC in the following dialogue regimes: "operator", "technologist" and "researcher", available and friendly for any user.

As a rule something, called know-how, lies between the best computer calculation and its successfull realization. The corner stone of production of complex shape parts is

hidden in the following problems: capsule design, choice of the best material for capsule, weld connections.

While producing "net-shape-parts", one should solve the problem of contamination of powder surface as a result of diffusion from the capsule or inserts material. This problem is tackled either under special HIP regimes, or through special treatment of the capsule's surface. We have worked out some techniques, in particular, the definition of either barrier, or diffusion coatings composition.

Another problem arises with the quality of the boundary zone in dual property parts and development of heat treatment regimes suitable for both materials. Here we have also worked out some statistical mathematical simulations and defined a number of couples of materials, posessing the requied properties. The main of them are:

-high-temperature + low-temperature material;
-high-strength + corrosion-resistant material;
-high-strength magnetic + high-strength non-magnetic material;
-high-temperature + weld material etc.

Taking into account all the above mentioned, we can formulate our concept approach to HIP as follows:

Many years of experience in HIP technology + new ideas + computer based intellect = new superior quality of PM parts and processes.

Examples of complex shape and dual chemical composition parts development

On the base of the technologies developed we are able now to produce parts up to 1m in dia, 2m in height, 2 ton in weight. Having started with aerospace materials and parts research, we spread this technology into civil machine-building and national economy. We have worked out capsules of special design, which are able to provide directional deformation during HIP and produce "near-net-shape" workpieces for turbine and compressor disks for various engines and power machines (Fig.1). We have mastered serial production of "as-HIP" disks and they are in successfull flight for years (Fig.2).

There are some examples of a "net-shape" part - body parts of the combustion chamber with non-machined internal surface made of a powder superalloy. (Fig.3)

Also we can produce dual property parts - wheels with blades made of directly solidified high temperature alloy, and disk made of a high-strength powder (Fig.4). Ceramic inserts provide geometry of the part. Shrinkage simulation enables to provide the geometry of the aerodynamic channel. "Net-shape" impeller wheel made of Ni-based alloy can be successfully bonded by HIPing with a steel shaft (Fig.5).

"HIP-cladding technology" became widely spread in national economy. Problems here are solved more easily because the casted or forged part acts as a capsule itself. Applying this technology to the production of "christmas-tree" body parts for oil and gas industry enabled them to operate in agressive media (Fig. 6). Such technologay is also successfully applied in production of metal-forming tool (dies, rolls, screws etc.)

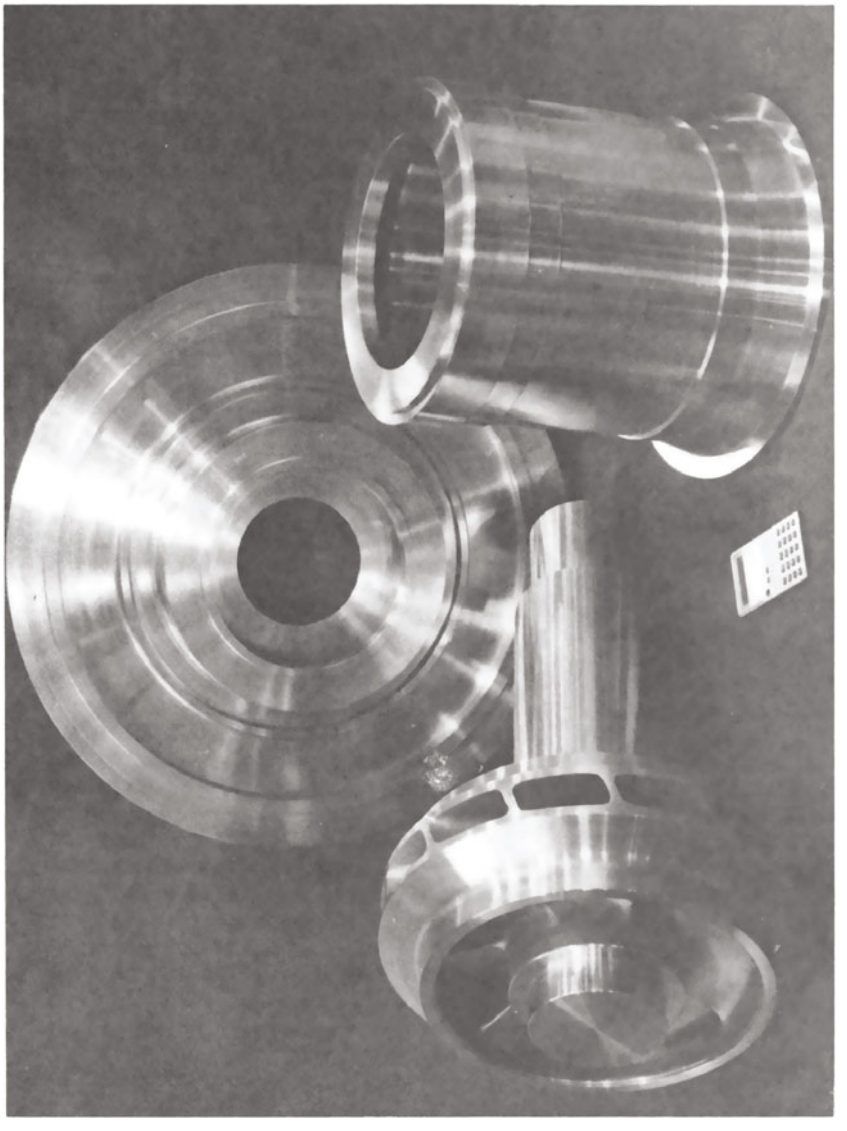

Fig. 1 Turbine and compressor disks "near-net-shape" workpieces

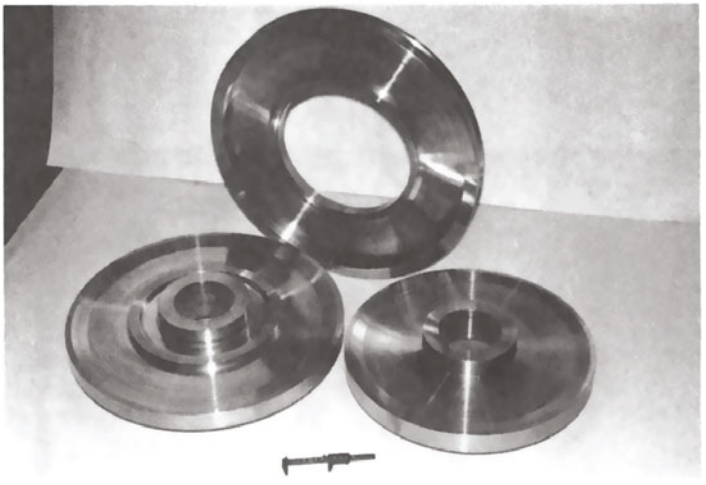

Fig. 2 Serially produced disks and shafts for jet engines

Fig. 3 Combustion chamber "net-shape" body part

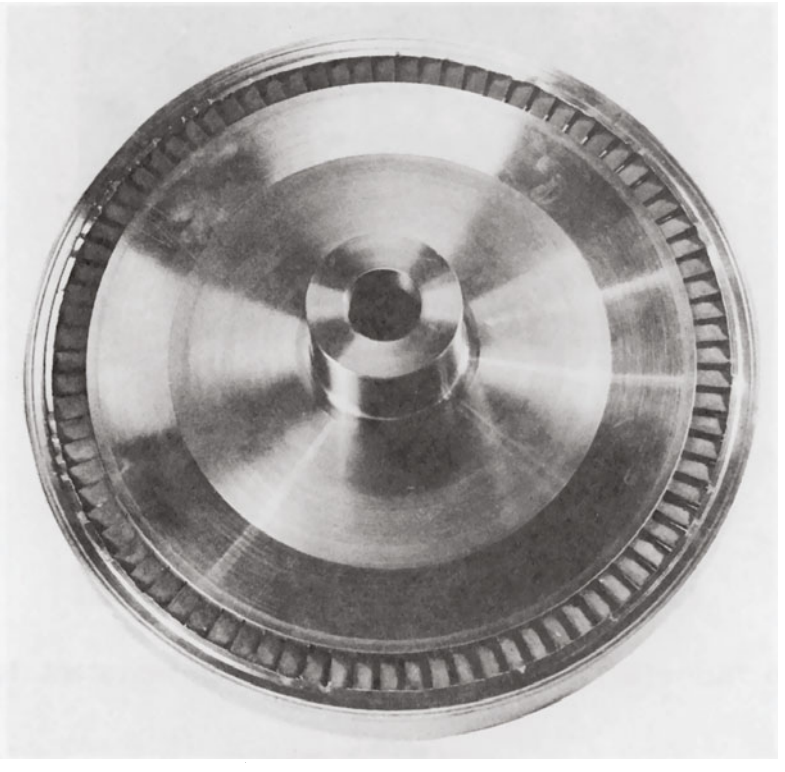

Fig. 4 As-HIPed bladed dual property disk

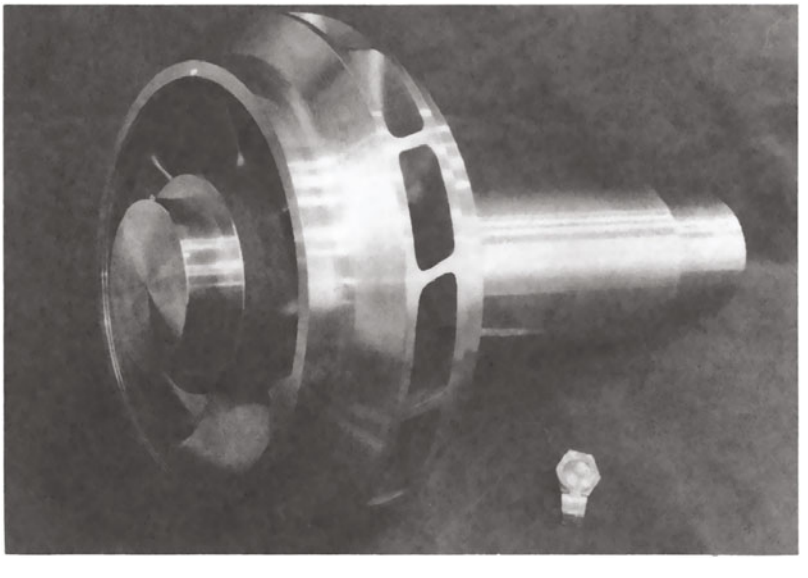

Fig. 5 "Net-shape" impeller wheel bonded with a steel shaft

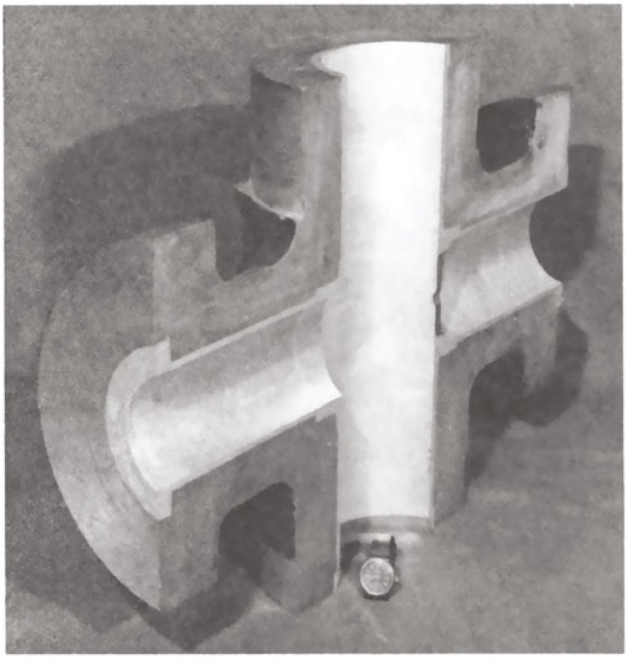

Fig. 6 "HIP-clad" body parts with corrosion-resistant layer

Fig. 7 Dual property rotor combined of magnetic and non-magnetic material

Production of parts with variable magnetic and electric properties for rotating electric machines can also present interest in this field (Fig.7).

Trends of HIP development in the USSR

In spite of the fact that HIP remains a rather expensive and exotic technology for civil engineers, it is slowly but surely developing and spreading into production of complex shape parts operating under severe conditions.

The main trends of such development in the USSR are the following:

-production of high strength "as-HIPed" PM parts with no plastic deformation;

-using powders of super high quality;

-numerical simulating of all elements of HIP technology and development of the software on its basis in dialogue regime available for any user;

-complication of "near-net-shape" parts;

-replacement of cast and welded parts with high strength "net-shape" parts;

-production of parts with variable cross-sectional properties meeting operational requirements;

-introduction of "high" aerospace technologies into national economy.

AFTERWORD

We have been working for more than 15 years in certain isolation. Now we are open to wide cooperation with both East and West. We hope that some peculiarities of our development and results achieved make us a rather interesting potential partner in both research and business. Of course this future cooperation should not be overcommercialized but still we can offer our perspective partners and customers the following:

-CAD software for capsules;

-"net-shape" technology;

-dual property part technology:

-HIP automative control systems.

EFFECT OF PRESSURE ON DIFFUSION OF ELEMENT CHROMIUM IN NICKEL DURING HOT ISOSTATIC PRESSING

PAN GANG, WANG SHENGHONG
Central Iron & Steel Research Institute
NO. 76 Xueyuan Nan Lu, 100081 Beijing, P.R. China

ABSTRACT

It is important to study the diffusion of element chromium in nickel-based alloys during hot isostatic pressing(HIP) treatment. In present paper the effects of pressures on interdiffusion coefficient of chromium in nickel were investigated by using Ni-Cr diffusion couples and diffusion coefficient was increasing with the pressures in the system and had a relation-ship of $D=nA^{P}$. The mechanism of increasing diffusion coefficient has been discussed as well. According to experimental results we believe that there are two types of diffusion mechanism, i.e. volume diffusion and diffusion along dislocation pipe and the later plays an important part in diffusion. Moreover, for further pressure increment this increasing tendency becomes slow down.

INTRODUCTION

Recently hot isostatic pressing(HIP) technology has been widely used in industry but there are only few reports in respect of effects of pressure on diffusion of elements in metals. P.G. Showmen[1], N.H. Nachtrieb et al.[2] had shown early the decressing effect on self-diffusion coefficient of lead, sodium and ordinary phosphous. These results were based on decreased amount of vacancies in the metals with increasement of pressure in the system, which causes increasing energy comsumption during diffusion and, consequently, decreases the diffusion coefficient of elements. But some others had different results. T. Vasilos and R.M. Spriggs[3] in their studying the hot-pressed process of Al_2O_3 and MgO found that the diffusion coeffcient was accelerated under pressure applied. R.L. Coble[4] in his serial works also

pointed out that mass-flow was increased with the pressure. Gatlinburg[5] found the increasement of self-diffusing of uranium and diffusion of iron in titanium under pressure, but no detail mechanism was reported. In our previous work[6] we found the treatment in a hot isostatic press unit was a more effective method than that of in a vacuum furnace to improve the homogeneity of alloying elements for K17 superalloy casting as well. Therefore, it is important to study the diffusion behavior of elements in metals under pressure in more detail. Because of complex structure of superalloys, Ni-Cr diffusion-couples were selected, for simplicity, to study the diffusion behavior of Cr element in Ni.

EXPERIMENTAL PROCEDURE

Diffusion-couples used in the study were comprised of 99.9% pure Ni plated with a layer of Cr. Pure Ni, as a matrix, was prepared by vacuum melting, followed by forging and test specimens measuring $20\times20\times10$mm were cut out from sheet obtained by forging. The surfaces were ground and degreased in acetone and ethanol and treated with acids before plating. Composition of plating bath : CrO_3-250g/l, H_2SO_4-2.5g/l. Technology parameters: Votage 5-6V, current density 55A/dm, plating bath temperature 50-55℃, plating time 10h, average thickness of Cr layer 400μm. The diffusion couples were cut perpendicularly to the bonding interface. The heat treatment regime under various pressures for diffusion couple samples were listed in Tab. 1.

TABLE 1
The heat treatment regime for diffusion couple samples

Samples	heat treatment regims			Type of treatment
	Temperature (℃)	Pressure (Mpa)	Time (h)	
V01	1140	-	4	Vacuum
H02	1140	85	4	HIP
H03	1140	120	4	HIP
H04	1140	200	4	HIP

Vacuum treatment was carried out in a furnace, Type TBB-4, and HIP treatment in ASEA Mini HIP at desired temperatures ±5℃. After different heat treatments the samples were examined by SEMQ-2 electroprobe to determine the composition of materials with a interval of 5μm and the measured results were mutually calibrated by the EDX and WDX which had been calculated by the aid of computer to obtain C-X curves of Cr. The diffusion coeffcient calculated according to Boltzman-Matann equation is given.

$$D=\frac{-1/2\ xdc}{-\frac{dc}{dx}} \qquad (1)$$

where dc/dx: slop at C-X curve
xdc: area obtain from Matano interface to C

EXPERIMENTAL RESULTS

C-X curves of Cr obtained by electronprobe examination from all samples treated under various pressures had been shown in Fig. 1. The width of diffusion band varies in a wide region and they became wider with increasing pressures in the system .

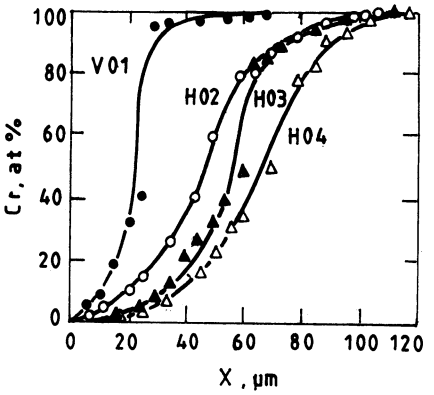

Figure 1. C-X curves of samples

Fig. 1 showed that the treated pressure of sample H02 was higher than that of sample V01 by 85Mpa and the width difference of diffusion band was 42μm . For the samples H04 and H02, H04 and H03 they were 115Mpa , 10μm and 80Mpa , 5μm respectively. These results indicated: the width of diffusion band increased with increasing the treated pressures in the system . There were no linear relationship here and these increasing rate of diffusion slowed down for further raising pressure .
According to the equation (1) and date obtained from above C-X curves , the diffusion coefficients had been calculated at different composition points , which were plotted against the pressures treated as shown in Fig. 2 .
In Pig. 2 it is clearly indicated that for the same composition the diffusion coefficient D was increased obviously with increasing pressure to certain degree, after that this increasing tendency

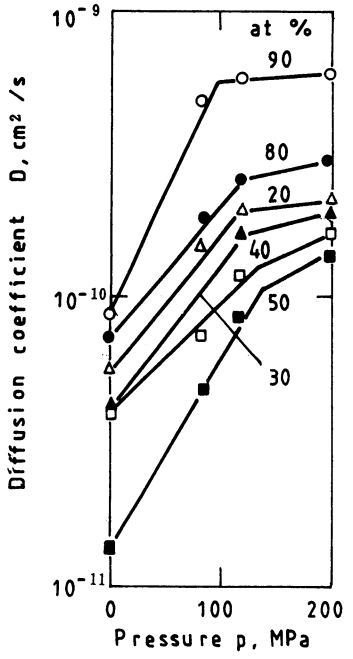

Fig. 2 Effect of pressures in system on diffusion coefficient

became slow down. In our cases, this decreasing tendency started when the pressure applied was greater than that of 120Mpa. Using linear regression treatment a common functional relation was given between diffusion coefficients and pressures treated

$$\log D = a + bP \qquad (2)$$

where D-diffusion coefficient, cm^2/sec; P--isostatic pressure treated, Mpa; a--constant; b--slope of the line

This equation can also be written

$$D = nA^{P} \qquad (3)$$

Equation (3) indicates the exponential function relationship of diffusion coefficient D to the pressure P in the system .

DISCUSSION

As the atom radius difference between Cr and Ni is small (1.28A and 1.24A respectively), it seems not possibly to be interstitial mechanism for them. The vacancy mechanism likely is a possible mechanism of diffusion in our cases, because in all crystals some of the lattice sites are unoccupied. The energy required for an

atom to jump into an adjacent vacancy is small. Like all crystal surface and grain boundary any structure defects would increase diffusion coefficient of metals, as well as for the dislocations. Dislocation line is a linear distortion region which is favour of diffusion of atoms in crystal. The role of dislocations as arteries of transport has been discussed theoretically and experiments have confirmed that the self-diffusion coefficient along dislocation pipes is greater by several orders than in the crystal lattica[7]. During the HIP treatment, alloys were subjected to high temperature and some deformation simultaneously which would cause the increment of dislocation density. Measurement of dislocation density for HIP treated samples under various pressures were made at Philips automatic X-ray diffraction apparatus , results of which were listed in Tab. II. In a well anealed metal single crystal any plane passed through the crystal will cut 10^6 to 10^7 dislocations per square centimeter. In the present test the dislocation density for sample V21 treated in vacuum at 1210℃ was 1.0318×10^7 which has good agreetment with reported value. The dislocation density was increased with the pressure and so did diffusion coefficient. A mathematical expression for diffusion coefficient which includes both parts of lattice diffusion and dislocation diffusion had been put[5].

$$D= (1-g)D_b + gD_d \qquad (4)$$

Where g--the fraction of time spent by the atom in the vicinity of dislocation; D_b--the bulk or lattice diffusion coefficient; D_d--the coefficient for diffusion along dislocations.
The above expression indicates that D_d must be taken into account and g is related to the dislocation density. The higher dislocation density, the higher diffusion coefficient will be.

TABLE II
The dislocation densities under various HIPing pressures

Samples	Dislocation density (lines/cm^2)	Conditions
Co	4.7860×10^9	original
V15	2.7060×10^9	1150℃, 2.5h in vacuum
HIP15	3.7549×10^{10}	HIPed 1150℃, 2.5h, 120Mpa
V21	1.0318×10^7	1210℃, 2.5h in vacuum
HIP21-1	1.1352×10^9	HIPed 1210℃, 2.5h, 120Mpa
HIP20	1.3987×10^{10}	HIPed 1210℃, 2.5h, 200Mpa

As mentioned previously that the diffusion coefficient along dislocation pipes is greater by several orders than in the crystal lattice. The values of diffusion coefficient of element all depends on the value of dislocation density which is enhanced with the increasing the pressure applied in the HIP system. The analysis has good agreement with the experiments. As the increasing tendency of dislocation density in specimen with further raising the pressure in the HIP system, there exist the exponential function relationship of diffusion coefficient D to the pressure P in the system.

CONCLUSIONS

The effect of pressure on diffusion of Chromium in Nickel during hot isostatic pressing was investigated.

1. The diffusion of Cr was carried out through vacancy mechanism and dislocation mechanism for Ni-Cr diffusion couple. Increased density of dislocation and criss-cross motion of dislocation with increasing the pressure in HIP system would enhance the diffusion coefficient. But this increasing tendency would slow down with further raising of preasure for reducing the vacancy and weakened enhancement of density of dislocation.
2. There exist a exponential function $D=nA^{P}$ relationship between diffusion coefficients and pressures, which has been concluded by calculation.
3. Since Cr is an important element in superalloys, the studying of the diffusion behavior of Cr with pressure is available to know the homogenization and structure changes of these alloys during the HIP treatment.

REFERENCES

1. P. G. Showmen, Diffusion in Solide (1963) 81-83.
2. N. H. Nachtrieb, et al., J. Chemical Physics vol. 31, No. 1 (1959) 135-8
3. T. Vasilos and R. M. Spriggs, J. Am. Ceram. Soc. Vol. 46 No. 10 (1963) 493-496.
4. R. L. Coble, PMI. Vol. 10, No. 3 (1978) 128-130.
5. Gatlingburg Tennessee, "Diffusion in Body-Centered Metals" Sep. (1964) 164, 343.
6. Wang Shenghong, et al., Central Iron & Steel Research Institute Technical Bulletin, 3(1985) 289-296.
7. S. E. Bokstein "Diffusion and Structure of Metals" 1985 P. 29

HIPPing Effects for Steel's Mechanical Properties

HIROSHI ONA*, SHIGEKI ICHIKAWA*, TOSHIHARU ANNDOU* and AKIRA NISHIOKA**
* Mechanical Engineering System, Takusyoku University. Hachiouji-shi, Tokyo 193, Japan.
** Nikkiso Co.,Ltd. Shibuya-ku, Tokyo 150, Japan.

ABSTRACT

After applying strain to carbon steel S45C for a mechanical structure, heat treatments were applied by 2 kinds of methods, which are vacuum annealing and HIP annealing, and the effects of these heat treatments on mechanical properties of material were investigated.

INTRODUCTION

HIP(Hot Isostatic Pressure) is attracting a great deal of attention as a manufacturing method for ceramics with high performance and high reliability with many studies having been carried out. Concerning metal materials, active developments and investigations are being carried out in the application field for removal of casting cracks, reclaiming of damaged parts due to fatigue or creep, solid diffusion welding, etc. However, reports on the evaluation of results of HIP forming are few, thus the publication of data is greatly desired. Accordingly, in present study, HIP annealing was applied to a carbon-steel plate for a mechanical structure, and the mechanical properties of HIP annealed metal was compared with vacuum annealed metal for examining the difference, and afterwards were arranged.

EXPERIMENT

Test pieces for tensile test were prepared from a carbon-steel plate for a mechanical structure(S45C, 1.6mm in thickness). For the removal of residual stress in this test piece, which was generated during preparation by mechanical working, vacuum annealing (10^{-4} torr) at 810°C for 30 min was applied. After vacuum annealing, the test piece was pulled with an Enstlon to apply strain in the range of 0 to about 4 %. Test pieces to

which strain were imposed, were subjected to HIP and vacuum annealing under the combinations of temperature and pressure which are shown in Table 1. After heat treatment, 2 kinds of test pieces were pulled again with an Enstlon and obtained stress-strain diagram, values which represent various mechanical properties of metals such as tensile strength, upper yield stress, yield elongation, uniform elongation, elongation

Table 1. Experimental condition to HIP and vacuum annealing

	HIP Pressure(Mpa)				Vacuum(Mpa)
Temperature(°C)	200	150	100	10	10^{-8}
810	▨	▨	▨	▨	▨
610	▨	▨	▨	▨	▨
510	▨				
410	▨				

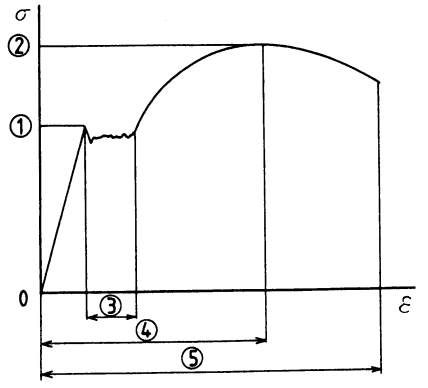

Fig.1 Measuring values to compare mechanical properties of HIP and vacuum annealed test pieces.
(1) Upper yield stress
(2) Tensile strength
(3) Yield elongation
(4) Uniform elongation
(5) Elongation after fracture

after fracture, etc. or values of hardness were obtained, then HIP and vacuum annealing were compared and discussed. These values are those in the outline of the stress-strain diagram in Fig.1. HIP cycle by the HIP apparatus (Nikkiso Co., Ltd.) is carried out by " HIP pattern of the pressure increment before temperature increment". Rising rate and lowering rate of the temperature of HIP were 10°C/min, rising rate of pressure was 1.67 Mpa/min.

RESULTS OF EXPERIMENT

1 Upper yield stress

The solid line in Fig.2 show a comparison of the values of the upper yield stress of the case when the temperature was held at 810°C for 30 min and pressure was changed from 10 Mpa to 200 Mpa in the HIP cycle, and also, in ordinary vacuum annealing. As shown in the figure , there is hardly any difference between the materials for HIP and vacuum annealing. The broken line in Fig.2 shows the case of annealing at 610°C. As shown in the figure, the broken line values (610°C) are higher by about 13 %

than the solid line (810 °C). In addition, HIP annealing at a higher pressure takes a lower value compared with vacuum annealing. The results that material for 610 °C annealing shows a higher value than material for 810 °C annealing following the pre-strain application. Furthermore, the fact that when HIP pressure is raised in 610 °C annealing, the value of the upper yield stress was made lower and reach closer to the values of the annealed material at 810 °C, is possible to interpret that HIP annealing has the effect of accelerating recrystallization. In other words, it suggests that there is a possibility of recrystalization by making HIP pressure higher, even at a temperature lower than recrystalization.

2 Tensile strength

The solid line in Fig.3 shows the relation between tensile strength by annealing at 810 °C and HIP pressure. As is clear from this figure, in the case of annealing at 810 °C, the difference between vacuum and HIP annealing can not be observed. The broken line in Fig.3 shows the case of 610 °C annealing. In this case the value of tensile strength shows a decrease following the increase in the HIP pressure. Moreover, in this case, the width of scattering grows larger due to the pre-strain values.

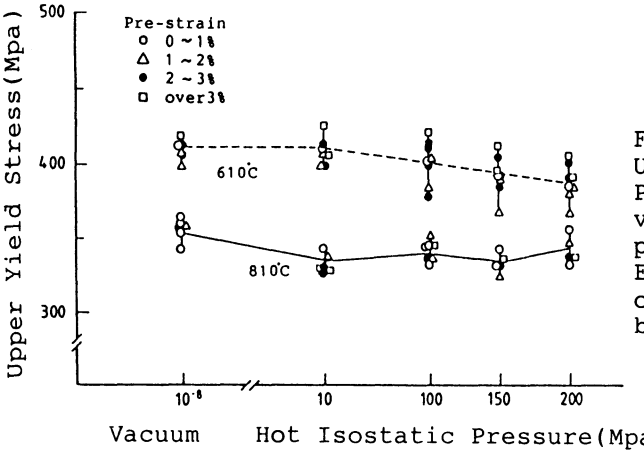

Fig.2 Relation between Upper yield stress and Pressure of HIP and vacuum annealed test pieces.
Each marks show values of pre-strain given before annealing.

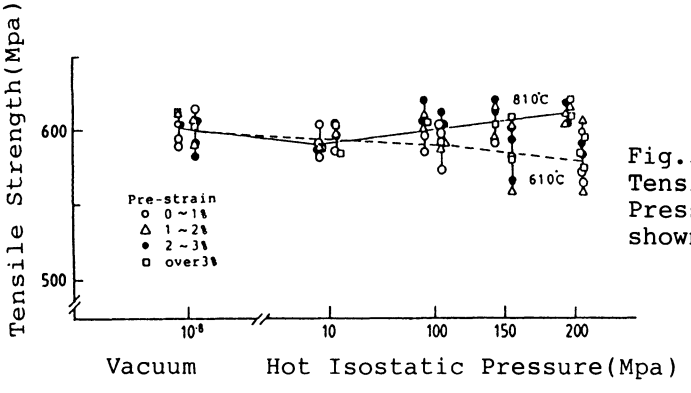

Fig.3 Relation between Tensile strength and Pressure of test piece shown in Fig.2.

3 Hardness

The solid line in Fig.4 shows the hardness of material annealed at 810 °C, and as is shown in the figure, no difference is observed between vacuum and HIP annealing. However, material for 610 °C annealing, which is shown by the broken line, shows the same values with the material of 810 °C annealing in 150 and 200 Mpa, but by vacuum annealing in the temperature range of less than 810 °C, hardness, and also the condition of scattering are larger than the case of 810 °C annealing. This is supposed also by work hardening, but it is important that even in the case of HIP annealing at a temperature less than the recrystalization temperature, if HIP pressure was made sufficiently higher, the same value with the case of the recrystalization temperature is possible to be obtained.

4 Yield elongation

As shown in Fig.5, by 810 °C annealing, when the HIP pressure is raised, yield elongation becomes lower compared with material for vacuum annealing. This suggests that yield elongation can

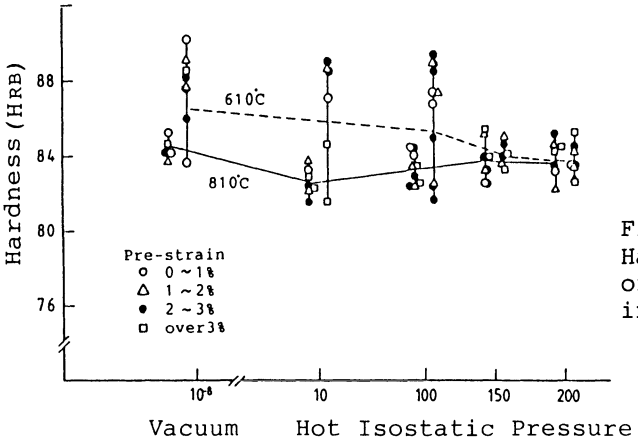

Fig.4 Relation between Hardness and pressure of test pieces shown in Fig.2.

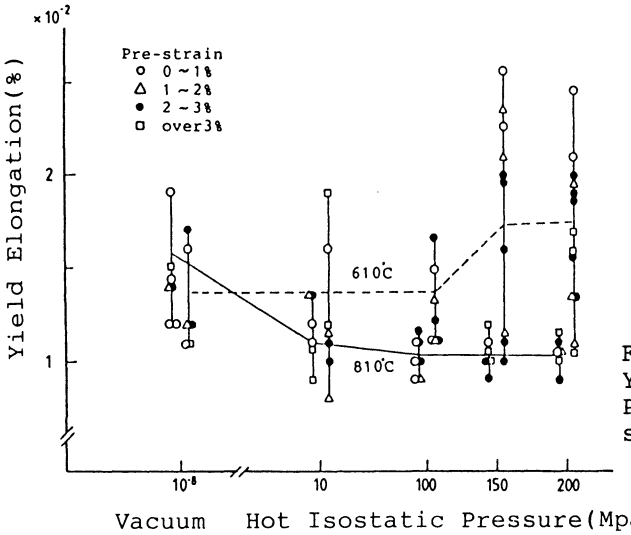

Fig.5 Relation between Yield elongation and Pressure of test piece shown in Fig.2.

possibly be improved if the HIP pressure is raised as annealing temperature is lowered. Figure 6 shows the result of an examination of the above by changing temperature under a high pressure of 200 Mpa. As seen in Fig.6, elongation shows a better result when the temperature is lower. This result is interesting, because it is opposite to that of the ordinary result that when the temperature is low, elongation property becomes lower because work hardness is not eliminated.

5 Uniform elongation

In the case of annealing at 810°C, as shown in Fig.7, the difference is not observed between materials annealed by a

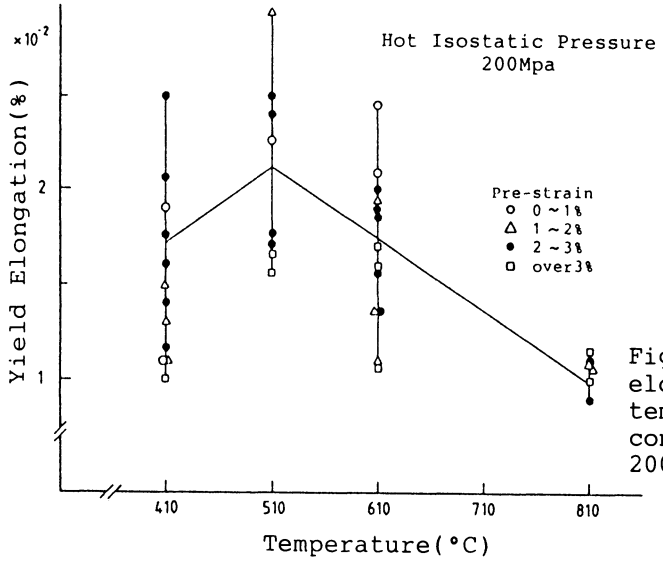

Fig.6 Change of Yield elongation by each temperature under constant HIP pressure 200 Mpa.

vacuum and HIP. However, in the case of 610°C annealing, which was shown in Fig.7, similar uniform elongation, with the case of 810°C annealing is obtained when high HIP pressure of 150 and 200 Mpa applied, but in vacuum annealing with less than 100 Mpa, elongation worsen. In omitted figure from this paper, in which the temperature was changed under a pressure of 200 Mpa, the lower the annealing temperature, the lower the elongation becomes, and this is remarkable when pre-strain was applied to a great extent. In this case, ordinary interpretation that work-hardening has had some influence, is applicable.

6 Elongation after fracture

Elongation of material which was annealed by HIP is better than material which was annealed by the vacuum method. This tendency is more remarkable when annealed at 610°C than the case of annealing at 810°C. In the case of a low annealing temperature with application of the high pressure of 200 Mpa, the value of elongation after fracture becomes lower. This result is caused by the same reason as in (5) above.

SUMMARY

(1) As for upper yield stress, difference is not observed

between vacuum and HIP annealing when treated at recrystallization temperature (810 °C). When treatment is carried out at a temperature less than recrystallization (610° C), the effect of work hardening is found to remain and upper yield stress shows a higher value than treatment at 810 °C. However, materials which were treated under high pressure, i.e., 150 Mpa, 200 Mpa, show values close to those of material which was annealed at 810 °C.

(2) Difference in tensile strength is not observed for materials which were annealed by the vacuum method and HIP

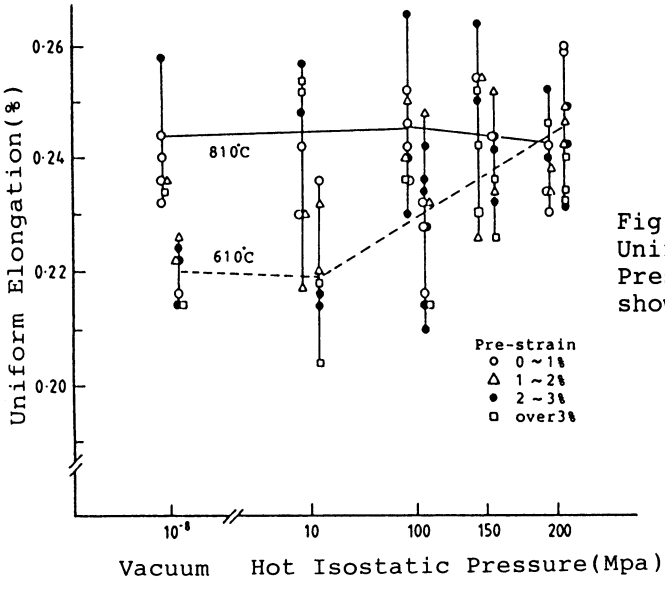

Fig.7 Relation between Uniform elongation and Pressure of test piece shown in Fig.2.

treatment when annealing was made at the temperature of recrystallization (810 °C). However, when pressures of 150 Mpa or 200 Mpa were applied at a temperature lower than that of recrystallization, values of tensile strength become lower than the value of vacuum annealing at 810 °C.

(3) Difference in hardness is not observed between materials of vacuum and HIP annealing when treatments were carried out at the recrystallization temperature (810 °C). When annealing is made at 610 °C, hardness is higher than that of material annealed at 810 °C, but when a higher HIP pressure is applied, the same value of hardness by annealing at 810 °C, is obtained.

(4) With annealing at 810 °C, yield elongation of material of HIP annealing is lower compared to the case of vacuum annealing. However, for the case of annealing at 610 °C, the results are opposite to that of the above, and a better elongation property is the result.

(5) Difference in uniform elongation is not found between materials of vacuum and HIP annealing when annealing was carried out at 810 °C. By vacuum annealing at a temperature of less than 810 °C, values of uniform elongation are lower than those of annealing at 810 °C, but the same value of elongation by annealing at 810 °C is possible to be obtained, provided HIP pressure is applied.

(6) Concerning elongation after fracture, the tendency is similar to that of (5).

NEW REGULARITIES OF THE SHAPE-CHANGING OF HOLLOW PARTS DURING HIP

Goloveshkin V. A., Samarov V. N., Seliverstov D. G.,
Kasberovich A. M.
All-Union Institute of Light Alloys (NPO VILS)
20 Gorbunov st. 121596 Moscow USSR

ABSTRACT

Regularities of HIP shrinkage of hollow axisymmetric parts are studied through numerical simulation, based on the idea of mutual high temperature plastic and creep deformation of monolite (capsule) and porous (powder) materials.

A complex study was carried out, investigating the influence of mechanical properties, materials rheology and the geometry parameters of the part on the regularities of deformation during HIP.

The analysis enabled us to reveal the area of parameter values which provide the non-monotonous and even reciprocal movement of the capsule surface and the materials borderline. A paradox possibility of growth of the borderline radius under external pressure was also detected.

INTRODUCTION

Production of hollow parts is an effective application of HIP technology. This can be explained by the fact that for the majority of materials such parts can be produced only by precision casting, but this method provides good geometry with poor properties.

Shrinkage under HIP conditions of hollow parts have some peculiarities due to the presence of the second free cylinder borderline and may be of quite a non-uniform character.

The developed numerical simulation of HIP process combined with the theory of mutual plastic high-temperature deformation of monolite (capsule) and powder materials helped us to study regularities of HIPing hollow axisymmetric parts.

This study enabled us to make the following thin-wall

hollow parts: gas engine shafts, high-pressure body-parts, working in agressive media, bi-metallic bushings with strictly defined borderline etc.

Physical and mathematical model of the process

First of all one should realize the cause of possible non-uniform deformation. Let us consider the distribution of stresses in a long tube under isostatic pressure P (Fig. 1).

σ_{R1} is always > σ_{R2} , i.e. P > σ_{R2} , so the outer wall will always move in radius decrease direction.

If σ_{r2} > σ_{r1} , radius of the inner wall will also decrease. So, as one can see, the inner wall movement depends on the stress variation character in powder. If σ_{R2} = σ_{r2} (the material has no shear strength i.e. acts as a "plastic gas"), σ_{r1} > σ_{r2} and the inner wall will move in outer direction. For a monolite or a low-porosity material σ_{r2} >> σ_{R2} , and the inner wall will shrink. So we must expect in some cases a non-monotonous movement of the capsule's walls, as the powder properties vary from those, close to the "plastic gas" properties, to those of monolite material.

Basic equations

Let us consider the approximate determination of the "Lame" problem for a three-layer tube (Fig. 2).

In zones 1 and 3:

$$\sigma_r = -P + 2\cdot\mu\cdot\frac{\partial U}{\partial r} ;$$

$$\sigma_f = -P + 2\cdot\mu\cdot\frac{U}{r} ;$$

$$\frac{\partial \sigma_r}{\partial r} + \frac{\sigma_r - \sigma_f}{r} = 0 .$$

Because of the imcompressibility:

$U = \frac{A}{r}$ in zone 1 and $U = \frac{D}{r}$ in zone 3;

$\sigma_r = -P_o$ when r=a and r=d.

In zone 2:

$$\sigma_r = \lambda_p\cdot\left(\frac{\partial U}{\partial r} + \frac{U}{r}\right) + 2\cdot\mu_p\cdot\frac{\partial U}{\partial r} ;$$

$$\sigma_f = \lambda_p\cdot\left(\frac{\partial U}{\partial r} + \frac{U}{r}\right) + 2\cdot\mu_p\cdot\frac{U}{r} ;$$

$$\frac{\partial \sigma_r}{\partial r} + \frac{\sigma_r - \sigma_f}{r} = 0$$

On the borderline between zones the values of σ_r and U are continuous.

The solution of the equation shows that the inner wall movement is determined by the following factor:

$$[2 \cdot \mu \cdot \frac{d^2 - c^2}{d^2} - 2 \cdot \mu_p]$$

So, if μ_p (powder shear modulus) is small, the inner wall will move in outer direction. With growth of density μ_p grows too, and it changes direction of movement.

Inner wall movement direction for long tubes at the initial moment is independent from the inner wall thickness.

But the analysis made is approximate and explaines this phenomenon only in qualitative way. In order to make a more accurate determination of influence of powder and capsule material rheology on the capsule wall movement, we have developed the following model of the process.

When modelling the flow process of a powder medium we've used mathematical application of the theory of irreversibly compressible materials' forming based on the continuity hypothesis (theory of visco-plastic flow of incompressible media). The essence of the theoretical study of HIP process is to solve the following set of simultaneous equations:

equilibrium equations

$$\sigma_{ij,i} = 0 ,$$

where σ_{ij} - components of the stress tensor.

kinematic relations for deformation rate components

$$\xi_{ij} = 1/2 \cdot (v_{i,j} + v_{j,i}) ,$$

where ξ_{ij} - components of the deformation rate tensor;
v_i - rates of displacements.

continuity equation:

$$\frac{d \ln \rho}{dt} + \operatorname{div} \vec{V} = 0,$$

where ρ - density of the material ;
t - time .

tension stress tensor and deformation rate tensor constitutive equations:

$$S_{ij}=2\cdot\mu\cdot\eta_{ij};$$

$$\sigma_0=3\cdot k\cdot\xi_0,$$

where $S_{ij}=\sigma_{ij}-\delta_{ij}\cdot\sigma_0;$

$\xi_{ij}=\xi_{ij}-\delta_{ij}\cdot\xi_0;$

$\sigma_0=1/3\cdot\sigma_{ii}; \quad \xi_0=1/3\cdot\xi_{ii};$

δ_{ij} - Kroneker's symbol.

μ and k are certain functions of powder's density and temperature $\mu = (\rho, T)$, $K = (\rho, T)$.

On the powder/can borderline we have accepted a hypothesis about the equality of displacements. On the outer borderline of the can

$$\sigma_{ij}\cdot n_j=0,$$

where P - external pressure.

Heat flow equations are the following:

$$c\cdot\rho\cdot\left[\frac{dT}{dt}+v\cdot\frac{dT}{dX}\right]=\frac{d}{dX}\cdot\left[\varkappa\cdot\frac{dT}{dX}\right]-p\cdot\frac{dv}{dX},$$

where c - const is the heat capacity of unit mass;
ρ - density of the material;
T - temperature;
ϰ - termal conductivity.

Plasticity criterium is the following:

$$T^2/f_1^2+\sigma_0^2/f_2^2=\tau_s,$$

Boundary equations:

$$\sigma_n=\sigma_n(t);$$

$$T=T(t),$$

where t - time.

The equations presented form a complete set and enable us to reach solution describing the shrinkage of a plastic can.

We applied a serial programm "ISOFORM" for complex shape capsule calculation to the numerical simulation of the process. It is based on the FEM method and mathematical application of the theory of viscous-plastic medium flow and

enables to simulate the HIP process, in particular for the complex shape powder parts.

We have studied the regularities of shape changing of hollow parts under HIP. We simulated this process on the PC in application to tube-shape parts (Fig. 3). The part's height related to it's outer diameter as 1.5 to 1. The powder layer thickness , inner capsule wall thickness and ratio of powder and capsule strength were the variables of simulation. Coordinates of characteristic points A, B, C, D, before and after HIPing were compared, and the diameter shrinkage was determined on the basis of this data. Furthermore, we carried out the analysis of characteristic point B movement during HIP.

At Fig. 4 one can see the obtained values of relative shrinkage in the characteristic points as a function of ratio of shear yield strengths of powder and capsule materials.

The chosen range of relations includes values for powder superalloy HIPed in a steel capsule (Tsp/Tsc=7) and steel powder HIPed in a steel capsule (Tsp/Tsc=1).

The results achieved prove the fact that if the compacted powder had low deformation resistance, it densifies due to the inner wall movement in the outer direction (away from the symmetry axis).

The calculations have also showen that when the powder layer is thin relative to the outer wall (the case under consideration), the inner wall movement in the outer direction still exists.

So we have revealed a strong influence of ratio of powder and capsule strength properties on the character of inner wall movement.

The next point of our investigation was the influence of workpiece's dimensions on shrinkage regularities. It was carried out in application to HIP of powder superalloy in a steel can.

Fig. 5 shows relative shrinkage (in the characteristic points) as a fuction of relation of thickness of powder layer to that of the outer wall. The outer wall of the can in any case moves in direction to the symmetry axis. The inner wall movement direction changes with the powder layer growth on the contrary. Intersection point of A and B curves means that the inner wall is practically immobile. Deviation of relative shrinkage from zero in this particular case can be explained by the height shrinkage of can, and for enough cans of enough height it comes to naught.

Fig. 6 shows the influence of inner wall thickness on the character of diameter shrinkage. It is clear that, when the inner wall is thin enough, shrinkage under HIP reduces to cladding of the outer wall with the powder. In this case change of the outer wall dimensions is negligible.

Having analysed the point B behaviour during HIP, we succeed in formulation the following regularities:

1. Fig. 7 - influence of the "powder/can" ratio of strength properties on the movement of the "powder/inner wall" borderline.

2. Fig. 8 - influence of the powder layer thickness on the movement of the "powder/inner wall" borderline.

3. Fig. 9 - influence of the inner wall thickness on the movement of the "powder/inner wall" borderline.

Results of the investigation prove the avobe mentioned supposition about the alternative movement of powder/can borderlines. It was shown that properties of powder and can materials, final density and initial thickness of powder layer determine the borderline movement direction. Furthermore, fig. 9 proves the conclusion, concerning the fact that the direction of the inner wall movement in the initial moment of time is independent from this thickness.

APPLICATIONS AND CONCLUSIONS

The above stated regularities were successfully applied to production of hollow parts, such as hollow jet engine shafts, thin-wall combustion chamber body-parts, christmas tree body-parts with a corrosion-resistant cladding. We succeed in ruling the shrinkage by means of special capsule design, i. e.:

1. Decrease the metal consumption when producing hollow shafts and obtain "near-net-shape" workpieces due to minimizing of the diameter shrinkage;

2. Obtain a complex "net-shape" outer surface of thin-wall body-parts due to preferential inner wall movement.

3. Achieve a required configuration of the borderline between powder and thick-wall body-part frame.

4. Decrease time and cost of R & D.

The developed software for HIP process is included in the capsule CAD system, worked out at the NPO VILS, realized in dialogue regime on the PC, and can be used by technologists in their practical work.

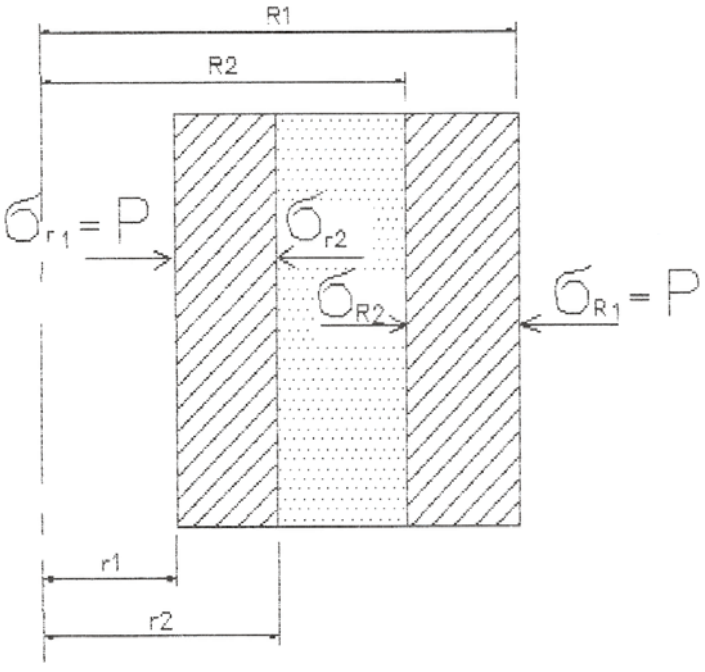

Fig.1 Scheme of stresses in a tube workpiece under HIPing.

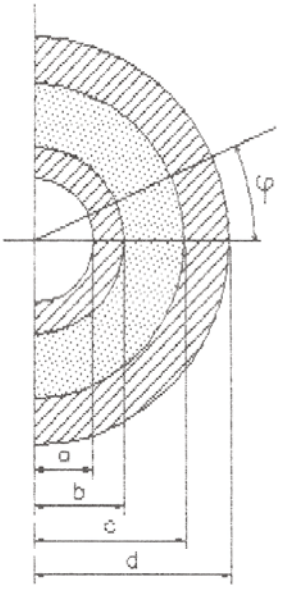

Fig.2 Scheme of a three-layer tube (for the Lame's problem).

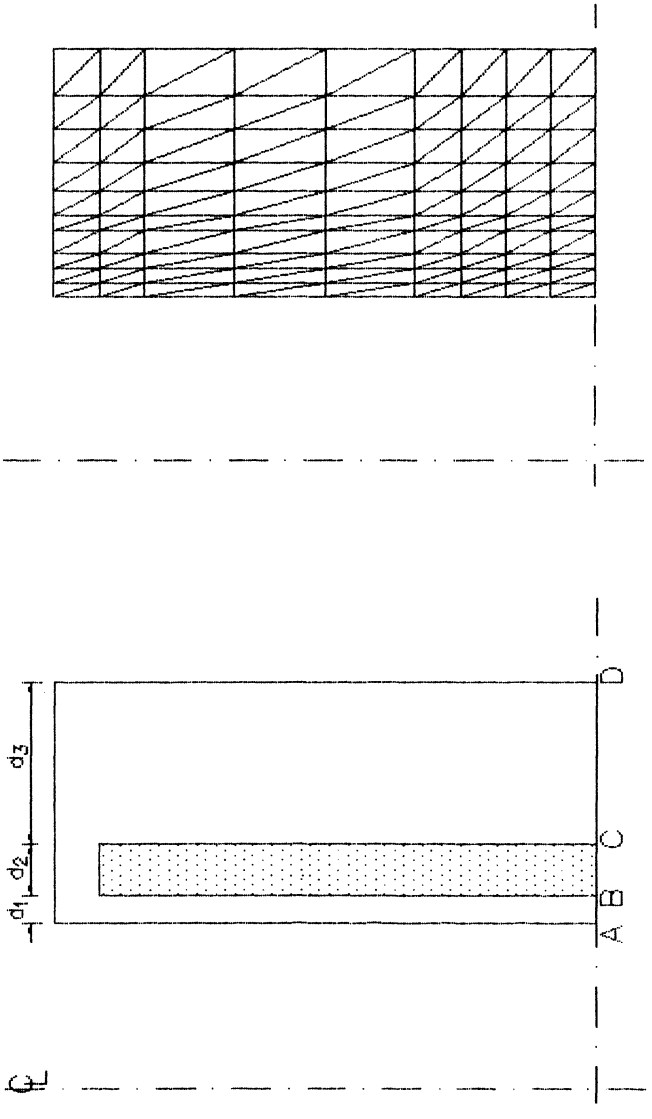

Fig.3 The workpiece inder investigation and its FEM model.

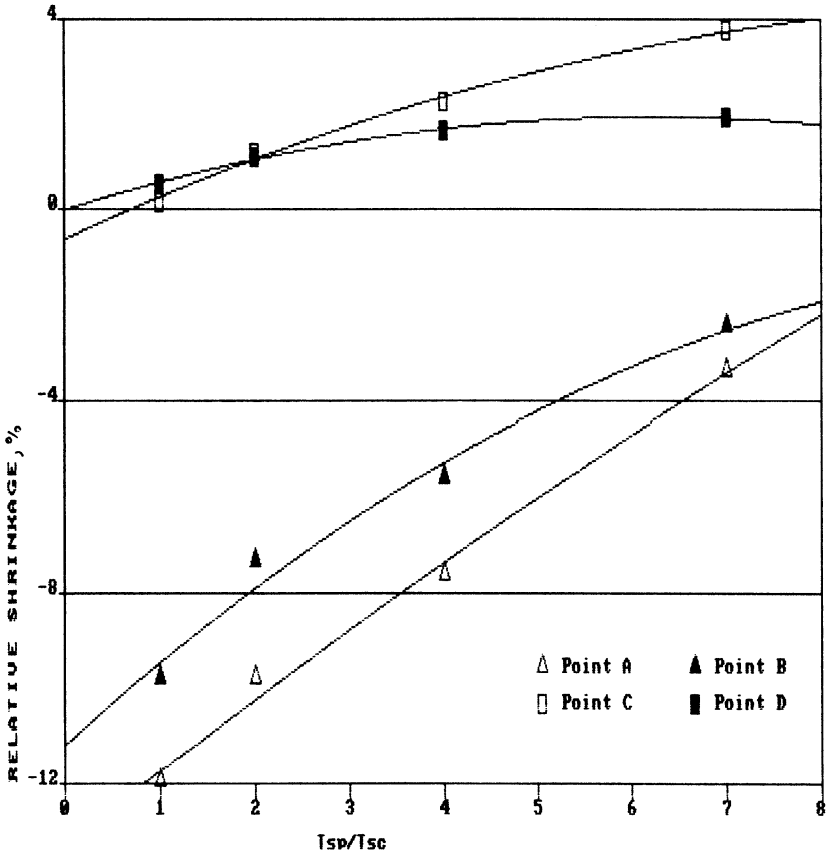

Fig. 4 Relative shrinkage in A,B,C,D points as a function of yield strength ratio of powder (Tsp) and can (Tsc).

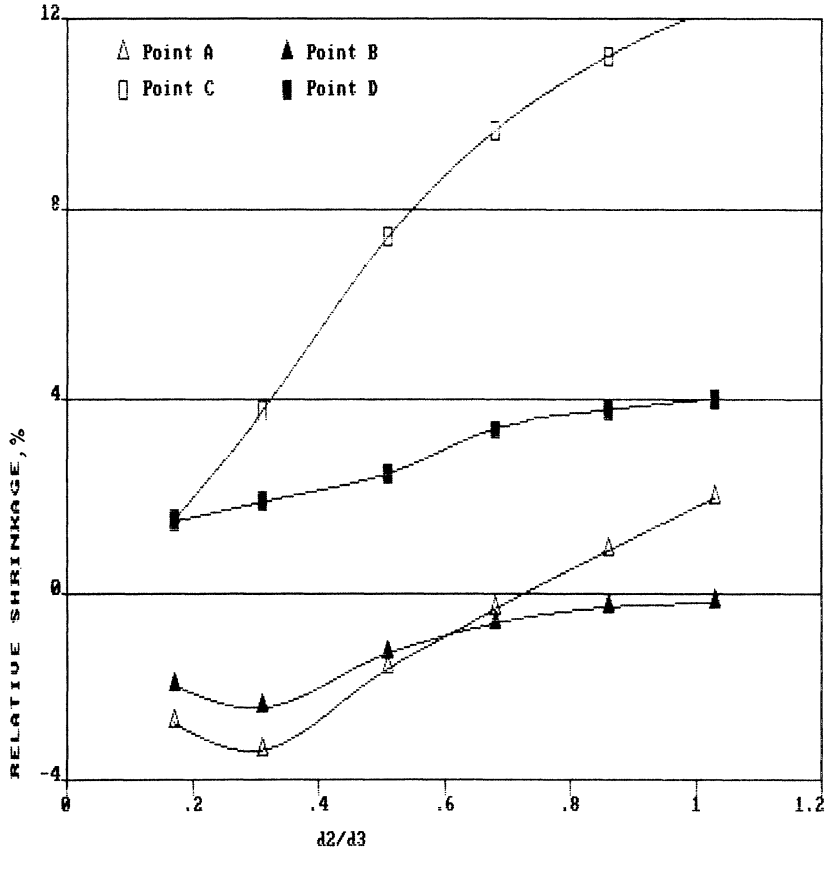

Fig. 5 Relative shrinkage in A,B,C,D points as a function of ratio of thicknesses of powder layer (d2) to that of outer wall (d3) (thicknesses of the outer and inner wall relate as 0.17).

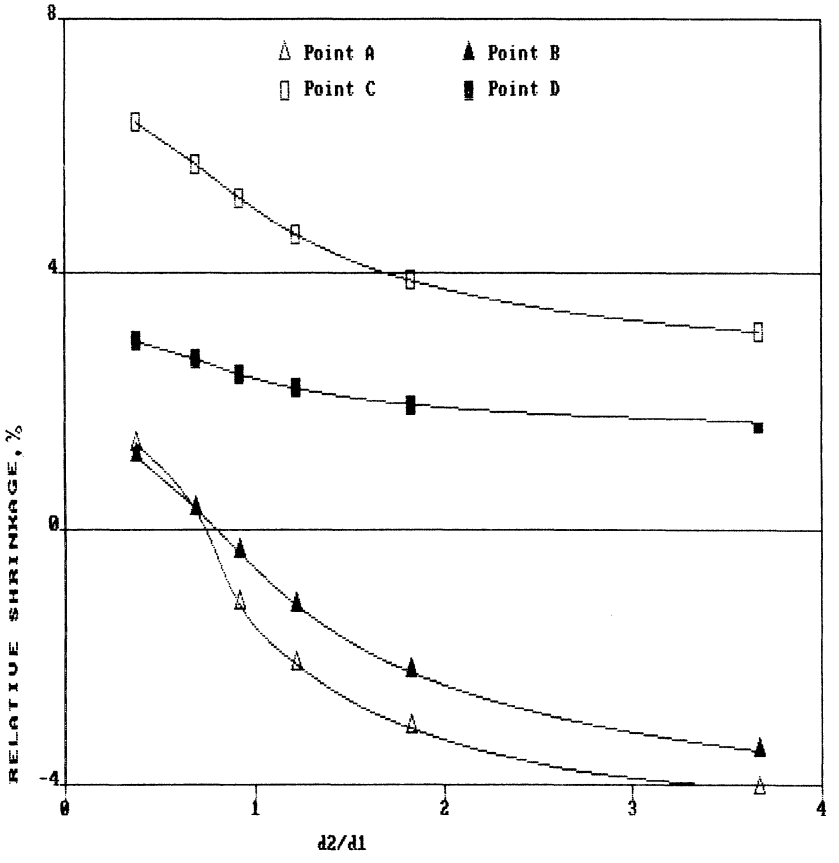

Fig.6 Relative shrinkage in A,B,C,D points as a function of ratio of thicknesses of powder layer (d2) to that of inner wall (d1) (thicknesses of powder layer and outer wall relate as 0.3).

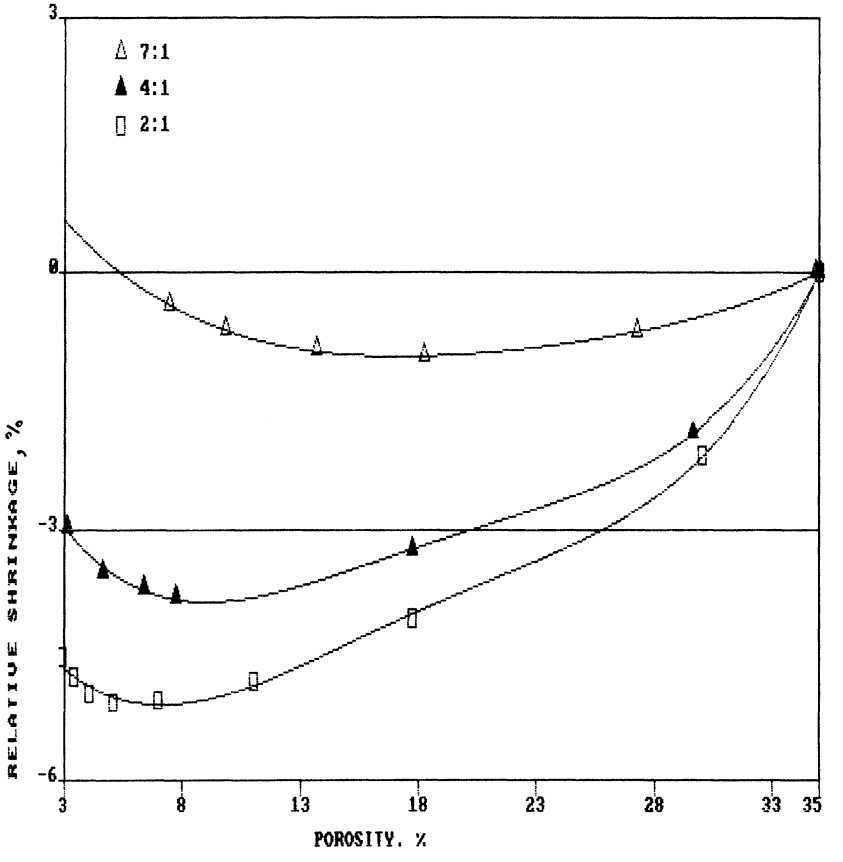

Fig. 7 Relative shrinkage in point B (on the powder/inner wall borderline) as a function of porosity, with various Tsp/Tsc ratios (thicknesses of powder layer and outer walls relate as 0.3).

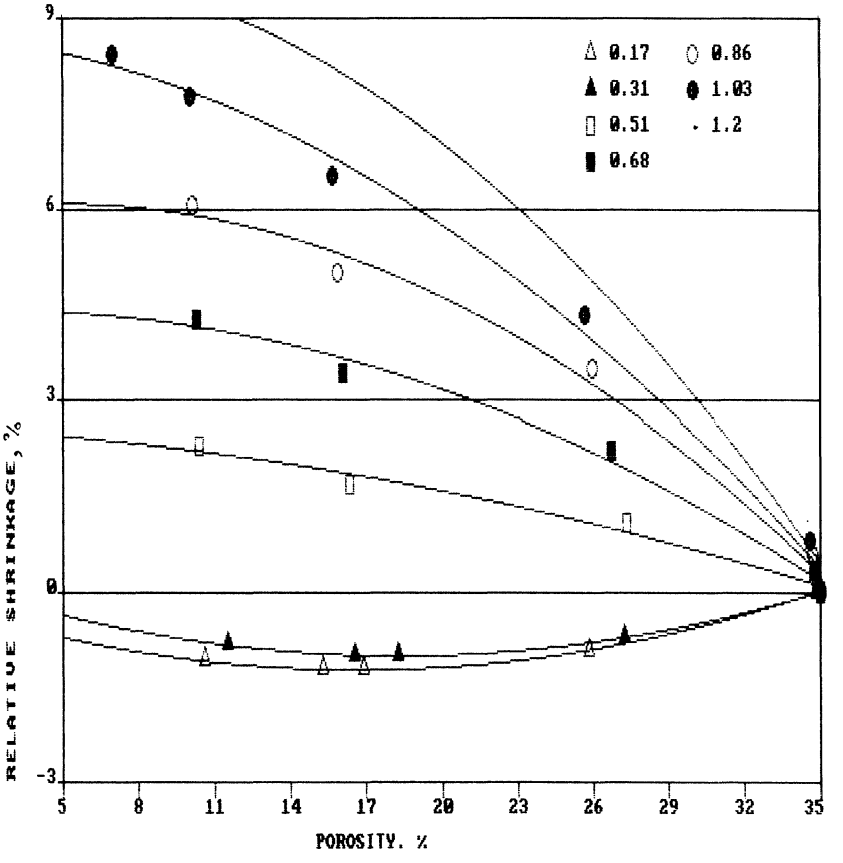

Fig. 8 Relative shrinkage in point B (on the powder/inner wall borderline) as a function of porosity, with various ratios of thicknesses of powder layer (d2) and that of outer wall outer wall (d3) (thicknesses of the outer and inner walls relate as 0.17).

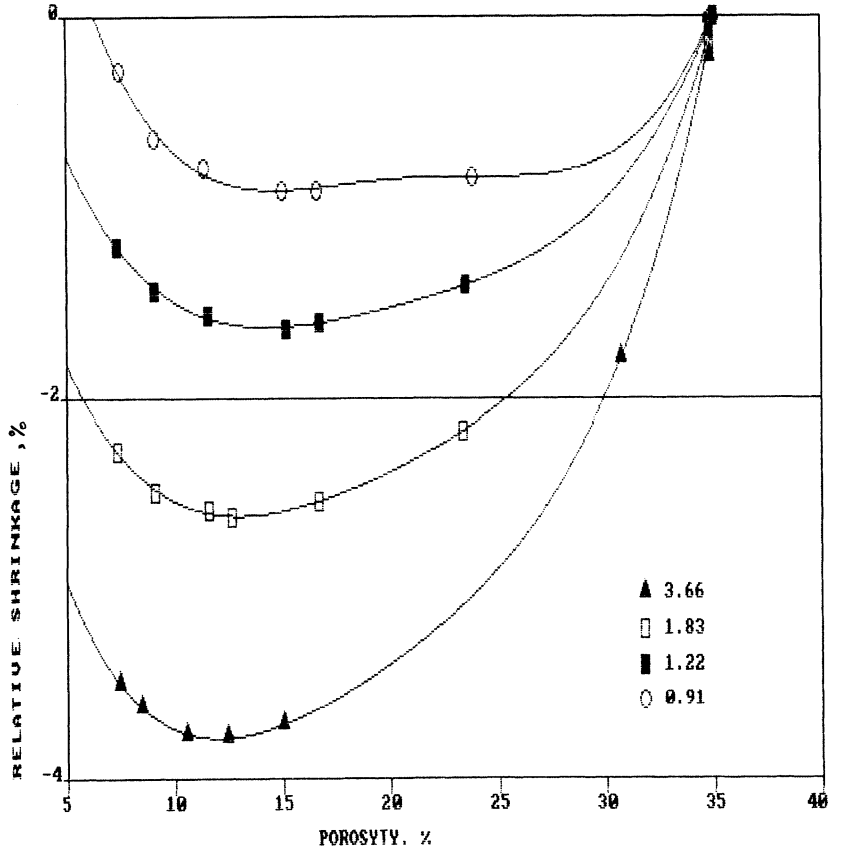

Fig. 9 Relative shrinkage in point B (on the powder/inner wall borderline) as a function of porosity, with various ratios of thicknesses of powder layer (d2) and that of outer wall inner wall (d1) (thicknesses of powder layer and outer and wall relate as 0.3).

SYNTHESIS OF TiAl INTERMETALLIC COMPOUNDS BY HIP-REACTION SINTERING

Atsushi Kakitsuji and Hiroki Miyamoto
Osaka Prefectural Industrial Technology Research Institute
Enokojima, Nishi-ku, Osaka, JAPAN

ABSTRACT

TiAl intermetallic compounds were fabricated by HIP-reaction sintering. Elemental powder mixtures of titanium and aluminum with composition Ti-45 to 55 at%Al were HIP treated after encapsulation with pyrex glass tube. At 1473K treatment, duplex phase of Ti_3Al and TiAl was detected in all compositions, but there was no lamellar structure typical for TiAl intermetallics. And as HIPing temperature rises, Ti_3Al/TiAl laminated structure was observed in the specimens of Ti-rich composition, which were almost fully densified and had a fine grain structure with mean size about 30μm. The DTA analysis showed exothermic peak at 923K, which indicates that the self propagating reaction takes place at the melting temperature of aluminum. It was considered that several compounds of Ti-Al system were synthesized by self propargating reaction at the first stage and densified by subsequent hot isostatic pressure and finally transformed to laminated structure by the effect of heat treatment.

INTRODUCTION

The TiAl intermetallic compounds is expected to be potential for high temperature application because of its low density and high yield strength at elevated temperatures (1). However, the lack of room temperature ductility has prevented using practically. To improve low temperature properties, various metallurgical attempts have been made such as grain refinement (2), distribution of second phases (3), and addition of third element like manganese (4) or vanadium (5). In the grain refinement, one possibility is powder metallurgy technique (6) together with thermo-mechanical treatment (7). Powder metallurgy techniques have the advantages of near-net shaping and easy microstructural control. Especially, HIP-reaction sintering, starting from elemental powders, has further advantage that densification is coincident with synthesis of TiAl intermetallics by the high temperature self propargating synthesis, and moreover, in this system, it can be easy to form net-shaping in the green body because of aluminum ductility.

In this present work, we tried to synthesize TiAl intermetallic compounds with dense and fine structure by HIP-reaction sintering. Special

attention was paid to the relationship between composition and HIP treatment temperature.

EXPERIMENTAL PROCEDURE

The raw materials of this study were elemental powders; titanium with two different particle sizes (-150 and -45μm) and aluminum (-70μm). These powders were weighed to nominal compositions shown in table 1, and blended using the ball mill without effect of the mechanical alloying. The powder mixture were then uniaxially compacted at room temperature into cylindrical pellets in diameter 16mm.

Tablel Nominal compositions of aluminum for this study.

mass%Al	31.6	34.2	36.0	37.9	40.8
at.%Al	45.0	48.0	50.0	52.0	55.0

The pellets coated with boron nitride powder were encapsulated in the borosilicate glass tube, after evacuation at 673K. HIP treatments were carried out under pressure of 198MPa at temperatures of 1073, 1273, 1473, 1523, and 1573K. In all treatments, gas pressure began to apply at 1073K, where the glass used in this investigation was softened enough.

Density determination, X-ray diffractometry analysis, and microscopic examination were carried out on the HIP'ed specimens.

The mechanical properties examined were Vickers micro hardness and room temperature compression test. The compression test was carried out on an Instron type tension/compression machine driven $_{2}$crosshead speed of 0.5mm/min. The specimens had a cross section of 3x3mm^{2} and gage length of 5mm, which were all electropolished after grinding by the emery paper.

RESULTS AND DISCUSSION

HIP-reaction sintering of stoichiometric TiAl

Compositions of titanium (particle size ;-150μm) and aluminum in equal atomic proportion to form stoichiometric intermetallic compound TiAl was

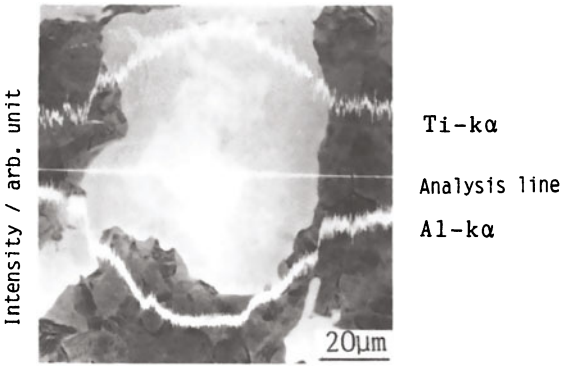

Fig.1 SEM micrograph and X-ray line analysis of Ti-50at%Al HIP'ed at 1473K.

HIP treated at 1473K. X-ray diffraction pattern of compact and HIP'ed specimen shows that the peaks of the starting materials were disappeared, and two kinds of another peaks were detected. One was TiAl as the matrix phase, and the other Ti_3Al, second phase. SEM images of this sample showed the duplex structure, with few pore observation. The X-ray line analyses revealed that this structure consisted of Ti-rich region surrounded by Al-rich matrix (Fig.1). Consequently, Ti-50at%Al specimen fabricated by HIP reaction sintering at 1473K has the nonhomogenous duplex phase structure with Ti_3Al dispersed in TiAl matrix in the form of large spherical shape. In addition, the size of Ti_3Al is smaller than about 150μm, corresponding to that of titanium powder of raw material. So, titanium powder with grain size -45μm was selected as Ti raw material and HIP treated at 1473K. Optical micrographs of this sintered specimen are shown in Fig.2(b).

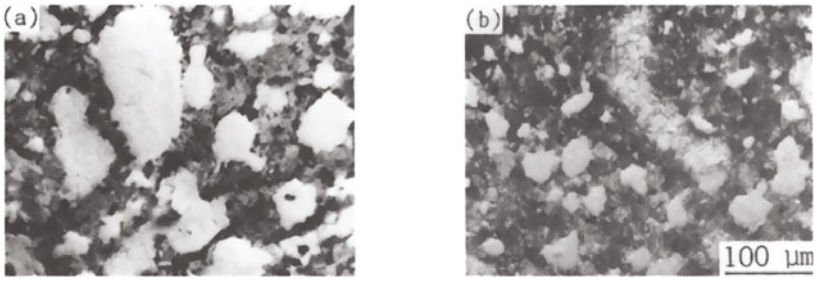

Fig.2 Optical micrographs of Ti-50at%Al HIP'ed at 1473K.
Ti powder size of raw material; a) -150um b) -45um

It is showed that the size of titanium powder affects the size of Ti_3Al particle and accordingly the homogeneity of sintered structure. This result suggests that more homogenous structure with small precipitated Ti_3Al particle could be obtained, if much finer titanium powder was used as raw material.

Effect of sintered temperature and composition on microstructure

It has been reported that TiAl intermetallic compound with duplex structure, which show $TiAl/Ti_3Al$ laminated structure, have more ductility than that with single phase structure, and that Ti-rich composition have more ductility than stoichiometric composition (8). But, as mentioned previous section, Ti-50at%Al specimen HIP'ed at 1473K had the duplex structure but not laminated structure. So, the effect of HIP temperature and deviation of compositions from stoichiometry on the microstructures was examined. Table2 shows the phases appeared in HIP'ed TiAl intermetallics with aluminum contents of 45, 48, 50, 52, and 55 at% and temperature at 1073, 1273, 1473, 1523, and 1573K. In this table, upper end shows the major phase and lower one shows the second phases determined from the height of the main peaks. At lower temperatures than 1273K, in the specimen with Al-rich compositions, $TiAl_2$ was detected as major phase and other phases were generated. As HIPing temperature rises, matrix phases change to TiAl, and second phase changes to the phase expected by Ti-Al binary equilibrium phase diagram according to the nominal composition.

Optical micrographs of sintered sample HIP'ed higher than 1423K were shown in Fig.3. These are result of the finer titanium powder (-45μm) used as raw material. At 1473K, in all compositions, similarly shown in Fig.1 and 2, Ti_3Al was precipitated island-likely in TiAl matrix. As the treatment temperature rises, drastic changes are occurred in microstructures. That is to say, $TiAl/Ti_3Al$ lamellar structure was observed in some grains except

Table2 Schematic phase diagram of Ti-Al system detected for this study.

1573					TiAl
1523	TiAl + Ti_3Al				
1473					
1273			TiAl + Ti_3Al		TiAl + $TiAl_2$
1073	TiAl + Ti_3Al	TiAl + $TiAl_2$	$TiAl_2$ + TiAl	$TiAl_2$ + Ti_3Al	$TiAl_2$ + TiAl + Ti_3Al + $TiAl_3$
Temp	31.6	34.2	36.0	37.9	40.8
(K)	Al contents / mass%				

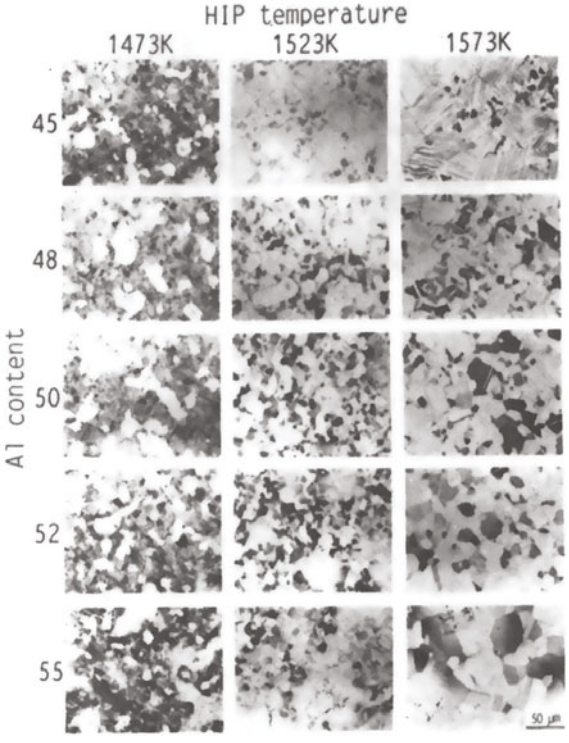

Fig.3 Change of microstructure by HIP temperature and compositions.

Ti-55at%Al sample. And at 1523K, grain coarsening was observed in all compositions. These specimens had the tendency that grain size with lamellar structure refines and the quantity ratio of duplex phase to single one decreases with increasing aluminum content. In Ti-50 and 52at%Al specimen HIP'ed at 1523K, mean grain diameter of laminated and non-laminated structure was eventually equalized in size about 30μm.

Figure4 shows the result of differential thermal analysis of Ti-50at%Al compact in Ar gas flow. At temperature around 923K exothermic peak was observed. This peak is caused by the self-propargating high temperature synthesis (SHS) reaction, and corresponds to melting point of aluminum (933K). This means SHS reaction take place in the vicinity of melting point

of aluminum. And at this temperature, glass tube is not softened sufficiently to act as seals, so gas pressure was not applied yet. It is assumed from these results that, in this process, at first several compounds of Ti-Al system were synthesized by SHS reaction, next densified by subsequent isostatic pressure and finally transformed to TiAl/Ti_3Al lamellar structure.

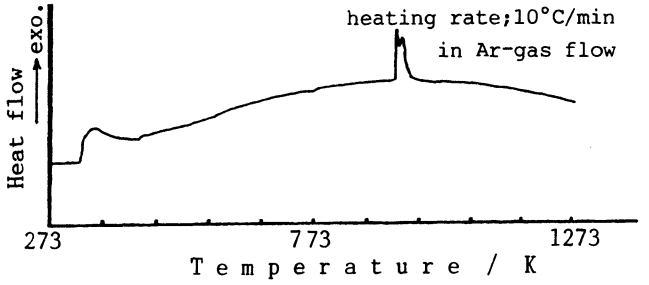

Fig.4 DTA curve of Ti-50at%Al compact.

Mechanical properties of reaction sintered TiAl

Figure5 shows the aluminum content dependence of the hardness of TiAl HIP'ed at 1073, 1273, 1473, and 1573K. Though the hardness of the samples treated at low temperatures ware not affected by aluminum content, minimum value was showed at stoichiometric composition in specimen HIP'ed at 1573K. In this sample, it is considered that increase of hardness in Ti-rich composition was caused by precipitation hardening of laminated Ti_3Al, and in Al-rich was deviation from stoichiometry typical for intermetallics.

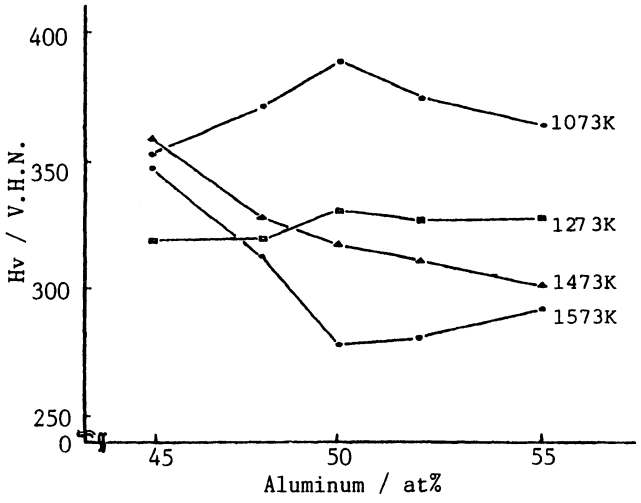

Fig.5 Hardness change of TiAl HIP'ed at several temperature.

The results of room temperature compression were shown in Fig.6. It seems that samples with lamellar structure have better ductility than no-laminated structure. In Ti-50 and 52at%Al samples HIP treated at 1573K, fracture strain more than 20% was observed at room temperature. In the TiAl intermetallic compounds, the fracture strain in compression is much larger than that in tension (9). However, the observed value indicates good tensile ductility at room temperature.

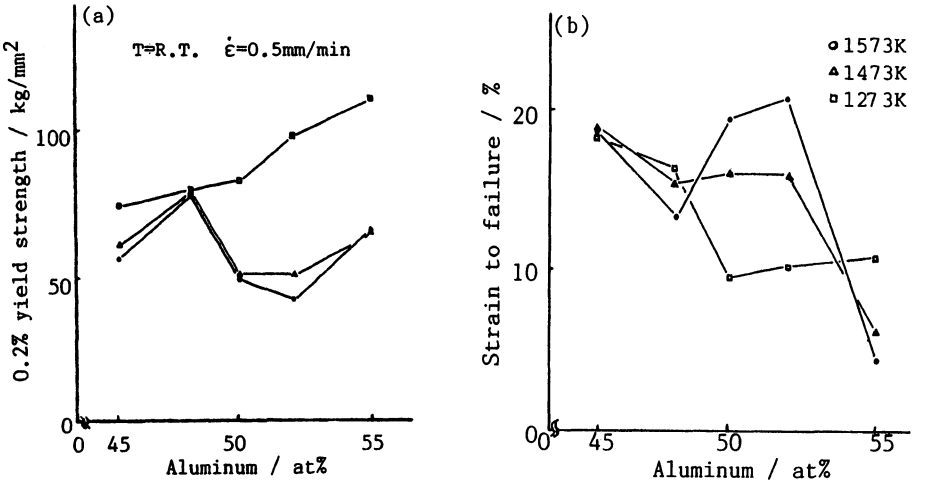

Fig.6 Effect of aluminum content on compressive properties.
a) 0.2% yield strength b) compressive strain to failure

SUMMERY

TiAl intermetallic compounds which contain aluminum from 45 to 55 at% were synthesized by HIP-reaction sintering using pyrex glass as seals. Powder mixture compact were capsuled and HIP'ed to give sintered materials of densified and fine grain structure. Sintered specimens were investigated by X-ray analysis, microscopic observation and room temperature compression test. Following results were derived.

1. Almost fully densified sintered body with laminated TiAl/Ti_3Al duplex structure was derived at 1523K treatment.
2. In this process, the steps of synthesis of TiAl intermetallic compounds was as follows;
   1). Synthesis of several Ti-Al compounds by SHS reaction
   2). Densification by isostatic pressure
   3). Phase transformation to TiAl/Ti_3Al lamellar structure by subsequent heat treatment effect
3. The fracture strain in the compression test at ordinary temperature was reached at 20%.

REFERENCES

1. D.Shechman, M.J.Blackburn and H.A.Lipsitt, Met.Trans., 5(1974),1373
2. M.Nobuki and Y.Asai,Proc. of 97th Meeting of the JPN Inst. of Metals, (1985),474
3. T.Tsujimoto, J. JPN Inst. Met.,36 (1986), 162
4. K.Hashimoto, H.Doi and T.Tsujimoto, Proc. Symp. on 'Plastic deformation of ordered alloys and intermetallic compounds', (1986), 17, Sendai, JPN Institute of Metals
5. W.Blackburn and M.P.Smith, U.S. Patent No.4292077
6. M.Nakamura and Y.Kaieda, Powder Met. 31 (1988), 201
7. J.B.McAndrew and M.P.Smith, U.S.Patent No.4294615
8. Y.W.Kim, J.Met, 41(1989), No.7, 24
9. T.Tsujimoto,K.Hashimoto,M.Nobuki and H.Suga, J.JPN Inst. Met.,48(1984), 435

FRACTURE TOUGHNESS OF ALUMINA-STEEL COMPOSITES PRODUCED BY HOT ISOSTATIC PRESSING

JENS BENDIXEN[1] & ANDREAS MORTENSEN[2]
1) Department of Industrial Metallurgy, Danish Technological Institute, DK-2630 Taastrup, Denmark
2) Department of Materials Science and Engineering Massachusetts Institute of Technology Cambridge, MA 02139, USA

ABSTRACT

Samples of eutectoid steel reinforced with alumina particles 200 to 300 μm in diameter were fabricated by hot isostatic pressing. The fracture behavior of the materials was examined by three-point bend tests on chevron-notched bars and instrumented impact tests. Significant matrix/particle decohesion was observed, indicating weak particle/matrix interfaces. Metallographic examination of the as-produced material revealed the presence of cracks along the particle/matrix interface after etching with nital. It is shown that the formation of these interfacial cracks in the as-produced composite may result from the volumetric expansion of the matrix upon transformation from austenite during processing.

INTRODUCTION

The reinforcement of steel with hard ceramic particles may result in an attractive material for use in abrasive wear environments [1,2,3]. As in most metal matrix composites, one of the main obstacles in the development of such materials is the reduction of toughness that results from the addition of a brittle ceramic to the metal. In this paper, we present results from a first exploration of the processing and fracture mechanisms of these materials, using an alumina particle reinforced eutectoid steel fabricated by powder metallurgy.

MATERIALS AND METHODS

Materials

HIP was used to produce the final dense composite material. Commercial water atomized iron powder (Atomet 25, Quebec Metal Powder, Canada) and carbon powder (graphite KS 15, Lonza) were used to produce a eutectoid matrix containing 0.8 wt% carbon. The reinforcing particles were alumina powder (Rhinalox) with an average diameter of 200-300 μm. The alumina occupied a volume fraction of 22 % in the composite. Three types of alumina powder were used: a white 99.6% pure alumina (designated as W), a brown 96.2% pure alumina, with impurities mostly of titanium oxide (designated as B) and a 96.2% pure alumina with titanium oxide impurities received after thermal treatment to cure and smoothen sharp edges and cracks at the powder surface (designated as C). Iron, carbon and alumina powders were blended in

ethanol, packed into mild steel containers, and dried for 18 hours under vacuum at 323 K. The containers were then evacuated at 973 K for 15 hours, and sealed, still in vacuum. HIP was performed at two temperatures, namely 1323 K (designated as L) and 1393 K (designated as H) at a pressure of 200 MPa for 30 mn. After pressing, the samples were allowed to cool slowly in the HIP press to 573 K in about 90 mn.

Bend test

Chevron notched three-point bend specimens, of square cross section 7 mm wide, with a 60 degree notch 0.5 mm wide were machined from the consolidated specimens. Testing was performed in an Instron universal test machine, at a crosshead speed of 0.05 mm per minute. Load point displacement was recorded with a linear variable dynamic transducer. Crack position was monitored during the test by observation of the chevron notch surface with an optical microscope at a magnification of 40. Loading-unloading cycles were performed during the tests, and used to construct a compliance calibration curve. This curve was then used to determine crack position from the compliance with a better precision than with the individual in-situ microscope measurements. The energy spent propagating the crack in each loading-unloading cycle was then divided by the increment in crack area, to obtain the fracture energy of the material in the present test configuration, following the procedure first proposed by [4]. Two to four specimens were used for each material. The ligament remaining on tested chevron-notched samples was broken after quenching in liquid nitrogen to differentiate its fracture surface from that generated during the test.

Impact test

Instrumented impact testing with inversed test geometry were performed at VTT (Technical Research Centre of Finland). The specimens were unnotched and with a square cross section of 7 mm. The impact velocity was 2.8 m/s and the impact energy was 146.4 J. Load and energy versus displacement and time were recorded. The test was repeated three times for each material.

RESULTS

Table 1 shows the reinforcement type and HIP temperatures. Samples are free of large voids, and the matrix is pearlitic with a lamellar spacing around 0.5 μm, Fig. 1. The samples exhibited considerable ductility in the bend tests, with the implication that resulting fracture data are at best a semi-quantitative indication of the material's toughness. Fracture energies in the bend test showed a complex dependence on crack position which varied with the nature of the material. This is most likely a result of the extensive plastic deformation that accompanied crack propagation in the tests, as well as the large particle size in relation to the test specimen size.

TABLE 1.
HIP temperatures and reinforcements
(* not in bend test)

Alumina type	HIP temperature	
	1323 K (L)	1393 K (H)
White (W)	WL	WH*
Brown (B)	BL*	BH
Cured (C)	CL	CH

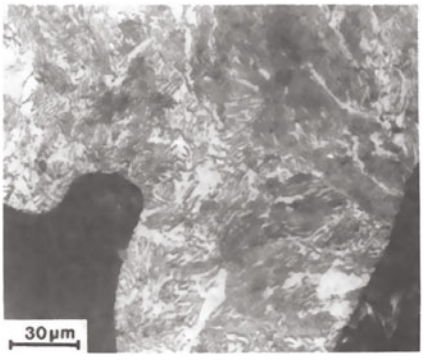

Figure 1. Microstructure in material designated WL.

To compare the various materials, therefore, the fracture energy spent propagating the crack from the first to the last unloading-loading cycle was computed, and is given in Fig.2. It is found that the difference in average fracture energy between the four materials in the bend test is within the range of variation for each material, indicating that there is no significant difference in fracture energy between the materials investigated here.

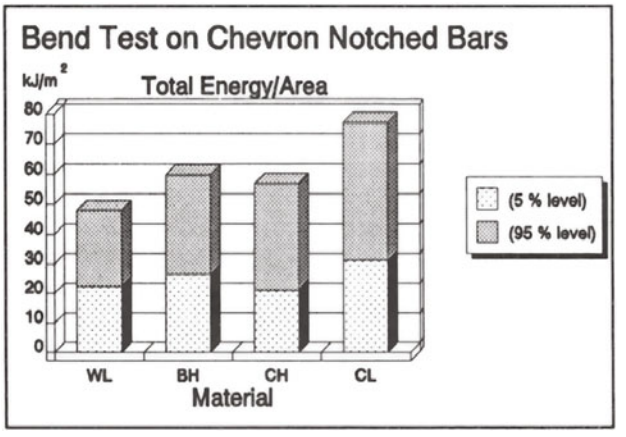

Figure 2. Fracture energy spent propagating the crack from the first to the last unloading-loading cycle in the bend test. 90 % confidence interval.

Fracture surfaces, Fig.3 and transverse cuts through the crack path, Fig.4, show that the crack propagates preferentially at the particle/matrix interface. In-situ monitoring of the intersection of the crack with the chevron ligament surface revealed that matrix cracking is preceded by the formation of voids at the particle/matrix interfaces. The extreme weakness of the particle/matrix interface was further revealed in one sample where a particle was observed to fall out of the crack during a test. A few broken particles were also found on the fracture surface. Given the weak particle/matrix interface, it seems most plausible that these particles were cracked during fabrication of the material.

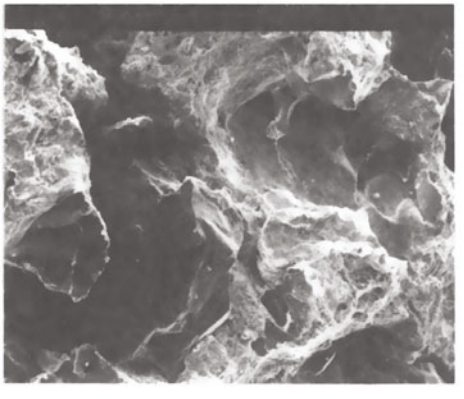

Figure 3. SEM of fracture surface showing particle/matrix interfacial debonding in material designated CH in the bend test.

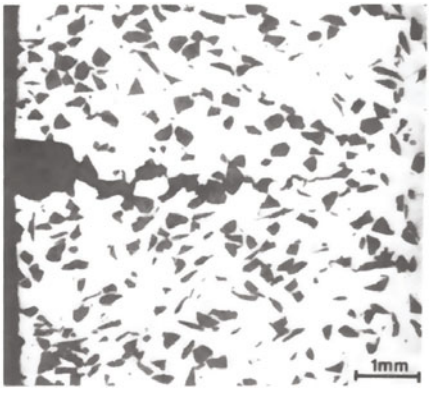

Figure 4. Transverse cut through the crack path in material designated BH in the bend test.

Examination of the as-processed material microstructure in the scanning electron microscope reveals that interfacial debonding might have been present in the material before testing, since a crack of width 0.1-0.2 μm is found at the interface all around the particles in polished flat metallographic samples etched with Nital, Fig.5. The crack around the particles is running along the interface between the particle and the ferrite, while the laminar cementite in the pearlite matrix mostly is in contact with the particles. Yet examination of non etched and Alkaline Sodium Picrate etched samples did not reveal any cracks. This could be because the Nital etchant has made the crack in a very reactive interface reaction layer or, alternatively, because polishing covered an existing crack by smearing a layer of the soft matrix material over the crack, which was removed by Nital upon etching of the ferrite. Additional microporosity was also found within the matrix, Fig.5.

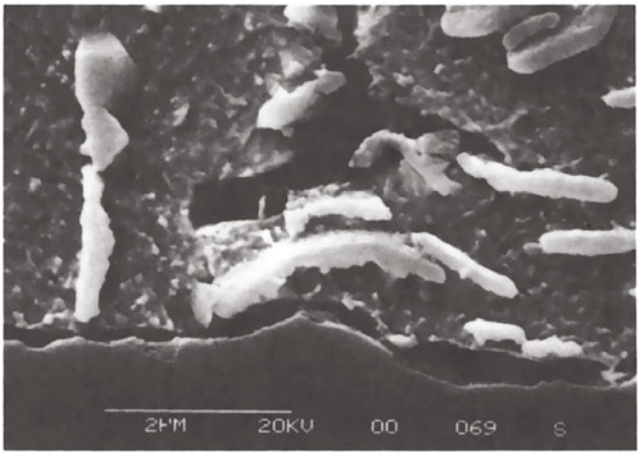

Figure 5. SEM of the particle/matrix interface, revealing interfacial decohesion in the as-processed material. Material Designated BH.

The fracture energies obtained with the impact test are given in Fig.6. As for the bend test, it is found that the difference in average fracture energy between the six materials is within the range of variation for each material. In the case of CH and CL the variation is most likely caused by large internal flaws in the material since some of the test bars did not break in the area where the applied stress was largest.

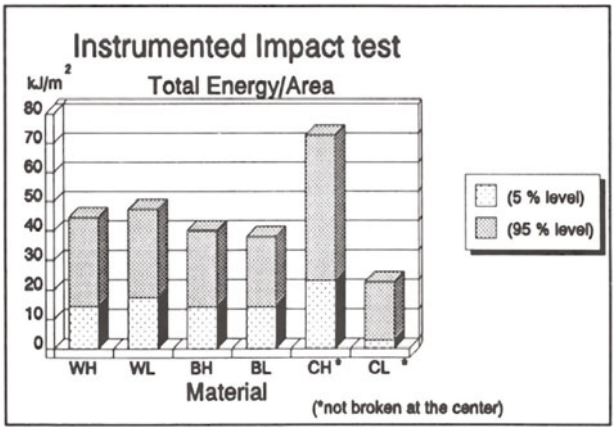

Figure 6. Fracture energy in impact test. 90 % confidence interval.

DISCUSSION

Interfacial decohesion in the as-processed material can be explained by the austenite to pearlite phase transformation during cooling from the pressing temperature at around 1000 K, coupled with a low interface strength at that temperature. The low cooling rate C ($\leq$ 1 K/s), of the samples corresponds to a strain rate in the matrix of about $\Delta\alpha_s C \simeq 5 \cdot 10^{-6}$ s^{-1} where $\Delta\alpha_s = 5 \cdot 10^{-6}$ K^{-1} is the difference in Coefficient of Thermal Expansion (CTE) between austenite and alumina. The flow stress of austenite at this strain rate is around $5 \cdot 10^{-4}$ G where G is the shear modulus of austenite [5]. This generates a compressive elastic strain of about 10^{-4} - 10^{-5} in the particle at the eutectoid temperature. The steel matrix then transforms to pearlite, and in doing so it expands by 2.9 vol.% [6]. This is much greater than the residual elastic strain in the particle due to contraction of the austenite, so interfacial decohesion takes place upon formation of pearlite, resulting in a crack of width about 0.01 times the particle radius. Thereafter, the pearlite shrinks more than the alumina, which reduces the interfacial gap width. The shrinkage strain of the pearlite is about $0.01 = a_{\alpha 1}$ [7], while that of the alumina is $6 \cdot 10^{-3} = a_{\alpha 2}$ [8] between 1000 K and room temperature. The final interfacial gap width in the material is then $(0.01 - a_{\alpha 1} + a_{\alpha 2}) = 0.006$ times the particle radius, i.e., 0.6 to 0.9 μm for particle radii ranging form 100 to 150 μm. This is slightly larger than, but of the same order of magnitude as, measured gap widths, which were 0.1 to 0.2 μm. The smaller experimental gap widths may be due to matrix flow after transformation to pearlite upon cooling in the pressurized HIP apparatus ($\approx$ 10 MPa at 1000 K), some amount of interfacial cohesion and the fact that the alumina particles are not spherical as assumed in the present interpretation. These results imply that alternative processing or greater interface strength are needed to fabricate steel matrix composites. Possible alloying additions that may increase interface strength can be inferred from the literature on inclusions in steel, and include Cr, Mo and Ti [9, 10, 11].

CONCLUSIONS

Particle/matrix interface bonding in these densified alumina-steel composites was tested by means of the chevron notch fracture toughness test method and instrumented impact tests. The chevron notch test revealed that failure is accompanied by extensive plastic deformation of the matrix and interfacial decohesion. Examination of the material microstructure revealed that the weak interfaces might be a result of a gap at the interface in the as-processed material. We interpret this gap as resulting from matrix expansion upon transformation from austenite to pearlite together with low interfacial bond strength at the transformation temperature. Calculations show that this cause can account for the measured gap widths.

ACKNOWLEDGEMENTS

This work was supported by a grant from The Danish Technology Council, Danit A/S, Grundfos International A/S and The Nordic Fund for Technology. Assistance from Pascal Metenier in conducting the chevron notch fracture tests is gratefully acknowleged as well.

REFERENCES

1. Parse, J.B., Semi-Solid Slurry Processing of Ferrous Matrix-Particulate Composites by Mechanical and Electromagnetic Stirring, M. Sc. Thesis, Department of Materials Science and Engineering, Massachusetts Institute of Technology, May 1985.
2. Chen, M., Kattamis, T.Z., Chambers, B.V. and Cornie, J.A., Processing and Abrasive Wear Resistance of Cast TiC-Ferrous Matrix Particulate Composites, Engineered Materials for Advanced Friction and Wear Applications, Conference Proceedings, F. A. Smidt and P. J. Blau, eds., ASM International, 1988, p.63.
3. Kattamis, T.Z. and Suganuma, T., Materials Science and Engineering, 1990, A128, p. 241-252.
4. Barker, L.M., Therory for Determining K_{Ic} From Small, non-LEFM Specimens, Supported by Experiments on Aluminium, Int. Journ. of Fracture, 1979, 15 (6), 515-536.
5. Frost, H.J. and Ashby, M.F., Deformation-Mechanism Maps, Pergamon Press, Oxford, 1982. chapter 5, p. 60.
6. Thelning, K.E., Steel and its Heat Treatment, 2nd ed., Butterworths, London, 1984, p. 584.
7. Smithells Metals Reference Book, sixth edition, Brandes, E. A. (editor), Butterworths, London, 1983, Section 14, p. 24.
8. Kingery, W.D., Bowen, H.K. and Uhlmann, D.R., Introduction to Ceramics, 2nd ed., John Wiley & Sons, New York, 1976, p. 591.
9. Van Vlack, L.H., The Metal-Ceramic Boundary, Metals Engineering Quarterly, ASM, nov. 1965, p. 7.
10. Fischmeister, H.F., Navara, E. and Easterling, K.E., Effects of Alloying on Structural Stability and Cohesion between Phases in Oxide/Metal Composites, Metals Science Journal, 1972, vol.6, p. 211.
11. Easterling, K.E., Fischmeister, H.F. and Navara, E., The Particle-to-Matrix Bond in Dispersion-Hardnened Austenitic and Ferritic Iron Alloys, Powder Metallurgy, 1973, Vol. 16, No.31, p. 128.

5. BONDING

HIP-BONDING OF ADVANCED STRUCTURAL MATERIALS AND SOME RELATED INTERFACIAL PHENOMENA

DETLEV STÖVER
Forschungszentrum Jülich GmbH, Institut für Angewandte Werkstofforschung, Postfach 1913, D-5170 Jülich, Germany

ABSTRACT

Bonding of complex structured materials is an unique applicational niche within the HIP process. Selected examples of metal-metal, ceramic-ceramic and metal-ceramic joinings are described. The resulting mechanical properties of the bond and the metallographic characterization are given with respect to the HIP parameter. Oxide Dispersion Strengthened (ODS) alloys were succesfully bonded employing a new, Low Pressure Plasma Spraying (LPPS), encapsulation technique. Silicon nitride interbonding of Sintered Silicon Nitride (SSN) material was studied and an optimum set of HIP parameters has been developed. The effect of HIP'ing plasma sprayed oxide coatings, on metal substrates, is described where plastic metal flow as well as chemical interface reactions are introduced as adhesive strength improvers.

INTRODUCTION

The manufacture of high temperature durable bondings of various materials can be best performed by the application of diffusion bonding and in many cases has been accomplished by the aid of HIP. This has been described in the literature for quite a large number of materials combinations [1-15].

By using HIP as the bonding method some related intrinsic advantages of the process are made use of: 1) Due to pressure accelerated plastic deformation and diffusional transport phenomena the processing temperature is lowered; 2) The process is not dependent on surface geometry of the parts to be bonded; 3) No macroplastic deformation (not more than a few percent), even under pressures exceeding the yield strength of the materials to be bonded, is taking place. Moreover, the capability of bonding a wide range of materials, of like and different compositions and irrespective of their geometrical complexity, is technologically attractive. HIP differs from

the nonisotropic uniaxial pressing, where in the latter the unbalanced applied stresses induce macroscopic plastic flow resulting in a distorted structure.

This paper describes some case studies of HIP bonded advanced materials. ODS alloys are an example of metal/metal bonding. HIP bonded silicon nitride was studied to some detail as a ceramic/ceramic bonding example, whereas plasma sprayed oxide coatings on metallic substrates are considered as a ceramic/metal bond systems.

ODS ALLOYS

Three different commercially available ODS alloys MA 6000, MA 754 and MA 956 have been investigated with respect to dominant HIP parameters and with respect to their pre-bonded surface condition. In addition, as an example of different materials, the alloy Incoloy 800 H was bonded to the ODS alloys. HIP bonding of ODS alloys has been described in the literature [7]. In comparision to the already reported results, this study utilizes a plasma sprayed encapsulation technique, recently developped [13], offering a possible simple and economical route.

Experimental

The specimens to be HIP bonded were each produced from two cylindrical rods with their bases brought to close proximity and then encapsulated. The roughness of the pre-bonded adjacent contact surfaces varied, as a result of a controlled grinding and polishing, in the range of R_a = 0,4 - 26µm. Prior to encapsulation, in order to remove oxides and other possible surface contaminations, the cylinders were sputtered by a transfer arc in the encapsulation chamber.

Gastight capsules were produced from a 500-800µm coating around the two cylinders. The coatings, made of the ferritic steel 100Cr6 or from the superalloy UDIMET-700 were applied by the LPPS operating at about 50mbar argon pressure. Prior to HIP the prefixed, encapsulated samples were He-leak tested.

The HIP bonding was carried out at pressures between 40 and 360MPa and at temperatures of 1050°C and 1150°C for holding time of 0,5 - 8h.

After HIP, the bonded rods were machined to tensile/creep test specimens. Tensile testings were respectively performed at ambient and 800°C temperatures. Ultimate tensile strength, yield strength and elongation were evaluated by adequate testing equipment.

Optical microscopy and SEM were employed to reveal the microstructure of the bonded zone. Elements distribution across the bonding interface was determined by EDX line profiling.

Results

In Fig. 1 and 2 the Ultimate Tensile Strength (UTS) versus HIP pressures and the pre-bonded surface roughness are respectively given. It appears that the UTS values of Incoloy 800H and MA 956 are not influenced by the HIP pressure. Since at 1150°C and pressures above 120MPa the yield strength of these two alloys

is already exceeded therefore, a further pressure increase causes no improvement in the bond strength.

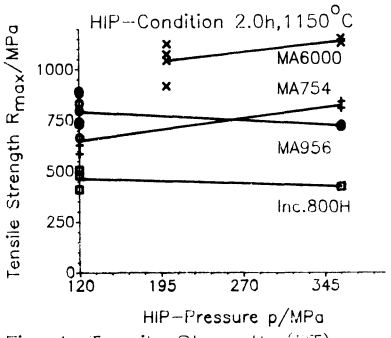

Fig. 1: Tensile Strength (RT) as f(HIP–Pressure)

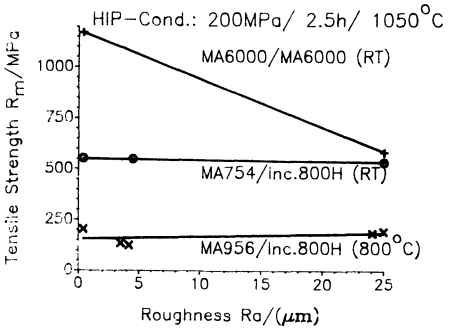

Fig. 2: Influence of surface roughness on bond strength

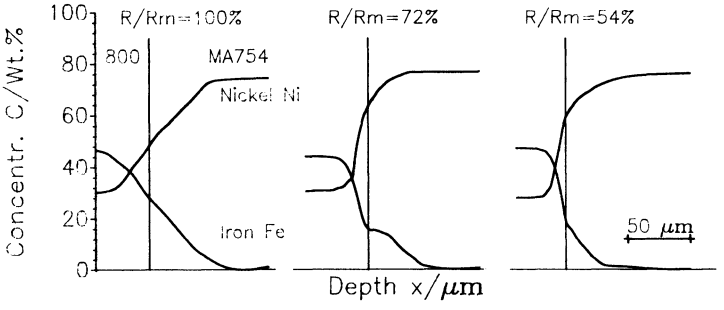

Diffusion profile of Nickel and Iron

Inc.800H/MA754–35k Inc.800H/Ma754–4b Inc.800H/Ma754–2a

Micrographs

Fracture in the bulk material Fracture in the bond zone Fracture in the bond zone

Fig.: 3 Bond strength, Ni and Fe interdiffusion and interface microscopy

On the other hand, the more temperature resistant alloys, MA 754 and MA 6000, show a clear increase in the UTS enhanced by the increasing HIP pressure, up to 360MPa. In these alloys the plastic deformability is lesser at 1150°C therefore, good quality bonds can only be established at the higher applied pressures.

The same approach as above holds for UTS dependence on surface roughness as in the pairing MA 6000/MA 6000, and which is demonstrated in Fig. 2. At 1050°C the pressure of 200MPa is insufficient to induce material flow and to fill roughness Ra ≈ 25μm deep. The bond strength decreases due to the

appropriate wording to verify contact of surface area between the partners to be bonded. These phenomena are in agreement with descriptions in a bonding model developed earlier [16]. Therefore, material partners like MA 754/Incoloy 800 H, and respectively, the MA 956/Incoloy 800 H are effectively bonded since at 200MPa the HIP pressure had already exceeded the critical yield strength in one of the partners. Consequently, no dependence on surface roughness can be detected (Fig. 2).

The role of alloying elements interdiffusion, the resulting strength and bond quality assessment are correlated in Fig. 3. Elements distribution profiles for interdiffusing nickel and iron are shown, following a sufficiently succesful bond processing of Incoloy 800 H/MA 754. In addition, the measured UTS, in relative units, as well as the metallographic views of the bond zones are also given in Fig. 3. The representative result example, with 100% bond strength, has a distinct interdiffusion zone with typical diffusion depths exceeding 50μm. Moreover, the fracture appears in the bulk material while the interface is well intact. On the other hand, the two remaining representative examples look quite different. The interdiffusion zone is scarcely extended, the element distribution is not uniform, the fracture appears at the primary interface and the bond strengths are reduced (72% and 54% respectively). The well developed element profiles of example 1 have been treated by Fick's diffusion law and they quantitatively adjust to self diffusion coefficients of the diffusing elements; in good agreement with already published findings [13].

Much of the results shown here, as well as other earlier findings of ODS alloy bonding [13], have been achieved by employing the LPPS encapsulation technique. The attempts made in bonding materials by the partial aid of LPPS promote the supposed applicability of this technique to fields such as stationary gasturbine structural parts development.

SILICON NITRIDE BONDING

As an advanced ceramic structural material, silicon nitride is in the last years intensively studied [1,2,5]. Although the main interest lies in powder technical sythesis of structural parts, bonding of silicon nitride to similar and different materials (metallic) partners is challenging, involving problems which may determine the engineering applicability of this outstanding material. As a case example of HIP bonding of ceramics, this part of the contribution introduces the results of a study, recently accomplished [18], on SSN and Hot Pressed Silicon Nitride (HPSN) Si_3N_4/Si_3N_4 bondings.

Experimental

Three different methods of encapsulation have been employed: 1) Quartz powder encapsulation. The area to be sealed is covered by a quartz powder. Following heating up to 1730°C, under nitrogen pressure of ≤ 5 MPa, the quartz softens and a gastight capsule is formed.
2) Quarz tube encapsulation. The samples were sealed under

vacuum in quartz tubes which were then introduced into the HIP chamber where under ≤ 5MPa nitrogen pressure and 1730°C the tube deforms to a sealed liner around the specimen.
3) LPPS. Molybdenum powder has been used as a spray material for encapsulation. Here HIP has been applied with the samples embedded in a BN powder.
HIP was performed at temperatures and pressures up to 1900°C and 360Mpa respectively and for dwelling times of 0.5-5h.
Bonds strength was evaluated by a four point (4P) bending test at ambient or at 1200°C temperatures.

Results

HIP temperature: The 4P bending strength, as given in Fig. 4 where each point refers to a single sample, increases respectively between 1750°C and 1900°C. Therefore, best strengths are obtained around 1900°C. From powder consolidation processes of SSN material it is well known that bonding is primarily established via liquid phase formation and sintering.

HIP pressure: As it appears in Fig. 5 a threshold pressure around 20 MPa is necessary to force the two partner surfaces to come into atomic contact. Once this initial pressure exceeds the critical value, bonding takes place. Therefore, higher pressures have only a small influence and no marked improvement in bond strength is observed.

HIP hold time: The influence of hold time during HIP on the 4P bending strengths is illustrated by a data field plotted in Fig. 6. As indicated, one hour contact time is necessary to establish satifactory bondings. It can be assumed that this critical hold time results from the kinetics of liquid phase formation, its movement across the interface and a further stabilization of a distributed glassy phase. Hold time longer than three to five hours have a minor influence on the bonding strengths and even promote an undesired Si_3N_4 grain growth.

Surface roughness: In Fig. 7 some results of the 4P bending strength, versus different roughness of the silicon nitride pre-bonded surfaces, are given. In general, large surface roughness tend to reduces the contact area between the adjacent partners. Moreover, due to the very low ductility of the ceramic, plastic deformation is not attainable. As a result, in large "peak-to-bottom" distances, only incomplete bonding can be expected. Therefore, a steep transient is observed in Fig. 7.

Argon ion irradiation: Some SSN specimen were argon ion irradiated in order to obtain a general idea whether changes in the surface activity, induced by the formation of lattice defect and other related phenomena, may promote bond properties. Prior to bonding the surfaces of the samples were exposed to an argon 300 keV ion beam with a cumulated dose of $10^{17}/cm^2$ at 300°C. The end results showed mostly a weak influence of irradiation on bond properties.

The production of perfect HIP bonds between silicon nitride materials requires a tight control of HIP parameters, temperature, pressure and time, at a minimal level. Three hours at 1900°C and 50 MPa pressure appear to be optimum conditions. Prolonged times and higher temperatures induce undesired grain growth. The encapsulation techniques employed had no detectable effect on the resulting bonding. On the other hand, when the encapsulation is not gastight, nitrogen atmosphere is strictly

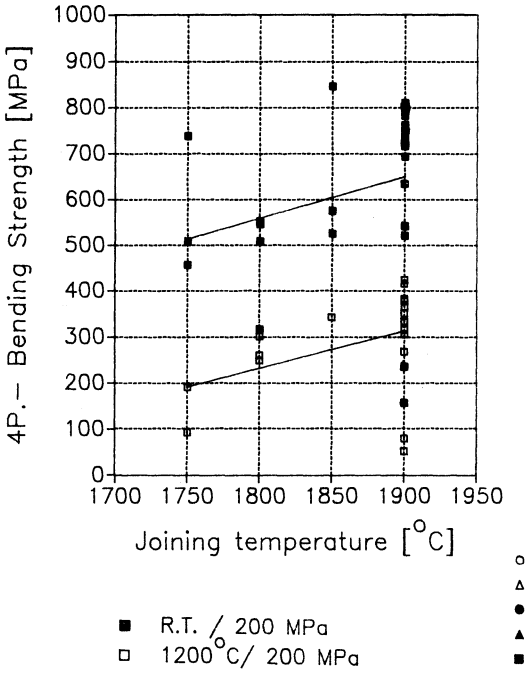

Figure 4: Bending Strength of SSN-SSN Joining

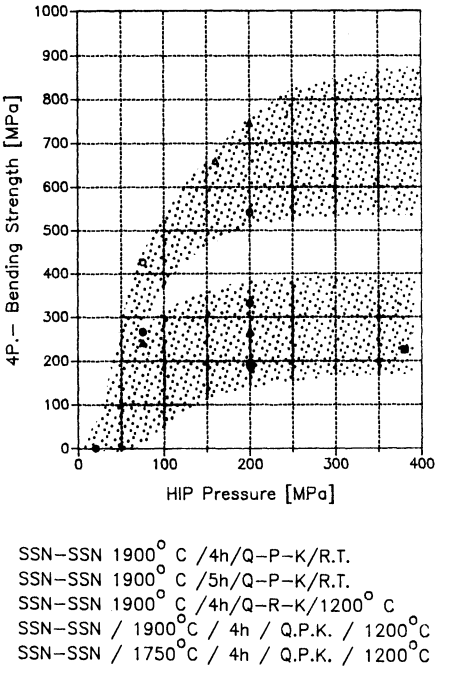

Figure 5: Effect of HIP-Pressure on Bending Strength

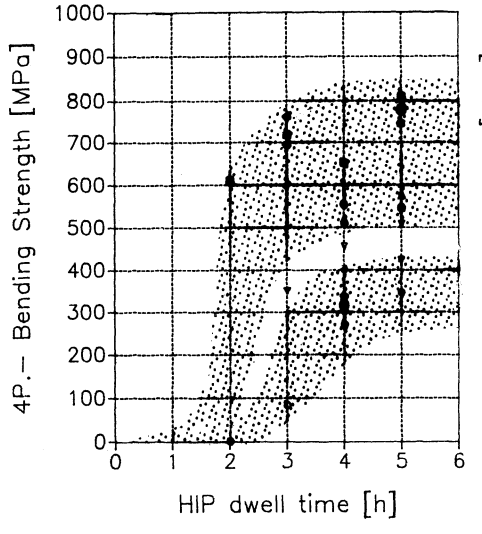

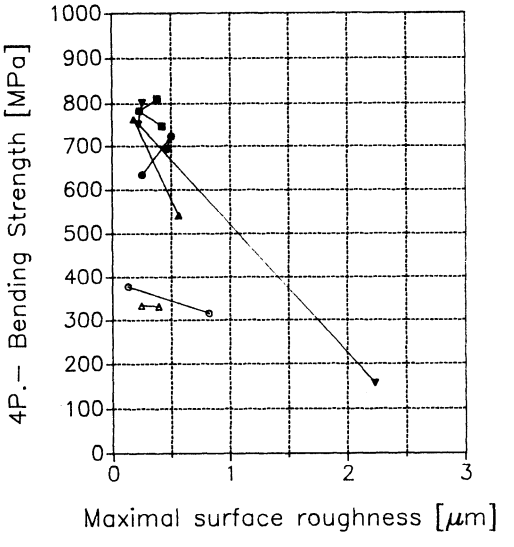

o SSN–SSN/ 1900°C/ 200 MPa/Q–P–K/1200°
▼ SSN–SSN / 1900°C/ 200 MPa/Q–R–K/1200°
▽ SSN–SSN / 1750°C / 200 MPa/ R.T. / Q–P–K
● SSN–SSN / 1800°C / 200 MPa/ R.T. / Q–P–K
▲ SSN–SSN / 1850°C / 200 MPa/ R.T. / Q–P–K.
■ SSN–SSN / 1900°C / 200 MPa/ R.T. / Q–P–K

o–o SSN–SSN / 1900°C, 5h, 200 MPa/ Q–P–K / 1200
Δ–Δ SSN–SSN / 1900°C, 5h, 200 MPa / Q–R–K / 1200
▼–▼ SSN–SSN / 1900°C 5h, 200 MPa/ Q–R–K / R.T.
●–● SSN–SSN / 1900°C 5h, 200 MPa/ V.P.S./ R.T.
▲–▲ SSN–SSN / 1900°C 4h, 200 MPa/ Q–P–K / R.T.
■–■ SSN–SSN / 1900°C 5h, 200 MPa/ Q–P–K / R.T.

Figure 6: Effect of dwell time on Bending Strength

Figure 7: Effect of Rmax on Bending Strength

demanded otherwise, nitrogen loss would avoid proper sintering and bonding behaviour. Since the materials used in this study contained La_2O_3 additions, bond formation took place largely via liquid phase sintering mechanisms. It should be noticed that no interlayers were introduced. Therefore, the bonds are temperature resistant, free of chemical interaction and thermal mismatch problems.

HIP TREATMENT OF PLASMA SPRAYED OXIDE COATINGS

Damage of composite materials for the most part originates from chemical, structural or thermomechanical incompatibility of the chosen material pairings. The same holds for plasma sprayed protective oxide coatings, which on a metallic substrate, function as a composite material. This chapter gives some selected results, from a larger study [17], mainly of $ZrO_2(Y_2O_3)$ coatings sprayed on two metallic alloy substrates, Hastelloy X and Inconel 617, which have been HIP treated after application. The process is given in detail elsewhere [17]. In general, 45mm in diameter and 2mm thick disk specimens were plasma sprayed with $ZrO_2(7\%Y_2O_3)$ to form 30-300 μm layers. The sprayed specimen were steel encapsulated either with oxide coatings face to face, or oxide in contact with metal.
The specimens were HIP'ed at 1200°C, 200 MPa for 2 hours.

Metallographical Findings
A typical cross section from Hastelloy X(M) sprayed with $ZrO_2(7\% Y_2O_3)$(C) and facing Hastelloy X(M) is given by the SEM image in Fig. 8. The interfaces I_1 and I_2 appear rough and closely connected, resulting from HIP induced metal flow into the rough surface structure of the ceramic. Metal flow assumption is supported by the line scan of some elements at I_2 where the irregular distribution, across the interface, of Zr, as well as the alloying elements of the substrate Ni, Cr and Fe, is noticed in Fig. 9. On the right side of Fig. 9 the element distribution, deeper in the oxide and at higher magnification, is given. The fact that alloy elements have penetrated deep into the oxide, to a constant concentration level of few percent, suggest the existance of two independent metal migration mechanisms: induced plastic flow and/or a surface/grain-boundary diffusion.
SEM image of a typical cross-sectioned Inconel 617(M) with $ZrO_2(7\% Y_2O_3)$(C) coating is given in Fig. 10. As before, both interfaces, I_1 and I_2, appear very deft indicating the above mentioned mechanical attachement induced by metal yielding. Moreover, in this case, the dark precipitates (P_1) which are concentrated at the interfaces have been mostly related to alumina. This interconnected oxide structure is probably formed by internal oxidation reactions of aluminum with oxygen released by ZrO_2. The results of such reactions can be observed in all aluminum containing substrates [17]. In addition, the light-grey areas (P_2) in Fig. 10 were identified as consisting of substrate metal and are embeded as separate isles in the ceramic. This metal enrichment finding is reproduced as an enlarged line scan in Fig. 11. (The EDX trace of the line scan

is visible in Fig. 10 as a vertical dark marking near P_1 and P_2).

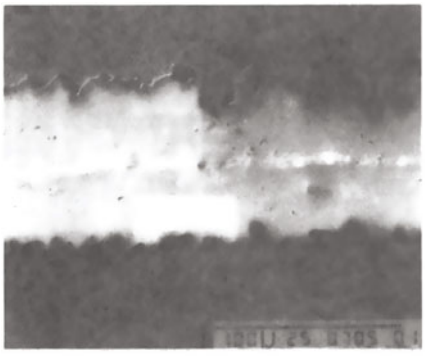

Figure 8

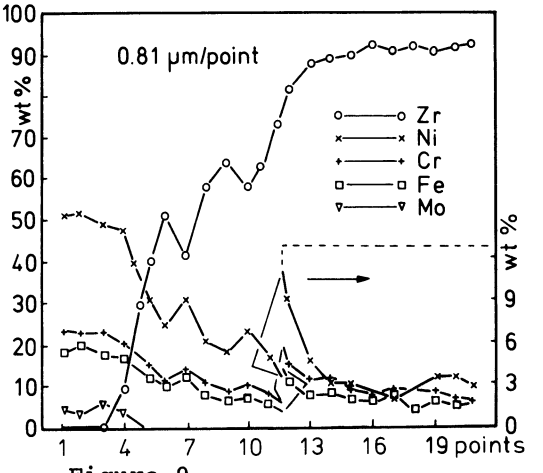

Figure 9

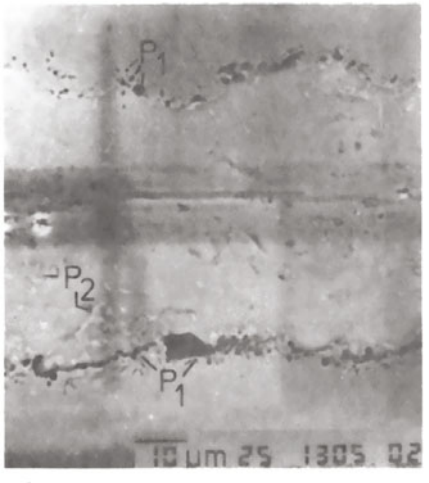

Figure 10

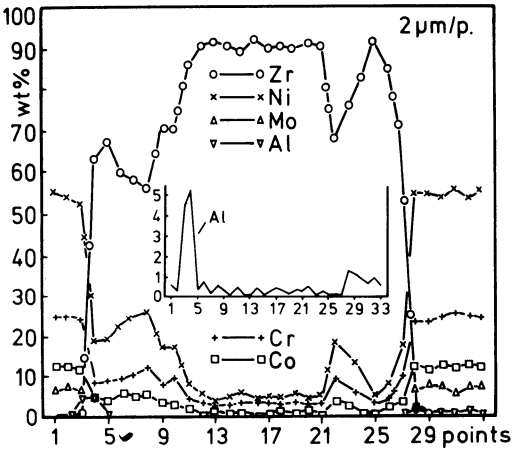

Figure 11

The insert in Fig. 11 represents the aluminum profile across the zirconia coating indirectly suggesting a possible alumina precipitation along the interfaces.

From the above results a massive infiltration of the ceramic by substrate material is assumed to take place under HIP conditions. Presumably, the open pores in the ceramic allow metal penetration by plastic deformation and are accordingly filled. This infiltration gives the impression of a dense ceramic structure with only few remaining pores. It should be mentioned that in thicker coatings, of about 100µm, the results are different; only 20-30µm zones near the interface are filled with metal while the other areas retain the same porosity as the non-HIP'ed coatings.

Consequently, the effect of HIP'ing zirconia, and possibly other oxide coatings, primarily promotes intensive interface interaction, of mechanical and chemical nature, between metal

and ceramic which, in turn, improve considerably the adhesion strength. The above does not imply that oxide cracking due to thermomechanical stresses can be avoided but the risk of spalling could be lower. The effect of densification of the oxides under HIP conditions seems to be of minor importance.

CONCLUSIONS

Sufficient bonding properties can be obtained under a controlled range of HIP temperatures and pressures.
Succesful bonding of commercial ODS alloys is a result of HIP enhanced interdiffusion across a tight, locally deformed, interface.
High temperature resistant alloys can be bonded at relatively high HIP pressures and low temperatures which in turn do not give rise to an undesired grain growth.
As a result of its high stiffness, HIP bonding of silicon nitride (SSN) is sensitive to pre-bonded surface quality and bonding can be accomplished without bond assisting interlayers and in different capsules with a limited range of HIP parameters.
The mechanisms acting in bond formation of silicon nitride are very similar to those governing the lanthanum doped SSN processing.
HIP assisted bonding of ceramic/metal systems is mostly marked by heavy interface interactions which are of different nature: metal flow, accelerated diffusion and chemical reactions in the presence of aluminium, imposing some difficulties to establish optimal processing conditions.
The bonding of oxide ceramic, plasma sprayed coatings, to a metallic substrate is mainly a result of an intimate contact with the metal substrate arising from plastic metal infiltration into the open porosity of the sprayed structure.
The applied encapsulation techniques, LPPS, introduces a possible route of joining component parts with curved surface shapes.
In general, HIP has the intrinsic advantage of bonding complex geometries, non weldable materials and can avoid the use of intermediate layers. Thus, new applications for advanced structural materials can be envisaged.

REFERENCES

1. Kaba, T., Shimada, M., Koizumi, M., Diffusional Reaction Bonding of Si3N4 Ceramics under High Pressure. J. of the American Ceramic Society, Vol. 66, No. 8, Aug. 1983.
2. Koizumi, M., Okamoto, T., Shimada, M., Suganuma, K., Diffusional-Reaction Bonding of Ceramics to Ceramics and to Metals under Pressure. J. of the American Society. Vol. 63 , No. 9, 1984.
3. Boncoeur, M., Maire, Ph., Valin, F., Diffusion Bonding by HIP of Titanium and Yttria. Proc. of the Int. Conf. on Hot Isostatic Pressing, Lulea(s) 15-17 June, 1987.
4. Jarvenpaa, M., Consolidation and Diffusion Bonding of Stellite and Stainless steel by Hot Isostatic Pressing. Proc. of the Int. Conf. on Hot Isostatic Pressing of Materials, Antwerp 25.-27. April, 1988.

5. Buchkremer, H., Hecker, R., Serpekian, T., Stöver, D., HIP-Bonding Tests of Si_3N_4-Parts, Proc. of the Int. Conf. on Hot Isostatic Pressing of Materials, Antwerp 25.-27. April, 1988
6. Kuribayashi, H., Suganuma, K., Migamoto, Y., Koizumi, M., Thermal Fatigue Testing of Plasma-Sprayed ZrO_2 Coatings on Metal Substrates Densified by HIP'ing, Proc. of the 3rd Int. Conf. on Isostatic Pressing, Nov. 10-12, 1986, London.
7. Verpoort, C., Nazmy, M., Jongenburger, C.P., HIP-Diffusion Bonding of ODS MA 6000, Proc. of the 3rd Int. Conf. on Isostatic Pressing, Nov. 10-12, 1986, London.
8. Hunold, K., Grellner, W., Heißisostatisches Verdichten von Siliziumcarbid, Proc. of the 3rd BMFT Statusseminar 1984, Keramische Bauteile für Fahrzeug-Gasturbinen, 13.15.2.84, Bad Nauheim.
9. Suganuma, K., Okamoto, T., Koizumi, M., Shimada, M., Effect of Thickness on Direct Bonding of Silicon Nitride to Steel. Journ. of the American Ceramic Society, Vol. 68, No. 12, Dec. 1985.
10. Syganuma, K., Okamoto, T., Koizumi, Shimada, M., Solid-State Bonding of Oxide Ceramic to Steel. J. of Nuclear Materials 133 & 134 (1985), 773-777.
11. Wing, R.G., Neunham, M., Dual-Alloy Turbine Blises. International Conference of Cranfield, 7.-8. July 1987.
12. Yiasemides, G.P., Diffusion Bonding using HIP. International Conference of Cranfield 7.-8. July 1987.
13. Hammelmann, K.H., et al., Diffusionsschweißen von ODS Legierungen mit Hilfe der HIP-Technik. JÜL Bericht 2381, September 1990
14. Atkinson, H.V., et al., HIP-Diffusion of Austenitic to Ferritic Steels. 2nd International Conference on D.B. at Cranfield , 28.-29. March 1990.
15. Klomp, J.T., Thermodynamics of Ceramic-Metal Interfaces. Proc. European, Colloquium, Designing Interfaces for Technological Applications. CEC-Joint Research Center, Petten, The Netherland, 1989, pp. 127-144.
16. Cline, C.L., Welding Journal 1966, pp 481-489
17. Schütz, H.G., Untersuchungen von Eigenschaften plasmagespritzter Oxidkeramiken auf metallischen Grundwerkstoffen. Dissertation RWTH Aachen 1991, to be published.
18. Sun Woo, J.H., Entwicklung und Charakterisierung von HIP Verbindungsverfahren an Si_3N_4-Werkstoffen. Dissertation RWTH Aachen 1991, to be published.

ACKNOWLEDGEMENT

Several persons have contributed to this paper. Especially Dr. H.P. Buchkremer, K.H. Hammelmann, Dr. A. Ruder, H.G. Schütz, Dr. T. Serpekian and J.H. Sun Woo are mentioned by name. The author gratefully acknowledges their valuable support.

DIFFUSION BONDING OF Si_3N_4 TO METALS BY HIP USED FOR HIGH TEMPERATURE APPLICATIONS

A.Frisch, W.A.Kaysser, W.Zhang, and G.Petzow

Max-Planck-Institut für Metallforschung
Pulvermetallurgisches Laboratorium
D-7000 Stuttgart 80, Germany

ABSTRACT

In the last few years there has been growing interest in the joining of metals to ceramics for use as structural materials. Diffusion bonding of Si_3N_4 to the new generation of ODS-superalloys, such as MA-6000, is a method considered to yield well joined metal/ceramic systems for high temperature applications. Joining of Si_3N_4 to MA-6000 bars was achieved by diffusion bonding during HIPing at 100 to 200 MPa at 1100 to 1400 ^{0}C. Stresses caused by the largely different thermal expansion coefficients were reduced by multiphase interlayers. An INVAR-alloy layer with high formability at elevated temperatures and small thermal expansion coefficient at low temperatures were combined with various reactive layers of transition metals, such as Ti, Nb and V. The reactions at the interfaces and the fracture surfaces were investigated by SEM, EDX and WDX analysis.
During bonding of Si_3N_4 to metals brittle phases are frequently formed at the interfaces which may lead to a failure of the joint. In systems with a large thermal mismatch, stress relaxation by thin soft interlayers is very limited. However, the formation of brittle reaction layers can be controlled by an interdiffusion layer technique and by the bonding temperature and -time. At special HIP-conditions, the damage of the joint can additionally be reduced by microcrack induced stress relaxation. Based on the thermodynamics of multicomponent systems, the interfacial reactions and the compatibility of the interlayers were calculated and compared with the experimental results. Calculations on the residual stresses in the metal/ceramic multilayer joints are presented.

INTRODUCTION

Diffusion bonding using Hot Isostatic Pressing (HIP) initiated the development of HIP technology. Although diffusion bonding by HIP is less important than powder or post densification, it has a great potential for combining materials with different properties such as metals and ceramics for complex structures. Metal/ceramic joints are used in the electronics field for insulators, capacitors or microchip substrates /1/ and increasingly considered as structural materials where high toughness and good resistance to wear, corrosion and erosion in operations at high temperature /1/ are required. Si_3N_4 and Ni-based superalloys, especially the new generation of ODS alloys, seem to be promising components for ceramic/metal joints used at high temperatures. Both the Si_3N_4 and the superalloy possess high strength, good creep and excellent corrosion resistance at high temperatures.

Direct bonds of Si_3N_4 to most metals fail during temperature changes /2,3/ due to the large difference in the thermal expansion coefficients of the components. During cooling from the joining temperature, the contraction of the metal part is usually much larger than that of the ceramic part. Residual stresses develop which may exceed the strength of either the ceramic parts themselves, the reaction products or the interfaces of the joints. Therefore, it was proposed to introduce ductile interlayers between the parts to be joined. These deform plastically during joining and cooling allowing stress relaxation near and at the interface /3/.

In Si_3N_4/metal joints, the insufficient chemical adhesion at the metal/Si_3N_4 interface can lead to failure by decohesion of the parts at small stresses. Due to the mostly ionic-covalent character of its interatomic bonding, Si_3N_4 possesses very little tendency for electron interaction with materials of strong metallic bonding character. Reactive coatings or thin films on Si_3N_4 have to be used to increase the chemical adhesion at the interface to the adjacent metal.

In the following, joining of Si_3N_4 to metals is presented. Soft interlayers and reactive diffusion bonding by HIP were used to obtain an increased adhesion and a relaxation of thermal stresses. The interfacial reactions and adhesions with various reactive interlayers at different bonding conditions are described and compared to the stress distribution in the joints after cooling calculated by an analytical estimation of residual stresses in multilayered metal/ceramic strips /4/. The interfacial structures and their correlation to strength measurements in four point bending tests are presented.

Experiments

Sheets of ODS-superalloy MA6000 and Si_3N_4 (2,5 x 3,5 x 16 mm^3) were joined with various combinations of interlayers by diffusion bonding during HIPing at 50 MPa and temperatures in the range of 1100 to 1300 ^{0}C. For an increased chemical adhesion, the use of various foils of transition metals, such as nickel, titanium, iron, vanadium or niobium between the ceramic and the soft metal was investigated. The INCO alloy Nilo 36 (Fe-36 wt% Ni) and pure Ni served as soft interlayers. Before joining, the surfaces of the structural components were ground and polished to an average roughness of 0.1 μm. The material combinations were placed into glass capsules which were evacuated and

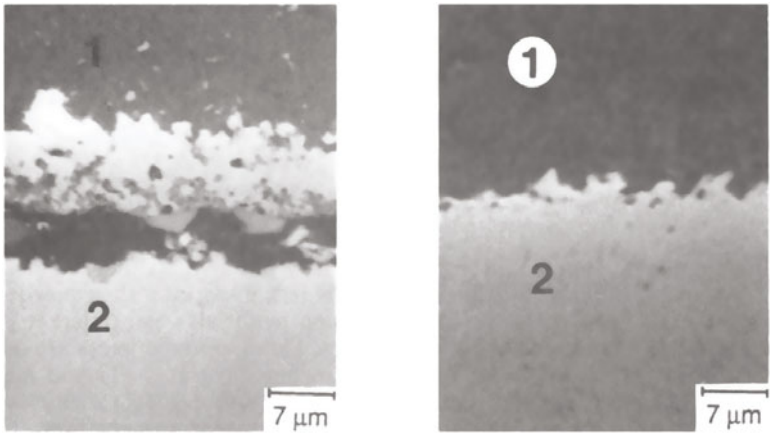

Figure 1: Si_3N_4/Fe-36wt.% Ni interface after bonding at 1200 ^{0}C (left) and 1100 ^{0}C (right). 1: Si_3N_4 2: Fe-36wt.% Ni

sealed before HIPing in a laboratory HIP equipment. The pressure was applied after the samples had reached the isothermal diffusion bonding temperature. After bonding, the metal/ceramic and metal/metal interfaces were investigated by SEM, EDX and WDX analysis. The mechanical strength was measured by four point bending tests at room temperature. The flexural bond strength σ_{bf} was determined from the fracture load F_c and the specimen dimensions:

$$\sigma_{bf} = \frac{3 \cdot F_c \cdot e}{B \cdot W^2}$$

B: width of the specimen
W: thickness of the specimen
e: distance between the upper and lower support

RESULTS

Figure 1 compares the metal/ceramic interfaces of Si_3N_4/Fe-36wt.% Ni/MA6000 joints bonded at 1200°C (Fig.1a) and 1100°C (Fig.1b). At the higher bonding temperature a large crack in the Fe-36wt.% Ni alloy parallel to the interface was observed. The dissolution of Si in the Fe-36wt.% Ni lead to a large amount of free N_2 (appr. 11 at.% N) because only a small fraction of the nitrogen can dissolve in the austenite (0.13 at.%). Therefore, N_2-filled voids are formed which may weaken the interfacial strength of the joint leading to crack formation in the interfacial area. A decrease of the bonding temperature results in reduced void concentration and an excellent bonding character at the metal/ceramic interface. However, large stresses arise in Si_3N_4 leading to crack formation in the ceramic part. The stress distribution in the Si_3N_4/Fe-36wt.% Ni/MA6000 joint calculated analytically after cooling of the joint from 1100°C (Fig. 2) predicts large tensile stresses up to 720 MPa in the ceramic part, which may exceed the mechanical strength. An increased mechanical stability is expected by trapping part of the free nitrogen either by strong nitride formers or by an increased solid solution in the

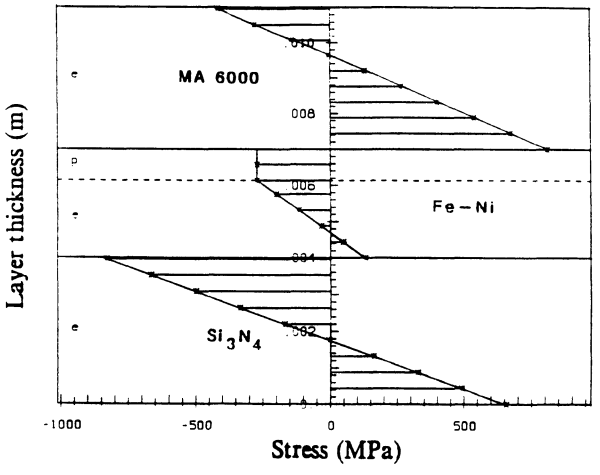

Figure 2: Stress distribution calculated for a Si_3N_4/Fe-36wt.% Ni/MA6000 joint after cooling from 1100 °C.

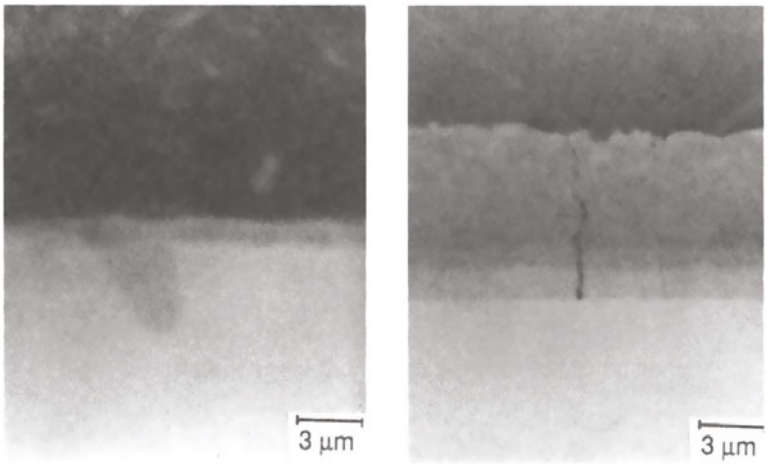

Figure 3: Si_3N_4/Nb- (left) and Nb/Fe-36wt.%Ni- interface (right) of Si_3N_4/Nb/ Fe-36wt.%Ni/MA6000 joint, bonded at 1100°C.

adjacent layer next to the ceramic. Further improvement of the joint properties should result from the use of soft interlayers possessing plastic formability to relax thermal stresses. Joints were produced with various adhesive transition metals, such as Nb, V, Ti, Hf and Fe. Figure 3 shows the interfaces of a Si_3N_4/Nb/ Fe-36wt.% Ni/MA6000 joint. A reaction layer (Fig.3a) was observed in the ceramic/metal interface which was proved to be NbN. Again, Si_3N_4 decomposed, but the free nitrogen reacted with Nb to NbN. No silicides were detected at the metal/ceramic interface. The nitride showed to be effective in forming a satisfying bonding layer at the Si_3N_4/metal interface. At the Nb/Fe-36wt.% Ni interface (Fig.3b), however, strong interdiffusion was observed leading to the formation of intermetallic compounds. The mechanical stability of the joint was excellent despite the fact that fine cracks running perpendicular to the interface were observed in the intermetallic phases.

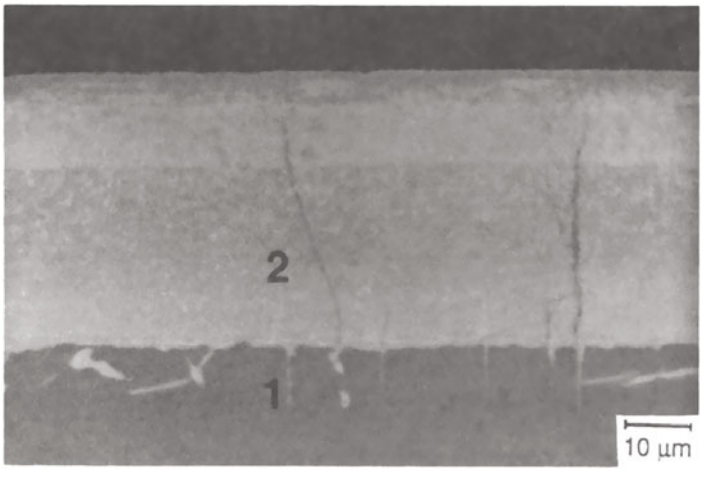

Figure 4: Si_3N_4/Hf-interface of a Si_3N_4/Hf/Fe-36 wt.%Ni/MA6000 joint.
1:Si_3N_4 2:Hf

Another example in which perpendicular microcracks were found beneficial for the mechanical stability of the joint is shown in Figure 4. It shows the microstructure of an initial layer sequence Si_3N_4/Hf/Fe-36 wt.% Ni/MA6000 in the joint area. In this case, a Hf-silicide layer was formed at the Si_3N_4 interface during bonding leading to a Si_3N_4/$HfSi_2$/Si-Hf-Fe-Ni/MA6000 sequence. Obviously, thermal stresses are relaxed by small cracks leading to an island structure in the brittle phase in contrast to other interlayer systems, such as Si_3N_4/V/Fe-36 wt.% Ni/MA6000, where cracks running parallel to the interface of the joint led to a high susceptibility for catastrophic interfacial damage.

In Figure 5 the ceramic/metal interface of a Si_3N_4/Fe/Ni/Fe-36 wt.% Ni/Ni/MA6000 joint is shown after bonding at 100 MPa and 1150°C for 2 h. The chemical adhesion and the mechanical stability of the joint were excellent. No reactions or formation of cracks parallel or perpendicular to the metal/ceramic or metal/metal interfaces were observed. Fe-36 wt.% Ni and Ni as soft interlayers seem to possess sufficient plastic deformation capability to relax thermal stresses during cooling of the joint.

Figure 6 shows the bending strength of a Si_3N_4/Fe/Ni(1)/Fe-36 wt.% Ni/Ni(2)/MA6000. The thicknesses for the Fe-Ni- and the Ni(2)-layer were held constant to 2 mm and 1 mm, respectively. The thicknesses of the Fe- and Ni(1)-layers were varied. The values were taken as mean values after six four point bending tests at RT for each material combination. Direct bonding of Si_3N_4 with Fe-Ni led to a low mechanical strength of σ_B = 75 MPa. An improvement of the mechanical stability was obtained by additional Fe- or Ni-layers. The combination of Fe-layer and Ni-layer increased the four point bending strength to 300 MPa. In contrast, the use of a stiff interlayer, such as a heavy metal alloy, which was has been proposed as being beneficial /5/, resulted in a decrease of the mean strength value to 255 MPa.

DISCUSSION

Si_3N_4 and the ODS-superalloy MA6000 are potential components for metal/ceramic joints at elevated temperatures. Due to the large thermal mismatch between both components, joints with interlayers are required which allow the relaxation of thermal stresses arising during thermal treatment. Calculations of the stress development and experimental investigations of Si_3N_4/MA6000 joints showed that stress relaxation by thin soft interlayers is very limited.

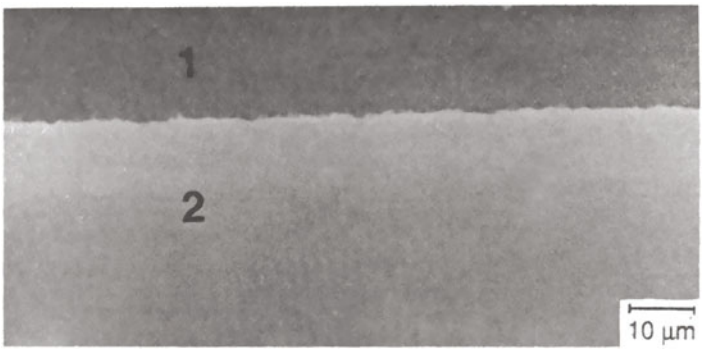

Figure 5: Si_3N_4/Fe- interface, bonded at 1150 °C for 2h. 1:Si_3N_4 2:Fe

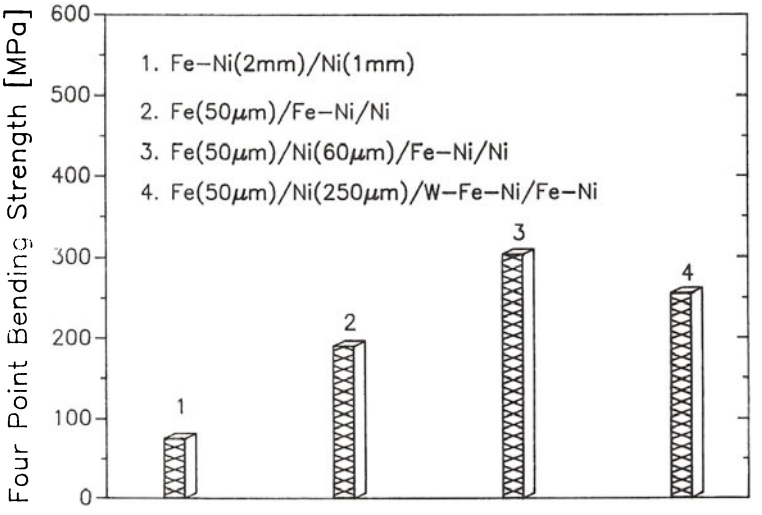

Figure 6: Four Point bending strength of Si_3N_4/MA6000 joints with different interlayer combinations.

During bonding of Si_3N_4 to metals, which are suitable as interlayers, brittle reaction products may be formed at the metal/ceramic interface. In systems with a low deformability of these stiff reaction layers, stress relaxation can be obtained in two ways as shown in Figure 7. If the stiff reaction layer possesses a high mechanical strength, the stress values at the interface may exceed the interfacial strength and result in stress relaxation along the interface by crack formation between the constituents. Another possibility is that the interfacial damage may be prevented by non-critical crack formation, if the stresses exceed the mechanical strength of the stiff reaction product. At first, microcracks may form perpendicular to the interface. Secondly, an additional stress relaxation could be obtained by crack blunting. Which of the mechanisms will proceed is influenced by the ratio of the Youngs modulus, the thickness of the reaction product and the ratio of the interfacial strength to the strength of the interlayer.

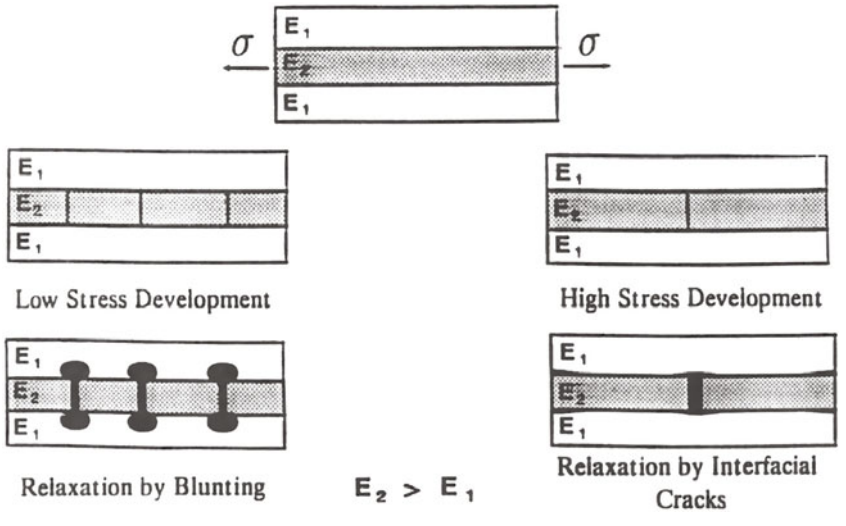

Figure 7: Two possibilities for stress relaxation in metal/ceramic systems with stiff reaction layers.

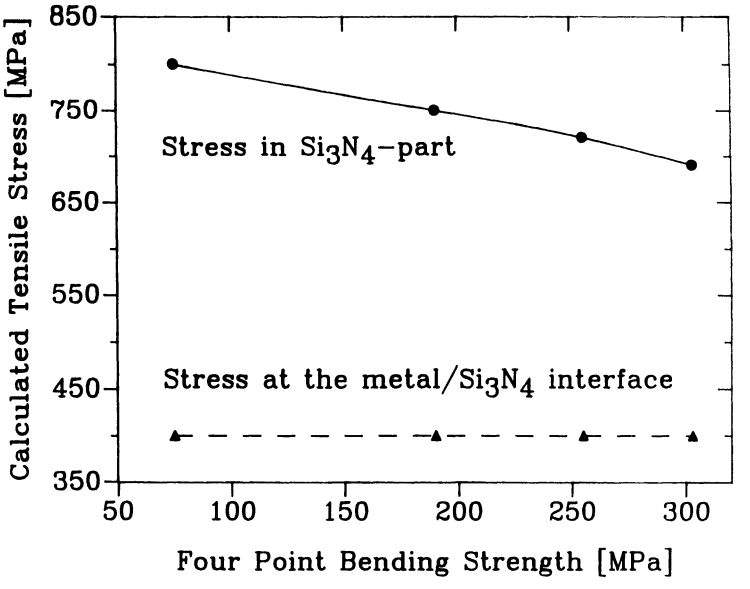

Figure 8: Maximum tensile stress (calculated) at in the metal at the interface and in the Si_3N_4-part as a function of the four point bending strength.

In systems without stiff interfacial layers the soft interlayers must be thick enough to allow sufficient stress relaxation during cooling of the joints. Figure 8 compares the mechanical strength with the calculations of the tensile stress in the metal at the metal/ceramic interface and the maximum tensile stress at the outer surface of the ceramic for the tested Si_3N_4/Fe/Ni(1)/Fe-36 wt.% Ni/Ni(2)/MA 6000 joints (see Figure 6). The tensile stress in the metal is constant for these material combinations. Thus, the mechanical strength of these joints seems to be determined by the stress distribution in the ceramic part because an increase of the strength is obtained with decreasing tensile stresses in the ceramic.

ACKNOWLEDGEMENT

This research was supported by the Volkswagen-Stiftung and by G.I.F., the German-Israeli Foundation for Scientific Research and Development.

REFERENCES

1. W.E.Borbigde, R.V.Allen and P.T.Whelan,"A Review of the Bonding Technique for Joining Ceramics to Metals", J. de Physique, 47 (1986), C1-131-137.

2. M.G.Nicholas and D.A.Mortimer,"Ceramic/Metal Joining of Structural Applications", Mater.Sci.and Tech., 1 (1985), 657-665.

3. K.Suganuma, T.Okamoto, and M.Koizumi,"Effect of Interlayers in Ceramic-Metal Joints with Thermal Expansion Mismatches", J.Am.Ceram.Soc., 67 (1984), C256-C257.

4. C.H.Hsueh and A.G.Evans,"Residual Stresses in Metal/Ceramic Bonded Strips", J.Am.Ceram.Soc., 68 (1985), 241-248.

5. A.Frisch, W.A.Kaysser, W.Zhang, R.Feldmann, amd G.Petzow, "Diffusion Bonding of Si_3N_4 To ODS-Superalloy MA-6000 by Hot Isostatic Pressing", "World Conference of Powder Metallurgy - PM'90", 2 (1990), 52-60.

HIP-PRODUCED BIMETALLIC CYLINDERS FOR FLUOROPLASTIC INJECTION MOLDING

Toshiyuki Minamide, Kouichi Umeda, Shigeki Nakamura,
Ichirou Kusabe, Masao Morishita
Kobe Steel,Ltd., Takasago, Japan

ABSTRACT

Bimetallic cylinders lined with a superior corrosion- and wear-resistant alloy were developed by using powder metallurgy and HIP diffusion bonding technology. The new alloy, whose chemical composition was Ni-17.5mass%Cr-24.0Mo-3.6B-2.9Si-1.0Cu(named C703), was obtained by reactive sintering between Ni-Mo-Si-Cu alloy powder and CrB powder during the HIP process. CrB particles were transformed into M_3B_2 particles during this process. The corrosion resistance to HF and HNO_3 of C703 was almost the same as that of Hastelloy C. Furthermore, the wear resistance of C703 was about 100 times superior to that of Hastelloy C. C703 was sintered and bonded to the inner surface of a Cr-Mo alloy steel cylinder body using the HIP process. This bimetallic cylinder met with good results for injection molding of fluoroplastic reinforced with glass fiber.

INTRODUCTION

Conventionally, a highly corrosion-resistant alloy, Hastelloy C, has been used for the cylinders of fluoroplastic molding machines because a corrosive HF gas is generated during injection or extrusion molding of fluoroplastics. However, since fluoroplastics become reinforced by the addition of hard materials (glass or carbon fiber, etc.) to improve its heat resistance, Hastelloy C has been accused of having low wear resistance. Therefore, it is vital that the alloys of the cylinders have wear resistance as well as corrosion resistance. In order to solve this problem, a new Ni-based corrosion- and wear-resistant alloy was developed through powder metallurgy. This new alloy was obtained by reactive sintering and bonded to the inner surface of a Cr-Mo alloy steel cylinder body during the HIP process.

EXPERIMENTAL PROCEDURE

Examination of the optimum alloy compositions

In a Ni base alloy, Cr and Mo are important alloying elements for improving

corrosion resistance to both the oxidizing agent, e.g. HNO_3, and the halogen agent, e.g. HF[1][2]. In addition, Cu is effective in reducing electrochemical cell corrosion[3]. Meanwhile, to improve wear resistance, it is desirable that fine particles, e.g. borides, are homogeneously dispersed and precipitated in the matrix. Hard borides significantly improve wear resistance. Furthermore, the addition of a certain amount of Si is necessary to improve the fluidity of the melt during production of the alloy powder by the vacuum melting-Ar gas atomization method[4]. Examination of the optimum alloy composition was conducted, taking the above mentioned matters into consideration. In order to determine the Cr and Mo contents, various Cr and Mo contents of the Ni-Cr-Mo-3Si-3B-1Cu alloys, as shown in Table 1, were arc melted. The Mo/Cr ratio was greater or equal to 1.0 when the Cr content was 15%, and the Mo/Cr ratio was less than 1.0 when the Mo content was 15%.

Table 1 Cr and Mo contents and Mo/Cr ratios of Ni－Cr－Mo－3.0Si－3.0B－1.0Cu arc melted alloys for corrosion tests.

Cr (mass%)	Mo (mass%)	Mo/Cr ratios
15	15	1.00
15	20	1.31
15	25	1.67
15	30	2.00
20	15	0.75
25	15	0.60
30	15	0.50

The corrosion resistance test pieces were cut from arc melted alloys. The size (mm) of the test pieces was $\phi 6.5 \times 10$. Their mass loss were measured after the corrosion test. Corrosion solutions were 10% HF and 6% HNO_3. The corrosion test temperature was 323K, and the time was 360ks(100h).

Application of the new alloy to HIP-produced bimetallic cylinders

In order to produce bimetallic cylinders lined with the new alloy using the HIP process, a manufacturing process, as shown in Figure 1, was designed. The capsule used as the cylinder body, which is made of Cr-Mo alloy steel, was assembled by welding it to the core bar. In this case, a core bar was used for forming the inside configuration of the lining alloy after HIP. After powder charging between the clearance of the capsule and core bar, the capsule was evacuated and then sealed by welding. Afterwards, the capsule was treated with HIP in Ar at 1223K under 98MPa. During the HIP process, the powder was sintered and bonded to the inside surface of the cylinder body.

To examine the corrosion and wear resistance of the HIP-ed alloy, each test piece was cut from the lining alloy of the HIP-ed bimetallic cylinder. The size(mm) of the corrosion test pieces was $5 \times 20 \times 1.4$. The test conditions were the same as in the case of the arc-melted alloy described above. The wear resistance of the alloy was evaluated

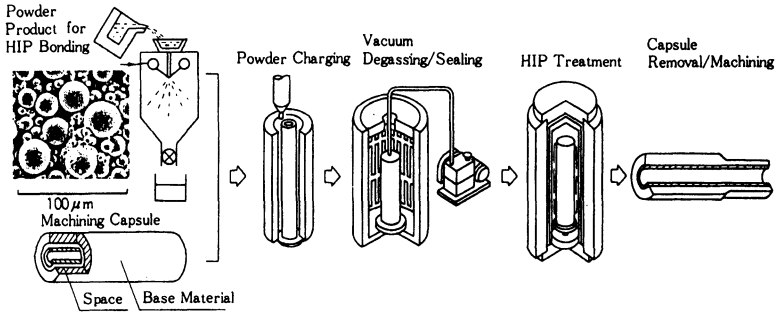

Fig.1 Manufacturing process of HIP－produced bimetallic cylinder.

by the Ohgoshi-type contact wear test[5], where the wear loss value indicated specific wear of $m^3/N \cdot m$. These tests were carried out to compare the results with the performance of commercial Hastelloy C. Furthermore, the bond region of the new alloy and the Cr-Mo alloy steel was cut from the HIP-ed piece and observed by electron probe microanalyser.

RESULTS AND DISCUSSION

Determination of the composition of the new alloy

First of all, the corrosion resistance of the arc-melted alloy was investigated. Figure 2 shows the effect of the Mo/Cr ratio on the corrosion resistance of Ni-Cr-Mo-3Si-3B-1Cu alloys shown in Table 1. Excellent corrosion resistance to the halogen agent (HF) was observed in the case of the Mo/Cr≧1.0 alloys. On the other hand, excellent corrosion resistance to the oxidizing agent (HNO_3) was observed in the case of the Mo/Cr< 1.0 alloys.

Based on these results and the reasons described below, the composition of the new alloy (named C703) was determined, as shown in Table 2. It was considered that the optimum Mo content was 24.0% because a large content of Mo increases the amount of the M_3B_2 boride phase[6～9] which improves wear resistance without decreasing corrosion resistance to the halogen agent. On the other hand, it was considered that the optimum Cr content was 17.5% because, in the case of an alloy containing only 15% Cr, the corrosion resistance to the oxidizing agent decreased when more than 15% Mo was added.

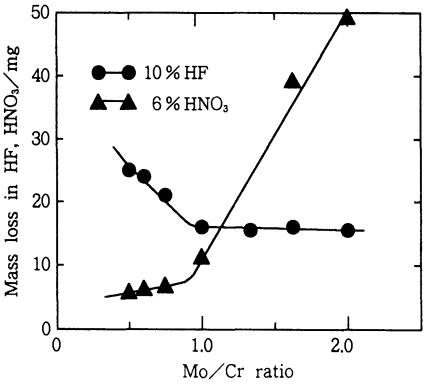

Fig.2 Effect of Mo/Cr ratio on mass loss of Ni－Cr－Mo－3.0Si－3.0B－1.0Cu alloys in 10% HF and 6% HNO_3.

Table 2 Chemical composition of the new alloy C703 (mass%).

Cr	Mo	Si	B	Cu	Ni
17.5	24.0	2.9	3.6	1.0	bal

Properties of the new alloy C703

It is difficult to produce alloy powder with this chemical composition by vacuum Ar gas atomization because of its high liquidus(1713K) and viscosity. Another process, taking advantage of powder metallurgy, should be studied to obtain this composition. In this study, a reactive sintering process during HIP was considered.

First, the Ni-31.0Mo-3.8Si-1.1Cu alloy powder was produced by the vacuum melting-Ar gas atomization method[4]. Then, this alloy powder (particle size:-100 mesh) and CrB powder (particle size:-325 mesh) were mixed for 32.5ks in Ar by using an attriter, where the relative proportion alloy powder to CrB powder was 79.0/21.0. This successfully compounded powder was expected to be reactively sintered during the HIP process.

Figure 3 shows the microstructure of the

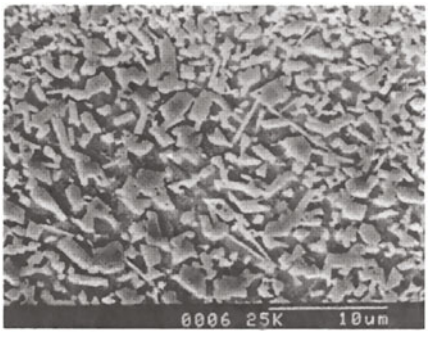

Fig.3 SEM photograph of the new alloy C703.

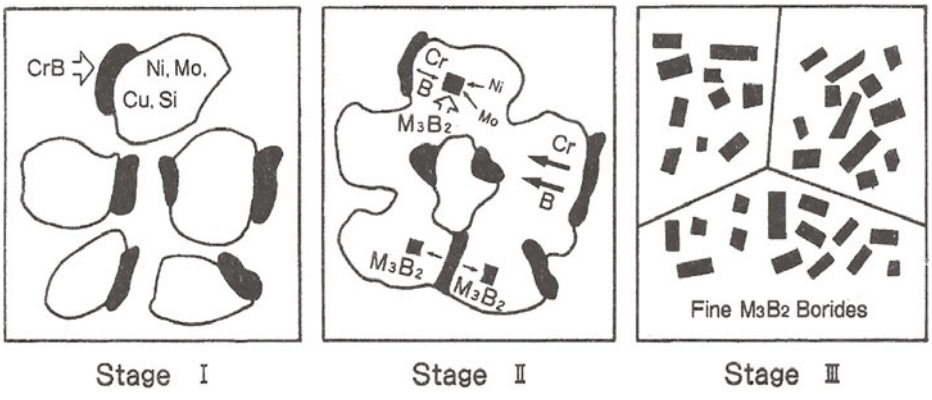

Fig.4 Schematic diagram of reactive sintering model.

new alloy C703 after HIP, which indicates that fine boride particles are homogeneously dispersed in the Ni-base alloy. It was identified by X-ray diffraction that this boride was M_3B_2(M:Ni, Cr, Mo) phase[6~9]. To clarify the mechanism of the fine dispersion of M_3B_2, the model shown in Figure 4 was examined. Stage I consists of the Ni-Mo-Si-Cu alloy powder and CrB powder after mixing. In this alloy, CrB is the non-equilibrium phase and M_3B_2 is the equilibrium phase. As can be seen in Stage II, during the HIP process, CrB particles decompose at the interface of the Ni-Mo-Si-Cu alloy powder. The decomposed Cr

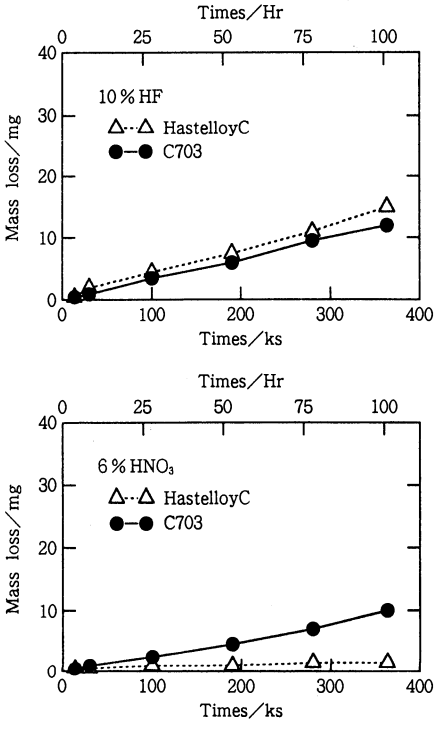

Fig.5 Mass loss of alloys in 10% HF and 6% HNO_3.

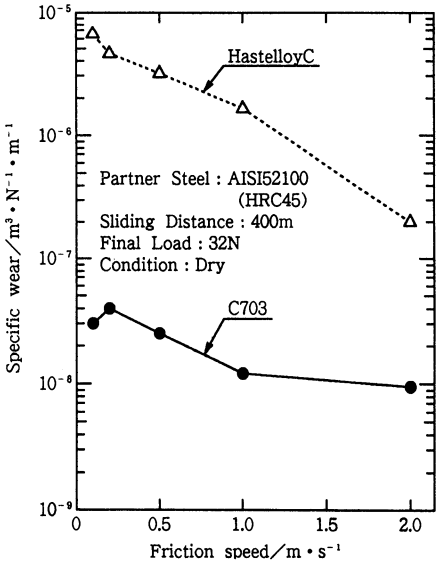

Fig.6 Results of Ohgoshi – type contact wear test.

and B are diffused into alloy powder and react with Ni and Mo. As a result, fine M_3B_2 boride particles reprecipitate in the alloy powder particles. Finally, the microstructure seen in StageⅢ is obtained.

Figure 5 shows the corrosion resistance of C703. The corrosion resistance to HF and HNO_3 of C703 was almost the same as that of Hastelloy C. Figure 6 shows the wear resistance of C703. The wear resistance of C703 was about 100 times superior to that of Hastelloy C, particularly under conditions of low friction speed. A low friction speed of 0.3m/s is the actual operating speed of plastic molding machines. It may be concluded that finely dispersed M_3B_2 particles improve wear resistance. Table 3 shows the mechanical properties of C703, which has high tensile and compression strength.

Table 3 Mechanical properties of C703.

Vickers hardness	786
Tensile strength (MPa)	1401
Compression strength (MPa)	2109
Elastic modulus (MPa)	28200
Poisson's ratio	0.28

Observation of the bond region of the HIP-produced bimetallic cylinder

Figure 7 is a cross-sectional photograph of a HIP-ed bimetallic cylinder. Figure 8 shows the electron probe microanalysis (EPMA) results of the bond region of C703 to Cr-Mo alloy steel. The diffusion layer was about 10 μm, and the main diffusion elements were Ni and Fe.

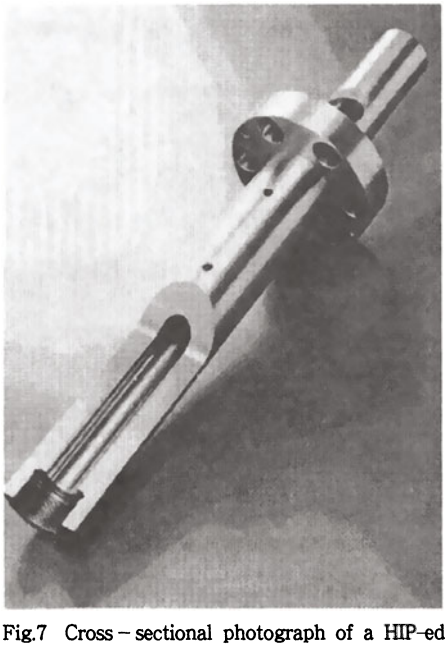

Fig.7 Cross-sectional photograph of a HIP-ed bimetallic cylinder.

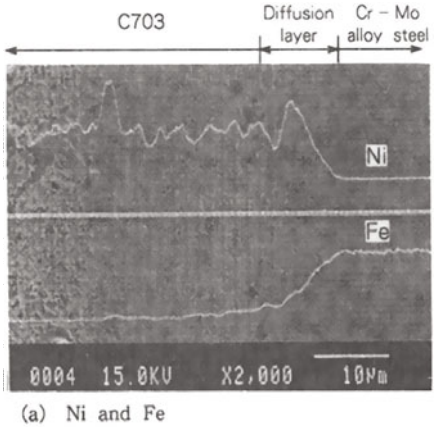

(a) Ni and Fe

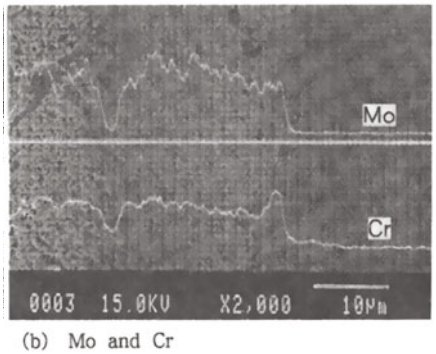

(b) Mo and Cr

Fig.8 EPMA results of C703 to Cr-Mo alloy steel.

RESULTS OF PRACTICAL APPLICATIONS

Since HIP-ed bimetallic cylinders lined with C703 were used for the injection molding of fluoroplastics reinforced by 3% to 5% glass fiber, the endurance life of these cylinders has reached more than two years and is still continuing, as compared with that of Hastelloy C, which is about three months. It may be concluded that the long endurance life of these cylinders was achieved by improving the wear resistance of Hastelloy C. C703 has also been applied to the twin barrels shown in Figure 9.

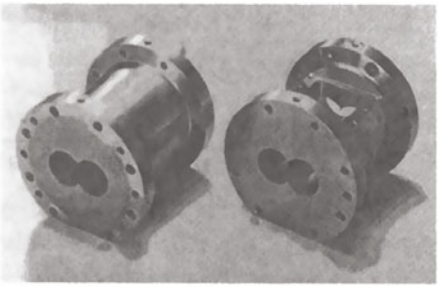

Fig.9 HIP-ed bimetallic twin barrels lined with C703

CONCLUSION

Bimetallic cylinders lined with a superior corrosion- and wear-resistant alloy were developed by using powder metallurgy and HIP diffusion bonding technology. The results were as follows:

1. The new alloy (named C703), whose chemical composition was Ni-17.5mass%Cr-24.0Mo-3.6B-2.9Si-1.0Cu, was obtained by reactive sintering between Ni-Mo -Si-Cu alloy powder and CrB powder during the HIP process. CrB particles were transformed into M_3B_2 particles during this process.
2. The corrosion resistance to HF and HNO_3 of C703 was almost the same as that of Hastelloy C. Furthermore, the wear resistance of C703 was about 100 times superior to that of Hastelloy C.
3. This bimetallic cylinder met with good results for injection molding of fluoroplastic reinforced with glass fiber.

REFERENCES

[1] Uhlig, H. H., Bond, P. and Fellor, H. J. Electrochemical Soc., 110, 650(1963).
[2] Weisert, E. D. Corrosion, 13, No.10, 659(1957).
[3] Satou, Y., Yoshikawa, K., Seki, Y. and Namba, K. Kobe Steel R&D Engineering Reports, 37, No.3, 3(1987).
[4] Kinzokubinran, ed. by Japan Institute of Metals, Maruzen, 756(1971).
[5] Tomoshov, N. D. Corrosion, 14(1958), 229.
[6] Kolomytsev, P. T. and Moskaleva, N. V. Porosh. Met., 71(1969).
[7] Ohmori, S., Hashimoto, Y. and Kohyama, K. J. High Temp. Soc., 7, 162(1981).
[8] Ohmori, S., Hashimoto, Y. and Kohyama, K. J. High Temp. Soc., 7, 167(1981).
[9] Ohmori, S., Hashimoto, Y., Kohyama, K. and Yamashita, M. J. Japan Inst. Metals, 48, 682 (1984).

MANUFACTURING OF HIP COMPOSITE ROLLERS THROUGH THE ROLLING PROCESS

TAKANORI KUROKI[1], HIRONORI KUROKI[2], KAZUHIRO OHKUBO[3],
TERUO ASAI[2], YUJI YANAGIDA[2] AND KAZUNORI HATTORI[2]

1 Kuroki Kogyosho Co., Ltd., Jinyama, Yahatanishi-ku, Kitakyushu 806, Japan
2 Kuroki Research Institute, Kuroki Kogyosho Co., Ltd., Jinyama, Yahatanishi-ku, Kitakyushu 806, Japan
3 Kuroki Composites Corporation, Kizuki, Kurate-machi, Fukuoka Pref. 807-13, Japan

ABSTRACT

In the manufacturing process of a HIP composite roller, powder is filled between a roller body and an outer cylindrical can, and sealed under vacuum. Then, powder is sintered and bonded to a roller body through HIP process. In the case of a roller not having a simple cylindrical shape but a more complex shape, for example, a hand-drum shape, manufacturing of an outer can is not an easy process. Authors have developed a method of manufacturing such a special-shaped HIP composite roller easily through the "rolling process". In the rolling process, a suitable amount of powder is poured between a handdrum-shaped roller body and a simple cylindrical-shaped can and then sealed into a vacuum. Then, the outer can is deformed into a handdrum-shape similar to the roller body by the rolling process. After the process, powder is distributed with uniform thickness between the roller body and the can.

INTRODUCTION

HIP composite rollers are manufactured by sintering and jointing powder to roller body with the use of HIP. In the manufacturing process of HIP composite roller, the powder is charged between the roller body and the outer cylindrical can and sealed in vacuum. Afterward, the powder is sintered and jointed to the roller body by the HIP treatment.

When the roller is not a simple cylindrical shape but a special shape such as a hand-drum shape, it is not easy to make the outer can. The authors developed the method making the HIP composite roller having such special shape by utilizing the "Rolling process". In this method, the

shape similar to roller body is obtained by charging an adequate amount of powder between the hand-drum-shaped roller body and the simply cylindrical can, and by sealing it in vacuum and then giving the rolling processing to the outer can. After this process, the powder is distributed by an uniform thickness between roller body and can. The workpiece processed by rolling is treated by HIP and machined into the product shape.

The HIP composite roller utilizing the rolling process has been used in various applications.

MANUFACTURING PROCESS OF HIP COMPOSITE ROLLERS

The manufacturing process of a hand-drum-shaped HIP composite roller is explained. Figure 1 shows the flow chart of manufacturing HIP composite roller.

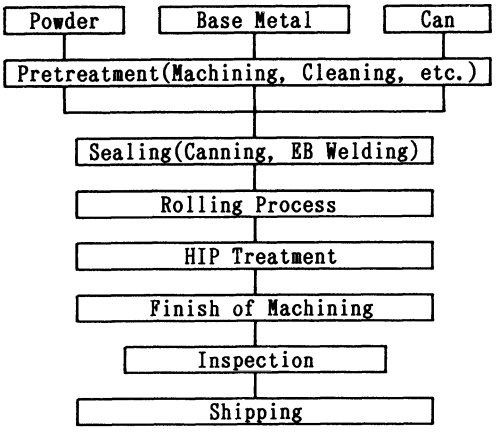

Figure 1. The flow chart of manufacturing HIP composite roller.

Raw materials

Figure 2 shows the raw materials for manufacturing the HIP composite roller. They are hand-drum-shaped roller body, cylindrical can, upper and lower lid, and powder. Powder material is utilized to form the surface layer of roller. High speed steel, Co-base hard alloy, etc. are used as powder material. Carbon steel is used as roller body material and then carbon steel or mild steel is used as can material.

Figure 2. The raw materials for manufacturing the HIP composite roller.

Assembly and seal

These roller body and can parts are rinsed and assembled. At first, the roller body and the cylindrical can are fitted and then the bottom lid is attached by an electron beam welding. Then, the required amount of powder is charged between the roller body and the cylindrical can as shown in Figure 3. In this case, the amount of charged powder is considerably less than the amount necessary to fill the space between the roller body and the cylindrical can. For example, it is approximately 1/4-1/2 of such space volume.

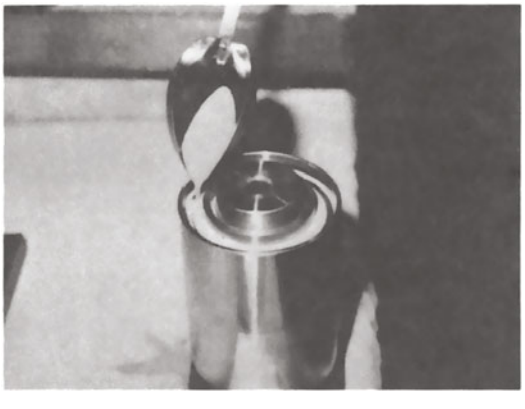

Figure 3. Charging the powder into the space between the roller body and the cylindrical can

After placing the upper lid, seal welding is done in vacuum by electron beam welding, thus causing the space with powder between the

roller body and the cylindrical can to be under vacuum. Figure 4 shows the roller workpiece after vacuum sealing.

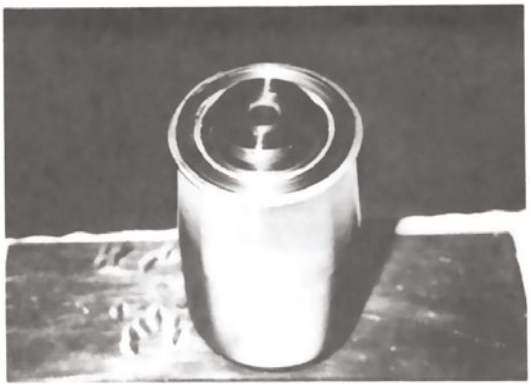

Figure 4. The roller workpiece after vacuum sealing.

Rolling processing

The roller workpiece assembled at the state of sealing powder in vacuum is formed through the "rolling process". The rolling processing is performed by lathe as shown in Figure 5. The cylindrical can is formed to the shape similar to the hand-drum-shaped roller body by pressing the rolling tool of the lathe to the cylindrical can. Figure 6 shows the appearance of shaped roller workpiece. The powder between the roller body and the outer can is packed very closely at this state.

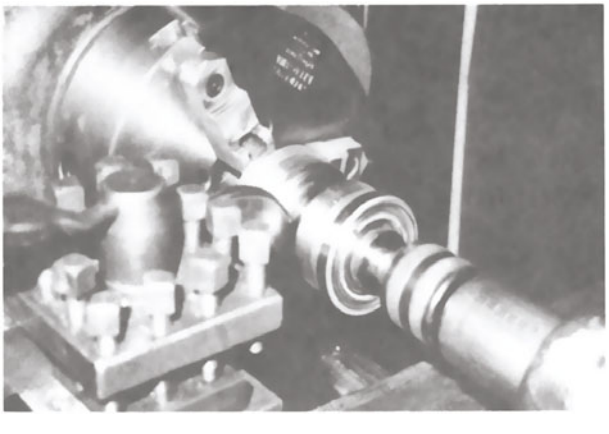

Figure 5. Rolling process.

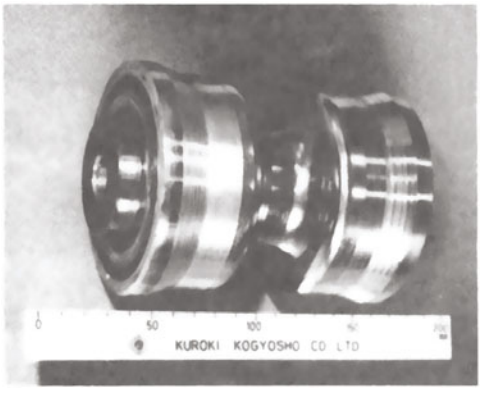

Figure 6. The roller workpiece shaped by the rolling process.

HIP treatment

The shaped roller workpiece is subjected to the HIP treatment. For the HIP treatment condition such as temperature, the condition causing the powder to be sintered and jointed to the roller body is to be selected. Figure 7(a) shows the workpiece after HIP treatment and, Figure 7(b) shows its sectional view.

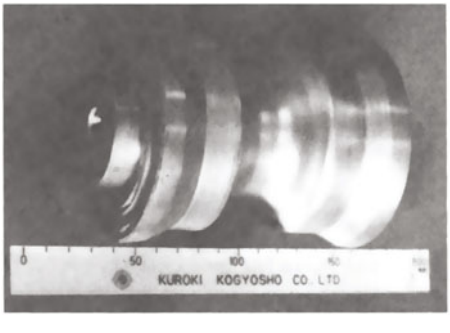

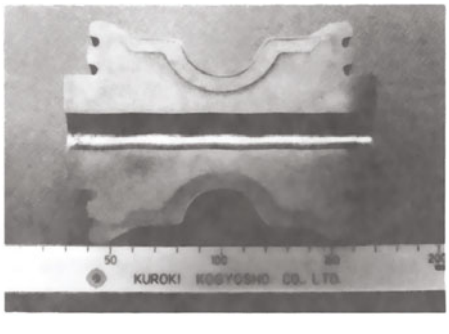

(a) The outer view. (b) The sectional view.

Figure 7. The roller workpiece after HIP treatment.

Finishing processing

The hand-drum-shaped HIP composite roller can be finished by machining the HIP treated workpiece. Figure 8(a) shows the finished product of the HIP composite roller and then Figure 8(b) shows its sectional view.

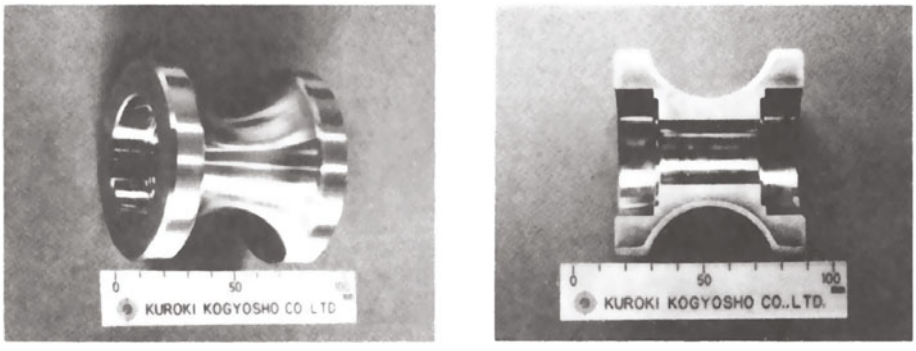

(a) The outer view. (b) The sectional view.

Figure 8. The finished product of the HIP composite roller.

MERITS OF UTILIZING THE ROLLING PROCESS IN MANUFACTURING THE HIP COMPOSITE ROLLER

1. The outer can is able to be manufactured very easily.
2. Utilizing the rolling process makes the amount of powder used lesser.
3. In the rolling process, the powder is packed closely before HIP, so there is no defect such as lack of thickness at surface layer.
4. The workpiece after HIP has the shape similar to the product, so the amount of machining of the hard layer is lesser.

APPLICATIONS OF HIP COMPOSITE ROLLERS MANUFACTURED THROUGH ROLLING PROCESS

The examples of the applications of HIP composite rollers manufactured through the rolling process are as follows:

1. Guide rollers for a wire rod rolling line.
2. Bar steel feeding roller in an automatic hot forging equipment.

REFERENCES

1. Kuroki, H. and Yanagida, Y., Diffusion Bonding by HIP. Bulletin of Japan Institute of Metals, 1989, **28**, 910-915.
2. Kuroki, H., Application of Diffusion Bonding by HIP. Preprint of International Symposium on New Joining of Materials, Kyushu Institute of Technology, Kitakyushu, Japan, April 1990, pp.9-15.

DIFFUSION BONDING OF SILICON NITRIDE ENGINEERING CERAMICS TO METALS USING HOT ISOSTATIC PRESSING

WEI SIMING WANG SHENGHONG
Central Iron & Steel Research Institute
No. 76 Xueyuan Nan Lu , 100081 Beijing , P. R. China

ABSTRACT

The bonding of Si_3N_4 to carbon steel by hot isostatic pressing (HIPing) has been investigted . The joining parameters such as temperature , holding time , pressure , surface roughness have been studied as well. To enhance the bonding and reducing the thermal stress after joining inserted interlayers which were Ti, Zr, Mo, Cu, Ni, Cu-Mo, Ni-Mo etc. were used . The eutectic reactions were found at interface during joining of Si_3N_4/steel and Si_3N_4/Ni . The highest tensile strength of 62Mpa was obtained for Ni-Mo insert . But fracture occured at interface resulting in formation of brittle phases for Ti , Zr , Mo inserts .

INTRODUCTION

Ceramics is expected to be applied as structural materials because of its excellent mechanical and thermal properties, but the hardformability and brittleness of ceramics are fatal weakness for structural components. Ceramics may always be used combining with other kinds of material, especially, with metals. Joining of metals to ceramics becomes an important subject on which many studies have been carried out recently. There are two essential problems in metal-ceramic joints. One is whether or not the ceramics and metals can be metallurgically bonded to each other. The other is whether or not the ceramics will be cracked by thermal stresses resulting from the difference of thermal expansion coefficient between ceramics and metals. As a structure material, special attention has been paid to silicon nitride for its com-

prehensive properties. As compared with oxide ceramics joining of which has been widely investigated nonoxide ceramics is more difficult to join with metals for their greater dissimilarity in physical nature. The common used methods of joining dissimilar materials are adhesion, mechanical joining, brazing and solid—phase bonding (1, 2). Joining by hot isostatic pressing (HIP) is one of prospective methods which has been reported recently (3, 4). The combination effects of solid-phase bonding and anchoring may make a strong bonding of silicon nitride with metals. Therefore, the purpose of this paper is to study the joining of Si_3N_4/steel by HIP using a tensile specimen instead of thin metal pieces and the effects of residual stress on bonding.

EXPERIMENTAL

Pressureless sintered silicon nitride used in this study was made in the same laboratory. It contained Al_2O_3 and Y_2O_3 with a relative density of 85-98%, hardness HRA 85-89 and 3 point bending strength 320-570Mpa. Steel used for joining was commercial ordinary carbon steel contained 0.45%wt. C. Pure metals Ti, Zr, Mo, Cu, Ni with purities of 99% or more and thickness varied form 0.08 to 0.7mm were selected as constituents for the joining. Low carbon steel capsules were used for HIPing. All tested materials were ground, cleaned ultrasonically with acetone and alcohol before use. Bondings were carried out in a HIP unit. The tensile strengths were measured with the specimens, dimensions of which are of $\phi 14\times 5$mm, $\phi 14\times 60$mm and $\phi 14\times 0.08$-1.0mm, for ceramics, steel and interlayers respectively (see Fig. 1). The interfacial reactions were observed by SEM-EDAX, XRD, TEM.

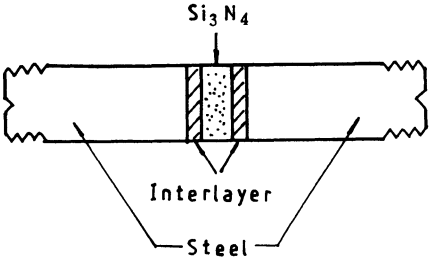

Figure 1. Schematic drawing of tensile specimens for Si_3N_4/steel joining

RESULTS AND DISCUSSION

1. The joining of silicon nitride to carbon steel

Fig. 2 showed the bonding strength of the Si_3N_4/steel joining as a function of bonding temperature. The fracture which is a "concave /convex" fracture mode due to the thermal expansion mismatch occurred in the silicon nitride side near the interface. The bonding strength was decreased by 40% with increasing the bonding temperature from 32Mpa at 1060℃ to 20Mpa at 1340℃, but it was only decreased by 13% at 1200℃.

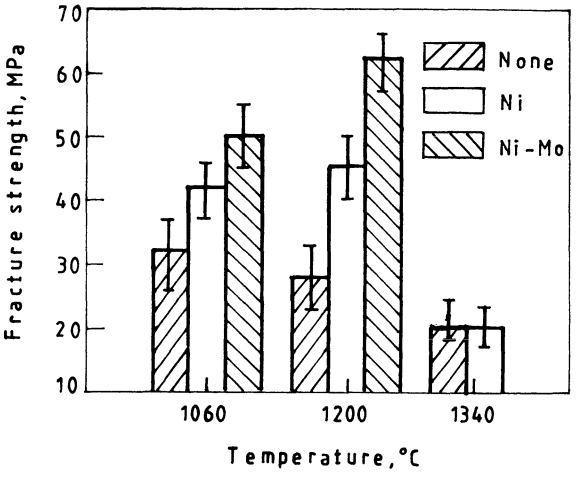

Figure 2. Effect of bonding temperature and interlayers on fracture strength of Si_3N_4/metal join, 100Mpa. 2hr.

Increasing the relative density of Si_3N_4 ceramics from 85% to 98% the bonding strength was also increased by a factor of 2 at 1200℃. Fig. 3 is the morphology of the interfaces of Si_3N_4/steel reacted at 1060℃, 1200℃ and 1340℃ which shows good contact between them. The surface irregularity of Si_3N_4 at 1200℃ could be seen obviously and it became more serious with raising bonding temperature. A transition layer with a microhardness of 2400Mpa was formed at the interface. The microhardness of this transition layer is higher than that of ferrite (2050Mpa) but lower than that of pearlite (3000Mpa) . The thickness of the layers changed with the bonding temperature. It was found by EDAX that silicon diffused deeply into the steel and the formation of Fe_5Si_3 was reconized

by XRD. This soft transition layer plays a role as compensation for thermal expansion mismatches between two parts. That is why small drop of bonding strength was made at 1200℃ for Si_3N_4/steel joints. Formation of eutectic liquid resulting in reaction of Si_3N_4 and iron had intensified the irregularity of reaction region. The change of pressure in the system had a little effects on bonding. Extending the time of bonding from 1hr to 5hr made this layer thicker but had a little effects on the bonding strength. Therefore, bonding temperature is the main factor by HIPing method.

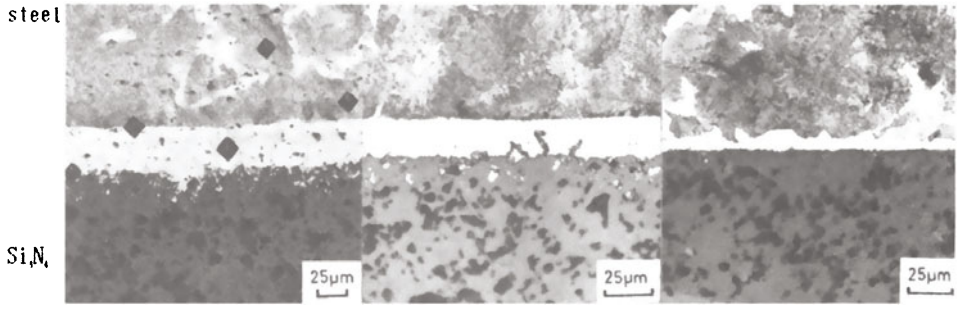

Figure 3. Morphology of Si_3N_4/steel interface at different bonding temperatures, 100Mpa, 2hr.
(a) 1060℃, (b) 1200℃, (c) 1340℃

Since surface prepartion was important for a good joining, 3 kinds of surface roughness of Si_3N_4 from 0.3μm to 0.8μm were tested at1060℃, 100Mpa for 2hr. But no effects on bonding strength were detected. Compression deformation of steel under HIPing conditions kept good contact at interface with ceramics. The advantages of joining with rough surface by HIP technology are less damage to ceramics during surface fine preparation, extend the contact area and more gripping force. To strengthen the bonding the ceramic specimen was inserted into a steel piece with a cylinderic hollow and the cylinder surface of ceramics was subjected to compression stress during the cooling which had enhanced the bonding strength of twopieces. The bonding strength was from 28Mpa up to 240Mpa (test bar with a thin layer of steel)but more detail calculation should be made before making a conclusion.

2. The joining of silicon nitride to carbon steel with inserted interlayers.

Low bonding strength of Si_3N_4/steel is related to thermal stress set up in the joined workpiece. The thermal stress may be relieved by inserting a ductile metal or a metal with approximately the same thermal expansion coefficient. In present investigation variousinsert metals were used. Fig. 4 is the morphology of bonding for Ni insert, which was similar to Si_3N_4/steel joint. The Ni_3Si phase was detected by XRD TEM at different joining temperatures and eutectic reaction was found as well. Higher bonding strengths were obtained as compared with Si_3N_4/steel with the highest bonding strength of 45Mpa at 1200℃ (see Fig. 2). The fracture was also occurred in the Si_3N_4 side. Addition of Mo layer which has a low thermal expansion coefficient and was adjacent to the Ni layer strengthens the bonding by a factor of two. Bad bonding with single layer of Mo fractured at interface was obtained at 1060℃, partial fracture occurred within Mo at 1340℃ which showed requirement of higher bonding temperature for Mo. At interface formation of brittle phases Mo_5Si_3 and Mo_3Si led to failure of bonding. More soft copper, as substitution of Ni was investigated for Si_3N_4/Cu/steel at 900-1200℃ and weak bonding was found with bonding strength less than 10Mpa. EDAX indicated the diffusion of Si but not any Cu-Si phases at interface. Bad wetting of Cu also made joining failure at 1200℃, though there was good contact at interface. Addition of Cu-Mo layer improved the joining but with low bonding strength. By using active metal layer (Ti, Zr, Ti-Cu, Ti-Ni, Zr-Ni) the formation of brittle phases, such as TiN, ZrN, Ti_5Si_3, Zr_5Si_3 etc., Leads to the failure joining at interfaces.

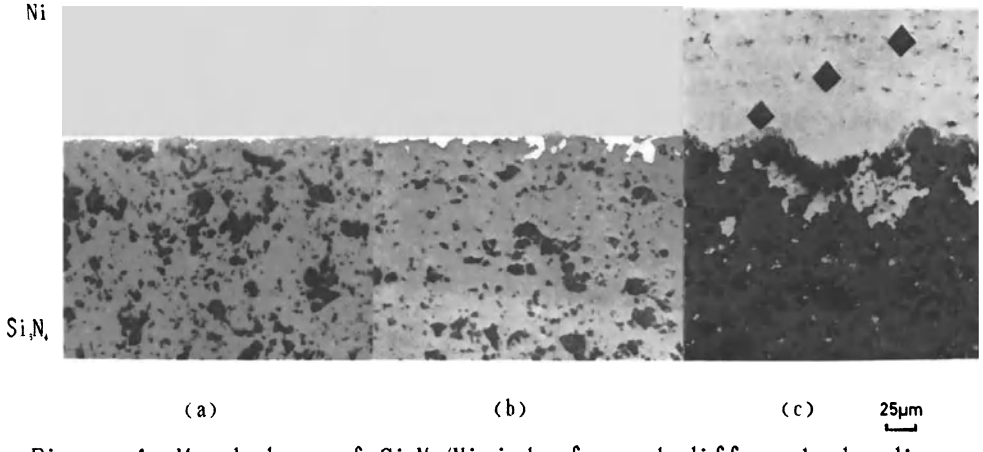

Figure 4. Morphology of Si_3N_4/Ni interface at different bonding temperatures, 100Mpa, 2hr.
(a) 1060℃ (b) 1200℃ (c) 1340℃

CONCLUSION

1. Eutectic joining with good contact at interface has been found for Si_3N_4/steel, Si_3N_4/Ni/steel joints. The later had higher bonding strength than that of Si_3N_4/steel and further improvement of strength has been achieved for Si_3N_4/Ni/Mo/steel joint.
2. Failure to join Si_3N_4/steel with active metal interlayer, such as Ti, Zr, Ti-Cu, Ti-Ni, Zr-Ni was found due to formation of brittle phases at interface. Joining with Cu, Cu-Mo interlayers was failured for its low reactivity with Si_3N_4.
3. HIP joining method can keep a complete contact and integrity interface regardless of roughness of workpieces, the metal may undergo plastic deformation and the irregular space of ceramics surface is filled with metal. In this way, the improved bonding was achieved by the anchoring effect.

REFERENCES

1. Elssner, G. and Petzow, G., Metal/Ceramic Joining. ISIJ International, 1990, 30(12), 1011-32.

2. Suganuma, K., Recent advances in joining technology of ceramics to metals. ISIJ International, 1990, 30(12), 1046-58.

3. Tanaka, K. and Ishizaki, K., Sintering of Advanced Materials--Applications of Hot Isostatic Pressing--, Uchida Rokakuho Publishing Co. Ltd., Tokyo, Japan, 1987, pp. 121-37.

4. Koizumi, M., Takagi, M., Suganuma, K., Miyamoto, Y, and Okamoto, T., Solid-State Bonding of Silicon Nitride to Metals Using HIP. In High Tech. Ceramics, ed. P. Vincenzini, Elsevier Science Publishers B. V., Amsterdam, 1987, pp. 1033-42.

STRUCTURE AND PROPERTIES OF THE BONDAGE AREA BETWEEN STEEL AND SUPERALLOY

Kratt E. P., Sobiev A. S., Blanter M. S., Burtsev A. G. Haykin R. A., Samarov V. N.

Abstract

A superalloy coating has been HIPed on cast low-carbon steel to protect it from corrosion and wear. The bondage area has a complex structure: it is narrow (25-35 m wide) on the steel side and wide (250-350 m) on the superalloy's. The part of the boundary area which is located in the superalloy consists of one sub-area and has no second-phase percipitations and two sub-areas containing various percipitations. The bondage strength turns out not to be lower than that of steel. Rupture initiates on fine second-phase particles. They contain Al, O and C distributed on the contact surface between steel and superalloy. Then rupture spreads from the contact surface into steel.

1. Introduction

Functional coatings on conventional materials enlarge ranges of their application without substantial raise of cost. E.g. christmas-tree body-parts are made of cast low-carbon steel and then are clad with corosion- and wear-resistant coating. The PM technique is successfully used here [ ]. Christmas-tree body parts are to have a high level of reliability which is provided by steel and bondage strength and cast quality. Henceforth the bondage area between steel and the coating is of the greatest interest. The aim of the work under consideration is to investigate its structure. This problem is also of general scientific interest as it helps to realise regularities of bonding of different materials under HIP conditions.

2. Experimental

2.1. Raw materials

Low-carbon steel was used in form of rods 15 mm in dia and 50 mm in length cut out from the casting. Chemical composition of the steel was the following (in weight %): 0.260-0.330 C, 0.80-1.10 Cr, 0.20-0.30 Mo, 0.40-0.90 Mn, 0.20-0.40 Si, less than 0.04 P and S each.

The superalloy powder was automized and was the following chemical composition (in weight %): 52.10-52.80 Ni, 8.0-10.0 Cr, 3.50-4.20 Mo, 4.80-5.20 Al, 5.20-5.90 W, 1.60-2.0 Ti, 2.50-2.80 Nb, approx. 0.05 Mn, 0.10-0.40 Hf, approx. 0.015 B and Zr each, approx. 0.01 Ce, 0.02-0.06 C, Ni bas.

2.2. Compaction

The steel rod was placed into a cylinder can and filled with the superalloy up to the height of 60 mm. Then the whole bulk was preliminarily pressed to the density of 5.5 g/sm^3 by means of vibration.

This sequence of operations allowed to obtain after sintering a massive rod 10 mm in dia by 80 mm in length, combined of steel and Ni alloy with boundary surface perpendicular to the axis of samples to be done.

2.3. Densification

Densification was obtained by HIPing

2.4. Mechanical tests

Tensile tests were carried out on cylinder samples with working part 5 mm in dia by 25 mm in length. The specimens were combined of the superalloy and steel with the boundary surface perpendicular to the sample's axis. Impact toughness was defined on the samples 5 10 55 mm with U-notch. The notch was cut out exactly in the contact surface. Also the hardness with the 0.05 N loading was defined. Before the tests all samples were subjected to standart heat

-treatment: oil quenching from 880+10°C (holding at the temperature within 15 min), tempering at 650+10°C, 2 hours, air cooling.

2.5. Microstructural study

Microsections were made perpendicularly to the boundary surface of steel and the superalloy. They were studied with transmission and scanning EM. In the latter case chemical composition was defined with MPCA. Fracture of the samples was studied with SEM and MPCA. Some cylinder samples with ring-shaped notch in the boundary area were ruptured under the temperature of liquid nitrogen in order to study their structure and chemical composition.

3. Results

3.1. Microstructure and chemical composition of the boundary area.

Fig.1 shows microstructure of boundary area in reflected electrons. Steel is in the upper part of the picture, superalloyin the lower. Areas studied with MPCA are marked with * sign, their chemical compositions are in Table 1. Fig.2 shows the bondage area under bigger magnification.

Points NN 2,3,4 are marked in the steel area; its composition has not changed during HIP. Point N 5 is marked in the boundary area, which is 25-35 m wide. Boundary area consists of steel enriched with Ni, Co, Cr, V from the superalloy. The initial contact surface is the zero point from which distance to different points is counted (look Table 1, positive direction is on the steel side, negative - on the superalloy's). There is a thin layer of Al and Ti rich particles on the boundary surface itself.

The diffusion zone in the superalloy is far more wide (approx. 250-350 m) according to the MPCA data. There are 3 sub-areas in it: the first one is about 20 m wide (point 6) and contains no second-phase percipitations, the second is about 50 m wide (points 7-

8) and contains white carbide percipitations, the third is up to 200 m wide and contains dark percipitations. Unevenness of this sub-area is proved by high local growth of concentration of elements on the boundary surface according to the MPCA data.

Hardness measurements (by the microhardness method) has also proved that all the variations of the chemical composition take place in the sub-area which is less than 250 m wide on both sides of the boundary surface.

An attempt to investigate the described sub-areas was made with the help of transmission electron microscopy, but failed because it cannot be defined which part of the boundary area is on the foil and the boundary surface itself isn't seen on the foil.

3.2. Bondage strength

Mechanical properties of the bondage area turn out to be the following: yield strength =645 MPa, tensile strength =770 MPa, specific elongation =10 %, specific contraction =30 %, impact strength =15 j/sm. Properties' values are close to those of steel after the same treatment (HIP + quenching + tempering) but the plasticity of steel is higher. At the same time the superalloy's strength is much more higher than that of steel and boundary area: σ_s =820 MPa, σ_ℓ =1185 MPa, δ =15 %, ψ =20 %. So HIPing doesn't decrease bondage strength which is limited by that of steel.

3.3. Fracture structure

Fig. 3 shows the typical fracture structure of the tensile sample at room temperature. The initial granule's surfaces are clearly seen, they consist of sells of various dimensions (three areas with sells of different dimensions are marked 1,2,3). MPCA showed high Fe, Al and Cr contents, i.e., rupture took place in the boundary area on the steel side.

Some zones of the fracture are located not only in steel, but in the superalloy as well. It means that the rupture crack may cross

various sub-areas of the boundary area. This is also proved by the difference between the three types of fracture (NN 1,2 and 3, Fig. 3). Fracture zones of the second type contain some more alloying elements (Ni, Ce, W, Mo, Ti) and less Al than the zones of the first and second type.

The second-phase particles are clearly seen in the fracture. Thus, in the steel zones particles 5-8 m in dia are present which are close to MnS in their chemical composition. Fig. 4 shows that the fracture sells include a lot of small particles 1-4 m in dia containing Al, O and C.

Samples subjected to fracture at the liquid nitrogen temperature ruptured also in the boundary area on the steel side. That was proved by the chemical composition of the fracture zone (75% Fe, 19% Ni, 1% Mo, 1.3% Cr, 1% Ti, 0.5% C in weight %).

4. Discussion

Boundary area between the steel and the superalloy is be assymetric, i.e., narrow on the steel side and wide on the superalloy's. The steel part of the boundary area is more homogeneous, and the superalloy's part includes at least 3 structural sub-areas. This might have been caused by the following:

-the superalloy had much more developed surface than steel as it was in powder state -C diffuses from steel and reacted with strong carbide-forming elements (Mo, W, Ti, Nb). That caused re-distribution of these elements in the boundary diffusion area and formation the sub-areas with white carbide percipitations and other phases' dark percipitations. Such reactions may displace Al onto the contact surface and form a chain of Al-rich particles on it (Fig. 2)

The boundary area on the steel side is enriched with Ni and other elements. That makes its chemical composition close to that of maraging steel. The relatively quick cooling from HIP temperature (1200°C) is equivalent to quenching, and tempering at 850 and 650 C - to ageing of such steel. Therefore the boundary area has enough strength. In spite of that rupture takes place in most cases in the

boundary area on the steel side. It initiates on the Al-rich particles as there is a lot of them in the fracture zone.

5. Conclusions

The main conclusions of the study are:

-strength of the combination "steel-superalloy" turn out to be not lower than that of steel -the diffusion area on the superalloy side is an order of magnitude wider than it is on the steel side and consists of several sub-areas -rupture of the combination initiates on the particles which are located on the contact and takes place mainly in the boundary area on the steel side.

6. List of illustrations

Fig. 1. SEM micrograph of the boundary area between steel and superalloy (330)

Fig. 2. SEM micrograph of the boundary area (×1500) Fig. 3. SEM micrograph of the fracture surface (× 300) Fig. 4. SEM micrograph of a fracture particle (a) and Al (b), O (c) and C (d) distribution (×3500)

Table 1

Chemical composition of the boundary zone stated by MPCA

Point number on the Fig. 1	Distance from the contact surface	Composition in weight %								
		Fe	Cr	Mo	Ni	Co	Al	Ti	Nb	W
4	+30	96.3	1.0	0.5	0.3	0.0	0.1	0.0	0.1	0.0
5	+9	70.0	5.1	1.6	15.8	6.0	0.7	0.0	0.0	1.5
6	-9	24.1	7.0	3.8	41.5	12.5	2.8	1.2	2.1	5.1
10	-84	0.3	8.9	3.8	58.9	16.1	5.3	0.7	0.7	5.3

Not all of the elements are included in the table so the concentration sum is not equal 100%.

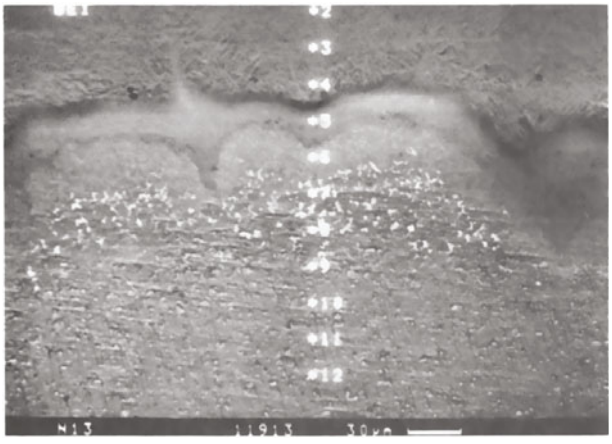

Figure 1

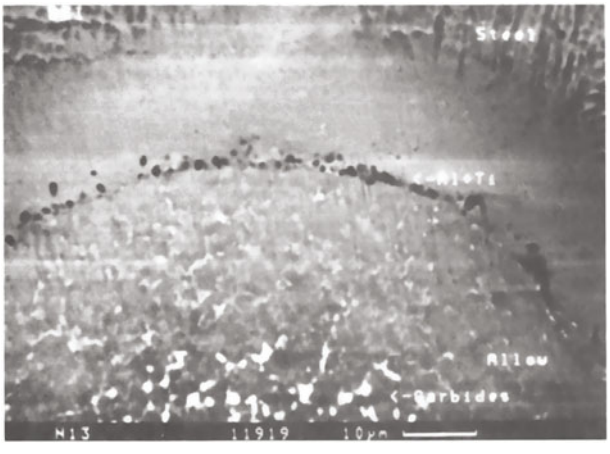

Figure 2

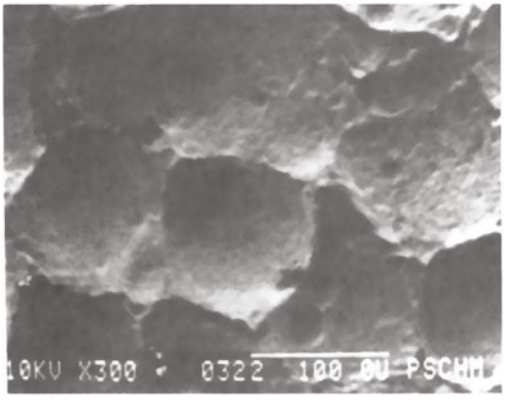

Figure 3

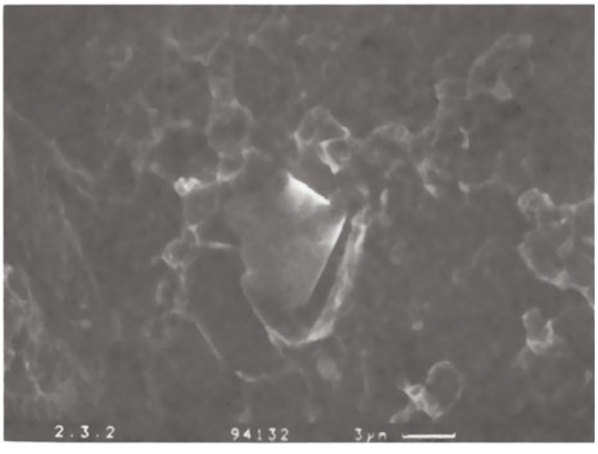

Figure 4a

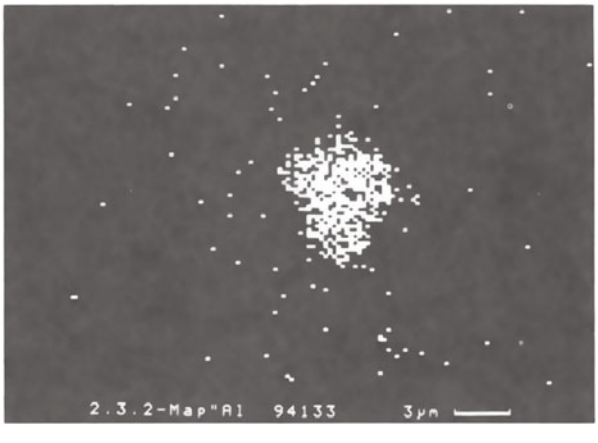

Figure 4b

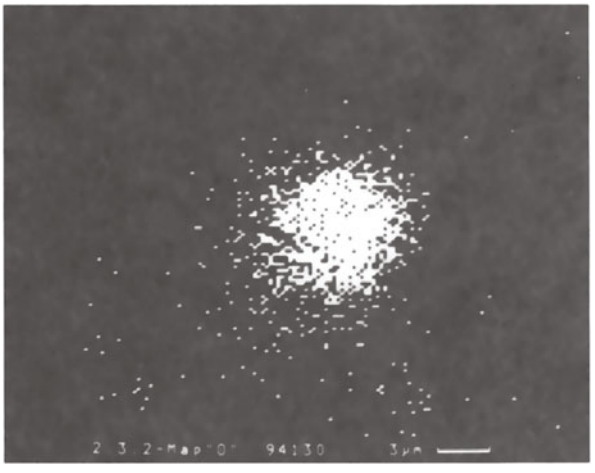

Figure 4c

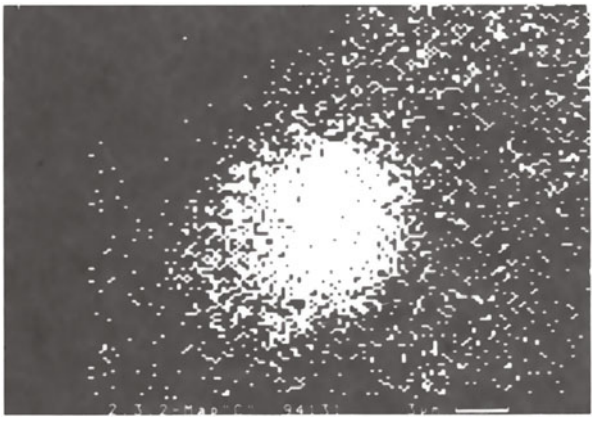

Figure 4d

6. HIGH TC SUPERCONDUCTORS

HIGH OXYGEN PRESSURE ($Po_2 \leq 3000$bar, $T \leq 1200°C$) INVESTIGATIONS IN THE $Y_2Ba_4Cu_{6+n}O_{14+n}$ FAMILY.

J.Karpinski, S.Rusiecki, E.Kaldis, E.Jilek, Laboratorium für Festkörperphysik
ETH 8093–Zürich.

Abstract.
A review of the phase diagram studies of the Y–Ba–Cu–O system under high oxygen pressure, is given. The structure and properties of the three superconducting phases are discussed together with some new defect structures.

1. Y–Ba–Cu–O superconducting phases and their properties.
In the $Y_2Ba_4Cu_{6+n}O_{14+n}$ family of compounds three members have been discovered up to now, corresponding to n=0,1 and 2.

a) n=0: $YBa_2Cu_3O_{7-x}$, the 123 phase has a T_c ($30<T_c<93$ K) dependent on the oxygen content. The maximum T_c corresponds not to the maximum oxygen content 7 but to 6.90 (1) or 6.94 (2). This is probably the most investigated HT_c superconductor because it is easier to synthesize. However, inspite of a large number of publications many basic properties of this compound remain still unknown. For example, it has been shown recently that the 123 phase is thermodynamically unstable under Po_2 = 1bar at the temperature $T \leq 750$C (3,4), which is in agreement with our phase diagram (5). This means that under the conditions considered to correspond to the stability range of the superconducting (orthorhombic) phase, the 123 compound is metastable and would tend to decompose to the stable phase 124. Only slow kinetics prevent this reaction. The "low temperature" synthesis from oxides of total composition of the 123 phase, at Po_2 = 1 bar and T = 750C, leads to the 124 phase (3,4). The decomposition proceeds much faster under increased oxygen pressure. Already under Po_2 = 40 bar at T=900C we have observed after 50 hours the decomposition of the 123 in the 124 phase, with $BaCuO_{2+x}$ and Y_2BaCuO_5 as byproducts.
In addition to the above mentioned instability of the cation lattice, also the instability of oxygen in the chains of the 123 structure (nonstoichiometry), is characteristic for the 123 phase. It is well known that this oxygen is unstable at

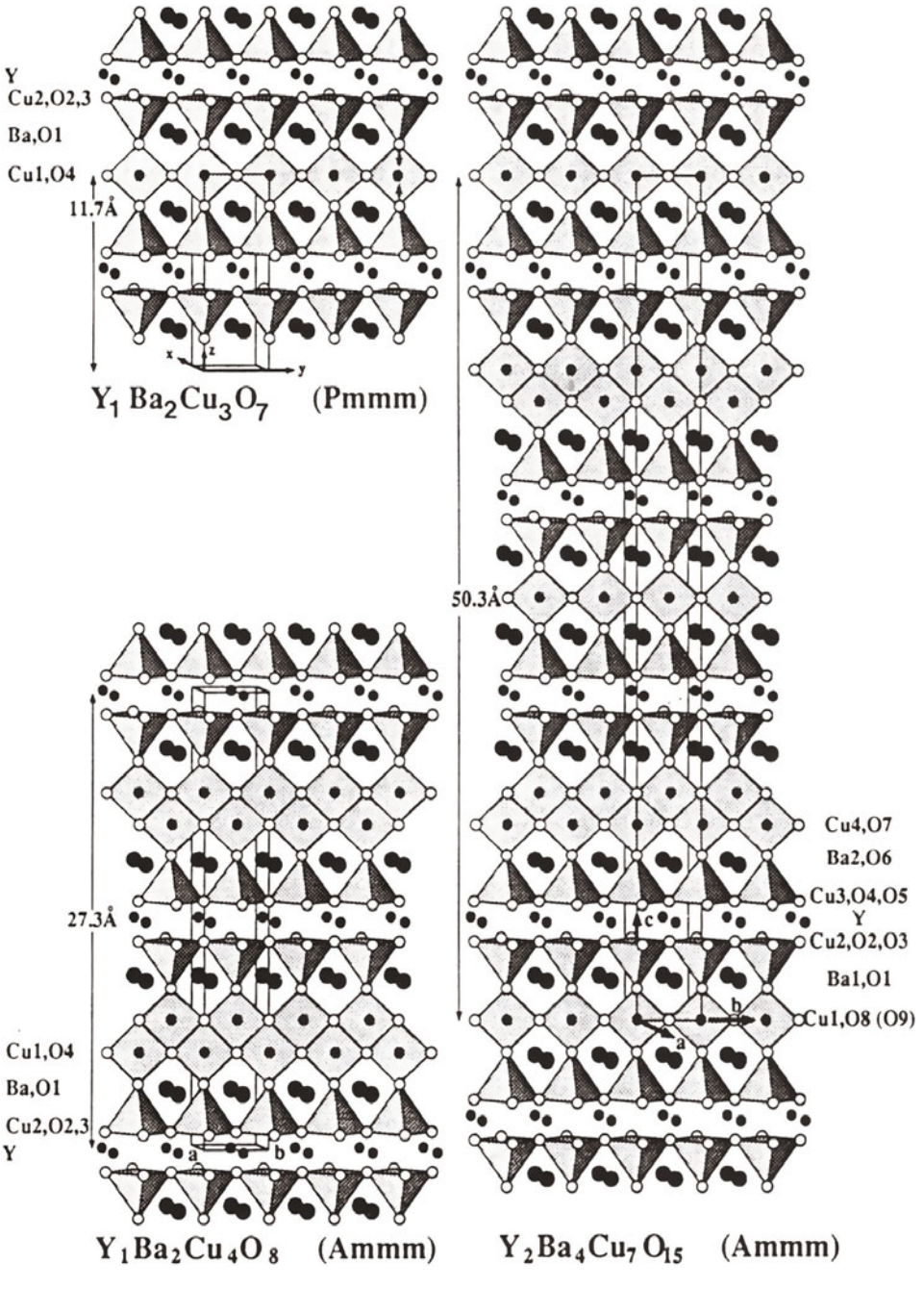

Fig.1. Three phases existing up to now in the $Y_2Ba_4Cu_{6+n}O_{14+n}$ family.

temperatures above 350C. At 650C in air every other oxygen in the chains dissapears, leading to a phase transition to the nonsuperconducting (tetragonal) phase. Due to the reversibility of this reaction, slow cooling in oxygen atmosphere allows the oxygen atoms to diffuse back in the structure. However, from the technological point of view one has to consider these two kind of instabilities as drawbacks. The problem of the phase instabilities will be discussed further in the phase diagram (sect.2).

b) n=2: $YBa_2Cu_4O_8$ (124, T_c=81K) This phase has been synthesised for the first time in bulk under high oxygen pressure (6). Also single crystals of the 124 phase have been obtained from the flux under high oxygen pressure (7,8,9). The 124 phase has four important advantages in comparison with the 123. It contains double (instead of single in 123) CuO chains, which leads to higher coordination of the equatorial oxygen of the chains (O_4 site). Each oxygen atom has three (instead of two in 123) nearest copper atoms. This higher coordination causes higher stability of the oxygen in 124 (up to 880C). This is the first advantage which leads to the second one – the 124 has oxygen stoichiometry fixed, which means it is insensitive to the method of cooling. The loading with oxygen during cooling is unnecessary, the oxygen content in the chains is fixed already at high temperature.

The third advantage is a direct result of the stoichiometric character. As no oxygen is lost, no twinning takes place in a–b plane (opposite to 123) and, therefore the a–b anisotropy can be for the first time measured (10).

The fourth advantage is the thermodynamic stability at T≤880C under Po_2=1bar, opposite to the 123 phase which is metastable at T≤750C.

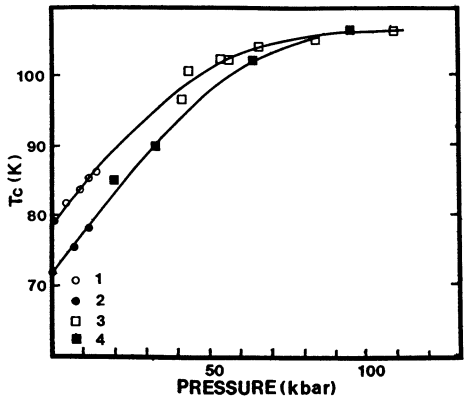

One of the most important properties of the 124 phase dicovered in our laboratory (11,12) is the strong pressure dependence of T_c (Fig.2). By application of very high hydrostatic pressure one could increase T_c up to 108 K (13,14). The pressure coefficient is very high :0.55 K/kbar. This brings up the idea of cation substitution in the 124 structure by atoms of different size in order to create internal pressure. Miyatake et al (15) succeeded in increasing the T_c of up to 90K by doping with Ca.

Fig.2. T_c dependence on hydrostatic pressure for the 124 phase; 1) ceramic material (11), 2) single crystal (11), 3) ceramic material (13), 4) single crystal (14).

These authors (15) believe that Ca^{2+} substitutes Y^{3+}, leading to the increase of the number of holes and T_c. Our investigations (16,17) showed, that opposite to that Ca^{2+} substitutes Ba^{2+} and the number of holes remains constant.
Therefore the increase of the T_c could be explained as an internal pressure effect due to the different size of ions. This is also supported by the fact that Ca doped 124 has smaller hydrostatic pressure dependence of T_c than undoped material. Part of the pressure effect has been already exhausted by the internal chemical pressure effect (12).

c) n=1: $Y_2Ba_4Cu_7O_{15-x}$ (247) is an intermediate compound containing alternating single and double chains. This compound has been obtained for the first time under high pressure (9) and its structure has been determined by x–ray diffraction on single crystals (18).
This compound has structural elements of both 123 and 124 phases. The double chains have fixed stoichiometry, but the occupation of the single chains varies. The T_c can be varied from 14 to 70 K (19) (Fig.3) by change of the oxygen stoichiometry from 14 to 15. Some authors achieved higher values of 95K (2,20) by loading more then 15 oxygen atoms per unit cell,15.3 in ref. (2). The dependence of the T_c on oxygen content in the single chains is linear, opposite to the two plateau behaviour of the 123 phase (Fig.3). This compound is also sensitive to the high hydrostatic pressure and the value of pressure coefficient is very high: 0.48 K/kbar. The strong dependence of T_c on oxygen content in single chains suggests that here the single chains play an important role in adjusting superconductivity. However, this phase is superconducting even with almost empty single chains ($x \cong 1$), opposite to the 123 phase which loses superconductivity with half filled single chains.

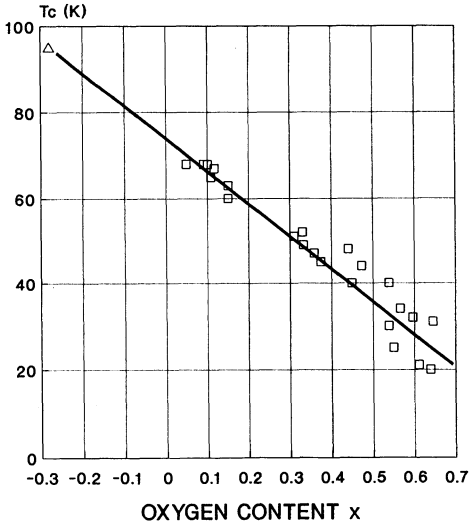

Fig.3 T_c dependence on oxygen content for $Y_2Ba_4Cu_7O_{15-x}$. Δ – point from J.–Y.Genoud et al (2).

2. P–T–x phase diagram for the composition range 123 to 124.

For fixed Po_2 and T one can consider the quaternary Y–Ba–Cu–O system as a ternary system of the three independent components Y_2O_3, BaO and CuO. Part of this system is shown in Fig.4. We have investigated the P–T–x dependence of a small portion of the ternary system – six compositions lying on the tie line 123–CuO. This is to our knowledge the most important part, where all superconducting phases in YBaCuO system appear. Up to now we have published only one part of this phase diagram, which combines the synthesis conditions of the 124, 247 and 123+CuO phases(21).

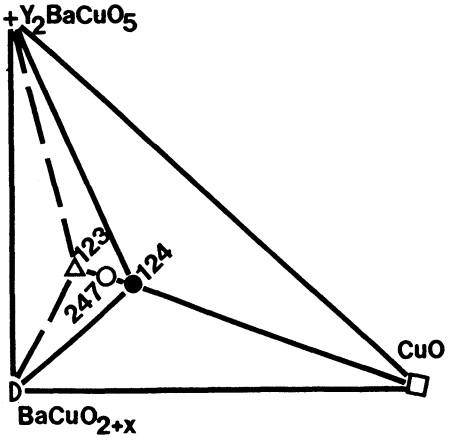

Fig.4. Part of the ternary system Y_2O_3–BaO–CuO.

There is a disagreement in the literature if the positions of the phase boundaries in the P–T phase diagram depend on the composition. Morris et al (22) investigated the P–T–x phase diagram of Y–Ba–Cu–O system at $Po_2 \leq 200$bar and $900 \leq T \leq 980$C and concluded, that the phase boundaries do not depend on the composition of the sample. Murakami et al (23) have investigated this phase diagram by heating oxides obtained by a gel method at $0.5 \leq Po_2 \leq 10$bar for 5 to 200h at temperatures 700 to 1000C. They observed that the positions of the phase boundaries are different for the 123 composition and for the 123.5, 124 and 125 compositions.

We have investigated the P–T–x phase diagram at $1 \leq Po_2 \leq 3000$ bar and temperatures 800 to 1200C. Mixtures of 123+CuO with total compositions 123, $123^1/_4$, $123^1/_3$, $123^1/_2$, $123^2/_3$, and 124 were used.

2a. Experiment.

For the high pressure experiments we have used the two–chamber autoclave described previously (24). The separation of the atmosphere of the sample from the atmosphere of the furnace allows the use of this autoclave for high oxygen pressures. The furnace works in argon atmosphere and oxygen is contained only in the internal ceramic vessel (crucible). This allows relatively high temperatures ($\approx$1300C) up to the melting temperature of high T_c superconductors. A sample consisting of pellets with a total weight 10–15g is placed in the alumina crucible and the free space is filled with

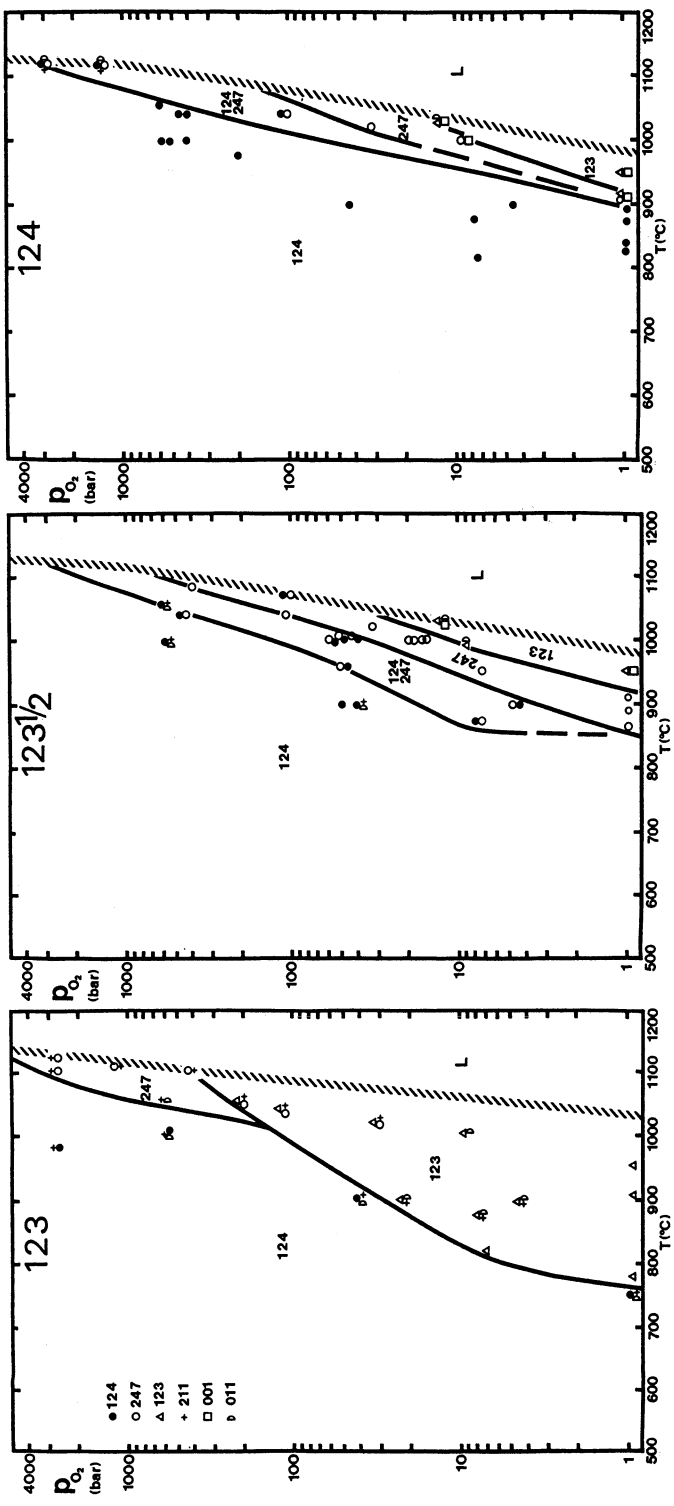

Fig.5. P–T cross–sections of the P–T–X phase diagram for three different compositions 123, 247 and 124. Except 123, 247 and 124 phases we observed also appearance of Y_2BaCuO_5 (211), CuO (001), $BaCuO_{2+x}$ (011 – high pressure form of $BaCuO_2$). The stability field of the 123 phase is probably smaller then shown, but slow kinetic of decomposition does not allow to determine exactly the phase boundary between 123 and 124.

alumina spacers. The dead volume in the crucible is very small – about $1cm^3$. This small dead volume makes the experiment safe and allows observation of the changes of pressure in the crucible during the experiments. Oxygen is pumped in the crucible and simultaneously argon pressure is supplied in the furnace. The equilibration of these two pressures is automatized (pneumatically controlled valves). The samples have been annealed at $1<P_{O_2}<3000$bar for 40–100 hours and quenched or fast cooled. In many cases additional annealings at 600C have been performed in order to load the samples with oxygen.

The identification of the phases has been done by means of x–rays, susceptibility, EDAX measurements and volumetric oxygen analysis (the latter only for pure phase samples).

2b.Results.

The first determination of the phase boundaries in the P–T space has been done from the variation of pressure over the mixture of 123+CuO. The starting pressures were chosen in the range $4<P_{O_2}<2000$ bar. The pressure increases, when the boundaries between the stability ranges of 124 and 247 or 247 and 123 are crossed and release of oxygen takes place during the decomposition reaction. The pressure increase takes place in the range of temperatures which corresponds to the existance of two–phase regions (124+247 or 247+123).

The various phases appearing in the samples are shown in Fig.5 by different symbols. One can easily notice that the positions of the phase boundaries depend on P_{O_2}, temperature and starting composition of the samples. The 123 stability range narrows with increasing CuO content. As we already mentioned, the 123 phase is unstable at $T \lesssim 750$C and $P_{O_2}=1$ bar or at high pressure at all temperatures. The 124 phase stability range increases with increasing CuO content and the 247 phase exists as a pure phase only in a narrow band between the 124 and 123 regions. In many experiments we have obtained samples, with two superconducting phases, 124+247 or 247+123, which indicated the existance of two–phase regions in the P–T–X phase diagrams.

These investigations have shown that the kinetics of the reaction play an important role. At normal pressure the reaction rate is rather slow, one has to wait many hours until the thermodynamic equilibrium is established. Under high oxygen pressure some of the reactions like: 123 + CuO $\rightarrow$ 124 proceed much faster probably because the equilibrium of this reaction is shifted towards higher temperature.

2c. Melting of the 124.

Similarly to 123, the 124 melts incongruently at 1 bar O_2 pressure. We have done several melting experiments of 124 samples under high oxygen pressures in the range of 1400 to 2800 bar. These experiments show that also at this pressure the 124 phase melts incongruently. The molten multiphase ingots contain Y_2BaCuO_5, $BaCuO_{2+x}$ and crystals of 124 and 247 phases.

2d. HIP process and phase diagram.

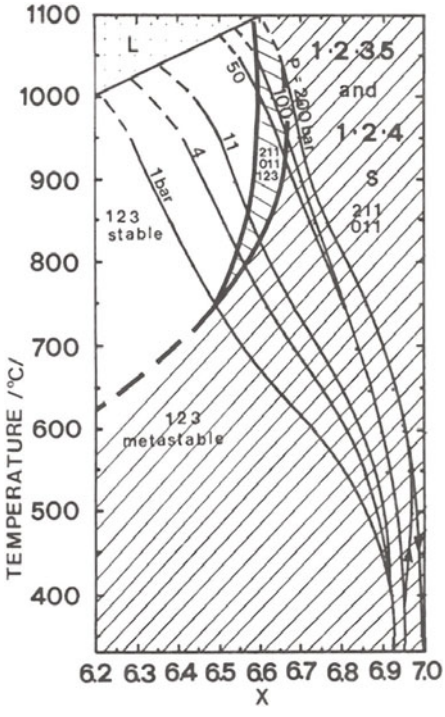

HIP processes take place under high pressure and high temperature conditions. It is difficult to determine the oxygen pressure in the encapsulated sample, but some conclusion could be made from our investigation of the oxygen content of the 123 samples in the metastable region $Po_2 \leq$ 200 bar (Fig.6). One sees, that if the oxygen content of 123 has to remain above x=6.6 at T=1000C, one expects $Po_2 \geq 70$ bars.

Fig.6. T–x phase diagram with p_{O_2} as a parameter. The 123 phase is thermodynamically stable only in a small part of the T–x space. The composition of the 123 has been measured in situ, in the high pressure autoclave.

However under these conditions, the decomposition of the 123 phase to Y_2BaCuO_5, $BaCuO_{2+x}$ and 247 or 124 should take place. The kinetic of this reaction may be rather slow. In agreement with the above, HIP experiments with 123 (25,26) showed decomposition and transformation to a mixture of 124, 211 and 011 phases. The 124 phase seems to be more suitable for the HIP process, because of its high oxygen pressure stability.

3. New defect–structures by TEM in the Y–Ba–Cu–O system.

One of the goals of the above systematic phase diagram studies was to find new phases in the Y–Ba–Cu–O system. Although, this was not possible, up to now, in bulk form, several new defect structures were found by means of TEM (27). These

structures show not only triple, but also fourfold and fivefold chains. Fig.7 shows three different sequences of CuO blocks, corresponding to compositions $123^1/_3$,$123^2/_5$ and 124 with alternating triple and single blocks. Clearly, it is not known up to now, if these defects correspond to thermodynamically stable structures or are kinetically driven intergrowths.

Fig.7 Different ordering of the CuO blocks observed by TEM (27): a) composition 124 – alternating triple and single blocks, b) composition $123^1/_3$ – 2 single blocks/1 double block, c) composition $123^2/_5$ – 3 double blocks/2 single blocks.

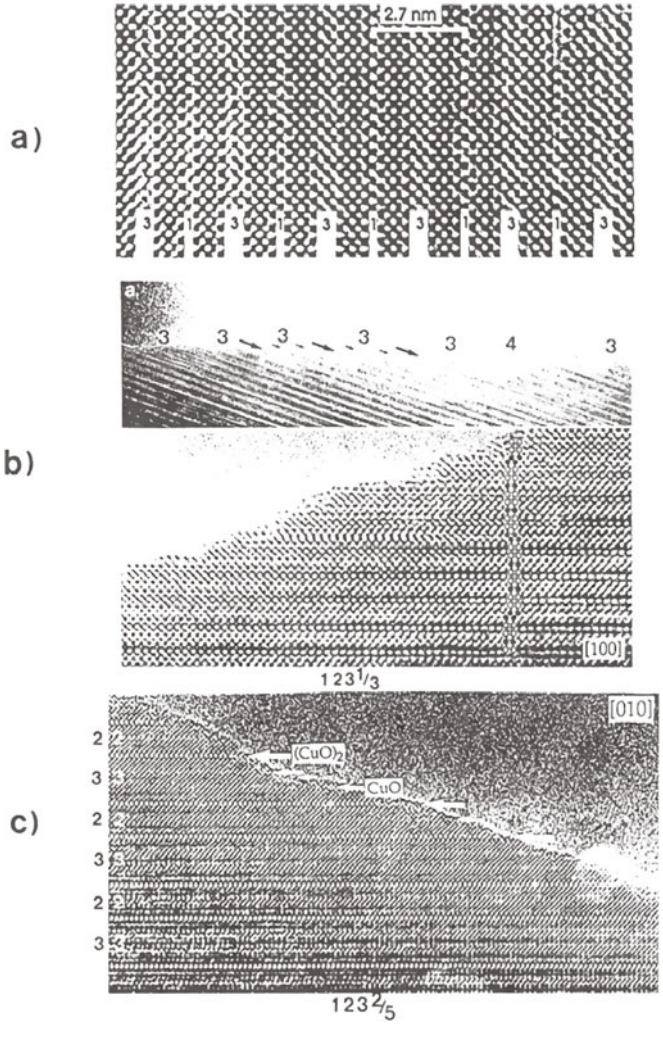

References

1. S.Rusiecki,B.Bucher,E.Kaldis,E.Jilek,J.Karpinski,C.Rossel,B.Pümpin,H.Keller, W.Kündig,T.Krekels,G.VanTendeloo, J.of Less Comm.Met 164/165(1990)31.
2. J.–Y.Genoud,T.Graf,A.Junod,D.Sanchez,G.Triscone,J.Muller, preprint.
3. M.Murakami,T.Suga,T.Noda,Y.Shiohara,T.Tanaka,J.J.Apl.Phys.29(1990)2720.
4. B.Seebacher et al, to be published.
5. E.Kaldis,J.Karpinski, Eur.J.Solid St.Chem. 27(1990)143.
6. J.Karpinski,E.Kaldis,E.Jilek,S.Rusiecki,B.Bucher, Nature 336(1988)660.
7. J.Karpinski,E.Kaldis,S.Rusiecki,E.Jilek,P.Fischer,B.Bordet,C.Chaillot,J.Chenavas, J.L.Hodeau,M.Marezio, J.Less Comm. Met.150(1989)129.
8. J.Karpinski,S.Rusiecki,E.Kaldis,E.Jilek, J.Less Comm. Met.164/165(1990)3.
9. J.Karpinski,C.Beeli,E.Kaldis,A.Wisard,E.Jilek, Physica C153–155(1988)830.
10. J.Schoenes,J.Karpinski,E.Kaldis,J.Keller,P.de la Mora, Physica C166(1990)145.
11. B.Bucher,J.Karpinski,E.Kaldis,P.Wachter, Physica C157 (1989) 478.
12. B.Bucher,J.Karpinski,E.Kaldis,P.Wachter, J.Less Comm.Met. 164/165(1990)20.
13. E.N.van Eenige,R.Griessen,R.J.Wijngaarden,J.Karpinski,E.Kaldis,S.Rusiecki, Jilek, Physica C168(1990)482.
14. D.Braithwaite,G.Chouteau,G.Martinez,J.H.Hodeau,M.Marezio,J.Karpinski, E.Kaldis, preprint.
15. T.Miyatake,S.Gotoh,N.Koshizuka,S.Tanaka, Nature 341(1989)41.
16. I.Mangelshots,M.Mali,J.Ross,H.Zimmermann,D.Brinkmann,S.Rusiecki, J.Karpinski,E.Kaldis,E.Jilek, Physica C172(1990).
17. M.Knupfer,N.Nücker,M.Alexander,H.Ramberg,P.Adelmann,J.Fink,J.Karpinski, E.Kaldis, preprint.
18. P.Bordet,C.Chaillout,J.Chenavas,J.L.Hodeau,M.Marezio,J.Karpinski,E.Kaldis Nature 334(1988)596.
19. J,Karpinski,S.Rusiecki,B.Bucher,E.Kaldis,E.Jilek, Physica C161(1989)618.
20. R.G.Buckley,J.L.Tallon,D.M.Poke,M.R.Presland, Physica C165(1990)391.
21. J.Karpinski,S.Rusiecki,E.Kaldis,E.Jilek, J.Less Comm. Met.164/165(1990).
22. D.E.Morris,A.G.Markelz,B.Fayn,J.H.Nickel, Physica C168(1990)153.
23. H.Murakami,T.Suga,T.Noda,Y.Shiohara,S.Tanaka, J.J.Applied Phys.12(1990)2720.
24. J.Karpinski,E.Kaldis, J.Cryst.Growth 79(1986)477.
25. Y.Yamada,M.Yata,Y.Kaieda,H.Irie,T.Matsumoto, J.J.Appl.Phys.28(1989)797.
26. R.K.Williams,K.B.Alexander,J.Brynestad,T.J.Henson,D.M.Kroeger, T.B.Lindemer,G.C.Marsh,J.O.Scarbough, J.Appl.Phys. 67(1990)6934.
27. T.Krekels,G.Van Tendeloo,S.Amelinckx,J.Karpinski,E.Kaldis, preprint.

THE PRODUCTION AND PROPERTIES OF HIGHLY DENSE $YBa_2Cu_4O_8$ PREPARED BY A REACTION HIP SINTERING PROCESS

JOHN V. NISKA AND BENGT LOBERG
Department of Engineering Materials, Luleå University of Technology, S-95187 Luleå, Sweden

ABSTRACT

A series of HIP runs have been made in which $YBa_2Cu_3O_7$ (123) and CuO have been reacted to form the $YBa_2Cu_4O_8$ phase (124). The reaction kinetics are examined and a densification model proposed for this sintering process. Densification is slow below 700 °C , but nearly fully dense materials are possible above about 900 °C with a HIP pressure of 200 MPa . The 124 phase is stable even under high pressure conditions, which makes it more suitable than the 123 phase for HIP densification. The material has a low fracture toughness typical of ceramic materials, which makes elimination of flaws important to obtaining high fracture strengths.

INTRODUCTION

A practical HIP process should be fast and yield a high quality product, which typically means fully dense and free from defects. Normally one wants to avoid chemical reactions when HIPing, and obtain a product which is chemically the same, but with a higher density. This has been attempted for the $YBa_2Cu_3O_7$ (123) superconductor, but decomposition occurs at the pressures required to reach nearly full density [1]. The stable phase at high oxygen pressures is the $YBa_2Cu_4O_8$ (124) superconductor, which apparently is stable at least to the maximum pressures used in HIPing (200 to 300 MPa) [2]. The practical requirement to HIP the 124 phase is to obtain closed porosity in a compact for use in an oxygen HIP or to use an encapsulation material which is nearly impervious and inert to

oxygen at high temperatures and pressures. The latter system was used in this work, by retaining the oxygen in a glass encapsulation.

Reaction Kinetics

In this case, a HIP using argon gas as the pressure medium was used, so that a borosilicate glass was chosen for the encapsulation to keep in the oxygen and out the argon. The following reaction stoichiometry occurs:

$$YBa_2Cu_3O_7 + CuO = YBa_2Cu_4O_8$$

This reaction equation does not show that the oxygen pressure is influential, but experimentally it is known that the oxygen pressure influences the formation of both superconductors. The 124 phase is stable even at 100 kPa oxygen at low temperatures, forming quite slowly at about 820 C, that is, in about 1-3 days. [3]. The reaction should proceed fast enough to make the process feasible in a HIP, that is, the kinetics of the reaction are important. Three methods of increasing the reaction rate are to add a catalyst, or to increase the temperature or to change the concentrations of the reacting species. It is known from the literature that a carbonate catalyst can be used to speed up the reaction at low temperatures [4], but fortunately the reaction rate can be increased sufficiently by the other two methods, so that the contamination created by the use of a catalyst can be avoided. The temperature (T) effect on the reaction rate (k) is given by the Arrhenius equation where ΔE is the activation energy for the reaction:

$$k = A \exp(-\Delta E/RT)$$

The reaction rate therefore increases exponentially with temperature, if the oxygen pressure is high enough to make the 124 phase the equilibrium phase. The effect of the oxygen partial pressure on the reaction rate must be determined experimentally. Ideally, a series of runs with different hold times, would give the reaction rate for a given temperature and pressure. This is rather difficult in a HIP, especially since a significant portion of the total time can be in the heating and cooling periods. A HIP run done with a setpoint temperature of 675 C with a 2 hr. hold period gave mostly the 124 phase. Only the use of a catalyst can approach this temperature at an oxygen pressure of one atmosphere [4], so that the high oxygen pressure increases the reaction rate sufficiently to avoid the use of a catalyst. This would mean that the oxygen acts as a reactant and the high oxygen pressure shifts the reaction equilibrium

towards the 124 phase. This could also be described as a lowering of the Gibb's free energy of the 124 phase, since the free energy change for a reaction is proportional to the logrithm of the reaction equilibrium constant.

Results

A fully dense and superconducting material is desired, therefore the conditions required to obtain this are of interest. A series of runs using a setpoint temperature from 675 to 980 C with a pressure of 200 MPa and a hold time of two hours have been made. The true temperature could be as much as 25 C higher due to thermocouple aging, but the setpoint temperatures will be used in this article. The resulting microstructures are shown in Figure 1. All the specimens showed 124 as the primary phase, by X-ray diffraction, but varying amounts of CuO can be seen as a secondary phase. A sample X-ray diffraction pattern is shown in Figure 2. The CuO is the light colored bodies in the optical micrographs, with the dark areas the porosity. It can be seen that already at 900 C, the material is nearly fully dense (>99% dense). The porosity at 940 C appears to be slightly higher than at 900 C, which is not expected, therefore there must be a difference in the two runs, such as in the starting powder morphology. The run at 675 C gave closed porosity, but on the order of 10% porosity by pore counting. A temperature of 750 C still gave a porous 124 microstructure for a similar cycle, and pore counting gave a porosity higher than that at 675 C, which may be again related to differences in the starting powder.

The final material has also been shown to be superconductive for the run at 980 C [5]. The resistivity versus temperature curve showed metallic behavior and a sharp drop in resistance at the critical temperature.

HIP Modelling

A large number of metals and ceramics have been modelled successfully with a computer program (HIP 487) that includes the effects of volume diffusion, grain boundary diffusion, power-law creep and Nabarro-Herring creep in a two stage process after the initial yielding of the powder compact [6]. This program does not model the release of gases by the powder or the effect of changing parameters due to reactions occuring in the HIP process. The reaction kinetics can be ignored if the kinetics of the reaction are much faster than the densification rate. The above runs showed that the 124 phase already forms at 675 C at 200 MPa, so that one can make the assumption, that one can model the densification as that of the 124 phase for HIPing times greater than 1/2 hour and temperatures above 700 C at 200 MPa. The $YBa_2Cu_3O_7$ phase is difficult to model

because of the gas release, and of little practical interest due to its instability at high oxygen pressures [2]. The oxygen generated can be removed using a reactive encapsulant (as steel) to give dense $YBa_2Cu_3O_6$, but it is not superconducting without an oxidation treatment to produce $YBa_2Cu_3O_7$ [1]. This oxidation treatment can lead to cracking due to differences in the density of the two phases. Modelling can be done on the 124 phase, but one should be careful about extrapolating the results to other temperatures and pressures, unless the effect of temperature and pressure on the reaction rate are included.

The mechanical and thermodynamic properties of 124 are still rather poorly known. This is due to several reasons including the difficulty of preparing large fully dense specimens on which to do mechanical testing, the anisotropy of the grains and therefore the properties of anisotropic bodies, and the problem of eliminating flaws and inhomogenities in a ceramic. The melting point as a function of temperature is given by Karpinski [2] . A value of 1430K was chosen for 200 MPa. The yield strength was estimated from hardness testing to be about 1 GPa [5]. A power law creep exponent of 5 was chosen, which might be expected for a ceramic. The activation energy for volume diffusion, creep, and surface diffusion were estimated as 185 kJ/mole, by adjusting the parameters to fit the results, using the approach given in HIP 487 [6]. Many of the parameters used in the HIP 487 program can be estimated from scaling relations and then refined from the actual HIP results. The final HIP map is shown in Figure 3. Note that diffusional densification mechanisms are dominant based on the parameters used, which leads to rather slow densification rates until one is near the melting point.

All the specimens showed some porosity, so that a pore-free material probably would require a very long hold time. This could be due in part to the anisotropy of the grains, in which grain growth on the *ab* -plane is much faster than in the *c*-axis. A pore bordered by three planar faces could be very slow to heal. The presence of flaws together with the low fracture toughness seen in superconductive ceramics make it likely to fail at stresses much lower than the yield strength.

Elimination of the residual CuO is difficult, since it is hard to make a very uniformly mixed, fine grained powder that is required to give good solid state reactions. An alternative method of forming dense 124 is to start with a 124 powder formed by the low temperature synthesis method. This was attempted, but the resulting material still had residual CuO.

Conclusions

Highly dense 124 superconductive ceramics are possible by a

HIP reaction sintering process using the 123 phase and CuO. Additional work is required to improve the process. One problem is the difference in the thermal expansivity of the 124 phase and the glass leads to cracking of the superconductor limiting the lengths of the specimens obtained. The process is sensitive to both the cycle used and the starting powder quality. A pure 124 starting powder should HIP densify using the same temperatures and pressures and allow intermediate grinding to improve the reaction with the CuO.

Acknowledgments

A special thanks to the work of L. Frisk for the help with the HIP encapsulations and for operating the HIP and to B. M. Andersson at Umeå University doing the superconductivity testing. Finally, this work was supported in part by the Swedish Board fo Technical Development (STU).

References

1. Niska, J. and Loberg, B., Retaining oxygen when HIPing the $YBa_2Cu_3O_7$ superconductor, Proceedings of the Second International Conference on Hot Isostatic Pressing, June 7-9, 1989, Gaithersburg, MD, ASM, 1990.

2. Karpinski, J., Kaldis, E., Jilek, E., Rusiecki, S., and Bucher, B., Bulk synthesis of the 81-K superconductor $YBa_2Cu_4O_8$ at high oxygen pressure, Nature, 1988, **336**, 660-662.

3. Liu, R.S., Janes, R., Edwards, P.P., and Campbell, A.M., Synthesis of high critical current $YBa_2Cu_4O_8$ submicron powders at one atmosphere pressure by the citrate-gell process, Physica B, 1990, **165&166**, 1667-1668.

4. Cava, R.J., Krajewski, J.J., Peck Jr, W.F., Batlogg, B., Rupp, L.W., Fleming, R.M., James, A.C.W.P., and Marsh, P., Synthesis of bulk superconducting $YBa_2Cu_4O_8$ at one atmosphere oxygen pressure, Nature, 1989, **338**, 328-330.

5. Niska, J., Andersson, B.M., Loberg, B., Easterling, K., and Sundqvist, B., Formation of the 124 phase superconductor $YBa_2Cu_4O_8$ by retaining oxygen in a reaction HIP sintering process, J. of Mat Sci Letters, 1990, **9**, 770-771.

6. Ashby, M.F., Hot Isostatic Pressing Diagrams- HIP 487, Engineering Dept., Cambridge, Uk, 1987.

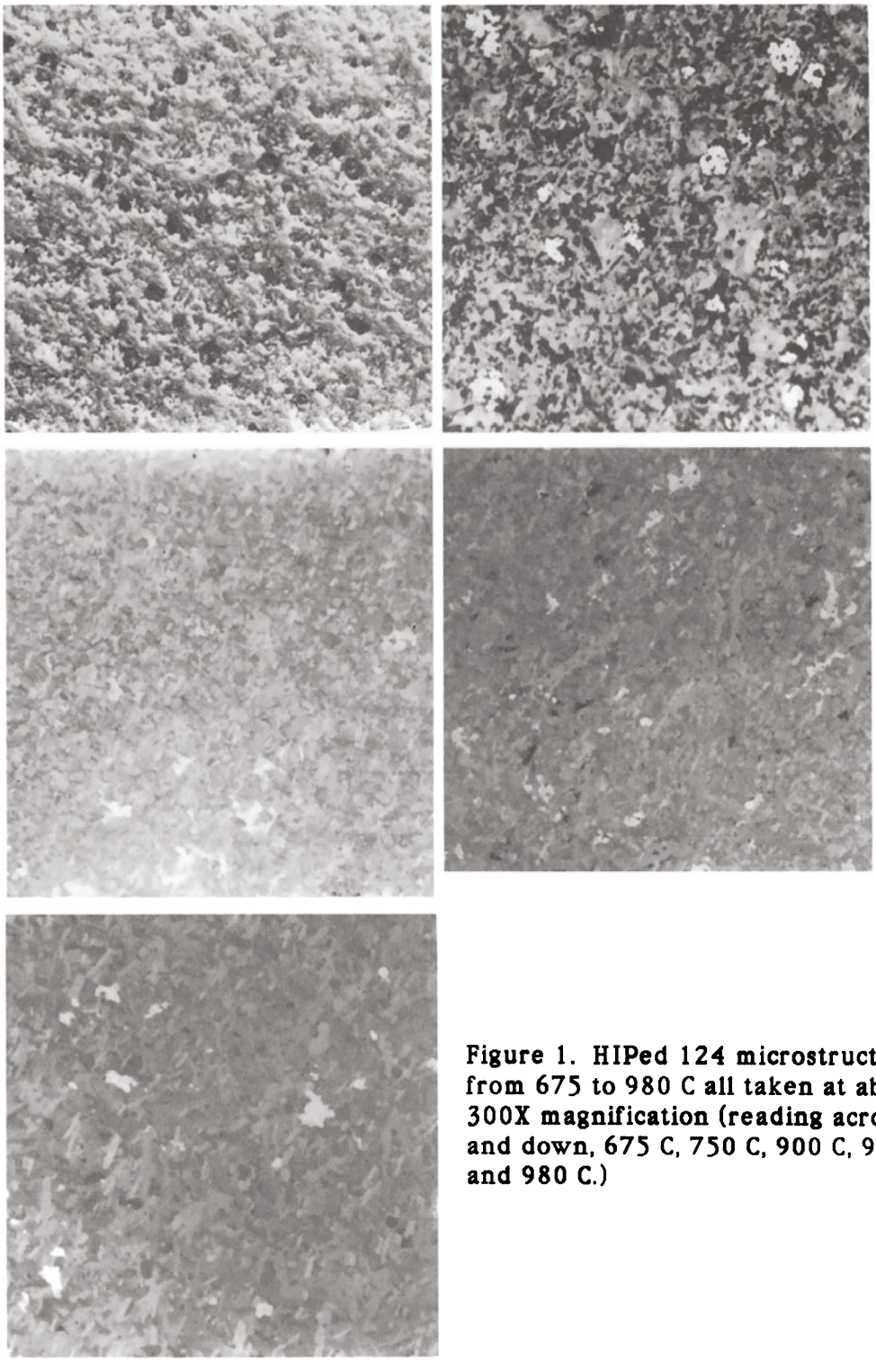

Figure 1. HIPed 124 microstructures from 675 to 980 C all taken at about 300X magnification (reading across and down, 675 C, 750 C, 900 C, 940 C and 980 C.)

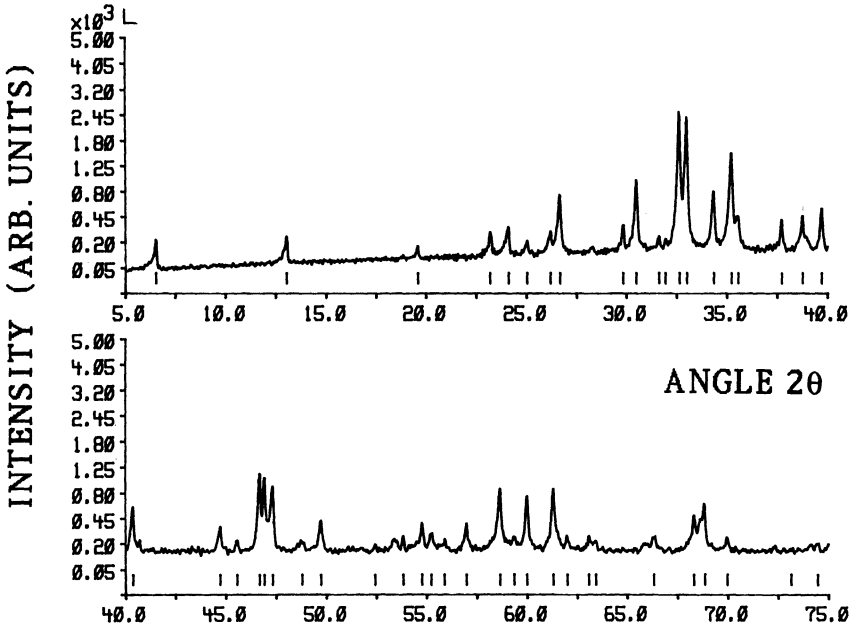

Figure 2. X-ray diffraction pattern for 124 formed at 750 C and 200 MPa (the "x" labels indicate impurity peaks).

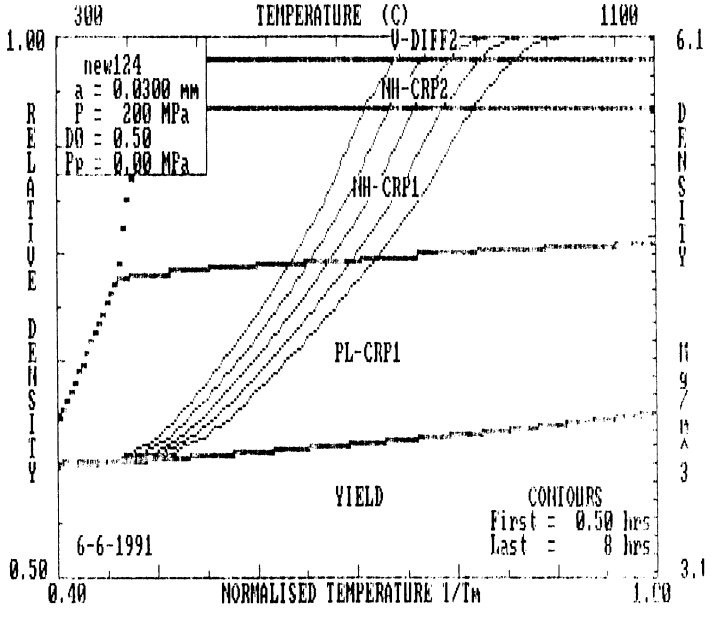

Figure 3. HIP map for the reaction-sintering densification of 123 and CuO at 200 MPa

EFFECTS OF OXYGEN PARTIAL PRESSURE AND TOTAL GAS PRESSURE ON STABILITY OF YBCO TYPE SUPERCONDUCTORS

Yuichi Sawai, Kozo Ishizaki
Department of Materials Science and Engineering, School of Mechanical Engineering, Nagaoka University of Technology, Nagaoka, Niigata, 940-21 Japan
Yutaka Narukawa
Kobe Steel Co.,Ltd., Kobe, Hyogo, 651 Japan*
and
Masasuke Takata
Department of Materials Science and Engineering, School of Electrical Engineering, Nagaoka University of Technology, Nagaoka, Niigata, 940-21 Japan

ABSTRACT

Phase stability of a YBCO type superconductor under variables of total gas pressure, oxygen partial pressure and temperature was studied by using oxygen hot isostatic process. A total gas pressure vs. temperature phase diagram at constant oxygen partial pressure (10MPa), and an oxygen partial pressure vs. temperature phase diagram at constant total gas pressure (200MPa) were obtained. AgO doped 124 phase was also synthesized by using O_2-HIP method. Doped AgO increased the critical temperature of the 124 phase from 75K to 77K.

INTRODUCTION

The oxygen pressure vs. temperature phase diagram of YBCO type superconductor was reported by Karpinski et al[1]. In their experiment, total gas pressure, $P_{tot}=P_{O_2}$. And the effects of P_{tot} and P_{O_2} could not distinguished. In the present work, three dimensional P_{tot}-P_{O_2}-T phase diagram in Y-Ba-Cu system were obtained and the effects of P_{tot} and P_{O_2} were distinguished. AgO doped 124 phase was also synthesized using oxygen hot isostatic process (O_2-HIP) at 1273K of T, 200MPa of P_{tot} and 40MPa of P_{O_2}.

EXPERIMENTAL

The starting materials are Y_2O_3, $BaCO_3$, CuO and AgO which had a purity of more than 99.9%. These raw powders were mixed in the atomic ratio of (Y:Ba:Cu:Ag) = (1:2:4:0), (1:2:3.96:0.04, i.e. 1at% of Cu), (1:2:3.8:0.2, i.e. 5at% of Cu), (1:2:3.6:0.4, 10at% of Cu), (1:2:3.2:0.8, 20at% of Cu), (1:2:0:4). These raw powders were mixed at each ratio and calcined at 1243K (970°C) for 48 hours in air. The obtained powder consisted of 123 phase with CuO. Then AgO was added at each ratio to the calcined powders and ground again. The sample without AgO was treated by O_2-HIP (Kobe Steel, O_2-Professor HIP) technique at various treatment temperatures, total gas pressures and oxygen partial pressures.

RESULTS

1.P_{tot}-P_{O_2}-T PHASE DIAGRAM

In figure 1, P_{tot}-T phase diagram at a constant P_{O_2} (10 MPa) is shown for P_{tot} range 10-200 MPa and T range 1200-1500 K. The open squares, the asterisks and the solid triangles show the condition at which the 124 phase, the 123.5 phase + CuO and the liquid phase were stable respectively. The A-A' curve shows the phase boundary between the 123.5 and the124 phases, and the B-B' is the melting line. Data points in brackets are from the results of Karpinski et al. [1]. In figure 2, P_{O_2}-T phase diagram at a constant P_{tot}(200MPa) is shown for P_{O_2} range 1-40

MPa and T range 1100-1500K. The solid circles show the condition at which the 123 phase + CuO was stable. All other marks have the same significance as in figure 1.

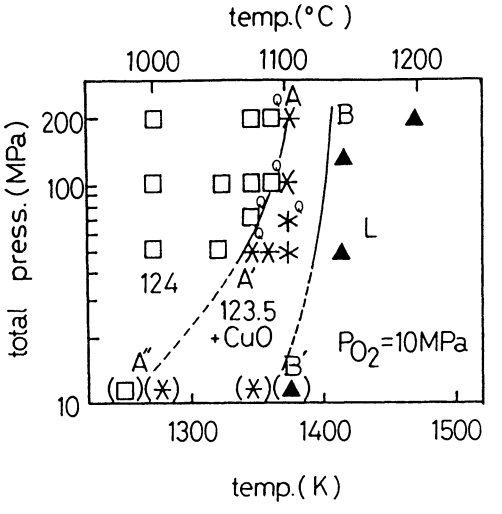

Figure 1. P_{tot}-T phase diagram at P_{O_2}=10MPa. The marks "Q" indicate quenched samples.

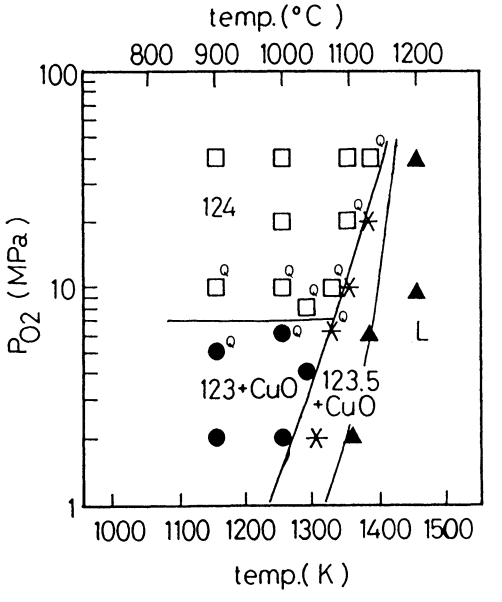

Figure 2. Phase diagram at P_{tot}=200MPa. All samples were kept for 5 hours or more at the indicated conditions.

2.AgO DOPING

The X-ray diffractograms were taken for all AgO doped samples. Superconducting 124 phase is formed in samples with 0, 1, 5, 10 and 20 at% AgO except the sample with 100at% AgO without CuO. The sample with 100 at% AgO without CuO was not superconductor. The intensities of (00$\underline{12}$) diffraction (2θ =39.7°) which comes from CuO_2 plane, and (00$\underline{14}$) diffraction (2θ =46.6°) which comes from CuO chain, become greater as the AgO doping fraction increases up to 10 at%, and they decrease at 20 at% of AgO doping fraction. The peaks of impurities such as Y_2O_3, Y_2BaCuO_5 (211 phase), $Y_2Ba_4Cu_7O_{15}$ (123.5 phase) and some compounds consist of Y, Ba and Cu decrease as AgO doping fraction increases. Small amount of Ag metal was detected for more than 5 at% AgO doped samples. On the other hand, AgO was not detected in each case.

The 124 phase with 5at% of AgO consisted of typical four kinds of grains. The amount of 124 phase was the highest, and other three grains were Ag, CuO and some compound consisted of Y, Ba and Cu. Silver can not be found in the grain of 124 phase by EDX method.

Critical temperatures, T_c, at which the resistivity of the specimen turns to zero, were measured as shown in table 2, and increase as the AgO doping fraction increases from 75K to 77K.

TABLE 1
Critical temperature of AgO doped samples.

AgO doping fraction (at%)	0	1	5	10	20	100
Critical temperature (K)	75	75	76	77	77	--

DISCUSSION

1.P_{tot}-P_{O_2}-T PHASE DIAGRAM

In figure 2, 123 phase + CuO transforms into 124 phase under about 7MPa of P_{O_2} for T range 1173-1373K. This results is quite different from that of Karpinski et al., who showed that the phase transition temperature from 124 phase to 123 phase + CuO is about 1100K in P_{O_2} range 0.1-0.6MPa[1]. Figure 2 also shows that phase transition temperature from 124 phase to 123.5 phase

+ CuO and from 123 phase + CuO to 123.5 phase + CuO depends on the P_{O_2}. Figure 1 shows the effects of the total gas pressure on the phase stability. Phase transition temperature from the 124 to the 123.5 phase + CuO, shown by the A-A' solid curve increases as P_{tot} rises. Using figures 1 and 2, the three dimentional P_{tot}-P_{O_2}-T phase diagram can be obtained as shown in figure 3. Figure 2 is included in figure 3 as the ABCD plane (P_{tot}=200MPa) and figure 1 is included as the EFGH plane (P_{O_2}=10MPa). Figure 3 also includes the results of Karpinski et al. in the OICD $P_{O_2}=P_{tot}$ plane. Considering the three dimentional phase diagram, the results obtained by Karpinski et al. are indeed at the condition $P_{tot}=P_{O_2}$, and well agreed with the present results.

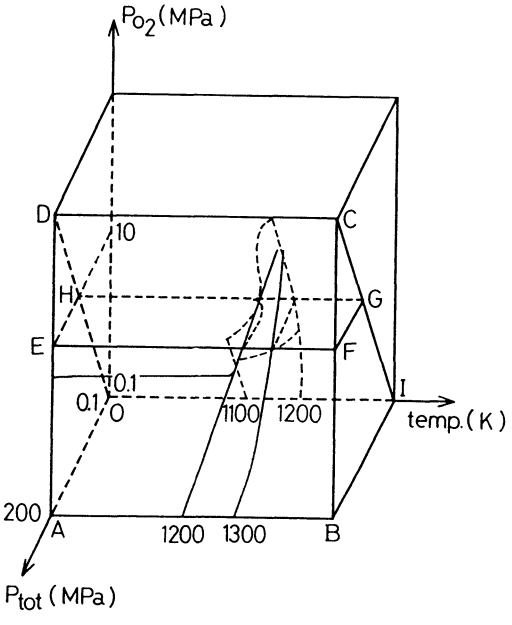

Figure 3. The three dimentional P_{tot}-P_{O_2}-T phase diagram of the YBCO type superconductor. Figure 2 corresponds to the ABCD plane, and figure 1 to the EFGH plane. Figure 3 also include the results of Karpinski et al. as OICD plane.

2.AgO DOPING

Some reports showed that the doped Ag improved T_c of 123 phase,

but it did not substitute for Cu[2-5]. In this work, the doped Ag also improved T_c of 124 phase. The substitution of Ag atom for Cu atom could not be confirmed by EDX method. But X-ray diffraction method shows the possibility of the substitution.

CONCLUSION

The doped AgO into 124 phase increased T_c from 75K to 77K. The evidence of substitution of Ag atoms in Cu sites could not be obtained by EDX method but the possibility of substitution was suggested by the peak intensity of X-ray diffractogram.

The three dimensional P_{O_2}-P_{tot}-T phase diagram of YBCO typesuperconductor has been determined. This $\log P_{O_2}$-$\log P_{tot}$-T phase diagram shows the following.

1. Phase transition temperature from 124 phase to 123.5 phase + CuO at 10MPa of oxygen partial pressure increases as total gas pressure rises.
2. Phase transition temperature from 124 phase to 123.5 phase + CuO and from 123 phase + CuO to 123.5 phase + CuO at 200MPa of total pressure depends on the oxygen partial pressure.
3. At total gas pressure of 200MPa, 123 phase + CuO transforms to 124 phase at 7MPa oxygen partial pressure for the temperature range 1170-1370K.

REFERENCES

1. J. Karpinski, S. Rusiecki, E. Kaldis, B. Bucher and E. Jilek, Physica C, 1989, 160, 449-57.
2. B. Dwir, M. Affronte and D. Pavuna, Physica C, 1989, 164, 351-2.
3. S. Zannella, L. Martini, V. Ottoboni, F. Parmigiani, A. M. Ricca and G. Ripamonti, Physica C, 1989, 164, 1179-80.
4. B. Shao, A. Liu, Y. Zhou, J. Zhang and J. Wang, Mat. Res. Bull., 1989, 24, 1369-73.
5. N. Imanaka, F. Saito, H. Imai and G. Adachi, J. J. Appl. Phys., 1989, 28, 580-2.

Superconductivity at 60K in $La_{2-x}Sr_xCaCu_2O_6$ ($0<x\leqq0.4$) synthesized using an O_2-HIP technique

Takeshi Sakurai, Toru Yamashita[1], H. Yamauchi and Shoji Tanaka
Superconductivity Research Laboratory, ISTEC. 10-13 Shinonome 1-chome,
Koto-ku, Tokyo 135, JAPAN

ABSTRACT

Superconducting $La_{2-x}Sr_xCaCu_2O_6$ (326 phase) samples (with x in range of $0<x\leqq0.4$) which have Tc^{onset} around 60K were synthesized using an O_2-HIP (hot isostatic press) technique. The samples were sintered at various temperatures (*Ts*) for 72h in flowing O_2 gas, and HIP-processed at various temperatures (*Ta*) for up to 100h in the mixture of 80%-Ar gas and 20%-O_2 gas of a total pressure of 1000atm. The present HIP-process is a specific annealing procedure under a high O_2 pressure. The HIP-processing temperature; *Ta* was found to be a key parameter for obtaining superconductivity (*superconductor-ization*) in the 326 samples, when the other parameters remain in the fixed ranges; $0<x\leqq0.4$ and $900℃\leqq Ts\leqq 1070℃$. The total pressure (P_T) and oxygen partial pressure (P_{O2}) in the O_2-HIP process seemed to have independent effects on the *superconductor-ization* of the 326 compound.

INTRODUCTION

Both systems of cuprates[1], $La_{2-x}Ca_{1+x}Cu_2O_6$ and $La_{2-x}Sr_{1+x}Cu_2O_6$, which are termed

[1] Present address: Electron Microscope Centre, University of Queensland, Brisbane, Queensland 4072, AUSTRALIA

326 compounds, posses crystallographic as well as chemical features common with conventional high Tc superconductor cuprates[2-4]. That is, the 326 compounds have double layers of CuO_5 pyramids and an effective valence per Cu ion which is higher than 2+ can be achieved by chemical doping to La (or "A(4e)") site. Among the perovskite related cuprates with double layers of CuO_5 pyramids, many of which have been known to be superconducting, the 326 compounds have the simplest crystallographic structure as shown in Fig.1.

Nonetheless, no one had been successful in making 326 compounds superconductive up until Cava. et.al[5] recently reported that they had synthesized $La_{1.6}Sr_{0.4}CaCu_2O_6$ which exhibited superconductivity at 60K. Cava, et.al. employed carbon-free reactants as starting materials and long time annealing under a high O_2 pressure of 20atm. In a previous work[6], though samples were annealed at 700℃ under the oxygen pressure of 200atm at the almost same chemical composition; $La_{1.6}Sr_{0.41}Ca_{0.99}Cu_2O_{5.9}$, superconductivity were not observed. The reason is suspected that the superconductor-ized "326" phase was stabilized by three thermodynamic parameters, i.e. temperature total pressure and oxygen partial pressure.

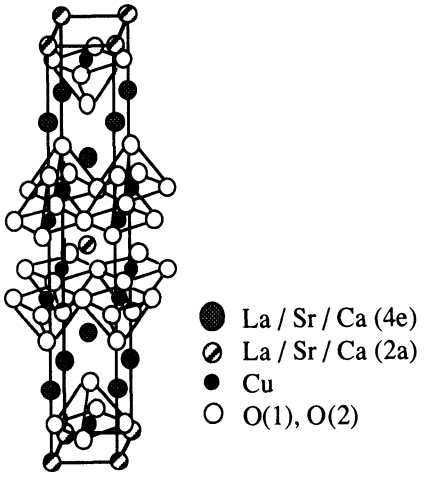

Fig.1. Schematic crystal structure of the "326" compound.

It is thought that when the parameters are well controlled, the "326" phase gets stabilized and exhibits suprconductivity. So, we attemped to search for the optimum condition to superconductor-ize "326" phase in terms of pressure and temperature using an O_2-HIP technique. The technique is thought more practical than the method employed by Cava's group[5] to produce relatively large amount of superconducting 326 samples.

EXPERIMENTAL PROCEDURE

The samples were prepared by a conventional solid-state reaction method plus an O_2-HIP process[7], using starting materials of highly purity (>99.9%) powders of La_2O_3, $SrCO_3$,

$CaCO_3$ and CuO. The samples sintered at a variety of temperatures, *Ts*, were HIP-processed at various temperatures, *Ta*, for various periods, t, in the range of 6h to 100h. For HIP-processing, the mixture of 80%-Ar gas and 20%-O_2 gas of the total pressure of 1000atm (oxygen partial pressure of 200atm) was utilized. Each of the $La_{2-x}Sr_xCaCu_2O_6$ samples with x=0.1, 0.2, 0.3 and 0.4 was heat-treated for 22 different combinations of (*Ts*, *Ta*).
The crystallographic structures of the samples were analyzed by x-ray diffraction technique. The lattice constants were determined by an extrapolation method using more than 15 diffraction peaks located in 2 θ range of 20° to 80° . Furthermore, a single-phase sample with the highest value of $Tc^{R=0}$(=50K) was analyzed by a joint x-ray/neutron diffraction at 300K in order to refine the structure parameters. Electrical resistivity was measured with respect to temperature using a conventional four-probe technique. The electrodes were formed using silver paste on the surface of the bar-shaped sample. The magnetic susceptibility was measured in a d.c. magnetic field of 10 Oe using a SQUID magnetometer (Quantum Design; MPMS).

RESULTS AND DISCUSSION

Superconducting 326 phase was detected in all samples with compositions x=0.1, 0.2, 0.3 and 0.4. The results in terms of the Sr content, (*Ts*, *Ta*)-combination, phases contained and superconducting temperature were examined thoroughly. The formed phases depended on *Ta*, but not significantly on *Ts*. Figure 2 shows the electrical resistivity -vs- temperature curves for the sample with x=0.2 which were HIP-processed at various temperatures for 6h under the total pressure of 1000atm. As *Ta* increases, the normal state resistivity decreases, and the narrower becomes the transition width, i.e. the difference between Tc^{onset} and $Tc^{R=0}$, while Tc^{onset} remains constant around 60K for all the samples except one which was HIP-processed at 920℃. Furthermore, when *Ta* exceeds 1070℃,

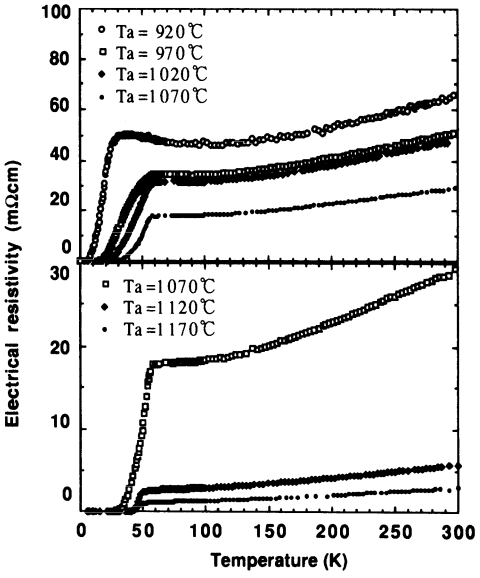

Fig.2. Electrical resistivity -vs- temperature for "326" samples; $La_{1.8}Sr_{0.2}CaCu_2O_6$, being HIP-processed at various temperatures; *Ta*=920℃, 970℃, 1020 ℃, 1070℃, 1120℃, 1170℃, when *Ts*=950℃.

Tc^{onset} temperature is deteriorated.

Although, the 326 phase requires a HIP-processing at a temperature higher than 970 ℃ in order to become a 60K-superconductor, it can be said that 1070℃ is the optimum value for *Ta* . Note that samples HIP-processed at 1020℃, 1070℃, 1120℃ and 1170℃ are all single phase.

Figure 3 shows the electrical resistivity -vs-temperature curves for the sample with x=0.2 which were HIP-processed at various periods up to 100h under the total pressure of 1000atm, when (*Ts*, *Ta*) combination is set at (950℃, 1020℃). As HIP-processing time is elongated, the normal state resistivity decreases and the transition width becomes narrower, while Tc^{onset} remains around 60K. It is suspected that the crystallinity of the samples is getting better during the HIP-processing. An evidence can be also detected in the magnetic susceptibility measurement. As the HIP-processing time increased up to 100h, the Meissner volume fraction became larger. On the contrary, Tc^{onset} determined from the magnetic susceptibility remained around 60K. So, it is supposed that the increase in the Meissner volume fraction is caused by the improvement of the crystallinity.

A joint x-ray/neutron powder diffraction study was made for the superconducting sample in order to study the reason for superconductor-ization[8].

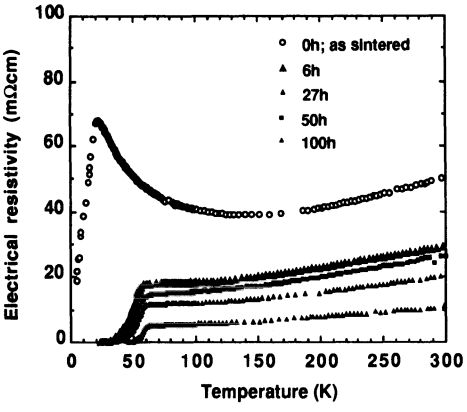

Fig.3. Electrical resistivity -vs- temperature for "326" samples; $La_{1.8}Sr_{0.2}CaCu_2O_6$, being HIP-processed at various periods; t=6h, 27h, 50h and 100h, when (*Ts*, *Ta*) is set at (950℃, 1020℃).

Table.1. Refined structure parameters for superconducting "326" samples.

	This work	Cava, et.al. [10]
Compound	La1.8Sr0.2CaCu2O6.01	La1.6Sr0.4CaCu2O5.94
Bond length		
Ca/La-O1 x8	2.4934(6)	2.498(1)
La/Sr/Ca-O1 x4	2.6530(9)	2.662(2)
La/Sr/Ca-O2 x4	2.7537(3)	2.735(1)
La/Sr/Ca-O2 x1	2.3459(19)	2.348(7)
Cu-O1 x4	1.91151(7)	1.912(1)
Cu-O2 x1	2.3068(20)	2.293(6)
Cu-O3 x1	1.6704(9)	-
Cation ratio		
La/Sr/Ca (2a)	0.14 / 0 / 0.86	0.191 / 0 / 0.815
La/Sr/Ca (4e)	0.83 / 0.1 / 0.07	0.708 / 0.2 / 0.096
Occupancy		
O1	1.02	1.02
O2	0.97	0.955
O3	0.03	-
Lattice parameter		
a	3.8207	3.8208
c	19.5434	19.5993
Copper valence	2.11	2.14

The sample, $La_{1.8}Sr_{0.2}CaCu_2O_{6.01\pm0.01}$, was prepared with the condition of (*Ts*, *Ta*)=(950℃, 1020℃) being HIP-processed for 50h. The oxygen content was determined by a coulometric titration technique[9]. By this method, the oxygen content can be determined to an accuracy of 0.01. In the final structural refinement by the Rietveld method, a cation ordering

was derived.

It was found that Sr^{2+} prefers A(4e) site having 9 co-ordination which was located in the rock-salt layer, but did not occupy 2a site having 8 co-ordination which was located between the double layers of CuO_5 pyramids. These results agree with another refinement data[10], as compared in Table 1.

Now, we consider the change in the free energy of the 326 phase, when a pressure is applied. When a high pressure field is applyed to the sample, the free energy of the sample increases. But, as temperature is fixed, other thermodynamic parameters should be changed in order to decrease the free energy. This may cause a cation ordering.

There is another effect, which mainly depend on oxygen partial pressure, that is, oxygen stoichiometory. As the Sr^{2+} ion substitutes for the La^{3+} ion at 4e site, oxygen defects are created in order to maintain the charge balance. If a number of oxygen defects are created, sufficient amounts of hole carriers were not introduced to the CuO_2 planes. It is suspected that a high oxygen pressure sufficiently introduces oxygen ions into the defects around the 4e site. So, in the 326 phase which is O_2-HIP-processed, the oxygen ions which were introduced around Sr^{2+} ion at 4e site should act as a hole donor to the CuO_2 plane.

CONCLUSION

The "326" compounds were successfully superconductor-ized by means of an O_2-HIP technique. The superconducting $La_{2-x}Sr_xCaCu_2O_6$ compounds were obtained in the range of $0<x\leqq0.4$, when the O_2-HIP-processing temperature, Ta, higher than 920℃. The optimum value for *Ta* was determined to be 1070℃, regardless the magnitude of *Ts*. Single phase compounds were obtained for the Sr content, $0.1\leqq x\leqq0.35$.

The cation ordering was determined by a joint x-ray/neutron diffraction technique, for the superconducting sample. That is, Sr ions occupied the 4e sites exclusively and Ca ions the 4e sites with a very low value of occupancy. The cation ordering occurred under a high pressure, i.e. during HIP-processing, is likely to be one of the reasons for the superconductor-ization of the 326 compounds.

ACKNOWLEDGEMENT

Authors are acknowledge to Dr. J. O. Willis of SRL-ISTEC and Dr. G. H. Kwei of Los Alamos National Laboratory for their helpful discussions. This work was supported by New

Energy and Industry Technology Development Organization as apart of program for R&D of Basic Technology for Future Industries

REFERENCES

1. Nguyen, N., Er-Rakho, L., Michel, C., Choisnet, J. and Raveau. B., Mater. Res. Bull., 1980, 15, 891.
2. Torrance, J. B., Tokura, Y., Nazzal, A. and Parkin, S. S., Phys. Rev. Lett., 1988, 60, 542.
3. Izumi, F., Takayama-Muromachi, E., Nakai, Y. and Asano, H., Physica C, 1989, 157, 89.
4. Caignaert. V., Nguyen, N., and Raveau, B., Mater. Res. Bull., 1990, 25, 199.
5. Cava, R. J., Batlogg, B., Van Dover, R. B., Krajewski, J. J., Waszczak, J. R., Flemming, R. M., Peck Jr, W. F., Rupp Jr, L. W., Marsh, P., James, A. C. W. P. and Schneemeyer, L. F., Nature, 1990, 345, 602.
6. Hiratani, M., Sowa, T., Takeda, Y. and Miyauchi, K., Solid. stat. comm., 1989, 72, 541.
7. Sakurai, T., Yamashita, T., Yamauchi, H. and Tanaka, S., J. Appl. Phys. 1991, 69, 3190.
8. Sakurai, T., Yamashita, T., Yamauchi, H., Tanaka, S., Willis, J. O. and Kwei, G. H., Physica C, 1991, 174, 187.
9. Kurusu, K., Takami, H. and Shintomi, K., Analyst, 1989, 114, 1341.
10. Cava, R. J., Santro, A., Krajewski, J. J., Flemming, R. M.,Waszczak, J. R., Peck Jr, W. F. and Marsh, P., Physica C, 1991, 172, 168

PRODUCTION OF SUPERCONDUCTING HIGH-T_C WIRES AND TAPES BY THERMOMECHANICAL TREATMENT USING THE HIP TECHNIQUE

P. WEIMAR, W. KRAUSS*
Kernforschungszentrum Karlsruhe GmbH.,
Institut für Materialforschung, Postfach 3640, W-7500 Karlsruhe, FRG
*E. Bühler, Postfach 1126, W-7454 Bodelshausen, FRG

ABSTRACT

Silver capillaries filled with BISCO powder were evacuated and sealed by welding. A predensification step by swaging was performed. This procedure was followed by several thermo-mechanical treatments as Hipping-Rolling- Annealing and final Hipping. The results of this work concerning improved microstructure and physical properties of these conductors will be presented.

INTRODUCTION

With the discovery of High T_c superconductivity by Bednorz and Müller [1] a worldwide boom was initiated to produce flexible wires and tapes from these brittle, ceramic materials [4,5,6,7,10]. There are many publications reporting on fabrication of clad and unclad specimen. Both directions however had no great success concerning superconductivity, whereas specimen with high densities could be obtained. The densification of Yttrium-Barium-Copperoxide (YBCO) proved to be more difficult [2,3] than densification of Bismuth-Strontium-Calcium-Copperoxide (BISCO). For both materials the current bearing capacity is very low after compaction. The terms "weak links" or "granularity" were defined. The important finding of these examinations was that it is necessary to give each oxide grain a distinct orientation in current direction - a so called texture. Textures can be gained by melting in a thermal gradient [9] or by a special thermomechanical treatment [8] . The latter procedure seems to have a great potential for fabrication processes. We adopted therefore this route.

Material

For the chosen way of thermo-mechanical treatment a silver clad high Tc-oxide of the following composition was chosen:

$$(Bi_{(1-x)}\,Pb_x)_2\,Sr_2\,Ca_2\,Cu_3\,O_{10}$$

Known as the so called 2223 composition with a Tc of 107 K.

The powder was produced by HITEC Cy at Karlsruhe/Germany, taking Bi-, Cu-, Ca-oxides and Sr-carbonate as starting material. The mean grain size was 3 μm.

Densification

Fig. 1 describes the densification procedure for the Ag-clad BISCO wires.

In the first step the BISCO powder was filled in a Ag-capillary (3.5 mm OD, 3.0 mm iD) by vibrating. After evacuating and sealing (Step 2), the tube was precompacted by swaging (step 3). Step 4 was a Hot Isostatic Compaction in a newly developed Laboratory HIP Unit (description below). The final step No. 5 consisted in rolling the Ag tube to a wire or tape.By a subsequent annealing step the formation of elongated (textured) BISCO cristallites should be provoqued.

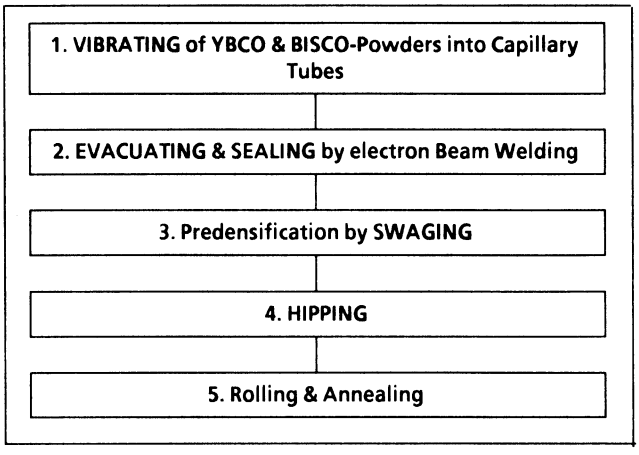

Figure 1: Fabrication route of BISCO/Ag wires

Technical Description of the HIP UNIT HIP 2000

The HIP-2000 was developed in collaboration with E. Bühler Co./FRG. It was constructed for densification, sintering and bonding of ceramic and metallic materials in R&D and for industrial application. Both, HIP and Sinter-HIP processes can be performed with this equipment.

The HIP consists od two parts - the pressing and the control unit - which can be installed independently.

- The maximum operation conditions are 2000 bar at 2200°C in Ar or N_2 atmosphere with CFC-heater.
- Sample dimension Ø 40 x 100 mm in height.
- The HIP system is designed for economic, save and easy handling.
- Low gas consumption (system volume 4 l).
- Fast pressurizing (2000 bar in 20 min, cold).
- Optimized cooling and heating systems.
- Operation by free programmable micro-processor system.
- Heating rate up to 100 K/min.
- Cooling rate up to 150 K/min.
- Power supply 380 V, 50 Hz, 16 kW
- Graphite, Mo or O_2 resistent furnaces optional.

Fig. 2 shows the HIP-2000 from BÜHLER Co. As can be seen, both end plugs of the autoclave are fixed by a double frame which can be moved aside for opening the pressure vessel. The top end plug is lifted by an hydraulic system and moved aside for charging or discharging. The isolation hood and the sample container can be discharged separately. All support and control systems are fixed separately at the lower (bottom) plug.

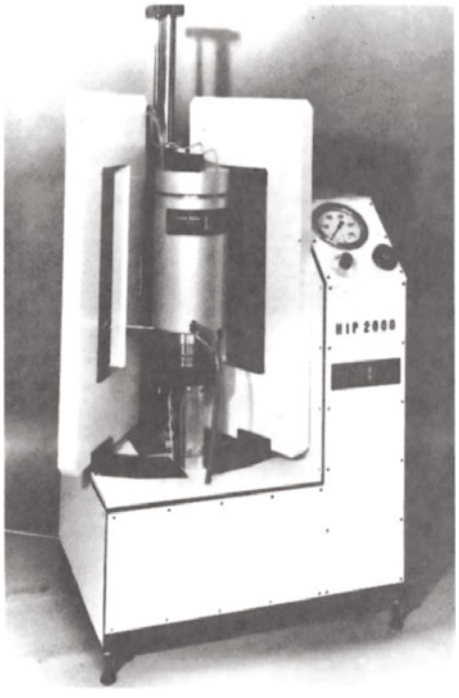

Figure 2. HIP-2000, Laboratory Hip Unit

Results

The different densification steps resulted in the following densities: (theoretical density of BISCO = 6.50 g/cm3)

- Filling of the capillary by vibrating: ~ 45 % T.D.
- Swaging of these capillaries: 85 % T.D.
- Hipping (1200 bar, 840 °C, 3h): 95 %T.D.
- Rolling (cold working steps with annealing): 98 % T.D.

Fig. 3 shows the X-ray diffraction pattern of the starting material in comparison to the as hipped specimen. As can be seen the original 2223-phase peak is now split into the 2223 (107 K) and in the 2212 (90 K) phase.

In the following 6 images (Fig. 4) we present one result of microprobe examination of a Hipped and cold worked (21 %) BISCO specimen. As can be seen we find now a very inhomogeneous elemental distribution.The elongated cristallites contain Cu, Sr, and Ca. In the grain boundaries we see Pb, Bi, and Sr again. The results of x-ray examination are confirmed.

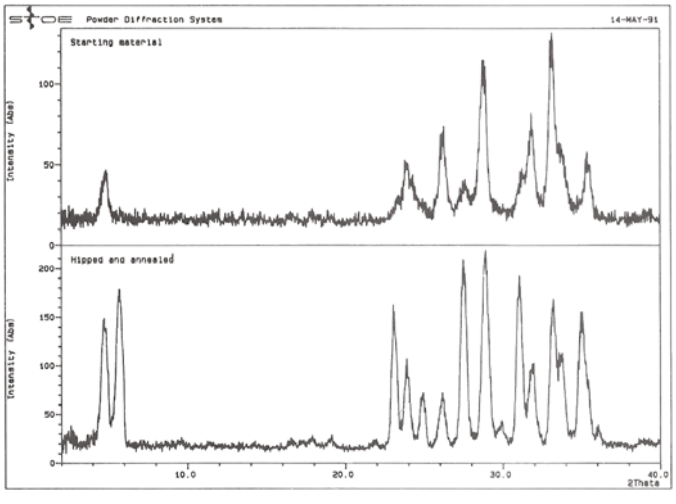

Figure 3. X-ray pattern of starting material and Hipped cold worked and annealed wire

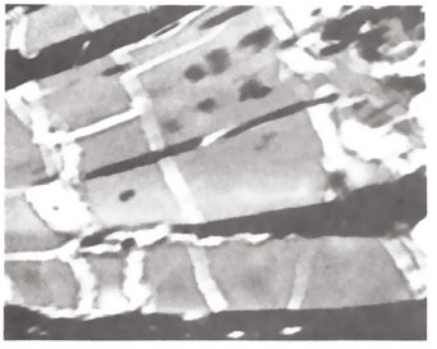

Figure 4.1

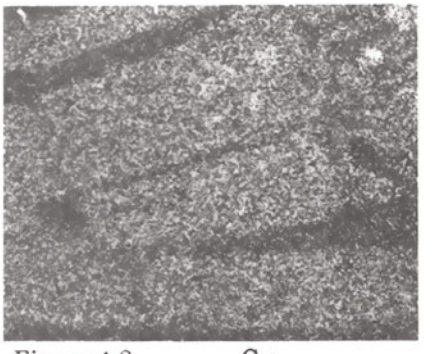

Figure 4.2 Cu

Figure 4.3 Sr

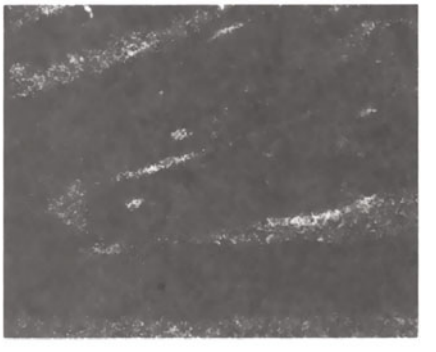

Figure 4.4 Pb

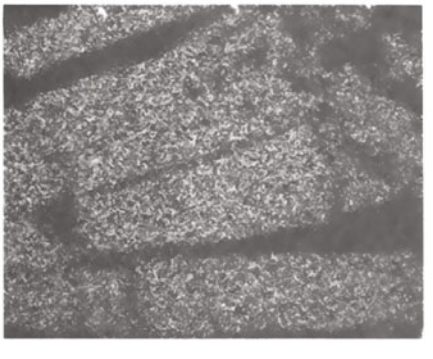

Figure 4.5 Ca

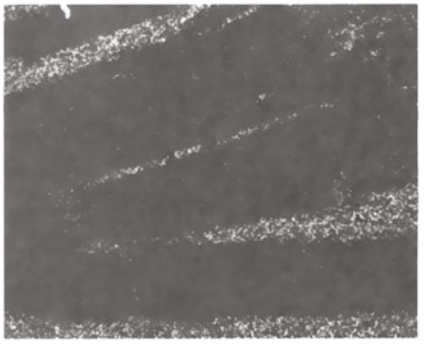

Figure 4.6 Bi

Figure 4. Microprobe examinations (elemental distribution)

Figure 5 shows a metallographic (longitudinal) section through a Ag/BISCO wire (hipped and 24 % cold worked). Figure 6 depicts a silver clad BISCO-coil and -wire.

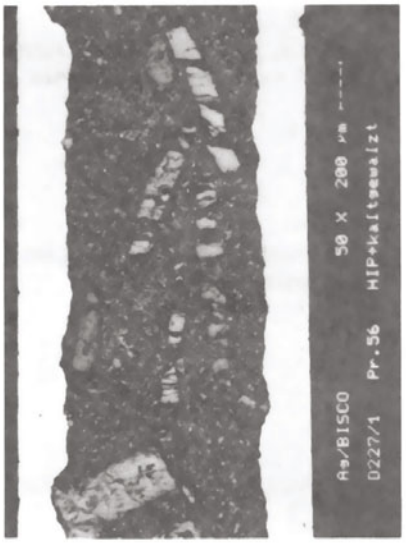

Figure 5. Ag/BISCO wire, (longitudinal section)

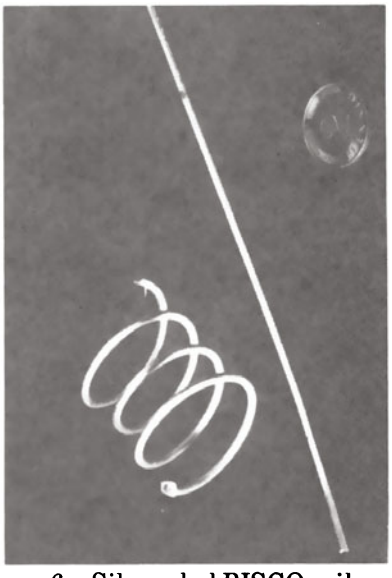

Figure 6. Silver clad BISCO coil and wire (as hipped)

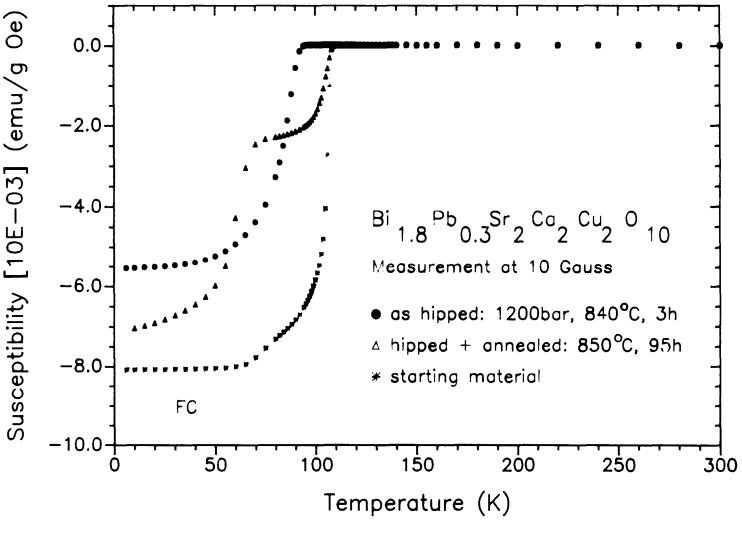

Figure 7. Susceptibility versus temperature for different thermo-mechanical treatments

Figure 7 presents the measurement of susceptibility versus temperature (SQUID-Measurement). As can be seen annealing of the hipped and cold worked specimen improves the position of Tc. Comparing with the starting powder there is still a gap for further investigations.

Conclusions

Thermomechanical treatment could be a remedy to improve the current bearing capacity of the high Tc-Superconductors. Future work must show if the problem of weak links can be overcome by this technique.

Acknowledgement

We thank our colleagues P. Graf for preparing the metallographic samples and H. Kleykamp for interpretation of the microprobe examinations.

REFERENCES

1. J.G. Bednorz, K.A. Müller. Possible High Tc Superconductivity in the Ba-La- Cu- O-System. Z. Phys. B 64 (1986), p. 189-193

2. W.D. MacDonald, A.J. Otto, E.J. Zwartz et al., Effect of thermally unstable noble metal oxide additions on structure and superconducting properties of $YBa_2CU_3O_8$ + delta, Conf. 4. Annual Northeast Regional Meeting of the Metallurgical Society on Processing and Applications of High Tc Superconductors: Status and Prospects, New Brunswick, NJ (USA), 9-11, 1988

3. S. Jin, R.C. Sherwood, T.H. Tiefel, G.W. Kammlott, R.A. Fastnacht et al., Superconductivity in the Bi-Sr-Ca-Cu-O compounds with noble metal additions, Appl. Phys. Lett (9 May 1988) v. 52(19), p. 1628-1630

4. S. Jin. R.C. Sherwood, R.B. Van Dover, T.H. Tiefel, D.W. Johnson, High TC superconductors-composite wire fabrication, Appl. Phys. Lett (20 July 1987) v. 51(3), p. 203-204

5. T.H. Tiefel, S. Jin, R.C. Sherwood, R.B. Van Dover, R.A. Fastnacht, M.E. Davis, D.W. Johnson, Fabrication and properties of high-Tc superconducting wires, J. Appl. Phys. (15 Nov. 1988) v. 64(10), p. 5896-5898

6. P. Weimar, H. Ketschkar, W. Krauss, C. Politis, Shaping of High-Tc Superconducting Ceramics Wires by Using a Modern Lab. HIP Unit, Conf. PM 90, London (July 1990), p. 241-243

7. P. Weimar, W. Krauss, Hot Isostatic Pressing of High Tc-Superconductors with a Newly Developed Lab. HIP Unit, 4th Intern. Conf. on Isostatic Pressing, Stratford upon Avon/UK (Nov. 5-7,1990)

8. K. Osamura, S.S. Oh, S. Ochiai, Effect of thermomechanical treatment on the critical current density of Ag-sheated B(Pb)SCCO tapes, Supercond. Sci. Tech. 3 (1990) p. 143-147

9. M. Muranami, T. Oyama et al., Melt processing of bulk high Tc superconductors and their application, IEE Trans MAG-27 (1991)

10. H. Krauth, K. Heine et al., Development of high Tc superconducting wires, Sov. J. Low Temp. Phys. (May 1990) v. 16(5) p. 355-356

PREPARATION OF THE HIGH DENSITY AND FINE-GRAINED $YBa_2Cu_3O_{7-y}$ BY CAPSULE HIP METHOD

Yasuharu Kodama, Keiko Kani, Masanobu Awano and Fumihiro Wakai
Government Industrial Research Institute, Nagoya
1-1, Hirate-cho, Kita-ku, Nagoya 462, Japan

ABSTRACT

As the first step for realizing a superplasticity in high-Tc oxide superconductors, a dense and fine-grained ceramic material of the tetragonal 123 phase was prepared by using a capsule HIP (hot isostatically pressing) method. A dense material with equiaxed grains of sub-micron order was successfully prepared by HIP at 750°C and at 90 MPa for 4 h. A possibility for realizing superplasticity was observed from a deformation property of a compression test. Recovery of oxygen content during annealing process was also investigated.

INTRODUCTION

Since the discovery of high-Tc oxide superconductors a lot of efforts have been devoted to many kinds of processing fields. Particularly remarkable results are developed in the field of thin films [1,2] and wires [3]. In the field of bulk body the materials prepared by melt process have good superconducting properties, high critical current and excellent pinning properties [4,5]. But materials prepared by sintering method have not shown remarkable development due to weak links at grain boundary. Because high-Tc oxide superconductors are materials difficult to form the desired shape, there are a few reports on forming bulk body into complicated shape [6,7]. The melt process is not convenient to form a complicated shape simultaneously on preparation because it requires the temperature gradient. Then a method which enables to form a complicated shape and improves superconducting properties is needed for the application of bulk body.

Although ceramic materials are generally thought to be difficult to be deformed, superplasticity which is defined as the ability of a material to exhibit exceptionally large elongations during tensile deformation [8] is observed in some ceramic materials with equiaxed grains of sub-micron order [9]. Since this discovery, fabrication of required shaped components of ceramic materials became possible by superplastic forming. Then the superplasticity is thought to be useful to form polycrystalline materials of high-Tc oxide superconductors. We consider that superplasticity of ceramic materials is a common nature to polycrystalline materials, because it is observed in many ceramic materials [10-12]. Therefore, if a ceramic material with equiaxed sub-micron order grains is prepared, superplasticity may be realized in high-Tc oxide superconductors.

HIP is a suitable method to prepare a dense ceramic material with equiaxed grains. It can reduce sintering temperature by enhancing the contact of grains, then reduces the rate of grain

growth. From the above mentioned HIP is advantageous in preparing a superplastic ceramic material, which is dense material with equiaxed grains of sub-micron order. In fact some superplastic ceramic materials were made by HIP [10,11]. Then it may be possible to prepare a candidate for superplasticity in oxide superconductors by HIP method.

In this paper, we attempted to prepare dense sintered materials of $YBa_2Cu_3O_{7-y}$ (123 phase) with sub-micron order grains which will show a superplasticity. We chose the tetragonal 123 phase as a target material, because it has the smallest anisotropy among the high-Tc oxide superconductors and an advantage to avoid pore formation during HIP process due to small oxygen desorption. We investigated sintering properties in a capsule HIP and deformation properties of sintered materials. And in order to induce a phase transition from tetragonal (non superconducting) to orthorhombic (superconducting) we also investigated a recovery of oxygen content by annealing in O_2 flow.

EXPERIMENT

A sintered material which consists of fine grains of sub-micron order was prepared by capsule HIP from calcined powders with a size of 100 nanometer . The calcined powder was prepared by a sol-gel method using metal alkoxides as starting materials. $Y(O\text{-}C_2H_4OC_2H_5)_3$, $Ba(O\text{-}C_2H_4OC_2H_5)_2$ and $Cu(O\text{-}C_2H_4OC_2H_5)_2$ were dissolved in a mixture of toluene and xylene and stirred at room temperature in N_2 atmosphere. After hydrolysis, the mixture was refluxed overnight and a brown precipitate was obtained. It was calcined at 690°C in vacuum for 20h. Details for preparing the calcined powder will be published elsewhere [13].

The calcined powder was pressed into pellet by uniaxial pressing and then pressed by cold isostatic pressing. The pellets were sealed in a pyrex glass tube at 650°C with evacuating. The sample was wrapped in gold foil before sealing in order to prevent a reaction between the sample and the glass tube. Then the capsuled sample was sintered at 750 - 800°C in an Ar atmosphere of 90 MPa for 1 - 4 h by using a HIP apparatus made by Kobe Steel Co. Ltd.

Observation of scanning electron microscope (SEM) on polished and fracture surfaces of sintered materials was used for a characterization of density and grain size. Some samples were used for compression tests in order to investigate the reduction of deformation stress by grain refinement. Compression tests were conducted by using a universal testing machine in air under a constant cross head speed condition. Recovery of the oxygen content by annealing was also investigated. Annealing was conducted at 400°C for 84 h in flowing O_2. The recovery of the oxygen content was characterized by observing lattice parameters, which were determined by X-ray diffraction (XRD) using Ge as an internal standard.

RESULTS AND DISCUSSION

Sintering by HIP

In the sample HIPed at 750°C for 2 h, the grain size was less than 1 μm. Pores with a size of 0.2 - 0.5 μm were observed inside of grains and at grain boundaries. (Fig. 1 a) In the sample treated at 750°C for 4 h grains had equiaxed shape and their size was 0.5 - 0.8 μm. A few pores with a size of 0.1 μm were also observed. (Fig. 1 b) In the sample treated at 775°C for 2 h the size of most grains was less than 1 μm, but some elongated grains with a size of 2 - 3 μm were observed. (Fig. 1 c) In the sample at 800°C for 2 h some elongated grains with a size of several micrometers were observed among equiaxed grains with a size of less than 1 μm. (Fig. 1 d) The size of pores observed in the samples at 775°C and 800°C was also 0.1 μm.

When the sample at 750°C for 2 h with a size of ϕ6 x 15 mm was removed from a capsule, it broke into many fractions each of which sintered tightly. But that situation did not happen in the case of the sample at 800°C for 2 h with the same size. Accordingly sintering of $YBa_2Cu_3O_{7-y}$ proceeded at 750°C, which was relatively low temperature, by HIP, but it was not sufficient to sinter the whole sample for 2 h. It is suggested that HIP at higher temperature for longer time is needed for full sintering of a large size sample, but sintering at higher temperature causes grain growth. Then HIP at 750°C and 90 MPa for more than 4 h is

necessary to prepare a sample for a demonstration of superplasticity, which needs a tensile test.

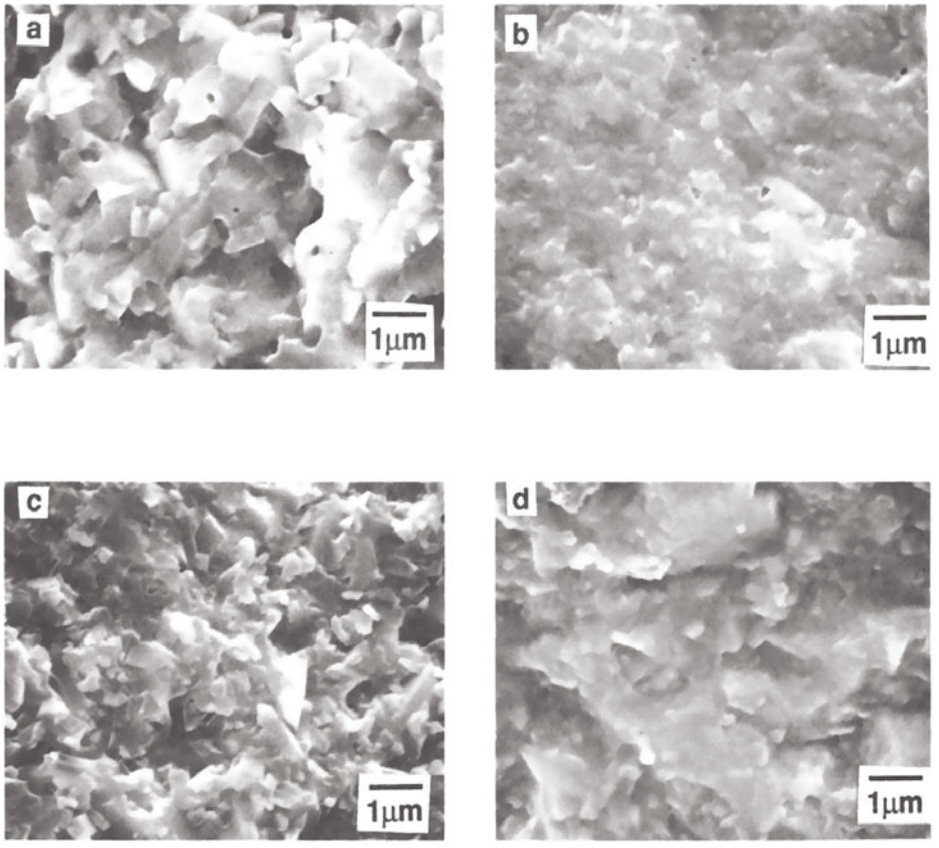

Fig. 1 SEM micrographs of the samples (a) HIPed at 750°C for 2 h, (b) at 750°C for 4 h, (c) at 775°C for 2 h and (d) at 800°C for 2 h.

Deformation properties

Figure 2 shows true stress - true strain curves of the sample HIPed at 750°C for 4 h (sample A) and at 800°C for 2 h (sample B). Test was performed at 750°C at the initial strain rate of 2×10^{-5} s^{-1}. We define true strain (ε) and true stress (σ) as

$$\varepsilon = \ln\left(\frac{L}{L_0}\right) \tag{1}$$

$$\sigma = \frac{P}{A_0}\,\frac{L}{L_0} \tag{2}$$

where L is the height of the sample, L_0 is the initial height, P is the load and A_0 is the initial cross-section area. The true stress of the sample A rapidly increases with the true strain until the true strain reaches -0.05, after that it gradually increases and its value is about 30 MPa.

The flow stress of 30 MPa was very low in the $YBa_2Cu_3O_{7-y}$ dense materials deformed at 750°C [14]. In the sample B, true stress - true strain curve behaves in the same manner as the sample A except for the stress value, which is three times larger than that of the sample A. The sample A consists of equiaxed grains with a size of 0.5 - 0.8 μm , whereas elongated grains with a size of several micrometers are mixed in the sample B. Higher true stress of the sample B is considered to be due to the difference of the microstructure, existence of elongated grains.

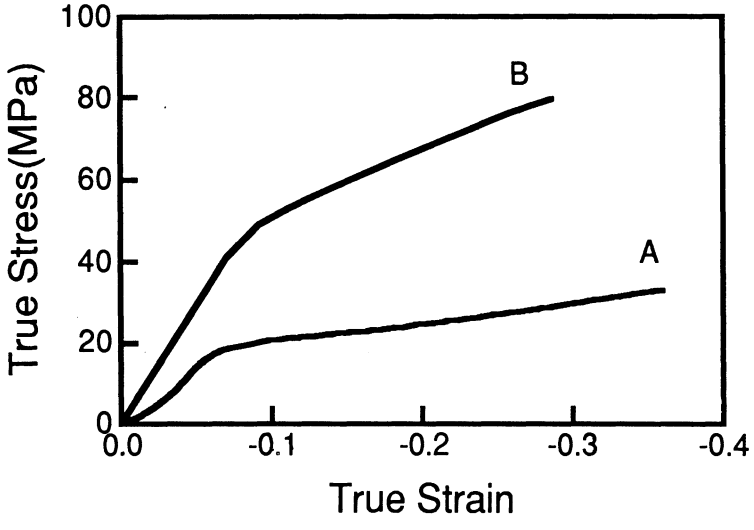

Fig. 2 True stress - true strain cureves for the samples HIPed (A) at 750°C for 4 h and (B) at 800°C for 2 h.

Some of superplastic ceramics are deformed at true stress of about 30 MPa [10-12], then we suppose that the superplasticity in the 123 phase can occur by preparing a ceramic material with equiaxed grains of sub-micron order.

Annealing

It is well known that the superconductivity of the 123 phase is very sensitive to the oxygen content. The relationship between the oxygen content and the lattice parameters is also well known [15-17]. Then we characterized the recovery of oxygen content from the lattice parameters by annealingthe sample. The oxygen content deduced from the lattice parameters shows the average of the whole sample by using the XRD pattern of the powdered sample. The sample for the annealing experiment was HIPed at 750°C for 2 h and its size was 3 mm x 3 mm x 1.5 mm. Figure 3 shows the XRD patterns of as HIPed and annealed samples. The peak separation between (200) and (020) indicates the recovery of the oxygen content by annealing. But the peak width suggests that the oxygen content in the whole sample is not uniform. The oxygen contents in the as HIPed sample and in the annealed sample were 6.0 and 6.7 unit, respectively. The lattice parameters and the oxygen contents are summarized in Table 1. An annealing for longer period is needed to obtain the fully and uniformly oxidized sample.

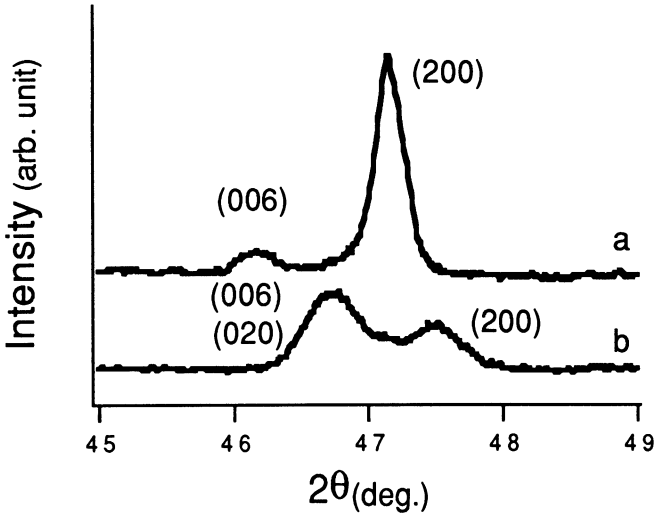

Fig. 3 XRD patterns of the samples (a) as HIPed and (b) annealed at 400°C for 84 h in O_2 flow.

Table 1
Lattice parameters and oxygen contents of as HIPed and annealed samples

	Lattice Parameters a(Å)	b(Å)	c(Å)	oxygen content
as HIPed	3.860	——	11.827	6.0
Annealed	3.823	3.880	11.698	6.7

CONCLUSIONS

For realizing a superplasticity in high-Tc oxide superconductors, preparation of a densely sintered material of the tetragonal 123 phase with sub-micron order grains was investigated by using a capsule HIP method. A dense material with equiaxed grains of a size of 0.5 - 0.8 μm was successfully prepared by HIP at 750°C and 90 MPa for 4 h. It was deformed at a stress of 30 MPa in the compression test performed at 750°C with an initial strain rate of 2×10^{-5} s^{-1}. This result suggests that a superplasticity is realized in the 123 phase by preparing a finely-grained sintered material. The annealing at 400°C for 84 h in O_2 flow was not sufficient to a full oxidation of the sample with a size of 3 mm x 3 mm x 1.5 mm.

REFERENCES

1. Koren, G., Gupta, A., Giess, E. A., Segmuller, A. and Laibowitz, R. B., Epitaxial films of $YBa_2Cu_3O_{7-\delta}$ on $NdGaO_3$, $LaGaO_3$, and $SrTiO_3$ substrates deposited by laser ablation. Appl. Phys. Lett., 1989, **54**, 1054

2. Witanachchi, S., Lee, S. Y., Song, L. W., Kao, Y. H. and Shaw, D. T., Critical current enhancement in multilayered $Y_1Ba_2Cu_3O_{7-y}/Y_1Ba_2(Cu_{1-x}Ni_x)O_{7-y}$ structures. Appl. Phys. Lett., 1990, **57**, 2133-2135
3. Kumakura, H., Togano, K., Maeda, H. and Miura, M., Bi(Pb)-Sr-Ca-Cu-O superconducting composite tapes prepared by the powder method using an Ag sheath. J. App. Phys., 1990, **67**, 3443-3447
4. Jin, S., Tiefel, T. H., Sherwood, R. C., van Dover, R. B., Davis, M. E., Kammlott, G. W. and Fastnacht, R. A., Melt-texyured growth of polycrystalline $YBa_2Cu_3O_{7-\delta}$ with high transport Jc at 77 K. Phys. Rev. B, 1988, **37**, 7850
5. Fujimoto, H., Murakami, M., Gotoh, S., Koshizuka, N., Oyama, T., Shiohara, Y. and Tanaka, S., Melt Processing of YBaCuO Oxide Superconductors. In Proc. ISS '89, ed. T. Ishiguro and K. Kajimura, Springer-Verlag, Tokyo, 1990, pp. 285-288
6. Minehara, E., Nagai, R. and Takeuchi, M., The TM010 Microwave Cavity Made of $YBa_2Cu_3O_{7-d}$. Jpn. J. Appl. Phys., 1989, **28**, L100-101
7. Shigematsu, K., Ohta, H., Hoshino, K., Takayama, H., Yagishita, O., Yamazaki, S., Takahara, H. and Aono, M., Magnetic Shield of High-Tc Oxide Superconductors at 77K. Jpn. J. Appl. Phys., 1989, **28**, L813-815
8. Edington, J. W., Melton, K. N. and Cutler, C. P., Superplasticity. Prog. Mater. Sci., 1976, **21**, 61-170
9. Wakai, F., Sakaguchi, S. and Matsuno, Y., Superplasticity of Yttria-Stabilized Tetragonal ZrO_2 Polycrystals. Adv. ceram. Mater., 1986, **1**, 259-263
10. Wakai, F. and Kato, H., Superplasticity of TZP/Al_2O_3 Composite. Adv. Ceram. Mater., 1988, **3**, 71
11. Wakai, F., Kodama, Y., Sakaguchi, S. and Nonami, T., Superplasticity of Hot Isostatically Pressed Hydroxyapatite. J. Am. Ceram. Soc., 1990, **73**, 457-460
12. Wakai, F., Kodama, Y., Sakaguchi, S., Murayama, N., Izaki, K. and Niihara, K., A superplastic covalent crystal composite. Nature, 1990, **344**, 421-423
13. Kani, K., Awano, M., Kodama, Y. and Takagi, H., SOL-GEL SYMTHESIS AND SINTERING OF Y-Ba-Cu-O POWDER. Submitted to Proc. 4th International Conference on Ceramic Powder Processing Science
14. Kodama, Y. and Wakai, F., Hot Deformation and Superconductivity of $YBa_2Cu_3O_{7-x}$ Ceramics. In Proc. ISS '89, ed. T. Ishiguro and K. Kajimura, Springer-Verlag Tokyo, 1990, pp. 113-116
15. Manthiram, A., Swinnea, J. S., Sui, Z. T., Steinfink, H. and Goodenough, J. B., The Influence of Oxygen Variation on the Crystal Structure and Phase Composition of Superconductor $YBa_2Cu_3O_{7-x}$. J. Am. Chem. Soc., 1987, **109**, 6667-6669
16. Cava, R. J. *et al.*, Studies of Oxygen-Deficient $Ba_2YCu_3O_{7-d}$ and Superconductivity Bi(Pb)-Sr-Ca-Su-O. Physica C, 1988, **153-155**, 560-565
17. Meuffels, P., Rupp, B. and Pörschke, E., PHYSICAL AND STRUCTUAL PROPERTIES OF $YBa_2Cu_3O_x$ PREPARED BY A DEFINED OXYGEN SORPTION TECHNIQUE. Physica C, 1988, **156**, 441-447

7. COMPOSITES

GAS-PRESSURE METAL INFILTRATION OF POROUS CERAMIC PREFORMS

H. Prielipp, M. Geerken, J. Rödel and N. Claussen
Advanced Ceramics Group, Technische Universität Hamburg-Harburg
Postfach 901052
D-2100 Hamburg 90

ABSTRACT

Gas pressure infiltration as a viable method to produce metal/ceramic composites by combining ceramics and non-wetting metals is described. The procedure is outlined via a discussion on two ceramic materials, RBSN and RBAO/SiC/Al_2O_3. Bending strength as well as fracture toughness are strongly influenced by the gas pressure applied during infiltration. The mechanical properties of 5 metal/ceramic pairs are listed and related to the properties of the ductile constituency. Finally an example of an interaction between a crack and a constrained metal ligament is given for an Al_2O_3/Al/SiC system.

INTRODUCTION

The incorporation of metal reinforcements into brittle solids, where they can act as crack bridging elements [1], is a viable way to increase the fracture toughness [2]. Various methods are available to produce these materials, as there are: squeeze casting, pressure filtration, direct metal oxidation (DMO), and infiltration [3]. Metal-reinforced ceramics are not only attractive from a mechanical properties point of view, but also offer advantages, such as: good joining possibilities, high thermal conductivity and therefore good thermal shock resistance.
In this paper we focus on gas pressure infiltration, exemplified by two materials, metal - infiltrated RBSN and metal - infiltrated RBAO (with SiC platelets and large particulate Al_2O_3 inclusions). The processing route will be introduced as well as resulting properties such as fracture toughness and bending strength given.

BASIC CONSIDERATIONS

Pressureless infiltration can be used to produce Si/SiC bodies [4]. The poor wetting behaviour of most metals with RBSN and RBAO does not allow us to use this route. Two approaches are possible to change the thermodynamics of the two-component system:

a) Change interfacial energies through either alloying of the metal component or coating the ceramic component [5] , similarly utilize the temperature dependence of interfacial energies [6].
b) Change thermodynamic equilibrium through pressure application[7].

The more straightforward and more general way is afforded by option b. The relationship giving the pressure needed to infiltrate a given pore with diameter, d, as a function of interfacial energy, γ, and wetting angle, Θ, is given in Eq. 1 [8]:

$$p = -4\gamma \cos \Theta / d. \qquad (1)$$

For Al/RBSN at 900 °C (γ=1 J/m^2 [9], d~0.16 μm, Θ=110° [10]), we find a value of p = 8.5 MPa from Eq. 1 . As the other metal/ceramic pairs allow similar predictions, we conclude that for the systems in question, metal (Al, Al-alloy, Ti/Al-alloy, Si) and RBSN as well as Al/Al_2O_3, pressure infiltration is required.

PRESSURE INFILTRATION

The experimental procedure is depicted in Fig.1. The porous body to be infiltrated is placed into an alumina crucible, surrounded by metal powder or metal plates. After evacuation, the system is heated up to the processing temperature and the metal molten. Pressure is applied through

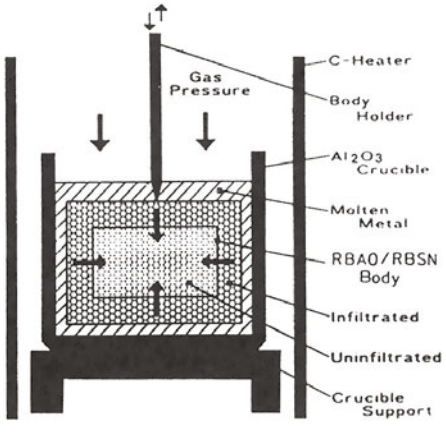

Figure 1. Schematic describing pressure infiltration apparatus.

an influx of argon gas. After a given holding time, the apparatus can be cooled under pressure and the sample finally extracted .

Let us describe the infiltration of the two ceramic materials under consideration , i.e. RBSN and RBAO . The RBSN [11] had a residual porosity of 18 % and a median pore diameter of 0.16 μm. RBAO [12] contained SiC platelets and alumina particulates in a fine grained alumina matrix with a residual porosity of 23 %. Metals for infiltration for RBSN were: pure Al, Al-alloy, Ti-39 wt.% Al and Si; for RBAO pure Al. Further details can be found in the respective publications [11,12].

RESULTS AND DISCUSSION

Pressure infiltration was successfully used to produce bodies with close to theoretical density with all the metal/ceramic pairs listed above. Two representive microstructures are shown in Fig. 2 , namely RBSN/Al [11] and RBAO/SiC/Al_2O_3/Al[12].

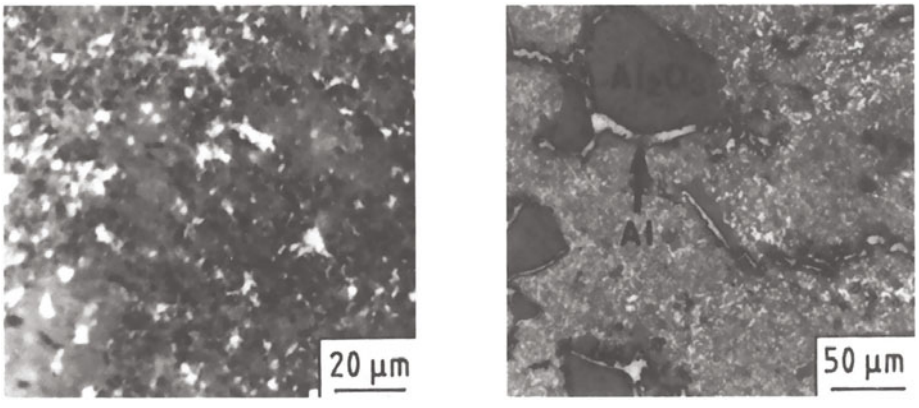

Figure 2. Optical micrographs of infiltrated a) RBSN/Al and b) RBAO/SiC/Al_2O_3/Al .

The influence of applied pressure on the mechanical properties of the resulting composite (RBSN/Al-alloy) is detailed in Fig. 3a,b. Incomplete pressure infiltration (below 60 MPa) is reflected in a lower achieved bending strength, which drops to the material strength of 220 MPa at 5 MPa pressure, which is comparable to the value of the uninfiltrated material. Similarly [13], the fracture toughness is decreased almost linearly with decreasing infiltration pressure from the peak value of the composite of about 4.5 $MPa \cdot m^{1/2}$ down to about 2.7 $MPa \cdot m^{1/2}$ for the porous RBSN . If we were to combine Fig. 3a, b and plot bending strength as a function of fracture toughness, we would find an almost linear relationship between both quantities. This result, in combination with

the simple Griffith theory seems to imply that the flaw population is unaffected by pressure infiltration. In this context, one might also note the good predictive capacity of the Washburn equation, Eq. 1, to compute the experimentally required pressure for full infiltration.

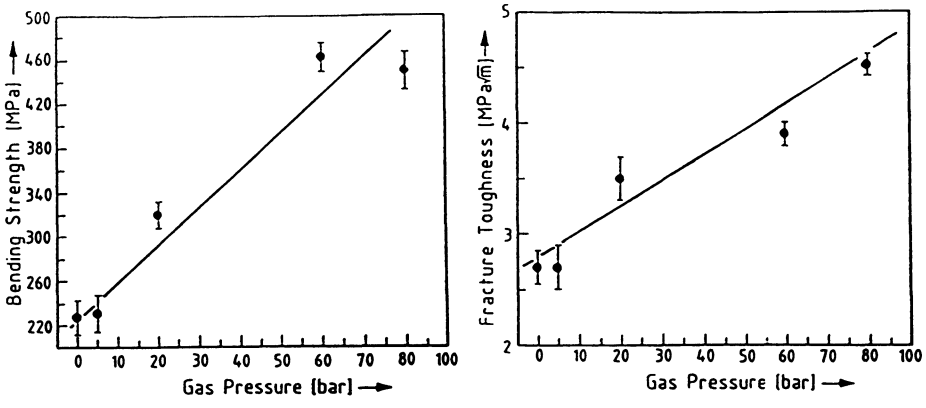

Figure 3. a) bending strength and b) fracture toughness as function of applied pressure for system RBSN/Al alloy [13].

A complete set of results of various metal/ceramic pairs with particular emphasis on bending strength (4-pt. bending) and fracture toughness (ISB) is given in Table 1 .

Table 1
Mechanical properties of metal-infiltrated RBSN and RBAO[11, 12]

	Material	Bending Strength [MPa]	Fracture Toughness [MPa·m$^{1/2}$]
RBSN (Annawerk)	not infiltrated	227 ± 15	2.70 ± 0.15
	Al (99.9%)	478 ± 15	5.00 ± 0.20
	Al-alloy	450 ± 18	4.52 ± 0.11
	Si (99.9%)	427 ± 20	3.90 ± 0.20
	Ti-39 wt-% Al	510 ± 20	n.m
RBAO	not infiltrated	90 ± 4.7	2.00 ± 0.10
	Al (99.9%)	336 ± 22	6.72 ± 0.72

Without further comparisons of specific metal/ceramic pairs we can make some generally valid statements:

- Bending strength has been increased by a factor of 2 - 3.5 compared to the uninfiltrated matrix.
- Fracture toughness has been increased by a factor of 1.5 - 2 (RBSN) and factor of 3.5 for RBAO compared to the uninfiltrated matrix.

The increase in fracture toughness goes almost parallel to the increase in bending strength; similar to the relation as discussed with respect to Fig. 3. The increment in toughness is governed by a series of interfacial as well as metal properties. Large debond lengths, paired with large metal ductility will result in a maximum of toughness increase (a trend observable in Table 1). Similarly, the metal deformation mechanism can either be dominated by necking (favoured by large debond lengths, high stacking fault energy and high metal purity [14]) or by metal cavitation (favoured by small debond lengths, low stacking fault energy, hard dispersions and incoherent or partially coherent precipitates [14]). Metal cavitation is demonstrated in Figure 4a,b, which was taken using an in-situ fracture stage in the SEM [15]. Although this particular sample was manufactured by the DMO process, the dilation of a constrained metal ligament in a ceramic matrix is a general response and not expected to depend greatly on manufacturing technique.

Figure 4. a) cavitation and b) cavity growth in $Al/Al_2O_3/SiC$ composite produced through DMO process, a) x (distance to the crack tip) = 360 μm, b) x = 410 μm.

ACKNOWLEDGEMENT

Funding was provided by the German Science Foundation under contract No. Cl 52/10-4.

REFERENCES

[1] Mataga, P., Deformation of crack-bridging ductile reinforcements in toughened brittle materials, Acta metall. Vol. 37, No. 12, 1989, 3349-3359.

[2] Krstic, V. and Nicholson, P., Toughening of glasses by metallic particles, J. Am. Ceram. Soc. 64 [9], 1981, 499-504.

[3] Toy, C. and Scott, W., Ceramic-metal composite produced by melt infiltration, J. Am. Ceram. Soc. 73 [1], 1990, 97-101.

[4] Kieffer, R., Eipeltauer, E. and Gugel, E., New in the field of cermets, Ber. Dt. Keram. Ges. 46, 1969, 486-492.

[5] Leimer, G. and Gugel, E., Infiltrations-Verbundwerkstoffe auf der Basis von Siliziumnitrid, Z. Metallkde. Bd. 66, 1975, 570-576.

[6] Nicholas, M., Mortimer, D., Jones, L. and Crispin, R., Some observations on the wetting and bonding of nitride ceramics, J. Mat. Sci. 25, 1990, 2679-2689.

[7] Jang, G., Kieffer, R., Gugel, E., Kollwentz, W. and Jicinsky, G., Anwendung der Infiltrationstechnik zur Cermetherstellung, Ber. Dt. Keram. Ges. 48, 1971, 262-268.

[8] Washburn, E., Note on a method of determining the distribution of pore sizes in a porous material, Proc. Nat. Acad. Sci. 7, 1921, 115-116.

[9] Dellanay, F., Froyen, L. and Deruyttere, A., The wetting of solids by molten metals and its relation to the preparation of metal-matrix composites, J. Mat. Sci. 22, 1987, 1-16.

[10] Loehman, R., Joining and bonding mechanisms in nitrogen ceramics, in Proc. Int. Meeting, Metal-Ceramic Joints 8, 1988, 3-16.

[11] Claussen, N. and Travitzky, N., Mechanical properties of reaction bonded silicon nitride-metal composites, in Processing of ceramic and metal matrix composites, ed. H. Mostaghaci, Pergamon Press, New York, 1989, 397-400.

[12] Wu, S., Travitzky, N. and Claussen, N., Processing of Reaction-Bonded Al_2O_3 (RBAO) Composites, in Structural Ceramics-Processing, Microstructure and Properties. Ed. Bentzen, J. et al., Roskilde, Denmark, 1990.

[13] Travitzky, N. and Claussen, N., Microstructure and properties of metal infiltrated RBSN composites, to be published in J. Eur. Cer. Soc., 1991.

[14] Lütjering, G., Gleitverhalten und mechanische Eigenschaften metallischer Werkstoffe, Deutsche Luft- und Raumfahrt - Fachbericht 70, 1974.

[15] Rödel, J., Kelly, J. and Lawn, B., In - situ measurements of bridged crack interfaces in the scanning electron microscope, J. Am. Ceram. Soc. 73 [11], 1990, 3313-3318.

FRACTURE TOUGHNESS BEHAVIOR OF β-SIALON COMPOSITES WITH CARBON-COATED SILICON CARBIDE WHISKERS

TATSUHITO TAKAHASHI and HIROAKI NISHIO
Advanced Technology Research Center,
NKK Corporation
Kawasaki-ku, Kawasaki 210, Japan

ABSTRACT

"β-SIALON" matrix composites with 10-30 vol% silicon carbide (SiC) whiskers, both uncoated and coated with carbon, were hot isostatically pressed (HIP'ed) by the glass-encapsulation method. TEM micrographs of the composites with carbon-coated whiskers showed that carbon layers remain between the whiskers and β-sialon grains. The fracture toughness of composites with 10-30 vol% carbon-coated whiskers increased with increasing whisker content, but composites with 10 vol% whiskers had almost the same toughness as monolithic β-SIALONs. Composites with 30 vol% uncoated whiskers had slightly less toughness than the monolithic sialons. The 100-hr oxidation test at 1350°C in air confirmed that the oxidation resistance of the composites with carbon-coated whiskers is excellent and equivalent to that of monolithic β-SIALONs.

INTRODUCTION

Silicon nitride and sialon ceramics offer desirable high temperature properties such as high strength and good oxidation resistance for structural components used in ceramic gas turbines. "β-SIALON" ceramics, which consist of β'-Si_3N_4 (β-sialon) and o'-Si_2N_2O (o-sialon), have high temperature strength and excellent oxidation resistance because of the lack of grain boundary phases [1-3]. However, the relatively low toughness (~3MPa•$m^{1/2}$) is a critical factor of monolithic β-SIALON that limits its use. The addition of whiskers is a method for improving the toughness of brittle ceramic materials [4]. The interface between the reinforcement material and the matrix is important for toughening composites. Commercial SiC whiskers coated with amorphous carbon are available for ceramic-ceramic composites. These whiskers can provide the carbon layer between the whiskers and sialon matrix. For the work reported herein, the stability of sialon composites with carbon-coated SiC whiskers during HIP'ing were first determined using thermodynamic data. Carbon-coated SiC whiskers

were then mixed with starting powders for a β-SIALON matrix and sintered using encapsulated hot isostatic pressing. The microstructure, fracture toughness behavior, and oxidation resistance were investigated for this sialon matrix composite with carbon-coated SiC whiskers.

THERMODYNAMIC ANALYSIS

Thermodynamic data for condensed phases and volatile species in the Si-C-N-O system used in this analysis were taken from the thermodynamic database [5]. This database does not include Si_2N_2O data but the reference data [6] was extrapolated up to 1800°C. Figure 1 presents stability diagrams of condensed phases in the Si-C-N-O system at 1800°C. P_{O_2}, P_{N_2} and P_C are the partial pressures of oxygen, nitrogen, and carbon gases, respectively. The designations (s) and (l) refer to the solid and liquid states. The lines in the diagram are boundaries between condensed phases. The dashed vertical line represents the vapor pressure of C(s). At the Si_3N_4-Si_2N_2O-SiC triple point with solid carbon, the phases Si_3N_4(s), Si_2N_2O(s), SiC(s), and C(s) co-exist at 1800°C with log P_{N_2} = 1.35 and log P_{O_2} = -16.77. At this point, P_{CO} and P_{SiO} are 0.095 atm and 0.002 atm, the highest and second highest partial pressures. For sialon phases [1], the slanted line of the boundary between Si_3N_4(s) and Si_2N_2O(s) moves slightly toward higher oxygen partial pressures, as shown by the dotted line in Figure 1. Consequently, while HIP'ing in encapsulated glass bottles at 1800°C under 200MPa, carbon and SiC of the whiskers co-exist with the β and o phases of the sialon matrix.

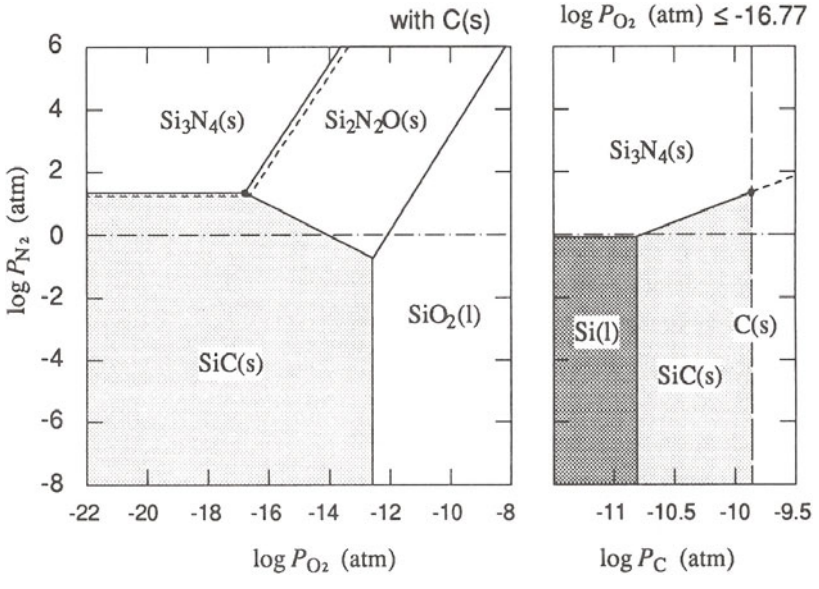

Figure 1. Stability diagrams in the Si-C-N-O system at 1800°C.

EXPERIMENTAL PROCEDURE

SiC whiskers (TWS-400, Tokai Carbon), both uncoated and coated with amorphous carbon (5nm in thickness), were used in the present study. These whiskers have an average diameter of 1.1 μm and aspect ratio of 10-30. Silicon nitride powder with 0.3 μm mean diameter (E-10, UBE Industries) and alumina powder with 0.5μm (RG-40, Iwatani Chemical Industry) were used as starting materials for the β-SIALON matrix (9wt% Al_2O_3). The total oxygen content in the silicon nitride powder was 1.1 wt%. Silicon nitride, alumina, and whiskers were dispersed with an organic binder in acetone using an ultrasonic homogenizer and then mixed for 15hrs in an attrition mill using Si_3N_4 balls. The mixture was dried in a rotary evaporator and screened to under 300μm. The resulting granules were die-pressed at 30MPa into compacts (80mm x 25mm x 20mm) and cold-isostatically pressed at 300MPa. The compacts were calcined for 5hrs in air at 500°C for de-waxing and then encapsulated in Vycor glass tubes under a vacuum at 1200°C. The encapsulated compacts were hot isostatically pressed at 1800°C for 2hrs at 200MPa in a HIP furnace (QIH-9, NKK-ABB). Composites with 10 to 30 vol% of carbon-coated SiC whiskers and those with 30 vol% of uncoated whiskers were produced.

Identification of the composite phases was carried out using an X-ray diffractometer (APD1700, Philips). TEM (EM420, Philips) was used to characterize the microstructure. The specimens were cut into 3mm x 4mm x 40mm bars, and finished with a #800 diamond grinding wheel for three-point bend strength and fracture toughness measurements. A universal testing machine (Autograph, AG-10TA, Shimadzu) was used with a crosshead speed of 0.5 mm/min. Fracture toughness was measured using SEPB method. Bulk densities were determined using the Archimedes method with deionized water. For oxidation examination, weight gains of specimens were measured after holding in air at 1350°C for 100hrs.

RESULTS AND DISCUSSION

Densities and phases

After encapsulated HIP'ing, the relative densities of the monolithic β-SIALON ceramics and the uncoated and carbon-coated whisker composites were more than 99%, as calculated from the bulk and theoretical densities. HIP is an excellent consolidation method for whisker-reinforced composites, which are usually difficult to sinter using conventional gas-pressure sintering because of the elongated whisker morphology. Powder X-ray diffraction analysis revealed β'-Si_3N_4 and o'-Si_2N_2O phases for monolithic sialon ceramics after HIP'ing. The β'-Si_3N_4, o'-Si_2N_2O, and β-SiC phases were observed in the carbon-coated and uncoated SiC whisker composites. No carbon phases were found in the carbon-coated whisker composites because of a small amount of carbon.

Fracture toughness and microstructure

Figure 2 shows the fracture toughness of the monolithic sialon ceramics and composites with carbon-coated and uncoated whiskers after encapsulated HIP'ing. The fracture toughness of the composites with 10-30 vol% carbon-coated whiskers increases with increasing whisker content. However, composites with 10 vol% carbon-coated whiskers have almost the same toughness as monolithic sialons. Composites with 30 vol% uncoated whiskers had slightly less toughness than the monolithic sialons. Whiskers should prevent grain growth of the matrix. Smaller matrix grains reduce the improvement in fracture toughness that can be obtained by the addition of up to 10 vol% of carbon-coated or 30 vol% of uncoated whiskers. Carbon-coated whisker additions of more than 10 vol% improves the fracture toughness of monolithic sialon over uncoated SiC whiskers. This suggests the importance of the carbon layer between the whisker and the sialon grains.

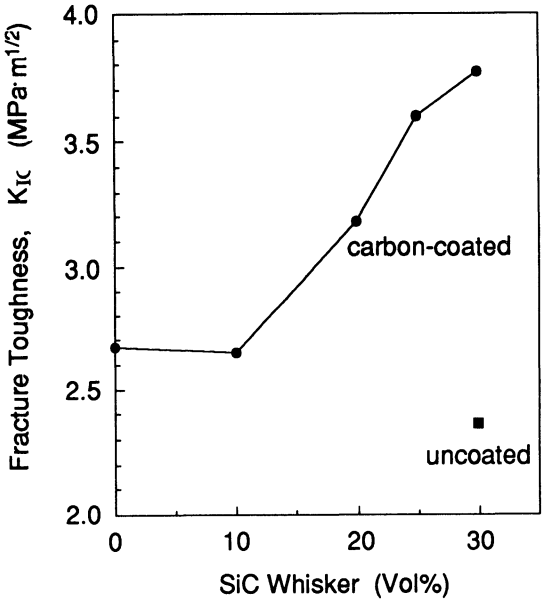

Figure 2. Fracture toughness vs SiC whisker content.

Room temperature fracture strengths were also measured, but are not presented in this paper. The strength of the composites were 800-1000 MPa or more over that of monolithic β-*SIALON* specimens. A correlation between whisker content and temperature was not evident, probably because of surface flaws introduced by machining.

TEM micrographs of HIP'ed composites with uncoated SiC whiskers are shown in Figure 3. The whiskers of 1-2 μm in diameter are uniformly distributed in the approximately 0.3 μm sialon grain matrix. No boundary layer or cracks were found between the whiskers and sialon grains. Figure 4 shows TEM micrographs of the composites with carbon-coated whiskers. The microstructure is almost same as that of the composite with uncoated whiskers except for the carbon layers between the whisker and sialon grains. The carbon layers remain on the SiC whisker after the encapsulated HIP'ing. This layer has the appearance of several graphite planes parallel to the whisker surface, as reported by Yamamoto et al. [7] While HIP'ing, amorphous carbon layer crystalized into graphite. The fracture toughness of carbon-coated whisker composites should be improved by slipping or flaking in the graphite interface between the whiskers and matrix.

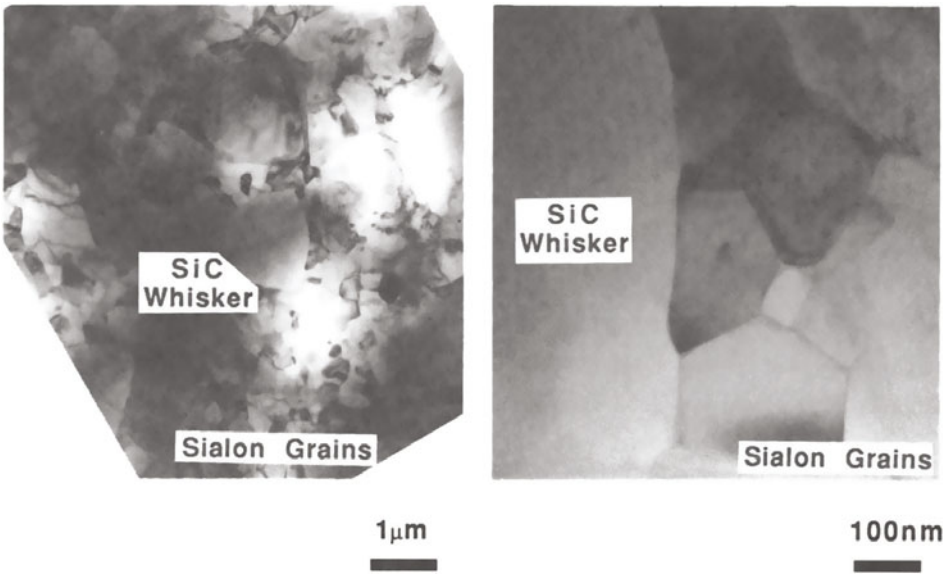

Figure 3. TEM micrograph of microstructure and grain boundaries of HIP'ed 30 vol% uncoated SiC whisker-sialon composite.

Oxidation Examination

The 100-hr oxidation tests at 1350°C in air confirmed the excellent oxidation resistance of sialon composites with carbon-coated whiskers. These tests gave values of 0.20mg/cm^2, which is equivalent to that of monolithic β-SIALON ceramics. Good oxidation resistance is observed because the carbon-coated whiskers are isolated from each other in the sialon matrix.

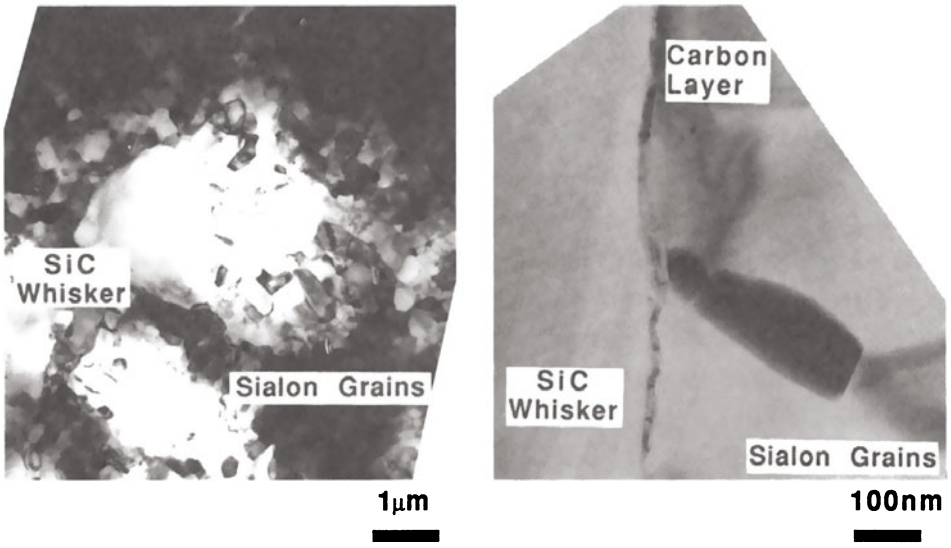

Figure 4. TEM micrograph of microstructure and grain bound-aries of HIP'ed 30 vol% carbon-coated SiC whisker-sialon composite.

CONCLUSIONS

The "β-SIALON" matrix composites with carbon-coated SiC whiskers were HIP'ed by the glass-encapsulation method at 1800°C under 200MPa. The carbon on the whiskers co-exists with the β and o phases of the sialon matrix and SiC whisker while HIP'ing. The fracture toughness of the composites containing 10-30 vol% carbon-coated whiskers increased with increasing whisker content. Oxidation tests in air at 1350°C for 100hrs on composites with carbon-coated SiC whiskers demonstrated excellent resistance to oxidation.

REFERENCES

1. Yabuta, K., Nishio, H. and Uematsu, K., Effect of phase composition on the mechanical properties of hot isostatically pressed sialon ceramics . J. Am. Ceram. Soc., 1991, **165**, 884-86.
2. Yabuta, K., Nishio, H., Kitamura, A. and Uematsu, K., Sialon ceramics by hot isostatic press encapsulation method. J. Mater. Sci. Let., (to be submitted).
3. Yabuta, K., Nishio, H. and Okamoto, H., High temperature bending strength and oxidation resistance of β-sialon prepared with minimal grain boundary phase. Ceramic Mat. & Components for Engines, ed. V.J. Tennery, Am. Ceram. Soc, 1989, pp. 622-30.
4. Wei, G.C. and Becher, P.F., Development of SiC-whisker-reinforced ceramics. Am. Ceram. Soc. Bull., 1985, **64**, 298-304.
5. The Society of Calorimetry and thermal analysis, Japan, MALT (Materials-oriented little thermodynamic data base for personal computers), 1985.
6. Ryall, W.R. and Muan, A., Science, 1969, **165**, 1363-64.
7. Yamamoto, M., Kida, T. and Sugihara, K., Characterization of surface-coated carbide whiskers for toughening ceramics. Whisker- and Fiber-Toughened Ceramics, ed. R.A. Bradley, D.E. Clark, D.C. Larsen and J.O. Stiegler, ASM International, 1988, pp.73-79.

HIPING EFFECTS FOR ZrO_2 STRENGTHENED Al_2O_3 BASED NANOCOMPOSITES

Koichi Niihara, Jianren Zeng, Atsushi Nakahira, Tohru Sekino, Yoshinari Miyamoto, Hiroshi Ohnishi* and Toshio Kawanami*
ISIR, Osaka University, 8-1 Mihogaoka, Ibaraki-shi 567, Japan
*NIKKATO CORP., 3-2-24 Orionocho, Sakai-shi 590, Japan

ABSTRACT

ZrO_2 strengthened Al_2O_3/SiC nanocomposites, Al_2O_3/5vol%SiC/20 vol% ZrO_2, were successfully fabricated by the pressureless sintering method. However, the pores and defects remained during pressureless sintering were found to decrease the fracture strength and toughness of Al_2O_3/SiC/ZrO_2 nanocomposites. To eliminate these pores and defects, the Al_2O_3/SiC/ZrO_2 composite was hot-isostatically pressed after pressureless sintering. The mechanical properties of Al_2O_3/SiC/ZrO_2 nanocomposites were significantly improved by the post HIPing. Especially, the fracture strength increased approximately twice by the HIP treatment.

INTRODUCTION

Al_2O_3 ceramics are promising materials for modern-day engineering applications, because of their desirable properties such as high refractoriness, good wear resistance and chemical stability[1]. However, Al_2O_3 ceramics show relatively low fracture toughness and strength, poor thermal shock resistance and rapid strength degradation at high temperatures. To improve these poor properties of Al_2O_3 ceramics, therefore, many ceramists have studied on Al_2O_3-based composites incorporated with second-phase dispersions such as ZrO_2, SiC, TiC and so on[2-4].

Recently, Niihara and his colleagues[5-8] revealed that the Al_2O_3 composites including only 5vol% nanometer-size SiC particle within Al_2O_3 matrix grains exhibited high strength over 1000MPa and excellent high-temperature mechanical properties. Furthermore, they showed that the mechanical

properties of Al_2O_3 with only 5vol% SiC nanometer-size particle can be improved by dispersing ZrO_2 particles[9]. These composites, however, have been fabricated by a hot-pressing technique.

The purpose of this work is to prepare ZrO_2-reinforced Al_2O_3/SiC nanocomposites by pressureless sintering and pressureless sintering/HIPing methods, which are more applicable to fabrication of complex-shaped components than hot-pressing techniques, and to examine effects of their micro- and nanostructures on the mechanical properties.

EXPERIMENTAL PROCEDURE

α-Al_2O_3 (average particle size of 0.5μm), 3mol% Y_2O_3 containing ZrO_2, 3Y-ZrO_2 (average particle size of 0.3μm) and β-SiC (average particle size of 0.3μm) were selected as starting powders in this experiment. The Al_2O_3 powder with 5vol% SiC and 20vol% ZrO_2 powder was mixed by the conventional ball milling in ethanol. The dried mixtures were isostatically pressed at 200MPa and sintered at 1650-1800°C for 2h in Ar atmosphere. The specimens pressurelessly sintered at 1700°C were further HIPed at 1400°C for 1h in Ar atmosphere under 1500atm.

The densities were measured by Archimedes method using distilled water. The phase identification was performed by X-ray diffraction. The fracture toughness was evaluated by the indentation microfracture method with an indenter load of 98N. The hardness was measured using Vickers hardness tester. The fracture strength was evaluated in 3-point bending on a 30mm span using 3x4x40mm test specimens at cross-head speed of 0.5mm/min. Tensile surfaces in the testing specimens were ground by #600 grid diamond wheel. The micro- and nanostructures were observed by transmission electron microscopy (TEM) and scanning electron microscopy (SEM).

RESULTS AND DISCUSSION

X-ray diffraction analyses revealed that the pressurelessly sintered Al_2O_3/5vol%SiC/20vol%ZrO_2 (Al_2O_3/SiC/ZrO_2) specimens were composed of α-Al_2O_3, β-SiC and tetragonal-ZrO_2 and free from other impurity phases.

Typical TEM picture of the Al_2O_3/SiC/ZrO_2 composites is shown in Fig. 1. As seen from this picture, the SiC particles were confirmed to be dispersed mainly within both Al_2O_3 and ZrO_2 grains. TEM observations also revealed that the finer ZrO_2 particles were dispersed within Al_2O_3 matrix grains, while the larger ZrO_2 particles located at the grain boundaries of Al_2O_3. The average grain size of Al_2O_3 sintered

at 1700°C was approximately 1 to 2μm. The particle size of SiC dispersed within Al_2O_3 matrix grains was less than 0.2μm, which was independent of sintering temperature. The particle size of ZrO_2 within Al_2O_3 grains was as large as that of SiC particle within Al_2O_3 grains, and the grain size of ZrO_2 at the grain boundaries of Al_2O_3 matrix was comparable to that of the Al_2O_3 matrix. These results indicate that $Al_2O_3/SiC/ZrO_2$ nanocomposites are successfully fabricated by pressureless sintering techniques.

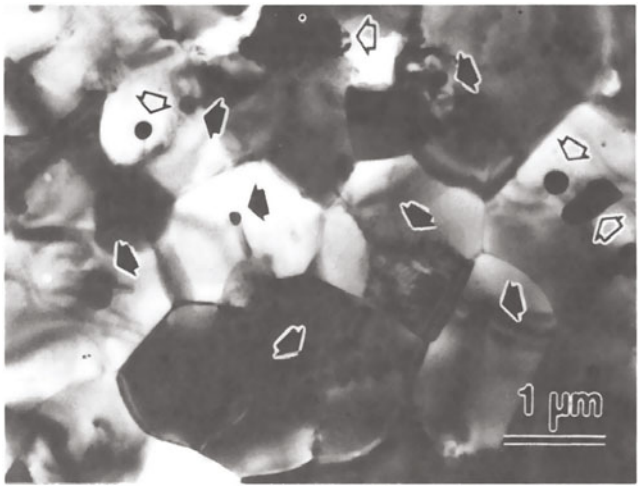

Figure 1 Transmission electron micrograph of Al_2O_3/5vol%SiC/20vol%ZrO_2 composite pressurelessly sintered at 1700°C. Black arrows indicate the SiC particles within Al_2O_3 and ZrO_2 grains. White arrows indicate the ZrO_2 particles within Al_2O_3 grains and at grain boundaries.

Fig. 2 shows the relative density of the pressurelessly sintered and pressurelessly sintered/HIP-treated $Al_2O_3/SiC/ZrO_2$ composites. Up to 99.6% relative density was obtained by the pressureless sintering at 1700°C. Furthermore, nearly full density was achieved by the HIP treatment. X-ray diffraction analyses and SEM/TEM microstructure observations indicated that there were no changes in the phase composition and the grain and particle sizes of the matrix and dispersions even after the HIP treatment at 1400°C.

The Vickers hardness of the pressurelessly sintered and pressurelessly sintered/HIPed $Al_2O_3/SiC/ZrO_2$ composites is given in Fig.3. Sintering-temperature dependence of the hardness showed a similar trend to that of the density. The hardness of these compositions was lower than that of Al_2O_3, as expected from the lower hardness of ZrO_2 dispersion. As apparent in Fig. 3, the hardness was improved slightly by the HIP treatment. This increase can be attributed to the increased density after the HIP treatment.

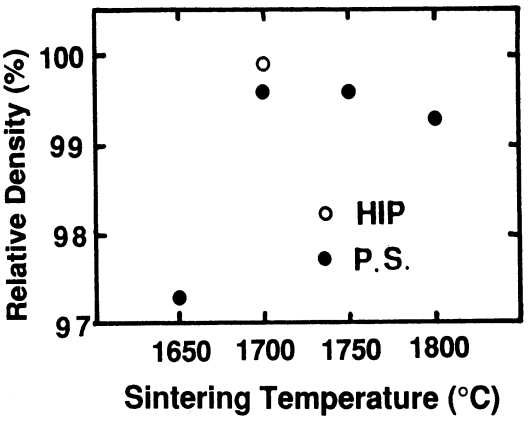

Figure 2 The relative density of Al_2O_3/5vol%SiC/20vol%ZrO_2 composites prepared by pressureless sintering and pressureless sintering/HIPing treatment.

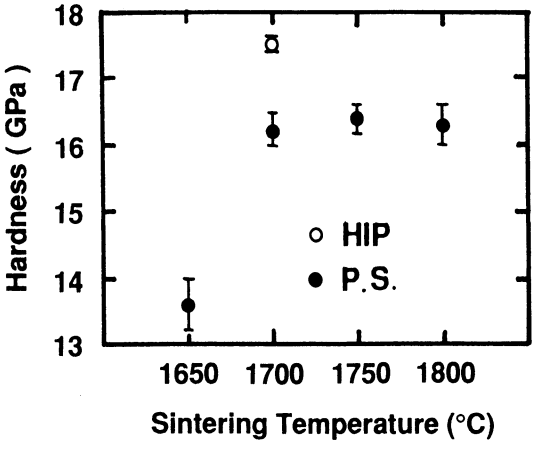

Figure 3 The Vickers hardness for Al_2O_3/5vol%SiC/20vol%ZrO_2 composites prepared by pressureless sintering and pressureless sintering/HIPing treatment.

Fig. 4 shows the bending strength and fracture toughness for the pressurelessly sintered and pressurelessly sintered/HIP treated Al_2O_3/SiC/ZrO_2 composites. The maximum strength and fracture toughness of the pressurelessly sintered composite at 1700°C are 870±60MPa and 4.7MPam$^{1/2}$, respectively. After the HIP treatment at 1400°C, the strength of the pressurelessly sintered composite increased to 1360±120MPa. The maximum strength was 1500MPa, which is comparable to the fracture strength for hot-pressed Al_2O_3/5vol%SiC/ZrO_2 nanocomposites (1700MPa).

A slight increase in fracture toughness was also observed after the HIP treatment as shown in Fig. 4. This increase is,

however, much less than that for the fracture strength. Therefore, the remarkable increase of strength by the HIP treatment is rationalized by the elimination of pores and defects by the HIP treatment.

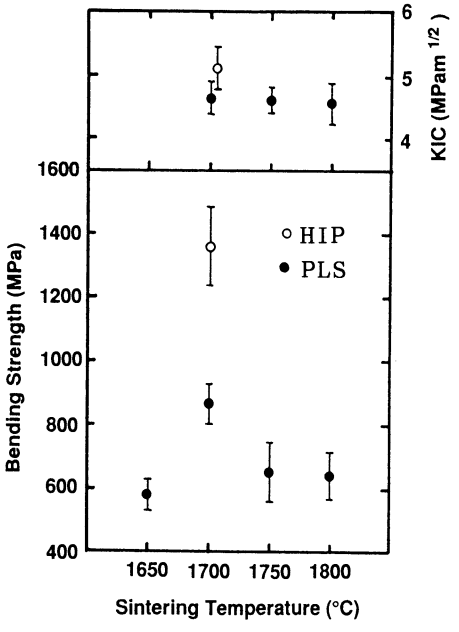

Figure 4 The bending strength and fracture toughness for Al_2O_3/5vol%SiC/20vol%ZrO_2 composites prepared by PLS and PLS/HIPing treatment.

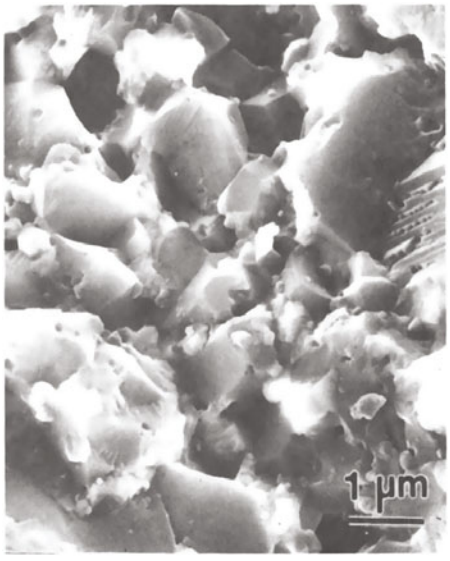

Figure 5 The fracture surface for Al_2O_3/5vol%SiC/20vol%ZrO_2 composites prepared by presureless sintering at 1700°C

Fig. 5 shows the fracture surface of the Al_2O_3/SiC/ZrO_2 composite pressurelessly sintered at 1700°C. The fracture mode is mainly transgranular. Similar fracture behavior was also observed for the pressurelessly sintered/HIP treated Al_2O_3/SiC/ZrO_2 composite. X-ray analyses of the fracture surfaces showed that the tetragonal-to-monoclinic transformation of 3Y-ZrO_2 for both pressurelessly sintered and pressurelessly sintered/HIPed Al_2O_3/SiC/ZrO_2 composites were less than that for 3Y-TZP. In addition, the Al_2O_3/20vol%ZrO_2 composites showed higher toughness than the Al_2O_3/5vol%SiC/20vol%ZrO_2 composites. This observation suggests that the SiC dispersions, in special, those within the ZrO_2 grains inhibit the tetragonal-to-monoclinic transformation of 3Y-ZrO_2. This inhibition of transformation of 3Y-ZrO_2 may be attributed to the residual compressive stresses around SiC particles within the ZrO_2 grains. Therefore, the slight increase in fracture toughness by the HIP treatment may be attributed to the crack deflection and increase in density rather than the transformation of ZrO_2.

CONCLUSIONS

Al_2O_3/5vol%SiC/20vol%ZrO_2 nanocomposites were successfully prepared by pressureless sintering and then HIPing.

1) The relative density up to 99.6% was obtained made by pressureless sintering at 1700°C. The fracture strength and toughness were 870MPa and 4.7MPam$^{1/2}$, respectively, which are much higher than those of monolithic Al_2O_3.

2) Finer SiC particles less than 0.2μm were dispersed not only within the Al_2O_3 matrix grains but also within the ZrO_2 grains, while ZrO_2 particles were dispersed within the Al_2O_3 grains and at the grain boundaries of Al_2O_3.

3) The nearly full density was achieved by the HIP treatment. The strength increased from 870$\pm$60MPa to 1360$\pm$120MPa, and the maximum strength was 1500MPa. This results suggest that pores and defects were eliminated by the HIP treatment.

4) The fracture toughness was also improved slightly by post HIPing, but the toughness value was much less than that expected from 20vol% ZrO_2 dispersion. This may be due to the inhibition of the tetragonal-to-monoclinic transformation of 3Y-ZrO_2 by SiC particles located within the 3Y-ZrO_2 grains.

REFERENCES

1. Abe, H., et al., Ceramic Science Series No. 5, GIHODO, Tokyo, 1984, pp. 22-3.
2. Lange, F.F., Transformation Toughening. J. Mater. Sci., 1982, 17, 225-62.
3. Niihara, K., Nakahira, A., Uchiyama T. and Hirai, T., High-Temperature Mechanical Properties of Al_2O_3-SiC Composite. In Fracture Mechanics, ed. R. C. Bradt, A. G. Evans, D. P. H. Hasselman and F. F. Lange, Plenum, New York, 1986, pp. 103-16.
4. Wahi, R. P. and Ilshner, B., Fracture Behavior of Composites Based on Al_2O_3-TiC. J. Mater. Sci., 1988, 15, 875-885.
5. Niihara, K., Ceramic Nanocomposites. Electronic Ceramics, 1988, 9, 44-8.
6. Niihara, K. and Nakahira, A., Development of Strong Al_2O_3-SiC Composites. Proc. of MRS Meeting on Advanced Materials, Vol.5, Tokyo, 1988, pp. 129-34.
7. Niihara, K., Nakahira, A. and Hirano, T., Particulate Strengthened Ceramics, Nanocomposites. Proc. of US-Japan Seminar on the Processing of Advanced Ceramics, Seattle, 1988, in press.
8. Niihara, K. and Nakahira, A., Strengthening of Oxide Ceramics by SiC and Si_3N_4 Dispersions. Proc. of Third Int. Symposium on Ceramics Materials and Components for Engines, 1989, pp. 919-26.
9. Nakahira, A., Fukushima, Y. and Niihara, K., Al_2O_3-SiC-ZrO_2 Composites. J. of Japan Soc. of Powder and Powder Metallurgy, 1989, 36, 116-21.

Gas-pressure Combustion Sintering of ($MoSi_2$-SiC) /TiAl Functionally Gradient Material (FGM) and its Residual Stress Analysis

Yuji Matsuzaki, Junzo Fujioka,
Shun-ichi Minakata, Yoshinari Miyamoto*
Akashi Technical Institute, Kawasaki Heavy Industries, LTD.
*Institute of Scientific and Industrial Research, Osaka University

ABSTRACT

Functionally Gradient Materials(FGMs) are expected to be applied, as advanced thermal barrier coating systems, to active cooling structures for air-frames and engines of hypersonic spaceplanes. In this paper, fabrication of ($MoSi_2$-SiC)/TiAl FGMs by the Gas-pressure Combustion Sintering is described and properties of the FGMs are discussed. Compositional distribution in the FGM was one of the most important determinants of residual thermal stress of an FGM, especially for radial stress on the $MoSi_2$-SiC surface. Residual stress after fabrication was examined by thermal stress analysis, and experimental results were compared with analytical results. Static thermal stress in actual high-temperature environments was also examined analytically, and it was considered to be less critical than residual thermal stress after fabrication.

INTRODUCTION

FGM is a macro-heterogeneous composite material having a micro-heterogeneous chemical composition which gradually changes from a heated-face to a cooled-face material(1). FGM has two purposes. One is to reduce heat flux entering the structural material through the use of thermal barrier systems in actual high-temperature environment, and the other is to disperse and minimize thermal stress concentration. The heated surface of the FGM must be a material with low thermal conductivity to produce a large temperature difference in the FGM, enabling it to resist extremely high temperatures and reduce the heat flux from a high enthalpy gasflow environment. The structural material should be a metallic one having excellent specific strength and high thermal conductivity at the operating temperature. At the same time, thermal stress in the FGM must be dispersed and minimized during both the fabrication process and use in the actual environment.

Research and development on FGMs has been promoted by the Science and Technology Agency of Japanese government since 1987. In the project, various kinds of material

systems are being studied by the processes including CVD(2), PVD(3), low pressure plasma spraying(4), powder sintering(5)(6) and SHS(Self-propagating High-temperature Synthesis) (7)(8).

In this study a $MoSi_2$-SiC composite, which has excellent oxidation resistance and a high temperature strength was chosen for hot-side material, and a TiAl intermetallic compound with a high specific strength for the cool-side material of FGM. The fabrication of ($MoSi_2$-SiC) /TiAl FGMs by the Gas-pressure Combustion Sintering method using the SHS and HIP processes is described and properties of the sintered FGMs are examined based on experimental and analytical considerations.

GAS-PRESSURE COMBUSTION SINTERING

Pressurized Combustion Sintering(9) is one of the processes used for sintering refractory compounds and their composite materials. In this process, the compounds are sintered simultaneously by synthesis from elemental powders during the SHS(Self-propagating High-temperature Synthesis) reaction under pressurized conditions. As the process is usually accompanied by rapid diffusion of elements at elevated temperatures up to 4000℃, various kinds of refractory non-oxide ceramics, intermetallic compounds and their composites can be sintered in a period of seconds. This process is especially suited for fabricating composite materials having macro-heterogeneous chemical compositions, because each portion of the material can be sintered independently at controlled temperatures, taking into account the chemical and physical properties of each portions. Several methods of pressurization for combustion sintering are proposed, such as spring pressurization(10), hydrostatic pressurization(11) and pulse-electromagnetic shockwave pressurization(12).

Gas-pressure Combustion Sintering(13), shown in figure 1, is one type of pressurized combustion sintering, which uses isostatic gas pressure for the pressurization of the synthesized products in the SHS reaction. In this process the SHS reaction of the reactants is initiated by the SHS reaction of the ignition powders such as the mixture of titanium and carbon.

Glass encapsulated reactants mixed into the ignition powders are pressurized by isostatic gas pressure at the glass's softening temperature. After that the ignition powders are ignited by electrical heating and the SHS reaction is induced. They react

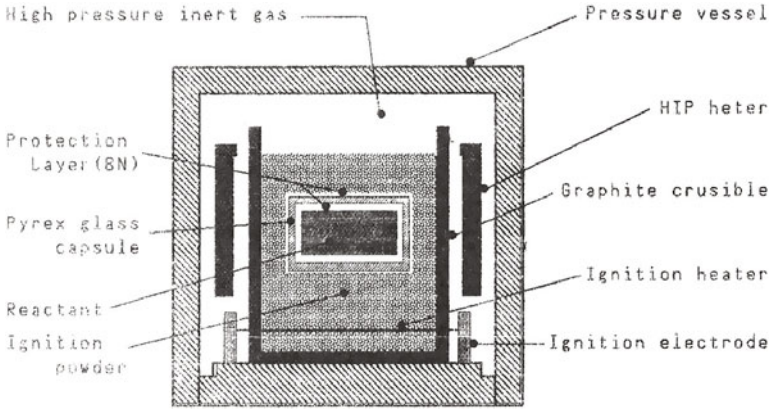

Figure 1 Gas-pressure Combustion Sintering

and are converted into a compound within a period of seconds, releasing a high enthalpy of formation. For example, the ignition powders of titanium and carbon release 170kJ/mole during their reaction and the combustion temperature reaches approximately 3000℃. Then the SHS reaction of the encapsulated reactant is initiated by combustion heat of the ignition powders. At this time the SHS product is sintered simultaneously by synthesis under isostatic gas pressure. For high-velocity combustion wave propagation, the reaction is conducted almost completely adiabatically which allows prediction of the combustion temperature with 95% accuracy using thermodynamical calculations. The high energy efficiency due to the extremely high sintering temperature and the isostatic gas pressure makes it possible to sinter various refractory materials such as borides, carbides, silicides, aluminides, and their composites with full density without sintering aids under lower pressure than that for ordinaly HIPing.

GLASS ENCAPSULATION TECHNIQUE

The glass bottle method of HIP(14) has been used for the Gas-pressure Combustion Sintering method. Although reliable encapsulation can be achieved by the method, the sizes and shapes of products have been limited. A new glass encapsulation technique, however, was devised for wider application of the Gas-pressure Combustion Sintering method(8). In this technique, a green compact is inserted into a pair of glass dishes, and then heated in a vacuum furnace up to the glass's softening temperature. Photograph 1 shows the glass dishes before sealing(left), an encapsulated green compact (middle) and a decapsulated product after the Gas-pressure Combustion Sintering(right). The sizes and shapes of products are not restricted and reliable encapsulation is possible with this method. Larger products with complex shapes can be fabricated by the Gas-pressure Combustion Sintering using this technique. If needed, a combined process of encapsulation-sintering would be possible by utilizing a sinter-HIP apparatus.

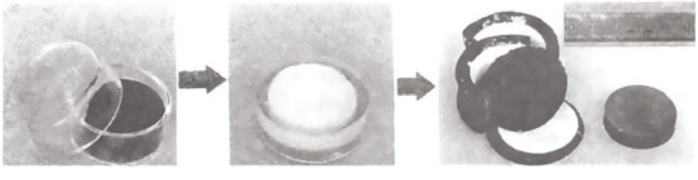

Photograph 1 Glass encapsulation technique, a compacted reactant and a pair of Pyrex glass dishes(left), an encapsulated reactant(middle), and a decapsulated product after sintering

PROCEDURE

Mo, Si, $MoSi_2$, SiC, and TiAl powders were weighed out and ball-milled for 12 hours. Green compacts were prepared by CIPing under 250MPa and encapsulated as stated previously. Gas-pressure Combustion Sintering was performed on the encapsulated reactants at a starting temperature of 700℃ under argon gas pressure of 100MPa. The chemical composition of the reactant powders was determined by thermodynamical calculations based on the combustion temperatures of the SHS reaction. Microstructures

were observed utilizing a scanning electron microscope and chemical compositions were analyzed by X-ray micro-analyzer. Properties including density, flexure strength, elastic modulous, coefficient of thermal expansion, thermal conductivity and specific heat of NFGMs (non-FGMs ; macro-homogeneous composite materials with different chemical compositions) were evaluated from RT up to max.1400℃ for heat transfer and thermal stress analysis.

FGMs were prepared by laminating 11 units of NFGM reactant powders and then Gas-pressure Combustion Sintering was performed. The effects of compositional distribution on the residual stress of the FGMs were evaluated experimentally. Thermal stresses after fabrication and in the static high-temperature environment were also evaluated numerically using the structural analysis program ABAQUS 4.8.

RESULTS AND DISCUSSION

Microstructure of FGM

Figure 2 shows the microstructure of ($MoSi_2$-SiC)/TiAl FGM and the elemental distributions in its cross-section. In the FGM, $MoSi_2$ is synthesized by the SHS reaction. The sintering temperature of all compositions is fixed at 1400℃. The NFGM products contained very few pores and were almost fully densified. The microstructure of the $MoSi_2$-33wt%SiC (0%TiAl) exhibited a network structure and the $MoSi_2$ matrix and SiC reinforcement were thermodynamically stable(15). As the content of TiAl increased, the microstructure changed into a dispersion composite structure. TiAl showed the typical $\gamma+\alpha_2$ eutectoid microstructure(16)(17).

Fabrication of FGM

The ($MoSi_2$-SiC)/TiAl FGMs are usually "warped" due to relative shrinkage of the TiAl side which has a larger coefficient of thermal expansion. This results in a generation of tensile stress on the $MoSi_2$-SiC surface which has a larger elastic modulous during the cooling process after sintering. The degree of residual stress in FGM is determined by the parameters below.

① Dimensional parameters (Ratio of the thickness of the hot-face, cool-face material, and gradient layer to surface area)
② Distributional parameters of the chemical composition
③ Process parameters (Sintering temperature, stress boundary conditions, and cooling rate after sintering)

The dimensional parameters are usually determined by the spaceplane system design concept, and the process parameters are restricted by the materials and processes.

Figure 3 shows the effect of compositional distribution on the residual stress of FGM after the process of fabrication. Each FGM is 30mm in diameter and 8mm in thickness. The left two photos show the $MoSi_2$-SiC and TiAl face of FGM having a chemical composition denoted by the distributional exponent of p=2.0 which means the content of TiAl increases in an inverse-parabolic manner from the hot side to the cool side in gradient layer. The right photos show those with a distributional parameter of p=0.5 meaning that the TiAl increases parabolically from the hot side to the cool side. The $MoSi_2$ surface of FGM with a distributional exponent of p=2.0 was clearly cracked and crack-free FGM was obtained at an exponent of p=0.5. It is believed that the degree of residual thermal stress is remarkably influenced by the macro-deformation of FGM in cooling process, which is determined by the compositional distribution.

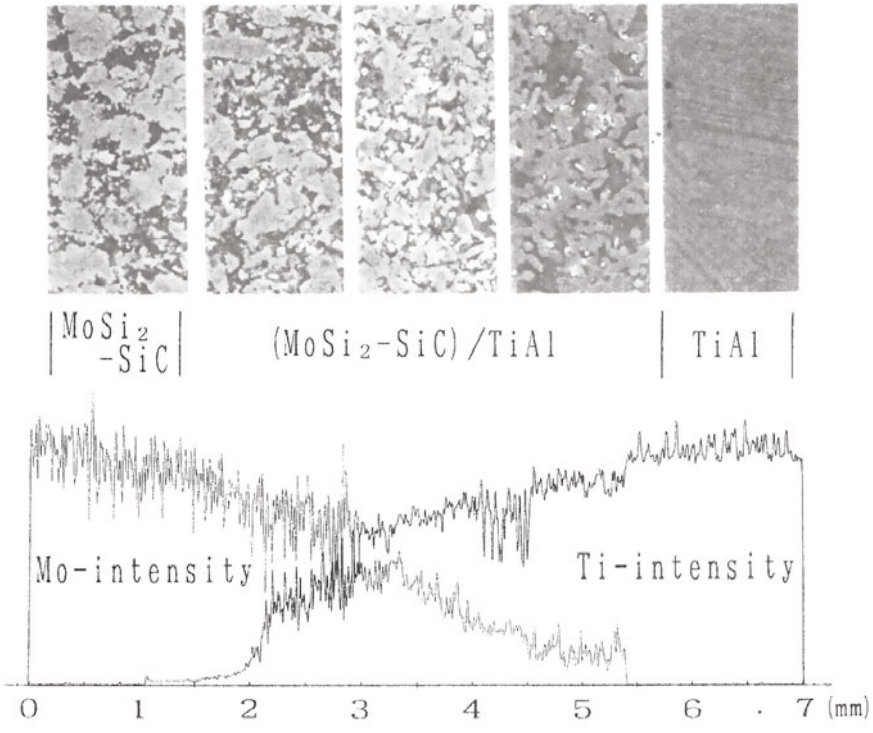

Figure 2 Microstructure of (MoSi2-SiC) /TiAl FGM and elemental distributions in its cross section

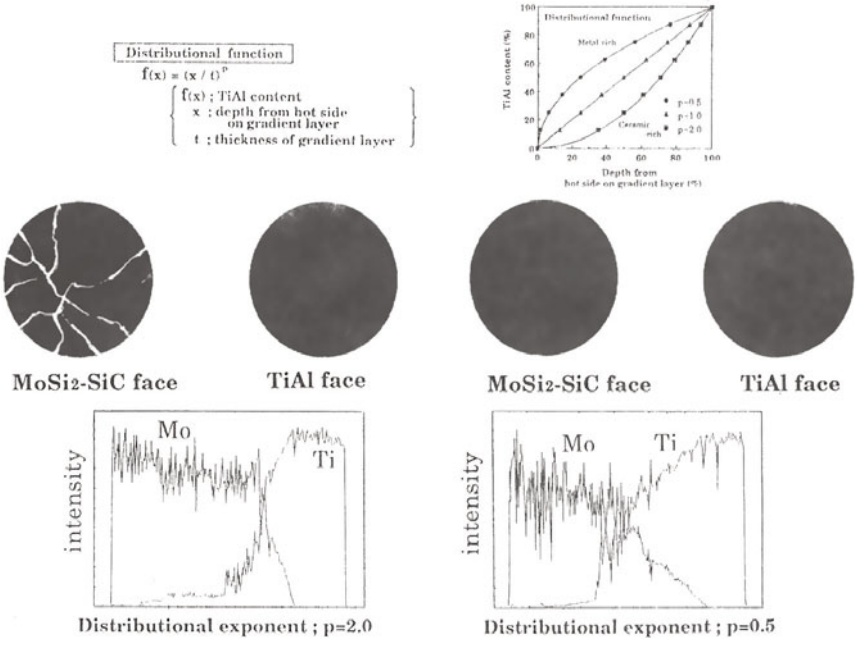

Figure 3 Macroviews of FGMs with different compositional distribution

Analytical Considerations

The results stated previously were also evaluated analytically using numerical calculations. It is clear that the residual thermal stress is critical on the $MoSi_2$-SiC surface having a larger elastic modulus and a higher elasto-plastic transition temperature, regardless of the compositional distribution. A residual tensile stress (Mises' equivalent stress) of 720MPa was generated on an $MoSi_2$-SiC surface of FGM with p=2.0 and it was larger than the flexure strength of $MoSi_2$-SiC which was 600MPa. On the other hand, with a p-value of 0.5, the residual stress on the surface was 200MPa, which was approximately 30% of the flexure strength of the $MoSi_2$-SiC composite.

In this FGM system the radial thermal stress was much larger than the circumferential stress, axial stress and shearing stress on $MoSi_2$-SiC surface. Figure 4 shows radial stress distributions on the $MoSi_2$-SiC surfaces of FGMs as a function of compositional distributions. The X-axis shows the distance from the center of the $MoSi_2$-SiC surface. The Y-axis shows the specific radial stress which is the ratio of calculated radial stress to the fracture stress of the surface material. The flexure strength was used for the fracture stress on the tension side, and ten times of the flexure strength on the compression side. From the experimental results, we see that a decrease in the exponent p-value resulted in reducing the residual stress on the $MoSi_2$-SiC surface, and crack-free FGM was obtained at a distributional parameter of p=0.5. The experimental results were compared with the results of numerical calculations. The critical level of reducing residual stress on $MoSi_2$-SiC surface below its fracture strength is considered to be the p-value reducing the maximum specific radial stress below approximately 0.4~0.5.

In practical use, FGM must be designed to minimize the critical thermal stress below an acceptable level in both the fabrication process and the actual high-tempareture environment. Analytical thermal stresses on the $MoSi_2$-SiC surface generated in a static high-tempareture environment are shown in figure 5. The thermal stresses were below the specific stress value of 0.4 regardless of the p-value and were mostly compressive stresses. In this analysis, the cooled side is bonded to a TiAl structure and the axial displacements on the bonded face are constrained. The hot face is heated at the static heat flux of 2.0MW/m^2 and the TiAl side is actively cooled at 800℃. The surface temperatures were approximately 1800℃ regardless of the p-value, which means the effective thermal conductivity is hardly influenced by the compositional distribution for this FGM system. The very close specific compressive stress values of FGMs with different compositional distributions in figure 5 is considered to be due to

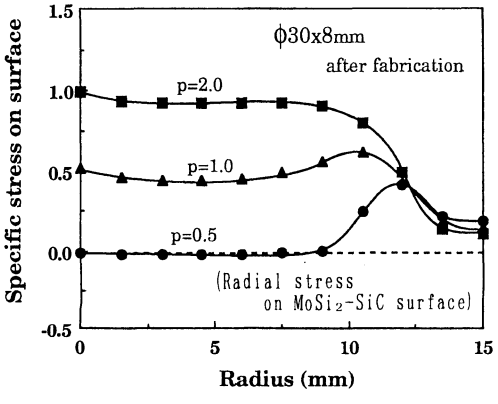

Figure 4 Specific residual radial stress on $MoSi_2$-SiC face after sintering

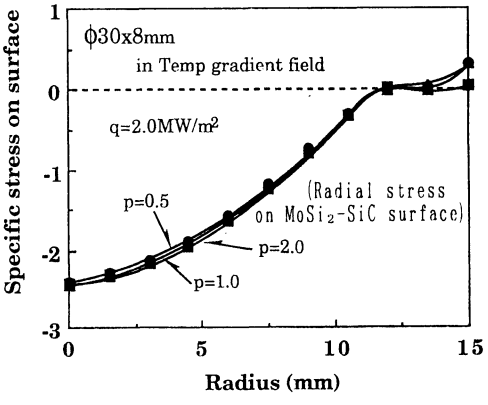

Figure 5 Specific radial stress on MoSi-SiC face in high-temperature environment

the small difference in the effective thermal conductivities and the constraints of the TiAl bonded face.

Figures 4 and 5 are summarized into figure 6. Generally, tensile thermal stress after the fabrication process is larger than the thermal stress in a static high-tempareture environment. We can say that the key problem with this FGM is the reduction of the residual thermal stresses in fabrication process. Further analytical considerations are required on wider range of the distributional and dimensional parameters for optimizing this FGM system.

Another possibility to reduce residual thermal stress is controlled temperature gradient sintering, which takes advantage of the SHS reaction as stated previously. The sintering temperature is the most important determinant affecting the residual stress after the fabrication process. It is believed that the difference in the thermal shrinkage between both sides of the material is reduced in the cooling process by sintering the ceramic side having a lower coefficient of thermal expansion at a higher temperature and the metal side with a higher coefficient of thermal expansion at a lower temperature, resulting in a reduction of residual stress after fabrication. For the purpose of performing temperature gradient sintering, the fundamentals of thermo-dynamical calculations, temperature controlling techniques, and elasto-plastic analysis are being examined currently.

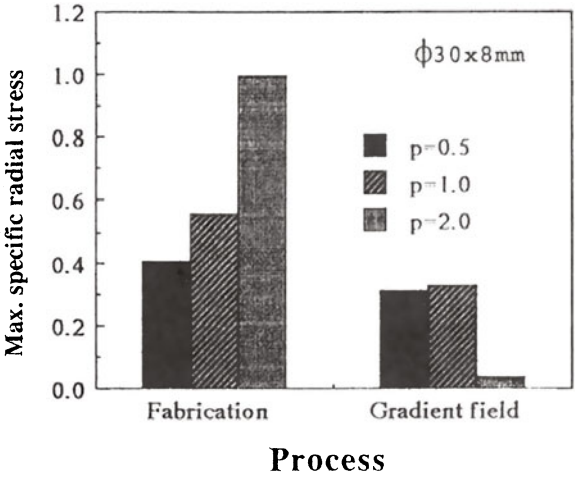

Figure 6 Comparison of max. spesific radial stresses after fabrication and in high-temperature environment

CONCLUDING REMARKS

The goal of this study is the application of advanced thermal barrier systems using Functionally Gradient Materials(FGMs) for the active cooling structures of hypersonic spaceplanes.

A process to synthesize Functionally Gradient Materials by the Gas-pressure Combustion Sintering method using SHS(Self-propagating High-temperature Synthesis) and the hot isostatic pressing was developed. Experimental and analytical considerations for residual thermal stress after Gas-pressure Combustion Sintering were performed on ($MoSi_2$-SiC) /TiAl FGMs. Furthermore, the thermal stress of the actual high-

tempareture environment was simulated and compared with the residual stress after the fabrication.

The residual stress after the fabrication process is remarkably affected by compositional distribution of ($MoSi_2$-SiC) /TiAl FGM. The critical conditions of the compositional distribution for sintering crack-free FGMs was considered to be those reducing specific stress value, which is the ratio of calculated thermal stress to flexure strength of $MoSi_2$-SiC composite, below approximately 0.4~0.5. Static thermal stress in the high-temperature environment was not as critical as the residual stress after the fabrication process.

ACKNOWLEDGMENT

The authors would like to acknowledge their support by grants from special coordination funds for R & D on Functionally Gradient Materials promoted by the Science and Technology Agency. They wish to express their gratitude to Mr. Hamano for his continuous assistance in experiments for this study.

REFERENCES

(1) M. Koizumi : The 1st International Symposium on FGM, Proceedings(1990), p.3.
(2) M. Sasaki and T. Hirai : The 1st International Symposium on FGM, Proceedings(1990), p.83.
(3) C. Kawai, S. Wakamatsu, S. Sakagami and T. Igarashi : The 1st International Symposium on FGM, Proceedings(1990), p.77.
(4) N. Shimoda, S. Kitaguchi, T. Saito, H. Takigawa and M. Koda : The 1st International Symposium on FGM, Proceedings(1990), p.151.
(5) M. Takemura, A. Yoshitake, H. Hayakawa, T. Hyakubu and M. Tamura : The 1st International Symposium on FGM, Proceedingth(1990), p.97.
(6) R. Watanabe and A. Kawasaki : The 1st International Symposium on FGM, Proceedings (1990), p.107.
(7) Y. Miyamoto, H. Nakanishi, K. Tanihata, I.Tanaka and O.Yamada : The 1st International Symposium on FGM, Proceedings(1990), p.257.
(8) Y. Matsuzaki, J. Fujioka, S. Minakata and Y. Miyamoto : The 1st International Symposium on FGM, Proceedings(1990), p.263.
(9) Y. Miyamoto, M. Koizumi, O. Yamada : J. Am. Ceram. Soc., vol.67, 1984, C224.
(10) N. Sata and J. Ikeuchi : J. Ceram. Soc. Japan, vol.95[2], 1987, p.243.
(11) N. Sata : Kinou zairyou, vol.8[2], 1988, p.47.
(12) Y. Matsuzaki, H. Hino, J. Fujioka, S. Minakata and N.Sata : The 5th International symposium of the Japan Welding Society, Proceedings[1], 1990.
(13) Y. Miyamoto, M. Koizumi : Proc. Int. Inst. for the Science of Sintering Symposium, "Sintering'87", Elsvier Science Publishing Co. Inc. 1, 1988, p.511.
(14) T. Fujikawa and H. Okada : Proceedings for the 5th. HIP seminar(1985), p.2.
(15) D. H. Carter, W. S. Gibbs, and J. J. Petrovic : Third international symposium on ceramic materials and components for engines, proceedings(1988), p.977.
(16) M. Yamaguchi : J. Japan Soc. for Heat Treatment, vol.29[5], 1989, p.248.
(17) S. Isobe : Sokeizai, vol.3, 1989, p.1.

HIPED PARTICULATE MMC:S FOR HARDWEARING APPLICATIONS

ULF BRYGGMAN, JAN-OLOV LINDQVIST AND TORE GARVARE
The Swedish Institute of Production Engineering Research (IVF)
S - 951 87 Luleå, Sweden

ABSTRACT

An investigation has been carried out to determine the production feasibility, by Hot Isostatic Pressing - HIP, and properties of some ironbase MMC:s. The MMC:s presented in this paper are divided into two groups dependent on the starting materials, "in-situ" MMC:s based on highly alloyed metal powder of cast iron type and particulate mixtures where a ceramic phase is added separately to the matrix powder. The particulate mixtures are based on different iron and steel alloys with Al_2O_3, of varying purity, and impure SiC as additions. The wear resistance of the MMC:s when exposed to pure grinding abrasion reaches 25 times that of tool steel AISI/SAE A2 while the wear resistance under mixed impact and abrasion is 2-3 times that of forged QT-steel.

INTRODUCTION

MMC:s with iron based matrices show great potential for use in low-cost, abrasion resistant wearparts. In order to develop and implement iron-base MMC:s a joint Nordic research project has been instigated and completed during 1988-1991. The combination of powderbased MMC:s with powderbased monolitic base-material using HIP has resulted in an interesting technique for the production of compound materials and parts.

MATERIALS AND METHODS

Base materials

Commercially available materials in the form of blasting particles and gas- and water-atomized metalpowder has been used. The size of the ceramic particles was 100-200 μm and the metal powder was <63 μm to obtain a contiuous matrix. The chemical composition of the used materials is shown in Table 1. The SiC particles were roasted, while stirred, in air at 1100 $^{\circ}$C for 10h to produce a protective SiO_2 layer on the surfaces of the particles.

TABLE 1
Analysis and composition, weight-%

Material				Material			
	SS 2240	APM 2311	3% C-iron		Al_2O_3		SiC
Substance				Substance	Corundum	Diruby	
C	0.33	2.0	3.19	Al_2O_3	95.8	99.4	not available
Si	0.39	0.6	0.03	SiO_2	0.7	0.1	"
Mn	0.44	0.7	0.30	Fe_2O_3	0.2	0.02	"
P	0.017	0.017	0.013	TiO_2	3.1	0.008	"
S	0.014	0.020	0.004	CaO	0.2	0.05	"
Cr	3.0	26.0		Na_2O	0.02	0.2	"
Ni	0.08	0.2		Cr_2O_3	-	0.25	"
Mo	0.58						
V	0.06	-		Hardness	~ 2000	~ 2200	~2600-2800
O	0.012	0.009	0.79	$HV_{100\ p}$			
N		0.06					

Mixing and encapsulation

The powders were mixed damp with methanol as mixing medium and packed in containers of cold drawn 2 mm steel. Hot evacuation was carried out to 700 °C/10^{-3} mbar and sealing was at ≈150 °C. Capsule removal after HIP was through conventional machining.

HIPing and heat treatment

HIPing was carried out at 2000 bars for 2 h. The temperatures used were 880 °C for the SiC-MMC:s and 1100 °C for the alumina MMC:s. Some tests with other duration and temperature were made to study the effect on ceramic-metal reaction. The SiC-MMC:s and the Al_2O_3-MMC:s with 2240 matrix were heat treated at 920 °C, 1 h followed by quenching in oil and double tempering 200 °C, 2 h. The MMC:s with 2311 matrix were heat treated at 1100 °C, 1h, air quenched and tempered 2 h at 500 °C.

Test methods

Both as HIPed (AS) and heat treated (QT) MMC:s were tested. The wear resistance was evaluated by using 2-4 bars of each MMC in a small rod mill (Ø 205 mm) for milling slurried 1-3 mm quartz sand (pH=7). The test situation contains both impact strains and pure abrasive wear. Dry abrasion was evaluated as a two-body case using sections of heat treated MMC bars. The sections were pressed against 90 μm SiC paper with 200 N force and 200 rpm counterrotating relative movement.

Tensile strength testing was carried out on 3-6 samples of each MMC and technical load-elongation curves were recorded. The elongation rate was 0.1 mm/s. Evaluation of the impact strength was carried out on an instrumentated impact test device using two unnotched bars with 10 mm square cross section per MMC. This test gave apart from energy loss, also the force-time relation.

Microstructural characterization

Light(LOM) and SEM microscopy, with EDS analysis, was used to study the resulting microstructures. The particle content of the MMC:s was determinated by LOM on polished and etched cross sections (5 per sample). The values of the particle content have to be regarded as good approximations and not as absolute values. Macro- and microhardness was determined using Brinell and Vickers indentation.

RESULTS AND DISCUSSION

SiC MMC:s, structure and reactions

There are different ways to prevent SiC from reacting with a surrounding matrix [1-2], but SiO_2-layers are naturally present on the SiC-particles and protective. A high content of C in the matrix also appears benificial while the Cr-content only has a small effect. The least reaction was obtained using a matrix with high contents of C and O, see Fig. 1. Initially SiC dissolves through a solid phase reaction where Si and C leaves the carbides and, mainly, Fe enters. In Fig. 2a) is shown how the initial reaction breaks open the SiO_2-layer on a SiC-particle. The rate of reaction is increased when a "melt film" of eutetic type is formed. This film is present even at temperatures below 880 °C. The existance of the melt film can be deduced from the reaction-transformed material. Fig. 2 b) shows the reaction in a Cr-iron matrix. Close to the particle is a zone with silicide precipitations , then a light etching layer followed by SiO_2 residues and partially transformed matrix. The Si-content is high in the silicide zone and decreases towards the matrix value outside the SiO_2-residues. The residues are enriched with S, Si, Cr and Mn, which indicates the previous existance of a melt film. In Fig. 3 a) precipitations, presumed to be graphite, can be seen.

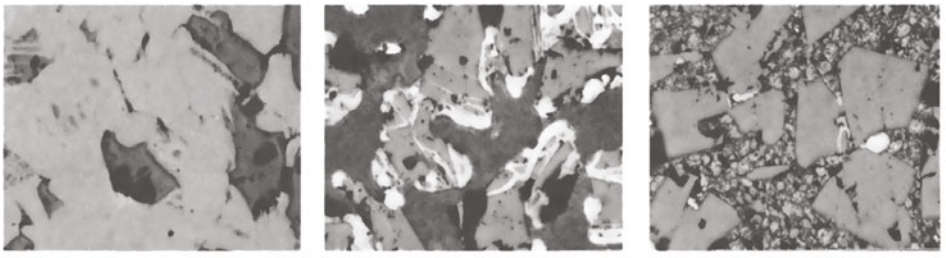

Figure 1. Roasted SiC in 2240, 2311 and 3 % C-iron matrix respectively (32X).

Figure 2. SiC in 2240 (800X) and Cr-iron matrix and the distribution of Si and Cr (160X).

Al_2O_3 MMC:s, structure and reactions

No macroscopic reactions between Al_2O_3 and matrix could be found except for some spinel-formation when using oxygen rich 3 % C-iron at 1100 °C HIP-temperature. Studies of the contact/bonding surfaces by LOM through Al_2O_3-crystals does show some reaction between particle and matrix, even at ordinary HIP-temperatures, cp Fig. 3b) and 3c).

Iron powder MMC:s

The two ironpowders used in the experiments can be regarded as directly prepared MMC:s. The powders contain 40-60 v/o carbide phase in the form of cementite and 3-carbide respectively. At higher HIP temperatures the carbide structures deteriorates and partial melting was reached at $\approx$1130 °C for the 3 % C-iron and $\approx$1250 °C for 2311 Cr-iron.

TABLE 2
Ultimate strength and elongation, total volume content hard phase and impact strength

Material		As HIPed (AS) σ_B	δ_B	Σ	Impact strength	Quenched and Tempered (QT) Σ σ_B	δ_B	Σ	Impact strength
Added volume constant hardphase/matrix-test		MPa	%	v/o hard phase*	J/mm²·10⁻³		%	v/o hard phase*	J/mm²·10⁻³
Corundum /SS 2240									
0	100	1415	19.5	-	-	>1860	no rupture	-	-
20	80	620	3.2	20	56	850	2.5	20	53
35	65	390	2.2	35	38	525	1.6	35	38
50	50	190	1.1	50	-	320	1.3	50	-
Diruby /SS 2240									
20	80	650	3.7	20	-	865	2.5	20	-
35	65	425	2.3	35	46	570	1.9	35	49
Diruby /APM 2311									
0	100	1150	5.0	46.0	94	1165	2.6	40.5	64
20	80	370	1.1	57.6	11	345	0.9	49.4	7
35	65	210	0.8	65.5	4	265	0.8	61.6	9
50	50	150	0.7	83.8	-	125	0.6	69.2	-
Corundum /APM 2311									
20	80	370	1.2	57.8	-	335	1.6	49.8	-
35	65	265	0.9	62.9	-	195	1.3	56.4	-
SiC/3.2 % C-iron									
0	100	700	2.6	60.5	28	1350	2.9	53.4	52
15	85	240	0.6	67.5	4	a)	a)	a)	-
30	70	165	-	73.2	-	a)	a)	a)	-

* The matrix material contains precipitated hard phases. SS 2240 contains a very small volume small particles which are neglected. APM 2311 contains 3-carbide ≤ 10 μm and the 3.2 % C-iron contains Fe_3C ≤ 100 μm.
a) The samples could not be heat treated at 920 °C due to reaction between the SiC and the container.

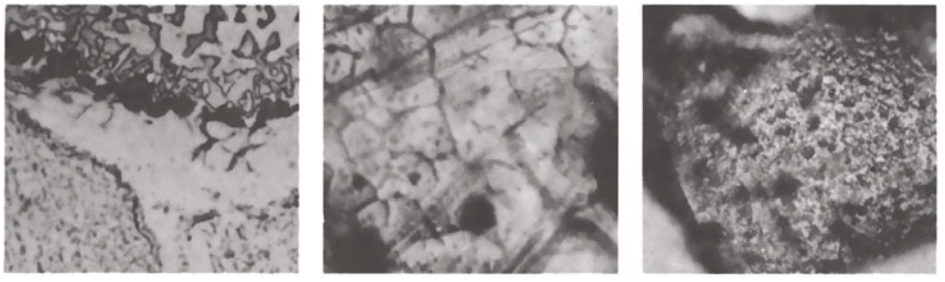

Figure 3. Flake precipitations (800X) and Al_2O_3 in 2240 and Cr-iron matrix (320X).

Strength and impact strength

The tensile strength was measured both on samples where the container had been removed by grinding and with the container remaining. The machined samples gave about 5 % higher values, after that the effect of the container was compensated for and the values given in Table 2 can therefore be regarded as minimum values. The elongation to fracture and strength drops quickly with additions of ceramic particles. Some of the MMC:s were also tested for impact strength. The tested materials and their results are found in Table 2.

Fracture surfaces

The MMC:s exhibit a mixed fracture behaviour. The fracture mainly follows the boundary

TABLE 3

Hardness and relative wear resistance

Brinellhardness: ϕ 2.5 mm hard metal. 187.5 N, 15 sec.

Material		As HIPed (AS)			Quenched and tempered (QT)		
		HB	a	Field	HB	a	ab
hardphase/matrix				test			
Corundum /SS 2240							
0	100	450	1.44	-	475	1.37	1.9
20	80	410	1.24	-	520	1.27	-
35	65	435	1.11	≥1.7	515	1.15	15.1
50	50	465	-	-	520	-	-
Diruby /SS 2240							
20	80	390	-	-	525	-	-
35	65	530	-	≈1.5	490	-	-
Diruby /APM 2311							
0	100	520	2.72	≥1.4	615	2.72	1.8
20	80	530	2.68	-	600	2.43	26.0
35	65	490	1.82	-	565	2.30	-
50	50	470	1.52	-	540	1.98	-
Corundum/APM 2311							
20	100	520	-	≈1.6	620	-	-
35	65	530	-	-	590	-	-
SiC/3.2 % C-iron							
0	100	325	1.30	≈1.3	490	1.77	1.2
15	85	425	1.11	≈1.8	(495)*	1.74	25.0
30	70	460	1.03	-	(525)*	1.53	-

* Uncertain values due to variations over the cross section area of the test samples.

between ceramic and matrix but also penetrates through the ceramic phase. SiC/3 % C-iron MMC, Fig. 4, shows a fracture type similar to quasi cleavage in the matrix while 2240 and 2311 show dimpeled, ductile fracture. Of special interest is that the Al_2O_3/steel MMC:s show sign of reaction in the form of patterns, both on the steel and on the Al_2O_3 particles. This could indicate that a chemical component in the bond between Al_2O_3 and steel is contributing to the strength of the composite.

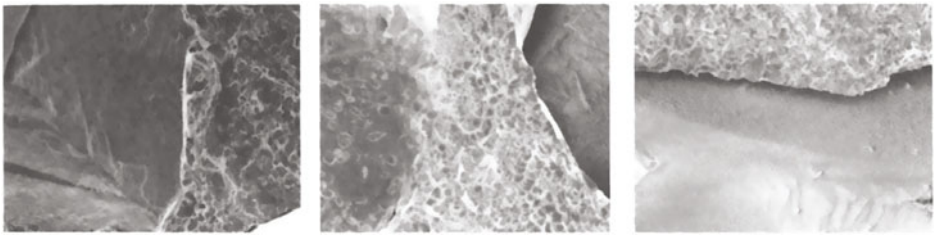

Figure 4. SiC/3 % C-iron, Diruby/2240, QT and Diruby/2311 AS (500X).

Wear resistance

Rod mill testing In total the MMC:s were tested for 144 h with weighing every 24 hours. In Table 3 is given measured hardness values and the wear resistance, related to QT steel. The wear resistance a = ΔWref/ΔWs, where ΔWref and ΔWs is the weight loss of the reference material and MMC:s respectively. The best abrasion resistance is expected at about 30-40 % hardphase [3] and this appears possible for diruby/2311, QT and SiC/3 % C-iron, AS and QT while corundum/2240 exhibits continuously decreasing wear resistance with increasing hard particle contents, probably due to the crushing out of hard particle fragments which efficiently contributes to the abrasion of the matrix.

Two-body abrasion Each test of three samples was run 3 x 5 min with a change of paper between test runs. The abrasion resistance ab = (ΔWref/Aref)/(ΔWs/As), where Aref and As are the areas of the reference sample and the tested MMC:s respectively. The hardness and the wear resistance, related to A2 steel, are given in Table 3.

Field testing Some MMC:s have been tested as compound teeth used in a log pre-treater for barking eucalypt-trees in Portugal. After two months of service preliminary results were as is described in Table 3. At present the tested MMC:s have given a total life-in-service three times that of forged QT steel.

CONCLUSIONS

SiC is unfortunately, even with protective SiO_2 layers, too reactive for HIPed iron base MMC:s except when using a carbon-and oxygen rich matrix. The Al_2O_3 MMC:s are mainly non-reactive, easy to manufacture and the bonding between oxide and ironbase matrix appears strong enough.

The MMC:s with cast iron powder as hard phase are also easy to manufacture but the Cr-iron powder contains a large fraction strategic and expensive alloying constituents and the 3 % C-iron only available as wateratomized powder, less suitable for the HIP-process.

The size of the added particles, 100-200 μm, influences the wear in the milling test through the crushing out of particle fragments. The resistance to pure abrasion is very good and the wear mechanism is here only chipping and crushing in microscale.

ACKNOWLEDGEMENT

This work has been financially supported by the Swedish National Board for Technical Development (STU) and Nordic Fund for Technology (NI). Kone-KMW AB, Sweden has performed the field testing and their cooperation is greatly appreciated.

REFERENCES

1. Schiepers, R.C.J., F.J.J. van Loo and G. de With: Reactions between α-silicon carbide ceramic and nickel or iron, J. Am. Ceram. Soc., **71** (6) (1988), C-284-C-287.

2. Bevolo A.J., G.J. Campisi, H.R. Shanks and F.A. Schmidt. Effectiveness of SiO_2 for preventing silicon-metal reactions at high temperatures, J. Appl. Phys., **51** (10) (1980), 5390-5395.

3. Zum Gahr, K.H., "Abrasive Wear of Two-Phase Metallic Materials with a Coarse Microstructure", Proc. Int. Conf. Wear of Materials 1985, Vancouver, ed. Ludema, ASME, New York, 1985, p. 45-58.

HOT ISOSTATIC PRESSING AND SINTERING BEHAVIOR OF YTTRIUM OXIDE DISPERSED TUNGSTEN

YUTAKA ISHIWATA, YOSHIYASU ITOH and HIDEO KASHIWAYA
Heavy Apparatus Eng. Lab., Toshiba Corp.
2-4 Suehiro-cho, Tsurumi-ku, Yokohama 230, Japan

ABSTRACT

Densification of tungsten with various yttrium oxide additions was investigated and the effect of capsule-free and encapsuled HIP treatment on density and bending strength at room and elevated temperature was examined. The sintered density of tungsten was greatly improved by addition of the yttrium oxide and a relative density above 99% was obtained by even in the case of capsule-free HIP treatment. Also, the bending strengh was much improved and improved homogeneity could be obtained by HIP treatment. Significant difference were not found between capsule-free and encapsuled HIP treated tungsten with yttrium oxide. It was clear that dense and homogeneous tungsten components can be produced by HIP treatment without encapsulation through the addition of small amount of yttrium oxide.

INTRODUCTION

In energy equipment, tungsten is an attractive metal not only for nuclear fusion reactor components such as the divertor or the first wall but also for cell components in isotopic separation such as crucible for melting of reactive metals. This is because of its high melting point and high strength at elevated temperature. However, the grain boundary of tungsten is selectively attacked by molten metal. Consequently, tungsten grains are dissolved into the molten metal. It has already comfirmed that yttrium oxide (Y_2O_3) included in tungsten results in excellent corrosion resistance in molten metals, as shown in Fig.1[1]. On the other hand, the corrosion resistance of tungsten alloys strongly depends on the sintered density as well as mechanical properties.

In this study, the sintering behaviors of tungsten containing from 0 to 20Vol.% Y_2O_3 were investigated. And also, the effects of HIP treatment on bending strength and densification of Y_2O_3 dispersed tungsten were made clear.

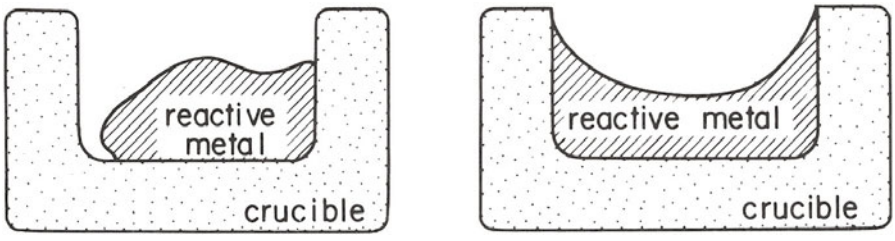

[Y_2O_3 dispersed tungsten] [pure tungsten]

Figure 1. Crosssections of a reactive metal melted in Y_2O_3 dispersed tungsten and pure tungsten crucible.

EXPERIMENTAL PROCEDURE

Sintering behaviors were examined for two kinds of tungsten alloys, Y_2O_3 dispersed and ThO_2 dispersed, in comparison with pure tungsten. The starting powders were tungsten (99.9% pure, supplied by Toshiba), Y_2O_3 (99.9% pure, supplied by Shin-Etsu Chemical) and ThO_2 (99.9% pure, supplied by Cerac). Chemical compositions and average particle size of used powders are shown in Table 1. Tungsten powders containing from 0 to 20Vol.% Y_2O_3 or 10Vol.% ThO_2 were mixed by ball-mill for 604.8ks. The mixed powders were molded into pellets about 60mm in diameter and 30mm in length by CIP at 196MPa. After pre-sintering at 1873K for 28.8ks in vacuum, the pellets were sintered at from 2073K to 2473K for 28.8ks in vacuum, HIP treatment was carried out for two cases, capsule-free and encapsuled. For the encapsuled HIP treatment, the sintered pellets covered with boron nitride powder were enclosed in a can made from niobium, and HIP treatment using argon gas was carried out at a fixed condition (at 2073K, 177MPa, for 14.4ks)[2].

The density of as sintered and HIP treated pellets were measured and the microstructure was observed. The specimens, 3x4x40mm, were ground, and four point bending tests were performed at room and elevated temperature (from 973K to 1573K), and 0.5mm/min. as the displacement rate, according to JIS R1601 -1981, using an autograph. Fractured surfaces were observed by scanning electron microscope.

TABLE 1
Chemical compositions and average particle size of used powders

(ppm)

W		Y_2O_3		ThO_2	
O	800	Dy_2O_3	<100	MgO	50
Mo	18	Ho_2O_3	<100	CaO	<30
Fe	8	Er_2O_3	<100	Al_2O_3	10
Ca	<5	Yb_2O_3	<100	CuO	10
Si	<5	SiO_2	<100		
W	>99.9%	Y_2O_3	>99.9%	ThO_2	>99.9%
2.10μm		0.87μm		1.63μm	

RESULTS AND DISCUSSION

SINTERING BEHAVIOR OF Y_2O_3 DISPERSED TUNGSTEN

The effect of sintering temperature on the relative density for tungsten with different Y_2O_3 additions is shown in Fig.2. The sintered density of all pellets tends to increase with the rise of sintering temperature. But for the pure tungsten and the tungsten with 10Vol.% ThO_2, the relative density is at most 90% after sintering at 2473K[3]. In contrast, the relative densities of Y_2O_3 added tungsten become above 96% at 2073K and above 98% at 2473K. As the sintered densities of tungsten with Y_2O_3 tend to increase with increasing the Y_2O_3 content, it might be thought that Y_2O_3 particles behave as a sintering aid for densification of tungsten. As a sintering aid for tungsten, Ni is a famous alloying element[4], but the fact that a metal oxide such as Y_2O_3 also has a similar effect is a very interesting phenomenon from the point of improving the strength and the corrosion resistance at elevated temperature.

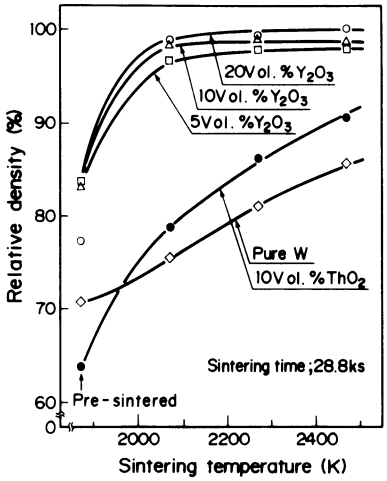

Figure 2. Effect of sintering temperature on relative density.

DENSIFICATION BY HIP TREATMENT

Figure 3 shows the relative density of as sintered and HIP treated pellets. For each pellet, the sintering temperature was 2073K. In the case of encapsuled HIP, the relative density of all tungsten alloys were above 99%. But, in the case of capsule-free HIP, only the densities of Y_2O_3 dispersed tungsten were almost equal to that of encapsuled HIP treated pellets. While, for the ThO_2 dispersed tungsten and the pure tungsten, a remarkable increase of relative density was not recognized after capsule-free HIP treatment. It might be surmised that residual pores in sintered tungsten with Y_2O_3 are almost closed pores. Microstructure of as sintered and HIP treated tungsten containing 10Vol.% Y_2O_3 are shown in Fig.4. Average size of Y_2O_3 and tungsten grains are about 1μm and 6μm, respectively, and grain size of HIP treated apecimen was almost equal to that

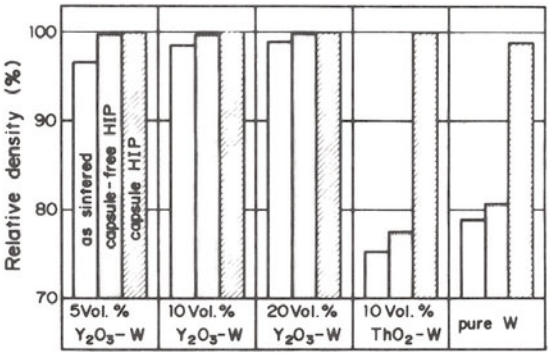

Figure 3. Relative densities of as sintered and HIP treated pellets (sintered at 2073K)

of as sintered specimen. It was recognized that little grain growth of Y_2O_3 particles was occured during HIP treatment and fine tungsten grain could be obtained by addition of Y_2O_3.

EFFECT OF HIP TREATMENT ON BENDING STRENGTH

Figure 5 shows the Weibull plots of bending strength of as sintered and HIPed tungsten with 10Vol.% Y_2O_3 and as sintered pure tungsten at room temperature. The relationship between the accumulated probability and the bending strength is well represented by a straight line for each specimen. For as sintered specimens, the Y_2O_3 dispersed tungsten (391MPa on average) had higher bending strength than pure tungsten (240MPa) due to the high sintered density. But the m value of these specimens was 5.9 and 7.5, respectively. there are quite low values. On the other hand, HIPed tungsten with Y_2O_3 had high bending strength (658MPa) and m value(m=12.1). These results show that the HIP treatment is very effective to improve strength and the homogeneity of sintered tungsten with Y_2O_3. A difference in bending strength between capsule-free and encapsuled HIP specimens was not observed. Bending strength and deflection of as sintered and HIPed tungsten with 10Vol.% Y_2O_3 at elevated temperature

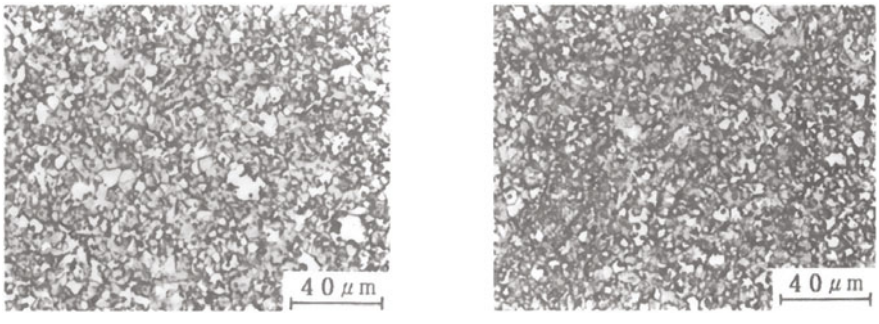

(a) as sintered (b) HIP treated

Figure 4. Microstructure of as sintered and HIPed tungsten with 10Vol.% Y_2O_3 (sintered at 2073K).

are shown in Fig.6. Both as sintered and HIPed tungsten with Y_2O_3 had high bending strength and a large deflection could be observed in comparison with the values measured at room temperature. For this temperature range, the bending strengths of HIPed specimens were higher than that of as sintered specimens. From fractographic observation, only intergranular fracture was observed in both specimens fractured at room temperature, but dimple fracture became dominant with the rise of testing temperature. However, the intergranular fractured areas of as sintered specimens tend to be much larger than those of HIPed specimens, HIP treatment is an effective method to improve not only density but also bonding strength between grains.

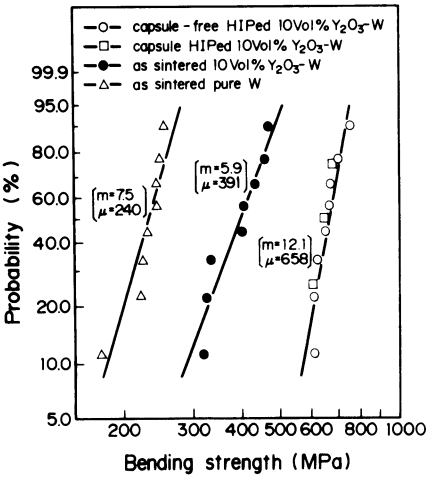

Figure 5. Weibull distributions of bending strength at room temperature.

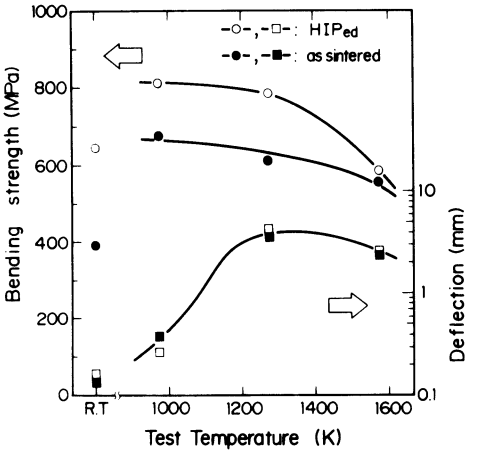

Figure 6. Bending strength measured at elevated temperatures.

CONCLUSIONS

Addition of small amount of yttrium oxide accelerates the densification of tungsten. The homogeneity and the bending strength of yttrium oxide dispersed tungsten at both room and elevated temperature could be much improved by HIP treatment even without encapsulation.

REFERENCES

1. Ishiwata,Y.,Itoh,Y. and Kashiwaya,H., Corrosion behavior of yttria dispersed tungsten in liquid metal. In Proc. The Japan Institute of Metals, 1990 autumn, 499.
2. Swinkels,F.B. and Ashby,M.F., A second report on sintering diagrams. Acta Met., 1981, 29,259-281.
3. Yih,S.W.H and Wang,C.T., Tungsten, Plenum press, New York 1979.
4. German,R.M., Powder Metallurgy Science, MPIF, Princeton, 1984.

STUDY OF DIFFERENT SINTERING TECHNIQUES FOR A Ti-Al-O-N SPINEL COMPOSITE

D S PERERA, S MORICCA AND S LEUNG
Australian Nuclear Science and Technology Organisation
Private Mail Bag 1, Menai, NSW 2234, Australia

ABSTRACT

A composite in the Ti-Al-O-N system consisting of a spinel matrix with a dispersion of TiN and AlN phases was fabricated from a mixture of TiO_2, Al_2O_3 and AlN powders by several sintering methods at 1800 °C. The composite formed from the starting composition $Ti_{0.6}Al_{3.2}O_{3.0}N_{2.0}$ was pressureless sintered, hot pressed, sinter + HIPed and HIPed. The density, porosity and microstructure were studied with respect to the sintering method. It was possible to produce a dense material with no open porosity and free of grain boundary glass. This spinel composite has the potential to be developed as a high temperature engineering ceramic.

INTRODUCTION

Nitrogen ceramics are prime candidate materials for use as engineering ceramics. Engineering ceramics are characterised by high hardness, high strength at elevated temperatures, resistance to corrosion and low thermal expansion. To achieve a high hot strength the material has to be free of glassy phases. In the Si-Al-O-N system, which has been widely investigated for engineering ceramics applications, there is a silicate glassy phase or a crystalline secondary phase at the grain boundaries. In the Ti-Al-O-N system which has been investigated to a limited extent there is no known glass formation [1-4]. In previous work [2,3] $Ti_{0.6}Al_{3.2}O_{3.0}N_{2.0}$ was hot pressed and its mechanical and physical properties were determined. In the present work the same composition was fabricated and sintered by different methods and the microstructure was examined in relation to the sintering technique.

EXPERIMENTAL

A powder mixture with the composition $Ti_{0.6}Al_{3.2}O_{3.0}N_{2.0}$ was prepared by ball milling powders of AlN (Elektroschmelzwerk Kempten GMBH), Al_2O_3 (Alcoa XA 16) and TiO_2 (Tiona AG, SCM Chemicals) in ethanol for 18 h. After drying, the powders were compacted into 20-50 mm diameter x 20-25 mm thick pellets of different sizes. The pellets used for hot pressing were uni-axially compacted at 15 MPa and the others at 35 MPa. One of the pellets was subsequently cold isostatically pressed at 172 MPa. The pellets were hot pressed at a pressure of 33 MPa in a dynamic nitrogen atmosphere at 1800 °C for 3h using a boron nitride lined graphite die and plunger. The pellets were pressureless sintered under the same conditions.

A pressureless sintered pellet was HIPed in argon gas at 100 MPa for 45 min at 1800 °C. The HIPing was carried out in a graphite furnace. A uni-axially pressed pellet was placed in a vitreous silica tube embedded in BN powder. After evacuation, the tube was sealed. This encapsulated pellet was HIPed under the same conditions as previously.

Polished and fracture surfaces were examined by scanning electron microscopy (SEM) and energy dispersive X-ray analysis (EDX). A thinned specimen was examined by transmission electron microscopy (TEM) and EDX. A diamond polished (10 μm) specimen was examined by optical microscopy.The bulk density and the porosity of selected specimens were determined by boiling in distilled water for 2 h and using a water displacement method. The X-ray diffraction (XRD) analysis was carried out on the fraction ground to -150 μm from a pellet after density determination.

RESULTS AND DISCUSSION

A typical XRD trace is shown in Fig 1, where the major phase is an aluminium oxynitride type spinel of unit-cell **a**= 0.7959 nm, with minor phases TiN and AlN. An optical micrograph shows (Fig 2) TiN (white) and AlN (light grey) grains less than 0.5 μm well dispersed in a matrix of spinel. These are the features of a good composite, in which the secondary phases are well dispersed.

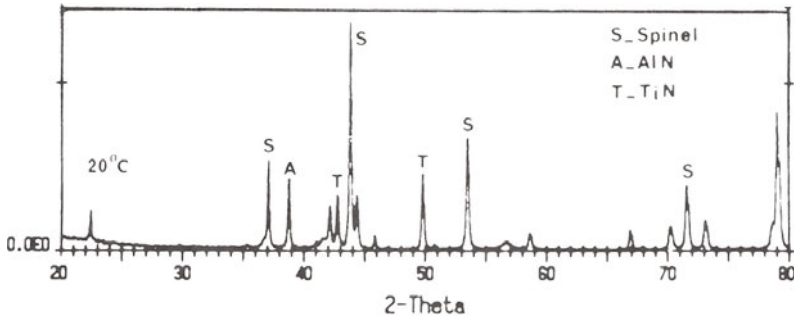

Figure 1. XRD trace of hot pressed tialon spinel composite (vertical axis represent counts in arbitrary units)

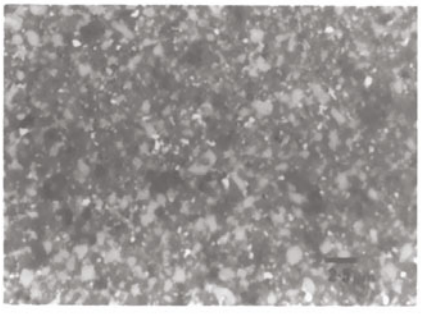

Figure 2. Optical micrograph of hot pressed tialon spinel composite (TiN= white, AlN= light grey, matrix= tialon spinel)

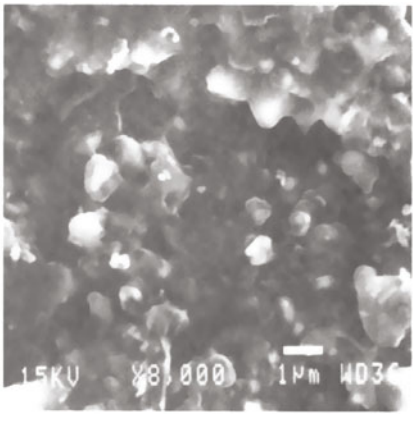

Figure 3. SEM micrograph of hot pressed tialon spinel composite; the spinel grains of the matrix

The SEM of a fractured hot pressed sample is shown in Fig 3 where the spinel grains are equiaxed and less than 0.5 μm. The EDX analysis showed the presence of Al and a small amount of Ti which indicated that the spinel is an aluminium oxynitride with Ti. A TEM micrograph of the same specimen shows (Fig 4) grains of spinel and TiN bonded to AlN. There are no glass or secondary phases at the grain boundaries. The EDX analysis of the spinel grain is shown in Fig 5, where Al is the major element and Ti is a minor element; this trace also shows a shoulder of nitrogen.

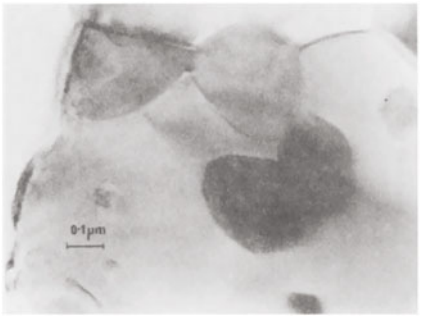

Figure 4. TEM micrograph of hot pressed tialon spinel composite (S= tialon spinel, T= TiN, A= AlN)

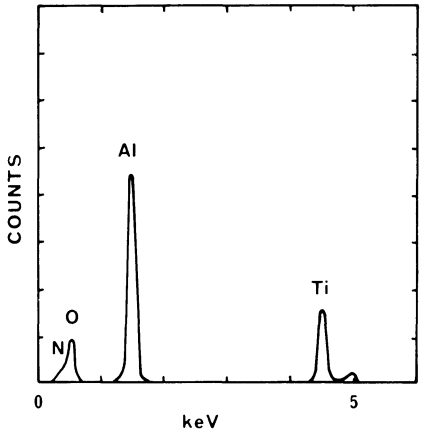

Figure 5. The EDX spectrum of the spinel grain in Fig 4

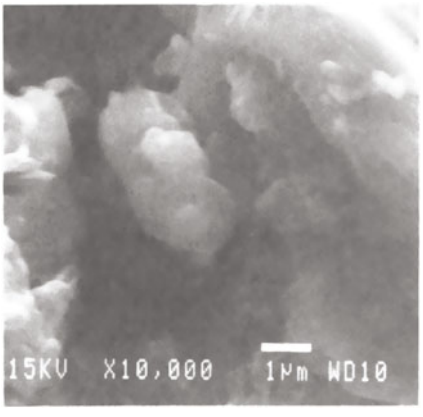

Figure 6. SEM micrograph of sintered tialon spinel composite

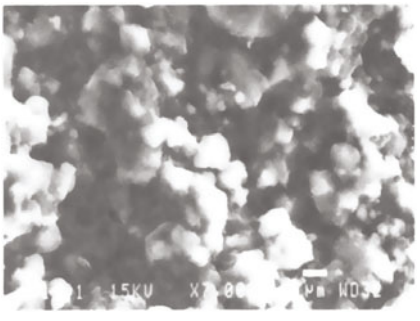

Figure 7. SEM micrograph of sinter + HIPed tialon spinel composite

The sintered samples were very porous and a typical SEM micrograph is shown in Fig 6. The microstructure of the sinter + HIPed sample cut from the interior of the pellet shows (Fig 7) smaller pores than that of the surface shown in Fig 6. Part of the pellet encapsulated in glass and HIPed shows (Fig 8) much less porosity. The glass envelope had exposed the pellet during the HIPing at some stage. Several different encapsulation techniques are being tested.

Figs 6,7 and 8 clearly show an increasing tendency to remove the pores moving from of sintering, sinter + HIPing and HIPing. However complete elimination of pores was not possible even in the hot pressed sample (Fig 3), which shows some closed porosity. The preliminary results suggest that it could be possible to eliminate even closed porosity with improved encapsulation and HIPing.

The bulk density and the apparent porosity of the samples are listed in Table 1. The hot pressed sample had the highest density and was free of open pores. Sinter + HIPing had only a marginal effect, as expected. Although the glass-encapsulation failed during HIPing, it had been effective during part of the cycle, as shown by the higher bulk density than that of sinter + HIPed sample.

The results show it is difficult to sinter this material without the application of

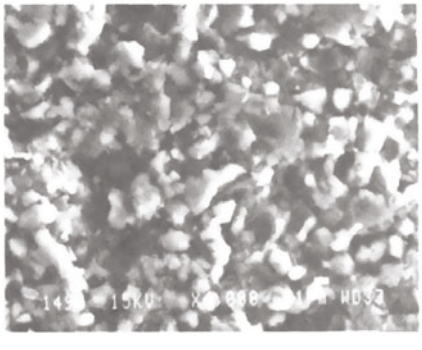

Figure 8. SEM micrograph of HIPed tialon spinel composite

TABLE 1
Density and porosity of the tialon spinel composite produced by different sintering methods

Sintering method	Bulk Density g/cm^3	Apparent Porosity %
Hot pressed	3.70	0.0
Pressureles sintered	2.37	49.1
Sinter + HIPed	2.39	42.6
HIPed (glass encapsulated)	2.55	32.1

pressure, although some liquid formation should occur above 1705 °C, the lowest eutectic in the TiO_2 -Al_2O_3 system [5]. At 1800 °C the grain growth is very small and hence is a reasonable temperature to aim for in reaction sintering. To make useful products the path to follow is HIPing with suitable glass encapsulation rather than hot pressing which is suitable for only limited shapes.

CONCLUSIONS

A composite of composition $Ti_{0.6}Al_{3.2}O_{3.0}N_{2.0}$ can be produced in the Ti-Al-O-N system with a Ti-containing aluminium oxynitride spinel as the major phase and TiN and AlN as secondary phases. There is no observed grain boundary glass in the composite. The grain size of the phases are fine and distributed uniformly, which are characteristics of a good high temperature composite suitable for development as an engineering ceramic. Glass encapsulation techniques to HIP this material are being investigated in order to produce a material free of closed porosity.

ACKNOWLEDGEMENTS

The authors thank the following Ansto staff: B Blackford, P Angel and J Warmeant.

REFERENCES

1. Mocellin, A. and Bayer, G. Chemical and microstructural investigations of high temperature interactions between AlN and TiO_2. J. Mater. Sci., 1985, **20,** 3697-704.

2. Perera, D. S. Phase relationships in the Ti-Al-O-N system. Br. Ceram. Trans. J., 1990, **89**, 57-60.

3. Perera, D. S., Cassidy, D. J. and Ripley, M. Ti-Al-O-N spinel composite - a new engineering ceramic. Key Engineering Materials, **48-50**, 338-43.

4. Hoyer, J. L., Bennett, J. P. and Liles, K. J. Properties of TiAlON/spiel composite. Ceram. Eng. Sci. Proc., 1990, **11,** 1423-39.

5. In Phase Diagrams for Ceramists, ed. E. M. Levin, C. R. Robbins and H. F. McMurdie. The American Ceramic society, USA, 1964, Fig 316.

GAS-PRESSURE COMBUSTION SINTERING OF TiC-Ni COMPOSITES USING HIP

Xianfeng Ma
Changchun Institute of Applied Chemistry, Academia Sinica,
Changchun 130022, China
Kimiaki Tanihata, Yoshinari Miyamoto
The Institute of Scientific and Industrial Research,
Osaka University, Osaka 567, Japan

ABSTRACT

Fully densified TiC-Ni composites with different Ni content from 0 to 65 vol.% and Ni were fabricated by the gas-pressure combustion sintering method using HIP. The composites were synthesized and densified simultaneously and rapidly under isostatic pressure of 100MPa Ar gas. Some mechanical and thermal properties such as flexural strength, Young's modulus, thermal conductivity and thermal expansion were measured for different Ni content. The microstructure changes were also observed by using SEM .

INTRODUCTION

The gas-pressure combustion sintering is a combined process of the self-propagating high temperature synthesis (SHS) and the hot isostatic pressing (HIP). This reaction sintering method can rapidly synthesize and densify some refractory ceramics and composites simultaneously without additives(1). It is attractive as an alternative to conventional ceramic processing due to its rapidity and energy efficiency for fabricating some refractory materials and composites that have a highly exothermic heat of formation.

As is known, titanium carbide and its composite with nickel are important refractory materials and widely used for super-hard abrasives, cutting tools, electric and electronic applications. Miyamoto et al.(2) once fabricated the TiC-Ni composite but some important mechanical and thermal properties were not measured because of the small size of the sample.

In this study, the $TiC_{0.8}$, the TiC-Ni composites with different Ni content and Ni were fabricated with both nearly theoretical density and larger size(32mm in diameter, 6-8mm in thickness), and some mechanical and thermal properties were measured in accordance with different content of Ni, while the microstructure changes were also observed.

EXPERIMENTAL PROCEDURE

The starting powders of titanium(<45 micron meter in size, >99.5% in purity), carbon(<0.5 micron meter in size, >96.3% in purity) and nickel(<1 micron meter in size, 99% in purity) were weighed and well mixed, then press-formed into a pellet with 37mm in diameter and 8-12mm in thickness. After cold isostatically pressed at 180MPa, the reactants were coated with BN powder and vacuum sealed into a glass container ($T_{sof.}$=1028K). The glass encapsulated green body was coated in BN powder spray and embedded into the ignition agent of Ti and C mixed powder in a graphite crucible. The BN was used for preventing the possible reaction between glass container and sample or ignition agent.

A HIP equipment was used for the gas-pressure combustion sintering. Inside of the pressure vessel was heated to about 1020K for making the glass container soften, and Ar gas pressure was subjected to 100MPa. Then, the ignition agent was burned by passing a current of about 80Amps for 4-6 seconds through a carbon ribbon heater for ignition. After combustion, the compact can be obtained. The $TiC_{0.8}$ can not be fully-densified by only Gas-Combustion Sintering method because of the poor mixture of Ti and C in green body due to the solid mixing and the size of Ti powder. So the sample was retreated by usual HIP sintering method at the condition P=170MPa, T=1973K, t=30min..

The crystalline status of the samples were analyzed by X-ray powder diffractometry. The microstructure, grain size and grain boundary were observed by SEM . The density was measured by Archimede's method, the flexural strength at room temperature by three-point bending test with cross head speed of 0.5mm/min.,and the span of 10mm, the Young's modulus and internal friction by the resonance vibration method for specimens cut into bars with dimensions 2x2x25mm, The thermal conductivity by Laser-flash method with the sample size of 10mm in diameter and 2mm in thickness, and the thermal expansion by using SHINKU-RIKO DL-7000H device from room temperature to 1473K in Ar.

RESULTS AND DISCUSSION

The fabricated samples were identified by X-ray powder

diffractometry, the peaks of TiC and Ni are sharp and there is no reaction between TiC and Ni(see Fig.1). Figure 2 shows the density of the fabricated composites: the relative density of $TiC_{0.8}$ is 98.7%, other's are more than 99.5%.

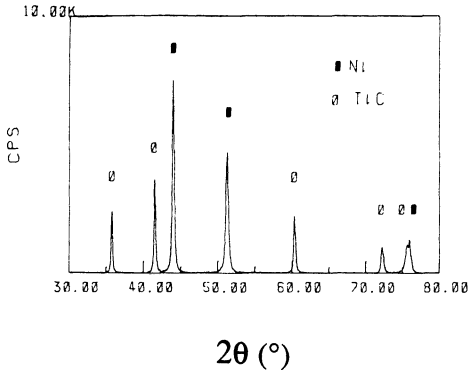

Fig.1 X-ray powder diffraction pattern of the TiC-40 vol.%Ni composite

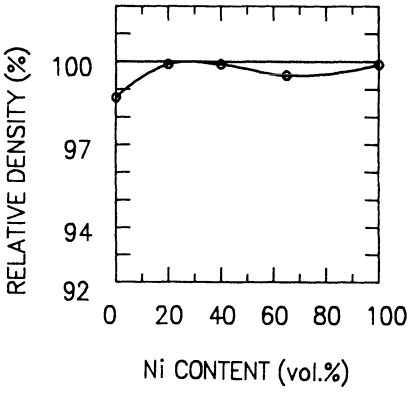

Fig.2 Relative densities of TiC-Ni composites

Figure 3 is the SEM photographs of fracture surface of TiC-Ni composites varying with Ni composition. The grain size of TiC decreases rapidly as the content of Ni increasing. The grain size is about 50 micron meter when there is no Ni, while it is only about 1 micron meter when 65vol.%Ni content. It can be explained by the different combustion temperature because of the different content of Ni. The Ni addition can dilute the reaction heat and then reduce the adiabatic combustion temperature, and the TiC can possess a relative small average grain size when the composite was synthesized at a relatively low temperature. In addition, the grain boundaries are strong for the monolithic TiC. So many cleaved grains were found in the fracture surface (see Fig.3 (a)). The combination between TiC and Ni is weak comparing with the TiC grain, and the fracture surface was made along the boundaries of TiC with Ni(see Fig.3 (b),(c),(d)).

Flexural strength at room temperature was given in Fig.4, where the curve has a maximum at about 50vol.%Ni content. The value for $TiC_{0.8}$ (no Ni content) is 332MPa that is less than the reported value(3), which may be the result of the sample having a little lower density and a relatively large grains.

Figure 5 and 6 plot the Young's modulus and internal friction respectively. the Young's modulus for $TiC_{0.8}$ is small

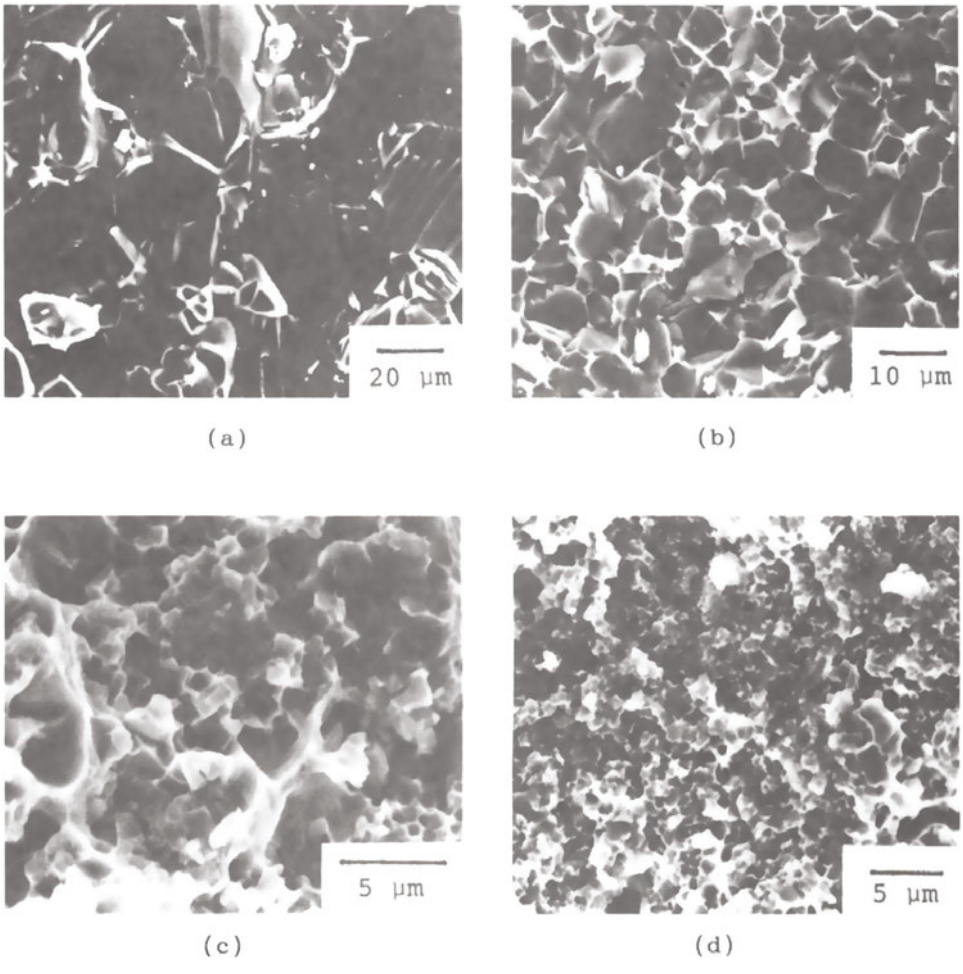

Fig.3 SEM photographs of TiC-Ni composites
(a).$TiC_{0.8}$ (b).TiC-20vol.%Ni
(c).TiC-40vol.%Ni (d).TiC-65vol.%Ni

comparing with the reported value(about 420GPa)(3), probably due to the same reason mentioned above. If the Young's modulus is supposed to obey the linear additive rule, the interpolated value to no Ni content will coincide with the reported one as indicated by a dotted line in Fig.5. The internal friction has a minimum between 20vol.% and 60vol.%Ni content. The microstructure observation indicates that the grains of TiC become smaller with Ni and the matrix phase changes gradually from TiC to Ni between 20 and 60 vol.% Ni content. It is of interest that the flexural strength and internal friction show the maximum and minimum peaks respectively at this transient compositions, although the reason is not clear now.

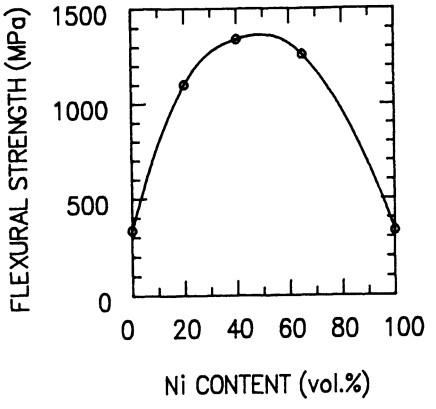

Fig.4 Flexural strength as a function of Ni content at room temperature

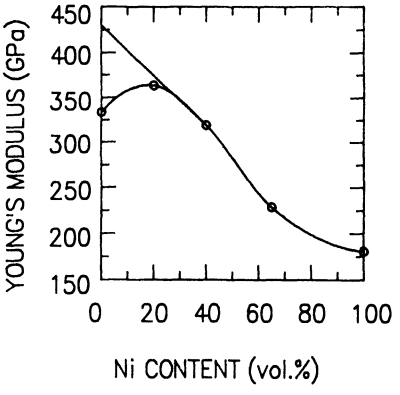

Fig.5 Young's modulus as a function of Ni content at room temperature

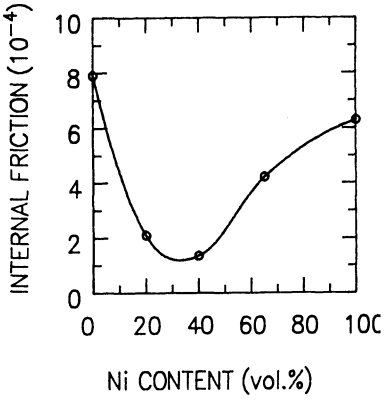

Fig.6 Internal friction as a function of Ni content at room temperature

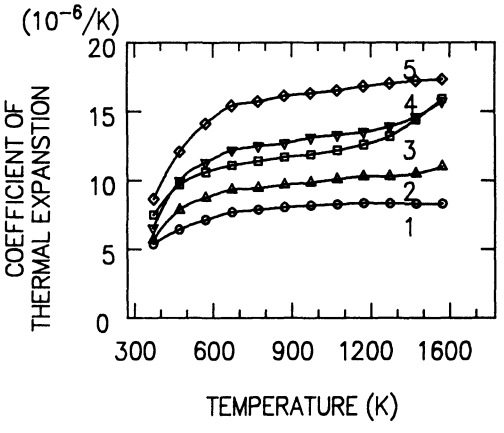

Fig.7 The coefficients of thermal expansion of TiC-Ni composites as a function of temperature

1.$TiC_{0.8}$ 2. TiC-20vol.%Ni 3. TiC-40vol.%Ni 4. TiC-65 vol.%Ni 5. Ni

Figure 7 shows temperature dependence of thermal expansion coefficients of the composites. They are increased rapidly from room temperature to 673K, while saturated at higher temperature. When the temperature is higher than 1373K, the thermal expansion coefficient of the composites with 20, 40 and 65 vol.% Ni begins to increase again. The Ni phase seems to play an important role for the expansion at elevating temperature over this temperature.

Figure 8 is the thermal conductivities for the composites as a

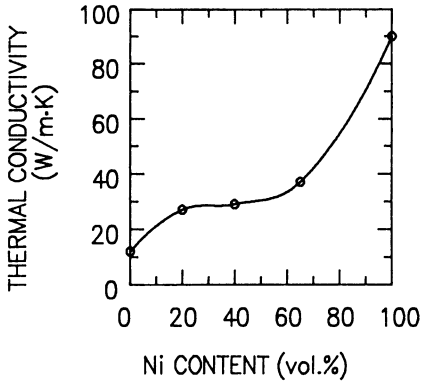

Fig.8 The thermal conductivity as a function of Ni content at room temperature

function of Ni content at room temperature. The curve is near steady at the transient compositions from the TiC matrix to the Ni matrix, and increase sharply toward the 100% Ni content.

SUMMARY

The TiC-Ni composites with 0, 20, 40, 65 and 100 volume percent were synthesized and densified simultaneously and rapidly under isostatic pressure of 100MPa Ar gas. The grain size of TiC decreases as the Ni content increases. The composites have a relatively high flexural strength at the Ni content around 40vol.%, where the matrix phase gradually changes from TiC to Ni.

ACKNOWLEDGMENT

The authors are grateful to Dr. Ken-ichi Matsushita for the help of the Young's modulus and internal friction measurements.

REFERENCES

(1) Yoshinari Miyamoto, "Processing Development for Gas-pressure Combustion", Memoirs of the Institute of Scientific and Industrial Research, Osaka University, 46,15-24(1989)

(2) Yoshinari Miyamoto, Hiroyuki Nakanish, Isao Tanaka,Taira Okamoto and Osamu Yamada, "Gas-pressure combustion of TiC-Ni FGM", 1st int. symp. on FGM Sendai, Oct. 8-9,1990

(3) G. V. Samsonov and I. M. Vinitskii, "Handbook of Refractory Compounds", IFI/Plenum pp. 287 (1980).

GAS PRESSURE COMBUSTION SINTERING OF MATERIALS IN THE Ti-Si-C-SYSTEM

Hagen Klemm, Kimiaki Tanihata* and Yoshinari Miyamoto*

Central Institute of Solid State Physics and Material Research, IKTM Dresden, Federal Republic of Germany

*The Institute of Scientific and Industrial Research, Osaka University, Ibaraki, Osaka 565, Japan

ABSTRACT

The processing of gas pressure combustion sintering (GPCS) to produce dense materials in the system Ti-Si-C was studied. By systematic variations of the reactants composition it was possible to produce different materials consisting of Ti_5Si_3, $TiSi_2$, Ti_3SiC_2, TiC or SiC. The complete densification of the samples was not in all the cases successful. It is speculated that the time at high temperatures was too short to densify the materials with more refractory character. Besides, not all the phases built up by combustion at high temperatures are stable at lower temperatures and some reactions occur during cooling influencing densification and properties of the final material. Some properties of full densified samples produced by GPCS are also given. The ceramic-metal composite produced by higher addition of Ti showed better mechanical properties in bending strength and fracture toughness.

INTRODUCTION

Gas-pressure combustion sintering is a process whose goal consists in obtaining synthesis and densification simultaneously and rapidly. For this purpose the execution of combustion synthesis is carried out under high isostatic gas pressure (1). With this method ceramic-ceramic or ceramic-metal composites can be produced. An advanced application of GPCS is the fabrication of Functionally Gradient Materials (FGM) (2). The FGM have a characteristic microstructure consisting of a metal phase which increases continuously within the ceramic matrix starting from a surface layer of pure refractory ceramic. The combustion sintering seems an excellent way to

produce FGM because the rapid reaction and sintering process can limit the phenomenon of diffusion process and maintain the compositional configuration of the starting body. For example, most recently some FGM materials consisting in silicides (e.g. $MoSi_2$) have been successfully produced (3) and attentioned for their design and excellent properties. The final goal of the present study would be the fabrication of a FGM titaniumsilicide material obtained by GPCS. However in this paper we report about a basic investigation concerning fabrication and properties of only the homogeneous materials.

EXPERIMENTAL

In the present study homogenous composites of the Ti-Si-C system were produced by GPCS. The raw materials Ti, Si, C and SiC* were mixed by a dry mixing method. Then the green bodies in the shape of disks with approximately 38 mm in diameter and 8 mm in height were produced by uniaxial (150 MPa) and isostatic pressing (250 MPa). A detailed description about the following processing and the gas pressure combustion sintering were given by Miyamoto et.al.(4). The compacts were analysed by X-ray diffractmetry using Cu-k_α radiation. The phase content was roughly estimated from the relative intensity of the main interferences from XRD. The density was measured by Archimedes Method. Some mechanical properties such as Vickers hardness, fracture toughness and bending strength were also evaluated. Fracture toughness was evaluated by intentation microfracture method (IM) by applying a load of 49 N for 15 s. The values were obtained from the measurment of crack length by using the equation given by Niihara et al. (5). In the case of the ceramic-metal composites it was not possible to use this method because of the plastical behavior. For that samples it was used a chevron notch method described by Munz (6). The bending strength was measured in 3-point bending geometry with a span of 15 mm on specimens 3x4x20 mm in dimentions. The tensile surface were polished and the edge removed prior the test.

RESULTS AND DISCUSSION

Phase composition of samples with different raw material ratio

Figure 1 shows the map of starting composition in the Ti-Si-C system. The phase composition of the samples after combustion sintering depends on the composition of the raw materials in the green body. A high content of Ti_5Si_3 was found when the content of Ti in the green body was higher. On the other side it is found more $TiSi_2$ in the silicon-rich corner of the phase diagramm. An example is given in table 1.

*Ti: TSPT 350 Osaka Titanium, SiC: Ultrafine Betarundum, Ibiden Co.LDT, Si: Si 2-3 um, Kojundo Kagaku, C: SP300, Nihon Kokuken

Table 1. Phase composition of two samples produced by GPCS

No.	content of raw materials mol%				phase composition after GPCS vol%			
	Ti	Si	C	Ti/Si	Ti_5Si_3	TiC	$TiSi_2$	SiC
1	24.5	45.5	30.0	0.45	-	20	47	33
2	53.9	11.6	34.5	4.65	40	60	-	-

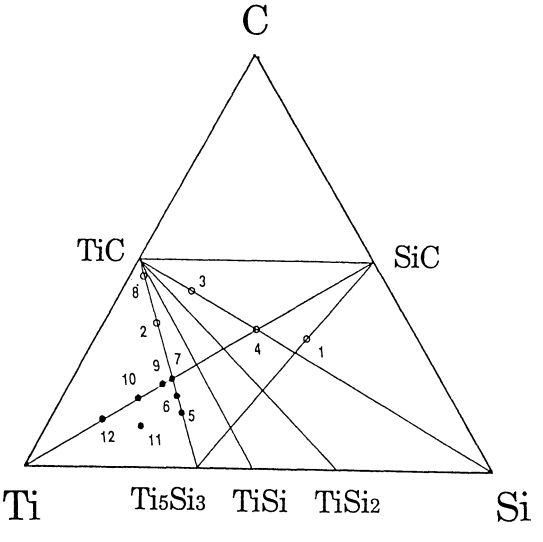

Figure 1. Phase diagramm of the Ti-Si-C system

In the discussion of the phase composition it is necessary to consider that the combustion process is a very rapid reaction. For that reason and also because of the quenching conditions after combustion the equilibrium state is not easily achieved. The reaction temperature in the case of using a titanium-carbon mixture as ignition powder is estimated between 2500 and 3000°C. Because of the high cooling rate (about 500 K/min at temperatures >1500°C) the time for reaction and sintering is very short. Also in the present Ti-Si-C system the phases built up during combustion at high temperatures are not in all cases stable after cooling. As an example, the behavior during cooling of Ti_5Si_3 and SiC built up and thermodynamic stable at high temperatures is discussed. When the temperature decreases the products will convert to $TiSi_2$ and TiC which are stable at temperatures below 1500°C (equation 1).

$$3Ti_5Si_3 + 7SiC \rightleftharpoons 8TiSi_2 + 7TiC \quad (1)$$

Reactions like that one reported in equation 1 will not occur when only Ti_5Si_3 and TiC are built up, it must also found silicon rich silicides like TiSi and $TiSi_2$ or SiC. TiSi was not detected by X-ray diffractmetrie. Probably it is combining with TiC to give the more stable Ti_3SiC_2 (equ. 2).

$$TiSi + 2TiC \rightleftharpoons Ti_3SiC_2 \quad (2)$$

In the phase diagram such reactions occur in the area between the Ti_5Si_3-TiC line and the Si-C line.It is supposed that at high temperatures the titanium-rich silicides are built up first. But after reaction they decompose during cooling to the more stable carbides. This assumption is supported by the comparisation of samples produced by combustion and a HIP-process (1850°C/170MPa/1h) where the time for reaction and cooling is longer. The phase composition of the HIPed samples shows higher content of carbides while the content of the titanium-rich silicides decreased (6).

Densification and properties

As shown in figure 1, a full densification of samples in the present system was not successful in all cases. One reason for this behavior is the too short sintering time specially for samples with high carbide-content. As an example the achieved density of Ti_5Si_3/TiC samples with increasing TiC-content is shown in figure 2. At a TiC-content as high as 50% fully densified samples were not obtained by combustion synthesis with a titanium-carbon-mixture as ignition powder.

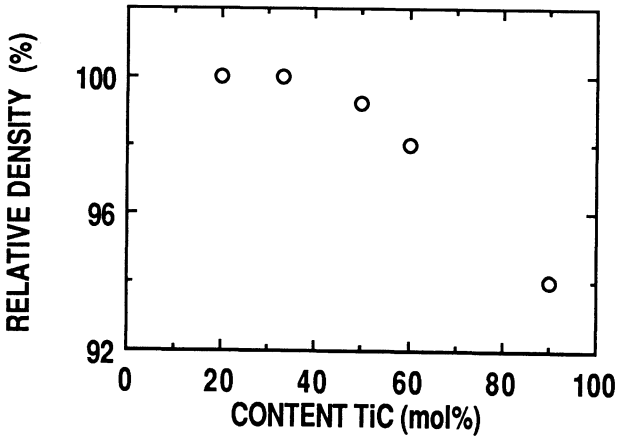

Figure 2. Density of Ti_5Si_3/TiC samples produced by GPCS with different TiC-content

The phenomenon of densification is very complex and this may be only one of the reasons for the not complete densification of these samples. It is supposed that because of the reaction occuring after combustion of the raw material and during cooling also the microstructure of the material changes. Furthermore, reactions as that shown in equation 1 produce TiC which has a higher density than the other components. In this way the volume phase of the products becomes smaller and pores are produced. A full densification of these samples should be possible by a HIP-process considering the temperatures where the reactions occur. Figure 3 shows the microstructure of the polished surface in sample 1. At the edge of the sample the material is fully densified, the conversation to $TiSi_2$ and TiC occurs first at this area because of the temperature gradient during cooling. The applied gas pressure is able to densify this region of the sample. When the process moves to the center, the edges are already stable and inhibit a complete densification.

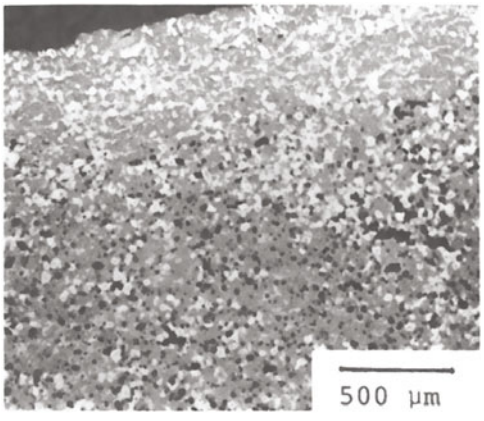

Figure 3. Microstructure of sample 1

Table 2. Mechanical properties of Ti_5Si_3/TiC/Ti-samples produced by GPCS

No	phase composition/vol%			ρ	σ^3	k_{1c}	HV
	Ti_5Si_3	TiC	Ti	(gcm^{-3})	(MPa)	(MPa $\sqrt{m}$)	(GPa)
5	81	19	-	4.52	350	4,23	12.40
6	74	26	-	4.52	350	4.10	12.88
7	67	33	-	4.52	355	3.45	13.32
9	63	32	5	4.52	350	3.94	12.28
10	49	23	28	4.49	580	6.05	11.05
11	56	13	31	4.47	770	-	9.80
12	31	15	54	4.49	1115	10.01	6.04

Some material properties of samples produced by GPCS are summarized in table 2. In materials containing additional Ti fracture toughness and bending strength can be improved significantly. Such high properties are usually found in similar ceramic-metal composites for example TiC/Ni or intermetallic compounds.

SUMMARY

The processing of materials in the system Ti-Si-C by GPCS was studied. By varying systematically the content of the raw materials it was possible to produce samples consisting in Ti_5Si_3, Ti_3SiC_2, $TiSi_2$, TiC and SiC. During cooling from the high temperatures after combustion some reactions occured and influenced phase composition, microstructure and properties of the samples. These reactions as well as the short sintering time are responsible for the not full densification of some samples. In the case of the composite containing Ti_5Si_3, TiC and Ti better mechanical properties were achieved.

REFERENCES

1. Y. Miyamoto, M. Koizumi, Potentiality of high pressure combustion sintering to produce ceramic based multi-phase components, Proc. IISS Symposium "Sintering 87" Tokyo 1987

2. Y. Miyamoto, M. Koizumi, O. Yamada, High pressure self combustion sintering for ceramics, J. Amer. Ceram. Soc. 67 (1984) C224

3. Y. Matsusaki, J. Fujioka, S. Minakata, Y. Miyamoto, Fabrication of $MoSi_2$-SiC/TiAl FGM by gas pressure combustion sintering, Proc. 1. Internat. Symp. on FGM, Sendai 1990

4. Y. Miyamoto, New ceramic processing approaches using combustion synthesis under gas pressure, Ceram. Bull. 69 1990 (686-689)

5. K. Niihara, R. Morena, D.P.H. Hasselmann, Further reply to "Comment on elastic/plastic intentation damage in ceramics: The median/radial crack system", J. Am. Ceram. Soc., 65 (7) C-116 (1982)

6. D. Munz, Fracture toughness calculation from maximum load in four point bend test of chevron notch specimen, Int. J. Fract. 16 R 137-R142 (1980)

7. H. Klemm, unpublished work

Si_3N_4-C(F) COMPOSITES SINTERED BY HIP

Hiroki Miyamoto, Toshiaki Katayama*, Kei Miyamoto,
Suguru Inamura, Yuzuru Takahashi, Masahiro Mori
and Yoshihiro Koya*
Osaka Prefectural Industrial Technology Research Institute,
Enokojima, Nishiku, Osaka, Japan
*Mitsubishi Kasei Ltd.

ABSTRACT

Si_3N_4-C(F)composites were fabricated by HIPing green compact formed by slip casting. Carbon fibre with length of 0.6 mm and diameter of 10 μm was used. Up to carbon fibre content of 15 vol%, well dispersed slurry was prepared. The green compact encapsulated in glass tube was HIPed at 1750°C for 2 hr. under 200 MPa of Ar pressure. Typical values of K_{1c} and bending strength for Si_3N_4-C(F) composites with 98 % of theoretical density are 10 $MPa \cdot m^{1/2}$ and 50 kgf/mm^2, respectively. The increase of K_{1c} was inferred to result from pull out effect of carbon fibres in the composites.

INTRODUCTION

Si_3N_4 composites with fibres such as SiC whisker, continuous carbon fibre and SiC/C fibre(Textron) have been extensively investigated in order to improve fracture toughness of ceramic materials. Among these composites, Iwata reported that Si_3N_4 composites with continuous carbon fibre showed fracture toughness of 28.1 $MPa \cdot m^{1/2}$ and bending strength of 690 MPa at room temperature(1).

In this study Si_3N_4 composites with chopped carbon fibre have been investigated to fabricate an isotropic Si_3N_4 composites with random orientation of carbon fibres. Slip casting method, which is applicable for production of desired shape, has been tried to form green compact. In order to obtain fully densified composites, HIP sintering of the green compact has been also attempted.

EXPERIMENTALS

Flow sheet of fabrication of Si_3N_4-carbon fibre[C(F)] composites is shown in Fig.1. Silicon nitride powder, thermally decomposed from imide compound(Ube-E10) is used as starting material. After the powder was dispersed in water by ball milling with sintering aids, Al_2O_3(5 wt%) and Y_2O_3(5 wt%), chopped carbon fibres with length of 0.6 mm and diameter of 10 μm were added to the dispersed slurry through #40 sieve to remove aggregates of the fibres.

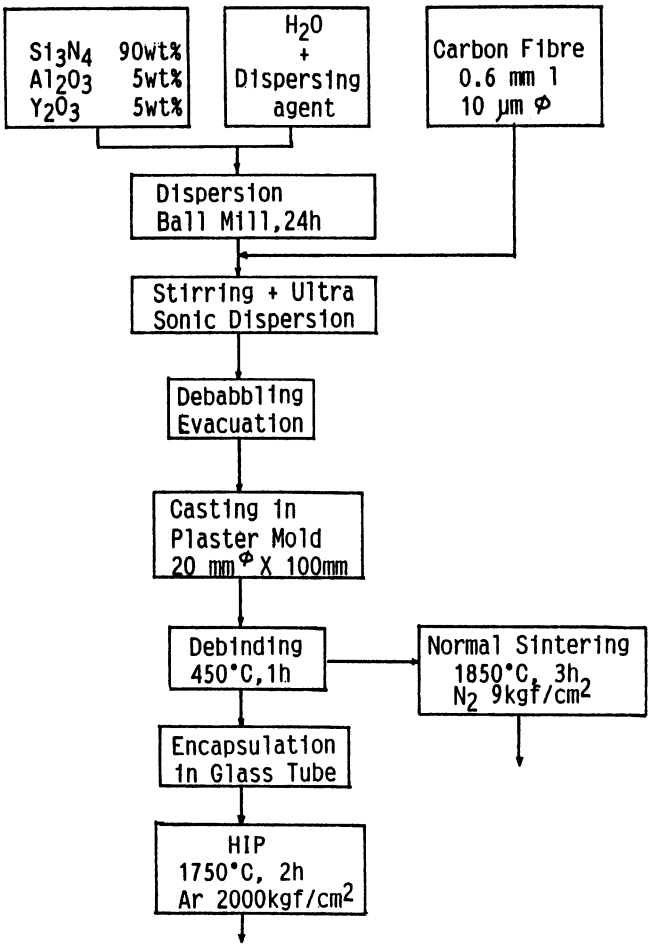

Figure 1. Flow sheet of fabrication of Si_3N_4-C(F) composites.

The prepared slurry was casted in plaster mold with 20 mm in diameter and 100 mm in length to form green compact. The green compact was debindered at 450°C for 1 hr in atmosphere. HIP sintering was carried out at 1750°C for 2 hr under 200 MPa of Ar gas pressure after the compact was encapsulated in pyrex tube. As a comparison normal sintering was also carried out at 1850°C for 3 hr under 0.9 MPa of N_2 gas pressure. The relative compressive strength of green compact was measured according to the illustration in Fig.2. Bending strength of the sintered body was measured by the conventional three point method, using a bar 3mm x 4mm x 40mm in size which was cut from the sintered body and polished in mirror surface. Fracture toughness was measured by I.M. method. The fractured surfaces were observed by SEM.

RESULTS AND DISCUSSION

1.Slip-casting of Si_3N_4-C(F) composites

Carbon fibres have a tendency to form aggregates in the slurry. This tendency makes it difficult to prepare a well dispersed slurry. Up to

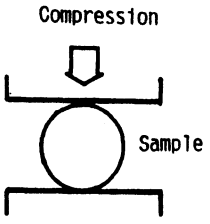

Sample Size: 26$^{\phi}$x L(9.5mm$^{\phi}$~17.5mm)
Speed of Load: 0.5 mm/min
Compressive Strength: Failured Load/L

Figure 2. Schematic illustration of relative compressive strength of green compact.

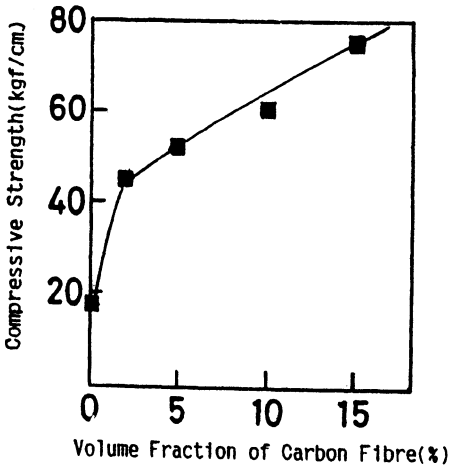

Figure 3. Effect of volume fraction of carbon fibre on relative compressive strength of slip-casted compact.

15 vol% of carbon fibre, a well dispersed slurry was successfully prepared by using chopped fibres with length of 0.6 mm.

In Fig.4, relative density of green compact is shown against volume fraction of carbon content. This linear increase of green density is explicable as ideal packing of large carbon fibres and small particles of starting powder. When fibres form aggregates or segregate during casting, relative green density is inferred to decrease from the density expected from ideal packing in composition range carried out in this experiment. In the green compact, carbon fibres are confirmed to disperse without aggregation in the starting powder by SEM.

A tendency that fibres oriented perpendicular to growth direction in casting process was observed. Therefor, purely isotropic dispersion of fibers is difficult to attain.

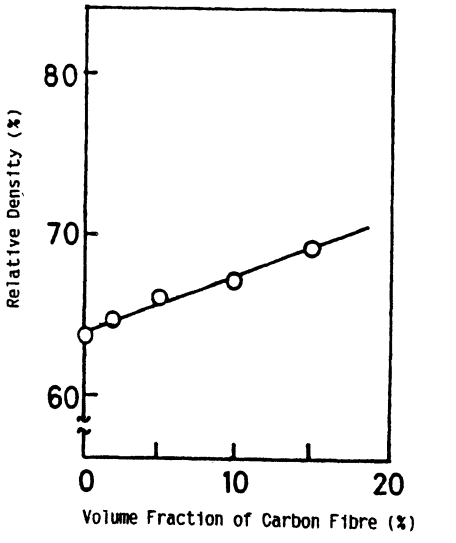

Figure 4. Relative density of slip-casted compact of Si_3N_4-C(F) composites vs volume fraction of carbon fibre.

The relative compressive strength showed a pronounced increase by adding a small amount of carbon fibre(2%) as shown in Fig.3. Above 2 % of carbon fibre content the relative compressive strength increased linearly with increase of carbon fibre content. The increase of green strength is beneficial for handling of green body.

2. Mechanical properties of sintered Si_3N_4-C(F) composites

Bending strength and fracture toughness were measured and summarized in Table 1. In normally sintered Si_3N_4, bending strength and fracture toughness were 100 kgf/mm^2 and 6.0 MPa.ml/2, respectively. Bending strength of normally sintered Si_3N_4 was greatly reduced by adding carbon fibres to Si_3N_4 matrix as shown in Table 1. Similar reduction of bending strength was observed in HIPed specimen. Si_3N_4 without carbon fibres, sintered by HIP, showed bending strength of 150kgf/mm^2 and fracture toughness of 6.2 MPa·m$^{1/2}$, respectively. By adding 10 % of carbon fibre, bending strength of HIP sintered specimen reduced to 50 kgf/mm^2, which is 1/3 of bending strength of HIPed Si_3N_4, although bulk density attained to 98 % of the theoretical density.

TABLE 1

Bending strength and fracture toughness of normally sintered(N.S) and HIP sintered Si_3N_4-C(F) composites

		Bending strength (kgf/mm^2)	Fracture toughness Klc (MPa·m$^{1/2}$)
HIP	CF-0 %	150	6.2
	CF-5 %	72.8	8.4
	CF-10 %	50	10.1
N.S.	CF-0 %	100	6.0
	CF-2 %	30	---
	CF-5 %	25	---

The specimen of HIP sintering showed 72.8 kgf/mm^2 of bending strength at 5vol % of carbon fibre, while that of normal sintering of the same composition showed 25 kgf/mm^2. The reduction of bending strength of HIP sintered composites is much smaller than that of normal sintering composites. On the other hand, the fracture toughness of HIP sintered specimens was improved from 6.2 MPa·m$^{1/2}$ without carbon fibre to 10.1 MPa·m$^{1/2}$ of 10 vol % of carbon fibre. It was difficult to measure fracture toughness of specimen of normal sintering because of its low density.

3.Microstructure of fracture surface

A typical pull out effect of fibres was observed in HIP sintered specimen as shown in Fig.5. In normal sintering pull out effect was not observed, because of void formation around carbon fibre as shown in Fig. 6. Distribution image of Si atoms are shown in the same figure. On the surface of the fibre Si exists clearly. This result indicates presence of reaction between carbon fibre and matrix. SiC formed presumably through gas phase reaction. Tight binding between fibre and matrix can not be expected.

On the other hand, distribution of Si on the surface of carbon fibre of HIP sintered specimen was poor in Fig.7. As a typical pull out effect was observed in the fracture surface of HIP sintered specimen, carbon fibre has kept its strength and is bound tightly to the matrix. Formation of void was not observed in the HIP sintered specimen. It is inferred that pressure applied in HIP sintering process suppressed SiC formation through the gas phase reaction.

The great reduction of bending strength of normal sintering is due to voids formed around fibres which act as fracture origin. The difference of reduction of bending strength between HIP sintering and normal sintering can be explained by the presence of voids formed around

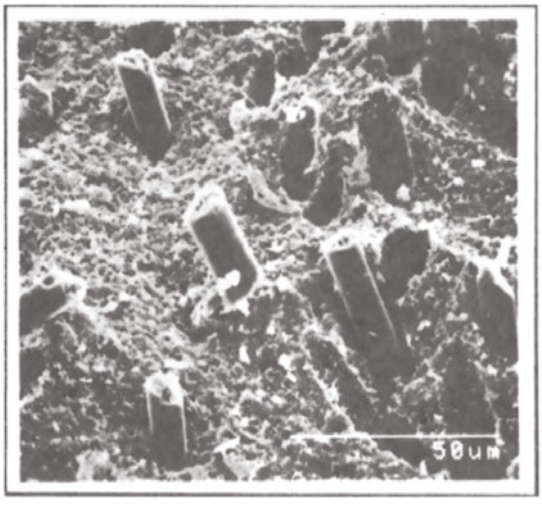

Figure 5. Pull out effect of fractured surface of HIP sintered Si_3N_4-C(F) composite.

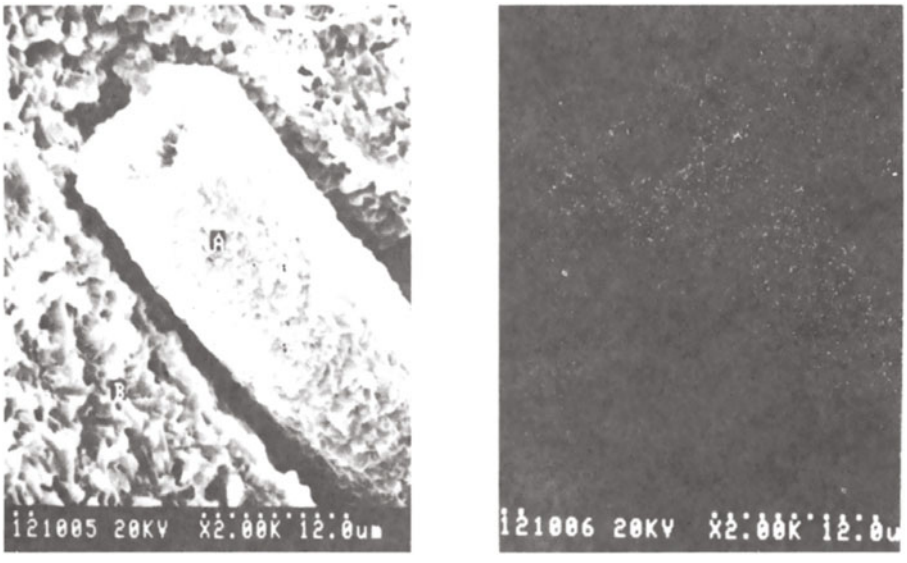

[SEM image] [Si]

Figure 6. SEM image of normally sintered Si_3N_4-C(F) composite and Si distribution.

[Secondary Electron] [Si]

[SEM image] [Si]

Figure 7. SEM image of HIP sintered Si_3N_4-C(F) composite and Si distribution.

fibres. The observed reduction of bending strength within HIP sintered samples may be attributed to defects introduced in the forming process of slip-casting like aggregates of fibres and babbles in the slurry.

CONCLUSION

Si_3N_4-C(F) composites were fabricated by slip-casting, followed by normal sintering and HIP sintering. The following results were concluded.

1. Homogeneously dispersed slurry of Si_3N_4 powder and chopped carbon fibres(0.6mm) is obtained up to 15 % of carbon fibre content.
2. Compressive strength of green compact shows a pronounced increase by adding a small amount of carbon fibres.
3. In HIP sintered Si_3N_4-10%C(F), K_{1c} is 10.2 $MPa \cdot m^{1/2}$ and bending strength is 50 kgf/mm^2. The composites are fully densified by HIP.
4. A typical pull out effect of carbon fibre is observed in HIP sintered composites. The increase of K_{1c} is inferred to result from pull out effect.
5. In normal sintering , carbon fibre reacts with the matrix. Bending strength greatly reduced in the composites, because of void formation around fibre.

REFERENCE

1. Misao Iwata, Fabrication of continuous fibre reinforced ceramics and improvement of mechanical properties. Powder and Powder Metallurgy, 1990,37,1108-1113

8. EQUIPMENT AND INSTRUMENTATION

HISTORICAL REVIEW OF HIP EQUIPMENT

by
CHARLES B. BOYER
Retired from Battelle/Consultant for Howmet Corporation
Columbus, Ohio U.S.A.

ABSTRACT

This paper is one person's endeavor to write a systematic account of the development of Hot Isostatic Pressing (HIP) equipment from the purchase of the first cold-wall HIP vessel through the first part of 1970.

Thirty-five years ago, the author, a mechanical engineer, joined Battelle's Fuel Element Development Division at the request of Henry (Hank) Saller. Hank wanted him to devote most of his time to the design and maintenance of the Division's equipment. It was shortly thereafter that the author accompanied Ed Hodge to one of Battelle's warehouse facilities, where a pressure vessel had been set into a pit. Since being introduced to this vessel, the author has been directly involved in the design, development, and application of Battelle's twelve HIP systems and has assisted most HIP suppliers and many of the HIP users with their equipment and systems.

Calling upon this varied experience, the many records and files that were maintained, and the acknowledged assistance of several experienced persons, it is hoped to present an accurate and interesting history of HIP equipment, with a philosophical explanation or accounting of their purpose.

INTRODUCTION

In this historical introduction, the events leading up to Battelle's acquiring the world's first cold-wall hot isostatic pressing (HIP) vessel are discussed.

The history of HIP spans a period of some 38 years. In the mid-1950's, gas pressure bonding was conceived by researchers at the Battelle Columbus Laboratories. These scientists were faced with the problem of developing a method of bonding zirconium to a zirconium-uranium alloy. This effort was an attempt to obtain a satisfactory cladding process, while maintaining strict dimensional control, for preparing a proposed pin-type fuel element. Conventional fabrication techniques, such as rotary swaging and drawing prior to diffusion anneal, and other methods involving hot deformation, proved unsatisfactory.[1,2,3]

In a staff meeting called by Dr. Russel Dayton, Battelle's Program Manager for the Navy Nuclear Programs, this bonding problem was discussed. Dr. Dayton suggested the idea of using an isostatic means to force the cladding into intimate contact with the core during the diffusion treatment. A gas was suggested as the best pressure media, due to the required high diffusion temperature.[4] Initial investigations, using equipment limited to a maximum of 2000 psi (13.78 MPa) at temperatures up to 1650 F (900 C), revealed promising results. This technique, called gas pressure bonding, was patented by four Battelle scientists, Dr. Russel Dayton, Henry Saller, Stanley Paprocki, and Edwin Hodge.[5,6,7]

The first investigations of these scientists were conducted in a vessel consisting of a 3-foot (91.44 cm) long piece of Type 304 stainless steel high pressure tubing 9/16-inch (14.29 mm) O.D. by 3/16-inch (4.76 mm) I.D. This tube was plugged and welded closed on one end while the other end was coned and threaded to accept a high pressure two-way straight valve.[8]

After inserting the sample pin all the way to the closed end, the valve was attached. A line was then connected between the valve and a helium cylinder, as illustrated in Figure 1. This small vessel was pressurized to approximately 2000 psi (13.78 MPa) or the pressure of the helium cylinder on hand. The closed end of the vessel was then inserted into a heat treat furnace at a temperature between 1500 F (816 C] to 1650 F (900 C). Encouraging results were achieved on specimens bonded at temperatures between 1550 F (843 C) to 1650 F (900 C) and pressures under 2300 psi (15.85 MPa). Considerable hold times, however, of 24 to 36 hours were required to obtain these bonds.

Figure 1. An illustrated demonstration of the first hot-wall gas-pressure-bonding system, as performed in the mid-1950's.

To accommodate larger test specimens, 1-inch (2.54 cm) I.D. reactor vessels of Type 410 stainless steel were procured.[9,10] Bonding studies were continued in these vessels with repeated cycles up to 36 hours. During this time, two of these utilized as hot wall units, did have rupture failures in the region of the heated end. These failures and the realization that the hot-wall vessel would be limited in size, temperature, pressure and life capabilities, brought about the idea of the cold-wall gas-pressure bonding vessel.

It should be pointed out, before continuing this historical review, that the HIP process has always seemed to lead the availability of adequate HIP equipment.[11,12,13]

GAS PRESSURE BONDING EQUIPMENT 1955 THROUGH 1957

The concept of obtaining a hot zone in a gas-filled vessel was a unique idea and was to require considerable inventiveness. A survey of the limited literature in the field of high pressure revealed no prior information of an internal heater.[14,15] Methods, however, of bringing insulated electrical leads into experimental pressure chambers were revealed. Following discussions with several high pressure equipment and furnace manufacturers, the equipment for the first cold-wall gas-pressure bonding system was placed on order.

The location selected for this system was approximately three miles from the Battelle campus. It was to be installed in one of Battelle's warehouses that had been converted, in name only, from an old casket factory. The decision was made, because of the limited overhead and safety reasons, to have the pressure vessel placed into a pit. Midway down the long North bay, approximately 3 feet (91.44 cm) from the center wall, a square pit was built. This pit was constructed of cement block measuring 6 feet (1.83 m) by 6 feet (1.83 m) wide and 9-1/2 feet (5.49 m) deep.

Late in 1955, a modified standard Type 304 stainless steel forged pressure vessel and an Andreas Hofer piston-type transfer compressor were acquired by Battelle from Autoclave Engineers, Inc. (A/E)[7,9] In addition, two single zone cartridge type furnaces were obtained from the K.H. Huppert Co. and Trent, Inc.

The 10,000 psi (68.9 MPa) vessel drawing, shown in Figure 2, was designed and built by A/E. It was 9 inches (22.86 cm) I.D. by 48 inches (121.92 cm) inside length (I.L.) and utilized a modified Bridgman/A/E closure with buttress-type threads on both ends.[16] The upper closure contained five openings, one 3/8-inch (9.53 mm) coned type gas inlet, two flat bottom packing electrical lead recess inlets, one flat bottom gasket inlet for a 1-inch safety disk assembly for 15,000 psi (103.4 MPa) at 72 F (22 C), and one internal coned type 5/32-inch (3.97 mm) inlet for the upper thermocouple-well tube. The lower closure had a single interval coned type 5/32-inch (3.97 mm) inlet centrally located for a bottom thermocouple well tube. These thermocouple wells were made from 3/8-inch (9.53 mm) O.D. by 5/32-inch (3.97 mm) I.D. Type 316 stainless steel tubing sealed on one end. A single 3/8-inch (9.53 mm) coned type opening had been machined into the vessel wall, approximately 1-inch (25.4 mm) above the top of the lower closure. It was intended to use this inlet as an evacuation port, as illustrated in Figure 3.

The vessel was placed in the center of the pit upon a 24-inch (60.96 cm) high stand, and the compressor positioned at the back of the pit on floor level, as shown in Figures 4 and 5.

On February 1, 1956, the author joined Battelle. One of the first tasks assigned him, by Stan Paprocki and Ed Hodge, was to assemble these components into a working system and to have the responsibility of maintaining and upgrading it. These tasks were in addition to other project assignments. The highest pressure the author had worked with, up to this time, was 100 psi (0.69 MPa) house air pressure.

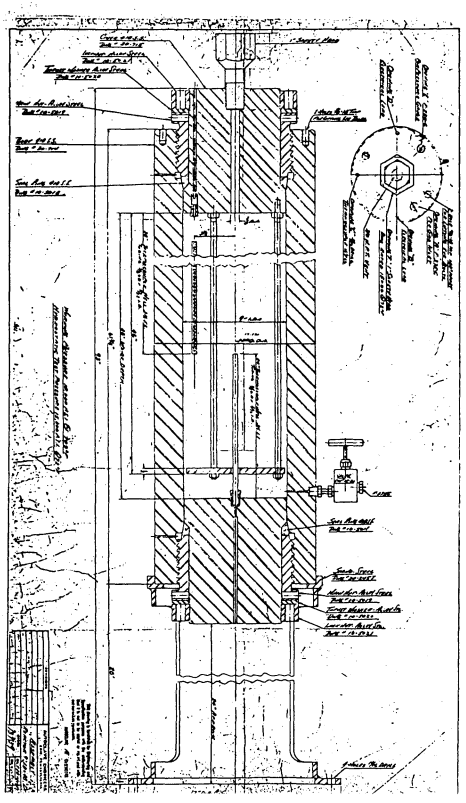

Figure 2. Autoclave Engineers' drawing of assembly reactor 9" I.D. x 48" depth, used by Battelle for gas-pressure-bonding. Note: Modified Bridgman or A/E closure. (Courtesy of Autoclave Engineers Group)

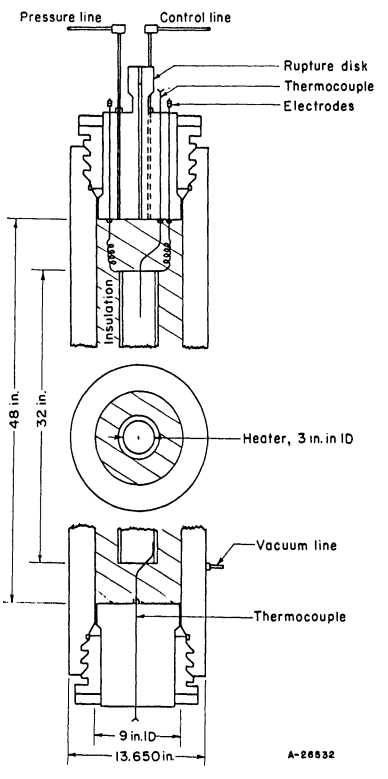

Figure 3. Sectional view of a high pressure cold-wall autoclave.

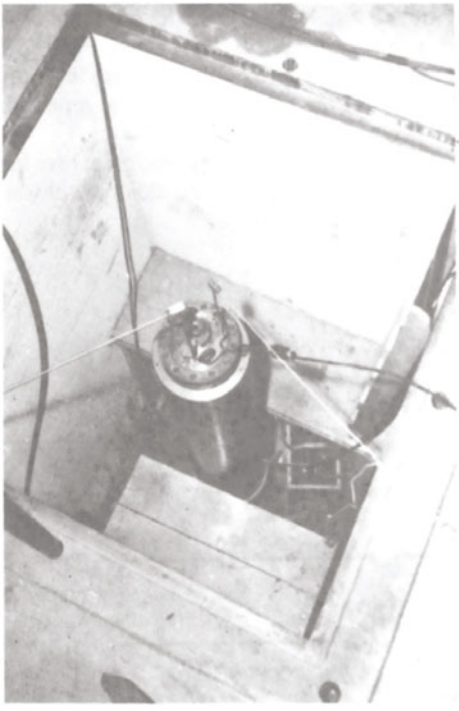

Figure 4. The first cold-wall gas-pressure-bonding vessel, as installed at Battelle in 1956.

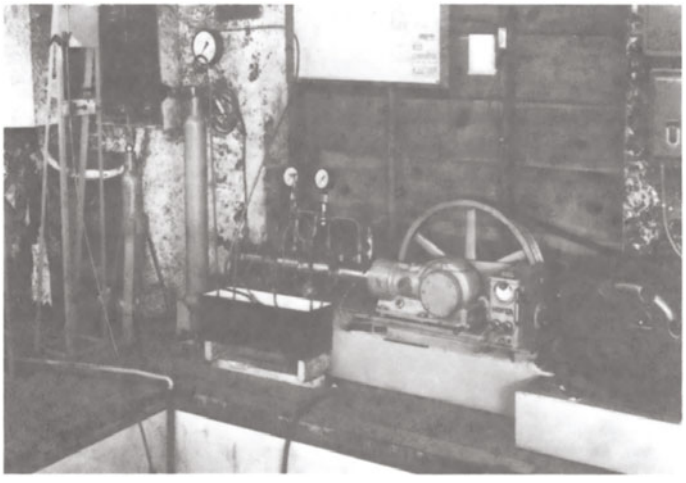

Figure 5. The Andreas Hofer piston-type transfer compressor, as installed at Battelle.

The components were assembled into a system per the preliminary flow sketched supplied by A/E; a copy of which is shown in Figure 6.[7,17] The system, Figure 7, was pressurized from the helium manifold to 500 psi (3.45 MPa). There were several gas leaks throughout the system. The leaks were noted and after releasing the pressure, they were repaired.

The metal seal closure, being a precision device, required great care in cleanliness and handling. After acquiring the skill of inserting and tightening this type closure, excellent results were obtained with numerous openings and closings.

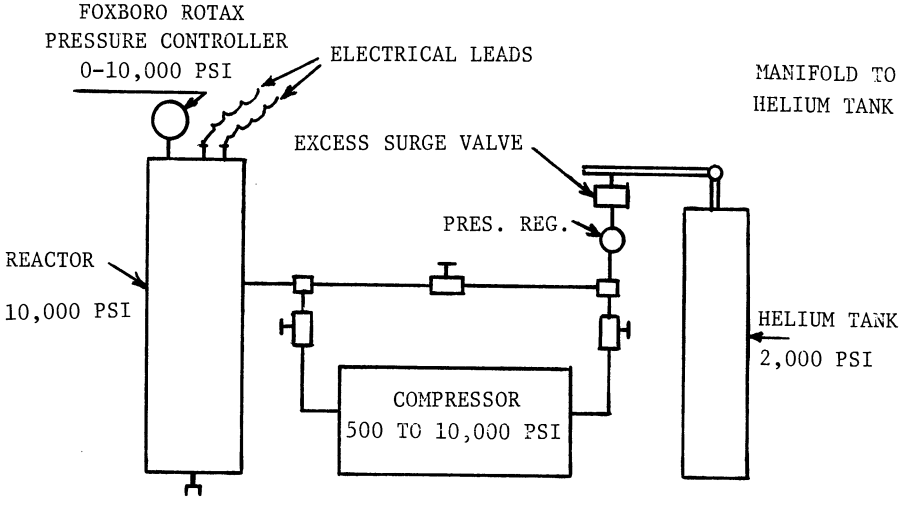

Figure 6. Flow sketch of gas-pressure-bonding system, supplied by Autoclave Engineers.

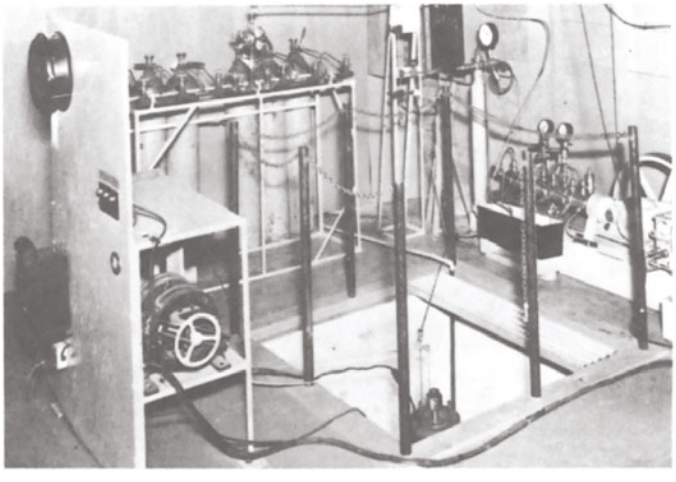

Figure 7. The initial cold-wall gas-pressure bonding system, as first assembled in 1956.

The electrical system was then checked for proper operation. The compressor was controlled by a Rotax Pressure Indicating Controller, and the furnace by a Foxboro Potentiometer Controller, and a 25 kw rotary switch transformer. Electrical power was brought into the furnace by two porcelain coated steel electrodes contained in the upper vessel cover. A recess was machined in this cover to contain and seal the electrodes with a packing of three Phenolite washers and a Garlock 834 packing. The electrodes did not hold pressure above 500 psi (3.45 MPa) and were satisfactorily replaced with three Phenolite washers, each having undersized I.D. openings, allowing for a press-fit onto the electrode and two Garlock packings.

Attention was given to the high-pressure compressor during installation of the various components. The Andreas Hofer piston-type transfer compressor had three stages with a suction pressure of 809 psi (5.5 MPa) and a discharge pressure of 10,000 psi (68.9 MPa). The instruction book was written in German, which we could not read. However, by looking at the various diagrams, using a borrowed book of German translations, and making several telephone calls to A/E, we soon acquired enough information to become knowledgeable in the operation of this machine. Special attention was given to the following: placement of a filter on the suction line, obtaining the proper recommended oil, the proper adjustment of the mechanical pressure lubricator, checking for proper flow of the cooling to each stage, and the draining, after each cycle, of the velocity oil separator.

The 24 ohm Trent cartridge type furnace was first tested in air to a temperature of 1300 F (704 C). This furnace, as sketched in Figure 8, consisted of a vertical grooved alumina tube, 2-inch (50.8 mm) I.D. by 36- inch (91.44 cm) long, wound with a single Chromel A wire to form a single zone with leads coming from the top and bottom.

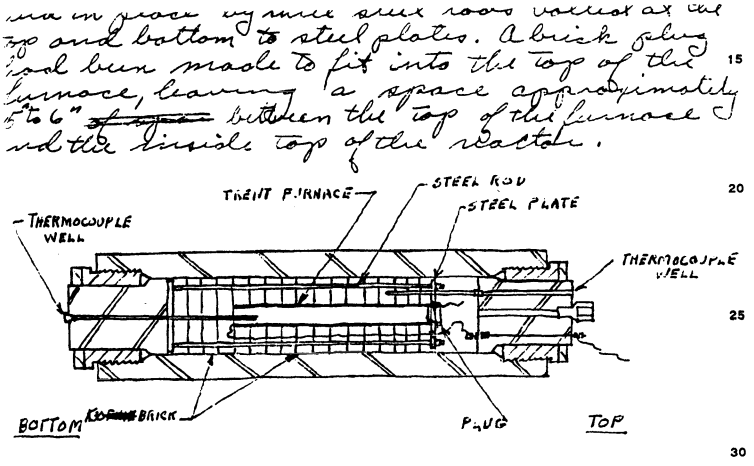

Figure 8. Sketch of cartridge type furnace, as installed into the pressure vessel.

K-30 fire bricks were used for insulation between the heater tube and the stainless steel outer jacket. The upper I.D. was filled with a plug made from a K-30 brick. The furnace was supported from the upper vessel closure by three steel rods that extended through the bricks to a steel plate at the bottom. The lower thermocouple well extended up through the bottom center of the heater tube approximately 14-inch (35.56 cm) and was used as the control couple. The upper thermocouple well extended down into the K-30 brick a distance of 1-1/4-inch (31.75 mm) from the heater element and approximately 18-inch (45.72 cm) down from the top of the heater. Type K thermocouples were made up and inserted into these wells.

After being installed and the vessel secured, the vessel was pressurized to 500 psi (3.45 MPa) and the furnace turned on. With each 100 F (37.8 C) rise of the furnace temperature, as measured by the thermocouple within the lower thermocouple well, a thermocouple monitoring the outer wall of the vessel rose an almost-equal amount. The pressure was increased to 1000 psi (6.89 MPa) while continuing to heat. After approximately 1-1/2 hours, the temperature of the furnace and the outer wall of the vessel were both at 600 F (316 C) indicating that with this arrangement, we could not have a successful system. At this time, the furnace power was turned off. For the first time, it was realized that the operation of a furnace in a high-pressure gas atmosphere was going to be a problem.

Unable to obtain outside assistance with this problem from the large furnace manufacturers, we approached it on our own. We attempted cementing between and over the faces of the K-30 bricks to reduce the heat flow path. A fibrous insulation (Fiberfrax) was used to fill the void between the top of the furnace and the inside top of the upper cover. Only a slight improvement was observed.

The Trent furnace was replaced with the Huppert furnace after making some of the same insulation modifications. The heater in this furnace, 3-inch (76.2 mm) I.D. by 24-inch (60.96 cm) long, used internal-vertical slotted half-shell ceramics, from Hevi Duty Electric Co., in place of the alumina tube. The heating elements were made from a 1/4-inch (6.35 mm) helically coiled Chromel-A wire. Each half of the heater had a resistance of 25 ohms. In making test cycles, an electrical short created a melt down in the lower part of the heater. This furnace was completely disassembled and the K-30 fire brick discarded. A new heater was built using six of the undamaged 4-inch (101.6 mm) long half-shell ceramics and lengths of the coiled Chromel-A wire. We obtained a heater 3-inch (76.2 mm) I.D. by 12-inch (30.48 cm) long having four elements. Stranded Chromel wire leads were welded to the leads of these four elements in a series/parallel connection to create a 10 ohm heater. This heater was placed in the center of the salvaged stainless steel jacket, with the intervening space tightly packed with a fibrous insulation, called Fiberfrax. End plugs and round spaces were made of K-30 brick to close the ends of the heater and as a specimen support. The upper thermocouple well was bent to be centered within the heater, making the tight packing of the insulation and the placement of the upper vessel closure very difficult. With this heater, we did obtain a temperature of 1525 F (830 C) at 10,000 psi (68.9 MPa) for a short period of time with a wall temperature of 80 F (27 C). This was an improvement and a step in the right direction.

Soon after, on April 20, 1956, a cycle was performed at 1500 F (816 C) and 10,000 psi (68.9 MPa) on a flat-plate fuel assembly specimen 1-inch (25.4 mm) square by 6-inch (152.4 mm) long. After 6 hours at these conditions, the outer vessel wall had reached a temperature of 234 F (112 C). Upon removal of the specimen, it was found that the upper end had melted, but the lower end was unbonded. However, a 1-inch long section in the middle revealed very good Zircaloy bonds, and with the exception of one channel that had shifted, excellent dimensional control was achieved.

With limited success, project support was obtained to proceed with our gas-pressure bonding development efforts.[3,7,18] Continued improvements were made to the furnaces and system components during the next 18 months. However, to allow for certain project work to continue, two Inconel X hot-wall vessels were purchased from A/E. These identical vessels were 2-inch (50.8 mm) I.D. by 6-inch (152.4 mm) O.D. with an I.L. of 21-inch (53.34 cm), and had a working pressure of 5,000 psi (34.45 MPa) at a wall temperature of 1500 F (815 C). They were closed on one end with a modified Bridgman/A/E closure (having two gas inlets) on the other end. A Marshall muffel furnace was purchased to heat the vessels. Marshall Products became interested

in the gas pressure bonding process and in our heater problems. Their assistance was very helpful over the next 15 years.

Using Hevi-Duty Electric Company's slotted semicylindrical high-purity refractory shells and Hoskins Type 835 helically coiled close-wound wire, a more efficient heater was constructed. It was found that with continued reuse of the Fiberfrax fibrous insulation, a greater packing density could be obtained, thereby achieving better insulating properties for our furnaces. To assist with resistance match up between the furnace and the rotary transformer, heater-cones of various resistances were series-wired into the furnace leads and mounted on top of the control panel, as shown in Figure 9. A main electrical power breaker switch, ohmmeter, potentiometer, vacuum meter, and various component switches were added to the control panel.

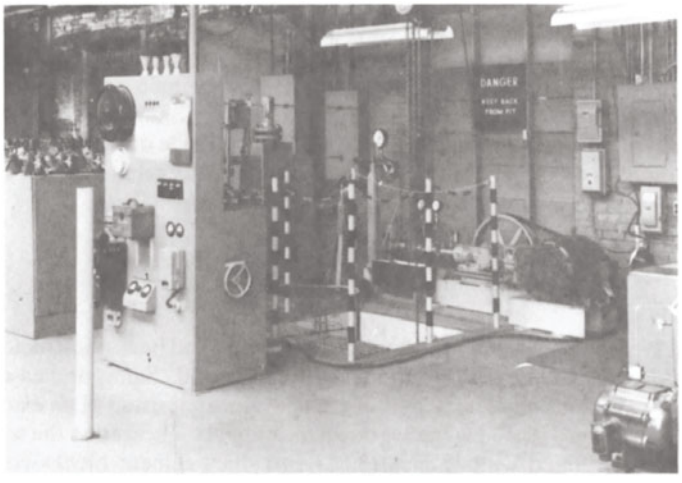

Figure 9. View of the HIP system and up-graded control panel.

It became apparent, with the addition of the fibrous insulation into the furnace and the rainy Spring weather, moisture could be a problem. Flushing of the sealed vessel with helium and then placing it under vacuum generally overnight helped reduce the moisture. The use of new insulation also called for heating while under vacuum.

Cycles to temperatures of 1925 F (1052 C) at 10,000 psi (68.9 MPa) were now being made for a delta-phase zirconium hydride cladding program.[19] A band containing four thermocouples had been installed around the O.D. of the vessel to measure its outer wall temperature. After a period of 2-1/2 hours at the above cycle conditions, the outer wall of the vessel did not exceed 250 F (121 C), well within the design temperature of 700 F (371 C).

It was during this period that we began experiencing electrical shorting of the electrodes within the packing seal recess in the upper closure. The shorts were caused by cracking of the porcelain coating. Generally, this would only require replacement of the electrode and packing. However, one severe short did damage the seal area of the packing recess and machining of the upper closure was required. When this was reported to A/E, they developed a new self-contained electrode unit. The body was machined with a flat bottom seal to fit into the upper cover recess and contained the packing within. This allowed for quick replacement of the electrode unit which contained a beryllium-copper electrode having better electrical properties. The electrical insulation was improved by spun-glass tubing.

With the higher temperatures and questionably improved hot zone, it was observed that the thermowell tubes were collapsing onto the thermocouples. This created shorting of the thermocouples and made replacement impossible. To obtain more thermocouples within the vessel, and to omit the two objectional thermowells, we designed a unit using four short lengths of a purchased 1/8-inch (3.05 mm) diameter magnesium oxide insulated stainless steel sheathed Type K thermocouple wire welded into a Type 304 stainless steel body. A short coned high pressure nipple was welded into the top of this body allowing the eight wires to pass through its I.D. and through the upper closure. This unit was tested and installed inside the upper cover of the vessel, allowing for the placement of four flexible thermocouples into and around the heater, as desired. There were no apparent leaks through the oxide in the sheathed wire and, being well out of the heated zone, no collapse of the sheathed wire occurred.

During the period from February 1, 1956 to December 31, 1967, with our limited system and project successes, the acquiring of additional equipment was considered. The designs for the new vessels were based upon the project needs of greater specimen size, higher temperatures, increased pressures, and the desire to use a helium-hydrogen gas mixture. This was an attempt to control the loss of hydrogen through dissociation of the hydride during cladding.[20,21] The design and location for a new laboratory to house this new equipment was also undertaken.

GAS PRESSURE BONDING EQUIPMENT 1958 THROUGH 1962

In the Spring of 1958, a new gas pressure bonding laboratory had been constructed on the back of a service building at Battelle's West Jefferson Site, Figure 10. Safety and ease of operation were given main consideration in its design. This laboratory consisted of an extension built of sheet metal with large glass scored windows down the outside. The wall to the service building (control area) was modified with 12-inch (30.48 cm) thick cement blocks containing steel reinforcement rods and steel door. The design was to allow for free expansion of the gases in all but one direction, should there be a major pressure failure. Further, personnel safety was accomplished by installation of four 8 foot (2.44 m) diameter by 12 foot (3.66 m) deep pits.

Figure 10. The new gas-pressure-bonding laboratory at Battelle's West Jefferson Site.

In April 1958, we started the transfer of the gas pressure bonding equipment to our new laboratory. By the Summer of 1958, Battelle had obtained two new 10,000 psi (68.9 MPa) vessels and a larger five-stage Hofer 15,000 psi (103.4 MPa) compressor from A/E. One vessel had the same inside dimensions as our first vessel, Figure 11, and the second was larger, having a 14-inch (35.56 cm) I.D. by 6 foot (182.85 cm) I.L., Figure 12.

Figure 11. Making electrical connection to the furnace in the new internal cooled 9-inch (22.86 cm) I.D. vessel.

A few of the more notable improvements incorporated into these two vessels were as follows:

(1) Both vessels of forged 4340 type steel had liners, having helical grooves machined on their O.D., shrunk into them. The liners, Type 316 stainless steel, 0.375-inch (9.525 mm) thick with 1/8-inch (3.175 mm) radius grooves on a 3/4-inch (19.05 mm) pitch for the smaller and Type 410 stainless steel 0.750-inch (19.05 mm) thick with 1/4-inch (6.35 mm) radium grooves on a 1-inch (25.4 mm) pitch for the larger, were installed to prevent possible hydrogen embrittlement of the vessel body. Each vessel had four fluid port entries into the liners. The passage of fluid through the grooved liners was expected to carry any hydrogen away that might permeate them. It should be noted that an unpredicted improvement, the cooling of the vessel to allow for extended cycle time or higher temperatures was achieved. A water solution of 10 percent water-soluble oil and 10 percent rust inhibitor was pumped through the grooved liners for cooling.

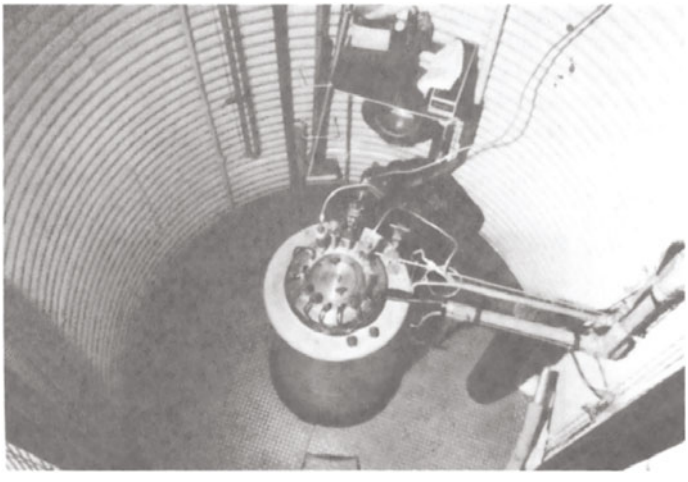

Figure 12. View of the 14-inch (35.56 cm) I.D. internally cooled vessel, as installed in its pit.

(2) Newly designed, self-contained beryllium-copper electrode bodies, four and six in the upper cover of the smaller and larger vessel, respectively, were employed. A close fitting rubber insulation cover was installed over each electrical connections. The beryllium-copper electrode is shown in Figure 13.

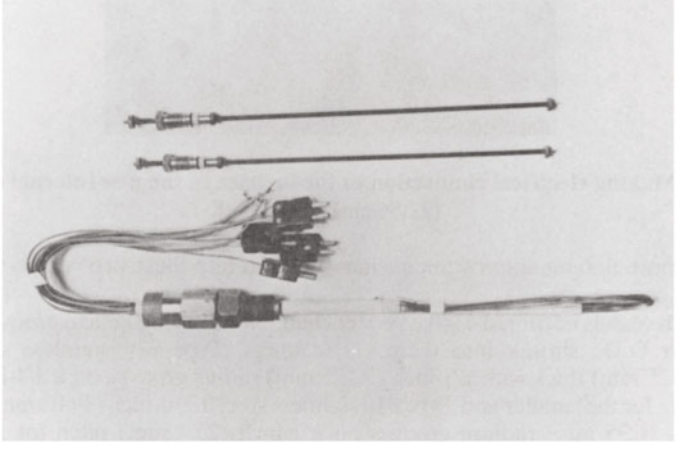

Figure 13. Beryllium-copper electrode assemblies and a multiple-wire thermocouple lead-through for 10,000 psi (68.9 MPa) service.

(3) A multiple-wire thermocouple lead-through unit had been obtained for 10,000 psi (68.9 MPa) services. Each unit contained six wires for three thermocouples. There was one unit in the upper cover of the smaller vessel and two units in the larger. Battelle personnel soon observed that the elastomer packing was being coextruded along with the thermocouple wires up through the alumina backup. The holes in the alumina backup were several mils larger than the Chromel-Alumel wire being used. We designed and acquired new alumina backup parts having holes with only a couple mils clearance with the T/C wire and backing this part with a thin, tight-fitting leather washer on the pressure side. No problems were encountered after this modification. The thermocouples were generally placed into the heater in bundles, as shown in Figure 14.

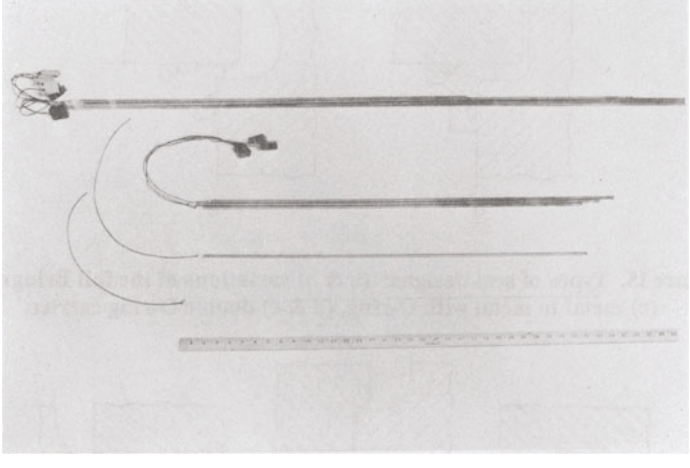

Figure 14. Multiple thermocouple bundle & method of assembly.

(4) The upper closure of the larger vessel was designed to have all gas openings and lead-throughs in a ring around the outer cover, so that an inner cover could allow for a 7-1/2-inch (190.5 mm) diameter free access to the furnace as illustrated in Figure 12.

(5) The smaller of the two vessels still used a modified Bridgman/A/E metallic closure and seal. The larger vessel used a tapered-bore O-ring closure for quick opening of the upper inner cover. Full Bridgman type packing seals were used on both the upper and lower vessel closures. The packing components, in the as-received vessel, were made up of two Neoprene washers sandwiched in between two Type 410 stainless steel washers. Having difficulties retaining helium pressure in the vessel, these were soon modified and replaced with a single Neoprene washer sandwiched between two aluminum foil packing washers and two Type 410 stainless steel washers. No leaks were observed with this modified seal; however, following several pressurizations, this type of seal was difficult to remove. Refer to Figures 15 and 16 for some of the various types of closure seals used for HIP vessels.

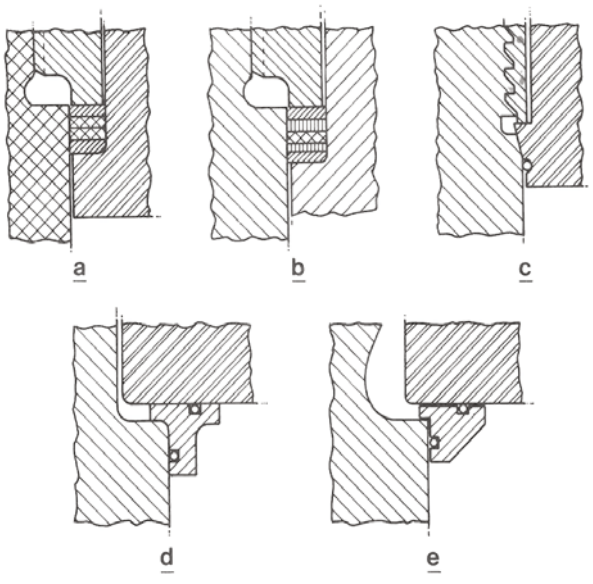

Figure 15. Types of seal designs: (a & b) variations of the full Bridgman, (c) metal to metal with O-ring, (d & e) double O-ring carrier.

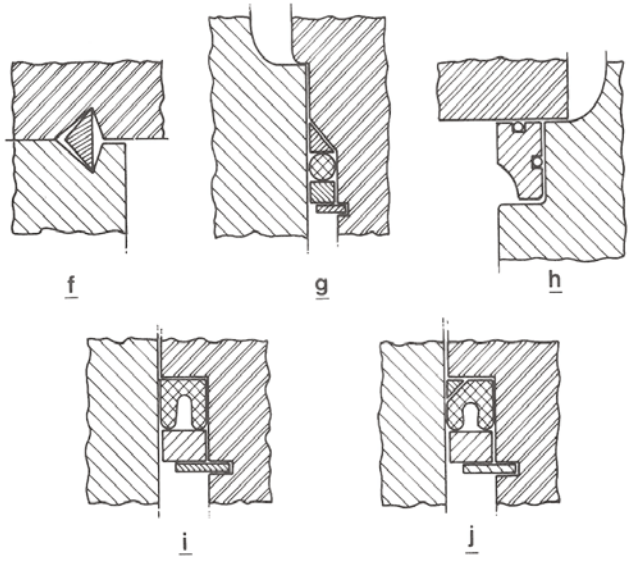

Figure 16. Types of seal designs: (f) delta-ring seal, (g) O-ring with anti-extrusion rings, (h) double O-ring with full bore opening, (i) U-ring seal, (j) U-ring with anti-exrusion ring.

Battelle personnel designed and installed multiple-zone ceramic furnaces in these two vessels. The small vessel had a 3-inch (76.2 mm) by 30-inch (76.2 cm) long furnace, and the larger vessel a 5-inch (127 mm) by 48-inch (121.92 cm) long three-zone furnace, Figure 17.[22] These consisted of resistance heating elements, for various temperatures, using Chromel-A, Kanthal, and Hoskins 835 and 875 alloys.

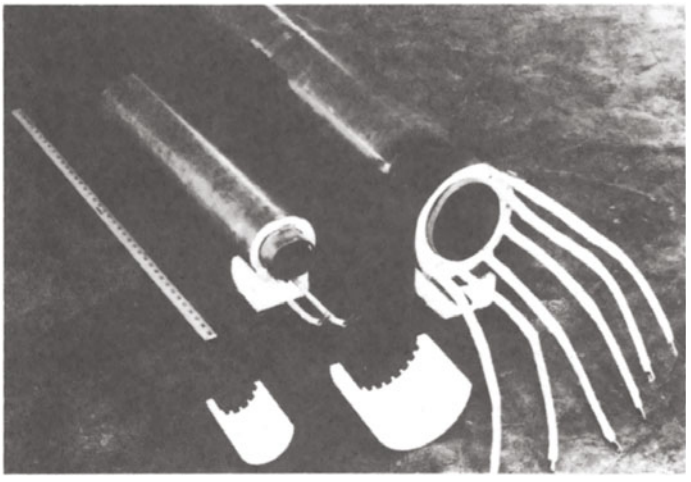

Figure 17. Typical ceramic shell type furnaces using FeCrAl alloy helically coiled wire.

We began using a fibrous insulating material in these furnaces called Microquartz, as illustrated in Figure 18. This insulation material replaced the Fiberfrax, as it could be used as a satisfactory thermal barrier to a temperature of 2000 F (1093 C). We also started using bubble alumina, in place of silica, in the heater void space, to cut down on the flue or chimney effect associated with a long vertically operated heater. This material was also used to support specimens. Large industrial sweepers were purchased for each HIP vessel, to assist in the handling both the fibrous and granular insulation materials.

An interesting sidelight was observed around this time concerning the economics of using porcelain thermocouple tube insulators instead of alumina. Upon opening of the vessel containing thermocouples with the porcelain tubes, we noticed a loud cracking sound. The helium had permeated the porcelain and the tubes were self destructing. So much for cost cutting.

New control panels, but very similar to our first, were built for each system. Each panel did contain three new 50 kW Powerstat variable autotransformers and a multi-point recorder to keep account of the additional thermocouples.

During this period of time, there was increasing project demand for furnaces with increased size and temperature range having reliability and a controllable hot zone. In response to these demands, a molybdenum wire-ceramic tube furnace with a 2-inch (50.8 mm) I.D. by 8-inch (203.2 mm) long, 2900 F (1593 C) hot zone, was designed and placed in operation. Both bubble and tabular alumina were used as a insulation next to the molybdenum windings.

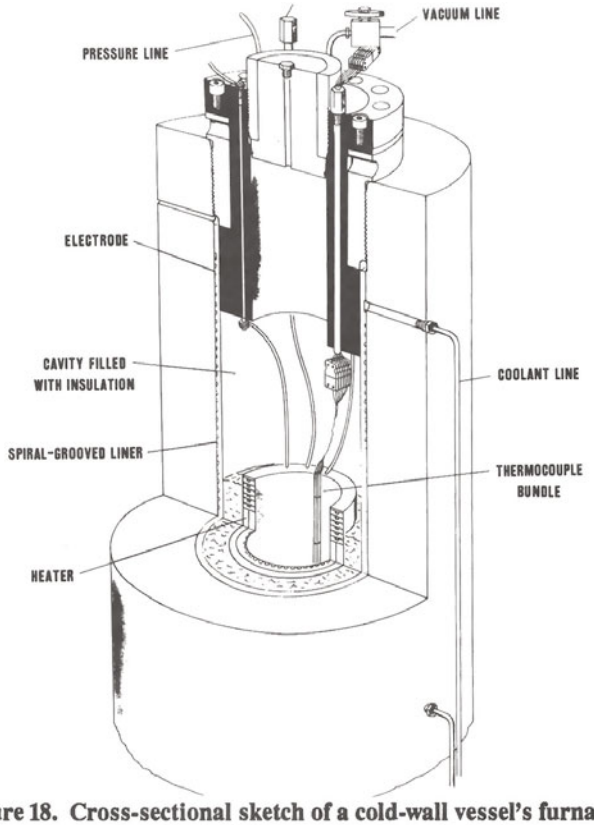

Figure 18. Cross-sectional sketch of a cold-wall vessel's furnace.

In the mid-1957's, work was undertaken by the Sylvania Corning Nuclear Corporation, Bayside, Long Island, New York, to investigate the bonding of various nuclear materials. They acquired and were using a hot-wall Inconel-X vessel 3-3/4-inch (95.25 mm) I.D. by 35-inch (88.9 cm) I.L. This vessel was designed by A/E to operate at 20,000 psi (137.9 MPa) at a temperature of 1112 F (600 C). A modified Bridgman/A/E closure was employed on both ends of the vessel. During 1958 at the suggestion of the AEC, to obtain a further development program, Sylvania decided to convert the hot-wall vessel into a cold wall vessel with the installation of an internal furnace. [23,24,25]

The following are a few of the more interesting elements of this system:

(1) The basic components and all other high pressure equipment were located in a reinforced concrete room below ground level. It was detached from their main building where they remotely located the control panel. The "isostatic room", as they referred to it, had explosion relief roof of wood construction.

(2) They used an Hofer transfer compressor to achieve system pressure, from an argon gas cylinder manifold. The pressure was measured by a Baldwin strain cell and a Foxboro pneumatic pressure transmitter connected in the high pressure line. The pressure was remotely read and controlled by a Baldwin strain indicator and a Foxboro controller on the control panel in the main building.

(3) The heat was supplied by a Kanthal internally wound heater rated at 1700 watts. It was 1-1/2-inch (38.1 mm) I.D. by 12-inch (30.48 cm) long. A variac was used to manually control the heater. Bubble alumina insulation was used between the heater and the vessel wall, with Fiberfrax insulation packed between the top of the heater and the upper vessel closure. They were using three internal thermocouples to measure and control the heater hot zone. The maximum conditions at which this vessel was operated were 2350 F (1280 C) at 12,000 psi (82.7 MPa) for sixty minutes.

(4) It should be noted that both the furnace leads and gas connections were made through the lower closure. The location or type of the thermocouple lead throughs was not known by the author.

The Bettis Atomic Power Laboratory became interested in gas pressure bonding in 1957, having been made aware of the encouraging results achieved by Battelle in the bonding of Zircaloy and its application in fuel element fabrication.[26] From 1957 to mid-1959, the Bettis effort was primarily directed toward gaining information in installing their own pressure bonding facility and overcoming equipment and construction problems. In early 1959, Bettis did acquire a pressure vessel designed for 10,000 psi (68.9 MPa) service and a five-stage Hofer 15,000 psi (103.4 MPa) compressor from A/E. The vessel was 14-inch (35.56 cm) I.D. by 11 feet (335.2 cm) I.L. being made of Type 4340 steel with a Type 410 stainless steel helical grooved liner. It was, except for length, identical to the Battelle vessel. It was Bettis' idea to emulate Battelle's gas pressure bonding facility, except for its name which they called the "Pneumastatic Bonding Facility".[27,28]

Some of the more interesting features of this system and its operation are as follows:

(1) Bettis constructed their first three-zone furnace with a 6-inch (15.24 cm) square inside configuration of unknown length. The heater contained an inner Type 310 stainless steel square can having flat ceramic shells, containing the resistance elements, set against the outer surface. This heater assembly was then placed in an outer square container with insulation packed between them. Major furnace problems were encountered by Bettis having the inner can buckling and the outer can bloating. They purchased a more rigid round furnace of a similar design; a 7-inch (17.78 cm) I.D. by 92-inch (233.68 cm) I.L., three zone furnace for 1650 F (900 C) operation.

(2) To improve the hot zone, copper shot was used to fill the void space inside the heater around the specimen. This had little effect on the hot zone. However, improvement was observed with the packing, of the void space, with long metal (copper or steel) plates.

(3) Bettis was encountering pressure leaks and shorting with their multi-wire thermocouple lead-throughs. They tried placing a silver soldered bead on each of the wires supported by a nylon washer to prevent the slow extrusion of the thermocouple wire through the standard ceramic backup. They soon followed Battelle's lead and obtained ceramic (alumina) backups with the correct 14-gauge holes. They also tested 16-wire lead throughs (available only with 20-gauge wire and with lava sealants) but did not put them into service.

(4) Like Battelle, Bettis' personnel also observed signs of strong convection flows within the furnace, viewed by holes that were blasted through the tightly packed insulation.

(5) The Ceramowire-type thermocouples (metal sheathed couples) were used within the Bettis heaters; however, they were typically replaced after six cycles due to compacting or pinching of the sheath. They again followed Battelle's lead in using high purity sintered alumina double bore insulator tubes to provide electrical insulation for the thermocouple. These were then loosely placed inside metal (Type 304 stainless steel) protection tubes that were sealed, welded on one end.

(6) Following several cycles, all attempts to remove the upper full Bridgman large cover had failed. It was suggested that internal pressure might be used to help break the seal and slowly edge the upper cover from the vessel. The outer/upper nut was removed entirely from the vessel and all connections were removed from the upper cover. The vessel was then slightly pressurized with helium. Instead of the 400 pound (181.4 kg) cover slowly raising out of the vessel, it jumped from the vessel several feet, spewing insulation over the entire area. Bettis and Battelle soon went to a new upper cover with a double O-ring seal, as shown in Figure 15, on both the outer and newly designed 9-inch (22.86 cm) inner cover.

By 1960, satisfactory laboratory processing of Zircaloy-clad flat-plate compartmental UO_2 fuel element measuring 0.135-inch (3.43 mm) by 4-inch (10.16 cm) by 40-inch (101.6 cm) long and incorporating 350 fuel compartments had been demonstrated at Battelle.[29,30] Bettis started investigating the production feasibility of the gas-pressure bonding process for the manufacture of these elements for PWR-2, the second Shippingport PWR core loading. During the next couple of years, Bettis built the first gas pressure bonding production facility. They obtained two 10,000 psi (68.9 MPa) vessels, 212-inch (53.34 cm) I.D. by 14 feet (426.72 cm) inside length and furnaces.[31] They were successful in manufacturing PWR-2 elements, approximately 5-inch (12.7 cm) wide by 102-inch (259.1 cm) long. A detailed description of the system or its equipment has not been found by the author.

Nuclear development studies were beginning to fade in late 1962 and attention was being turned to the commercial development for the compaction of powders.

Battelle, in order to further pursue this technology and increase their size, temperature, and pressure capabilities, purchased two more vessels with associated compressors from A/E in 1962. The first vessel was rated for 15,000 psi (103.4 MPa) and had a 16-inch (406.4 mm) I.D. by 108-inch (274.32 cm) I.L. This vessel was installed at Battelle's Nuclear Site, to support continuing development programs. We wanted this facility to be an ultra-safe laboratory. The following precautions were taken with the design and operation:

(1) The vessel was placed into a 10-foot (3.05 m) I.D. by 20-feet (6.1 m) deep metal pit that had concrete reinforcement around its top and extending several feet down. Two sets of rails were installed on either side of this pit. The outer set of rails allowed for the mobility of an A-frame hoist and the inner to allow for a 24-inch (60.96 cm) thick, wood plank, sand, steel plate, and concrete blast shield to electrically move to cover the pit when the vessel was to be pressurized. There was also an explosion relief port directed toward an open field away from the control and compressor rooms.

(2) There was a high pressure line leading straight from the rupture disk assembly into a relief tank designed to receive all the helium gas from the empty pressure bonding vessel at 15,000 psi (103.4 MPa). Operation of the vessel was strictly limited to 10,000 psi (68.9 MPa) when processing nuclear materials.

(3) This vessel was designed similar to our 14-inch (35.56 cm) I.D. vessel in that it had a coolant liner and 2-piece upper closure. All gas inlets and lead-through openings were contained in the outer cover, so the inner head could be free from quick opening for 10-inch (254 mm) furnace access.

(4) All closure seals on this vessel were of the double O-ring carrier design. The carriers were made of an SAE 4340, the same as the vessel.

(5) Due to difficulties with the clogging of the coolant grooves in our other two internally cooled vessels, a closed loop heat-transfer oil cooling system was designed for this vessel. Its success lead to the change over, from water-soluble oil, to a new system using a commercial heat-transfer oil at our other laboratory. The pressure in the new system was controlled to keep the temperature range for the returning cooling fluid from the vessel at 120 to 180 F.

The second vessel, which was to assist in our new areas of project development, was rated for 50,000 psi (344.7 MPa) operation and was our first unit purchased as a packaged system.[32] This vessel was set into one of two new 10-foot (3.05 m) I.D. by 20-foot (6.1 m) deep pits that were contained in the expansion of our gas pressure bonding laboratory. Plans for a large 15,000 psi (103.4 MPa) vessel were being considered for the second pit.

Some of the most interesting features of this system are as follows:

(1) This externally cooled vessel, 9-inch (228.6 mm) I.D. by 108-inch (274.32 cm) I.L., was forged of a Modified 4340 steel and then autofrettaged.

(2) The vessel was designed with an upper and lower closure each containing a beryllium-copper double O-ring seal. The upper closure contained an inner closure, with the same type seal, for quick access to the heater.

(3) The vessel contained a graphite furnace, as shown in Figure 19. The heater was machined of a graphite tube containing a grooved portion approximately 8-inch (203.2 mm) long placed toward the middle of its 102-inch (259.08 cm) length. The current came through coolant cooled beryllium-copper electrodes in the upper closure, through the graphite heater tube, and out through coolant cooled electrodes in the lower closure. Concentric tubes of graphite and carbon with layers of carbon cloth and felt between them served as insulation for the vessel wall. Though argon appeared to be the more appropriate gas for this furnace, due to its low thermal conductivity, it soon became apparent that helium was more suitable.

Through the concerted efforts of Autoclave engineers and Battelle personnel, cycles were more or less performed on a routine basis at temperatures of 5000 F (2760 C), pressure of 20,000 psi (137.9 MPa) for periods of 1 to 2 hours. Some of the other unique features of this system and its operation are as follows:

(1) We discovered that if we were to have any success in obtaining a controllable hot zone in this heater, we had to prepressurize before heating. We found that a helium pressure of approximately 8,000 psi (55.2 MPa) would allow us to heat within our power capabilities and obtain a final pressure of approximately 20,000 psi (137.9 MPa) at 5000 F (2760 C). Power was supplied from a 240-volt, single-phase, 75 KVa line through a saturable core reactor to an impedance-matching, 4:1 isolation transformer.

To carry this high current, which reached 1450 amperes upon occasions, four size 0000 flexible cables were used for each electrode. The isolation transformer was set into the pit, near the vessel, to cut transmission losses to a minimum.

(2) Pressure was obtained for this autoclave by the use of a 36,000 psi (248.2 MPa) single stage Hofer booster compressor having a 950 scfh capacity. This compressor used inlet gas from a matched 15,000 psi (103.4 MPa) multistage compressor.

(3) The specimens were loaded into the hot zone of the graphite heater onto a graphite pedestal. The temperature was measured through a single crystal sapphire sight glass on the bottom of the pedestal by a Brown Radiomatic unit. This instrument measured the total radiant energy and converted it to a voltage which was then read out in degrees, starting at 1500 F (896 C) on a Honeywell universal recorder-controller. Temperature corrections were made for the error introduced by the sapphire window, but not the gas atmosphere.

(4) An early cycle incident occurred while testing this unit. We were measuring a pressure close to 20,000 psi (137.9 MPa) with no temperature being recorded. The author entered the pit with a safety harness in place. Peering up through the Radiomatic unit into the vessel, he saw a white hot surface. Shooting from the pit, all power was cut to the heater. Following let down and disassembly of the furnace, we found that the graphite heater's 1/2-inch (12.7 mm) grooves had completely collapsed from over temperature. Upon removal of the sapphire from its plug, it was observed that the sapphire had cracked on about a 45 degree angle, which allowed all the radiant energy to be directed away from the element in the Radiomatic unit. The Radiomatic unit was soon modified by attaching it to the lower cover with a precision-hinged mount so that the unit could be moved to one side. This allowed us to make observations, through a chain of front-surface mirrors to form a periscope, into the heater while a cycle was being performed by not entering the pit.

During late 1962, other organizations were becoming interested in developing their own gas-pressure-bonding facilities. These included the Oak Ridge Y-12 Plant, General Electric's Evandale Plant, Lawrence Radiation Laboratory, and B.S.A. Group Research Center, Birmingham, England.[33,34,35]

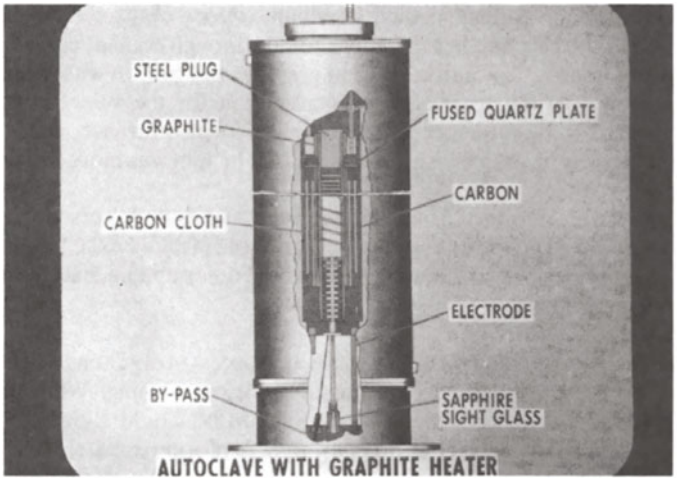

Figure 19. Sectional drawing of the graphite heater contained in a high-pressure autoclave.

GAS-PRESSURE BONDING EQUIPMENT
1963 THROUGH 1966

An additional 15,000 psi (130.4 MPa) vessel 27-inch (68.6 cm) I.D. by 108-inch (274.31 cm) I.L. and a six-stage piston type Hofer compressor were purchased by Battelle from A/E in November of 1963, shown in Figures 20 and 21. To replace the use of cylinders and to allow us to recycle the helium a new gas storage facility was designed and put into operation. By a step-down reclaim of the bonding vessels into each of the four banks of two tubes each, we could reclaim a large percent of the helium.

Figure 20. View of the 27-inch (68.6 cm) gas-pressure vessel within a 10-foot (3.05 m) I.D. pit.

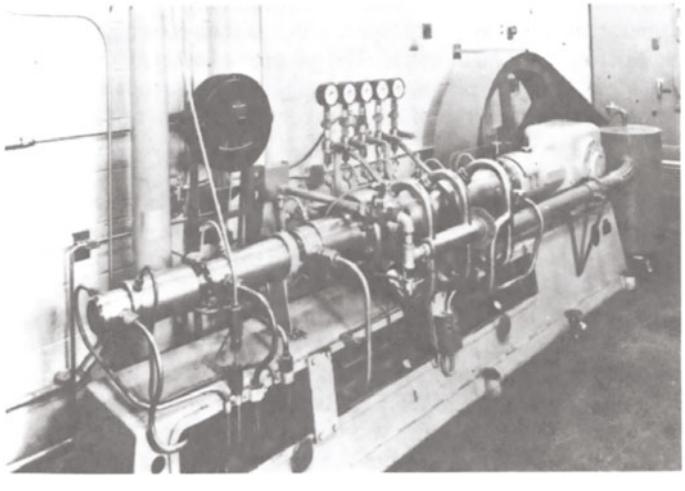

Figure 21. View of a Hofer multistage piston-type compressor, with a capacity of 4250 scfh at 15,000 psi (103.4 MPa).

The following are a few of the more interesting features of these units:

(1) Soon after placing our first vessel into operation, using helium, we observed overheating of the exhaust valve. This reverse Joule-Thomson effect with helium was of no real concern until we started gas reclaim. We solved this problem by placing a heat exchanger, coiled high pressure tubing in a coolant bath, just beyond the exhaust valve exit.

(2) The vessel was designed with ten 1/2-inch (12.7 mm) diameter beryllium-copper electrodes. Five 50 KVA silicon-controlled rectifier (SCR) units, a relatively new device, were acquired to control the five zone heater. The zones of this heater were electrically isolated from each other with the aid of an isolation transformer.

(3) Improved furnace designs of ceramic resistance type heaters were being designed for all Battelle vessels. There were three furnaces for this vessel, with heaters ranging in temperatures from 1800 F (982 C) to 3000 F (1650 C) with respective inside diameters of 13-inch (330.2 mm) to 8-inch (203.2 mm).

(4) We had experienced some oil carry-over into the pressurized gases, the amounts varying from each piston compressor and gas used. Double ended, pressure vessels, tightly packed with a glass wool material and backed up with a fine stainless steel screen, were placed into the pressurizing line just beyond the velocity oil separators on each compressor. These were frequently removed from the line, filler material removed, checked for signs of oil, cleaned and repacked. There was greater amounts of oil carry over observed when argon was used.

During this period, we at Battelle, were using 1/8-inch (3.175 mm) diameter electrodes, as thermocouple lead throughs for pressures above 15,000 psi (103.4 MPa). In the 50,000 psi (344.7 MPa) vessel, four electrodes were used for three Type-K thermocouples. We were trying a new thermocouple lead through in our vessel. It contained a sealant made of a dental compound, as we later discovered, and four wires for two Type B thermocouples. After several cycles to 30,000 psi (206.8 MPa), it failed. The helium pressure, coming out of this approximately 1/8-inch (3.19 mm) diameter sealant, was at atmospheric in less than 60 seconds. In so doing, it picked up some of the Microquartz and alumina. The gas eroded away all the sealant and the threads of the gland, slicing it into three pieces, while cutting out the threads and a half-inch V-notch in the upper cover. The three sections of the gland dented but did not penetrate the sheet metal roof.

Following this incident, a test bunker was built in back of the gas pressure lab. The full testing of all new vessel components was completed before allowing them to be used in the vessels. We ran both high pressure hydrostatic and gas lines into this bunker.

Helium gas was still being used for pressurization in most applications. Experience to this time indicated that helium presented less severe problems with control of the hot zone and convective circulation within the vessel than did argon. Heat flow analyses of these systems were undertaken by Battelle and others.[32,36,] At Battelle, a cylindrical glass condenser, to simulate a furnace, was immersed in water which was contained in a large glass vessel used to simulate the autoclave. This unit was set-up to study the flow patterns in a pressurized gas system. The simulated autoclave was filled with water to simulate the pressurized helium gas, with the simulated furnace being totally immersed. Steam was fed through the condenser as the heat source. The flow patterns were traced by the injection of dye, and temperature gradients

recorded. The general arrangement and a typical flow pattern observed in shown in Figure 22. The results of the water analog study were extended in one of the gas-pressure bonding vessels using 24 thermocouples to record the temperature gradients. The indicated results supported the existence of convective gas flow through the furnace and vessel. It was observed that the degree of convective flow was greater in bubble alumina insulation than in densely packed Microquartz.

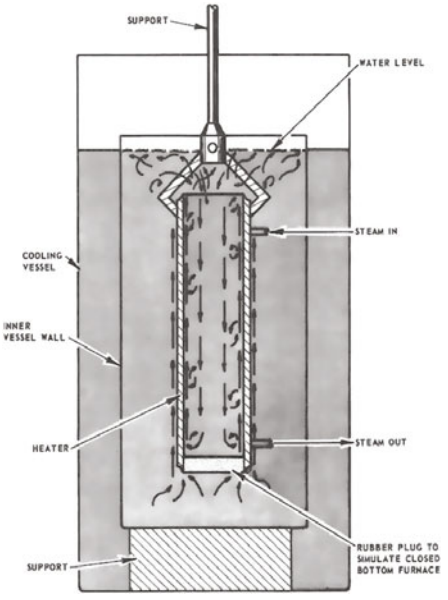

Figure 22. Illustration of a flow pattern in the water analog.

From the developmental heat flow studies, it was concluded that convective flows within the furnace and vessel had to be stopped or minimized if an acceptable hot zone was to be achieved. The development of the inverted container furnace seemed to meet the requirements. A three zone furnace of this design, illustrated in Figure 23, was built using molybdenum wire wrapped on a high-purity alumina tube. This furnace was placed into our 50,000 psi (344.7 MPa) vessel.

Cycles using this inverted container-type, 3-inch (76.2 mm) diameter by 30-inch (76.2 cm) long molybdenum furnace were routinely made at 3180 F (1750 C) and 30,000 psi (206.8 MPa) for periods up to 3 hours, with a 16-inch (406.4 mm) hot zone.[32] A 50:50 moly-rhenium wire, used in place of the molybdenum wire, performed with great success and long life. Heaters could be rewound with wire that had been used to temperatures of about 3000 F (1650 C).

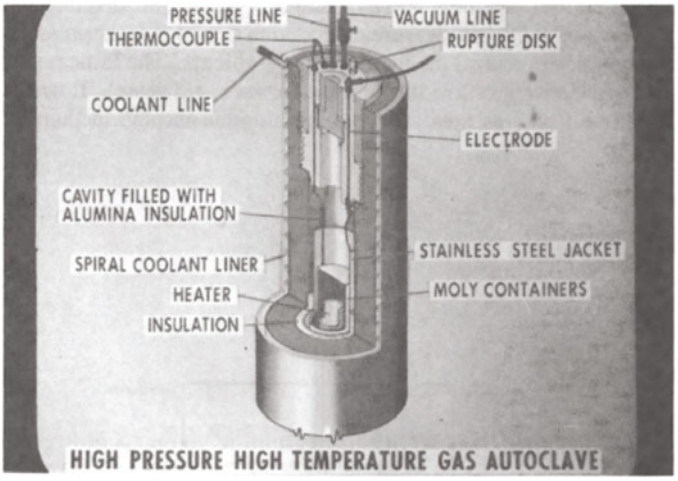

Figure 23. A sectional drawing of a molybdenum-wire-wound tube heater with an inverted container.

At the end of 1963, work in the area of pressure bonding and compaction were being carried out in Europe. The B.S.A. Group Research Center in Birmingham, England, after considering various types of pressure apparatus, did determine that a cold-wall autoclave would satisfy their requirements of 10,000 to 15,000 psi (68.9 to 103.4 MPa) at 2192 to 2732 F (1200 to 1500 C).[35] They designed a vessel, built by Messrs. Hadfields Ltd., Sheffield, of an EN24 material with an internal cooling chamber. It had a 10-inch (254 mm) I.D. by 23-inch (584.2 mm) I.L. It contained a molybdenum wire ceramic tube heater 3-inch (76.2 mm) I.D. by 23-inch (584.2 mm) long. The unit was designed to operate in a horizontal position to ensure minimum heating of the end-closures by gas convection and for general convenience in operation. They did, however, mount the vessel in a cradle pivoted at its center on trunnion bearings. The unit was run in a vertical position with some modifications. The CEA, in France, also purchased a gas-pressure bonding production system from A/E. The vessel was rated for 14,300 psi (98.5 MPa) at 1832 F (1000 C) and had threaded closures.[37] The French also elected to position and operate this vessel in a horizontal position. The vessel, after several unsuccessful cycle attempts, was placed into a vertical position for its future operation.

By 1964, efforts by a staff engineers at Union Carbide's Oak Ridge Y-12 Plant had started the conversion and modification of a large existing 30,000 psi (206.8 MPa) isostatic pressure vessel into a gas pressure bonding system.[33] After modifications were completed, the converted vessel had a 28-inch (71.12 cm) I.D. by 46-inch (116.84 cm) I.L. The decision was made to lower the operational pressure to 20,000 psi (137.8 MPa). A similar vessel to this gas pressure bonding vessel had failed in 1956 under a hydraulic pressure of approximately 28,500 psi (196.5 MPa).[38,39] A few interesting features about this system are as follows:

(1) The furnace design team at Y-12 took an approach diametrically opposite to other facilities. Instead of minimizing convection currents, they attempted to maximize them. They designed a furnace that consisted of a 3-phase bottom plate ribbon element heater having a 17-1/2-inch (44.45 cm) I.D. by 50-inch (127 cm) I.L. Over this heater was placed two insulated metal bell jars. Within these jars, an inner metal shell was placed to allow the convection currents to freely move during heat up for a fast

response. At hold conditions, these currents were to slow down to give a desired hot zone.[40,41] It was later reported that at 1833 F (1000 C) and 15,000 psi (103.4 MPa), they did have to decrease the heater height, obtaining an excellent hot zone in a 16-inch (40.64 cm) I.D. by 16-inch (40.64 cm) high heater.[42]

(2) The Y-12 engineering staff elected to use argon as the gas for this gas-pressure bonding system. They selected to use a cryogenic pump that was designed and built by the Cosmodyne Corporation.[43] The 20,000 psi (137.9 MPa) intensification unit pumped at a rate of 1.8 gpm/200 scf/m. It was reported to be a very trouble-free means to pressurize the vessel.

(3) This vessel was mounted in a reinforced concrete containment cell approximately 16 by 16 by 45 feet (4.88 by 4.88 by 13.72 m) high.

(4) Engineers at Y-12 were concerned with the long pressurization and heating cycles required for the gas-pressure bonding process, along with its expense and hazardous operation. They proposed a hydrostatic hot pressing system. This was accomplished by high-pressure oil acting directly on a heated specimen via a sand medium. Temperatures of 5432 F (3000 C) and pressures of 15,000 psi (103.4 MPa) were reported to have been used.[44] After considerable experimental effort, this compaction process was abandoned.[43]

In this period, gas pressure bonding took on a new name, hot isostatic processing (HIP). At the same time, it began to be recognized as a viable materials processing method and developed into commercial applications.

Fully dense structures of refractory metals, stainless steel, ceramic, carbon and beryllium powder and electronic component materials were achieved.[45] The more notable process development at this time frame was the hot-isostatic compaction of spherical tungsten powder to a fully dense structure.[48] This brought about the installation of a commercial hot-isostatic system at Allied Chemical Companie's Baton Rouge Plant. The system had a 15,000 psi (103.4 MPa) vessel, 36-inch (91.5 cm) I.D. by 108-inch (274.3 cm) I.L. This vessel, for the first time, utilized the Autoclave Engineers' resilient spring closure (Gasche Resilient Thread).[47] It contained a cooling liner and had upper cover cooling capabilities, as shown in Figure 24. All three closure seals were of the double O-ring design, using Viton O-rings. The system installation was modeled after Battelle's laboratory. Due to the high water table, great difficulty was encountered in the construction of their 10-foot (3.05 m) I.D. by 20-foot (6.1 m) deep pit.[48]

In 1964, additional HIP systems were installed in several government laboratories. Four of these HIP systems are as follows:

(1) The General Electric Company's, Hanford Atomic Products Operation, installed a HIP system manufactured by Pressure Products Industries, Inc. (PPI). It had a 20,000 psi (137.9 MPa) vessel 10-inch (25.4 cm) I.D. by 28-inch (71.1 cm) I.L. The vessel had two threaded upper closures and a one piece lower closure, using an O-ring, with a metal wedge for back up, on all three closures. It contained a cooling liner and a special cooling unit opening in the upper outer closure. This device, which consisted of two concentric tubes and some seven seals, was to allow the helium to be cooled during reclaim. Soon after being placed into operation, the vessel which was under

vacuum, filled with coolant leaking from this unit. Steps were taken to remove the device and to cool the helium external to the vessel. A single PPI, two-stage diaphragm compressor was used to pressurize this GE system.[49]

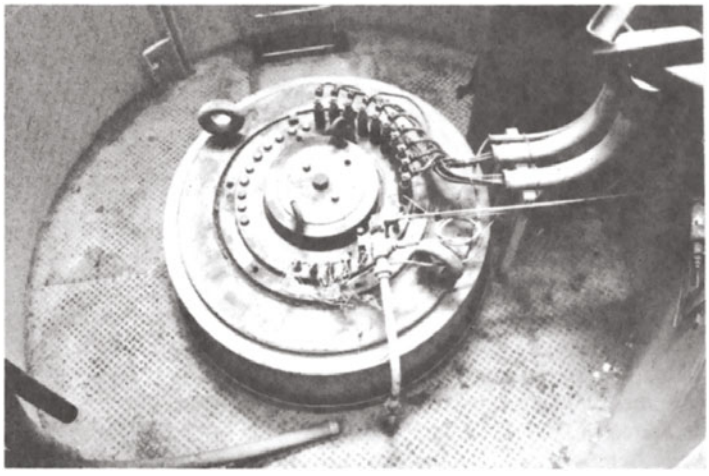

Figure 24. Autoclave Engineers first resilient thread closure vessel, as installed at Allied Chemical. It had a 36-inch (91.5 cm) I.D. rated for 15,000 psi (103.4 MPa) (Courtesy of Autoclave Engineers Group)

(2) Another similar HIP system by PPI was installed at the NASA Lewis Research Center. This system contained a 50,000 psi (344.7 MPa) vessel having a coolant liner and two upper threaded closures and a single lower closure; all using the single O-ring with a metal wedge ring. The vessel measured 12-inch (30.48 cm) I.D. by 42-inch (106.7 cm) I.L. and contained a 3-inch (76.2 mm) by 32-inch (81.28 cm) long furnace.[50] Two PPI diaphragm compressors were used for pressurization of this system.

(3) The Lawrence Radiation Laboratory installed two HIP systems built by A/C. One system was a 16-inch (40.64 cm) I.D. by 108-inch (274.32 cm) I.L. for 10,000 psi (68.9 MPa) vessel and the other a 18-inch I.D. (45.72 cm) by 72-inch (182.88 cm) I.L. for 50,000 psi (344.7 MPa) vessel.[51] Both these vessels were placed into individual pits, which were housed in reinforced-concrete cells. The cells had fully automatic ventilation systems. The first system was pressurized with helium by an air-driven 10,000 psi (68.9 MPa) Haskel piston compressor and the second utilized a five-stage 15,000 psi (103.4 MPa) Hofer piston compressor and a single stage 50,000 psi (344.7 MPa) Hofer booster to obtain pressure. The first vessel contained a 3-zone resistance heater, while the second a 5-zone resistance heater. Both heaters used SCR power units and the second included an automatic Trendtrack unit for programming. An LRL incident was reported pointing out the danger of compressed fluids. An employee placed his finger over the end of a 6,000 psi (41.36 MPa) helium line, to determine if the line was plugged. The gas punctured his finger and inflated the tissue of his left arm to almost twice its size. Because it was helium, it soon permeated the tissue and skin with no permanent damage reported.[52]

(4) The Argonne National Laboratory installed and placed into operation a 50,000 psi (344.7 MPa) A/E-HIP system.[53] This composite wall vessel had internal cooling and was 13-inch (33.02 cm) I.D. by 75-1/8-inch (190.82 cm) I.L. It had two upper covers

and a single lower cover as had become more or less standard at this time for top loading units. A/E had designed and supplied new electrodes and T/C assemblies. The 1/2-inch (12.7 mm) diameter fluid cooled Berylco electrodes had a silicon impregnated spun glass insulation and a combination of Teflon, Dilecto, and steel sealing washers. The T/C assembly was constructed of a steel plug, with a single O-ring seal, and a gland nut. In the steel plug were brazed four steel sheathed, platinum versus platinum 10 percent rhodium compensated lead wires. Both of the above assemblies were hydrostatically tested to 75,000 psi (517 MPa). The system was pressurized, with a six-stage Hofer piston compressor, to 15,000 psi (103.4 MPa) and a single stage Hofer booster compressor on up to 50,000 psi (344.5 MPa). Their three zone molybdenum furnace was wired for two 12 KVA and one 100/50 KVA, 1 phase, 60 cycles saturable reactors, and controlled by three Series 620 SCR Barber-Colman Company power controllers.

The period of 1963 and 1966 brought about a number of changes and improvements in the components that go to make up a HIP system. The equipment manufacturers began to engineer and offer complete packaged HIP systems. In addition to Autoclave Engineers, Inc., and Pressure Products Industries, Inc., other high pressure manufacturers started supplying HIP systems. These included the National Forge Company, American Instrument Company, Harwood Engineering Company, Inc., and most notably, due to its unique wire wound design, ASEA, as illustrated in Figure 25.

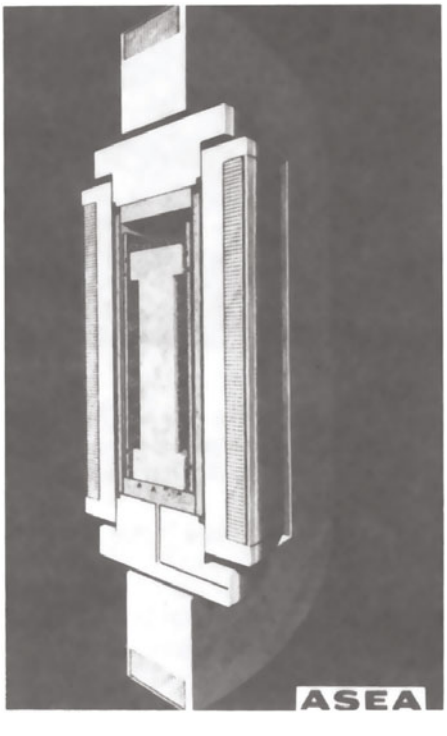

Figure 25. Sectional view of a wire-wound pressure vessel and supporting frame. (Courtesy of ABB Metallurgy AB)

The first hot isostatic press built by ASEA, in 1965, was intended for operation for both HIP with an argon pressure of 29,000 psi (199.9 MPa) and cold isostatic processing (CIP) with a fluid pressure of 46,000 psi (314.1 MPa). The cylinder was wire wound, with threaded closures. ASEA had used this design, in 1939, to build the world's first wire wound press for development of synthetic diamonds. This HIP/CIP press, as shown in Figure 26, was used at ASEA's high pressure laboratory in Robertsfors, Sweden, for development of materials and machine technology. For HIP operation, it contained a 2640 F (1450 C) molybdenum furnace, having a hot zone 9-inch (228.6 mm) I.D. by 4 3-inch (109.2 cm) I.L.[54]

Figure 26. The first HIP press built by ASEA. The cylinder was wire-wound with threaded closures.
(Courtesy of ABB Metallurgy AB)

Battelle had undertaken and assisted Alcoa in a program to heal the defects in aluminum castings. Significant improvements were shown in the aluminum castings processed by HIP. Alcoa was granted a patent on the process but did not place it into commercial practice.[55] Alcoa's management, at this time, was unsuccessful in locating an equipment manufacturer who would build a large enough vessel to make HIP'ing of aluminum profitable.

In 1965, Kennametal, with Battelle's assistance, began its adaptation of the HIP process to the improvement of tungsten carbide parts.[56] With the application of HIP, internal porosity was removed, improving the properties of cemented carbide parts and in many cases, eliminating pits and flaws. Kennametal purchased their first production HIP system from A/E in 1967 under

strict secrecy.[38] They called their process KEZIZ. Their first vessel, shown in Figure 27, was of monoblock construction with an external cooling jacket and the usual threaded closures arrangement. The 20,000 psi (137.9 MPa) vessel was 24-inch (60.95 cm) I.D. by 140-inch (355.6 cm) I.L. and contained a moly furnace having a hot zone at 2700 F (1483 C) of 10-inch (25.4 cm) I.D. by 50-inch (127.0 cm) long. Kennametal started their KEZIZ (HIP) manufacturing operation in 1967.[57]

Figure 27. The loading of a tungsten carbide part into one of Kennametal's KEZIZ vessels. (Courtesy of Kennametal, Inc.)

The General Electric's Evandale Plant purchased a HIP system, for the experimental compaction of metal and cermaic powders, from the Harwood Engineering Company, Inc. in 1966.[58,59] The dimensions of the 10,000 psi (68.9 MPa) are not known, but it contained a molybdenum furnace with a 3000 F (1650 C) hot-zone 5-inch (127 mm) I.D. by 24-inch (60.96 cm) long. A 2-stage Harwood compressor was used to pressurize the vessel with helium.

Around this same time period, the Materials Department at A.W.R.E., England, after obtaining some experience with a small laboratory-scale isostatic hot pressing unit, purchased a large installation from an American manufacturer. The vessel was 26-inch (66.04 cm) I.D. by approximately 6-feet (1.83 m) I.L. and was internally cooled by pumping an oil and water mixture through the helical passages of a liner shrunk into the inside of the main cylinder. The vessel had the usual two upper threaded closures and one bottom threaded closure. As a safety precaution, they designed a yoke which surrounded the vessel to retain the end plugs in the event

of a thread failure. Helium, after first being unsuccessful using argon, was used to pressurize the vessel to 10,000 psi (68.9 MPa) using a five-stage Hofer piston compressor. A three-zone molybdenum furnace with a hot-zone of 6-inch (152.4 mm) I.D. by 48-inch (218.4 cm) long was supplied with the system. They experienced difficulties in temperature control due largely to uncontrolled gas convection currents. A.W.R.E., as an example, made one run with a charge of steel bars, melting point 2642 F (1450 C), that melted despite the fact that none of the thermocouples adjacent to the bundles of rods indicated temperatures in excess of 2282 F (1250 C). While the supplier of the system was attempting to rectify the performance of the furnace, A.W.R.E. engineers developed their own furnace. Several practical considerations indicated that it would be advantageous to mount the vessel and furnace with their axes horizontal, as the small scale vessel had first been mounted. Using a vertically-mounted, well-baffled, multi-zone furnace, insulated with fine dense alumina powders and tightly packed ceramic wool, they achieved some success.[60]

It should be noted that A.W.R.E., while making test cycles, experienced a similar thermocouple plug incident to that at Battelle. They reported that while at 10,000 psi (68.9 MPa), a thermocouple plug developed a leak and the escaping gas carried with it some of the fine alumina powder from within the top of the vessel. This quickly ground the inside of the base of the coupling away and pierced the barrel of the plug in three places. The scouring became progressively more rapid until finally, the ceramic insets were blown from the coupling and these, together with the jet of abrasive powder, quickly pierced and eroded a large hole in the hardboard ceiling and corrugated aluminum roof, about 10 feet (3.05 m) away.

In early 1966, Battelle again expanded their HIP facility and obtained another vessel to increase their capabilities. A 20-inch (50.8 cm) by 108-inch (274.3 cm) I.L., 30,000 psi (206.8 MPa) vessel purchased from the National Forge Company, as shown in Figure 28. This was this manufacturers first HIP vessel. It was soon placed into operation, but was limited to a maximum pressure of 15,000 psi (103.4 MPa). At this time, there were no multi-wire lead-throughs available for pressures above 15,000 psi (103.4 MPa). This problem was solved by placing a 24-point rotary switch inside the vessel, synchronized to a 24-multipoint recorder, outside the vessel. To obtain up to 24 thermocouple readouts from within the vessel required only five electrical lead-throughs.[61,62]

Several attempts were made to make our first 30,000 psi (206.8 MPa) cycle in this vessel; however, at a pressure of around 19,000 psi (301 MPa), a leak would develop in the lower closure. After careful examination, it was discovered that during the hydrostatic testing at 45,000 psi (310.2 MPa), an unsupported area in the coolant liner had yielded. This was an area where the helix-groove joined the cylindrical outlet groove and just happened to be in the exact location of the lower O-ring seal. It should be noted that the O-ring was backed up with a metallic wedge ring. A new cooling liner was designed with the same groove diameter but with a modified junction. After replacement with the new liner, excellent results were achieved with this vessel. We were continuing to bring all gas, thermocouple and electrical convections out the top of the vessel. this vessel also had an outer cover, containing lead throughs, and a quick-opening work loading cover. The small inner cover had an interrupted buttress thread and a 3/4-inch (19.05 mm) diameter vacuum port with valve.

In addition to the Battelle HIP vessel, National Forge Company also supplied HIP systems to two other laboratories; a 30,000 psi (206.8 MPa) system for 2500 F (1371 C) operation to the Boeing Company and a 50,000 psi (344.7 MPa) system for 3000 F operation to the Bell Telephone Laboratories.[63]

Figure 28. A 30,000 psi (206.8 MPa) HIP vessel designed and built by the National Forge Company. Note: the interrupted thread on the small closure.

At Battelle, the development of more reliable furnaces with greater size capability was again given high priority during this period. Furnaces were constructed at Battelle utilizing ceramic insulator units and molybdenum elements to obtain temperatures of 2800 F (1538 C) to 3000 F (1649 C), with hot zones 10-inch (254 mm) diameter by 36-inch (88.9 cm) long.(64] A furnace was designed and patented which utilized the inverted container concept and metallic construction, eliminating the dependence on a ceramic muffle support.[65] This so-called "spool-type furnace", as illustrated in Figure 29, created a controllable and reliable hot zone which occupied a larger portion of the vessel cavity. The furnace was 18-inch (45.7 cm) I.D. by 64-inch (162.6 cm) I.L. and had a hot-zone length of over 48-inch (121.9 cm) at 1900 F (1038 C) and 15,000 psi (103.4 MPa).

Some innovations or information that were developed and put into practice by Battelle for various research and development programs were as follows:

(1) A method to out-gas specimen containers, through the upper vessel cover, during pressure compaction.

(2) A method to hot-isostatically form sheet materials.[66]

(3) Though it was of questionable value, a transistor radio, with antenna, batteries, and speaker outside, was placed inside a vessel and taken to 10,000 psi (68.9 MPa). It performed well to about 8,000 psi (55.1 MPa), then faded. On depressurization, it again began playing at approximately 7,000 psi (48.3 MPa). It continued to play for many years.

(4) Development of a method to perform high pressure melting and casting, within the HIP unit, was demonstrated.

(5) A device was designed and placed into practice to hot load and unload an idling HIP furnace through the upper vessel opening. This unit was used several times to load and unload large beryllium components.[67]

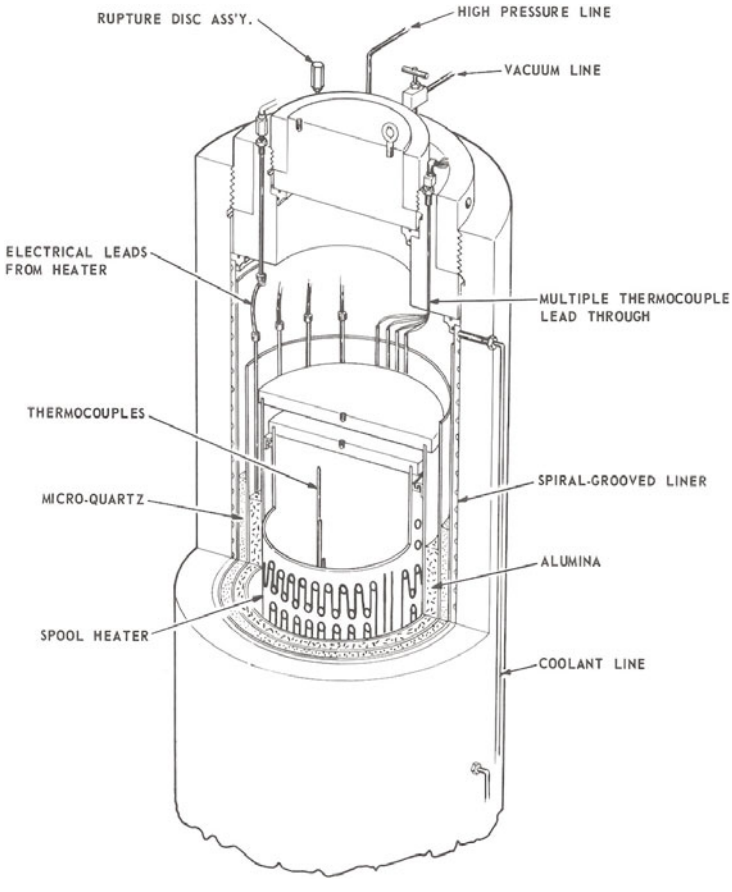

Figure 29. Battelle's spool-type furnace.

(6) Developed the plug-in furnace concept, which allowed for the insertion and removal of furnaces from within a vessel, with no manual connection required. This concept was first placed into practice in the internally cooled 9-inch (228.6 mm) vessel.[62]

(7) For a production application, the concept of multiple-furnaces for a single HIP vessel was proposed as illustrated in Figure 30. This allowed one furnace to be unloaded and reloaded with parts while the second furnace was being HIP cycled. The idea was further developed to include both hot-loading and hot-unloading of a HIP vessel using multiple furnaces.[62]

(8) During this time period, the idea of bottom-loading a HIP vessel was considered. This approach was discussed with an ASEA engineer as one method to keep the molybdenum inverted containers in place during loading. The idea was later developed and placed into practice by ASEA.[68-72] It was also developed later by Battelle in its modular inverted-container design furnaces.[73]

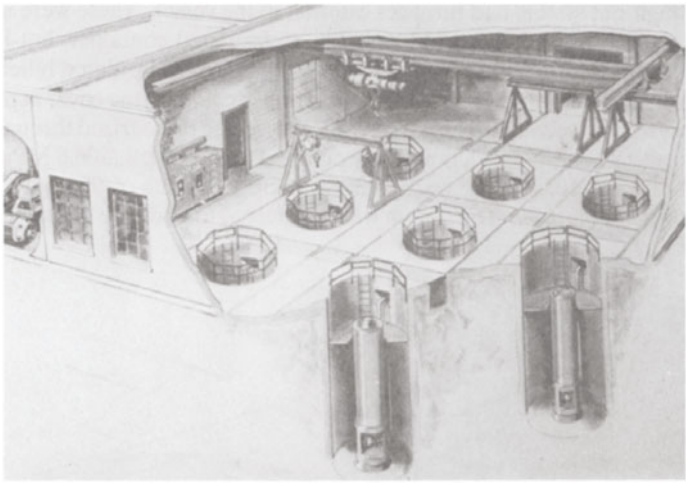

Figure 30. Illustration for a proposed production application.

(9) One of the hot wall vessels was modified to perform hot-gas extrusion. This isostatic method of extrusion was successfully carried out on both copper and 1100 aluminum materials. No further development was carried out due to lack of interest in the process in the United States. There was an interest in Russia for the application of hot-gas extrusion, as discussed by L. F. Vereschagin, Institute for High Pressure Physics, U.S.S.R., at the III AIRAPT International High Pressure Conference held in Aviemore, Scotland.

(10) An isostatic pressure transmitting apparatus was designed and placed in operation in our 30,000 psi (206.8 MPa) HIP vessel. This unit allowed us to perform needed hydrostatic compaction within this vessel without any contamination and allowing quick turn-around between hot isostatic and hydrostatic processes.[74]

(11) As early as 1964, Battelle's personnel had started performing in-house engineering studies to determine if HIP vessel sizes could be increased. During this time period, however, with the commercialization of HIP being realized, Battelle's efforts were expanded into the feasibility of considerably larger hot isostatic pressing than had previously been considered.[73]

HOT ISOSTATIC PROCESSING (HIP) EQUIPMENT 1967 THROUGH 1969

The HIP process was beginning to receive worldwide recognition and with this came many ideas for its possible utilization for new processing applications. Many of these processing applications would require unique use or changes in the HIP equipment.

During the previous couple of years, Battelle had worked with the Crucible Steel Materials Research Center to develop HIP to fully dense compacts of their atomized high-speed tool steel powders. This being accomplished, Battelle set about to assist Crucible in the development of an economical P/M production HIP method.[75,76] This brought about the development of the rapid through-put system in 1967. Working with A/E, a pin-closure vessel was designed, built, and installed at Battelle.[37]

The rapid through-put system had furnaces external to the vessel. These were used to heat the process billets, which were then encompassed in an insulated container, hot-loaded into the vessel for rapid compaction and hot unloading.[77,78] Once the insulated billet was within the vessel, the automatic hydraulic head handling mechanism could set the cover in place and secure it by a pin in less than 45 seconds. The process vessel was then pressurized through high pressure valves from an accumulator vessel, previously pumped to 30,000 psi (206.8 MPa), to a working pressure of 15,000 psi (103.4 MPa) in 20 to 30 seconds. A sketch of this system was set up at Battelle as shown in Figure 31. The system was transferred to Crucible's commercial operation in 1968.[79]

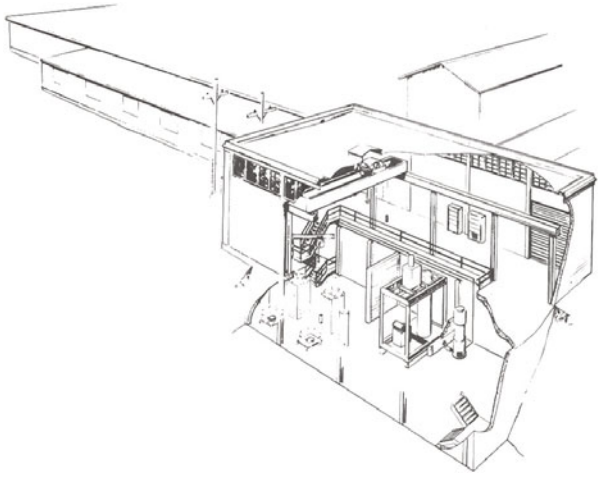

Figure 31. Illustration of Crucible's rapid through-put system as set-up at Battelle.

During this period, A/E sold three more research and development systems as follows:[37]

(1) A low pressure, 2,200 psi (15.3 MPa) at 1832 F (1000 C), HIP system was delivered to GE, Evandale for diffusion bonding of titanium hollow turbine blades.

(2) The Union Carbide's Oak Ridge Plant received a 22,000 psi (151.7 MPa) HIP system rated for 1832 F (1000 C) to perform carbon impregnation applications.

(3) The most interesting HIP system delivered at this time had a pressure vessel rated for 150,000 psi (1033.5 MPa) operation. The vessel delivered to Battelle was 3-inch (76.2 mm) I.D. by 24-inch (6.10 cm) I.L. and contained a 1-inch (25.4 mm) diameter furnace with a 3-inch (76.2 mm) long hot zone at 2300 F (1260 C). For safety considerations, this vessel was placed into one of our deep pits and set into a trunnion stand for vertical loading, but horizontal operation. Due to the small diameter and short hot zone required for our experiments, the horizontal operation to pressures of 120,000 psi (827.2 MPa) were successful. Pressurization was achieved with a reciprocating intensifier, high pressure check valves, and a 50,000 psi (344.7 MPa) accumulator vessel. To use this system, both the HIP and accumulator vessels were pumped to 50,000 psi (344.5 MPa) before utilizing the intensifier. Even with the relatively small volume of the intensifier, it took only a few strokes to reach the pressure of 120,000 psi (827.2 MPa).

ASEA had also supplied HIP systems for research and development to the following:[54]

(1) The first HIP system with a wire wound cylinder and frame, to take the axial forces instead of threads, was delivered to ASEA's own lab in 1969, shown in Figure 32. It had a hot zone of 6.3-inch (160 mm) by 11.8-inch (300 mm) I.L. for a temperature of 2640 F (1450 C) at a pressure of 45,000 psi (310.2 MPa).

(2) A HIP system, almost identical to the one manufactured for their own lab, was delivered to the Kelsey Hayes Company in the United States in early 1970.

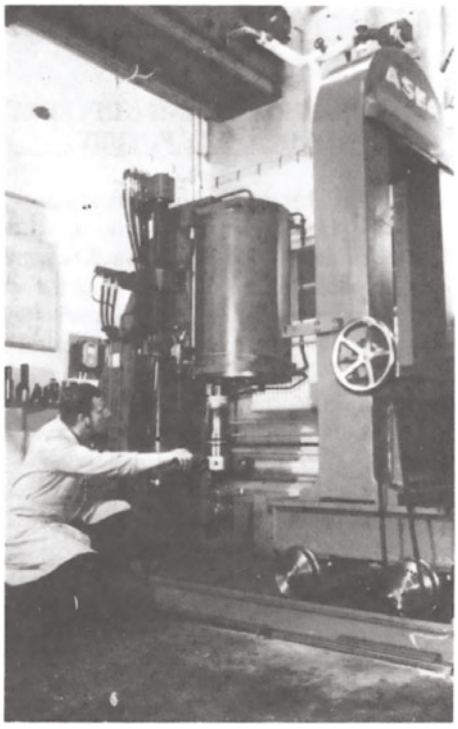

Figure 32. ASEA press installed at their lab in Robertsfors, Sweden. Wire-wound cylinder and frame. (Courtesy of ABB Metallurgy AB)

The National Forge Company, during this period, also delivered HIP systems for research and development to the following:

(1) A HIP system was supplied to the General Electric Company in Cincinnati, Ohio, in early 1968. The vessel for this system was externally cooled with threaded closures on both ends. Its inside dimensions were 16-inch (40.6 cm) I.D. by 60-inch (152.4 cm) I.L.

(2) A total HIP system was provided to Industrial Materials Technology, Inc. (IMT) on January 15, 1968 for R&D processing. However, IMT and the National Forge Company soon established a joint venture to offer what was probably the first independent toll-HIP facility in the world.[80] This system had an internally cooled double-ended threaded closure vessel, for 15,000 psi (103.4 MPa), having a 14-1/8-inch (36.2 cm) I.D. and 48-inch (121.9 cm) I.L. It contained a furnace with a 2500 F (1371 C) hot zone 9-inch (22.9 cm) I.D. by 17-inch (43.2 cm) I.L. It was pressurized with a Hofer 15,000 psi (103.4 MPa) piston compressor.

In 1969, additional interest was being shown for the HIP process. A greater interest by both HIP users and manufacturers was seen in the continued development and improvement of HIP equipment. These included advancements in the processing, components, furnaces, controls, vessels, and systems.[81-94]

HOT ISOSTATIC PROCESSING (HIP) EQUIPMENT 1970 INTO THE FUTURE

From February 1956 to the end of 1969, the author had a hands-on working experience with both Battelle's HIP equipment and most of the other installations. After this period, however, with other responsibilities and the expanded numbers of HIP facilities, my direct involvement became impractical. The seventies, also, brought on a broadening of the scope of both the application of HIP and its equipment. It seemed appropriate, with these statements in mind, to bring this reporting on the history of HIP equipment to a close with the end of 1969.

In conclusion to this paper, it should be understood that the progress and development of HIP equipment, from 1970 to the present, has been well documented.[12,95-97] It will, however, remain for others to compile these into a historial format, possibly into a book.

A few of the high points, as seen by the author, will be briefly presented as follows:

(1) The interesting account of the ASEA-STORA plant for the manufacture of large tool steel billets by means of gas atomized powders and HIP compaction.[54,98,99] Figure 33 shows an exploded view of the facility at Stora Kopparberg.

(2) The installation and operation of the large HIP system at Battelle, as shown in Figure 34, with its successful transfer to the Crucible Compaction Metals operation.[73,100] The A/E-designed vessel contained a Battelle-designed 48-inch (122 cm) I.D. by 115-inch (292 cm) I.L. furnace for 2300 F (1260 C) operation at 15,000 psi (103.4 MPa).

(3) The modification of the HIP equipment to perform the high-pressure impregnation/carbonization process (HiPIC). The first systems were developed and placed into operation at Oak Ridge and Battelle.[101.102]

(4) The installation and operation of the A/E HIP system at Henry Wiggin, a Division of International Nickel. The system, as installed, had a row of three preheat furnaces plus a cold-loading station in line with the 15,000 psi (103.4 MPa) vessel. Used primarily to consolidate superalloy powders.[96]

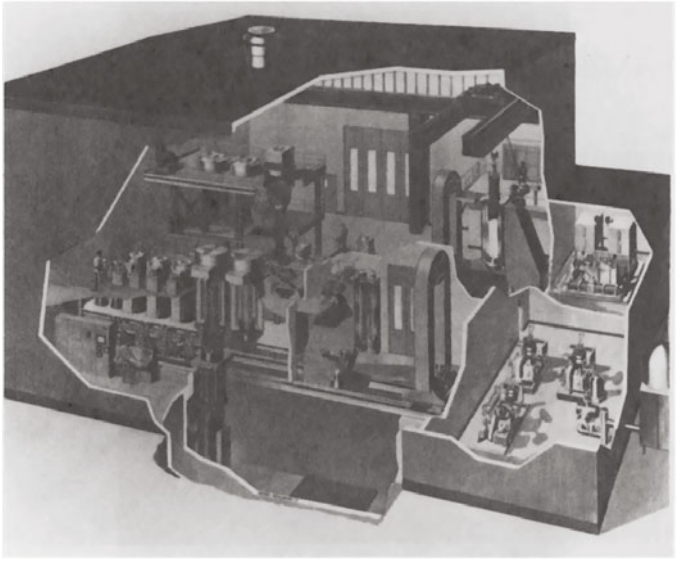

Figure 33. Illustration of the ASEA-STORA HIP facility used for the production of high-speed toolsteel from powder. (Courtesy of ABB Metallurgy AB)

(5) The large HIP system placed into operation by ASEA at Pratt & Whitney was transferred to the Howmet Corporation's Whitehall HIP Division. This wire-wound vessel and supporting frame presently contains a 51-inch I.D. (129.5 cm) by 73-inch (185.4 cm) I.L. furnace for operation at 2280 F (1250 C) at 29,000 psi (200 MPa), as shown in Figure 35.[96,103]

(6) The interest shown in HIP by Japanese users and equipment manufacturers has had a steady growth since 1973.[104,105] Kobe, as the leading HIP manufacturer, has developed many innovative HIP systems and associated equipment, as were presented at the 6th HIP Seminar at Kobe Steel in November 1986.

(7) IMT's installation of the world's largest HIP system, Figure 36, having a 15,000 psi (103.4 MPa) vessel with a 76-inch (193.1 cm) I.D. by 160-inch (406.4 cm) cavity. The vessel contains a furnace, capable of temperatures to 2350 F (1288 C), with a hot-zone of 64-inch (162.6 cm) I.D. by 120-inch (304.8 cm) I.L.[106]

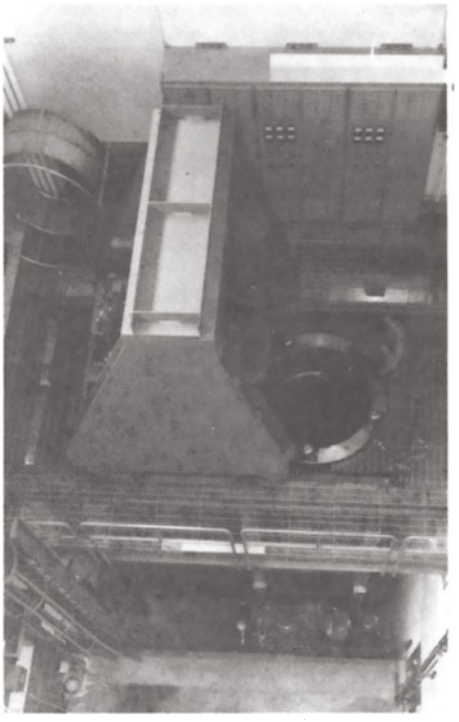

Figure 34. The large HIP vessel, as installed at Battelle, to be transferred to the Crucible Compaction Metals Operation. (Courtesy of Crucible Steel)

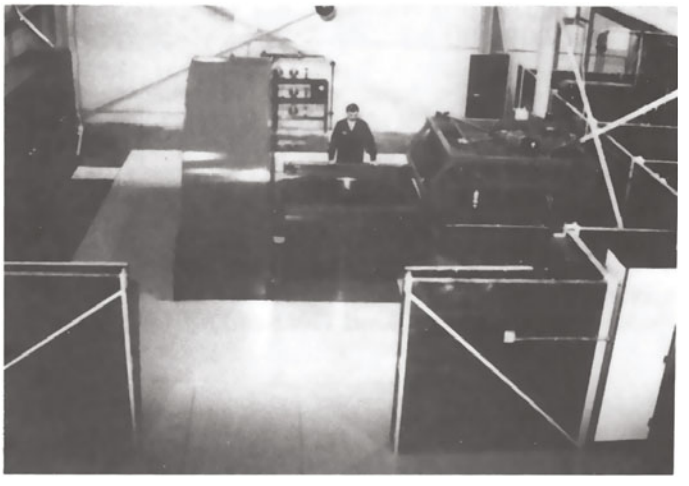

Figure 35. View of Whitehall HIP Division's large production HIP vessel. (Courtesy of Howmet Corporation)

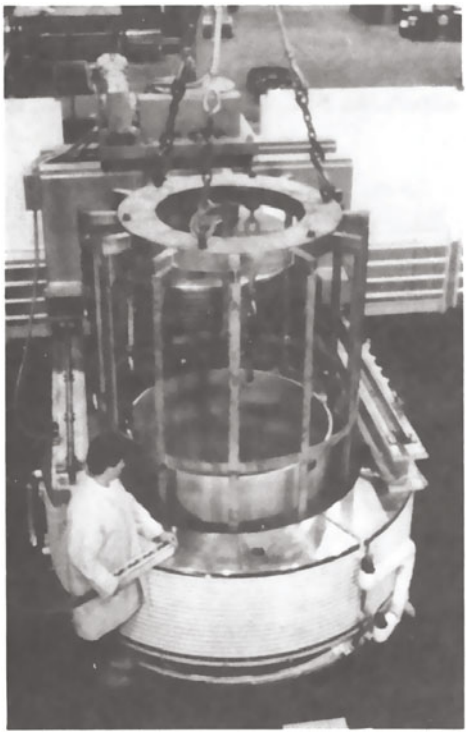

Figure 36. IMT's 60-inch (152.4 cm) working diameter, HIP unit is being unloaded after a cycle. (Courtesy of IMT)

ACKNOWLEDGMENTS

I first want to thank my family (Marty, Jan, and Eric) who have given me the needed understanding and support in my career involving HIP over the past 35 years. Second, my very grateful thanks to those faithful Battelle technicians without whom our successes with the HIP systems could not have been accomplished.

I am very grateful to the following for the information and pictures supplied to me for this paper:

(1) Franz X. Zimmerman, ABB Autoclave Systems, Inc.
(2) Jan Westerlund, ASEA Brown Boveri (ABB) Metallurgy.
(3) Andrew S.D. Crum, National Forge Company, Pressure Systems Division.
(4) Greg Butzer, Howemet Corporation, Whitehall HIP Division.

In addition, I want to express my gratitude to the organizing committee for this invitation to present this paper at the 3rd International Conference on Hot Isostatic Pressing.

REFERENCES

1. Saller, H.A., Paprocki, S.J. and Hodge, E.S., "Cladding of Zirconium-Uranium Alloys with Zirconium", Report No. BMI-960, Battelle Memorial Institute, Columbus, Ohio, October 25, 1954.

2. Dayton, R.W. and Saller, H.A., "The Fabrication of Zirconium Alloy SIR Fuel Elements", Report No. BMI-941, Battelle Memorial Institute, Columbus, Ohio, August 13, 1954.

3. Hodge, E.S., Pioneer Reviews Developments in Hot Isostatic Pressing, in Metal Powder Report, May 1987, Vol. 42, 5, pp 379-80.

4. Paprocki, J.S., Private communication, January 10, 1991.

5. Saller, H.A., Paprocki, S.J., Dayton, R.W., and Hodge, E.S., A Method of Bonding, U.S. Patent 687-842 (classified).

6. Saller, H.A., (deceased), Hodge, E.S., Paprocki, E.S., and Dayton, R.W., Method of Bonding, Canadian Patent No. 680,160, February 18, 1964.

7. Boyer, C.B., Pressure Bonding, Laboratory Record Book No. 11683, Battelle Memorial Institute, Columbus, Ohio, February 2, 1956 to August 12, 1956.

8. High Pressure Autoclaves (Valves and Fittings), Catalog 200, Autoclave Engineers, Inc., Erie, Pennsylvania, 1952.

9. Paprocki, S.J. Hodge, E.A., and Boyer, C.B., "Preparation of Reactor Components by a Gas-Pressure Bonding Technique", Second International Conference on the Peacetime Uses of Atomic Energy, held at Geneva, Switzerland, September 1-13, 1958.

10. Paprocki, S.J., "Pressure-Bond Technique and Fuel-Element Cladding", Unpublished paper, Battelle Memorial Institute, Columbus, Ohio, June 1956.

11. Boyer, C.B., "The Evolution and Future of HIP Systems", in 2nd International Conference on Isostatic Pressing (Stratford-Upon-Avon), Vol. 2, MPR Publishing Services Ltd., Shrewsbury, 1982, pp 7-0 - 7-40.

12. Clauer, A.H., Meiners, K.E., and Boyer, C.B., "Hot Isostatic Processing", MCIC Report No. MCIC-82-46, Metals and Ceramics Information Center, Battelle Columbus Laboratories, Columbus, Ohio, September 1982.

13. Boyer, C.B., "The History of HIP and Its Status in the United States", in Proceedings 6th Hot Isostatic Pressing Seminar, (Japan: Kobe Steel), Kobe, 1986, pp 1-35.

14. Bridgman, P.W., "The Physics of High Pressure", 1949 Supplement, G. Bill and Sons, Ltd., Londone, 1952.

15. Commings, E.W., High Pressure Technology, McGraw-Hill, New York, 1956.

16. Frederick, D.D., "Pressure-Vessel Closures", Machine Design, May 11, 1967, pp 183-6.

17. Boyer, C.B., "Development of Techniques for Gas Pressure Bonding", Laboratory Record Book No. 12263/continued from No. 11683, Battelle Memorial Institute, Columbus, Ohio (August, 13, 1956).

18. Paprocki, S.J., Hodge, E.S., Boyer, C.B., and Getz, R.W., "Gas-Pressure Bonding of Flat-Plate Fuel Assemblies", Report No. BMI-1312, Battelle Memorial Institute, Columbus, Ohio (January 20, 1959).

19. Paprocki, S.J., Hodge, E.A., and Boyer, C.B., "The Cladding of Delta-Phase Zirconium Hydride", Report No. BMI-1244, Battelle Memorial Institute, Columbus, Ohio (December 27, 1957).

20. Paprocki, S.J., Hodge, E.S., and Carmichael, D.C., "Pressure Bonding of Zircaloy-Clad Flat-Plate Uranium-Dioxide Fuel Elements", in Nuclear Metallurgy, American Institute of Mining, Metallurgical and Petroleum Engineers, New York, Vol. V, 1958, pp 13-24.

21. Paprocki, S.J., Hodge, E.S., and Boyer, C.B., "Cladding of Delta-Phase Zirconium Hydride", in AIME Nuclear Metallurgy, Transactions of The Metallurgy Society of AIME, New York, Vol. VIII, October 1960, pp 73-9.

22. Hodge, E.S., Boyer, C.B., and Orcutt, F.D., "Gas Pressure Bonding", Industrial and Engineering Chemistry, January 1961, Vol. 54, No. 1, pp. 30-5.

23. Fugardi, J. and Zambrow, J.L., "Bonding of Various Metals and Alloys By Isostatic Pressing at Elevated Temperatures", Nuclear Engineering and Science Conference, sponsored by American Institute of Mining Metallurgical and Petroleum Engineers, preprint V-104, Cleveland, Ohio, April 6-9, 1959.

24. Sheinhartz, I. and Fugardi, J., "Ceramic Fuel Elements Made By Hot Isostatic Pressing", Report No. SCNC-311, Sylvania-Corning Nuclear Corporation, Bayside, New York, September 1960.

25. Sheinhartz, I. and Fugardi, J., "Isostatic Pressing of UO_2 in High Temperature Metals", Report No. SCNC-312, Sylvania-Corning Nuclear Corporation, Bayside, New York, September 1960.

26. Weber, J. and Frankhauser, W.L., "Theory and Mechanism of Zircaloy Pressure Bonding", Report No. WAPD-305, Bettis Atomic Power Laboratory, Pittsburgh, PA, July 1966.

27. Cochrun, L.F., "BMI Pressure Bonding Equipment", Internal Report, Bettis Atomic Power Laboratory, Pittsburgh, PA, April 10, 1959.

28. Cochrun, L.E., Manual for Fourteen Inch I.D. Pneumastatic Bonding Facility, Internal Report, Bettis Atomic Power Laboratory, Pittsburgh, PA, July 16, 1959.

29. Paprocki, S.J., Hodge, E.A., Sayer, E.H. Wintucky, E.G., Gripshauer, P.J., and Carmichael, D.C., "Further Development of Gas-Pressure Bonding of Zircaloy-Clad Flat-Plate Uranium Dioxide Fuel Elements", Report No. BMI-1436, Battelle Memorial Institute, Columbus, Ohio, May 11, 1960.

30. Paprocki, S.J., Hodge E.S., Gripshauer, P.G., and Carmichael, D.C., "Fabrication of a Compartmented Flat-Plate Ceramic Fuel Element", Symposium on Fabrication of Fuel Elements, Vienna, Austria, May 1960.

31. Hodge, E.A., "Pressure Bonding Handles Dissimilar Metals", Steel, September 12, 1960, pp 144-5.

32. Boyer, C.B., Orcutt, F.D., and Conaway, R.M., "High Temperature High Pressure Autoclaves", Chemical Engineering Progress, May 1966, Vol. 62, No. 5, pp 99-106.

33. Muzzall, C.E., Compendium of Gas Autoclave Engineering Studies, Report No. Y-1478, Union Carbide Corporation, Y-12 Plant, Oak Ridge, Tennessee, November 2, 1964.

34. Working With Pressure at LRL, Report No. M-015, University of California, Lawrence Radiation Laboratory, Livermore California, 1969.

35. Sands, R.L., Herbert, E.P., and Morgan, W.R., An Apparatus for Hot Isostatic Compaction with Pressurized Gas, Powder Metallurgy, 1965, Vol. 8, No. 15, pp 129-41.

36. Bett, K.E. and Saville, G., "Heat Transfer in Packed Beds Under Pressure", Department of Chemical Engineering and Chemical Technology, Imperial College, London, July, 1965.

37. Zimmerman, F.X., Unpublished correspondence, April 4, 1991.

38. Photo, H.A., "Aspects of the Brittle Fracture Failure of a 30-inch I.D., 30,000 psi Isostat with Threaded Closure", Report No. Y-1758, Union Carbide Corporation, Y-12 Plant Oak Ridge, Tennessee, April 30, 1971.

39. Photo, H.A., "Brittle Failure of a large High-Pressure Isostat and a Comparison Analysis of Its Twin Vessel", Report No. Y-1989, Union Carbide Corporation, Y-12 Plant, Oak Ridge, Tennessee, August 20, 1975.

40. Neeley, A.C., Pfeiler, N.A., and Valentine, C.K., "The Hot Isostatic Pressing Experience of the Oak Ridge Y-12 Plant", Report No. Y-1683, Union Carbide Corporation, Y-12 Plant, Oak Ridge, Tennessee, July 18, 1969.

41. Pfeiler, W.A. and Valentine, C.K., Hot-Isostatic-Pressing Apparatus, U.S. Patent 3,419,935, January 7, 1969.

42. Valentine, C.K., Unpublished communication, June 6, 1966.

43. Valentine, C.K., Unpublished communication, June 6, 1968.

44. Levey, R.P., "Isostatic Hot Pressing", Report No. Y-1487, Union Carbide Corporation, Y-12 Plant, Oak Ridge Tennessee, June 9, 1965.

45. Hodge, E.S., "Elevated-Temperature Compaction of Metals and Ceramics by Gas-Pressure", Powder Metallurgy, 1964, Vol. 7, No. 14, pp. 168-201.

46. Properties of Allied Chemical Tungsten, Technical Report, Allied Chemical Co., Morristown, N.J., (1963).

47. Frederick, D.D., "Resilient Vessel Closures and Connections for High-Pressure-Temperature Service", Technical reprint 2751, Autoclave Engineers, Inc., Erie, Pennsylvania, February 1968.

48. Tassin, M.A., Unpublished communication, May 6, 1964.

49. Thiede, R.A., Unpublished communication, July 20, 1965.

50. Hoover, R.J. Unpublished communication, June 24, 1964.

51. Mechanical Engineering High Pressure Laboratory Manual, Mechanical Engineering Department Technician Division, Lawrence Radiation Laboratory, University of California, Livermore, January 28, 1971, M-019, pp 143-157.

52. Working with Pressure at LRL, Mechanical Engineering Department Hazards Control Department, Lawrence Radiation Laboratory, University of California, Livermore, January 1969, M-015, pp 5.1 - 5.16.

53. Pugacz, M.A., Unpublished communication, March 9, 1964.

54. Westerlund, J., Unpublished communication, March 25, 1991.

55. Kerr, D.L., Lemon, R.C., and Stonebrook, E.E., Castings, U.S. Patent No. 3,496,624, Feb. 20, 1970.

56. Boeckeler, B.C., "Development of Keziz Process", Keziz Seminar, Kennametal, Inc., Latrobe, PA, Sept. 1, 1971.

57. Smith, E.N., Unpublished communication, September, 1971.

58. Necker, W.C., "A New Tool for Complex Operation", Research/Development, February 1967, pp 40-3.

59. Hardwood Engineering Products, Hardwood Engineering Company, Inc., Walpole, Massachusetts, 1973.

60. Snowden, P., "Design of Furnaces for Use in High Pressure Systems", Proceedings of the Institute of Mechanical Engineers, 1967-68, Vol. 182, Pt 3C, pp 283-287.

61. Boyer, C.B., Conaway, R.M., and Orcutt, F.D., Remote Switching Device, U.S. Patent No. 3,466,656, (Sept. 9, 1969).

62. Boyer, C.B., Hatfield, J.E., and Orcutt, F.D., "Hot Isostatic Processing", Mechanical Engineering, February 1971, pp 33-9.

63. Crum, A.S.D., Unpublished communication, April 19, 1991.

64. Boyer, C.B., and Orcutt, F.D., High Pressure Furnace, U.S. Patent 3,427,011, February 11, 1969.

65. Boyer, C.B., Orcutt, F.D., and Hatfield, J.E., "Hot Isostatic Bonding and Compaction Developments", Industrial Heating, January, 1970.

66. Gripshover, P.J., Boyer, C.B., and Harth III, G.H., Isostatic Forming, U.S. Patent 3,633,264, January 11, 1972.

67. Boyer, C.B., Orcutt, F.D., Shaw, R.L., and Gregg, G.C., Apparatus for Loading a High-Pressure Furnace, U.S. Patent No. 3,741,718, (June 16, 1973).

68. Lundstrom, H.T. Furnace for Heat Treating Objects Under Pressure, U.S. Patent 3,695,597, October 3, 1972.

69. Isaksson, S.E., Furnace for Sintering Powder, U.S. Patent, 3,703,278, November 21, 1972.

70. Larker, H.T., Cylindrical Elongated Furnace for Treating Material at High Temperatures and Under High Pressure, U.S. Patent 3,732,078, May 8, 1973.

71. Lundstrom, H.T., Method of Sintering Powder Bodies, United Kingdom Patent, 1,291,458, October 23, 1969.

72. Lundstrom, H.T., Plant for Performing Hot Isostatic Compaction Processes, United Kingdom, Patent 1,204,344, October 6, 1967.

73. Boyer, C.B., Woessner, D.S., and Rhodes, T.C., "Development and Operation of a Large Hot Isostatic Pressing System", in High-Pressure Science and Technology, Sixth AIRAPT Conference, Vol. 2, Plenum, New York, 1977, pp 664-678.

74. Boyer, C.B. and Conaway, R.M., Isostatic Pressure Transmitting Apparatus and Method, U.S. Patent 3,523,148, January 4, 1968.

75. Dulis, E.J. and Neumeyer, T.A., "New and Improved High Speed Tool Steels by Particle Metallurgy", Progress Powder Metallurgy, TN695, pp 129-142, 1972.

76. Thompson, V.R., Method for Producing Dispersioned Hardenable Steel, U.S. Patent 3,450,528, June 17, 1969.

77. Boyer, C.B., Apparatus for Rapid Fluid Compacting, U.S. Patent No. 3,543,345, December 1, 1970.

78. Boyer, C.B., Heat Insulating Casing, U.S. Patent No. 3,599,281, August 17, 1971.

79. Dulis, E.J., High-Speed Tool Steels by Particle Metallurgy, Chapter 16, Powder Metallurgy for High Performance Applications, Chapter 16, Syracuse Univ. Press, (1972).

80. Williams, B., IMT Keeps up the Pressure in Toll HIPing, Metal Powder Report, Septebmer 1984, Vol. 39, No. 9, pp 524-26.

81. Smith, Jr., C.W., Gas Pressure Bonding Furnace, U.S. Patent 3,548,062, December 15, 1970.

82. Lundstrom, H., Furnace for Heat Treating Objects Under High Pressure, U.S. Patent 3,606,286, September 20, 1971.

83. Lundstrom, H., "Furnace for Heat-Treating Objectives Under Supra-Atmospheric Pressure, United Kingdom Patent 1,271,116, September 11, 1969.

84. Havel, C.J., Hot Isostatic Pressing Using a Viterous Container, United Kingdom Patent, 1,190,123, April 29, 1970.

85. Lundstrom, H., Method of Sintering Powder Bodies, United Kingdom Patent 1,291,458, October 23, 1969.

86. Boyer, C.B., Hot Isostatic Processing, presented at 64th Annual Meeting of the AICHE in San Francisco, California, November 28-December 2, 1971.

87. Witkin, D.E., Comparison of National Forge Standard Threaded Closure with Pin Type Closure for Pressure Vessels Subject to Cyclic Service, Pressure Systems Division of National Forge Company, 1970.

88. Witkin, D.E., Design of Closures for High Pressure Vessels, Pressure Systems Division of National Forge Company, 1970.

89. Witkin, D.E., Use of Interaction Analysis to the Design of High Pressure Vessels, Pressure System Division of National Forge Company, 1970.

90. Gripshover, P.J., Boyer, C.B., and Harth III, G.H., Isostatic Forging, U.S. Patent 3,633,264, January 11, 1972.

91. St. Onge, C.D. and Poohto, H.A., High Temperature Furnace for High-Pressure Argon Gas Operation, Report No. Y-1629, Union Carbide Corporation, Y-12 Plant, Oak Ridge, Tennessee, February 17, 1969.

92. Isaksson, A-E., Method for Manufacturing an Object from Iron-Based Alloy by Isostatic Compaction, U.S. Patent 3,772,009, October 8, 1972.

93. Obrzut, J.J., PM Tool Steels Come Out Swinging, Iron Age, January 4, 1971, pp 51-3.

94. Lundstrom, H., Furnace for Heat-Treating Objects Under High Pressure, U.S. Patent 3,628,779, December 21, 1971.

95. Fischmeister, H., "Isostatic Hot Compaction", Powder Metallurgy International, 1978, Vol. 10, No. 3, pp 119-23.

96. Winship, J.T., Upsurge in Isostatics, American Machinist, McGraw-Hill, Inc., New York, April 1984, pp 99-114.

97. Zimmerman, F.X., Hot Isostatic Pressing Equipment Development, in paper presented at 2nd International Conference on Isostatic Pressing, September 21-23, 1982, Vol. 2, pp 22-22-23.

98. Hellman, P., Larker, H., Pfeffer, J., and Stromblad, I., The ASEA-STORA Process, International Powder Metallurgy Conference, New York, 1970.

99. Stromblad, I., Experience from the Commissioning of the World's First ASEA-STORA Plant, Swedish Technical Week, Tokyo, February 21-25, 1972.

100. McTierman, B.J., Modern Production Method for Superalloy and Titanium Aluminide Powders, Metal Powder Report, January 1991, Vol. 46, No. 1, pp 22-5.

101. Cook, J., Lambdin, F., and Trent, P., Discontinuous Carbon-Carbon Composite Fabrication, Report No. Y-1719, Union Carbide Corporation, Y-12 Plant, Oak Ridge, Tennessee, May 20, 1970.

102. Lambdin, F. and Cook, J.L., Fabrication of Discontinuous, High-Fiber-Content, Isotropic Carbon-Carbon Composites, Report No. Y-1784, Union Carbide Corporation, Y-12 Plant, Oak Ridge, Tennessee, October 7, 1971.

103. Hot Isostatic Pressing, Howmet Corporation publication, Whitehall HIP Division, Whitehall, Michigan, 1988.

104. Isostatic Pressing Trends in Japan, Metal Powder Report, March 1991, Vol. 46, No. 3, pp 17.

105. Ishii, T., Tsuzuki, H., and Inoue, Modular-Type, Hot Loading-Type, and Compact Hot Isostatic Pressing Systems, in papers presented at 2nd International Conference on Isostatic Pressing, September 21-23, 1982, Vol. 2, pp 20-20-24.

106. Widmer, R., World's Largest HIP System Goes on Stream at IMT, Metal Powder Report, April 1987, Vol. 42, No. 4, pp 302.

NEW CONCEPTION OF AUTOMATIC CONTROL SYSTEMS DESIGN FOR HIP AND CIP PROCESSES

I. Burovoy, A. Romashkin, D. Andreev, A. Balashov, I. Kanyshev
Moscow Institute of Steel and Alloys
4, Leninsky prospect 117049 Moscow USSR

ABSTRACT

A HIP process automatic control system is described. It performs both traditional direct digital control functions and functions which use the artificial intellect methods, such as the optimal cycle program elaboration, operator's and researcher's intellectual support. This approach results in increasing of the process reliability and quality as well as reducing of the production cost.

INTRODUCTION

Practical experience of last years shows the high efficiency of HIP process for large complex makes production. However, the HIP technology adoption meets some noticeable difficulties as high cost and duration of new process elaboration; exacting demands upon staff skill; low reliability of some equipment elements etc., which result in low productivity and high cost of isostatic treatment.

METHODS

To overcome these difficulties it's necessary to build a HIP process automatic control system (ACS) of a new type. This control system performs both traditional direct digital control functions and optimal HIP cycle program elaboration, operator's and researcher's intellectual support. These new functions provide the improvement of the HIP process reliability and quality. The ACS contains a technological knowledge base and uses modern automatic control theory achievements as well as artificial intellect methods.

RESULTS

The ACS ensures the HIP process monitoring and control in both automatic and hand-operated modes. The ACS has two hardware levels: the lower level based on a programmable microprocessor controller and the upper level based on IBM-compatible personal computer. The ACS consists of the basic "HIP cycle control" system and two additional functional blocks - "Operator's technical support" and "Intellectual support"

THE "HIP CYCLE CONTROL SYSTEM"

accomplishes the following tasks:

- puts the technological equipment into its initial state;
- collects, processes and represents the information about the current HIP cycle state;
- controls the HIP cycle in the automatic mode according to the set cycle program;
- monitors the equipment state;
- shuts down the HIP cycle in the case of the equipment breakdown.

This system provides:

- HIP cycle reproducibility which results in the constant treatment quality;
- elimination of spoilage caused by operator's errors;
- improvement of the HIP process reliability and safety;
- increasing of the equipment service life;
- reducing of the total treatment cost.

The ability of a dinamic cycle program adjustment performed by other functional blocks in a real-time mode is provided.

The special features of this sub-system are:

- complete control logic which works according to the current situation when the equipment faults;
- using of the latest achievements in automatic control theory which provide the uniform temperature field within the furnace and the minimal time of achieving the requested process parameters (if desired);
- various ways of the HIP cycle shuting down when a breakdown occurs.

Special attention is payed to the heating system control. As distinct from the principles of heating system control used by ABB group, we take into account the reciprocal influence of the heating zones.

For the heating process simulation we accepted the following suppositions:

- the furnace volume is breaked up into cells corresponding to the heating zones;
- the gas within each cell is mixed perfectly;
- heat- and mass-exchange between the cells take place;

- the gas pressure values in all the furnace volume are identical.

With these suppositions a non-linear model of heating process with undefined parameters was built.For this approximate model the temperature field stabilization problem is solved with the binary automatic control methods [1].

THE "OPERATOR'S TECHNICAL SUPPORT" FUNCTIONAL BLOCK

accomplishes the following tasks:

- calculation of the charge volume;
- calculation of the initial pressure;
- support of a data base on standard cycle programs;
- support of a data base on completed HIP cycles.

The initial pressure calculation is performed on the base of real gas models (taking into account its compression). The precize initial pressure calculation results in the reducing of the working gas consumption as well as the HIP cycle duration.

THE "INTELLECTUAL SUPPORT" FUNCTIONAL BLOCK

helps to master existing HIP technologies and to develop new ones within the shortest time. It includes the following sub-systems:

- operator's intellectual adviser;
- technologist's and researcher's intellectual adviser;
- operator's trainer;
- shape-forming tool CAD system.

The intellectual advisers are built on the base of HIP cycle simulation, the data base on materials and fluids properties, the data base on completed HIP cycles and the data base on the equipment working time.

THE "INTELLECTUAL OPERATOR'S ADVISER" SUB-SYSTEM

- predicts the possible process faults;
- offers the operator the sequence of actions for the HIP cycle continuation.

This sub-system contains the technological knowledge base. For decision making the simulation of HIP cycle stages and the data bases are used.

This sub-system provides:

- improvement of the HIP process safety and reliability;
- reducing of the maintenance costs;
- increasing of the number of successfully completed HIP cycles.

THE "RESEARCHER'S INTELLECTUAL ADVISER" SUB-SYSTEM

is intended for:

- identification of HIP cycle mathematical models in accordance to the equipment state;
- development of the optimal HIP cycle program in accordance to the equipment capabilities;
- prediction of the HIP cycle results on the base of simulation and on-site information.
- planning of the experiment for development of new technologies for makes with requested properties production.

This sub-system provides:

- reducing of the technology elaboration period;
- reducing of R & D cost;
- increasing of the equipment productivity.

THE "HIP CYCLE SIMULATION" SUB-SYSTEM

contains:

- vacuumizing models;
- gas pressure equalizing models;
- pumping models;
- heating and cooling models;
- makes compacting models which take in account the geometrical shape.

HIP cycle simulation may be used for prediction of the cycle duration, equipment failure diagnostics and the HIP treatment technology selection (the number of expositions and their parameters).

THE "DATA BASES" SUB-SYSTEM

provides

- stock-taking of makes;
- revealing of the connection between the parameters and the results of treatment;
- accomplishing of the simulation, diagnostics , optimization, etc.

THE "OPERATOR'S TRAINER" SUB-SYSTEM

is intended for operators' and technologists' training in HIP processes performance and equipment control. This purpose is achieved by:

- HIP cycle simulation;
- standard and non-standard situations generation;
- evaluation of operator's actions in non-standard situations.

This sub-system provides:

- reducing of the equipment mastering time;
- improvement of the staff skill without the equipment wear;
- evaluation of operator's skill.

The trainer includes an expert system which is similar to one used in the "Operator's intellectual advisor" sub-system.

THE "SHAPE-FORMING TOOL CAD" SUB-SYSTEM

is intended for:

- simulation of shape-forming of axis-simmetrical makes;
- calculation of capsules parameters;

This sub-system provides:

- data output in AutoCAD format;
- reducing of capsules elaboration time;
- reducing of the R & D costs;
- reducing of the powder consumption;
- reducing of allowances for mechanical treatment;
- reducing of makes costs.

CONCLUSIONS

Existance of all the functional blocks in one ACS is not necessary. The ACS functional composition depends on the equipment purpose. For industrial HIP units which implement standard cycle programs and use large set of auxiliary equipment, it's not necessary to use the "Technologist's intellectual advisor" sub-system. In this case the special attention must be payed to data bases and diagnostic sub-system. For laboratory HIP units it's not necessary to use the "Operator's intellectual support" sub-system and the special attention must be payed to the "Technologist's intellectual advisor" sub-system.

REFERENCES

1. Emelyanov S.V., Binary Automatic Control Systems, MIR Publishers, Moscow, 1987.

GLASS ENCAPSULATION IN HIP CHAMBER

DESCRIPTION OF METHODS USED IN PRACTICE

OLE HUUSMANN
Danish Technological Institute, Industrial Metallurgy,
Gregersensvej, DK-2630 Taastrup, Denmark

ABSTRACT

The DANISH TECHNOLOGICAL INSTITUTE (DTI) has developed a method for encapsulation of products or powders in the HIP chamber during the HIP process.

The principle is that the products/powders (packed or not) are placed in a glass container. The container is then placed in a graphite or steel crucible with a special glass stopper on top of it. The whole thing is placed in the HIP chamber and the HIP is closed. The HIP is heated up, creating vacuum in the chamber. When the glass has reached the softening temperature (approx. 900°C for pyrex glass), the gas is let into the HIP chamber. The gas presses the glass stopper and the glass container together. The encapsulation is finished and the HIP cycle can continue.

INTRODUCTION

The Danish Technological Institute (DTI) has been using the HIP process since 1989. DTI's HIP is of the ABB QIH 9 type, with the furnace dimensions ø 150 mm x 300 mm. Max. temperature 2000°C and max. pressure 2000 bar. This is the only HIP unit in Denmark.

The HIP is mainly used for prototype production of new materials, both in-house at DTI and for other research institutions in Denmark. The new materials are usually made with powder as base material, either by making a "green product" by conventional powder pressing, followed by glass encapsulation and pressurization in the HIP or by direct glass encapsulation of the powder before HIP'ing.

The glass encapsulation used to be done by placing the green product/powder in a glass container, removing the air from the container by means of a vacuum pump and sealing the container under vacuum before placing it in the HIP.

However, practical experiments have shown that the sealing of the glass container - under vacuum - can be done in the HIP chamber provided specially designed glass containers are used. The latest experiments in this field have shown that encapsulation in the HIP chamber can also be done with other encapsulation materials, for example lead or teflon.

PRACTICAL EXPERIMENTS

The first experiments with glass encapsulation in the HIP chamber were carried out with Al_2O_3 discs made by cold pressing the powder. The dimensions before HIP'ing were ø 85 mm x 3 mm, and pyrex glass bowls were used as containers. The bowls were placed one on top of the other as shown in fig. 1, and different protection materials were tested with a view to preventing contact between the Al_2O_3 discs and the glass bowls.

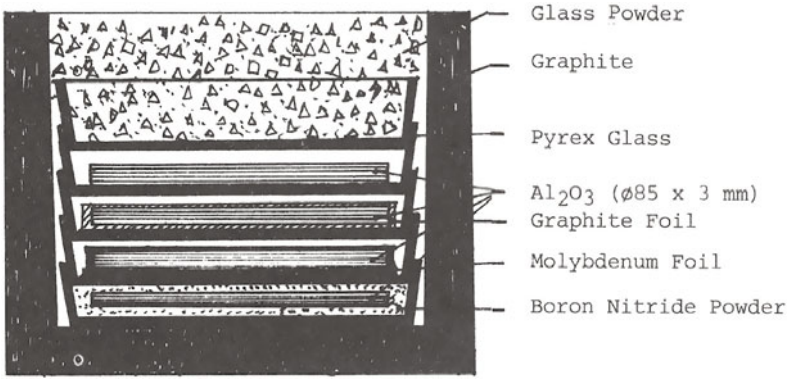

Fig. 1. Sketch of pyrex glass bowls with Al_2O_3 discs and protection materials.

The glass bowls are placed in a graphite crucible, which is then placed in the HIP. The process - which is outlined in fig. 2 - is arranged so that the temperature in the HIP chamber is increased to 900°C under vacuum. At 900°C, the glass bowls become very soft and therefore form lids for each other when pressure is applied in the HIP chamber.

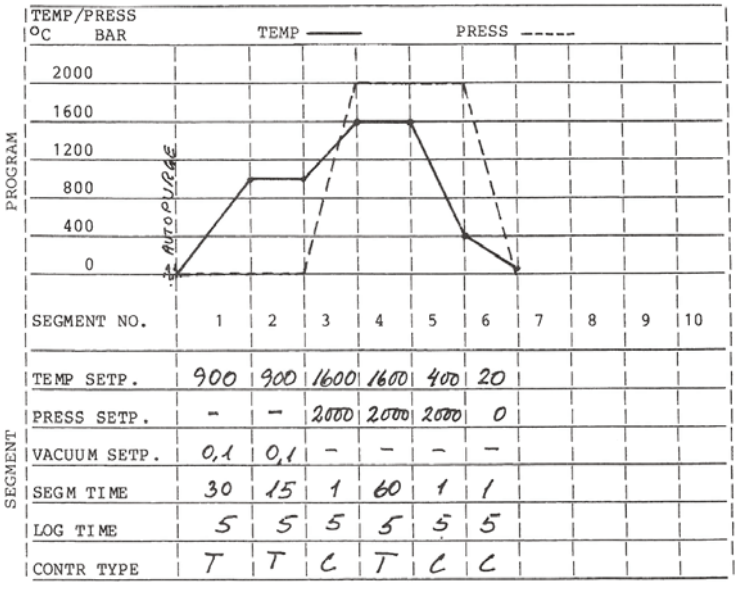

Fig. 2. Process in connection with pressurization of pyrex glass bowls with Al_2O_3 discs.

Fig. 3 shows the Al_2O_3 discs placed together with the protection material in the pyrex glass bowls, and fig. 4 shows an Al_2O_3 disc before and after HIP'ing, together with the graphite foil used as protection during the HIP'ing.

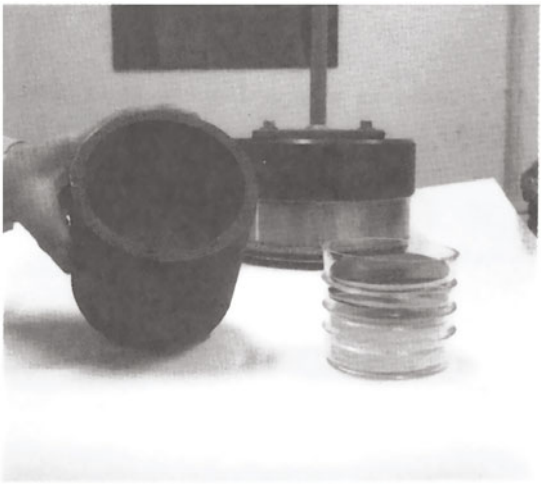

Fig. 3. Al_2O_3 discs in pyrex glass bowls together with the protection material.

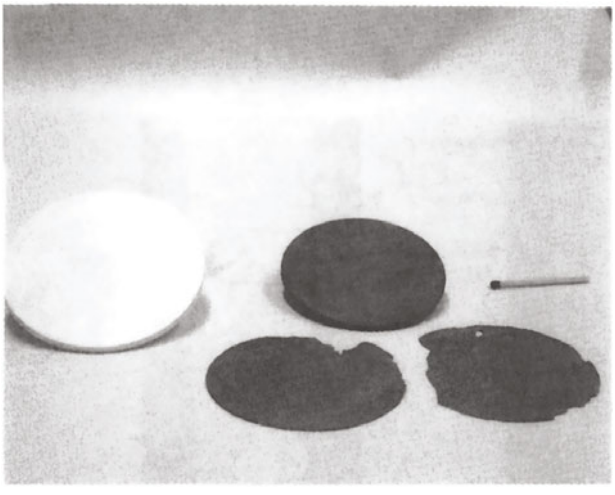

Fig. 4. Al_2O_3 disc before and after HIP'ing, together with the graphite foil used as protection.

The glass encapsulation method which DTI usually uses is pressurization of powder in a cylindrical container with a conical stopper - both parts being made of pyrex glass. The glass container with the powder is placed in a graphite crucible which a conical hole in it. After HIP'ing, the glass container can be removed from the graphite crucible without damaging this. To facilitate removal of the glass container after HIP'ing, the hole in the graphite crucible can be brushed with boron nitride before insertion of the glass container.

Fig. 5 shows the glass container with powder before and after HIP'ing.

Fig. 6 shows the glass container with powder before HIP'ing, and fig. 7 shows the HIP'ed product, the graphite crucible, and the remains of the glass container.

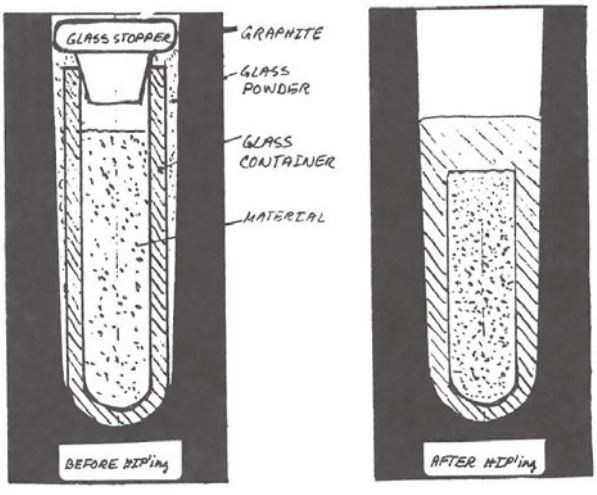

Fig. 5. Principle of glass encapsulation.

Fig. 6. Glass container with powder before HIP'ing.

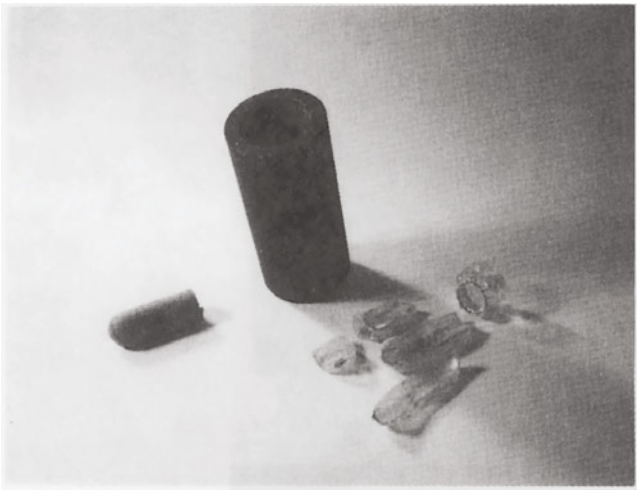

Fig. 7. The container from fig. 6 after HIP'ing.

A variant of the methods described is shown in figs. 8, 9, 10 and 11. With this method, the graphite crucible is destroyed after each HIP'ing.

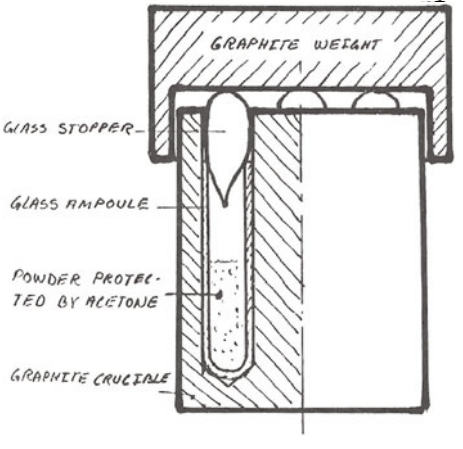

Fig. 8. Glass ampoule with powder. The powder is protected against oxidation by acetone.

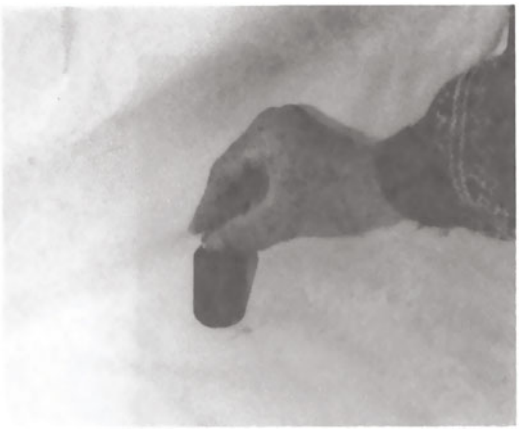

Fig. 9. Placing of glass ampoules in graphite crucible.

Fig. 10. Cutting of ampoules after HIP'ing.

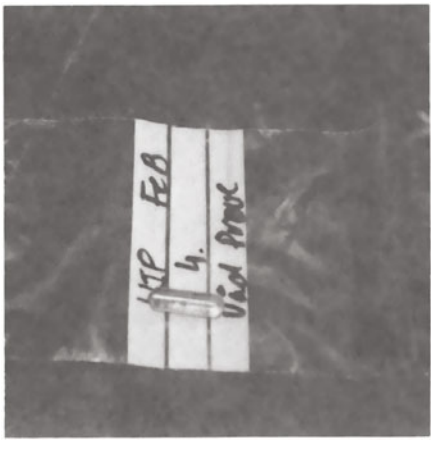

Fig. 11. Glass ampoule with HIP'ed powder.

The method with glass encapsulation in the HIP chamber has been used in the temperature range 900°C to 1650°C without problems, but it is also considerable desirable to be able to perform HIP'ing at lower temperatures. Therefore, experiments are in progress with other materials than glass for the encapsulation, and good results have so far been obtained with teflon and lead in the temperature range 250°C to 300°C.

CONCLUSIONS

The method of glass encapsulation in the HIP chamber, using self-sealing containers, has considerably simplified the work of developing new materials.

The method of using self-sealing containers is expected to be developed through use of other container materials than glass, so that the whole of the HIP's temperature range can be utilized. Good results have been achieved with lead and teflon containers.

REFERENCES

* Larker, Hans T.,"Hot Isostatic Pressing for the Forming and Production of Ceramics", ASEA Journal, Vol. 54, No. 4, 1981.

* Larker, H.,"Hot Isostatic Pressing of Shaped Silicon Nitride Parts", Sixth AIRAPT Conference, June 25-29,1977, High-Pressure Science and Technology, Vol. 2, Plenum Press, New York, 1979.

* Havel, C.J., Hot Isostatic Pressing Using Vetrous Containers", U.S. Patent No. 3,622,313, November 27, 1971.

Mini-HIP Research In CISRI

CHEN HONGXIA , ZHOU ZHONGFU
Central Iron and Steel Research Institute, 21 DEP., Beijing, P.R.China

ABSTRACT

The structure and safety of the plug screw-HIP is analyzed in this paper. It is suggested that to use coarse pitch thread, improve the transition region of the vessel and reduce the R_t-value for increasing K_R-value of the vessel is a necessary measure to lower the stress concentration and guarantee the safety. The heating, insulating and temperature measuring of HIP with high temperature and high pressure are discussed in the paper.

INTRODUCTION

The Mini-HIP at working temperature up to 2000℃ and pressure up to 200 MPa has been developed since 1980 at CISRI. The varieties of HIP developed are listed in table 1. The HIP used in laboratory can adopt the simple plug screw structure, but the thread zone has to possess good fatigue property and small stress concentration (uneven load distribution) . The RD100 HIP used in laboratory at CISRI belongs to this type, as shown in fig.1, and fig.3, but CISRI focus on developing frame structure. The main points occured in developing above mentioned equipments are reviewed.

§ 1. Safety-key factor to plug screw vessel

The plug screw vessel, including Buttress and V-thread, was discussed in detail at the 2nd International High Pressure Congress [4] [5] in 1975. In some articles, the load on the trough at the bottom of first thread were analyzed by finite element method and experimental approvement. It is considered that the load distribution on thread can be predicated by D. G. Sopwith technique and the stress condition can be

analyzed by finite element method. Furthermore, the stress suffered in Buttress thread is higher than that of V-thread, but there is no difference in fatigue life in the experiment and the Buttress's life is even higher if yielding is not evident. The opposed prediction is to be continuously investigated.

The RD100 HIP developed in CISRI is of plug screw structure, as shown in fig.1 and fig. 3. Some results of D.G. Sopwith [9] are used in design to improve the imhomogeneity of axial load and stress concentration in thread zone. To adopt Buttress thread with coarse pitch ($D_o/t=8.2$) in structure, properly increase the tooth angle, select the short plug screw ($L/D=0.44<0.6$), etc., play an important role in protecting the thread zone from brittle fracture. However, the local peak stress occured in the thread zone can still excess the maximum working stress of vessel, even higher than its σ_s. For this reason, the following complemental measures are adopted in design.

§1. 1. Increase the micro-plastic parameter $(K_R/\sigma_s)^2$ of vessel material to release the peak stress. Due to the full toughness of materials, even if micro-flaw appears, it can be limited to slow expanding state, because the critical crack length $[(K_R/\sigma_s)^2/3.8]$ is lengthened and make the vessel reach the predicted working life. The fracture toughness (K_R=4900 $Nmm^{-3/2}$) of vessel material used in RD100 HIP is 1. 5 times higher than that of constructional steel , expected to ensure the safety in operation. With reference to the CIP400 with plug screw structure developed in the sixties at CISRI, the toughness of vessel material, which was lower initially, attains to $\alpha_k \approx 0.588 Nm/mm^2$ (correspond to higher K_R) by repeated heat treatment, it has been in operation for more than 20 years and with no trouble. As contrasted with another CIP100 of the same structure, the vessel material has lower toughness ($\alpha_k \approx 0.392$ Nm/mm^2, correspond to lower k_R), it was broken when worked less than 200 times at peak stress state. Therefore, The peak stress can be released by increasing k_R-value, to make material have full toughness and realize safty in operation.

§1. 2. Increase the height of under-cut of thread to make smooth transition between sections to avoid overlapping effect of different stress from upper and lower position of under-cut of thread. The axial stress and bending stress of the first thread at upper under-cut of thread end is about four times of the average stress and the sealing zone at lower end of it bears radial stress (σ_r)and shear stress (σ_t) resulted from working medium. Longer under-cut of thread and smooth transition of upper and lower joint can be free from fracturing due to stress overlapping or three dimensional stress produced .

The height of under-cut of thread according to normal standard is not enough. The suitable height may be assumed about half diameter of vessel. Too short of under-cut of thread was one of main reasons resulting in threaded rod breaking of CIP130 manufactured at CISRI in 1960 s.

The design of thread zone mentioned above is realized by improving the conventional thread. But in 1970s, the elastic thread had been applied to larger thread vessel in USA, which is also worthy to be noticed and developed.

§ 2. Main problems in developing high temperature HIP

Most of advanced engineering ceramics are non-oxide ceramic, which formed at about 2000℃ in Nitrogen or Argon atmosphere. At so high temperature, it should be considered in design that the structure of furnace must suit for it. The temperature in the furnace has to be uniform and mutual reactions of various materials in furnace and harmful substance must be avoided.

§ 2.1. High temperature

For heater requiring 2000℃ or so, the graphite is generally used as heating element and insulating material, because it keeps stable mechanical properties below 2500℃ and can be self-supported. High purity graphite does not volatilize harmful substance usually, but it is necessary to adopt low voltage and high current because of its low resistance. For this reason, it should reduce the power loss of lines before and after electrode in power supply system in order to make the effective power, as much as possible concentrate on heating body. Moreover, radiation plays an important role in heating at high temperature, so the power supply at every zone in heater must be rational adjusted to achieve uniform temperature required by the process.

§ 2.2. Medium

Many products, such as nitrede, are fabricated usually at nitrogen atmosphere. This is benefical to suppress affective substance in products volatilizing, but not good for heating furnace, insulating system and measuring system. It is noted especially that nitrogen can react with some free carbides to form very toxie substance, such as HCN. At high temperature, once it is leaking, it will pollute environment and is harmful to personal health. In addition, when the volatilized substance drops on the surface of insulant, it will make its insulating capacity lower or lose. Hence, when using nitrogen as protecting atmosphere, the rational operating system must be cautiously worked out. Resently so trouble is not occured when woking temperature is normally below 1800℃.

§ 2.3. Selection of insulating material under high temperature.

In conventional HIP, Al_2O_3 and other oxide ceramic are usually used as insulant. When it is heated up to 2000℃, its insulating performance strongly drops, unstablitizes and reacts with nitrogen medium of high temperature to form harmful deposits. As a result, a good insulant, i.e. "BN", which is stable at high temperature of up to 2000℃, is selected. It has not only excellent high temperature strength and insulating capacity, but also good machiniability, as well as simple assembly. It shows good result in operation.

§ 2.4. High temperature uniformity

It is well know that the physical properties of argon and nitrogen varies with temperature change [7]. In heating furnace, heat transfer is realized by conduction, convection and radiation, convection and radiation are dominant in HIP. The "Bouryoncy effect " resutled from high density medium at high temperature leads to temperature

gradient in furnace, making the temperature far lower at lower part than that at upper part and greatly in non-uniform distribution. So, to heat workpiece with cyclic flow of the upper and lower medium, so called convective heat transfer, is used to eliminate temperature non-uniformity.

To simplify the structure of heat furnace, the convective heat transfer is usually adopted by bottom heating, as shown in fig.5. As heating, the high temperature gas flows to the top of furnace. A flow-leading unit is installed in furnace to make the gas flow top back to bottom for reheating and realizing cyclic heat supply. This bottom heating type has features of simple structure and uniform temperature in furnace. Another heating method is radiation as shown in fig. 4, which suits for high temperature heating. Its heating element is placed on the side wall of the furnace, because of lower density of medium at high temperature and poor heat supply by natural convection. This design takes following measures: adopting radiation heating combined with convection heating; rationally distributing the radiating area at upper and lower part in furnace and equipping with suitable control system to strictly control the furnace temperature. Consequently, the main technical index, including fast temperatune rising, furnace temperature uniformity meets the requirement of the process.

§ 2.5. Temperature measurement under high temperature and high pressure

The W-Re thermocouple can be satisfied for HIP. In present design, a new type of W-Re thermocouple which can measure the temperature as high as 2300℃ has been developed in CISRI. This thermocouple requires clearness in furnace and no contacting with harmful volatiles, otherwise the service life will be greatly reduced. For that reason, the thermocouple wire is sheathed into a protective tube made of sealing refractory material. The tube must be elongated to low temperature zone of working room where the orifice of its lower end is sealed with filling, so as to keep the thermocouple from pollution, hold sensitivity and stablization of measuring signal and extend its life.

It demonstrates in practical application that the new thermocouple can keep the measuring signal stable and carry out the HIP process according to some typical technological system as shown in fig.6 and fig.7.

Recently, Sweden and other countries have developed a modern optical pyrometer, which has successfully applied to temperaure measuring in HIP, offers a good result. This is worthy to be noticed.

CONCLUSION

As mentioned above, the modification of Mini-HIP RD100, including structure improvement of thread vessel; adoption of radiation combined with convection to heating furnace and use of a new W-Re thermocouple, are successful. It suits for R & D laboratory use.

However its structure and performance should be further improved.

Today, the Mini-HIP is developed quickly in the world. New types of quality HIP and specific HIP for special application, such as ultra-high temperature HIP operated at ≥2300～2700℃ and rapidly cooling (100～200℃ /min) HIP with advanced temperature device are continuously developed. These show that HIP technique is striding to higher level.

TABLE 1

Mini-HIP developed at CISRI

Type	Pressure MPa	Temperature ℃	Working chamber (D×H)mm	Medium
RD100	200	2000Ar 1800N_2	100×120	Ar N_2
RD120	200	2000Ar 1800N_2	120×240	Ar N_2
RD180	200	2000Ar 1800N_2	180×200	Ar N_2

REFERENCE

1. ASEA-QUINTUS
   Isostatic Pressing Technique
   1975. 02. 01.
2. Proceeding of the International Conference on Hot Isostatic Pressing
   -Lulea, /15～17, June 1989
3. 周仲甫，《超高压容器安全分析》
   《钢铁研究总院学报》, Vol. 7, No.4, 1988 P.101～109
4. M.G.GRAY, R.J.PICK, Fatigue of threaded closures of high pressure vessels
   1977 HIGH PRESSURE ENGINEERING
5. D.M.Fryer, C.W.Smith, Threaded closures for large high pressure vessels
   1977 HIGH PRESSURE ENGINEERING
6. Anders Traff, Now Developments in Hot Isostatic Press (HIP)units
   MPR April 1990, P.279～282
7. M. KOIZUMI, Development and New Application of HIP Technique
   Pressure Technology, Vol. 25, No.6 1987
8. Hot Isostatic Pressing Technology at NKK in Japan
   MPR September, 1989, P.621～623
9. Frist International Conference on High Pressure Engineering
   1967 London

ANNOUNCEMENT:

The Fig,1— Fig,7 see appendix diagrams in next page.

APPENDIX DIAGRAMS

(Fig. 1—Fig. 7)

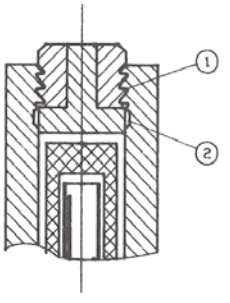

1. thread 2. under-cut

Fig.1 HIP of plug screw type

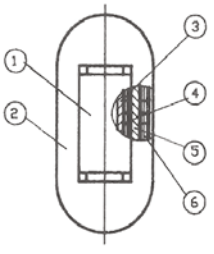

1. vessel 2.frame 3. cylinder
4. steel wire 5. pillar 6.steel wire

Fig.2 HIP of winding type

Fig.3 Thread used in RD100 HIP of plug screw type

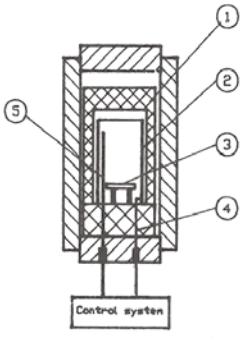

1. heating barrier 2.heating element
3.working chamber 4. power lead rod
5. thermocouple

Fig.4 Operating principle of heat, insulating and temperature measuring in mini-HIP

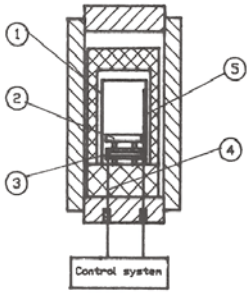

1. flow-leading barrier 2. working chamber 3. heating element 4. power lead rod 5.thermocouple

Fig.5 Bottom heating system of mini-HIP

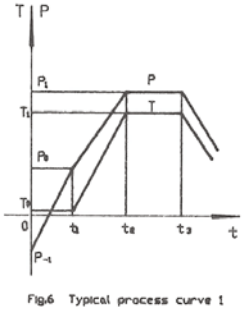

Fig.6 Typical process curve 1

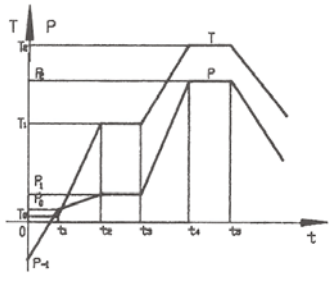

Fig.7 Typical process curve 2

RECENT DEVELOPMENT OF O_2-HIP EQUIPMENT

Yutaka Narukawa, Takao Fujikawa*, Yoshihiko Sakashita**, Takeshi Kanda**

No.2 Engineering Section, Engineering Dept., Industrial Machinery Group, KOBE STEEL,LTD., Kobe, Hyogo 651, Japan

*Technology Development Center, Engineering & Machinery Division, KOBE STEEL,LTD., Kobe, Hyogo 651, Japan

**Mechanical Engineering Research Laboratory, Technical Development Group, KOBE STEEL,LTD., Kobe, Hyogo 651, Japan

ABSTRACT

Progress in the development of O_2-HIP equipment is described in this paper regarding safety and the achievement of a new high temperature O_2-HIP apparatus.
Firstly, since safety is the most important factor in the design of O_2-HIP equipment, the materials which are used in this equipment are described in detail, paying special attention to ignition phenomena of metals and organic materials under Ar+max.20%O_2 high pressure gas atmosphere.
Secondly, furnaces which utilize Fe-Cr-Al or Pt-Rh heating element have been developed and have already been supplied commercially. However, a new high-temperature O_2-HIP with ZrO_2 heating element has recently been developed.

INTRODUCTION

Since the invention of HIP equipment, available pressure and temperature have reached higher levels, and the rate of operation of the equipment has increased. Moreover pressure medium gases have been used according to the workpiece, for example, N_2 gas for Si_3N_4. In this regard, O_2-HIP has recently become popular for the HIP treatment of oxide ceramics.
In this paper, the fundamental applications of O_2-HIP are

introduced and some of the recent developments of HIP units at Kobe Steel are described.

Safety of O_2-HIP apparatus

Outline of O_2-HIP

The aim of O_2-HIP, where $Ar+O_2$ mixture gas is used as the pressure medium, is to carry out HIP treatment while maintaining the resolution of oxide ceramics.
Soft-ferrite, PZT, and TiO_2 have already been commercially treated to avoid reduction during HIP treatment. Structural ceramics can be treated to improve characteristics or control color [2]. Oxide superconductors are treated for the enhancement of oxygen difusion, which leads to improved superconductive characteristics. [3, 4]
Fig. 1 shows O_2-HIP temperature of some applications and the typical heating element utilized in O_2-HIP. Fe-Cr-Al was already being utilized for HIP treatment of soft-ferrites. In addition, Pt-Rh was widely in use, especially in experimental-scale O_2-HIP apparatus.

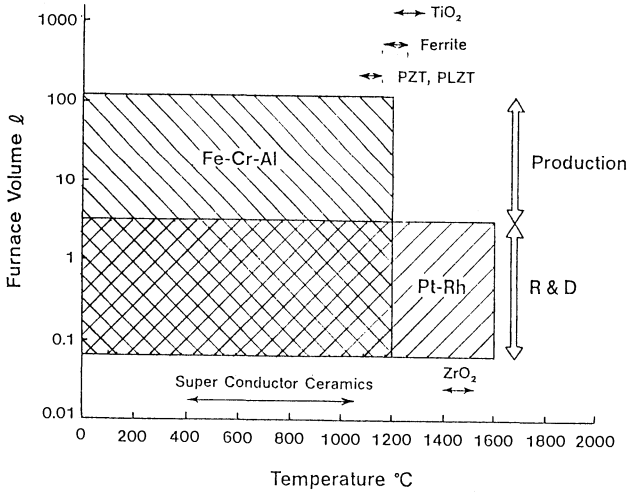

Figure 1. Materials of heating element and furnace volume

Safety of O_2-HIP apparatus

O_2-HIP equipment is very different from the conventional HIP, because it has to be designed in consideration of safety due to the use of high-pressure and high-temperature oxygen gas.
Therefore, safety considerations have been determined as follows:

1. Restricting the materials which can be used in O_2-HIP equipment
2. Adhering to the operation and maintenance procedures given

in the operating manuals
3. Equipping each apparatus with safety devices by the manufacturer
4. Running trial tests and simulations
5. Following safety procedures to prevent accidents

Ignition experiment in O_2-HIP furance

Safety has been confirmed by various experiments, for example, the ignition experiment which investigates the ignition temperatures of materials used in O_2-HIP equipment and the rapid gas-discharge experiment which supposes that high-temperature and high-pressure oxygen will cause gas leakage.

The ignition experiment is described in this paper.

Fig. 2 shows the materials and sizes of testpieces.

The temperature at which the recorded temperature begins to rise suddenly is defined as the ignition temperature.

When the furnace temperature was increased with the use of at O_2-HIP apparatus in Kobe Steel, ignition temperatures were recorded by thermocouples whose measuring point touched the testpieces.

Condition of the experiment : max.196MPa, max.20%O_2+Ar

Fig. 2 shows the results of the ignition experiment.

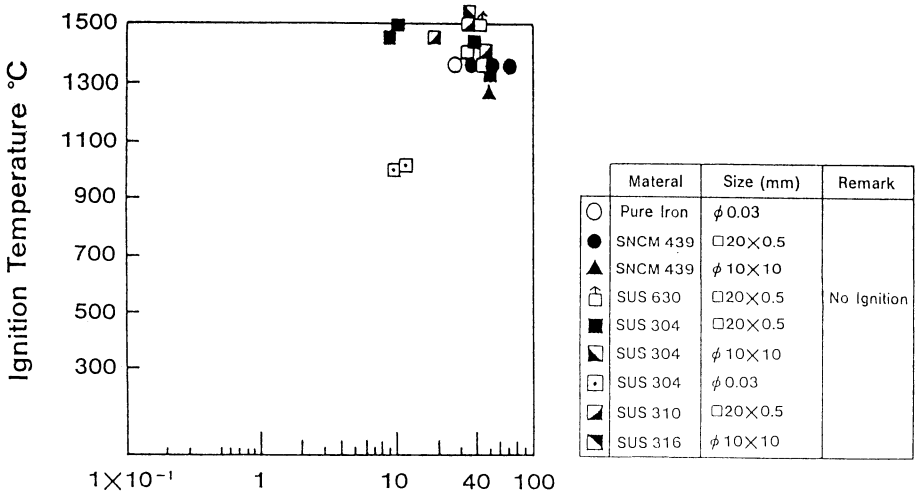

Figure 2. Relation between ignition temperature and oxygen partial pressure

The following results were obtained at an oxygen partial pressure of less than 39.2MPa:

(1) SUS304 and SUS316 ignited over 1001℃.
However, SUS630 did not ignite under 1500℃.
(2) Silicon rubber ignited over 321℃, PES over 364℃, EP over

411℃, fluorinated rubber over 350℃, and PTFE over 478℃.
(3) Copper alloys ignited over 1069℃.
Accordingly, O_2-HIP units have been designed and manufactured in Kobe Steel based on these data.

Example of O_2-HIP equipment

TABLE 1 shows the specifications of the experimental scale O_2-HIP apparatus (O_2-Dr.HIP) developed at Kobe Steel, utilizing a Pt-Rh heating element. Because this unit can also be equipped with molybdenum and graphite furnaces, it is widely used for fundamental research on the HIP process.

TABLE 1
Specifications of O_2-Dr.HIP

	O_2-Dr.HIP		
Heater	Pt-Rh alloy	Graphite (Optional)	Molybdenum (Optional)
Gas	Argon+oxygen (Max.20%)	Argon, Nitrogen	Argon
Hot zone dimensions	40mm dia. × 50mm H	50mm dia. × 70mm H	60mm dia. × 100mm H
Max. temp.	1600℃	2000℃	1500℃
Max.press.	2000kgf/cm²		

The technical features of O_2-Dr.HIP are as follows:
(1) Pressure vessel, closures, and gas cylinder of compressor are made of high strength stainless steel.
(2) High pressure seals at the top closure are protected from heat.
(3) 2000℃ inert gas HIP process is made possible by the replacement of the heating cartridge.
(4) There is an automatic discriminator between the cartridge for the O_2-HIP process and those for other processes.
(5) Gas compressor is designed to prevent oil from getting into the gas cylinder.

High temperature O_2-HIP

Following the current trends to increase the temperature of HIP in conventional units, a high temperature O_2-HIP apparatus has been developed.

Structure of high temperaure O_2-HIP apparatus

The basic structures and features are as follows:

(1) The heating element, insulating mantle, and support of workpieces are made of porous ZrO_2 ceramics which are effective agaist heat shock.
(2) As ZrO_2 heating element is used, pre-heating is necessary.
(3) The pre-heating element is set under the ZrO_2 heating element.
(4) The shape of the ZrO_2 heating element is a self-supported cylinder with two opposite slits.
(5) The radial size is compact because of item (3) and (4).
(6) The furnace size is 25mm in diameter × 50mm in height.

Operation

The resistance values of the ZrO_2 heating element are different by O_2 partial pressure.

Fig. 3 shows the relation between ZrO_2 heating element resistances and absolute temperature. When measuring, the ZrO_2 heating element was set as the workpiece in the atmospheric furnace and in the O_2-HIP furnace. It was found that the resistance value in the O_2-HIP furnace was about 10% less than in the atmospheric furnace.

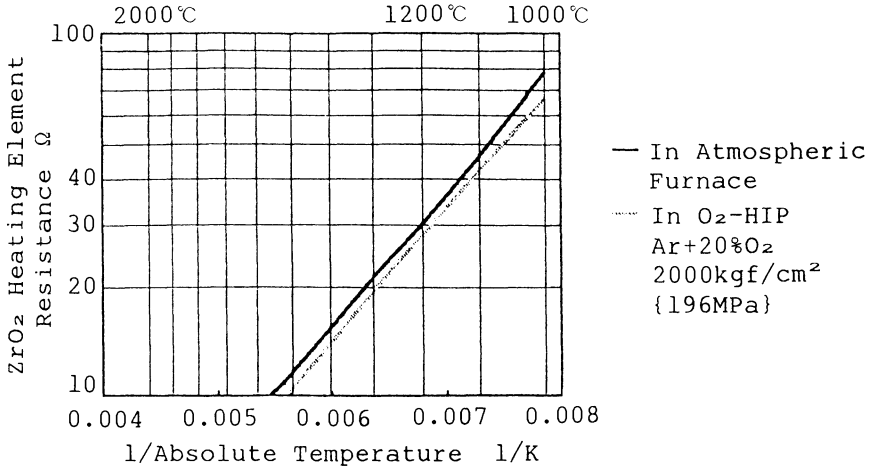

Figure 3. Relation between ZrO_2 heating element resistance and absolute temperature

Next, the operating process of high temperature O_2-HIP is described.

For pre-heating, the temperature is increased to the appointed temperature (ex. 1200℃). The pressure is increased initially or simultaneously. While keeping the pre-heating temperature constant, an electric current is applied to the ZrO_2 heating element, and the temperature is then increased at a constant

rate. After reaching a stable temperature and pressure, the temperature is lowered at a constant rate to avoid damaging the ZrO_2 heating element.
As a result, high temperature O_2-HIP has been achieved in this way.(Fig. 4)
Moreover, 2000℃ O_2-HIP has been reached by using the optical method among some temperature measurement systems in Kobe Steel, for example, by the use of new thermocouples, dilatometric temperature measuerment system, etc.

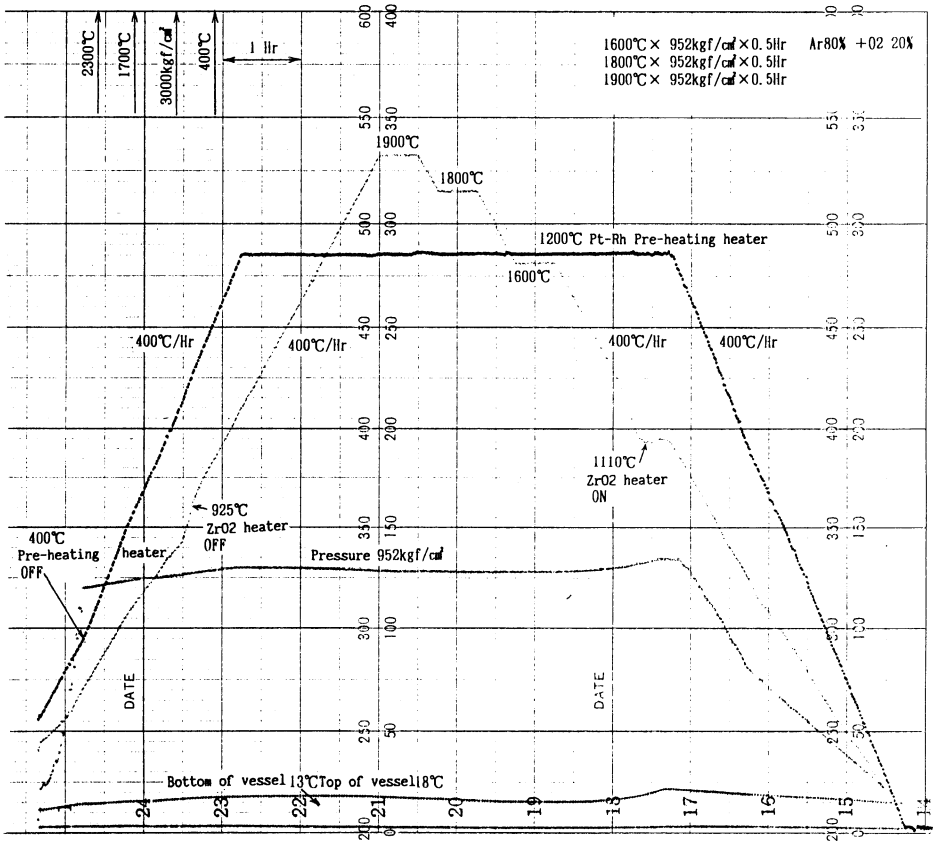

Figure 4. Chart of 1900℃ test run of high temperature O_2-HIP apparatus

Conclusion

HIP equipment has made a step forward in O_2-HIP due to the successful application of pressure medium gas, that is oxygen,

to workpieces.
We believe O_2-HIP equipment will have various uses because high temperatures have been achieved and most ceramics are oxides. Kobe Steel plans to carry on the technical development of O_2-HIP and hopes to continue to contribute to the advancement and promotion of isostatic pressing technology.

ACKNOWLEDGEMENT

This work was partially supported by the Mon-busho (Ministry of Education and Culture) under a cooperative program (Kyo-do Kenkyu) with Nagaoka University of Technology on O_2-HIPping. The authors wish to express their gratitude to these organizations.

REFERENCES

1. Fujikawa, T., Miyatake, T., and Okada, H., Control of oxidizing atmosphere in HIP. Text of KOBELKO 7th HIP Seminar, Kobe, Japan, November 1987.
2. Manabe, Y., Fujikawa, T., and Narukawa, Y., Effect of O_2 HIP for oxide ceramics. Proc. Second. Int. Conf. HIP, Gaithersburg, MD, USA, June 1989.
3. Seino, H., Ishizaki, K., and Takata, M., High total and high oxygen partial pressure effects on Bi-Sr-Ca-Cu-O superconductor during O_2-HIP Sintering. Jpn. J. Appl. Phys., 1989, 28(3) L371
4. Miyatake, T., Synthesis and superconducting properties of $YBa_2Cu_4O_8$. Text of KOBELKO 10th HIP Seminar, Kobe, Japan, December 1990.

HIP QUENCHING

by Carl Bergman and Anders Träff
ABB Metallurgy AB, S-721 66 Västerås, Sweden

Abstract

This paper presents a new method of heat-treatment that combines hot isostatic pressing (HIP'ing) and uniform rapid cooling. This method reduces costs, saves time, and produces better quality.

HIP Quenching in 2000 Bar Argon Gas

This new method of heat-treating turbine parts offers several advantages in comparison with the conventional method of first HIP'ing the part and then reheating and quenching it in a furnace designed for 6 bar.

Cost reduction and time savings:

The quenching is combined with conventional HIP'ing at the same cost as HIP'ing only. The parts are cooled more uniformly and consequently the average cost of correcting distortion will be lower.

Quality improvement:

The new method permits very close control of cooling rates and better uniformity in the cooling of the parts. The grain growth will be reduced due to the shorter time at high temperature.

To cool parts uniformly requires a high and uniform heat transfer coefficient (α) from the parts to the cooling medium and close control of gas temperature as a function of time. This is what HIP Quenching provides. Cooling rates of up to 500°C/minute can be programmed in the computer.

Typical pressure in HIP Quenching is 1000 - 2000 bar.

The heat transfer coefficient at 2000 bar is approximately 30 times higher than at 6 bar (100 to 300 W/m² °C compared with 3 to 9 W/m² °C).

Theoretically the heat transfer coefficient at 6 bar could be raised by blowing the gas by fan over the surfaces of the parts. However, the speed needed to achieve the same heat transfer is of the order of 110 m/s. As it is impossible to have a gas flow of that speed sweep every square inch of the charge, the heat transfer will differ up to 100 times between the different surfaces of the charge, resulting in very uneven cooling.

With HIP Quenching, the very high and uniform heat transfer coefficient assures that the surface temperature of all parts of the charge will follow the temperature of the high pressure gas very closely.

At 2000 bar the argon gas is a unique cooling medium that assures freedom from surface reactions. It has a density comparable with and a kinematic viscosity far lower than water.

The temperature in the furnace hot zone is kept uniform by stirring the gas during the rapid cooling.

The heat from the charge is dissipated through a powerful heat exchanger situated in the high pressure vessel but outside the furnace. Typical heat exchanger power is approximately 15,000 kW at 900 °C furnace temperature.

Physical data of argon gas at 900°C:

Pressure, bar	**6**	**1000**	**2000**
Density, kg/m^3	2.5	330	570
Specific heat, Cp WS/kg°C	510	540	540
Kinematic viscosity, m^2/s	$30 \cdot 10^{-6}$	$0.25 \cdot 10^{-6}$	$0.13 \cdot 10^{-6}$
Thermal conductivity, W/m°C	0.05	0.06	0.08
Coefficient of volumetric expansion, /°C	$0.86 \cdot 10^{-3}$	$0.68 \cdot 10^{-3}$	$0.58 \cdot 10^{-3}$
Typical heat transfer coefficient at free convection α, W/m^2 °C *	8	180	280

* The α values can be about 5 times higher at forced convection.

Fig. 1: Physical data of argon gas at 900°C.

The very high density of the argon gas at 2000 bar makes it a unique cooling medium. Even a very slow convection flow yields enormous cooling power.

Close coupling between gas and part's surface temperature:

The problem is illustrated below by studying a plate during quenching (see fig. 2).

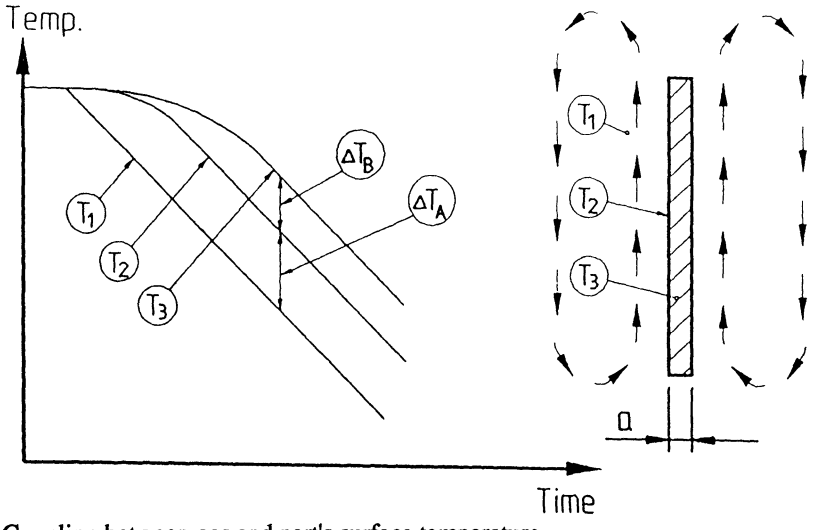

Fig. 2: Coupling between gas and part's surface temperature.

The gas temperature (T_1) has to be lower than the surface temperature (T_2). The difference in temperature, $T_2 - T_1 = \Delta T_A$, depends on the following factors:

- The cooling rate R
- The thickness of the metal a
- The density of the metal ρ
- The specific heat of the metal C
- The heat transfer coefficient α

$$\Delta T_A = \frac{K_1 \rho C R a}{\alpha}$$

See figs. 2 and 3.

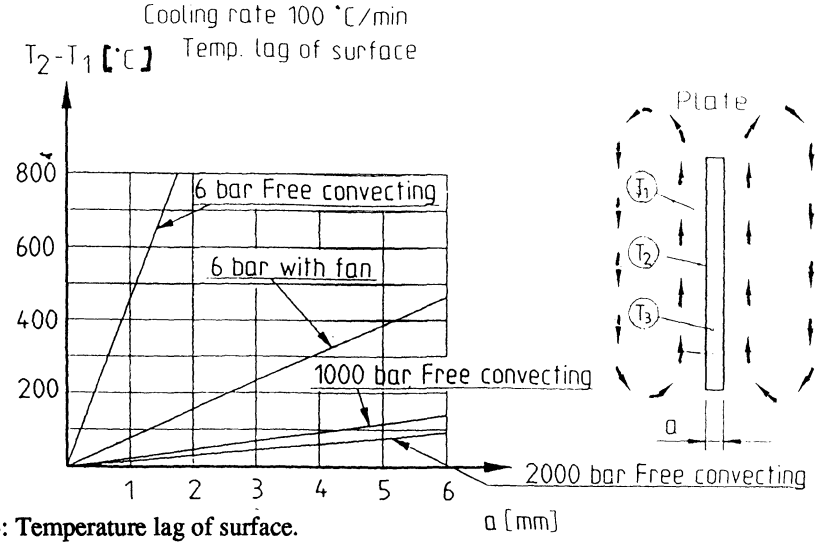

Fig. 3: Temperature lag of surface.

The difference in temperature inside the workpiece, between the surface and the core, $T_2 - T_3 = \Delta T_B$, depends on the following factors:

- The cooling rate R
- The thickness of the workpiece a
- The specific heat of the metal C
- The thermal conductivity λ
- The density of the metal ρ

$$\Delta T_B = \frac{K_2 \rho C R a^2}{\lambda}$$

See figs. 2 and 4.

Note that ΔT_B is independent of the α value.

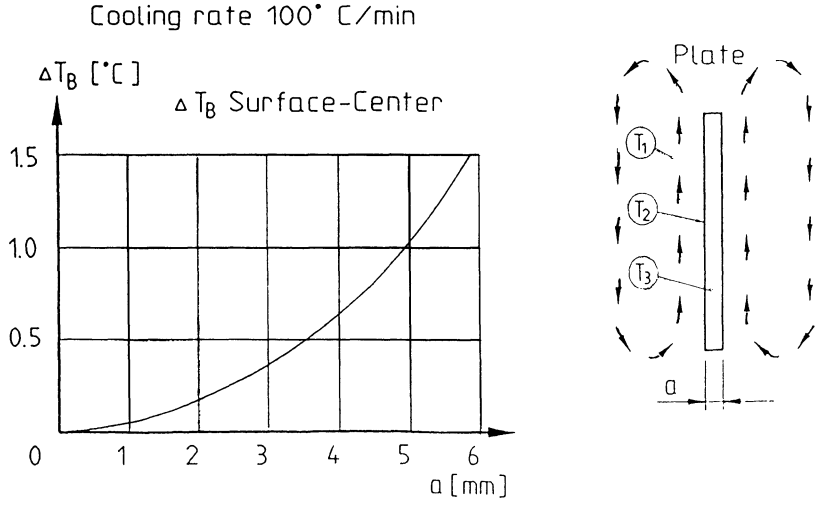

Fig. 4: Center temperature.

Distortion

Distortion is always a risk if the temperature differences in the workpiece are too big.

If the workpiece is made up of different thicknesses (see figs. 5 and 6) it is especially important to have a high α value to lower the distortion risk. A high α value yields smaller differences in temperature between thick and thin sections of the workpiece.

The furnaces for quenching at 6 bar normally incorporate a fan to increase the α value. The average speed of the gas is normally 5 to 10 m/s, which will give an α value of max 40-55 W/m^2 °C, but this will depend very much on the following factors:

- The shape of the workpieces.
- The positioning of the workpieces.
- The design of the charge basket.

We are here dependent on very complicated laws of gas flow dynamics which make it very difficult to predict the true α value. Parts of more complicated shape will cool very unevenly because of disturbances in the high velocity gas flow, which increases the distortion risk.

When quenching in a HIP working at 2000 bar it is not essential to place the parts in the same position each time. Here self convection of the highly dense gas alone will assure very high α values and thus minimum temperature differences and little distortion risk.

QUENCHING of a part according to figs. 5a and 5b has been computer-simulated to illustrate the influence of the heat transfer coefficient on the temperature differences in the part.

Necessary average cooling rate between 1200°C to 800°C was assumed to be 68°C/minute in the heaviest section of the part.

A comparison is made between the quenching process in a gas quencher operating at 6 bar and using a powerful fan to raise the α value (case a) and the quenching process in a HIP QUENCHER operating at 2000 bar and using only free convection (case b).

Figs. 5a and 5b (see page 6) illustrate the temperature distribution at the moment when the thickest section has reached 800°C. It can be observed that there is a difference of 328°C in the part quenched in the 6 bar quencher while there is a difference of only 160°C in the part quenched in the HIP QUENCHER. The risk of distortion due to uneven temperature is of course smaller in the HIP QUENCHER.

The diagrams in fig. 6 (see page 6) illustrate the temperature in the thinnest and the thickest sections and in the cooling gas as a function of the time. To get the desired cooling rate the gas in the 6 bar quencher has to have a much lower temperature than the part. The coupling between the gas temperature and the temperature of the part is much better in the HIP QUENCHER.

HIP QUENCHING opens up new quenching process control possibilities due to the following:

1. High heat transfer coefficient assures small temperature differences between gas and part surfaces.

2. Gas temperature can be accurately computer-controlled as a function of time.

3. Very high cooling power is available.

6 bar with fan.
Average cooling rate 68.5°C/min.
1200 - 800°C in the thickest section.
Time = 350 seconds

Fig. 5a

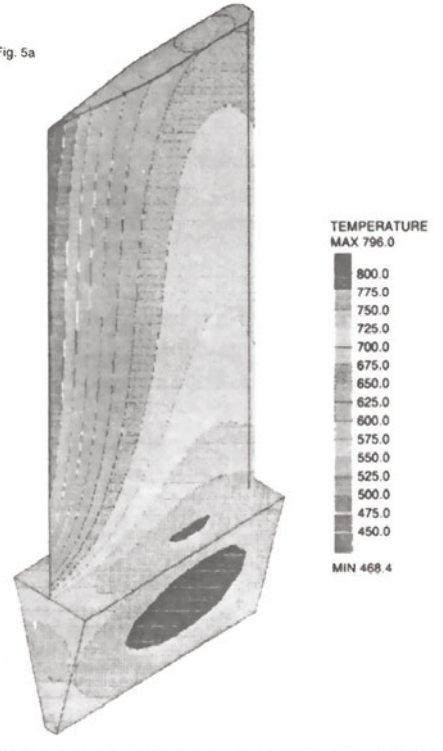

2000 bar free convection
Average cooling rate 68.5°C/min.
1200 - 800°C in the thickest section.
Time = 350 seconds

Fig. 5b

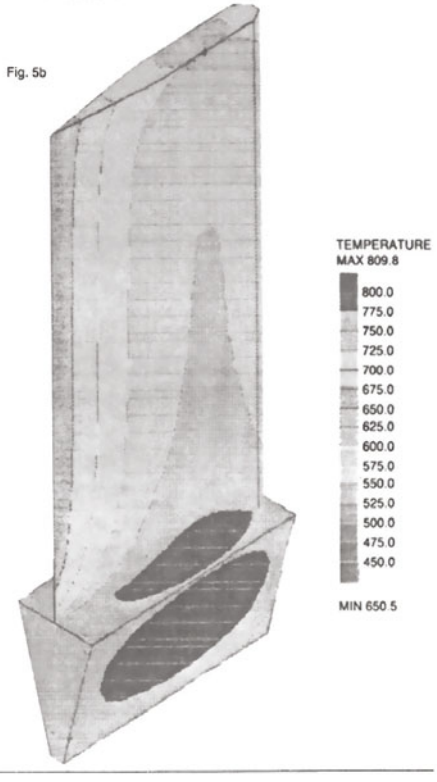

Fig. 6

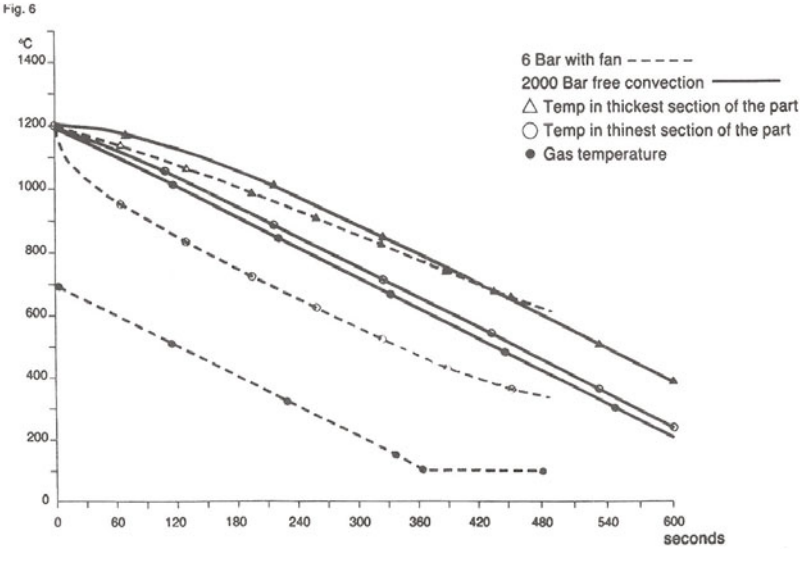

OXIDATION RESISTANT ODS-SUPERALLOYS FOR HIP-EQUIPMENTS

LOTHAR BRUECKNER
PM Hochtemperatur-Metall GmbH
P.O. Box 144, A - 6600 Reutte/Tyrol, Austria
EGON OKORN
Metallwerk Plansee GmbH
A - 6600 Reutte/Tyrol, Austria

Abstract

HIP-treating in oxygen containing atmospheres enables new material processing techniques e.g. the densification of ceramic superconducting or magnetic materials. In these circumstances HIP-equipments require oxidation and creep resistant materials. Exhibiting superior isothermal and cyclical oxidation resistance up to temperatures of 1440° C (2552° F), the new oxide-dispersion-strengthened iron-base superalloy PM 2000 is designated for applications in HIPs.

Introduction

Oxide-dispersion-strengthened ODS-superalloys on nickel- or iron-basis combine excellent strength and oxidation resistance up to temperatures close to the melting point. By the powder metallurgical production route of mechanical alloying [1] finely dispersed yttrium oxide particels can be introduced into the matrix. This dispersoid is stable in longtime service and is along with a coarse grain structure very effective for a high creep resistance. Chemical compositions with high chromium and aluminum content contribute to a high oxidation resistance.

Materials

PM Hochtemperatur-Metall GmbH is producing ODS-superalloys on iron-base (PM 2000) and nickel-base (PM 1000 and PM 3030) (Tab. 1).

Table 1
Chemical compositions of PM - ODS-alloys.

Alloy	Ni	Fe	Cr	Al	Ti	Mo	W	Ta	Zr	B	C	Y_2O_3	
PM 1000	bal.		20	0.3	0.5							0.6	wt.%
PM 2000		bal.	20	5.5	0.5							0.5	wt.%
PM 3030	bal.		17	6		2	3.5	2	0.15	0.01	0.05	1.1	wt.%

The production route of the materials contains as the principle step "mechanical alloying", where the powder feedstock is homogenized in chemical composition and a fine dispersion of oxide particles is obtained. Depending on the product form the mechanical alloyed powder is consolidated in steel capsules by hot extrusion or hot isostatic pressing. The grain size of this material is less than 1 μm and contributes to considerable metal forming capabilities to produce a wide range of semi-finished products and fabricated components. At last a final recrystallisation heat treatment results in a coarse grain structure (Fig. 1), that is responsible for a high creep resistance at very high temperatures [2, 3].

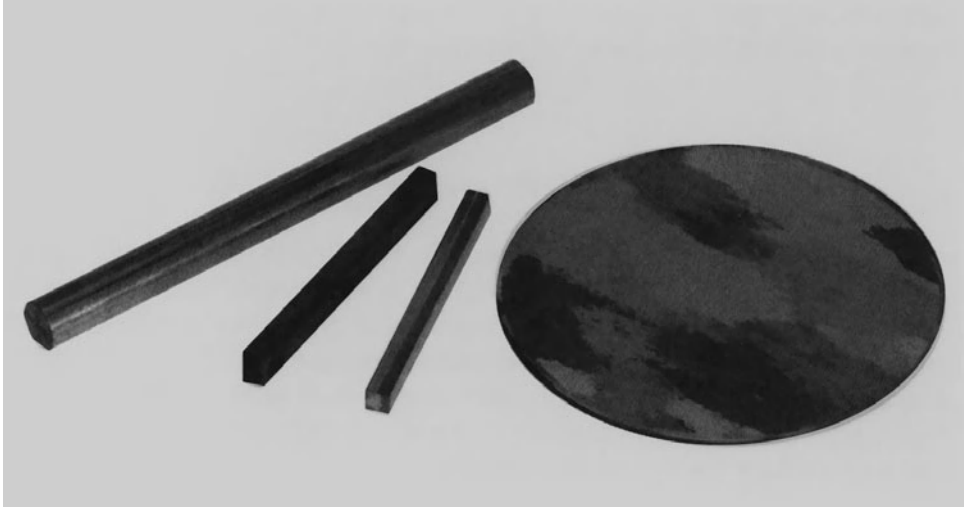

Fig. 1: Coarse grain structure in bar and sheet material of PM 2000.

Mechanical properties

Mechanical properties of PM - alloys at high temperatures are shown for tensile and creep strength in Fig. 2 and 3. Above temperatures of about 800° C the hot strength of ODS - alloys is superior compared with conventional heat resistant alloys [2]. The ODS - strengthening mechanismen is effective up to the melting point and the creep strength shows a relative small temperature dependance. In principle the strength level of nickel-base ODS-alloys is higher than for iron-base ODS-alloys, but the maximum application temperature for nickel-base ODS-alloys (PM 3030: T=1150° C) is lower.

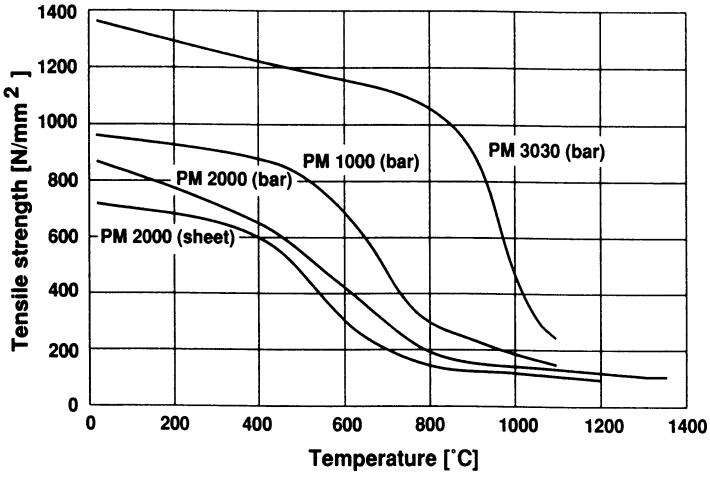

Fig. 2: Tensile strength of PM - ODS-alloys.

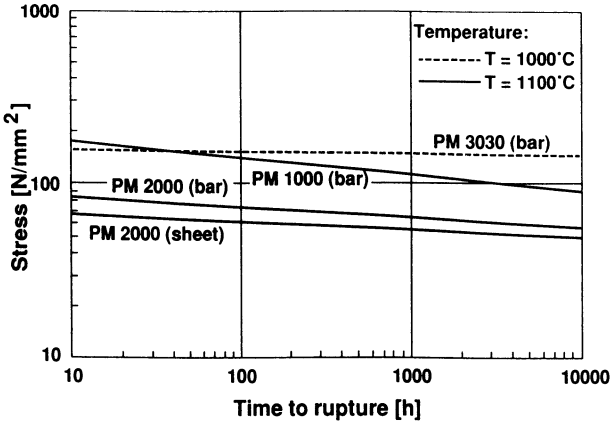

Fig. 3: Creep strength of PM - ODS-alloys.

During longtime application the yttrium oxide dispersion is stable and aging by coagulation of the particles does not occur.

Oxidation properties

An indication of the oxidation properties of PM 2000 in air atmosphere is shown in Fig. 4. At a temperature of T = 1350° C a small weight increase is observed for isothermal and cyclical test condition. Due to the high Al-content PM 2000 is protected from oxidation by the formation mainly of an Al_2O_3-scale on the surface, that is slowly growing and strongly adherent to the surface. In case of damages of the oxide-scale defects are quickly healing by diffusion of Al from the bulk.

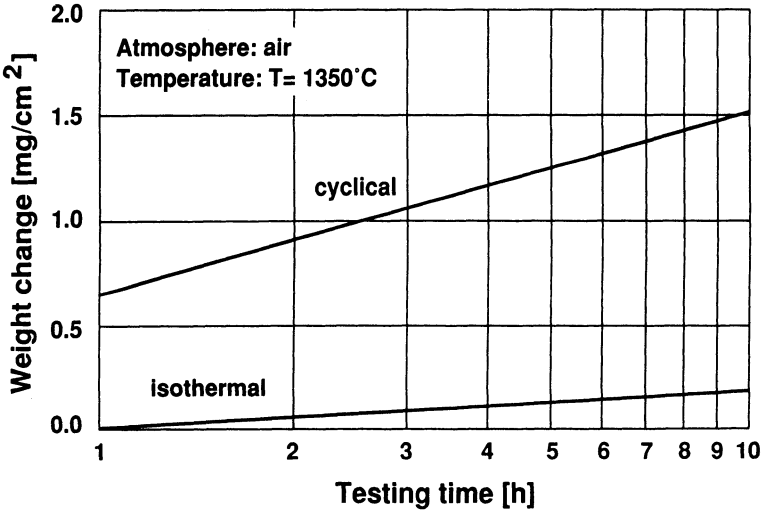

Figure 4. Isothermal and cyclical oxidation behaviour of PM 2000.

In Fig. 5 the cyclical oxidation behaviour of PM 2000 and PM 3030 are compared in air atmosphere for T = 1100° C. The test cycles of 60 min. included heating from room temperature to test temperature in 3.5 min. and cooling in 2 min. Under these severe test conditions the total weight increase was found for PM 2000 only 9 mg/cm^2 after 1000 cycles and indicats the excellent corrosion resistance. The oxidation behaviour of PM 3030 is attended by spalling of oxide layers resulting in a weight decrease. The high aluminum content in PM 3030 (6 wt.%) is less effectiv for the corrosion resistance as in the iron-base alloy, but provides a superior corrosion resistance in comparison with other nickel-base superalloys [4].

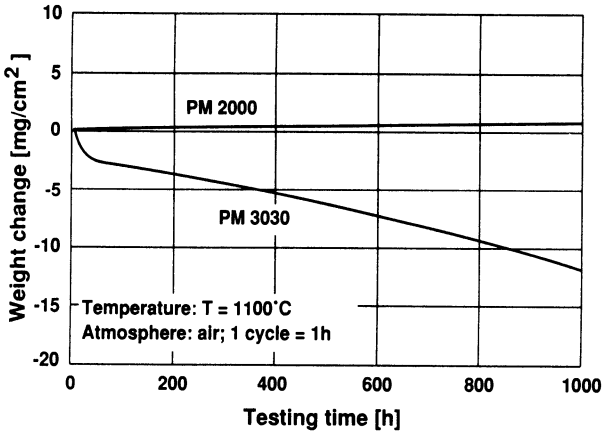

Figure 5. Cyclical oxidation behaviour of PM 2000 and PM 3030 in comparison.

Joining of PM 2000

Joining of PM 2000 is possible by electron and laser beam welding, TIG- and friction welding, diffusion bonding, brazing and riveting [5]. Fusion welding techniques affect the microstructure by melting the material in the weld pool, so that the coarse grain structure is destroyed and a coagulation of the dispersoids take place. Therefore reduced mechanical properties of weldings have to be accepted. In the case of electron beam welding the best tensile strength properties at higher temperatures are obtained (Fig. 6), whereas friction welding provides good results concerning creep strength. Fusion welding of PM 2000 is not restricted by pore formation in the weld pool like it is known from some other ODS-alloys.

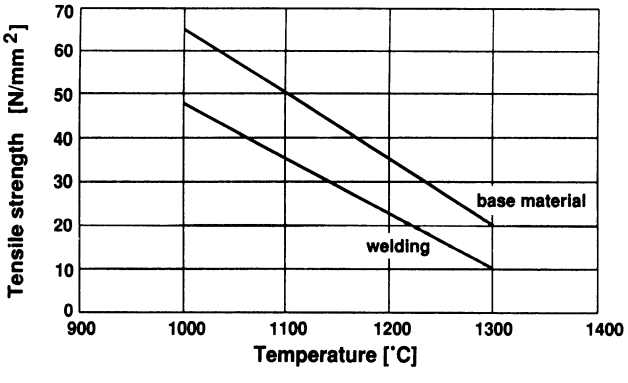

Figure 6. Tensile strength of PM 2000 electron beam weld at high temperatures.

Product forms of PM 2000

Some examples of PM 2000 product forms are presented in Fig. 7. Manufacturing techniques like forging, spinning, bending, cutting and machining are possible. To a certain extent the material properties can be adjusted to the application requirements by variing the metal forming conditions.

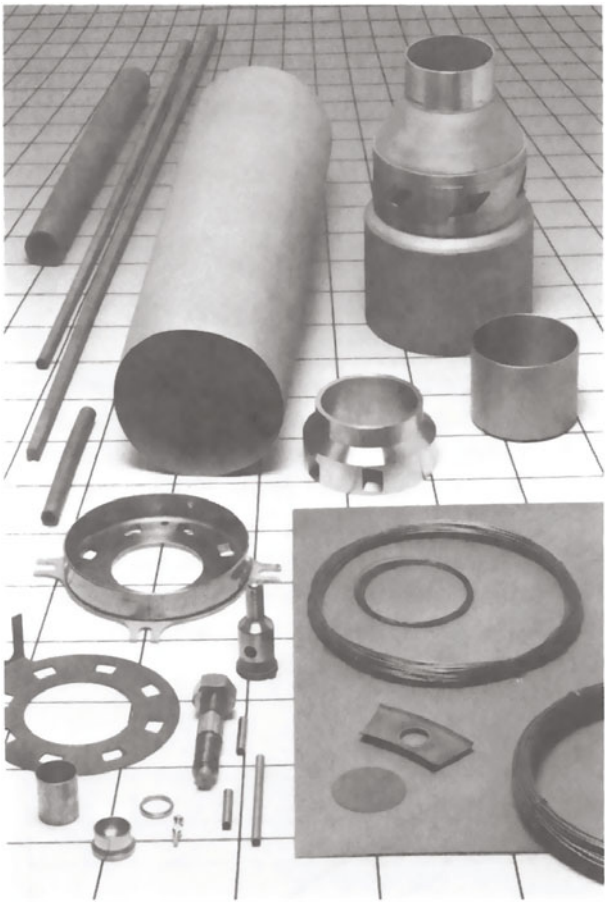

Figure 7: Examples of PM 2000 product forms.

Conclusion

In the circumstances that new production techniques require HIP-treatments under oxygen containing atmospheres new material solutions are necessary for HIP-equipments. The new iron-base ODS-alloy PM 2000 can be a reliable material solution for HIP-cylinders, charge carriers and thermocouple sheaths in fact of a high application temperatur in combination with a high creep strenght and hot gas corrosion resistance.

References

[1] Benjamin, J.S.: New materials by mechanical alloying techniques. Ed. E. Arzt and L. Schultz, Informationsgesellschaft-Verlag, Oberursel, 1989.

[2] Korb, G.; Rühle, M.; Martinz, H.-P.: New iron-base ODS-superalloy for high demanding applications. Presented at the Int. Gas Turbine and Aeroengine Cong. and Exposition, ASME, Orlando, FL, 3.-6. June 1991.

[3] Matucha, K. H.; Drefahl, K.; Korb, G.; Rühle, M.: Neue oxid-dispersions-gehärtete Legierungen für Hochtemperaturanwendungen. VDI-Ber. Nr. 797, 1990, p. 125-152.

[4] Quadakkers, W. J.; Schuster, H.; Schubert, F.; Nickel, H.: Behaviour of nickel based ODS alloys in oxidizing/sulphidizing environments at temperatures $\geq$ 1000° C. Will be presented at the conference Eurocorr '91, Budapest, 21-25.9.1991.

[5] Hedrich, H.D; Mayer, H.G.; Haufler, G.; Kopf, M.: Joining of ODS-superalloys. Presented at the Int. Gas Turbine and Aeroengine Cong. and Exposition, ASME, Orlando, FL, 3.-6. June 1991.

NUMERICAL SIMULATION OF RAPID-COOLING HOT ISOSTATIC PRESSING

SHIGERU WATATANI * , TOMOMITSU NAKAI ** , TAKESHI KANDA *
Mechanical Engineering Research Laboratory, *
Isostatic Pressing Center, **
Kobe Steel Ltd.
1-5-5 , Takatsukadai, Nishi-ku, Kobe, Hyogo, Japan

ABSTRACT

Transitional temperature distribution in Rapid-Cooling HIP process is indispensable information, both in designing the apparatus and in carrying out a successful treatment of workpiece. The experimental approach has limitations in estimating it on every occasion with wide range of furnace size and HIPping conditions. Eventually, numerical analysis of heat transfer mechanism is necessary in predicting the temperature profile. In analysis, the velocity distribution of the pressure medium should be pursued, while the region of the analysis should be extended to the whole apparatus.

In this paper, the gas velocity profile is calculated by adopting the $k-\varepsilon$ turbulence model. Simultaneously, transitional temperature distribution of the whole apparatus is determined. The outline of the analysis and the initial results are presented.

INTRODUCTION AND PROBLEM DEFINITION

A Rapid-Cooling HIP improves productivity. In addition, it is also possible to apply this apparatus to the heat treatment process.

In the HIP operating cycle, Rapid-Cooling is conducted by circulation of the pressure medium gas between the inside of a furnace and the outside, after held at HIPping temperature. The schematic view of Rapid-Cooling process is shown in Fig.2.

In Fig.2, the gas flow is caused by natural convection, however, various cooling patterns are made by increasing and controling the amount of the gas flow by mechanical methods, such as a fun operated by a motor.

In this Rapid-Cooling process, some problems which have not appeared in conventional HIP occer. The convectional heat transfer of the pressure medium flow is dominant in the apparatus, so that the temperature profile changes drastically from that of the conventional type. And the temperature profile varies more rapidly. The transitional temperature distribution is influential in making successful HIPping products, and in designing a cost effective furnace with a long lifespan.

Consequently, estimation of transitional temperature distribution in the HIP apparatus is absolutely necessary. However, there is a limitation to estimate on every occasion experimentally due to the demand to apply to wide range of furnace size. Numerical simulation is expected to have such flexibility. Since the circulation of the medium gas inside the vessel have a great role to transfer heat in Rapid-Cooling process, heat transfer analysis should be conducted on a region of HIP apparatus as a whole.

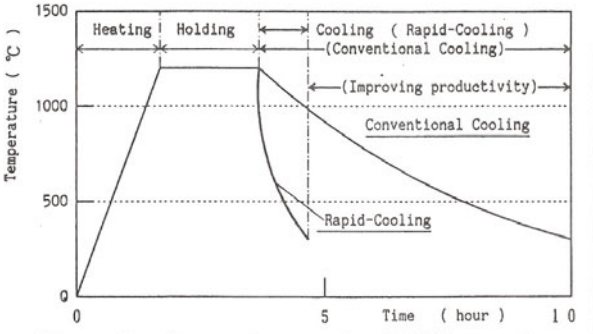

Figure 1. Temperature cycle of HIP operation

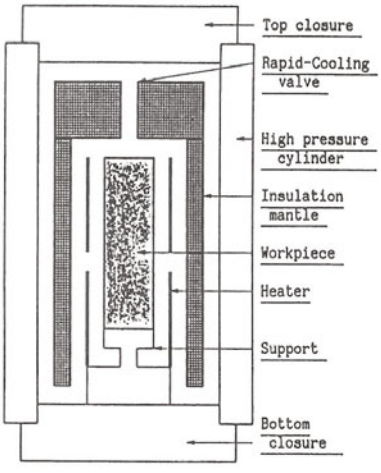

Figure 2. Simplified view of Rapid-Cooling HIP : Natural Convection type

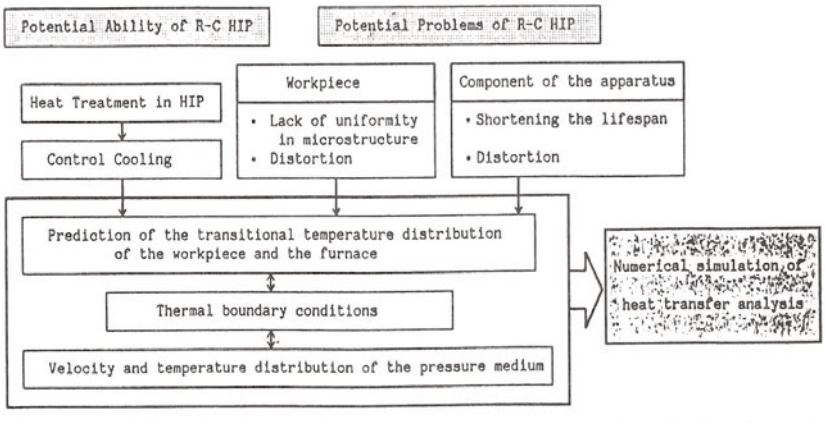

Figure 3. Schematic block diagram explaining necessity of the simulation

UNIQUENESS OF THE SIMULATION

Uniqueness of the simulation is attributed to the characteristics of the high pressure gas (100～200 MPa) properties (Fig.4,5). Kinetic viscosity is the major influential property when the heat transfer mechanism in fluid medium is considered.

Pressure dependence of the medium gas density is much larger than that of coefficient of viscosity, which means high pressure Ar gas is heavy as liquid but at the same time, has mobility as gas. As a result, heat transfer coefficient under high pressure gas is more than 100 times bigger than one under normal pressure.

Such relations are shown in Fig.6.

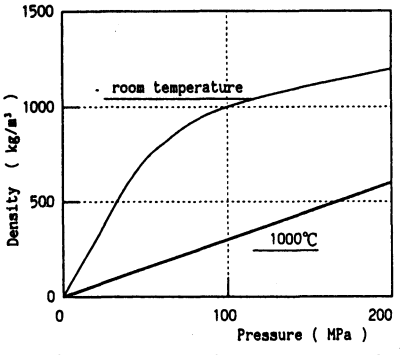

Figure 4. Pressure dependence of density (Ar)

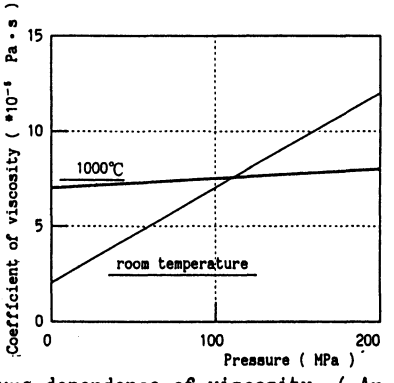

Figure 5. Pressure dependence of viscosity (Ar)

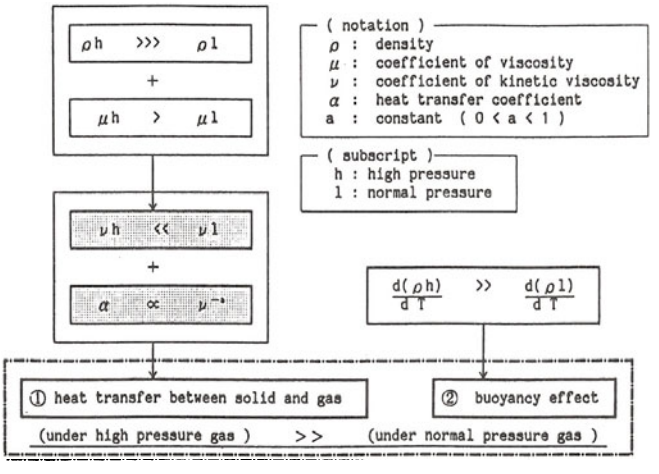

Figure 6. Schematic block diagram explaining uniqueness of the Simulation

MODELING AND CONDITIONS

The velocity of the medium is rather slow ($10^{-2} \sim 10^{0}$ m/s), however, low kinetic viscosity and the disturbance of the furnace components make the gas flow turbulent.

Gas flow distribution of the high pressure medium is simulated by k - ε model and calculated by supercomputer(VP-200).
The simulation was carried out under the following conditions.

TABLE 1
Conditions of Rapid-Cooling simulation

Initial conditions (HIPping conditions)	Pressure medium : Ar Pressure : 100 MPa Temperature : 1150 ℃
Furnace size	Φ 300. mm H 600. mm
Workpiece	Dummy (A column made of steel)
Cooling mechanism (2 cases)	a) Natural convection b) Forced convection (A fan installed in the bottom of the furnace)

RESULTS

The examples of the numerical simulation results are presented. All of the figures are the simulated results at 3 minutes after the beginning of Rapid-Cooling. A rough description of each case is in the following Table 2..

TABLE 2
Explanation of the results

Rapid-Cooling mechanism	Natural Convection (Fig.7-(a),Fig.8-(a))	Forced Convection (Fig.7-(b),Fig.8-(b))
Advantages	*Structually simple *Low running cost	*Isothermal atmosphere *Relatively fast cooling
Disadvantages	*Undesirable temperature differences	*Structually complicated *High running cost

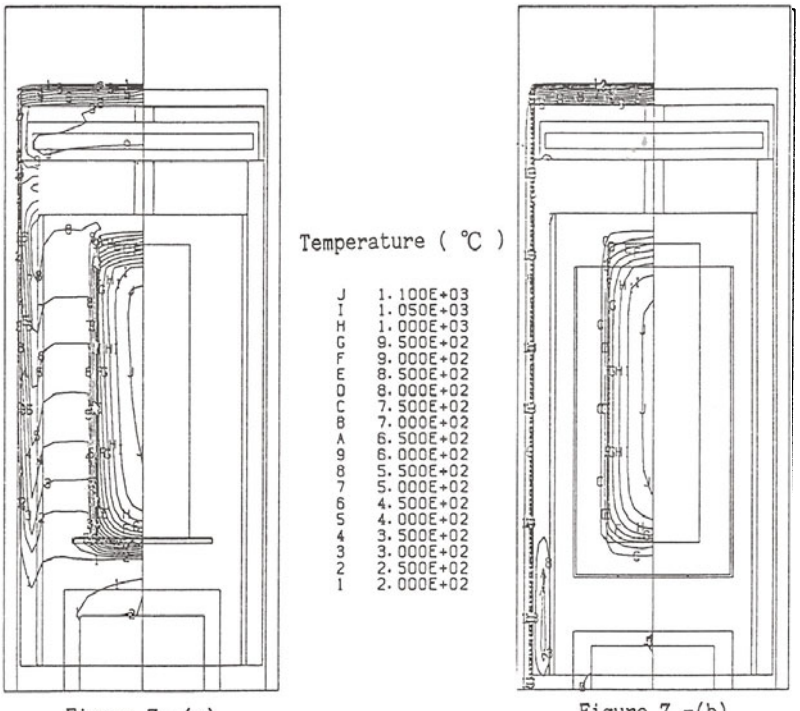

Figure 7.-(a) Figure 7.-(b)

Figure 7. Temperature profile of Rapid-Cooling HIP apparatus
(a): Natural Convection type (b): Forced Convection type

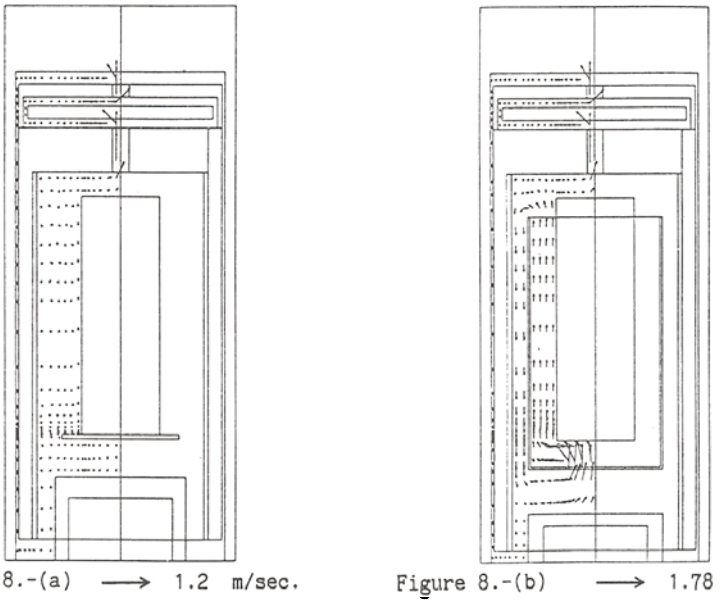

Figure 8.-(a) ⟶ 1.2 m/sec. Figure 8.-(b) ⟶ 1.78 m/sec.

Figure 8. velocity profile of pressure medium in Rapid-Cooling process
(a): Natural Convection type (b): Forced Convection type

The temperature range at the beginning of Rapid-Cooling process in the whole apparatus is wide enough to present in one figure. The inadequate temperature contour lines near the inner surface of the vessel is a problem of visualization. Actually, the transitional temperature profile of the vessel was obtained, which assures the possibility of practical applications.

CONCLUSION

The transitional temperature distribution of the whole HIP apparatus in Rapid-Cooling process was simulated.
In the process, the temperature and velocity distributions of the pressure medium gas were predicted numerically.
The simulated results proved to be available considering the comparison with the experimental ones, which assures the successful probability of practical applications of this simulation technique.

EQUIPMENT FOR NEW TECHNOLOGICAL PROCESSES OF HIP

G.A.Krivonos, V.I.Snop, A.A.Ezhov
Soviet-British Joint Venture METMACHECOSSE
Rjazansky prospect 8a, Moscow,USSR

T.R.Dick
Soviet-British Joint Venture METMACHECOSSE
P.O.BOX 8 HAMILTON ML3 OEL SCOTLAND

ABSTRACT

Along with HIP processes succesfully using Hot Isostatic Presses for commercial production of advanced materials (casting defect healing, powder metallurgy of superalloys, intermetallics and engineering ceramics) intensive research works are under development now in different countries and in different fields of science and techniques. There are such advantages fields as impregnation of porous materials with chemically active either liquid or gas medium under high pressure and temperatures. These processes may be utilised in order to design and manufacture new materials with unique preprogrammed properties. Another fascinating and rewarding development is in applying the HIP technique in manufacturing optical and ceramic materials along with Self-Propagating High-Temperature Synthesis. The developments of these fields haven't achieved yet the widely accepted level. That is why there is a demand not only for big but also for compact and high efficient laboratory Hot Isostatic Presses, equipped with the perfect modern tooling and instrumentation enabling users to carry out intensive material and technological researches.

INTRODUCTION

"Over the last thirty years hot isostatic pressing (HIP) has gone through the transformation from a laboratory curiosity to a widely accepted industrial process." [1]

Sharing this view we non the less can remark that said curiosity not only has been satisfied but an ever increasing number of researchers in different fields of science and industry tries to satisfy it again and again. Improvement of equipment opens new opportunities in tailoring materials and parts with unique properties. These materials help to improve equipment still more and so on without end. The carbon-carbon composites may serve as a very good example of the said endless progress. Now these materials manufactured by HIP are widely used for heaters and thermoinsulation in hot isostatic presses , that permits to increase working temperature up to more than 2000°C offering possibilities for the development of a new and novel family of composites exhibiting improved properties.

IMPREGNATION BY HIP

The production of carbon-carbon composites using HIP can include the impregnation of the porous base from a strong continues carbon fiber with a melted carbon pitch under high temperature and pressure. When heated contaminating gas components are released from the pitch affecting the systems of the hot isostatic press. This is the reason for that safe separation of these gases from inert (neutral) working medium in the vessel is an important engineering task. One of the possible solutions is a sealed retort inside the press working chamber with the treated workpiece and pressure synchronization between chambers.

Hot isostatic presses of Metmachecosse do have not require such the complete separation. Two mediums contact at the bottom of the working chamber. The temperature of the mediums at that place is comparatively low (up to 100°C) and due to the specially organized labyrinth two mediums are not mixed in the hot zone of the press. This design was tested in laboratory and industrial presses. Control of the gas chemical composition was achieved by the programmed input and output of appropriate components with feedback by the amount of the controlled gas component.

The tests proved high reliability of the systems and effective separations of the inert (neutral) medium from contaminated medium inside the working zone.

There are many other examples of such processes where a porous base is impregnated with melted material.

Results of many laboratory studies promise a big future for HIP in those cases.

SELF-PROPAGATING HIGH-TEMPERATURE SYNTHESIS (SHS)

Another example of HIP unusual application is production of ceramic parts using Self-Propagation High-Temperature Synthesis. The experimental processes demonstrate that there is considerable potential for engineering new materials in a controlled and reproducible method by utilizing HIP technology. Boron, aluminium and silicon were under study. Samples of preformed powders of these materials were placed in the working zone of the hot isostatic press.

The starting density was not less than 65%. High pressure of nitrogen (200 Mpa) and high temperature (2200°C) were used for achievment of about 100% density.

But combination of these conditions resulted in overheating and spontaneous reaction with nitrogen gas in a whole volume of the sample. This affected the quality of the product. It was found that said parameters had to be provided but only after completion of the exothermal reaction with a precalculated velocity of self-propagating. The development of a new heating system ensured the energy saving, the simplicity of the process, the relative purity of the products and simultaneus formation and densification of the product. The main feature of that system was capability to rise the temperature with the high speed (above 200°C/min) and heat transfer to the sample with a low speed (less than 20°C/min). The design of the thermoinsulation and material for it guarantee that the temperature of the sample was below the ignition point. As soon as combustion propagated the generated heat rised the temperature around the sample inside the thermoinsulation. After completion of the reaction the temperature there became higher than that of the heater. But a low temperature level was higher than allowed for begining the solidification. The heating system of a special design had been tested on the laboratory press. Results were very promising and now a new heating system for an industrial press is under development.

HIP OF FIBER OPTICAL MATERIALS

The compaction of a fiber optical materials is severaly restricted in todays tradition pressing equipment due to the stringent requirements on the uniformity of the temperature distribution. The use of high isostatic pressure and temperature provides a dramatic reduction in processing time of their treatment. The main feature of the process is the need for a precise and prolonged cooling with a very low speed. To use the unique and expensive equipment efficiently it is preferable to discharge the hipped product from the hot isostatic press and locate it into the furnace with subsequent programmed cooling the batch of such a product after some sycles of HIP.

Gas releasing and product discharge are to be carried out when the heater is not switched off and product is still hot but the press charging has to be done in a cooled working chamber. Thus heating system should work in oxidizing atmosphere and have means for a fast cooling between discharging and charging operations. As a rule the compaction of these materials is to be performed in glass containers. Manufacture of sealed containers is very complicated and expencive process, but it was found possible to produce them directly in the chamber during the HIP. This route is much easier than traditional process of container production and provides perfect quality of the product.

PRESSURIZING SYSTEM

In many HIP processes especially in laboratory presses rapid isostatic treatment considerably widen the scope of HIP application.

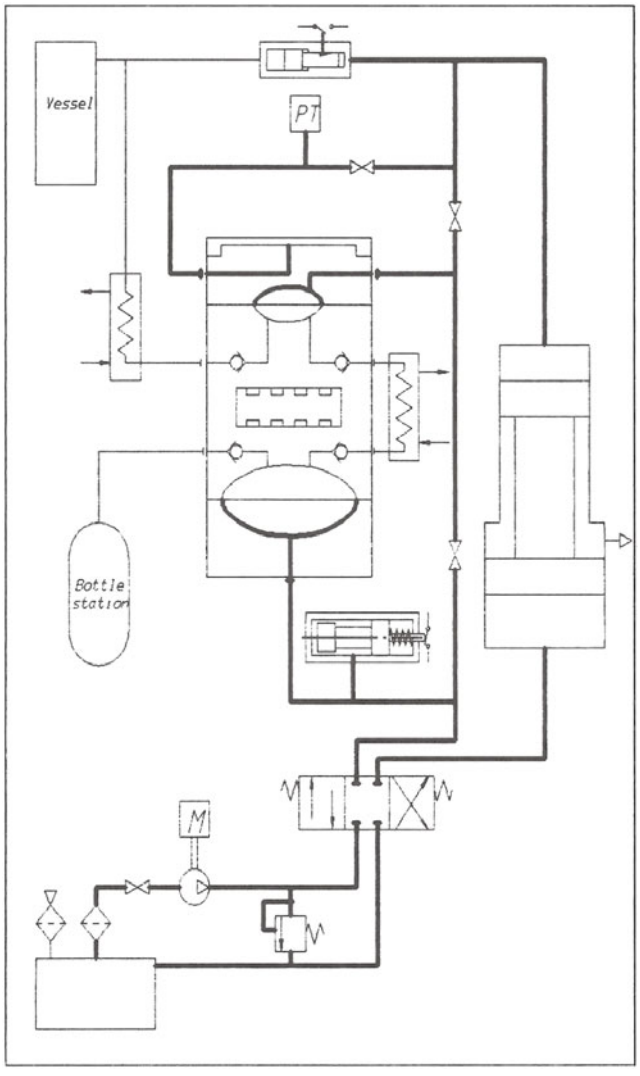

FIGURE 1. SCHEMATIC DIAGRAM OF THE HYDRAULIC AND PNEUMATIC SYSTEMS OF THE COMPRESSOR MME 20-44R WITH RUBBER DIAPHRAGMS.

PNEUMATIC

HYDRAULIC

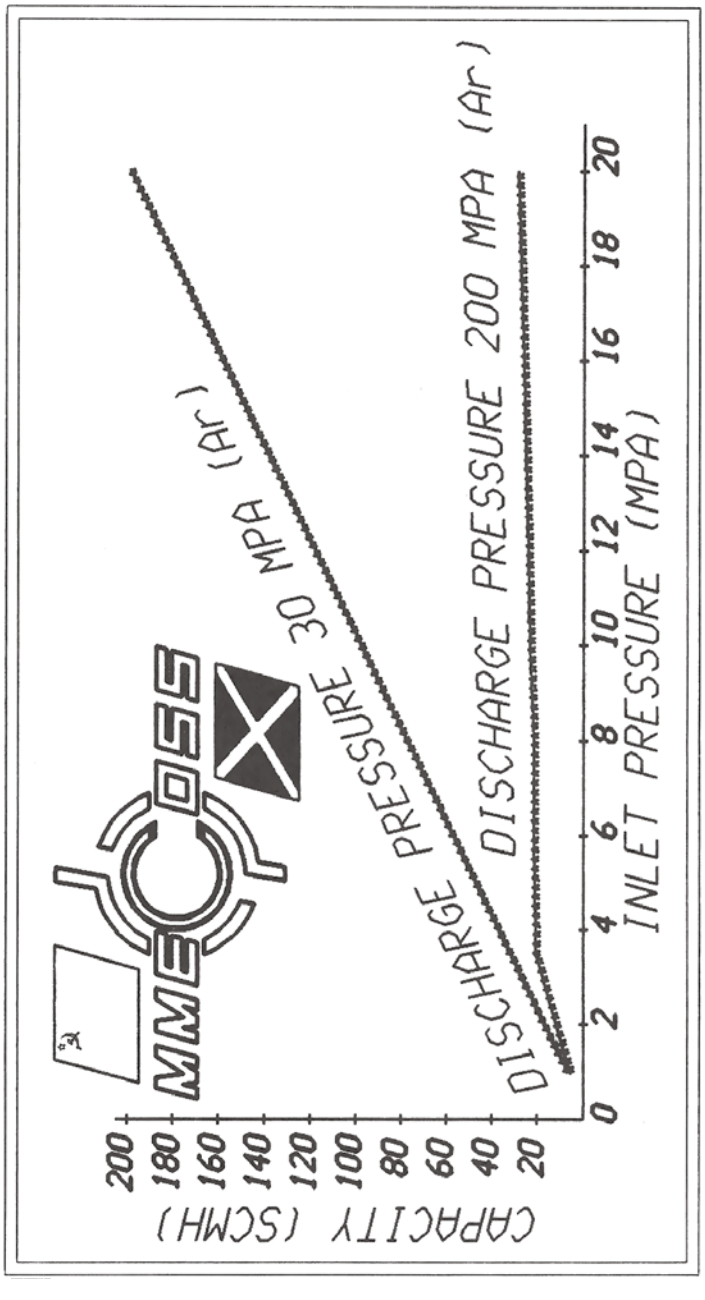

FIGURE 2. PERFORMANCE CURVE FOR COMPRESSOR MME 20-44R.

The processing time is defined basically by capacity of pressurizing system. All hot isostatic presses are equipped now with noncontaminated gas compressors of different designs. Their capacity varies directly with the dimensions and costs.It is accepted that the main problems dictating the choice of the compressor are pressure level, reliability, dimensions and cost. The capacity till now is not a critical parameter especially for laboratory presses. But rate of pressurizing as well as rate of heating is a processing parameter of HIP.
The most popular compressors are of steel diaphragm and piston types. Both of them are limited in capacity because of use threaded parts for pressure force holding. The volume of discharge there is also limited and increase in the capacity depends on the number of the strokes per minute. The higher the number of strokes the lower efficiency because of worse cooling conditions.
It has been manufactured and tested compressor of new design with flexible diafragm: minimum inlet pressure - 5 bars, maximum discharge pressure - 2000 bars.
The flexible diaphragm and autonomous hydraulic drive allow to discharge a few litres of compressed and cooled gas per cycle. Prestressed wound frame guarantees the safety and simple operation of the compressor.
Utilization of this compressor has proved its reliability and high efficiency along with compactness and reasonable price.
Perfomance curve and schematic diagram of the hydraulic and pneumatic system of the compressor MME-20-44R with rubber diahragms are shown in FIGURES 1 and 2.

CONCLUSION

The HIP method has found and is finding new applications in processing industry. Improvements in the field allows to widen horizons of science and technique. It is very difficult to guess the trends of further developments, but it is clear that HIP will "play a unique role where no other known processes can solve the problem" [1].
One thing which may be guaranteed surely is that only most efficient and equipped laboratory hot isostatic press will save money and time modelling now the equipment and processing for future.

REFERENCES

1. Widmer R., Current Status of HIP Technology and its Prospects for the 1990's.
The Fourth International Conference on Isostatic Pressing, Stratford, UK, 5-7 of november 1990.

HIP EQUIPMENT FOR THE EXTREME TEMPERATURES (3000°C)

SHOTARO HARANO, KEISHI AKIU, KOSAKU WATANDO
Engineering Division, NKK Corporation
2-1, Suehiro-cho, Tsurumi-ku, Yokohama, 230 JAPAN

ABSTRACT

NKK and ABB delivered the first hot isostatic press (HIP) for 3000°C in the world to a major Japanese company. The press successfully underwent test runs up to the maximum temperature. This press, built for a maximum temperature of 3000°C, is equipped with a graphite furnace of NKK-ABB's patented design having a hot zone volume of 2.5ℓ. The two individually controlled heating zones make it possible to achieve excellent temperature accuracy over the whole temperature and pressure ranges. Under vacuum conditions the maximum temperature is 2000°C, while the corresponding value at pressure up to 200 MPa is 3000°C. All types of material can consequently be densified in a wide spectrum of sintering cycles. Further, high-temperature materials can be tested under realistic conditions.
The press is equipped with NKK-ABB's proprietary High-Temperature Measuring System (HTMS), which permits operation with the above-mentioned combinations of temperature and pressure.
The delivery of the present 3000°C press marks an important step in the further development of the application range of HIP equipment. Such equipment can be operated reliably under well-defined conditions up to the most extreme parameters for the first time. This gives scientists total freedom in the selection of suitable sintering cycles.

HIGH TEMPERATURE MEASURING SYSTEM

The key to successful high temperature operation is the temperature measurement system. The upper limit for reliable use of thermocouples is about 1700°C with careful selection of clean insulators. An optical system has the drawback that it can only be used for reference measurement. The

refractive index of the gas depends on the pressure and the gas itself glows. It is thus very difficult to focus at a specific point with an internal lens system, thereby denying the possibility to use the signal for heater control for a multizone furnace.

The new proprietary NKK-ABB system can register temperatures up to 3000°C at individual points like a thermocouple with accuracy comparable with tungsten rhenium (in the temperature range where they are stable).
The concept is shown in Fig. 1 and the features are described as follows:

(1) The temperature range is 20 ~ 3000°C

(2) The measuring accuracy is equivalent to W-Re thermocouples, and the life is much longer.

(3) The sensor components are made of graphite, and no deterioration occurs due to carbonization.

(4) The calibration and the treatment of electrical signals are easy with a microcomputer.

(5) The measured results are linearized to generate output signals of either 0 ~ 10V or 0 ~ 20 mA.

(6) The influence of pressure on the measuring signals is compensated automatically.

(7) The computer is a small encapsulated unit which is installed inside a cabinet or an el-cubicle. The computer unit can handle the signals from two temperature transducers.

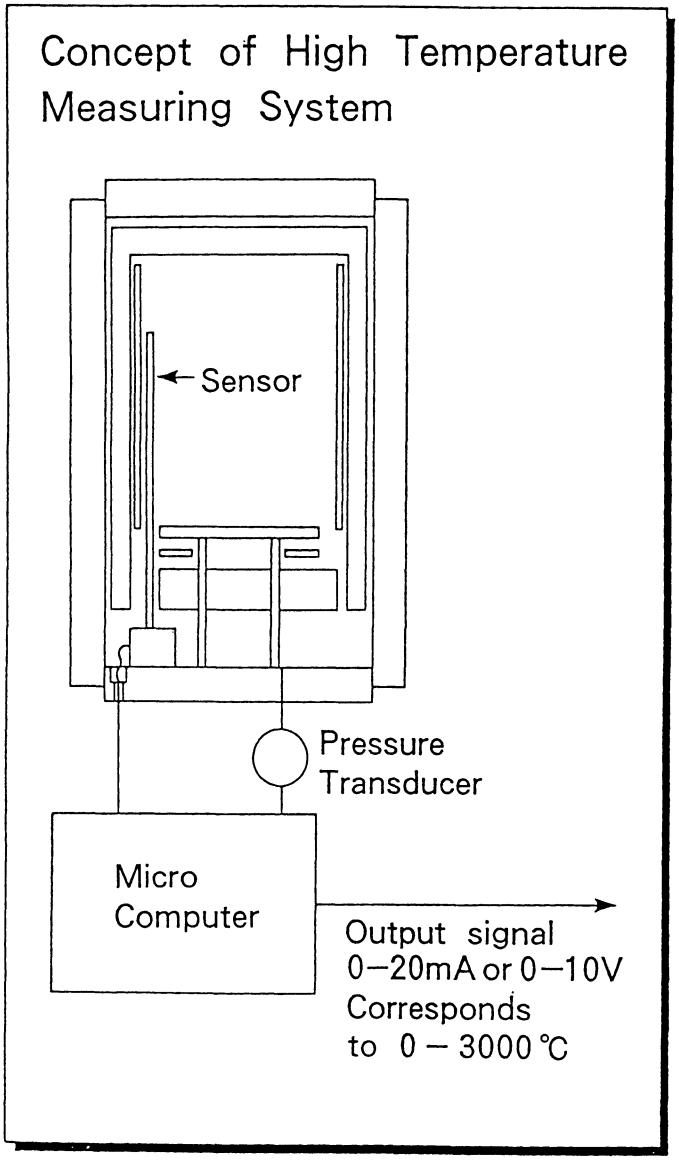

Figure 1. NKK-ABB High-Temperature Measuring System for HIP equipments

DATA OF HIGH TEMPERATURE MEASURING SYSTEM

The operation data are shown in Fig. 2 and 3.

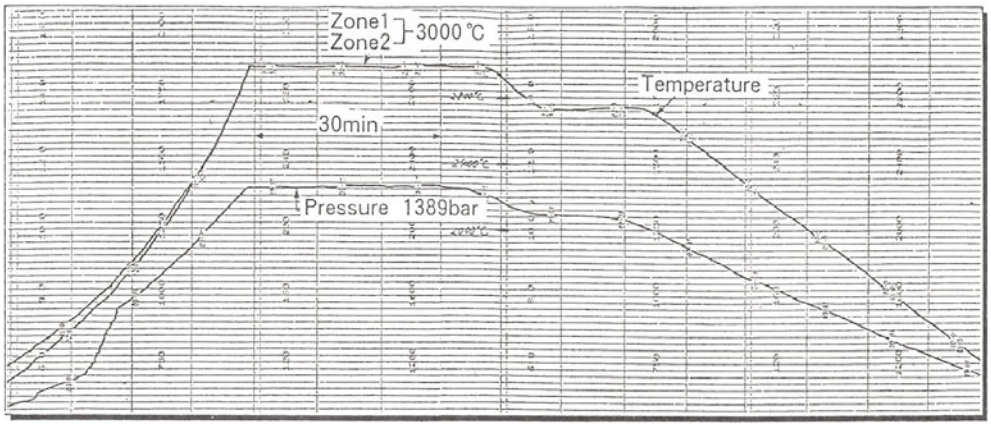

Figure 2. 3000°C Operation at high pressure

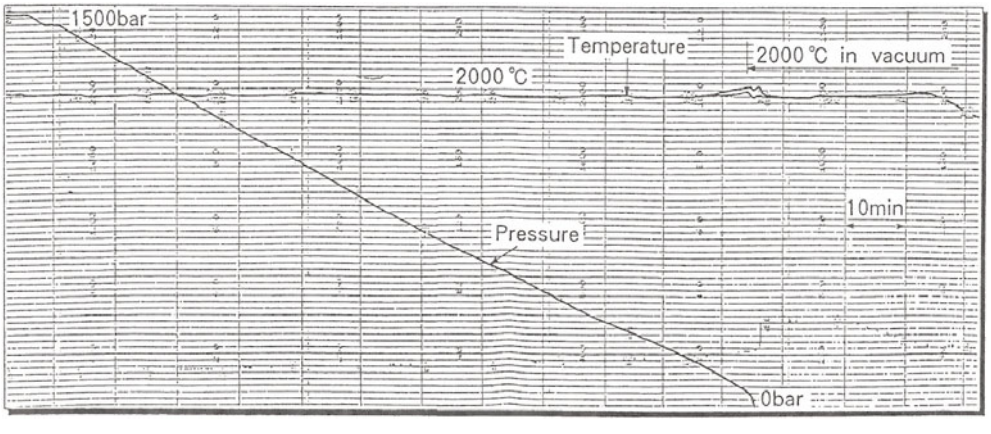

Figure 3. 2000°C Operation in vacuum and pressurization process

CONCLUSIONS

This high temperature measuring system is intended primarily for use at temperatures above 1700°C, where its reliability and repeatability are far superior to thermocouples. By using High-Temperature Measuring System in high temperature cycles (above 1700°C), faulty treatment of valuable charges due to thermocouples drift or break down can be avoided as well as time and costs for replacement of thermocouples.

NKK-ABB's HIP equipment for the extreme temperature provides the users with a powerful and cost-efficient production tool for advanced materials.

RECENT TRENDS IN COLD ISOSTATIC PRESSING

TOSHIKATSU NAOI, NORIYUKI NAKAI
No.2 Engineering Section, Engineering Dept., Industrial Machinery Group
Kobe Steel, Ltd., Kobe, Hyogo 651, JAPAN

TAKESHI KANDA
Mechanical Engineering Research Laboratory
Kobe Steel, Ltd., Kobe, Hyogo 651, JAPAN

ABSTRACT

Recently, interest in high-pressure food processing, such as processing relating to sterilization, has been growing rapidly because of its potential compared with the ordinary thermal type of processing. To meet this demand, Kobe Steel, Ltd. has developed a laboratory-size standard high-pressure food processor, using a thermal range from -20°C to 80°C.

INTRODUCTION

CIP (Cold Isostatic Pressing) is a process based on Pascal's principle, and it is said that this method first became known when a patent was granted in the U.S.A. in 1913 for a method developed to produce tungsten billets. The development of application techniques for this process was very slow due to the delay in the development of extra-high pressure technology. However, new attention was given to this process in the 1940's when it was applied to produce special materials for military applications, and this triggered rapid progress in technology involving CIP in the U.S.A. and Europe.
Japan was also influenced by this trend. Research into CIP related technology began in the 1950's, and this research led in the 1960's to industrial applications of CIP for high melting point metals, such as molybdenum, ceramics, such as alumina balls and fire resistant materials, such as immersion nozzles. At the same time, dry systems employing rubber molds were introduced. In the 1970's, the molding of ferrite was accompanied by a rapid growth in the application of small, wet-type equipment. The application started to cover the molding of ultra-hard alloys and carbon blocks in the late 1970's, and this was followed by the introduction of medium to large equipment. This continued until the middle of 1983.

After 1984, CIP was applied to high-quality products, such as non-oxide ceramics. The range of equipment has now diversified, and automatically-operated equipment is now being used to achieve high productivity. As for recent development, research is being done into applications of CIP in the food industry for sterilization, transformation and storage, and future progress in this area, or WIP (Warm Isostatic Pressing), is awaited with much interest.
This paper describes the most recent developments in CIP/WIP equipment.

Application to the Food Industry and Future Prospects

Application of High Pressure in the Food Industry

Since man discovered the use of fire, heat has been used for cooking, processing and sterilization of food. Recently, however, attention is being given to high-pressure processing as a replacement for heat, and the Ministry of Agriculture, Forestry and Fisheries has organized a project concerning this.
Protein undergoes denaturation without chemical change, as illustrated in Figure 1, when it is subjected to a pressure of several hundred MPa. It has also been confirmed that high pressure has the effect of sterilizing bacteria, such as colon bacilli, and affects enzymes, starch and lipids, and it is expected that these reactions will be used extensively for practical purposes in the near future.

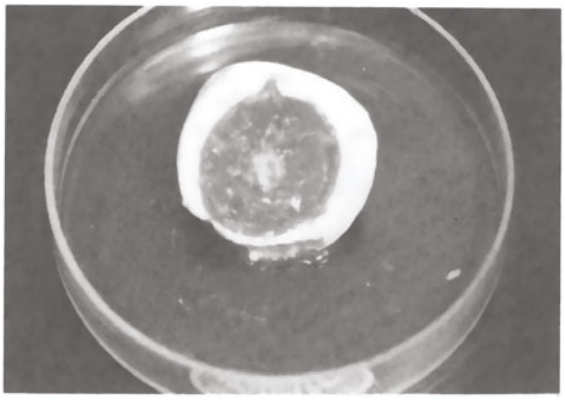

Figure 1. CIP'ed egg

High-Pressure Processing Equipment for Food (WIP Equipment)

When we consider the application of high-pressure equipment to food processing, the basic structure of CIP equipment can be retained, but the following points must be particularly taken into account: 1) the assurance of sanitation; 2) the assurance of safety; 3) simple operability and maintainability.
An experimental facility developed by our company for research into the application of high-pressure equipment for food processing (700 MPa, 60 mm in diameter and 200 mm high, RT-80°C) is illustrated in Figure 2.

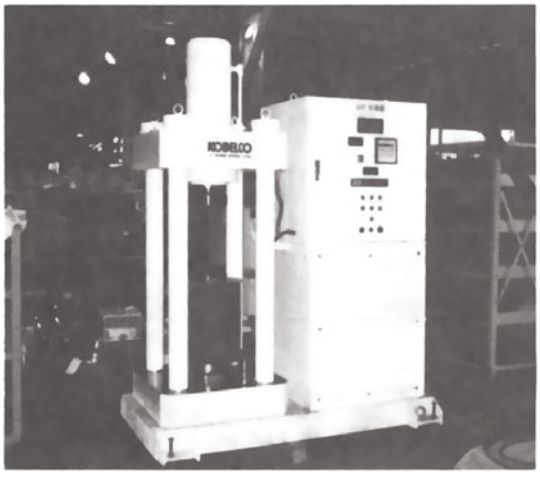

Figure 2. High pressure food processor

This equipment is a piston-drive, direct-pressurization type. A piston cylinder is provided in the upper inner side of the press frame, and a high pressure container is located at the lower side. The hydraulic system is installed on a common base, together with the control panel. The surface in contact with the liquid is made of high-strength, stainless steel, and drinking water is used as the working medium in order to maintain sanitary cleanliness. High safety is assured by the press-frame system and the single cylinder made of multiple-layer shrink fitting.
The charging and discharging of the processed object is carried out by a simple procedure, as the piston automatically rises to open the container when depressurization is completed. The heating of the container is provided by a sheath heater which is fitted around the periphery of the high-pressure cylinder. This equipment is provided with an internal temperature measurement system as standard, so temperature can be then recorded together with the pressure.

Production System

A high-pressure processing system for production use can be designed with adequate safety standards based on the design technology of CIP equipment, but more challenging problems are the assurance of cleanliness and the reduction of processing costs.
The simplest way of maintaining cleanliness is to use drinking water as the pressure medium and to pack the processed object like a retort pouch. When the processed object has a shape like a sausage, the application of dry CIP seems to be effective. It is possible to have liquid food products directly charged to the high-pressure container without packing, but it is important to maintain sterile conditions when the objective of processing is sterilization. Suitable equipment is a high-pressure sterilization unit for liquid food products, in which the processed object is pressurized via a flexible barrier, and the product is discharged by means of gas. Sterile charging should be possible if we use sterile gas.
It should be possible to reduce processing costs by a reduction of the processing pressure and the processing time, and by automation of the

processing procedure. In reducing the processing pressure and time, the use of various temperatures in combination with pressure should be taken into account as far as possible. It should be possible to use an automated CIP system as the equipment, and automate the stations for product packing, insertion into the basket, pre-heating, high-pressure processing, drying, removal from the basket, and crating, to formulate a system which can efficiently process a large amount of packed products. Continuous batch operations may be the practical way to reduce cost.

Development of a Standard CIP Series

Dr. CIP

In response to the request of researchers in various circles to "have CIP equipment which is handy to use", our company has developed and put into commercial use the compact, wet-type CIP equipment (named Dr. CIP, 400 MPa, 100 mm in diameter and 300 mm high), which is shown in Figure 3.

Figure 3. Dr. CIP

The operating circuits of this equipment have been simplified, and handling has been made easy by adopting a manual operation for the opening/closing operations of the press frame and for handling the valves which reduce pressure. The thrust force is produced by the press-frame system, and the high-pressure cylinder is simply made without threads. Sufficient safety features, as well as a mechanical interlocking system, to prevent over-pressure. The equipment is compact, the dimensions being 1.3 (W) x 1.1 (D) x 1.3 (H) meters, thereby making the equipment quite suitable for installation in a small space.

As the processing pressure of Dr. CIP is a maximum of 400 MPa, it can be used for molding oxide ceramics, non-oxide ceramics and metal powders. In addition, a dry attachment, (which has a patent pending), has been

developed to facilitate research on dry molding, thereby expanding the scope of application of Dr. CIP. The dry attachment consists of the attachment proper which incorporates pressurizing rubber, and a casting mold which is filled with powder. In operation, the attachment proper is positioned inside the container, and only the casting mold is taken out. In the molding operation, pressure is applied only in the radial direction via the pressurizing rubber mold and the casting mold.

The Standard Wet CIP Series; "ADW CIP"

As the scope of application of CIP expands, demands for medium- and small-sized wet CIP equipment for production use have increased. In response to such needs, our company has put on the commercial market the ADW (advanced wet-bag) CIP series, that is, standard wet CIP models with "high performance, low price and short delivery time". Table 1 shows the 28 combinations of specifications which can be found in the two series of this model.

Table 1
Specifications of "Advanced Series" wet-bag CIP

Series	Rated Press. MPa	Vessel Size mm	
		Diameter	Height
700	100	400	400
	200	300	500
	400	200	600
	500	150	
800	100	500	500
	150	400	600
	200	400	700
	300	300	800

In this series, too, emphasis has been placed on safety design, and a system with a "simple cylindrical container plus a press frame" has been adopted. At the same time, workability and maintainability have been enhanced, based on past experience, by adopting a "rotating-type press frame", (which has already been patented) and providing a wide working deck. A sheet key panel was used for the operating panel in order to improve the visual design and to prevent the ingress of dust. In addition, the hydraulic counter-facing type volumetric control system (which has already been patented), is provided as standard equipment for the operation of the secondary pressure reduction process below 20 MPa, in which delicate control is required. This makes it possible to implement the pressure reduction steps with high accuracy and reproducibility. The outside appearance of the 800 Series is shown in Figure 4.

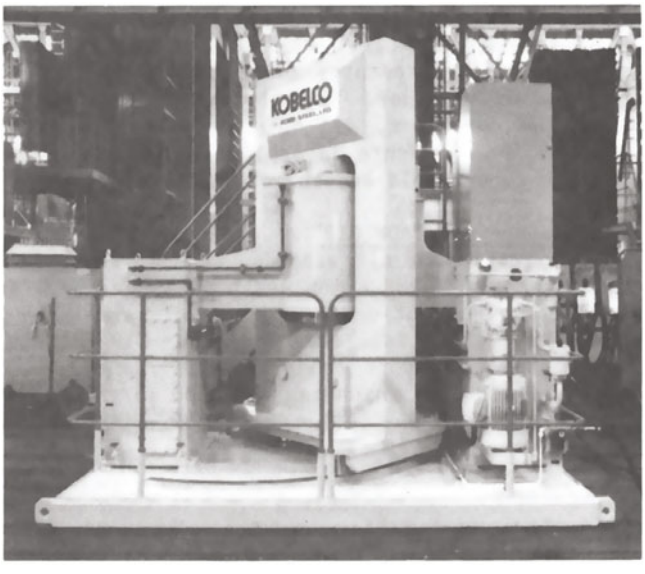

Figure 4. ADW CIP series (800 series, 200 MPa, ϕ400x800Hmm)

The World's Largest CIP Equipment

Extra-Large CIP Equipment

The increase in demands for refractories for steel and isotropic graphite materials, plus the stringent requirements on the high quality of these materials, have turned the needs of refractory and carbon product suppliers concerning wet CIP equipment towards larger and higher-pressure models. In response to this trend, our company has manufactured the world's largest equipment with a processing pressure of 200 MPa, with processing chamber dimensions of 2 m in diameter and 3 m high, and whose thrust force reaches as high as 618 MN.

In manufacturing the press-frame and high-pressure cylinder, the wire winding method was adopted, after considering the need for enhanced reliability under high pressure and large thrust force, ease of manufacture and transportation, and reduction of installation space.

For high-pressure cylinders, pre-tensioned piano wires with square cross-sections are wound on the periphery of the alloy cylinder having high tensile strength. For the press frame, the piano wires are wound on the left and right columns and on the upper and lower semi-circular yokes.

This structure has the following features, owing to the high precision wire winding technology of our company: 1) The equipment weight is reduced to 40 to 50% of that of conventional structures; 2) The mass effect produced by a large equipment component is reduced; 3) The stress distribution is simple, making it possible to increase the accuracy of calculation.

Dry CIP Equipment

Recent Trends in Dry CIP Equipment

There are two systems of dry CIP equipment; in-line systems in which the raw powder filling the rubber mold is supplied in high-pressure containers, and off-line systems in which the powder fills the mold outside the container.

The in-line system is used when powders having a superior filling performance are used to mold products having simple geometry, and the series of operations from powder feeding to the discharge of the molded product is generally performed automatically. In addition, there is a dual cylinder system, in which two containers have common pressurizing/depressurizing systems and press-frames for the purpose of enhancing productivity.

The off-line system is used for powders having an inferior filling performance or for molding products of complex geometry, and in general only the feed and discharge of the rubber mold are automated. The off-line, fully-automated, dry CIP equipment manufactured by our company has a processing pressure of 200 MPa, and has a rubber mold 200 mm in diameter and 200 mm high.

In this CIP equipment, all operations starting from the feeding and filling of the powder in the rubber mold to the discharging of the rubber mold can be performed automatically and continuously. Special features of this equipment are that powders which are not granulated and are, therefore, difficult for feeding and filling, can be handled, while products with different geometries can be molded continuously.

CONCLUSION

This paper has discussed recent trends in CIP/WIP equipment with an emphasis on the applications and structures of the equipment. It is anticipated that the needs of high-pressure processing will increase in the future, not only in relation to powder processing, but also to food processing. As the applications diversify in the future, the features of the various systems will also be diversified corresponding to the areas of application. We are anxious to continue the development and commercialization of new equipment under close cooperation with the users.

9. NEW APPLICATION

PROGRESS OF HIGH PRESSURE USE IN FOOD INDUSTRY

RIKIMARU HAYASHI
The Research Institute for Food Science, Kyoto University,
Uji, Kyoto 611, Japan

ABSTRACT

As temperature is used in cooking, pressure can also be used for food processing and preservation. Now in Japan there grows a recognition of two cooking methods by heat and pressure. In this report, principle of high pressure use for food, its merit, and present status of research and development are described.

INTRODUCTION

From more than a century ago, it has been known that bacteria are generally inactivated when they are placed under high pressure [1]. In 1914, P.W. Bridgman observed that "egg albumen" coagulated by high pressure [2]. Since these findings, many data about the pressure effects on living organisms and living matters have been accumulated [3].

The author started to study on the application of these phenomena to food in 1989. The research and development, therafter, are described in this report [I-III,1-11].

RESULTS AND DISCUSSION

An Egg Placed under High Hydrostatic Pressure [I,4,8]
When an egg is compressed in water by high pressure of several thousands bar, the egg is not crashed, although sometimes develops small crevices. In this experiment, there is water outside and inside the egg, and volume of the egg decreases by 15% at 6,000 bar. This small shrinkage results in no crashing of the egg shell.

After the pressure-treatment, egg proteins coagulate being cold: egg yolk coagulates at 4,000 bar or higher, and egg white does at 6,000 bar or higher.

The boiled egg and the pressure-coagulated egg are different in properties. Especially, the pressure-coagulated yolk is natural and vivid in color. Taste and flavor of the pressurized egg are natural

or raw without cooked flavor. Heat-sensitive vitamins, such as retinol, tocopherol, and folic acid are not destroyed by the pressure-treatment. Texture of the pressure-coagulated egg is unique: it is soft, grossy and not broken by pushing. Protease digestibility is improved by the pressure-treatment as well as the heat-treatment but former provides better digestibility of egg white.

In summary of the experiment with egg compresssion, a high pressure induces denaturation of proteins without causing chemical changes although high temperature sometimes destroys covalent bondings. This implies that high pressure-treatment generally coagulates proteins, therefore inactivates enzymes, gelatinizes starches, sterilizes microorganisms, and kills insects and parasites without destruction of nutrients and change in flavor and taste. Thus, high pressure is useful in food processing and preservation with unique merits (Table 1).

TABLE 1
Various Uses of High Pressure in Cooking, Processing and Preservation of Food as compared with High Temperature.

Phenomenon	Temperature	Pressure
Coagulation and denaturation of protein	0	0
Gelatinization of starch	0	0
Chemical changes[a]	0	X
Enzyme inactivation	0	0
Sterilization of microorganisms	0	0
Inactivation of bacterial spores	0	0[b]
Killing of insects and parasites	0	0
Stimulation of seed germination	0	0
Thawing of freezed food[c]	0	0
Non freezing preservation below 0°C[c]	X	0

[a] Maillard reaction, off-flavor, vitamin destruction, etc. [b] Possible by pressurization at elevated temperature. [c] See References II and III.
0, possible; X, impossible.

Pressure-Treatment of Food [I-III]

Food processing by high pressure: Soy protein suspended in water and packed in plastic tubes is completely coagulated at 4,000 bar.

Beef pressurized at 4,000 bar and room temperature for 10 min is like a raw ham and the taste of the pressurized beef is intact and a little sweet. When the surface of the pressurized beef is slightly baked, it tastes like a rare steak.

Generally saying, pressure-coagulated protein foods such as eggs, soy protein, beef, pork, and fish meat, are more glossy, transparent, dense, smooth and soft than boiled ones [9]. These unique textural properties obtained by pressurization offer new food materials.

Pressure effects on food proteins including meat, fish meat and plant are recent concerns [12-18]. Pressure control of intracellular proteases may be applied to meat tenderization [19].

Boiled shrimps turn red and curve, and the meat coagulate, but apparently there is no change after the pressurization at 4,000 bar for 10 min, although the meat coagulates as boiled one. When the pressurized shrimp is boiled, that turns red, curves and develops the flavor and

taste of the boiled shrimp. Raw oisters apparently show no change after pressurization at 3,000 or 4,000 bar and room temperature for 10 min, keeping the raw taste and flavor. This pressurized oisters may be safe without developing a stomachache [II,III].

Starches of potato, corn, and wheat are gelatinized by pressure-treatment, but the pressurization produces unique properties being different from heat-gelatinization[7]. The pressure-treated starches are digested very well by amylolytic enzymes such as alpha-amylase. This is similar to the phenomenon that the pressure treatment of proteins increases the proteolytic susceptibility. Thus, pressure-treatment opens a way for processing of starches with a minimum use of heat.

Food sterilization by high pressure: Bacteria, yeasts, and molds in foods including meat, fish meat, and agricultural products are sterilized by high pressure [20-24].

As an example [20,21], the pressurization at 3,000 to 4,000 bar is enough to sterilize vegetative cells of microorganisms, although spores of Bacillus sp. are not killed [II]. The pressure effect is higher at 45°C than at 25°C. Orange and mandarin juices pressurized at 4,000 bar for 10 min can be stored at room temperature for 5 monthes keeping good taste and flavor. However, pectin esterase is partly inactivated to produce precipitation during the storage.

Pressurized juice should be preserved by chilled conditions to keep the fresh flavor and taste in better conditions, and to reduce the development of precipitates. This is also the case for other foods, fresh taste or flavor of which is important such as pressure-processed jams.

To keep taste and flavor of traditional pickles, pressure-sterilization is useful though heat-sterilization deteriolates the flavor and taste [III]. In general, pressurization may be used for sterilization of fermentation foods while keeping their taste and flavor intact.

In summary, the prominent merit of high pressure sterilization for food preservation is to keep flavor, taste, and nutrients natural. This merit is effectively applied for the production of partially-prepared foods or oven-ready foods in combination with their chilled transportation. However, The Food Sanitation Act should be cleared for commercial selling.

Pressure Machine and Industrial System for Foods [I-III]

Recently, high pressure technology has greatly progressed and various equipment have been practically used in industry. Especially, CIP (cold isostatic pressing) is widely used to form powdered materials such as ceramics. In this process, water is pressurized to apply a uniform pressure to rubber molds containing ceramics powder. Huge CIP machines which compress several thouthands litters of water to 3,000 bar are operated in ceramics industries. However, machines for ceramics can not be directly applied for food processing.

In order to meet the requirments in food science and technology including food safety, test equipment for food have been developped in several machine manufactures. A typical equipment has the capacity of 500 ml and the maximum operating pressure of 7,000 bar. Pressurizing and depressurizing speeds are very fast and it takes only 90 seconds for pressurization. Temperature of the pressure medium water is regulated by an electric heater surrounded the pressure vessel. Thus, in this machine, hydrostatic pressure is directly applied to foods immersed in

the pressure vessel with high speed under regulated temperature without any harmful contaminants.

Industrial machines for food treatment by Mitsubishi Heavy Industries are operated in some food manufactures. Cycle time of the pressure operation is very short: it takes only 15 min for food sterilization or food processing, although a big pan takes about 1 hr for heating and cooling. Therefore, a pressure vessel of 50 liters corresponds to a heating vessel of 200 liters in quantity.

An industrial system for high pressure processing of foods is similar to the conventional heating process: raw materials are treated preliminarily, filled in plastic bags, sealed in vacuum, and pressurized. Final products are obtained after just drying.

Different from the heating process, metal cans and glass wares are not suitable for the pressure-treatment [II,III]. It may be pointed out that the use of pressure is energysaving and clean in comparison with the use of temperature.

Background of High Pressure Use in Food-Treatment

In Japan, foods of high quality, instead of the over-heated foods such as retort poches or autoclaved foods, are required by consumers. To meet the requirement, non-heating processes for sterilization and processing of foods become major concerns of food industries. Introduction of pressure-processing to food industries is natural and essential results. Heavy industries or machine industries have supported and developed the high pressure-processing of foods during these four year. This situation is a background of the development and interest in the high pressure use for food in Japan.

Already, almost 50 food manufactures have equipped high pressure test machines in these three years, and have been performing research and development for new foods. The author has organized five symposia on the subject of the high pressure use in food. On July in 1989, The Ministry of Agriculture, Forest, and Fishery in Japan has supported to found the Association of High Pressure Application in Food Industy. The Association includes 10 food and 7 machine manufactures.

Pressure-processed foods have been placed on the market on April 23 in 1990 by Meijiya Food Company. Those are three kinds of jam (strawberries, kiwis, and apples) made by high pressure-treatment without any heating process. They are vivid and natural in color and tast [25]. These jams are the first pressure-processed foods in the human history.

CONCLUSION

High hydrostatic pressure is useful for cooking, processing, sterilization, and preservation of foods, as is high temperature. The prominent merit of the high pressure is to keep flavor, taste, and nutrients natural. This merit should be effectively applied for partially-prepared foods in combination with their chilled-transportation system. Recent progresses of high pressure-technology support the production of machines for food industry.

In order to develop this philosophy, studies of biochemistry and food science under high pressure are required. High pressure science and technology have been developed in this century on the basis of physics, chemistry, and technology. Now, combined with bioscience, the high pressure science is going to be applied to the field of food,

medicine, and pharmacology for human welfare.

REFERENCES

Extensive symposium reports on this topic are

I. Hayashi, R. (ed.), High Pressure Use in Food, San-Ei Shuppan, Kyoto, Japan, 1989.

II. Hayashi, R. (ed.), Pressure-Processed Food: Research and Development, San-Ei Shuppan, Kyoto, Japan, 1990.

III. Hayashi, R. (ed.), High Pressure Science for Food, San-Ei Shuppan, Kyoto, Japan, 1991.

Literature cited

1. ZoBell, C.E., Pressure effects on morphology and life processes of bacteria. In High Pressure Effects on Cellular Processes, ed. A.M. Zimmerman, Academic Press, New York, 1970, pp. 85-130.

2. Bridgman, P.W., The coagulation of albumen by pressure. J. Biol.Chem., 1914, **19**, 511-2.

3. Hite, B.H., Giddings, N.J. and Weakley, C.E., The effect of pressure on certain microorganisms encounted in preserving fruits and vegetables. West. Va. Univ. Agr. Expt. Sta. Bull., 1914, **146**, 1-67.

4. Hayashi, R., Possibility of high pressure technology for cooking, sterilization, processing, and storage of foods. Shokuhin to Kaihatsu, 1987, **22(7)**, 55-61.

5. Hayashi, R., Kawamura, Y. and Kunugi, S., Introduction of high pressure to food processing : Preferential proteolysis of beta-lactoglobulin in milk whey. J. Food Sci., 1987, **52**, 1107-8.

6. Hayashi, R., Application of high pressure to food processing and preservation: Philosophy and development, Engineering and Food, Vol. 2, ed. Spiess, W.E.L. and Schubert, H., Elsevier Appl. Sci., England, 1989, pp. 815-26.

7. Hayashi, R. and Hayashida, A., Increased amylase digestibility of pressure-treated starches. Agric. Biol. Chem., 1989, **53**, 2543-44.

8. Hayashi, R., Kawamura, Y., Nakasa, T. and Okinaka, O., Application of high pressure to food processing: Pressurization of egg white and yolk and properties of gels formed. Agric. Biol. Chem., 1989, **53(11)**, 2935-39

9. Okamoto, M., Kawamura, Y. and Hayashi, R., Application of high pressure to food processing: Textural comparison of pressure- and heat-induced gels of food proteins, Agric. Biol. Chem., 1991, **54**, 183-9.

10. Okamoto, M., Hayashi, R., Enomoto, A., Kaminogawa, S. and Yamauchi, K., High-pressure proteolytic digestion of food proteins: Selective

elimination of beta-lactoglobulin in bovine milk whey concentrate, Agric. Biol. Chem., 1991, 55, 1253-57.

11. Tamaoka, T., Itoh, N. and Hayashi, R., High pressure effect on Maillard reaction, Agric. Biol. Chem., 1991, 55, 2071-4.

12. Matsumoto, T. and Hayashi, R., Properties of pressur-induced ges of various soy protein products, Nippoon Nogeikagaku Kaishi, 1990, 64, 1455-9.

13. Shoji, T., Saeki, H., Wakameda, A., Nakamura, M. and Nonaka, M., Gelation of salted paste of Alaska pollack by high hydrostatic pressure and change in myofibrillar protein in it, Nippon Suisan Gakkaishi, 1990, 56, 2069-76.

14. Ko, W.C., Tanaka, M., Nagashima, Y., Mizuno, H. and Taguchi, T., Effect of pressure treatment on depolymerization of fish F-actin, Nippon Suisan Gakkaishi, 1990, 56, 2109-12.

15. Suzuki, A., Watanabe, M., Iwamura, K., Ikeuchi, Y. and Saito, M., Effect of high pressure treatment on the ultrastructure and myofibrillar protein of beef skeletal muscle, Agric. Biol. Chem., 1990, 54, 3085-91.

16. Yamamoto, K., Miura, T. and Yasui, T., Gelation of myosin filament under high hydrostatic pressure, Food Structure, 1990, 9, 269-77.

17. Shimada, A., Kasai, M., Yamamoto, A. and Hatae, K., Changes in the palatability of foods by hydrostatic pressure, Nippon Shokuhin Kogyo Gakkaishi, 1990, 37, 511-9.

18. Shigehisa, T., Ohmori, T., Saito, A., Taji, S. and Hayashi, R., Effect of high hydrostatic pressure on pork slurries and inactivation of microorganisms associated with meat and meat products, Intl. J. Food Microbiol., 1991, 12, 207-16.

19. Ohmori, T., Shigehisa, T., Taji, S. and Hayashi, R., Effect of high pressure on the protease activities in meat, Agric. Biol. Chem., 1991, 55, 357-61.

20. Ogawa, H., Fukuhisa, K. Fukumoto, H., Hori, K. and Hayashi, R., Effects of hydrostatic pressure on sterilization and preservation of freshly-squeezed, non-pasteurized citrus juices. Nippon Nogeikagaku Kaishi, 1989, 63, 1109-14.

21. Ogawa, H., Fukuhisa, Kubo, Y. and Fukumoto, H., Pressure inactivation of yeast, molds, and pectinesterase in Satsuma mandarin juice: Effects of juice concentration, pH, and organic acids, and comparison with heat sanitation, Agric. Biol. Chem., 1990, 54, 1219-25.

22. Hara, A., Nagahama, G., Ohbayashi, A. and Hayashi, R., Effects of high pressure on inactivation of enzymes and microorganisms in non-pasteurized rice wine (Namazake), Nippoon Nogeikagaku Kaishi, 1990, 64, 1925-30.

23. Shimada, K. and Shimahara, K., Decrease in high pressure tolerance

of resting cells of Escherichia coli K12 by pretreatment with alternating current. Agric. Biol. Chem., 1991, 55, 1247-51.

24. Watanabe, M., Makino, T., Kumeno, K. and Arai, S., High-pressure sterilization of ice nucleation-active bacterial cells, Agric. Biol. Chem., 1991, 55, 291-2.

25. Horie, Y., Kimura, K., Ida, M., Yosida, Y. and Ohki, K., Jam preparation by pressurization, Nippoon Nogeikagaku Kaishi, 1990, 65, 706-7 and 975-980.

LIST OF CONTRIBUTORS